MODELING AND OPTIMIZATION OF MICRO-EDM OPERATION FOR FABRICATION OF MICRO HOLES

Himanshu Mishra

Mechanical Engineering
National Institute of Technology Rourkela

MODELING AND OPTIMIZATION OF MICRO-EDM OPERATION FOR FABRICATION OF MICRO HOLES

Dissertation submitted to the

National Institute of Technology Rourkela

in partial fulfillment of the requirements

of the degree of

Doctor of Philosophy

in

Mechanical Engineering

by

Himanshu Mishra

(Roll Number: 511ME134)

under the supervision of

Prof. Kalipada Maity

January, 2017

Department of Mechanical Engineering

National Institute of Technology Rourkela

Mechanical Engineering
National Institute of Technology Rourkela

January 14, 2017

CERTIFICATE OF EXAMINATION

Roll Number: 511ME134
Name: Himanshu Mishra
Title of Dissertation: Modeling and Optimization of micro-EDM operation for fabrication of micro holes

We the below signed, after checking the dissertation mentioned above and the official record book (s) of the student, hereby state our approval of the dissertation submitted in partial fulfilment of the requirements of the degree of Doctor of Philosophy in Mechanical Engineering at National Institute of Technology Rourkela. We are satisfied with the volume, quality, correctness, and originality of the work.

Kalipada Maity
Principal Supervisor

Sushanta Kumar Sahoo
Member (DSC)

Manoj Mishra
Member (DSC)

Mithlesh Kumar
Member (DSC)

Sushanta Kumar Panigrahi
Examiner

Ranjeet Kumar Sahoo
Chairman (DSC)

Mechanical Engineering
National Institute of Technology Rourkela

Prof. Kalipada Maity

Professor

January 14, 2017

SUPERVISOR'S CERTIFICATE

This is to certify that the work presented in this dissertation entitled "*Modeling and Optimization of micro-EDM operation for fabrication of micro holes*" by "*Himanshu Mishra*", Roll Number 511ME134, is a record of original research carried out by him under my supervision and guidance in partial fulfillment of the requirements of the degree of *Doctor of Philosophy in Mechanical Engineering*. Neither this dissertation nor any part of it has been submitted for any degree or diploma to any institute or university in India or abroad.

Kalipada Maity

DECLARATION OF ORIGINALITY

I, *Himanshu Mishra*, Roll Number 511ME134 hereby declare that this dissertation entitled “Modeling and Optimization of Micro-EDM operation for fabrication of micro holes” represents my original work carried out as a doctoral student of NIT Rourkela and, to the best of my knowledge, it contains no material previously published or written by another person, nor any material presented for the award of any other degree or diploma of NIT Rourkela or any other institution. Any contribution made to this research by others, with whom I have worked at NIT Rourkela or elsewhere, is explicitly acknowledged in the dissertation. Works of other authors cited in this dissertation have been duly acknowledged under the section "References". I have also submitted my original research records to the scrutiny committee for evaluation of my dissertation.

I am fully aware that in case of any non-compliance detected in future, the Senate of NIT Rourkela may withdraw the degree awarded to me on the basis of the present dissertation.

January 14, 2017
NIT Rourkela

Himanshu Mishra

ACKNOWLEDGMENT

I wish to express my deep sense of gratitude to **Prof. Kalipada Maity** my supervisor for his esteemed guidance, valuable encouragement, moral support, free to act on my ideas and scholarly inputs from early stage of research work that in still confidence in me during the research duration. Above all, his priceless and meticulous supervision at each and every phase of work has been the cradle of illumination for me. This thesis could not have been completed without his accordant suggestions, motivation, constant encouragement and crucial contribution, which have enriched value of my thesis.

I express my sincere thanks to **Prof. Siba Sankar Mohapatra**, Head, Mechanical Engineering Department for providing me all departmental facilities to carry out the research work.

I am also highly obliged to **Prof. Animesh Biswas**, our Honourable Director and **Prof. Banshidhar Majhi**, Dean (Academic Affairs), National Institute of Technology, Rourkela for their academic support and concern about requirements to carry out the research work at the Institute.

I also greatly acknowledge the financial support given by the Ministry of Human Resource Development, Government of India during my tenure of stay at National Institute of Technology, Rourkela.

I always cherish association with my friends and co-research scholars **Abhijeet Ganguly**, **Panchanand Jha**, **Anshuman Kumar, Swastik Pradhan**, **Sambit Mohapatra** who made my stay at NIT, Rourkela pleasant and memorable.

The thesis would remain incomplete without my parents for their inseparable support and encouragement at every stage of my academic and personal life to see this achievement come true. I am greatly indebted to them for sincerely bringing me up with care and love. I am highly thankful to my father for bearing the inconvenience of stay away from me.

Generally, people say no man succeeds without a good woman behind him. I specially thank my wife **Ranjana** for her enthusiastic cooperation, forbearance and sympathetic understanding to me in all times. Last but not the least I will always be thankful to my daughter **Aparna** for giving his cute smiles and doing all the naughty activities, which always releases all the stresses running in my mind.

Above all, I owe it all to Almighty God for granting me the wisdom, health and strength to undertake this research task and enabling me to its completion.

Himanshu Mishra
NIT Rourkela Roll Number:511ME134

Abstract

Rapid developments in the micro-machining and innovations in advanced engineering materials have led to the increased demand for micro-structures in various industries such as aerospace, biomedical equipment's, fuel injection nozzles and for producing micro-holes in a turbine blade for cooling effect in aeronautics applications. These typical applications require rigid design requirements and close tolerances in manufactured products. In recent years, numerous developments in micro-EDM have focused on the fabrication of micro-holes, micro-tools and micro components. However, micro-holes are fabricated by different manufacturing methods micro-EDM proves to be one of the most promising and reliable manufacturing technologies. Products in miniaturized compact volumes with additional functions are embedded in the products. This requires advancement of micro manufacturing; hence industrial research on micro-machining has become considerably critical and widespread. To meet these challenges, non-conventional machining processes are being employed to achieve higher metal removal rate, better surface integrity characteristics with high degree of pre-specified accuracy. It is an efficient machining process for the fabrication of a micro-hole. Micro-EDM process is based on the thermoelectric energy between the workpiece and electrode. There are many electrical and technological parameters of micro-EDM process which play significant role in the machining characteristics and affect geometrical shape and surface quality of the machined parts. Electrode with inherent micro features is used to cut its mirror image in the workpiece, it is necessary to investigate the machining efficiency of the electrodes used. Furthermore, to improve the machining efficiency, it is vital to consider the effect of various influencing input and output parameters.

In this study, a series of experiments were carried out with various electrodes such as copper, graphite and platinum of 0.5 mm diameter as a tool electrode and Inconel 718 and Titanium grade 5 as workpiece material to fabricate micro holes. Micro-holes are fabricated as per the Central composite design using response surface methodology. The combination of gap voltage, peak current, pulse on duration and pulse of time are considered as process variables. Furthermore, Material Removal Rate (MRR), Overcut effect (OC), Recast layer thickness (RCL) and Taper angle are considered as process responses. The main aim was to identify the electrode material which facilitates highest MRR simultaneously maintaining surface quality characteristics. Analysis of variance technique was used to identify process variable, significantly affecting the process responses. Experimental results were used for development of neural network models for prediction of process responses. Multi-

objective optimization using nature inspired algorithms like Teaching learning based optimization (TLBO), Differential evolution(DE) and Artificial bee colony optimization (ABC) were employed for determining pareto set of solutions which were further ranked by fuzzy ranking method.

Further a comparative study has been carried out in order to investigate the effect of process variables on process responses. Finally, an axisymmetric three-dimensional model for temperature distribution in the micro electrical discharge machining process has been developed using the Finite element method to estimate the MRR by using a combination of different electrode materials during fabrication of micro holes in Inconel 718 and Titanium 5 as workpiece materials. Additionally, the effect of process variables like pulse on duration and peak current on plasma flushing efficiency has been carried out.

Based on the experimental results, an analysis was made to identify the performance of various electrodes during fabrication of micro holes considering Inconel 718 as well as titanium as workpiece materials. It was found that that platinum followed by graphite and copper as electrode material exhibited higher MRR for both the workpiece materials but on the other hand platinum showed higher values of OC, RCL and TA respectively when compared to graphite and copper. The variation of temperature distribution in radial and depth direction with different process parameters has been determined for Inconel 718 and Titanium 5. Theoretical cavity volume was calculated for different process parameter settings for both workpiece materials and it was found that Titanium 5 exhibited higher cavity volume then Inconel 718.

This research work offers new insights into the performance of micro-µ-EDM of Inconel 718 and Titanium5 using different electrodes. The optimum process parameters have been identified to determine multi-objective machinability criteria such as MRR, angle of taper of micro-hole, the thickness of recast-layer and overcut for fabrication of micro-holes.

Keywords: Artificial bee colony optimization; Differential evolution; Inconel 718; Material Removal Rate; Overcut effect; Recast layer thickness; Taper angle.

TABLE OF CONTENTS

List of Figures

List of Tables

List of Abbreviations

EDM	Electro discharge machining
MRR	Material removal rate
OC	Overcut effect
RCL	Recast layer thickness
TLBO	Teaching learning based optimization
DE	Differential evolution
ABC	Artificial bee colony
TA	Taper angle
MEMS	Micro electro mechanical systems
IEG	Inter electrode gap
DC	Direct current
μ-EDM	Micro electro discharge machining
WEDG	Wire electro discharge grinding
FEA	Finite element analysis
TWR	Tool wear rate
HAZ	Heat affected zone
WC	Tungsten carbide
SEM	Scanning electron microscopy
EDD	Electro discharge drilling
ANOVA	Analysis of variance
CVD	Chemical vapour deposition
PCD	Poly crystalline diamond
SD	Sintered diamond
SR	Surface roughness
NGM	Neuro grey modelling
ANN	Artificial neural network
GRA	Grey relational analysis
ANFIS	Adaptive neuro fuzzy interface system
GA	Genetic algorithm
ROC	Radial overcut
RSM	Response surface methodology
FEM	Finite element modelling
DOE	Design of experiments
HSTR	High strength temperature resistance
ETLBO	Elitist teaching learning based optimization
DEA	Differential evolution

	algorithm
FL	Fuzzy logic
FIS	Fuzzy interface system
MFs	Membership funtions

List of Symbols

µs	Micro seconds
V	Voltage
I_p	Peak current
T_{on}	Pulse on duration
T_{off}	Pulse off duration
Amp	Ampere
Hz	Hertz
kHz	Kilo hertz
MHz	Mega hertz
R_a	Surface roughness
R	Resistor
RC	Resistor capacitance
mm^3	Cubic millimeter
B_4C	Boron carbide
SiC	Silicon carbide
Cu	Copper
CuW	Copper tungsten
Gr	Graphite
T_m	Machining time
D_t	Top diameter of micro hole
D_b	Bottom diameter of micro hole
h	Thickness of workpiece material
D_a	Average diameter of micro hole
D	Tool diameter
ɵ	Taper angle
D_{entry}	Entrance diameter of micro hole
D_{exit}	Exit diameter of micro hole
Δw	Weight change
E	Error function

CHAPTER 1

INTRODUCTION

1. INTRODUCTION

In recent years, manufacturing industries have experienced rapid advances in material technology as well as miniaturization of components. With the increasing demand for micro components in many industries, and rapid developments in micro-electro-mechanical systems (MEMS), micro-manufacturing techniques for producing these parts has become increasingly important. The machining of hard to cut materials is an important issue in the field of manufacturing. Since these materials possess excellent mechanical properties which can be useful in many important applications, machining of them can open up opportunities of utilizing them comprehensively. In order to overcome the technical difficulties in conventional machining and the high costs associated with the elevated hardness and intrinsic brittleness, non-conventional machining has been developed.

1.1 ELECTRICAL DISCHARGE MACHINING – FEATURES

In 1970, the English scientist, Priestley, first detected the erosive effect of electrical discharges on metals. More recently, during research (to eliminate erosive effects on electrical contacts) the soviet scientists, B. R. Butinzky and N. I. Lazarenko, decided to exploit the destructive effect of an electrical discharge and develop a controlled method of metal machining. In 1943, they announced the construction of the first spark erosion machining. The spark generator used in 1943, known as the Lazarenko circuit, has been employed over many years in power supplies for EDM machines and an improved form is being used in many current applications (Pandey et al. 2003). The EDM process can be compared with the conventional cutting process, except that in this case, a suitably shaped tool electrode, with a precision controlled feed movement is employed in place of the cutting tool and the cutting energy is provided by means of short duration electrical impulses. The EDM has found ready application in the machining of hard metals or alloys (necessarily electrically conductive) which cannot be machined easily by conventional methods. It has

proved valuable and effective in machining of super tough, hard, high strength and temperature resistance of conductive material. These metals would have been difficult to machine by conventional methods. It thus plays a major role in the machining of dies and tools made of tungsten carbides, stellites or hard steels. Alloys used in the aeronautics industry, for example, hastalloy, nimonic could also be machined conveniently by this process. The EDM is also used to machining of exotic materials, refractory metals and hard enable steels. This process has an added advantage of being capable of machining complicated components and making intricate shapes. Most of the surgical components are being machined by this process since the EDM is one of the unconventional processes which can produce better surface quality.

1.2 PRINCIPLE OF ELECTRIC DISCHARGE MACHINING

Figure 1.1 shows the concept of EDM. Pulsed arc discharges occur in the "gap" filled with an insulating medium, preferably a dielectric liquid like hydrocarbon oil or de-ionized (de-mineralized) water between tool electrode and workpiece. The insulating effect of the dielectric medium has some importance in avoiding electrolysis effects on the electrodes during an EDM process. As the electrode shape is copied with an offset equal to the gap-size, the liquid should be selected to minimize the gap (10-100 μm) to obtain precise machining. On the other hand, a certain gap width is needed to avoid short circuiting, especially when electrodes that are sensitive to vibration or deformation are used. The ignition of the discharge is initiated by a high voltage, overcoming the dielectric breakdown strength of the small gap. A channel of plasma (ionized, electrically conductive gas with high temperature) is formed between the electrodes and develops further with discharge duration. As the metal removal per discharge is very small, discharges should occur at high frequencies (103 -106 Hz). For every pulse, discharge occurs at a single location where the electrode materials are evaporated and ejected in the molten phase. As a result, a small crater is generated both on the tool electrode and workpiece surfaces. Removed materials are cooled and resolidified in the dielectric liquid forming several hundreds of spherical debris particles, which are then flushed away from the gap by the dielectric flow. After the end of the discharge duration, the temperature of the plasma and the electrode surfaces contacting the plasma rapidly drops, resulting in a recombination of ions and electrons and a recovery of the dielectric breakdown strength.

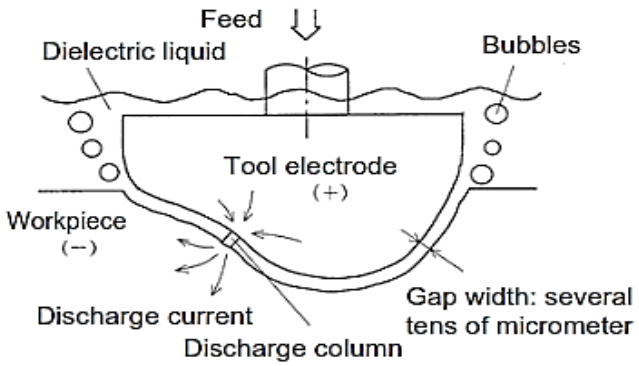

Figure 1. 1 : Concept of EDM (Kunieda et al. (2004))

As a result, a small crater is generated both on the tool electrode and workpiece surfaces. Removed materials are cooled and resolidified in the dielectric liquid forming several hundreds of spherical debris particles, which are then flushed away from the gap by the dielectric flow. After the end of the discharge duration, the temperature of the plasma and the electrode surfaces contacting the plasma rapidly drops, resulting in a recombination of ions and electrons and a recovery of the dielectric breakdown strength. To obtain stable conditions in EDM, it is essential for the next pulse discharge to occur at a spot distanced sufficiently far from the previous discharge location. Such a spot may be the place where the gap is small or contaminated with debris particles which may weaken the dielectric breakdown strength of the liquid. Accordingly, the interval time between pulse discharges must be sufficiently long so that the plasma generated by the previous discharge can be deionized and the dielectric breakdown strength around the previous discharge location can be recovered by the time the next pulse voltage is applied. Otherwise discharges occur at the same location for every pulse, resulting in thermal overheating and a non-uniform erosion of the workpiece. The schematic of an EDM machine tool is shown in Figure 1.2 The tool and the workpiece form the two conductive electrodes in the electric circuit. Pulsed power is supplied to the electrodes from a separate power supply unit. The appropriate feed motion of the tool towards the work piece is generally provided for maintaining a constant gap distance between the tool and the work piece during machining. This is performed by either a servo motor control or stepper motor control of the tool holder.

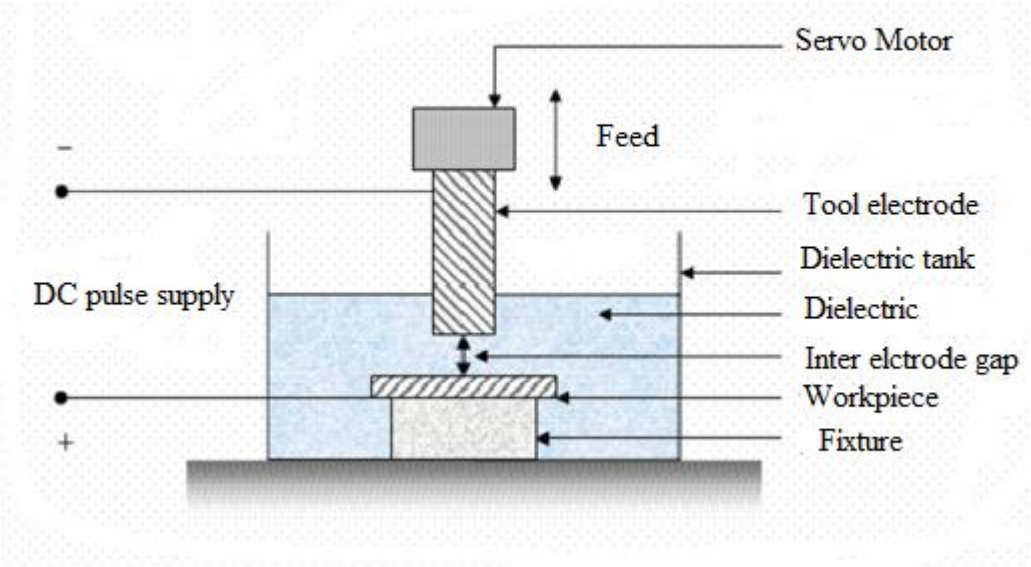

Figure 1. 2: Schematic of an Electric Discharge Machining (EDM) machine

As material gets removed from the work piece, the tool is moved downward towards the work piece to maintain a constant Inter Electrode Gap (IEG). The tool and the work piece are plunged in a dielectric tank and flushing arrangements are made for the proper flow of dielectric in the IEG. Typically, in oil die-sinking EDM, pulsed DC power supply is used where the tool is connected to the negative terminal and the work piece is connected to the positive terminal. The pulse frequency may vary from a few kHz to several MHz. The IEG is in the range of a few tens of micro meter to a few hundred micro meter. Material removal rates of up to 300 cubic mm/min can be achieved during EDM. The surface finish (Ra value) can be as high as 50 µm during rough machining and even less than 1 µm during finish machining.

1.3 DEVELOPMENT OF MICRO-EDM

EDM has become an indispensable process in modern manufacturing industries because of its ability to produce complex shapes with high degree of accuracy in difficult-to-cut but electrically conductive materials. If the size of the spark is substantially reduced by appropriately selecting the machining parameters to create micro-features with high accuracy and better surface finish on micro and macro components, the process is called electro-discharge micromachining (micro-EDM) or ‘Micro-EDM’. Thus, in micro-EDM, the key is to limit the energy in each

discharge to make micro-featured products with high accuracy and good surface finish. Micro-EDM is the application of EDM in micro-field. It has similar characteristics as EDM except the size of the tool, discharge energy and axis movement resolutions are in micro-level. The basic principle of micro-EDM is the same as that of the EDM process. In EDM, a potential difference is applied between the tool and workpiece. Both the tool and the work material are to be electrically conductive, submerged in dielectric fluid. Generally, EDM oil kerosene and deionized water is used as the dielectric medium. The sparking phenomena during micro-EDM can be separated into three important phases named as preparation phase for ignition, phase of discharge, and interval phase between discharges (Schumacher 2004). When the gap voltage is applied, an electric field or energy column is created, which gains highest strength once the electrode and surface are closest. The electrical field eventually breaks down the insulating properties of the dielectric fluid. Once the resistivity of the fluid is lowest, a single spark is able to flow through the ionized flux tube and strike the workpiece. The voltage drops as the current is produced and the spark vaporizes anything in contact, including the dielectric fluid, encasing the spark in a sheath of gasses composed of hydrogen, carbon, and various oxides. The area struck by the spark will be vaporized and melted, resulting in a single crater. Due to the heat of spark and contaminates produced from workpiece, the alignment of the ionized particles in the dielectric fluid is disrupted, and thus, the resistivity increases rapidly. Voltage rises as resistivity increases and the current drops, as dielectric can no longer sustain a stable spark. At this point, the current must be switched off, which is done by pulse interval. During the pulse off time, as heat source is eliminated, the sheath of vapour that was around the spark implodes. Its collapse creates a void or vacuum and draws in fresh dielectric fluid to flush away debris and cool the area. Also, the re-ionization happens which provides favorable condition for the next spark.

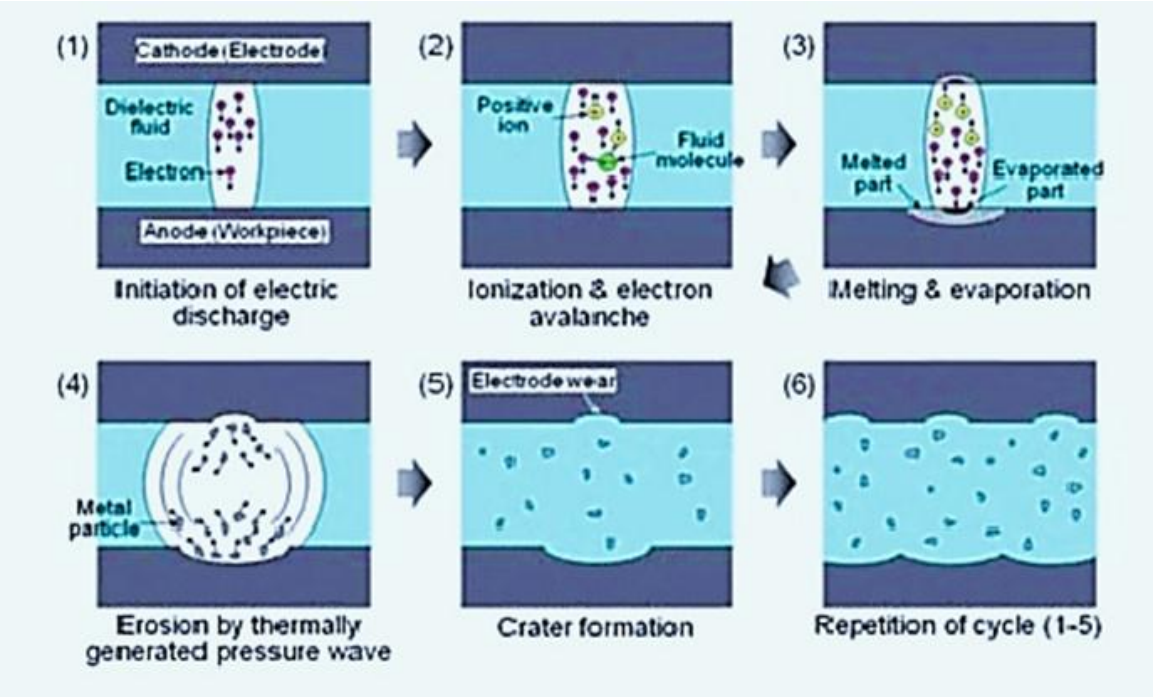

Figure 1. 3 Illustration of the principle of micro-EDM (Takahata 2009)

1.4 DIFFERENCES BETWEEN MACRO AND MICRO-EDM

Even though micro-EDM is based on the same physical principle of spark erosion, it is not merely an adoption of the EDM process for machining at micron level. There are significant differences in the size of the tool used, fabrication method of micro-sized tools, the power supply of discharge energy, movement resolution of machine tools' axes, gap control and flushing techniques, and processing techniques. For example, micro-EDM milling, wire electro-discharge grinding(WEDG), and repetitive pattern transfer are commonly employed in and more specific to the micro-EDM process. Some other differences between the macro and micro-EDMs are listed below:

- The most important difference between micro-EDM and EDM (for both wire EDM and die-sinking EDM) is the dimension of the plasma channel radius that arises during the spark. In conventional EDM, the plasma channel is much smaller than the electrode, but the size is comparable to micro-EDM (Jahan et al. 2014).

- Smaller electrodes (micro-WEDG and micro-BEDG can produce electrodes as small as Ø5 mm and thin wires can be < Ø20 mm) used in the micro-EDM process present a limited heat conduction and low mass to dissipate the spark heat. Excessive spark energy can produce the wire rupture (or electrode burn in die-sinking micro-EDM), being the maximum applicable energy limited by this fact in micro-EDM (Jahan et al. 2014).
- Together with the energy effects, the flushing pressure acting on the electrode varies much in micro-EDM with respect to the conventional EDM process. In micro-EDM, the electrode pressure area is smaller, but the electrode stiffness is lower, increasing the risk of electrode breakage or tool deflection. The debris removal is more difficult in micro-EDM because the gap is smaller, the dielectric viscosity is higher, and the pressure drop in micro-volumes is higher (Katz et al. 2005).
- In the conventional EDM, the higher precision can only be achieved if electrode vibrations and wear are controlled. On the other hand, the precision and accuracy of the final products are much higher in micro-EDM (Jahan et al. 2014).
- For each discharge, the electrode wear in micro-EDM is proportionally higher than conventional EDM. The electrode is softened, depending on the section reduction in the spark energy.
- In micro-EDM, the maximum peak energy must be limited to control the unit removal rate per spark (UR) and use small electrodes and wires. Therefore, the crater sizes in micro-EDM are also much smaller than those in conventional EDM (Uhlmann et al. 2005).

1.5 MICRO-EDM SYSTEM COMPONENTS

1.5.1 TRANSISTOR-TYPE PULSE GENERATOR

The transistor-type pulse generator is widely used in conventional EDM as it provides a higher removal rate due to its high discharge frequency. The pulse duration and discharge current can arbitrarily be changed depending on the machining characteristics required. A series of resistances and transistors are connected in parallel between the direct current power supply and the discharge gap. The discharge current proportionally increases to the number of transistors, which is

switched on at the same time. The switching ON – OFF of the gate control circuit is operated by the FET. In order to generate a single pulse, gap voltage is monitored to detect the occurrence of discharge and after preset discharge duration, the FET is switched off. However, there is a delay in signal transmission from the occurrence of discharge to the switching off of the FET due to the time constants in the voltage attenuation circuit, pulse control circuit, and insulating circuit and gate drive circuit for the FET (Han et al. 2004). The applications of the transistor-type generator in micro-EDM were first studied by (Masuzawa et al.1980), and they reported on successfully generating a discharge pulse used for rough machining. (Nakazawa et al.2000) and (Hara et al.2001) also conducted studies on the development of the transistor-type generator for micro-EDM and reported that it was difficult for them to make sure that electrical breakdown occurs whenever open voltage is applied because the discharge delay time is not always shorter than the pulse duration (Han et al. 2004). One of the major advantages of the transistor-type pulse generator is that the discharge process can be easily controlled by detecting the discharge state in the gap in the transistor-type pulse generator. If the transistor type is used, it takes at least several tens of nanoseconds for the discharge current to diminish to zero after detecting the occurrence of discharge because the electric circuit for detecting the occurrence of discharge, the circuit for generating an output signal to switch off the power transistor, and the power transistor itself have a certain amount of delay time. Hence, it is difficult to keep the constant discharge duration shorter than several tens of ns using the transistor-type pulse generator (Han et al. 2004).

1.5.2 RC-TYPE PULSE GENERATOR

The RC-type pulse generator was the first type used for EDM, and it is still used in finishing and micromachining because the conventional transistor pulse generators do not produce a constant-energy pulse that is sufficiently short (Kunieda et al.2005). In an RC or relaxation type circuit, discharge pulse duration is dominated by the capacitance of the capacitor and the inductance of the wire connecting the capacitor to the workpiece and the tool (Rajurkar et al 2006). The frequency of discharge (discharge repetition rate) depends upon the charging time, which is decided by the resistor (R) used in the circuit. Therefore, R should not be made very low because arcing phenomenon can occur instead of sparking and a critical

resistance is desirable that will prevent arcing (Wong et al.2003). Discharge energy is determined by the used capacitance and by the stray capacitance that exists between the electric feeders, tool electrode holder and work table, and between the tool electrode and workpiece. This means the minimum discharge energy per pulse is determined by the stray capacitance. In the final finishing, when minimum discharge energy is necessary, the capacitor is not wired and machining is conducted with the stray capacitance only (Rajurkar et al.2006). It can easily generate pulses with high peak current values and short duration, allowing efficient and accurate material removal, and meanwhile achieving the required surface quality. Finally, pulse conditions with shorter discharge duration and higher peak current provide better surface roughness due to a smaller discharge crater (Kunieda et al.2005). Figure 1.4 shows the schematic representation of basic transistor- and RC-type pulse generators. However, machining using the RC pulse generator usually has an extremely low removal rate from its low discharge frequency due to the time needed to charge the capacitor. In addition, a uniform surface finish becomes difficult to obtain because the discharge energy varies depending on the electrical charge stored in the capacitor before dielectric breakdown. The RC pulse generator has no way to control the pulse interval. Moreover, thermal damage can easily occur on the workpiece if the dielectric strength is not recovered after the previous discharge and the current continues to flow through the same plasma channel in the gap without charging the capacitor (Han et al. 2004).

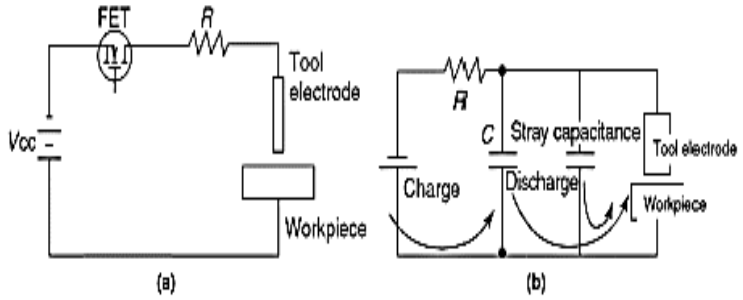

Figure 1. 4 :Schematic representation of basic circuit diagram of (a) transistor-type and (b) RC-type pulse generator

1.6 ADVANTAGES OF MICRO-EDM

The use of micro-EDM has many advantages in micro parts manufacturing micro-components with excellent dimensional accuracy close, shape precision, good surface finish and a large batch of production. It can machine complex shapes with very negligible forces. As a low cost non-traditional machining technology, it has special advantages in machining complex micro-structures. The mechanical forces are very small because the tool and the work material do not come into contact during the machining process (Ekmekci et al. 2009). Very small process forces involved and good repeatability and reliability of the process have made micro-EDM the most sought-after technique in micro-machining for achieving high-aspect-ratio micro-parts/ holes. The growing popularity of micro-EDM can also be attributed to its advantages, including low set-up cost, high aspect ratio of parts, enhanced precision and large design freedom (Lim et al. 2003).

1.7 APPLICATIONS OF MICRO-EDM

Parts produced by micro-EDM are widely used in MEMS, biomedical applications, automotive industry, and defense industry. There have been several successful attempts in producing micro parts such as micro pins, micro nozzles and micro cavities using micro-EDM. The main goal of micro-EDM is to achieve a better stability and higher productivity of the micro-holes. Machining capability of micro-EDM using conductive materials with high precision regardless of material hardness creates a wide range of application area with the increasing demand for miniaturized parts and components such as holes, gears and micro cavities. It is also used to make gasoline injector spray nozzles, dies for extrusion, liquids and gas micro fields, needles for the medical field and in semi-conductor industries to produce electrolysis needles (spiral electrodes) in semi-conductor industries. Micro-EDM has also wide application in the new fields such as MEMS, medical and surgical instruments. It has also become popular with its potential applications in pharmaceutical industry, orifices for biomedical devices, micro-fluidic channels, cooling vents for gas turbine, turbine blades of jet engines, military affairs, aerospace industries, automobile industries, heat exchangers, micro-gears, micro-robot, micro-robotic arm and micro-stage.

1.8 SCOPE OF THE PRESENT WORK

The scope of the present work can be presented in three parts:

The first part deals with experimental investigation during fabrication of micro holes on aerospace materials namely Inconel 718 and Titanium grade 5 as workpiece materials. These materials have attracted many researchers because of their inherent

characteristics like high hardness, high strength at high temperatures, affinity to react with tool materials and low thermal diffusivity. Still, the available research data in the form of papers and books pertaining to EDM of these materials is scanty. Furthermore, the fabrications of micro holes on these materials have been carried out with different electrode combinations like copper, graphite and platinum. The machining characteristics of Inconel 718 and Titanium Grade 5 have been described with in input parameters. In second part of this work, prediction based modelling along with FEA have been carried out for better understanding of process dynamics and involved complexities. In third part of this work optimal combinations of input parameters are obtained by employing various optimization techniques. This part provides guidelines to the engineers working in the field of EDM to select the proper combinations of input parameters for the best process performance.

CHAPTER 2

LITERATURE REVIEW

2.1 INTRODUCTION

Electrical Discharge Machining (EDM) is a non-traditional machining process that has become a well-established machining option in manufacturing industries throughout the world. It has replaced drilling, milling, grinding and other traditional machining operations in different aspects. Micro-EDM, a recent development, is found to be a cost-effective process for fabrication of micro-tools, micro-components and micro-features with good dimensional accuracy and repeatability. This chapter provides a review of the published literature on EDM and micro-EDM to place the research problem in perspective.

2.2 DIFFERENT ISSUES IN MICRO-EDM

There are many parameters that influence the machining performance of micro-EDM, some of which are given in Figure 2.1. Several studies focused on the influence of the most relevant micro-EDM factors to achieve high MRR, low TWR and good surface finish. The performance and influences of different electrodes and the outcome of the different parameters such as MRR, OC, RCL and TA. MRR is defined as the volume (mm^3) of the material removed, divided by the machining time (min). Overcut effect (OC), is the radial distance between the two concentric geometrical circles. Overcut is the measure of concentricity, associated with form/geometric accuracy. The sparks produced during the EDM process melt the metal's surface, which then undergo ultra-rapid quenching. A layer forms on the workpiece surface defined as a recast layer (RCL) after solidification. The sparks produced during the EDM process melt the metal's surface, which then undergo ultra-rapid quenching. A layer forms on the workpiece surface defined as a recast layer after solidification have been investigated.

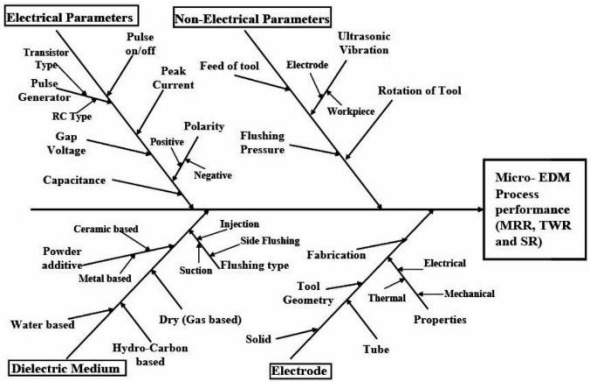

Figure 2. 1:Fish-bone diagram of various influencing parameters

2.2.1 INFLUENCES OF DISCHARGE ENERGY

The factors influencing the machining performance largely depend on the discharge energy applied for machining. The various issues such as surface roughness, heat affected zone, micro-hardness and crack formations and machining quality of the workpiece are determined by the amount of energy released in every spark (Masuzawa 2000).

Jahan et al. (2009a) studied the performance of die-sinking micro-EDM of tungsten carbide using different electrodes. They observed that the lower discharge energy shows better surface finish. Lower input energy proves to show reduction in surface roughness and burr width.

Somashekar et al. (2010) investigated the influence of discharge energy and predicted that the increase in discharge energy leads to increase in MRR. Wong et al. (2003) developed a single spark generator to study the erosion characteristics from the micro-crater size. The result shows that the volume and size of the micro-craters are found to be more consistent at lower energy discharges and the specific energy required to remove the material is found to be significantly less at lower energies (< 50μm) when compared with that at higher energies. The estimated erosion efficiency of MRR at low-energy discharges is found to be seven to eight times higher than that at higher-energy discharges. This can be due to occurrence of

resolidified or recast layer largely associated with high energy discharges, apart from arcing problems.

Gostimirovic et al. (2012) examined the influence of discharge energy during the micro-EDM process of manganese-vanadium tool steel using copper electrode. The results revealed that MRR and HAZ increase due to increase in discharge energy.

2.2.2 INFLUENCES OF DIELECTRIC FLUIDS

The two most commonly used fluids are petroleum-based hydrocarbon mineral oils and deionized water. These dielectrics have the proper effects of concentrating the discharge channel and discharge energy but they might have a difficulty in flushing the discharge products. Research has been done using different dielectric fluids like kerosene and de-ionized water.

The basic need of dielectric in EDM is to provide a momentary plasma column/channel for electron to flow maintaining sparking only. In order to maintain the desired integrity of workpiece and to enhance the performance of micro-EDM, it is essential to properly choose a dielectric and associated spark discharge. Discharge depends on pyrolysis (plasma) effect in dielectric fluid. Since different dielectrics have different cooling rates and compositions, the choice of dielectric plays an important role in the micro-EDM process. Many research works proved that ceramic powder added to dielectric increases the breakdown characteristics of the dielectric fluid.

Chung et al. (2007) investigated with micro electrical discharge milling using tungsten carbide (WC) as tool electrode and stainless steel plate as workpiece, with deionized water as a dielectric fluid. They used deionised water with high resistivity to minimize the machining gap and investigated machining characteristics such as tool wear, machining gap and machining rate. When the resistivity of deionised water increased, the machined gap decreased to minimize the gap resistance.

Kibria et al. (2010), examined the performance criteria like MRR, TWR, overcut, diameter – variation at entry and exit of the drilled hole and surface integrity during machining of titanium alloy (Ti-6Al-4V) using different types of dielectric such as kerosene and deionised water. The boron carbide (B_4C) powder was suspended in kerosene and deionised water. The experimental results revealed that MRR and TWR were higher using deionised water than kerosene. It is surprising to observe that despite higher order TWR; MRR may be higher. This could be due to setting of smaller inter-electrode gap inducing occasional (transient) arcing. When dielectrics with suspension of boron carbides are used, MRR is found to increase. Scanning electron microscopy (SEM) indicates that the thickness of white layer is less on

machined surface when deionised water is used as compared to kerosene. Presence of particles like B_4C can reduce the dielectric constant of the dielectric material facilitating high order spark intensity and higher MRR.

Song et al. (2009) made an attempt to produce an electrolytic, corrosion-free hole in micro-electrical discharge drilling (EDD) of WC-Co with deionised water. The WC-Co is susceptible to electrolytic corrosion when deionised water is used as the working fluid with a DC power source for the RC circuit. To suppress this electrolytic corrosion, a bipolar pulse power source reduces the positive polarity period of the workpiece by periodically alternating the polarity of the workpiece and electrode and decreases the average gap voltage at the machining gap. Since the electrolytic corrosion is an electrochemical reaction between the side of the electrode and the surface of the workpiece, the usage of the triangular electrode with small side area reduces these reactions. The bipolar pulse power source is more effective in reducing electrolytic corrosion with low electrode wear and high machining speed than the DC power source for an RC discharge circuit. Normally hard, brittle materials like WC are spark eroded with reverse polarity and also dielectric such as kerosene or paraffin is used to avoid such problem.

Prihandana et al. (2009) reported the effect of micro-powder suspension and ultrasonic vibration in micro-EDM processes using the Taguchi method. They observed an increase in MRR using copper as a workpiece material with the addition of micro-MoS_2 powder to dielectric and superimposed ultrasonic vibration.

Yeo et al. (2007) investigated the effects of using silicon carbide (SiC) nano powder suspended in dielectric like Idemitsu synthetic electric spark oil and Daphne cut HL-25 on crater characteristics for micro-EDM. The results show that the craters with smaller diameters and more consistent circular shapes and depths are produced for dielectric with additive than without additive. The presence of nano powder can control the plasma channel (resistance) and thereby avoid any surge effects.

Kagaya et al. (1990) experimented with the deep micro-hole drilling using water as a working fluid for the fabrication of narrow slit. The optimum condition for narrow slit fabrication was investigated concerning the electric discharge circuit and combinations of electrode, workpiece materials and electrode polarity. The result shows that it is possible to fabricate fine slits as narrow as 20μm wide and 3mm long with fairly fine surface roughness of around 1μm.

Chow et al. (2007) investigated micro-slit EDM process along with small discharge energy and SiC powder in pure water (distilled water). The results indicated that the addition of SiC powder would increase working fluid electrical conductivity,

extrude the debris easily and increase the MRR. It is seen that SiC suspended deionised water facilitates higher order depth of removal and machining is mostly insensitive to pulse duration. However, plain deionised water exhibits lower order machining depth sensitivity to pulse duration. The use of deionised water as dielectric is preferred to kerosene, owing to increased MRR. However, deionised water can cause problems such as hydrogen embrittlement, corrosion and occasional explosion. This requires a lot of caution in using deionised water. Addition of particles such as B_4C, SiC can enhance the machining performance. EDM with dielectric containing suspended particles has been used to enhance the hardness of work materials. In sinking EDM, however, hydrocarbon dielectrics are normally used because surface finish is better and tool electrode wear is lower compared to de-ionized water (Kunieda et al. 2005).

Kaminski and Capuano (2003) investigated the machining of micro-hole and stated that the dielectric fluid used is composed basically from hydro-carbons that are cheaper than synthetic dielectric fluids. To sum up from the literature highlighted, the hydro-carbon oil is also one of the most suitable dielectric for the micro-EDM process.

2.2.3 INFLUENCE OF PULSE CHARACTERISTICS

As micro-EDM is a thermo-electric process, the pulsed discharge is responsible for removing metal through melting and evaporation.

Han et al. (2004) developed a new transistor type iso-pulse generator and servo feed control to improve the machining characteristics of micro-EDM. They observed that the pulse duration can be reduced to around 30ns which is ideal for finishing and obtained a removal rate of about 24 times higher than that of the conventional RC pulse generator with a constant feed rate (in both semi-finishing and finishing conditions). The advantages of using servo feed control in finishing are considerably greater than in semi finishing, whereas the transistor type iso-pulse generator proved more useful in semi-finishing than in finishing. However, it is difficult to infer the contribution of an individual parameter (pulse duration and servo feed) to machining performance. Reduction in pulse duration can minimize the spark intensity and consequently favors better surface finish. However, minimizing the pulse on duration, with consequent increasing pulse off duration can impair the machining. Thus, one can anticipate a mixed mode of conflicting influence.

Kim et al. (2010) introduced a novel hybrid micromachining system using a nanosecond pulsed laser and micro-EDM. The feasibility and characteristics of the hybrid machining process were compared to conventional EDM and laser ablation. It was experimentally proved that the machining time can be effectively reduced in both EDM drilling and milling by rapid laser pre-machining prior to micro-EDM. Laser ablation can enhance the hardness of the surface (effect of laser glazing), and consequently facilitate improved micro-EDM.

Son et al. (2007) investigated the influences of EDM pulse condition on the micro-EDM properties. Voltage, current, and on/off time of the pulse were selected as experimental parameters based on their relationship to the MRR. The pulse condition is significant, in that it particularly focuses on tool wear, MRR, and machining accuracy. The experimental results showed that the duration of pulse off/on (t_{off}/t_{on}) time considerably affects machining properties and comparatively shorter pulse on duration is preferable to make accurate machining with a higher removal rate and lower TWR. More than pulse on, pulse off duration is a key factor in sustaining the process. The wear of tool electrode was measured and the results are shown in Figure 2.2.

Koyano and Kunieda (2010) proposed an electrostatic induction feeding method to achieve high accuracy and removal rate in micro-EDM. In the new method, only a single discharge occurs for each cycle of the periodic pulse voltage. The results showed that the machining speed is four times higher and the heat damage on the machining surface is less compared to the conventional machining with pulse generator.

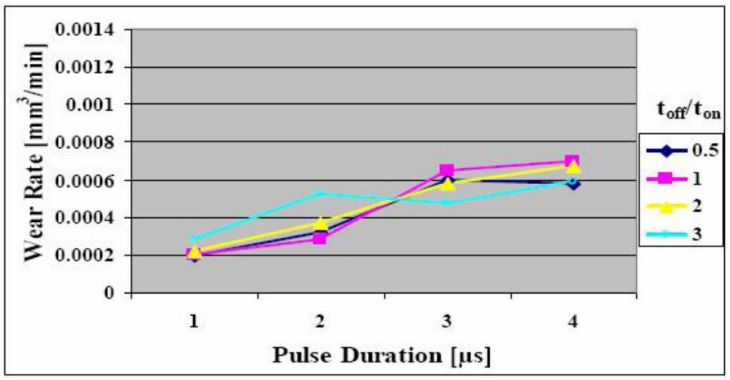

Source: Son et al. (2007)

Figure 2. 2: TWR vs on-off time conditions of micro-EDM pulse

Yeo et al. (2009a) developed a new pulse discriminating technique for monitoring micro-EDM. The developed system employed current pulse as the main detecting

parameter and it was tested on micro-EDM drilling and micro-EDM milling; pulse distributions were analysed. The experimental results showed that the system was able to reduce the machining time by more than 50%. The accuracy of the resulting features is increased.

Jahan et al. (2009b) investigated the influence of major operating parameters on the performance of micro-EDM of WC with a focus on obtaining quality micro-holes with both transistor and RC-type generators. The experimental results showed that RC-type generator could produce micro-holes with good surface quality with rim free of burr-like recast layer, good circularity and dimensional accuracy. The comparative values of spark gap for transistor and RC circuit, respectively, at different setting of machining conditions for the micro holes are shown in Figure 2.3. As the discharge energy can be reduced easily in RC type using very low capacitance, it is more suitable for fabricating micro-structures and RC type pulse generator can produce smoother surface compared to that of transistor type in the micro-EDM of WC. This also supplements the need for reverse polarity for spark erosion of WC.

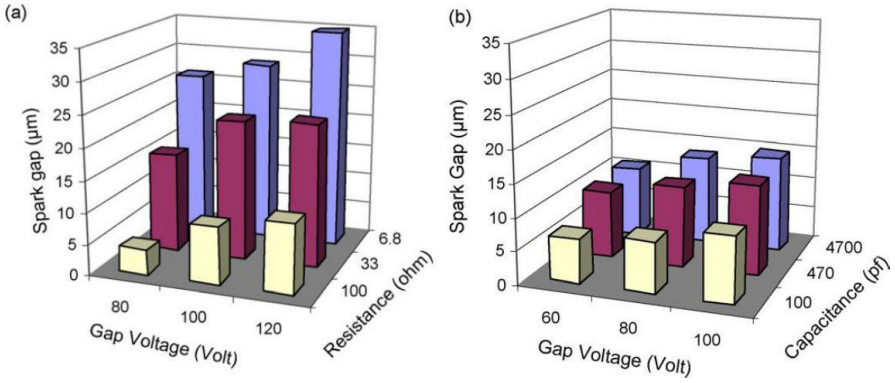

Source: Jahan et al. (2009b)

Figure 2. 3: Comparison of spark gap of micro-holes for transistor-type and RC-generator

It is seen that with transistor type generator a wide variation in spark gap, gap voltage and resistance occurs. However, in RC circuit, only limited order of variation can be seen.

Liu et al. (2010) investigated the influence of pulse generator to produce small input energy pulses with high precision systems. An in depth analysis was also made on the correlation between the discharge pulses and the machining parameters in order

to have an overview of process capability. The results revealed that high accuracy machining in the range of less than 1μm could be achieved.

Long et al. (2012) studied the new micro-EDM deposition process using transistor type and RC-type generators. From the results, it is observed that pulse generators can be applied in the micro-EDM deposition process in both cases. However, in the transistor type, the short circuit damages the deposited material even though it is easy to obtain the same single discharge energy. But the RC type generator is extensively used in micro-EDM.

2.2.4 INFLUENCE OF VARIOUS ELECTRODES

Jahan et al. (2009a) experimented with ultra-die-sinking micro-EDM of WC using different electrodes and found that CuW electrode achieving the highest MRR followed by AgW.

Muttamara et al. (2010) studied the micro-EDM performance on silicon nitride using different electrode materials and observed that Cu electrode with the highest MRR, followed by the CuW and AgW electrodes.

Sanchez et al. (2001) investigated the machining of B_4C and SiSiC, using different electrode materials and observed that Cu and Cu-Gr electrodes achieve maximum MRR. The graphite as electrode material shows the highest electrode wear rate.

Ramaswami and Louis Raj (1973) studied erosion of high speed tool steel HSS with three different electrodes such as copper, brass and aluminum. It was proved that copper was having better MRR, wear ratio and surface finish than other electrodes. The machining performance of AISI H13 die steel using differently shaped copper electrode was carried out by Pellicer et al. (2009).

Singh et al. (2004) investigated the electrical discharge machining of hardened EN-31 tool steel using copper, copper tungsten, brass and aluminum electrodes and concluded that copper was comparatively a better electrode because of good surface finish, high MRR, low diameteral overcut and less electrode wear. The good surface finish with high MRR and low tool wear was attributed to possible side erosion of the machined holes. The results also revealed that the output parameters of EDM increase with the increase in pulsed current and the best machining rates were achieved with copper and aluminum electrodes.

Yeo et al. (2009b) studied the micro-EDM performance using tungsten rod electrode, copper and brass electrodes, it was observed that tube electrodes experienced lower tool wear than rod electrodes. This was due to the enhancement of heat transport through a larger tool electrode area that was exposed to the dielectric. Also tubular electrodes facilitate central flushing tendency.

Soni and Chakraverti (1995) studied the effect of material properties of different electrodes such as copper, brass, copper tungsten, graphite and titanium in electrical discharge machining of HCHCr die steel. It was observed that surface roughness and dimensional accuracy increase with increase of thermal conductivity. It was also found that copper–tungsten was the best electrode material for finish machining whereas for rough machining, graphite is better. Size of crater increased with increase of current which ultimately affects the surface finish.

Nguyen et al. (2012) performed micro-EDM on tempered carbon steel using tungsten electrode. The results revealed that MRR was higher while using deionized water than hydrocarbon oil. It was also observed that MRR reduced with high frequency and short duration of pulse.

Lee and Li (2003) investigated the effect of machining parameters upon machining characteristics in EDM of WC using Cu, CuW and graphite electrodes and found that the CuW electrode performed better compared to other two electrodes for the EDM of WC.

2.3 PERFORMANCE MEASURES IN MICRO-EDM

The observation of various machine setting parameters such as MRR, TWR, SR, circularity error, overcut, micro-cracks and HAZ in micro-EDM process is reviewed in this section.

2.3.1 MATERIAL REMOVAL RATE

Sundaram et al. (2007) investigated ultrasonic assisted micro-electro discharge machining. They found that introducing ultrasonic vibration of workpiece was significant for higher MRR.

Jahan et al. (2010), investigated the feasibility of machining deep micro-hole in two difficult-to-cut materials, cemented carbide (WC-Co) and austenitic stainless steel (SUS 304), using micro-EDM drilling. The higher MRR was observed for WC-CO then SUS 304 They observed that higher hardness and melting point of WC-Co was a good condition for EDM, in preference to SUS 304.

Put et al. (2001) investigated MRR by altering electrode polarity on a zirconia-based composite and concluded that negative polarity gave the most stable machining conditions with. a noticeably lower risk of arcing. Carbide and nitride gave higher MRR with positive polarity, whereas boride gave faster machining with negative polarity. However, to minimize the chance of thermal shock and consequence cracking mostly the negative polarity was preferred.

Beri et al. (2008) investigated the influences of electrodes made through powder metallurgy in comparison with conventional copper electrode during electric discharge machining. It was found that the higher MRR was achieved for Cu electrode then that of Cu-W made by powder metallurgy.

Sanchez et al. (2001) studied the performance of various electrodes on ceramic material. It was found that maximum MRR was achieved using copper (Cu) as electrode and minimize MRR with graphite electrode (Gr).

Wang et al. (2011) investigated the influence of adhesion composed of heat-resolved carbon and graphite during the machining of poly crystalline diamond by micro-EDM. The results revealed that an appropriate volume of adhesion on the tool electrode increased MRR and reduced TWR by protecting the electrode.

Lim et al. (2003) investigated the machining performance of high-aspect ratio micro-structures using micro-EDM and it was observed that more material was removed with increase in capacitance.

Gupta et al. (2010) studied the performance analysis of micro-EDM process using pyrolytic carbon. ANOVA was performed to identify the effect of process parameters on the process responses. The results revealed that MRR increases with the increase of gap voltage and a smoother surface was obtained at 110V gap voltage and low capacitance.

Zahiruddin et al. (2012) studied the comparison of energy and removal efficiencies between micro and macro-EDM. The main difference identified is the ratio of energy consumed for material removal with regard to energy distributed into the workpiece and the ratio of total removal volume per pulse with respect to the molten area volume. It was also found that the power density in micro-EDM was approximately 30 times greater and consequently energy efficiency and removal efficiency were significantly greater than macro-EDM.

2.3.2 TOOL WEAR RATIO

Tool wear ratio (TWR) is defined as the ratio of volume of electrode to the volume of workpiece removed. One of the most difficult output parameters is to calculate TWR in micro-EDM process. Four methods are used to measure the electrode wear ratio by means of measuring weight, length, shape and total volume, respectively.

Yu et al. (2004) proposed a recently developed uniform wear method integrated with CAD/CAM software to generate 3D micro cavities. They found that the uniform wear method compensated the tool wear and helped in regaining the tool shape during machining. The compensation for wear maintains the desired inter electrode gap.

Yoshida and Kunieda (1999) studied the mechanism for minute tool electrode wear in dry EDM. The tool electrode wear is almost negligible for any pulse duration because the attached molten workpiece material protects the tool electrode surface against wear. However, this is subjected to polarity adapted in micro-EDM. Also, attachment/transfer of molten workpiece material to the electrode changes its status by way of release of electrode and related gap condition.

Uhlmann and Roehner (2008) investigated on the reduction of tool electrode wear in micro-EDM using novel electrode materials. The investigation results revealed that novel materials such as electrically conductive boron doped CVD diamond (B-CVD) and polycrystalline diamond (PCD) were suitable to minimise the wear of tool electrode. However, one has to look for the stability of the diamond wits spark erosion environment.

Yu et al. (2003) developed a simulation model for uniform wear method. The proposed method was based on one-dimensional wear model and predicted the longitudinal tool wear length.

Bigot et al. (2005) investigated the suitability of electrode wear compensation methods, during the micro-EDM process. Electrode shape deformation and random variation of the volumetric wear were studied as the main factors and as an indicator for the achievable accuracy with the micro-EDM process. The measured wear ratio does not appear to be constant which does not allow for the use of compensation method. Usage of suitable sensor for gap measurement, with necessary adaptive control technique can ensure sustained machining.

Wang et al. (2009) experimentally investigated a wear-resistant electrode for micro-EDM. The results proved that Cu-ZrB_2 composite (copper-zirconium diboride) coated electrodes have better wear resistance than pure copper electrodes. They also found that it was feasible to use the wear compensation method on the basis of the difference between the wear ratio of matrix and that of coating material to maintain electrode shape precision.

Aligiri et al. (2010) developed a new micro-EDM drilling method, in which the material removal volume was estimated as machining progresses. A real-time, material removal volume estimator was developed based on the theoretical electro-thermal model, number of discharge pulse and pulse discrimination system. The result showed that the proposed method is more reliable as compared to the uniform wear method. In drilling micro-holes of 900μm depth error can be reduced to 4% using the proposed method.

Tsai and Masuzawa (2004) evaluated the wear resistance of the electrode in micro-EDM. They found that the volumetric wear ratio of the electrode becomes small for the electrode material with high boiling point, high melting point, and high thermal conductivity. The result also showed W and Cu are good candidates for electrode.

Yan and Lin (2011) presented a novel multi-cut process planning method and a new electrode wear compensation method based on a machine vision system for three-dimensional (3D) micro-EDM. Experimental results indicated that the proposed multi-cut process planning and electrode wear compensation methods can improve machining time.

Uhlmann et al. (2010) investigated the influence of grain size of the boron-doped CVD diamond coating on the wear behavior in micro-sinking EDM.

Experimental investigations showed that nanocrystalline coatings exhibit smaller discharge craters compared to those for microcrystalline diamond coatings. The microcrystalline coating also shows melted material around the discharge crater. However, it is subjected to further investigations.

In sum, the literature on TWR in micro-EDM emphasizes the need for wear compensation and associated adaptive control strategy.

2.3.3 SURFACE ROUGHNESS

Zhang et al. (2005) studied the roughness of the finished surface of AISI 1045 steel using copper as the electrode. The result revealed that surface roughness increased with an increase in the discharge voltage, discharge current and pulse duration.

Ogun et al. (2004) investigated the various machining parameters which influenced the surface profile of 2080 tool steel. It is found that surface roughness increases with increased in discharge current, pulse duration and dielectric flushing pressure.

While studying the molecular dynamics simulation of the material removal mechanism in micro-EDM, Yang et al. (2011) observed that the existence of micro pores in the workpiece material increased the depth of the discharge crater and melted area which resulted in the increase of machining surface roughness.

In micro-EDM, the machined surface is covered with many craters, micro-cracks and heat affected zones (HAZ) that are generated by sparks. The machined surface is covered by a multitude of overlapping craters whose geometry depends on the process parameters used, the physical properties of the electrodes, and the type of dielectric medium (Kurnia et al. 2009).

Nakaoku et al. (2007) experimented with the micro-EDM of sintered diamond (SD) and found that the surface roughness of SDs is sufficiently good for micro mould applications and the surface property of SDs with large diamond particles is quite different from that of metals.

Kiran and Joshi (2007) developed a model based on the configuration of a single-spark cavity formed as a function of process parameters to predict surface roughness of micro-EDMed surfaces.

Yeo et al. (2009b) machined zirconium-based bulk metallic glass using micro-EDM. They employed three different electrodes, tungsten rod electrode, copper and brass tube electrodes, to elucidate the effects of different machining conditions on the machined surface roughness, burr width and tool wear. The results showed that the surface roughness is reduced when lower input energy is used. Also, tungsten electrode outperforms other electrode materials in finish machining.

Jahan et al. (2011) investigated the feasibility of improving surface characteristics of carbide in fine-finish sinking and milling micro-EDM using graphite nano-powder-mixed dielectric. The experimental results proved that the fine-powder-mixed micro-EDM of WC-Co with the addition of semi-conductive graphite nano-powder in dielectric oil provides smooth and defect-free surface. This is due to more surface area being exposed to machining at improved machining stability.

Chung et al. (2009) investigated the micro-EDMed surface based on electro chemical dissolution using deionised water. The results showed that the inner surface of the hole can be finished successfully via electrochemical dissolution in deionised water. Normally, electro chemical dissolution needs an electrolyte. Hence, the role of deionised water in electrochemical dissolution requires better understanding. It is seen that the introduction of tool rotation results in effectively removing the resolidified/recast layer of the inner surface and facilitates better surface finish consequently.

2.3.4 CIRCULARITY ERROR/OVERCUT

The circularity of spark machined holes is influenced by two types of electric sources. These are RC-type generator and transistor-type generator. It is proved from the experimental results that good surface finish and circularity is achieved by RC type generator (Jahan et al. 2009a).

In micro-EDM drilling error occurs due to the vibration of the electrode high roundness (Ali et al. 2009). The surface finish and circularity are also influenced by the rotation of the electrode (Egashira et al. 2010).

During machining process, overcut occurs due to side erosion and removal of debris. Overcut is also one of the major parameters to be considered to evaluate the machining performance of die-sinking micro-EDM.

Pradhan et al. (2009) observed from the experimental investigations that the peak current and pulse-on time used in the machining process influence the overcut of the machined micro-holes. Overcut increases due to the increase of gap voltage and gap width as the higher voltage allows breakdown of dielectric at a wide gap due to the higher electric field (Jahan et al. 2009a).

In EDM, the machined surface is covered with many craters, HAZ and even micro-cracks (Rajurkar et al. 2006). In the micro-EDM process, three layers are categorized on the surface of the machined component. Pandey and Jilani (1986) observed from the micro-EDM process that the transverse section of workpiece has three distinct zones namely white layer, HAZ, and unaffected parent metal. The top surface contains a thin layer of spattered material which can easily be removed by flushing. Underneath the spattered material a thin layer called re-cast layer is formed due to the rapid cooling effect of dielectric and adheres to the machined surface. Recast layer is extremely hard, brittle and porous and may contain micro cracks. The next layer is the HAZ which is affected due to the amount of heat conducted with the material. As in the case of welding, when adjoining the molten / solidified deposition, formation of HAZ occurs. In EDM also, the heat of machining and subsequent depth (based on thermal diffusibility) facilitates formation of HAZ. Rajurkar and Pandit (1984) studied the recast layer and HAZ of EDMed AISI 4130 steel and observed that the damaged layer is estimated to be about 30 - 100μm with pulse on time of 100 to 300μs.

2.3.5 MICRO-CRACKS

Panda (2012) studied the surface damage caused due to thermal stress during electrical discharge machining process and identified that the crack formation on the surface is based on the nature and magnitude of the stress developed.

Ekmekci et al. (2009) studied the micro-hole machining of mould steel using tungsten carbide tool electrode and a hydrocarbon-based dielectric liquid. They observed that discharged pulse energies influence the surface and they identified crack formation by utilizing low pulse energies during machining. The crack density is inversely proportional to the thermal conductivity of the work material (Lee et al. 1992) and as the content of carbon within the white layer increases (transfer from dielectric liquid), surface crack intensity increases rapidly.

Tsai et al. (2003) experimented with the micro-hardness of EDMed surface using Cu electrode and Cu-Cr composite electrode. The Cu metal electrode was having higher micro-hardness than that of composite electrodes. They also observed that the cracks and pores were present in the recast layer (attributable to rapid heat extraction) of Cu electrode.

Patowari et al. (2010) machined C-40 grade steel with WC/Cu powder metallurgy electrodes. They observed relatively a few micro-cracks in recast layer. The EDMed surface has a relatively high micro-hardness, which is due to the migration of carbon from the oil dielectrics to the workpiece surface forming iron carbides in the white layer (Kruth et al. 1995).

Ekmekci et al. (2006) observed that the micro-cracks are associated with the increase of thermal stresses exceeding the ultimate tensile strength of the material. The significant causes of the thermal stress in the machined surface are the drastic heating and cooling rates and the non-uniform temperature distribution. They observed only minor cracks while using tungsten and silver tungsten electrodes rather than copper and copper tungsten. Therefore, they recommended that micro-cracks present on the machined surface should be minimized to improve its service life.

2.3.6 HEAT AFFECTED ZONE (HAZ)

Extremely high temperature resulted (Das et al. 2003, Ekmekci et al. 2005a) in the formation of multi-layered HAZ, including a hardened layer that possesses high brittleness and reduced fatigue strength of the work-material.

Shabgard et al. (2011b) studied the depth of HAZ in EDM of AISI H13 tool steel and observed that increase in pulse currents results in decrease of depth of HAZ. Payal et al. (2008) investigated the machining performance of micro-EDM of EN-31 tool steel using different electrodes such as copper, brass and graphite. Analysis revealed that graphite electrode shows volcanic eruption and cracks due to non-uniform distribution of heat on work surface. Moreover, graphite electrode exhibits deeper HAZ than brass and copper electrodes.

Shabgard et al. (2011a) predicted the white layer thickness and HAZ on AISI H13 tool steel using copper as an electrode of EDM process. A numerical model was developed and it was concluded that increase in pulse on-time shows increase in white layer thickness and depth of HAZ.

Ekmekci et al. (2009) reported that when de-ionized water is used as dielectric fluid

only minimum amount of retained austenite phase and the intensity of micro cracks are identified in the white layer of the plastic mould steel than with kerosene as dielectric. It is possible that pickup of carbon can induce brittleness /cracking, sulphur in kerosene can also cause damage in HAZ.

Kahng and Rajurkar (1977) analyzed the texture of eroded surface and reported that the application of higher discharge energy results in deeper HAZ and subsequently deeper cracks.

Thao and Joshi (2008) identified the area of HAZ around the micro-electrical discharge machined holes and thereby reduced the micro-hardness of the bulk material around the hole. However, presence of HAZ needs not bring down hardness, unless there is any depletion of chemistry.

Liu et al. (2005) studied the micro-EDMed high nickel alloy micro-holes and reported that the overcut was identified around the micro-holes. It may be due to side erosion / inadequate electrode stiffness. It is seen that during micro-EDM process, there is a possibility to attain varying size / geometry of holes varying HAZ characteristics and varied response to MRR and texture depending on the types of electrode used and associated machining conditions.

Paul et al. (2012) also observed that smaller overcut dimensions of crater can be identified with low energy discharge with a decrease in MRR, during the micro-EDM process of γ-titanium aluminide alloy using steel rod as electrode.

Ekmekci et al. (2005b) found that the pulse energy influences the thickness of heat-damaged layer than the shape of the pulse forms. To attain higher performance, it is necessary to overcome the problem of crack formation. The topography of micro-electrical discharge machined surface was investigated by electron microscope. The increased pulse duration also allows more heat to sink into the workpiece and spread which results in deeper HAZ (Garg et al. 2010).

Peng et al. (2008) investigated the micro growth process and characteristics of deposited material in micro-EDM deposition. They found that the micro-EDM deposition process can be used to fabricate finer micro structure with thinner electrode.

Jahan et al. (2010) investigated the migration of different sources of materials to the machined surface during fine finishing micro-EDM of cemented tungsten carbide (WC-Co). They revealed that the major source of material transfers to both workpiece and electrode is the diffusion of carbon and that migration occurs more frequently at lower gap voltages due to low spark gap and stationary tool electrode.

It is evident from literature review that during micro-EDM process, there is a possibility of attaining global maximum of high MRR, good surface finish, low order dimensional overcut and wear. The presence of definite HAZ minimizes the hardness of bulk material around the hole.

2.4 OPTIMIZATION METHODS

2.4.1 TAGUCHI METHOD

Taguchi method has been widely used in engineering analysis as it can optimize performance characteristics through the settings of process parameters and reduce the sensitivity of the system performance to sources of variation. It is a powerful tool to design a high quality system (Lin et al. 2009).

Bigot et al. (2005) proposed Taguchi method for machining parameters optimization. They investigated the optimization of machining parameters for rough and fine machining in micro-EDM.

Vijayaraj et al. (2009) experimentally investigated the micro-WEDM of Ti alloy and the process is optimized using Taguchi method. Their work revealed that the

Taguchi method was a powerful approach used in design of experiment. The high quality of machining characteristics is achieved without increasing the operation cost. Recently, the Taguchi method was widely employed in several industrial fields and research work. Lin et al. (2002) adapted the Taguchi method to obtain the optimal machining parameter of the electrical discharge machining process. Pradhan et al. (2009) studied the optimization of micro-EDM parameters for machining Ti-6Al-4V super alloy by using the Taguchi method for the responses of MRR, TWR, overcut (OC) and taper. They also identified optimal combination levels using ANOVA and S/N ratio graphs.

Prihandana et al. (2009) used the Taguchi method to identify the optimal process parameters to increase the material removal rate of dielectric fluid containing micro-powder in micro-EDM using an L_{18} orthogonal array.

Tosun et al. (2004) used the Taguchi method to explore the effects of MRR and kerf of wire electrical discharge machining. Their works revealed that the Taguchi method was a powerful approach used in design of experiment. Furthermore, the Taguchi method can be used to optimize only single performance characteristics. Hence, in order to optimize multiple performance characteristics, researchers used grey relational analysis as a suitable theory.

Mitra et al. (2011) studied the effect of different dielectric medium in micro-EDM of γ-titanium aluminide. They analyzed both in the absence (dry conditions) and in presence of dielectric (EDM Oil) and observed circular craters in both the conditions. Further investigation to find the most influencing factors using ANOVA revealed that capacitance of RC-Circuit contributes significantly to crater formation followed by pulse frequency.

2.4.2 GREY RELATIONAL ANALYSIS

The grey relational analysis is a method for measuring the degree of approximation among the sequences using a grey relational grade. Theories of the grey relational analysis have attracted considerable interest among researchers. Many researchers have also examined the optimization of process parameters.

Somashekhar et al. (2009a) used a new approach for the optimization of the micro-WEDM process with multiple performance characteristics based on ANOVA with the grey relational analysis. Chiang and Chang (2006) applied the grey relational analysis to optimize the WEDM process with the multiple performance characteristics such as MRR and the minimum surface roughness.

Taguchi method coupled with grey relational analysis has a wide area of application in manufacturing processes and can solve multi-response optimization problem simultaneously. Datta et al. (2008), Esme Ugur (2010) and Natarajan and Arunachalam (2011) have done the optimization of multiple performance characteristics using the Taguchi method and grey relational analysis. From this analysis, the optimal parameters in EDM of 304 stainless steel are identified and the improvements in performance characteristics have been obtained using grey relational analysis.

Jung and Kwon (2010) also employed the Taguchi method and grey relational analysis to find the optimal machining parameters to satisfy the multiple characteristics of the EDM process.

Shen et al. (2012) determined the optimal combination of the process parameters during EDM process of 1Cr17Ni7 using Cu as electrode using Taguchi-based grey relational analysis. From the analysis it was inferred that the performance of MRR, TWR and SR were improved.

Muthukumar et al. (2010) identified the optimum levels of parameters by grey relational analysis and percentage contribution of all the parameters by ANOVA to study the optimization of machining parameters.

Panda (2010) employed a new-hybrid approach of neuro-grey modeling (NGM) for modeling and optimization of multi-process attributes of electro-discharge machining process. The study proved that combining ANN and GRA in NGM was found to be suitable to provide generalized solution pertaining to parameter design of the process.

2.4.3 ARTIFICIAL NEURAL NETWORK (ANN)

An ANN can work satisfactorily as a knowledge-acquisition tool for diagnosis problems.

Sarkar et al. (2010) presented an integrated approach for optimization of wire EDM of gamma titanium aluminide (γ-TiAl) with the assistance of ANN modeling. Aravind et al. (2009) attempted to model the MEDM process for MRR using ANN. Experiments were performed for all possible combinations with three levels using design of experiments considering voltage, capacitance, feed and speed of the electrode as input parameters and MRR as output parameter.

Somashekhar et al. (2009b) proposed an ANN model to represent the relationship between MRR, overcut and input parameters of micro- wire electro discharge machining (WEDM) process. The results showed that a well-trained ANN system is very helpful in estimating performance characteristics.

Pellicer et al. (2009) investigated the influence of different process parameters and tool electrode shape on performance measures for copper electrode and AISI H13 steel workpiece in sinking type micro-EDM process. They used advanced process models using ANNs to obtain a better process-prediction.

Ramakrishnan and Karunamoorthy (2008) developed ANN models and multi-response optimization techniques to predict and select the best cutting parameters of WEDM process.

Somashekhar et al. (2010) analyzed the material removal of micro-EDM using ANN. They developed a neural network model using MATLAB programming and the trained neural network is simulated. They also employed genetic algorithms (GAs) to determine optimum process parameters for any desired output value of machining characteristics. Experimental results showed that the process optimization through ANN modeling and GA technique is very effective in optimizing the performance of the micro-EDM process.

Suganthi et al. (2013) proposed adaptive neuro-fuzzy inference system (ANFIS) and back propagation (BP) based artificial neural network (ANN) models for the prediction of

multiple quality responses in micro-EDM operations. They observed that the predicted values of the responses were in good agreement with the experimental values. The ANFIS model was found to be better than the BP-based ANN. To evaluate the effect of machining parameters on performance characteristics, a specially designed experimental procedure is required. Classical experimental design methods are too complex and difficult to use. Additionally, a large number of experiments have to be carried out when the number of machining parameters increases (Lin 2002, Yang and Tarng 1998).

2.4.4 MATHEMATICAL MODELING

Kurnia et al. (2008) predicted process performance measures in micro-electrical discharge machining such as MRR, TWR and SR. They proposed a theoretical model to analyze the approximation of performance measures based on the crater prediction. The results of comparison between analytical and experimental data of MRR and TWR revealed a variation of up to 30% and 24% respectively.

Luis et al. (2005) studied the influence of MRR and electrode wear in the die-sinking EDM of siliconized silicon carbide. To achieve this, design of experiments (DOE) and multiple linear regression statistical techniques were employed.

Dhar et al. (2007) employed a second order non-linear mathematical model to evaluate the effect of current, pulse-on time and air gap voltage on MRR, TWR, radial overcut (ROC) on electrical discharge machining of Al-4Cu-6Si alloy-10wt% SiCp composites. They revealed that MRR, TWR and ROC increased significantly with the increase of current and pulse duration. Moreover, gap voltage shows minimum influence on the three responses.

George et al. (2004) studied the most important input parameter of EDMed carbon-carbon composite using regression models and response surfaces method. They identified spark current as the most influencing factor.

Shabgard and Shotorbani (2010) developed mathematical models for relating, TWR and SR to machining parameters such as current, pulse-on time and voltage.

Bhattacharyya et al. (2007) analyzed the influences of major machining parameters such as peak current and pulse-on duration on different materials machined through EDM. They employed mathematical models based on response surface methodology (RSM) and found that the lower peak current and pulse-on duration shows minimum SR and white layer thickness.

Pradhan et al. (2008) used RSM to identify the influencing parameter on MRR in EDM process of AISI D2 tool steel with copper electrode.

2.4.5 FEA MODELING

Optimum utilization of the µ-EDM process requires the selection of an appropriate set of machining parameters that would result in the minimum thickness of the recast layer and the depth of heat affected zone (Shabgard et al. 2013) . Several studies have been carried out to determine optimum ED machining parameter combinations from the aspect of surface integrity (Alfano and Crisÿeld 2001). However, these studies were based on the use of experimental approaches and statistical analyses. In a few studies, mainly numerical models have been developed to analyse the outputs of the EDM process, using FE or analytical methods(Das et al. 2003) .For instance, (Ben Salah et al. 2006) developed a numerical model to study the temperature distribution in the EDM process, for prediction of the material removal rate using the thermal model. They reported that taking into account the thermal conductivity of workpiece material was of crucial importance to the accuracy of the numerical results and gave a better correlation with experimental observations. (Marafona and Chousal 2006) employed an FE model for predicting removed material from both anode and cathode. They reported that the anode material removal efficiency was smaller than that of the cathode because there was a high amount of energy going to the anode and also a fast cooling of this material. They stated that this phenomenon could be explained by the differences of thermal conductivity of the cathode and anode. (Joshi and Pande 2009)introduced an intelligent process modeling and optimization of EDM process. In their model, FEM was used to estimate the output parameters of EDM process including MRR and %TWR. The dependency of material properties on the temperature and spark radius to the discharge duration has been emphasized in their investigation. Considering the existing tendency for improving the quality of EDMed product, it is essential to develop numerical models to estimate the relationship between the predominant EDM machining parameters and the resulting machined surface integrity, i.e., white layer thickness and depth of HAZ. In Kansal's study (Kansal et al. 2008) an axisymmetric two dimensional model for powder mixed dielectric has been developed using finite element method.

2.5 SUMMARY

The following observations can be drawn from the detailed literature review as the bases of this research.

Micro-EDM has some distinct characteristics and the literature review has established clear techniques/ strategy for achieving higher MRR and lower TWR. In addition to extending the wide applications of micro-EDM, it is desirable to have a better surface finish. In die-sinking micro-EDM, maximum MRR, minimum TWR and better surface finish can be achieved based on the properties of the electrodes used.

The literature survey clearly indicated the need for selection of proper dielectric, electrode material and even current source for achieving desired results in EDM, especially in micro-EDM.

The influence of various dielectrics has been presented. Both de-ionized and paraffin exerts their influence. With regard to electrode, copper, graphite, tungsten-based electrodes have been tried out. The result showed that material specific electrodes are to be selected for desired results. Various research works have been carried out with different workpiece materials such as tool steels, ceramics, composites, tungsten and titanium alloys. However, there is report of inadequate work on micro-EDM operation of high strength aerospace material such as Inconel 718 and Titanium etc. The micro holes are inherent features of different micro products.

From the available literature it can be seen that the parametric optimization and modeling of MRR, Overcut effect, Taper Angle and Recast layer thickness by employing different electrode materials has not been reported yet. Therefore, there is an urgent need for performance analysis of various electrodes on Inconel 718 and Titanium Grade 5 to produce quality micro-holes. The major challenges of die-sinking micro-EDM were identified and the research problem was formulated. The objectives of this work were also outlined. Based on the objectives, the research methodology was sketched out. Based on the proposed methodology, the experimental procedure is discussed in the next chapter.

2.6 OBJECTIVES OF THE RESEARCH

The main aim of the present study is to understand and improve the performance characteristics during fabrication of micro holes in a die-sinking type micro-EDM. The objectives are as follows:

1. To carry out experimental investigations for fabrication of micro-holes using Inconel 718 and Titanium Grade 5 using Micro-EDM operation.

2. To evaluate the influence of process variables on the performance of micro-EDM process to determine the optimum conditions.

3. To determine optimum process parameters in order to obtain maximum MRR with minimum Recast Layer thickness overcut effect and taper angle using response surface methodology.

4. To investigate the parametric effects of different operating parameters such as gap voltage, peak current, and pulse on duration, pulse off duration on the performance characteristics.

5. To evaluate and compare the performance of different electrodes in producing micro-holes

6. To determine optimal parameters settings for obtaining higher MRR, minimum recast layer thickness, overcut effect and taper angle of the micro-hole using nature inspired optimization algorithms like Teaching learning based optimization(TLBO), Differential evolution(DE) and Artificial Bee colony algorithm(ABC).

7. To develop ANN model for fabrication of micro-holes in order to predict responses

8. To develop ANFIS model for fabrication of micro-holes in order to predict responses.

9. To model the micro-EDM process relating the machining performance with machining conditions using Finite element method.

CHAPTER 3

EXPERIMENTAL METHODOLOGY

3. EXPERIMENTATION

3.1 INTRODUCTION

An experimental study was carried out to investigate the performance of different electrodes in die-sinking micro-EDM for fabrication of micro holes in Inconel 718 and Titanium as workpiece materials. The experimental set-up and experimental procedures used for machining of Inconel 718 and Titanium grade 5 in this study are presented. An overview of the set-up includes a brief description of machine tool, preparation of workpiece, various electrodes and dielectric material. Various measurement methods and equipment's are also highlighted. The methodology followed for the present study is highlighted in the final section. The experimental plan is based on Central composite design for each electrode.

3.2 EXPERIMENTAL SET-UP

This section includes a brief description of machine tool, workpiece material, various electrodes and dielectric fluid used. Increasing demands in the field of high precision machine technology require a higher quality standard of machining systems. Limitations in conventional machining are a result of inaccuracies such as axial and radial run out of the machining spindle, resolution of the measurement and control system, fluctuations in temperature, air pressure and humidity in the quality of the machining systems. To overcome all these problems.

3.2.1 MACHINE USED

Switzerland built AGIETRON 250 die-sinking EDM machine with computer numeric control has been used for conducting experiments. Figure 2 depicts the EDM machine that was used for conducting experiments.

Figure 3. 1 AGIETRON 250 EDM machine

This machine was used for conducting the micro-EDM experiments. This machine is energized by a pulse generator which can be switched to both transistor-type and RC-type. The maximum travel range of the machine is 700 mm(X) * 500 mm (Y) *500 mm (Z) with the resolution of 0.1 mm in X, Y and Z directions and full closed-feedback control ensures sub-micron accuracy

3.2.2 WORKPIECE MATERIALS

The workpiece materials used in this study are Inconel 718 and Titanium Grade 5 owing to their applicability in aerospace applications. They are renowned for their high strength and wear resistant properties.

3.2.3 TOOL MATERIAL

The selection of electrodes plays a vital role as it influences the machining performance of die-sinking micro-EDM. In this study, three electrodes made of Copper, Graphite and Platinum with a diameter of 0.5 mm each, respectively, were used. The electrode material's specific thermal conductivity and thermal stability (melting point) influence the machining performance significantly. Graphite and platinum as electrode materials provides a higher metal removal rate than copper with less wear and higher electrode stability.

3.2.4 DIELECTRIC

EDM oil 3033 was used as dielectric fluid for this study owing to its relatively high flash point, low pour point, high auto-ignition temperature and high dielectric strength. EDM 3033 was used as a dielectric instead of distilled water because of its low resistivity and electro- chemical action (Jeswani 1981).

3.3 EXPERIMENTAL PROCEDURES

As electrodes plays a vital role in die-sinking process, careful tool preparation and optimal conditions are essential to produce good quality micro-holes. This section describes the electrode dressing and workpiece preparation.

3.3.1 DIE-SINKING MICRO-EDM PROCESS / MICRO-HOLE MACHINING

The study focuses on die-sinking micro-EDM of Inconel 718 and Titanium, using different electrodes combinations such Copper, Graphite and Platinum. The selection of electrode polarity is significant before setting various parameters. Hence, the suitable electrode polarity was selected based on MRR, and surface quality obtained during micro-EDM of Inconel 718 and Titanium. It was identified that the negative electrode polarity provided higher MRR, and good surface finish (Put et al. 2001, Wang et al. 2011). Normally positive workpiece polarity gives higher removal rate whereas negative workpiece polarity gives higher surface finish. Generally micro EDM is used for higher surface finish. Hence negative workpiece polarity is utilized for Micro EDM. Therefore, the experiments were carried out with electrode as negative polarity and workpiece as positive. In die-sinking micro-EDM, after machining each hole the electrode was dressed using a sacrificial block of electrodes. The dressing was necessary as the electrode became tapered after machining of each micro-hole. Thus, the worn out height of the electrode was dressed after machining each hole.

3.4 PARAMETERS CONSIDERED

In the die-sinking micro-EDM, the influencing machining parameters are listed below:

3.4.1 INPUT PARAMETERS

- Gap voltage
- Peak current
- Pulse on duration
- Pulse off duration

3.4.2 OUTPUT PARAMETERS

- Material removal rate (MRR)
- Overcut (OC)
- Recast Layer thickness (RCL)
- Taper Angle (TA)

3.5 DESIGN OF EXPERIMENTS (DOE)

DOE technique is an experimental strategy used to reduce the number of experiments without affecting the quality of the performance. Orthogonal arrays are important means of DOE and the experiments were conducted based on the following calculations

highlighted in the section. The experimental layout was based on the Central composite design. The design consists of 30 experiments with 16 (24) factorial points, eight star points to form a central composite design with α=±2, seven centre points for replication. The design was generated and analysed using Design expert ® 9.0 software package. Based on literature survey and preliminary investigations, four significant process parameters were selected as source voltage (V), Peak current (I_p), Pulse on duration (T_{on}machining time (Tm) and Pulse off duration (T_{off}) (Ahmad and Lajis 2013). The process factors and their levels for Inconel 718 and Titanium grade 5 have been presented in Table 3.1 and 3.2 respectively.

Table 3. 1 :Process parameters and their levels for machining experiments(Inconel 718)

Process parameters	Units	Low	High
Voltage(V)	Volt	30	40
Peak Current (I_p)	Ampere	8	32
Pulse on duration (T_{on})	µs	20	40
Pulse off duration (T_{off})	µs	30	60

Table 3. 2: Process parameters and their levels for machining experiments (Titanium grade 5)

Process parameters	Units	Low	High
Voltage(V)	Volt	30	60
Peak Current (I_p)	Ampere	10	40
Pulse on duration (T_{on})	µs	40	80
Pulse off duration (T_{off})	µs	20	30

3.6 MEASUREMENT OF MACHINING PERFORMANCE

The overview of various measurement methods involved to measure output parameters such as MRR, Recast Layer thickness (RCL), and Overcut effect (OC) and Taper Angle (TA) in this section are discussed.

3.6.1 MATERIAL REMOVAL RATE

MRR for micro-EDM process can be calculated by dividing the total volume of material removed and the total machining time. In the present study, MRR was calculated based on the depth of the hole with respective to time.

MRR was calculated by using the following formula:

$$MRR = \text{Volume of material removed} / \text{Machining time}(T_m)$$

3.6.2 OVERCUT & RECAST LAYER THICKNESS (RCL)

Overcut is the difference between the radius of the micro-hole and the radius of the electrode. This can be measured by using SEM. The diameter of hole at entrance side was measured by scanning electron microscope. In this study, the overcut was represented in terms of percentage and was calculated as the ratio of the radial difference between the hole on the workpiece and the radius of the electrode divided by the radius of the electrode. Recast layer thickness was examined using Scanning electron microscope. The measurement was done from various positions and an average value has been considered.

CHAPTER 4

EXPERIMENTAL INVESTIGATION OF MICRO HOLE DRILLING ON INCONEL 718

4.1 INTRODUCTION

The miniaturization of the product is the index of progress in the present day scenario of the industrial growth. Especially innovations in material science technology have led to the development of various hard to cut materials like Titanium, Inconel and other high strength, temperature resistance (HSTR) nickel-based super alloy. These materials are widely used in aerospace industry, gas turbines, rocket motors, nuclear reactors and pumps. These typical applications require stern design requirements and close tolerances in manufactured products. Conventional machining of such materials proves to be a challenging task because of their inherent properties like high toughness, high hardness, and high work hardening rate. Moreover, traditional machining methods often fail to meet the desired accuracy and precision required during fabrication of such products. Electrical discharge machining (EDM) is a non-contact process that eliminates mechanical stresses, chatter and vibration related issues, therefore production of micro and fragile pieces with high accuracy level can be achieved to machine any electrically conductive materials regardless of its hardness (Ho and T 2003)**.** Therefore, it is very effective in machining small holes, blind holes, and deep holes. The capability of an EDM process in producing micro-features is well known. Tiwary et al.(2015) studied the influence of various process parameters on material removal rate (MRR), tool wear rate (TWR), overcut (OC), and taper of µ-EDM during machining of Ti–6Al–4V by using response surface methodology for mapping the relationship between the input process parameters with the resulting process response. The research and development activities of the last few years have named the new variant of EDM for micro-machining as µ–EDM. In recent year's µ –EDM has emerged as a promising technology for achieving high-aspect-ratio micro-features. Inherent features like small process forces and good repeatability has made this process more prevalent in micro machining area. As µ-EDM process is speculative and random in nature, it is very difficult to predict the output characteristics accurately by mathematical equations.

In the present investigation, fabrication of micro-holes in Inconel-718 has been carried out using copper, graphite and platinum as electrode tool material. Micro-holes are fabricated as per the Central composite design using response surface methodology. MRR, the thickness of recast layer, radial overcut and taper angle of the micro-hole have been measured as the responses. The qualities of micro-holes have been investigated. The effect of the process-parameters on process responses have been analyzed using analysis of variance analysis. Further, artificial neural network modeling has been carried out for prediction of the process responses. Finally, multi-objective optimization has been carried out using popular nature inspired algorithms like Elitist Teaching learning based optimization (ETLBO), Differential evolution algorithm (DEA) and Artificial Bee colony algorithm (ABC).

4.2 EXPERIMENTAL DETAILS

Experimentation work has been carried out in three different phases. In first phase fabrication of micro holes was drilled by using electrolytic copper in the form of cylindrical rod, whereas in the second and third phase micro holes have been drilled using Graphite and Platinum electrodes.

4.2.1 DESIGN OF EXPERIMENTS

The experimental layout was based on the rotatable central composite design. The design consists of 30 experiments with 16 (2^4) factorial points, eight star points to form a central composite design with $\alpha=\pm2$, six centre points for replication. The design was generated and analyzed using evaluation version of Design expert® 9.0.5 software package. Table 4.1 presents process factors and their levels.

Table 4. 1: Process parameters and their levels for machining experiments

Process parameters	Units	Low	High
Voltage (V)	Volt	30	40
Peak Current (I_p)	Ampere	8	32
Pulse on duration (T_{on})	µs	20	40
Pulse off duration (T_{off})	µs	30	60

4.2.2 EXPERIMENTAL SETUP AND MATERIALS USED

The AGIETRON 250 die-sinking EDM machine with computer numeric control has been used for conducting all the experiments. Figure 4.1 depicts the EDM machine used for conducting the experiments. The holes were fabricated on a rectangular shaped work piece specimen made of Inconel 718 having a mean thickness of 1 mm, length 25 mm, and width 15 mm which is presented in Figure 4.2. The physical properties of workpiece have been presented in Table 4.2. The tool was made up from electrolytic copper in the

form of cylinder with 0.5 mm diameter. Electrolyte was fed externally to the cutting zone through the dielectric pumping system incorporated with machine. EDM 3033 oil was used as a dielectric instead of distilled water because of its low resistivity and electrochemical action (Jeswani 1981). Based on literature survey and preliminary investigations, the source voltage (V), Peak current (I_p), Pulse on duration (T_{on}) and Pulse off duration (T_{off}) (Ahmad and Lajis 2013) were selected as four significant process parameters.

Figure 4. 1 AGIETRON 250 EDM machine

The machining time (T_m), recast layer thickness (RCL), Overcut (OC) and taper of micro-hole were measured. The hole overcut and recast layer thickness were examined using Scanning electron microscope. SEM was used for measurement because along with measurement of micro hole diameter at entry side as well as exit side it also incorporated the measurement of Recast layer thickness and other geometrical form tolerances. Moreover, the resolution of SEM is higher than optical microscope. Table 4.3 shows experimental design matrix along with results in the form process responses.

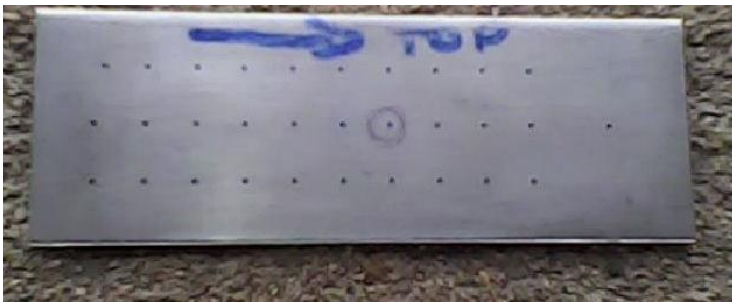

Figure 4. 2 Inconel 718 workpiece

The measurement was done from four different positions namely horizontally, vertically and diagonally further, an average value has been considered for determination of entry as well as exit diameter. For determining machined hole overcut, the diameter of hole at entrance side was measured by scanning electron microscope. The microscopic view of micro drilled holes measured from both top and the bottom surface of workpiece are shown in Figure 4.3(a).

Table 4. 2: Properties of Inconel 718

Property	Value (Units)
Density	8090 (kg/m^3)
Thermal Conductivity	11.4 (W/m/°K)
Specific Heat	435 (J/kg °K)
Melting Point	1609 K
Electrical Resistivity	820 (micro-ohm-mm)
Hardness	70 (HRB)
Tensile Strength	586 (MPa)

Table 4. 3: Experimental design matrix along with results

S. No	Parameters				Material Removal Rate (MRR) in mm^3/min	Overcut (OC) in µm	Recast layer thickness (RCL) in µm	Taper Angle (TA) in degrees
	Voltage (V)	Peak current (I_p)	Pulse on duration (T_{on})	Pulse off duration (T_{off})				
1	30	8	20	30	0.766	0.168	92.370	2.777
2	30	8	40	60	0.556	0.238	113.079	1.960
3	30	8	20	60	0.784	0.202	105.555	1.853
4	30	8	40	30	0.538	0.236	79.032	2.153
5	30	20	30	45	0.748	0.192	118.483	1.890
6	30	32	20	30	0.588	0.188	89.041	3.831
7	30	32	20	60	0.427	0.165	87.999	3.037
8	30	32	40	60	0.593	0.193	116.060	2.449
9	30	32	40	30	0.458	0.168	87.249	2.917
10	35	8	30	45	0.614	0.205	112.308	1.174
11	35	20	30	45	0.651	0.212	104.857	1.525
12	35	20	30	30	0.682	0.183	102.237	2.369
13	35	20	30	45	0.766	0.127	105.472	1.525
14	35	20	30	45	0.627	0.130	102.943	1.565
15	35	20	30	45	0.659	0.124	104.857	1.525
16	35	20	30	45	0.682	0.197	95.173	1.453
17	35	20	30	45	0.748	0.220	103.514	1.565
18	35	20	40	45	0.673	0.193	106.391	0.788
19	35	20	20	45	0.659	0.161	103.891	1.541
20	35	20	30	60	0.689	0.146	106.408	1.567
21	35	32	30	45	0.725	0.134	102.560	2.201
22	40	8	20	30	0.715	0.220	57.926	1.897
23	40	8	20	60	0.627	0.222	64.348	1.467
24	40	8	40	30	0.623	0.185	68.854	2.584
25	40	8	40	60	0.518	0.195	73.287	2.775
26	40	20	30	45	0.627	0.217	87.390	1.415
27	40	32	40	60	0.601	0.222	83.250	2.775
28	40	32	40	30	0.816	0.240	78.322	2.184
29	40	32	20	60	0.582	0.187	64.077	1.987
30	40	32	20	30	0.725	0.222	68.791	1.490

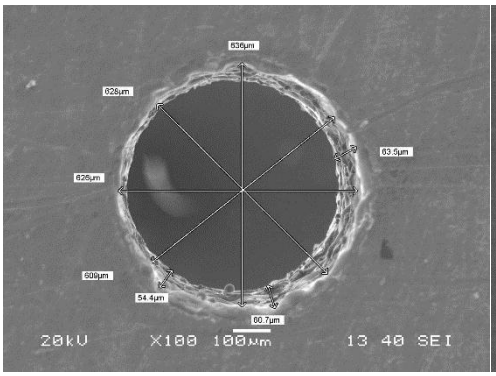

1st Hole Top view

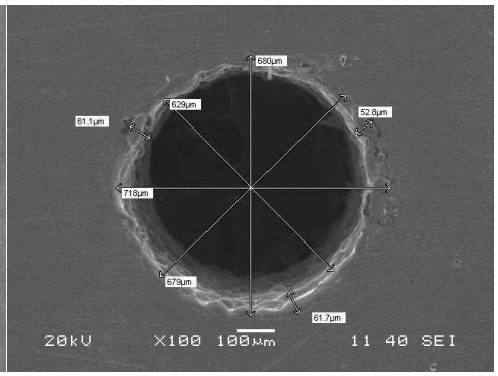

1st Hole Bottom view

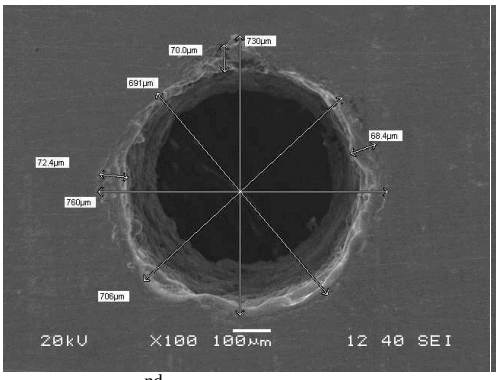

2nd Hole Top view

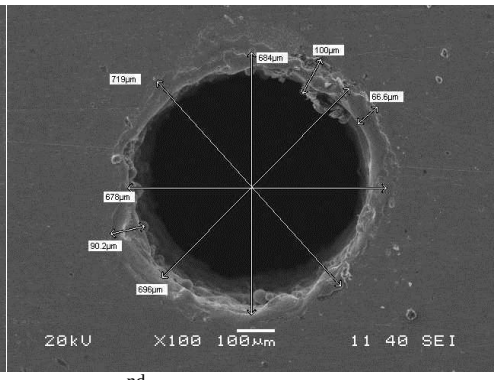

2nd Hole Bottom view

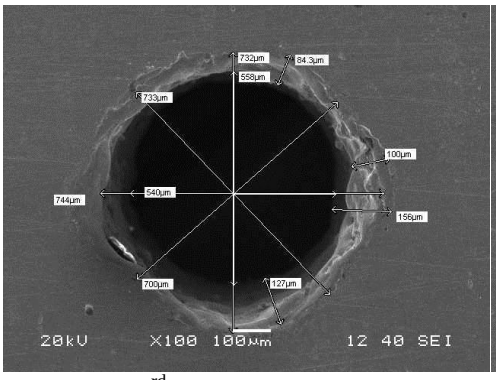

3rd Hole Top view

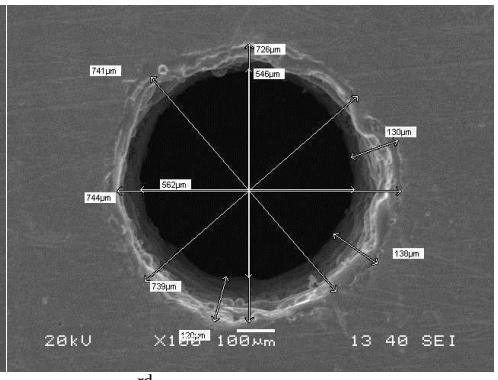

3rd Hole Bottom view

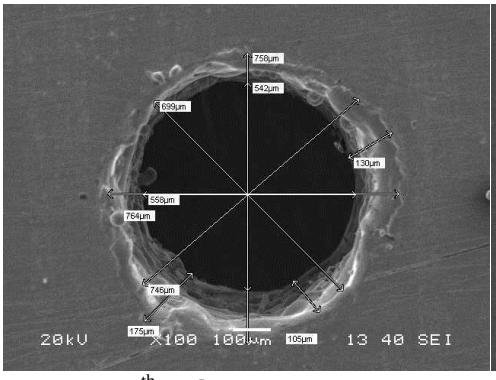

4th Hole Top view

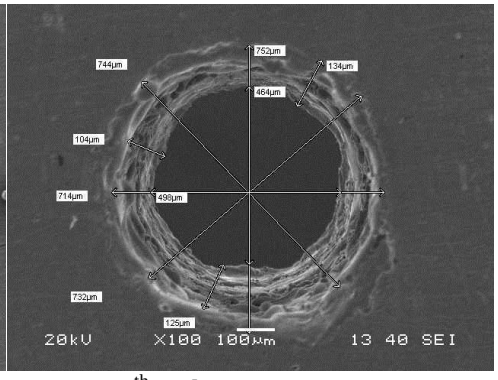

4th Hole Bottom view

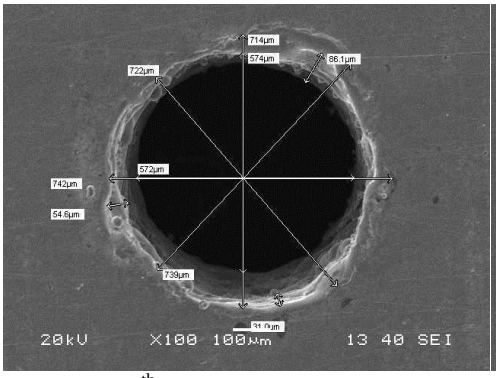

5th Hole Top view

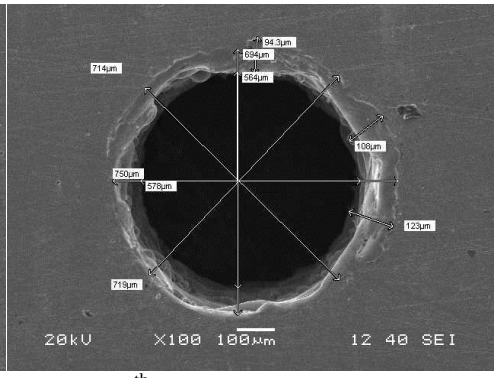

5th Hole Bottom view

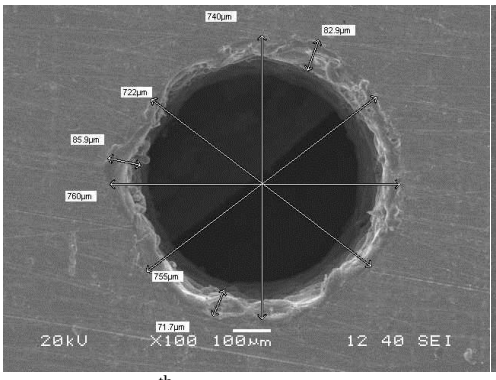

6th Hole Top view

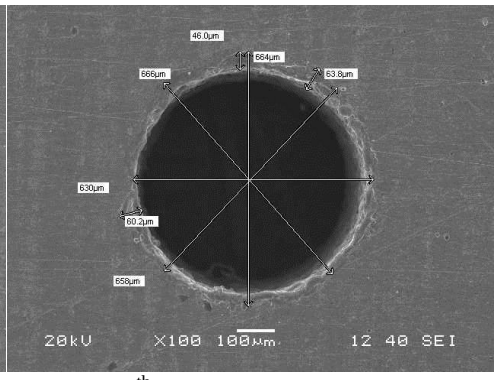

6th Hole Bottom view

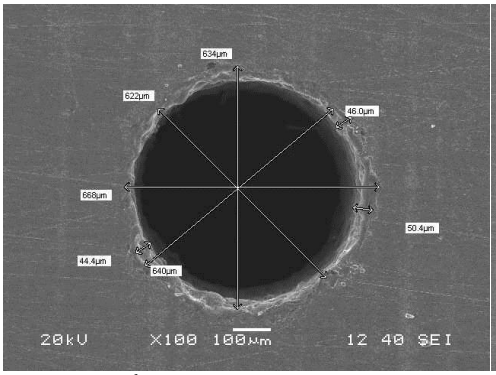

7th Hole Top view

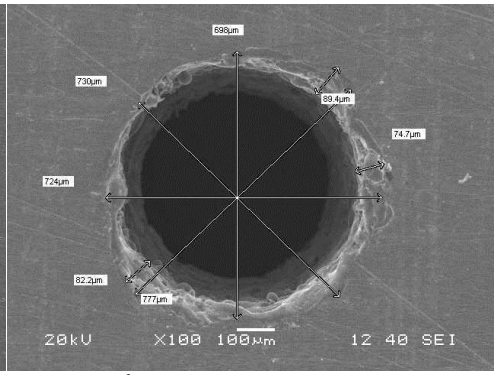

7th Hole Bottom view

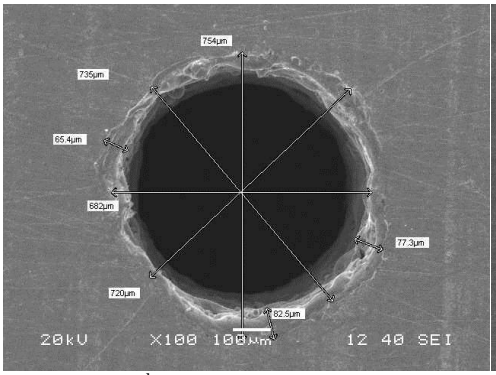

8th Hole Top view

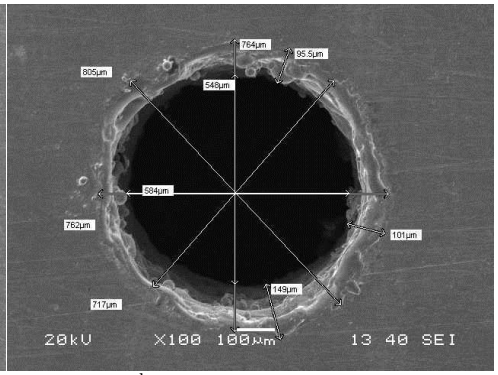

8th Hole Bottom view

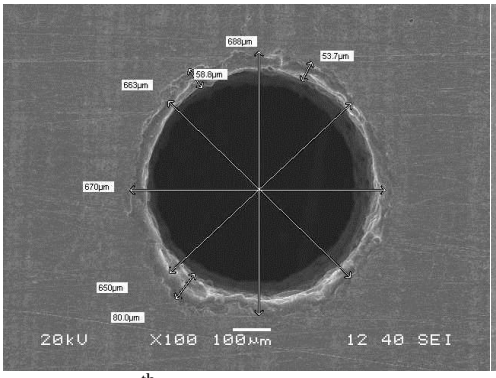

9th Hole Top view

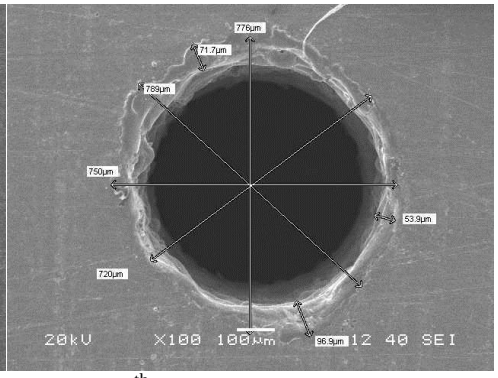

9th Hole Bottom view

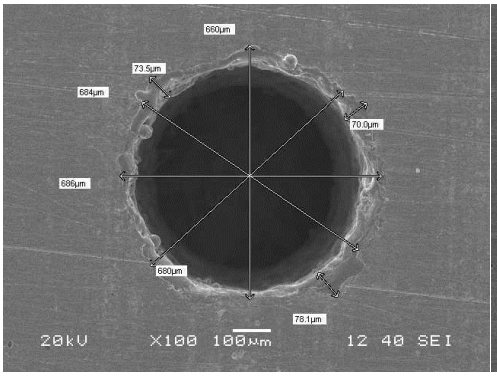

10th Hole Top view

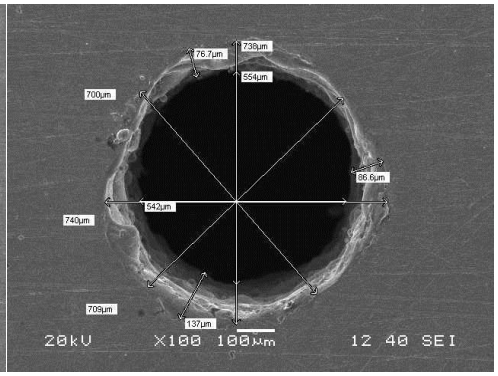

10th Hole Bottom view

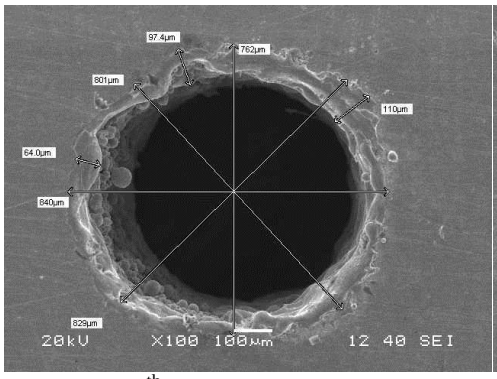

11th Hole Top view

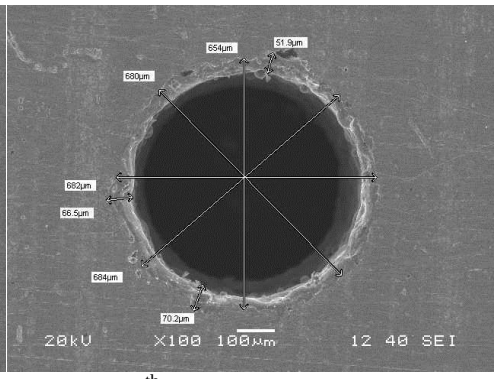

11th Hole Bottom view

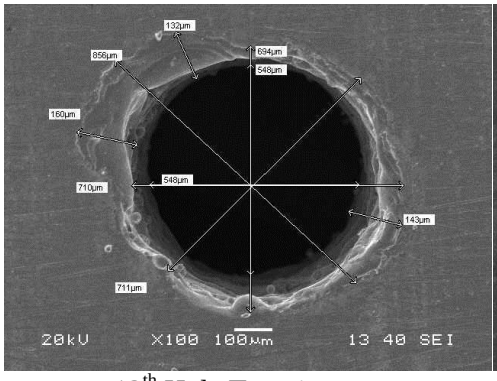

12th Hole Top view

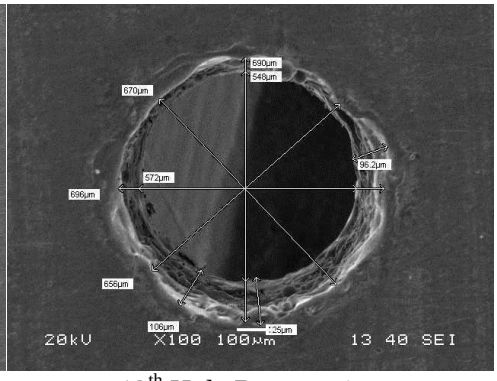

12th Hole Bottom view

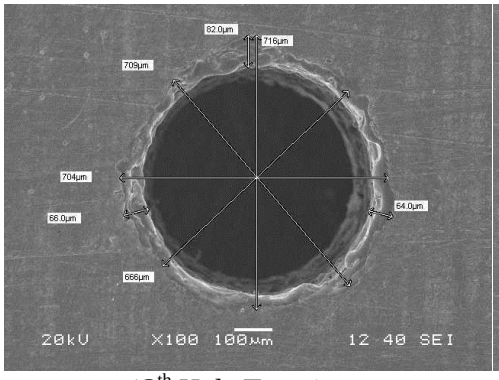

13th Hole Top view

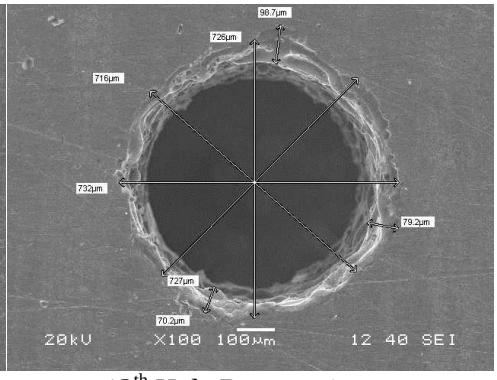

13th Hole Bottom view

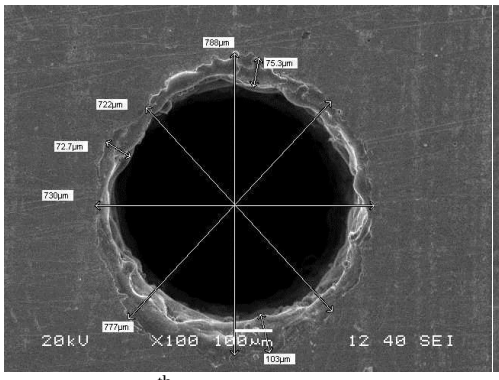

14th Hole Top view

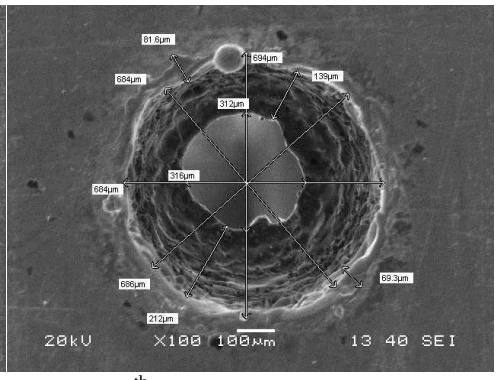

14th Hole Bottom view

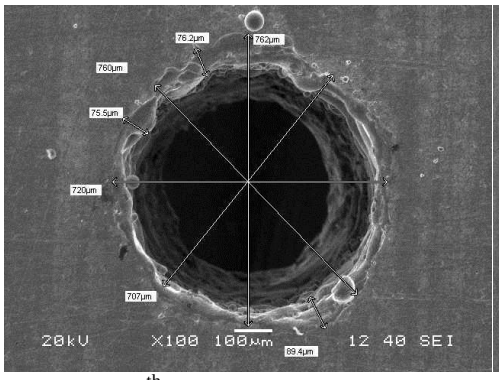

15th Hole Top view

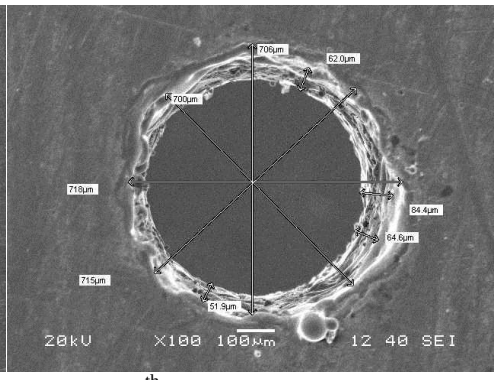

15th Hole Bottom view

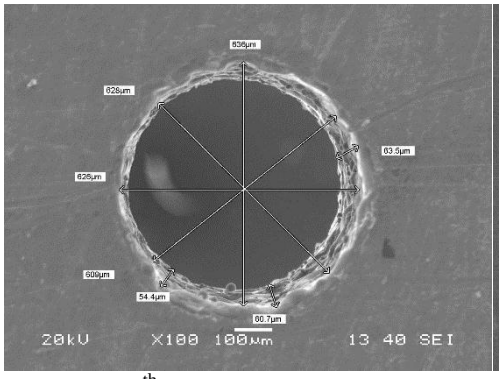

16th Hole Top view

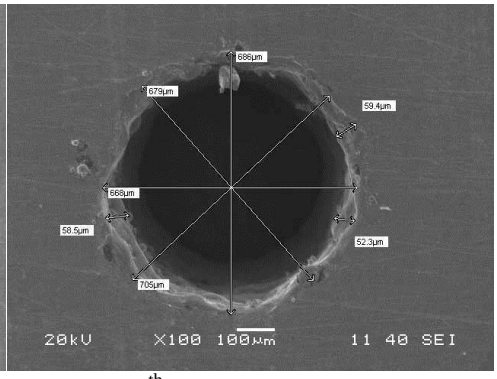

16th Hole Bottom view

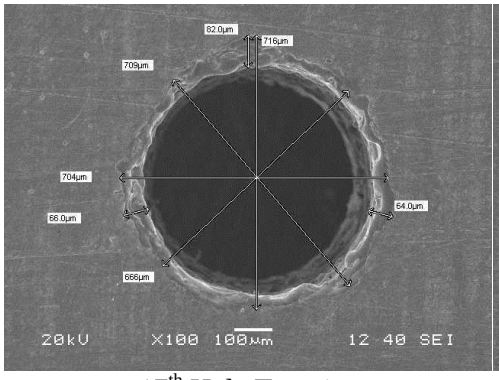

17th Hole Top view

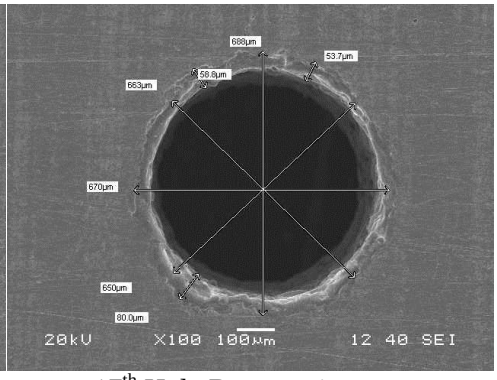

17th Hole Bottom view

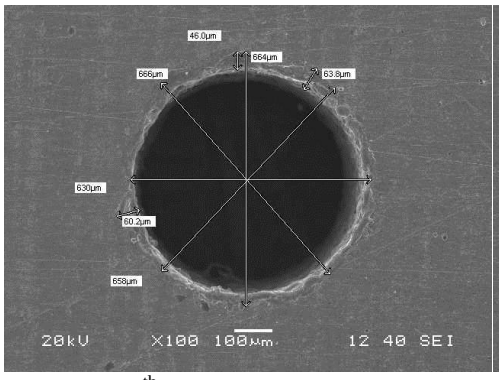

18th Hole Top view

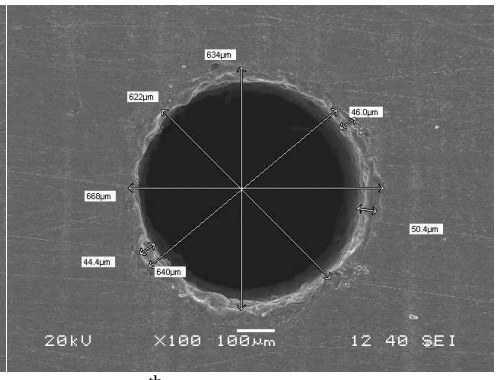

18th Hole Bottom view

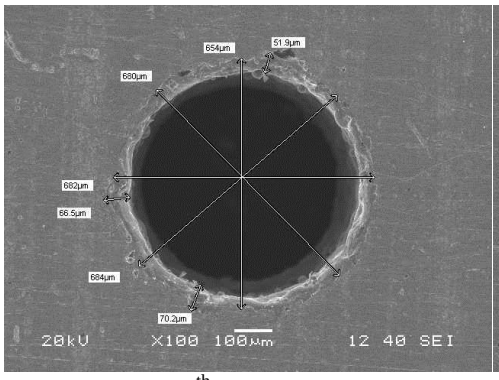

19th Hole Top view

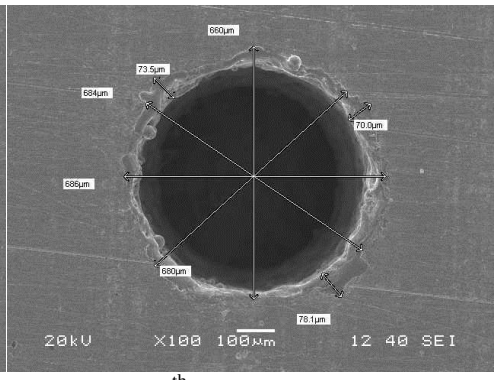

19th Hole Bottom view

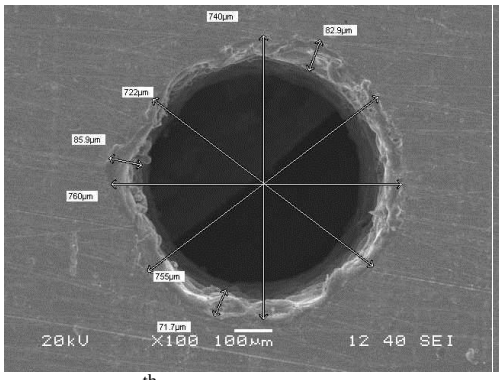

20th Hole Top view

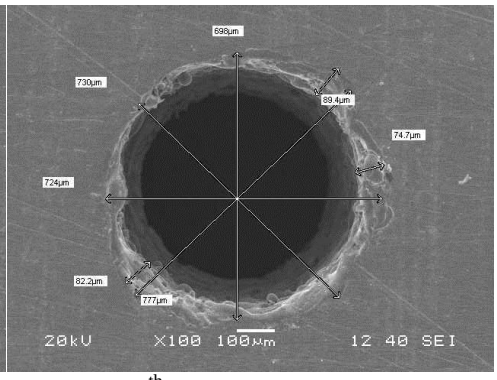

20th Hole Bottom view

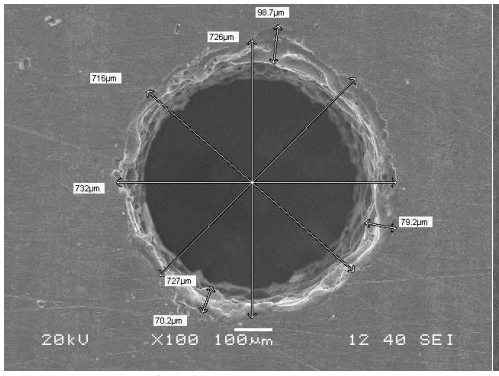

21st Hole Top view

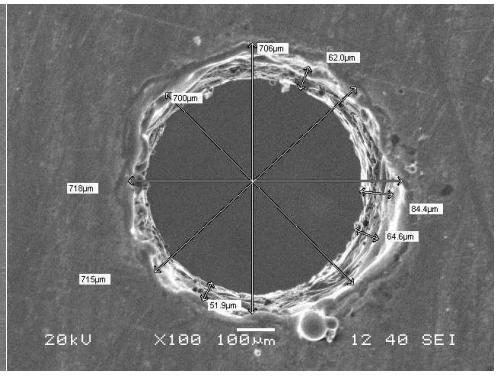

21st Hole Bottom view

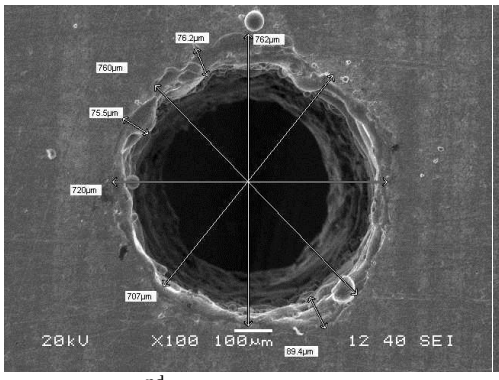

22nd Hole Top view

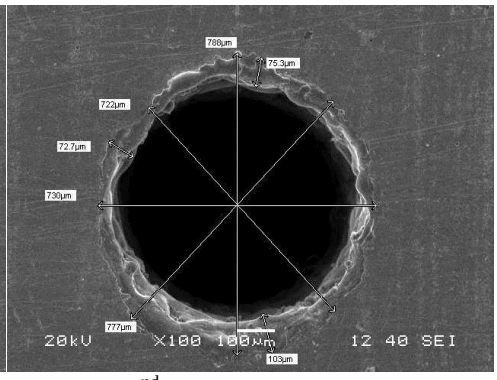

22nd Hole Bottom view

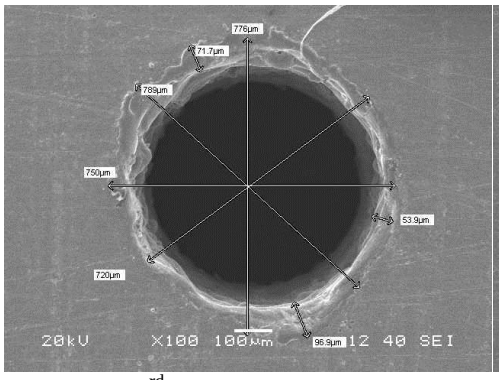

23rd Hole Top view

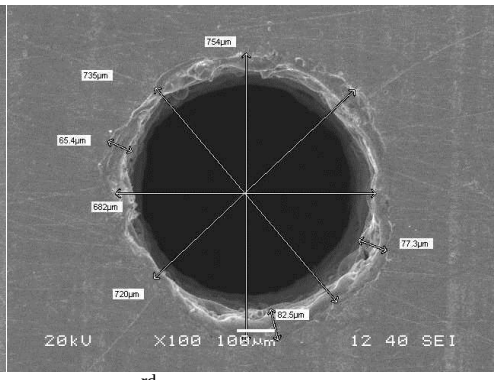

23rd Hole Bottom view

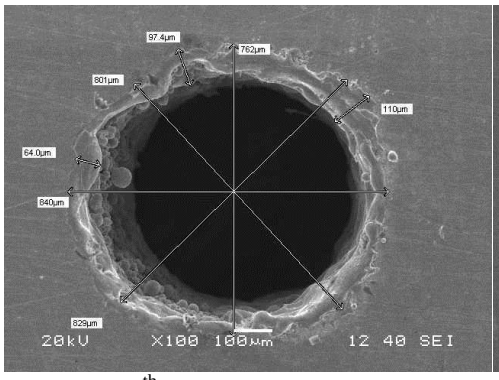

24th Hole Top view

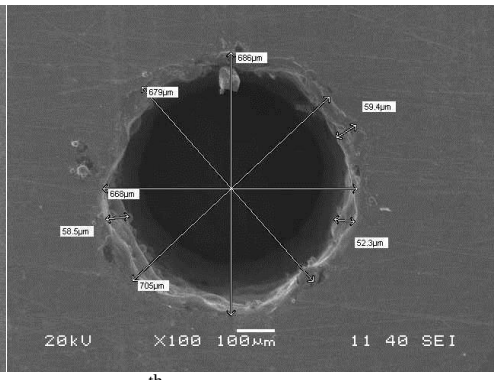

24th Hole Bottom view

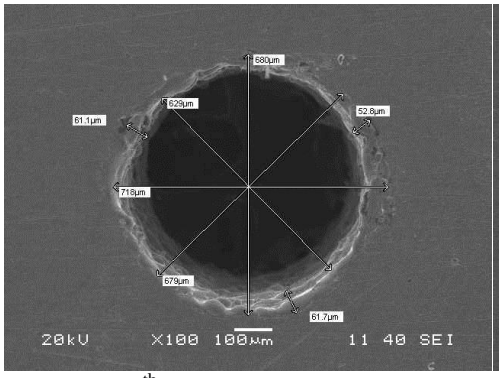

25th Hole Top view

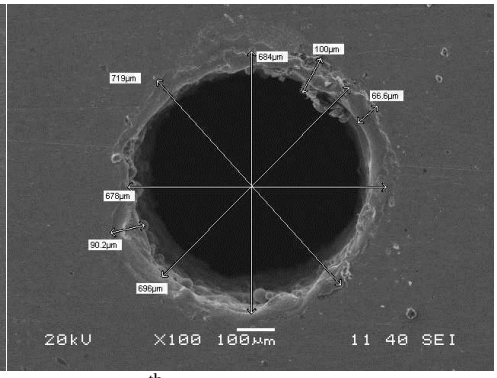

25th Hole Bottom view

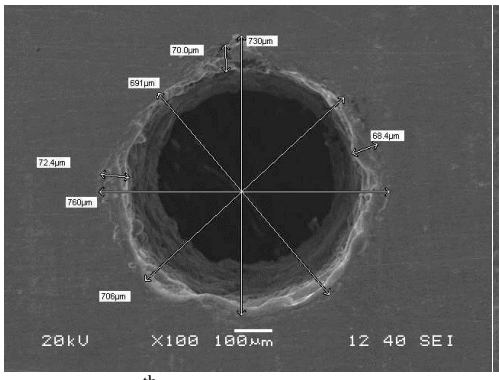

26th Hole Top view

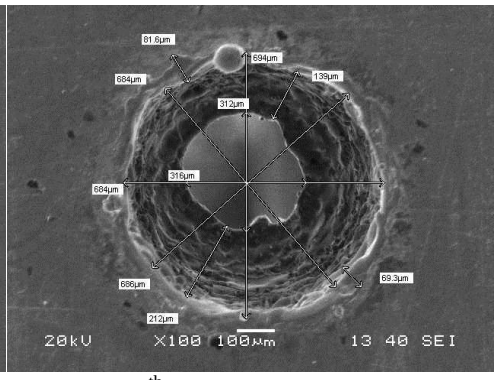

26th Hole Bottom view

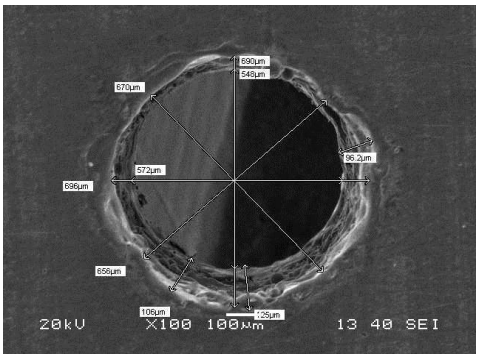

27th Hole Top view

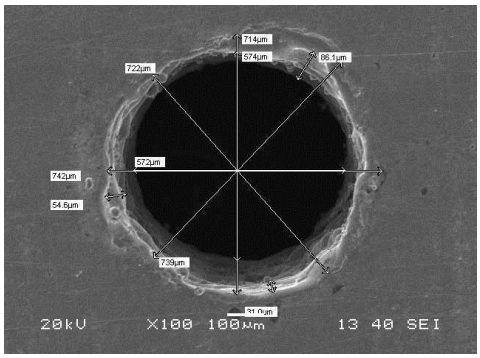

27th Hole Bottom view

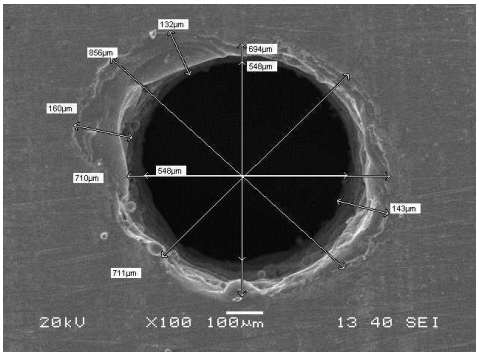

28th Hole Top view

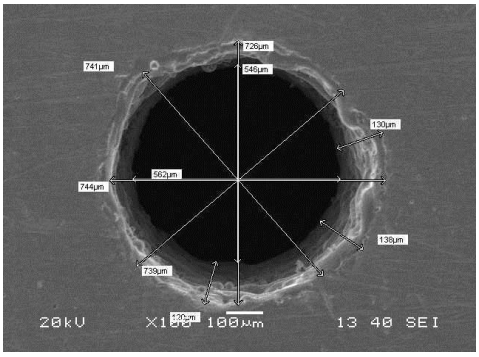

28th Hole Bottom view

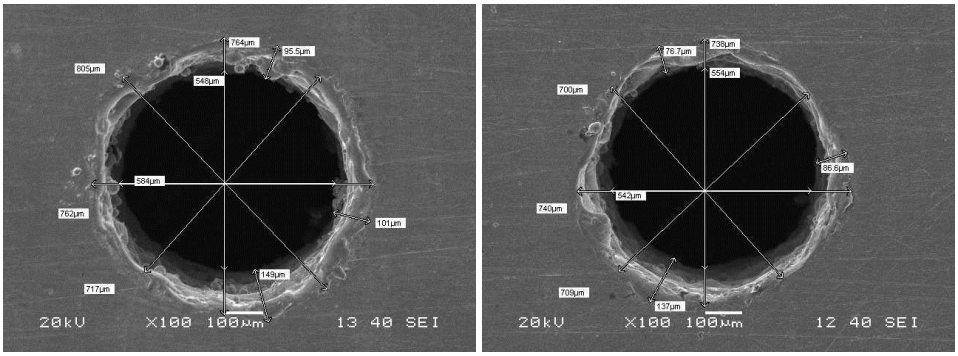

29th Hole Top view 29th Hole Bottom view

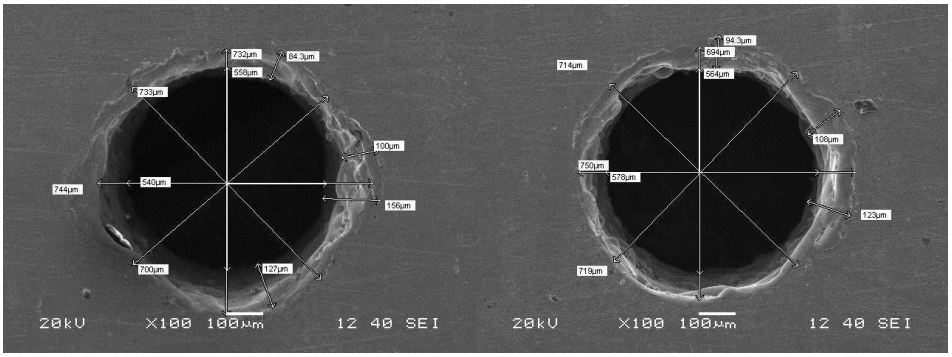

30th Hole Top view 30th Hole Bottom view

Figure 4.3: (a) SEM Images of Micro Holes

MRR was calculated considering the geometry of micro-hole and machining time. The MRR has been determined as the average volume of the material removed to the machining time and expressed in cubic millimeter per minute. General Volume formula considered for MRR in workpiece is the volume of a conical frustum which is as follows:

$$\text{MRR} = \text{Volume of material removed} / \text{Machining time } (T_m) \quad (4.1)$$

$$\text{Volume of material removed} = \frac{\pi h}{12}(D_t^2 + D_t^2 * D_b^2 + D_b^2) \quad (4.2)$$

where D_t is the Top diameter of micro-hole.

D_b is the Bottom diameter of micro-hole.

h is the thickness of workpiece material.

T_m is the machining time.

The calculation of Overcut and Taper has been determined using Equations 4.3 and 4.4 respectively. The value of OC was calculated by diametric difference of tool as well as machined as illustrated in Figure 4.3(b) and 4.3(c) respectively

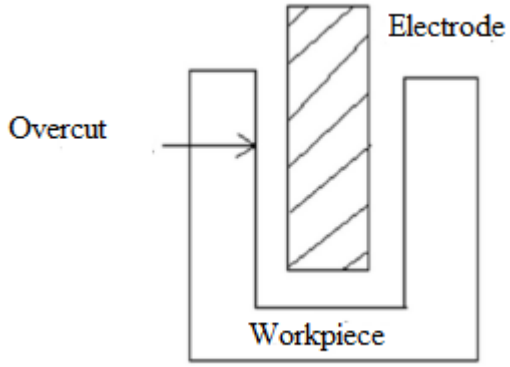

Figure 4.3 (b) Measurement of overcut

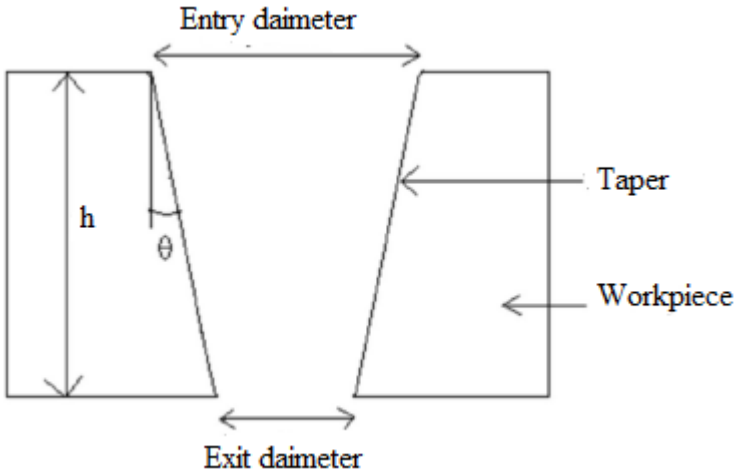

Figure 4.3 (c) Measurement of Taper angle

$$\text{Overcut} = \{(Da - D)/2\} \tag{4.3}$$

$$\text{Da} = \{(D_t + D_b)/2\}$$

where D_a is the average diameter of micro-hole produced.

where D_t is the Top diameter of micro-hole produced.

D_b is the Bottom diameter of micro-hole produced.

D is the tool diameter.

The taper angle of the micro-holes is measured as:

$$\theta = \tan^{-1}\left(\frac{D_{entry} - D_{exit}}{2t}\right) \tag{4.4}$$

where θ is the taper angle, D_{entry} is the entrance diameter, and D_{exit} is the exit diameter of the micro-hole and t is the machined depth.

4.2.3 ANOVA APPROACH USING RESPONSE SURFACE METHODOLOGY

As per Montgomery, response surface method is a collection of mathematical and statistical techniques that are helpful for modeling and analysis of problems in which response is influenced by several input variables, and the main objective is to find the correlation between the response and the variables inspected (Montgomery 2011). Response surface method has many advantages, and has effectively been applied to study and optimize the processes. It offers enormous information from a small number of experiments. In addition, it is possible to detect the interaction effect of the independent parameters on the response. The model easily clarifies the effect for binary combination of the independent process parameters. Furthermore, the empirical model that related the response to the independent variables is used to obtain information. It has been widely used in analyzing various processes, designing the experiment, building models, evaluating the effects of several factors and searching for optimum conditions to give desirable responses and reduce the number of experiments (Gopalakannan and Senthilvelan 2013). Response surface methodology (RSM) is an interaction of mathematical and statistical techniques for modeling and optimizing the response variables which incorporates quantitative independent variables. In this present work, a second-order polynomial was selected for developing the empirical model relating the response surface and independent parameters as shown below:

$$y = b_0 + \sum_{i=1}^{n} b_i x_i + \sum_{i=1,\, j=1}^{n} b_{ij} x_i x_j + \sum_{i=1}^{n} b_{ii} x_i^2 \pm \Psi \quad (4.5)$$

where y and x are output response and input factor respectively. Furtherb_0,b_i, b_{ij} and b_{ii} are the polynomial constants. Lastly, Ψ is the error constant. The coefficients of regression model can be estimated from the experimental results by Design expert software. The significant terms in the model were identified by backward elimination process. The backward elimination considers all the predictors in the model. The variable least significant i.e., the one with the largest p value is removed and the model is refitted. Each subsequent step removes the least significant variable in the model until all remaining variables have individual p values smaller than some value equal to 0.05. The regression coefficients are calculated using the uncoded units. Analysis of variance (ANOVA) was carried out to check the adequacy of the developed models. Table 4.4 shows the ANOVA for MRR after applying backward elimination process and as it can be seen from Table 4.4 that it comprises of only significant terms. The p value for the model is lowers than 0.05 (i.e., at 95% confidence level) indicates that the developed model is statistically significant. Further the model F-value of 7.87 implies the model is significant. There is only a 0.01% chance that an F-value this large could occur due to noise. In this case A, C, D, AC, AD, BD are significant model terms. The same and similar analyses were carried out for OC, RCL and TA. Furthermore, after backward elimination process the R-Squared value for MRR, OC, RCL and TA were found to be 0.6725, 0.9652, 0.7061 and 0.9995 respectively. However, the truncated models have lower R-Squared value than that of full quadratic model exhibiting significance of relationship between the response and the variables. This shows that second order models can explain the variation in the MRR, OC, RCL and TA up to the extent of 67.25%, 96.52%, 70.61% and 99.95% respectively. The "Predicted R-Squared" values are in reasonable agreement with the "Adjusted R-Squared ‘‘values.

Table 4. 3 Truncated model for MRR. (After elimination)

Source	Sum of Squares	Degree of Freedom	Mean Square	F Value	p-value Prob > F	Percentage Contribution (%)
Model	0.12	6	0.021	7.87	0.0001	66.667
A-Voltage	0.014	1	0.014	5.19	0.0324	7.778
C-Pulse on duration	0.012	1	0.012	4.44	0.0462	6.667
D-Pulse off duration	0.035	1	0.035	13.41	0.0013	19.444
AC	0.016	1	0.016	6.12	0.0212	8.889
AD	0.015	1	0.015	5.69	0.0256	8.333
BD	0.032	1	0.032	12.38	0.0018	17.778
Residual	0.060	23	2.625E-003			
Lack of Fit	0.047	18	2.613E-003	0.98	0.5655	Insignificant
Pure Error	0.013	5	2.668E-003			
Corrected Total	0.18	29			R-Squared	0.6725
					Adjusted R-Squared	0.5871
					Predicted R-Squared	0.4616

The percentage contribution of different process variables on MRR is presented in Figure 4.4 and it can be seen that pulse off duration has a significant effect on MRR followed by voltage and pulse on duration.

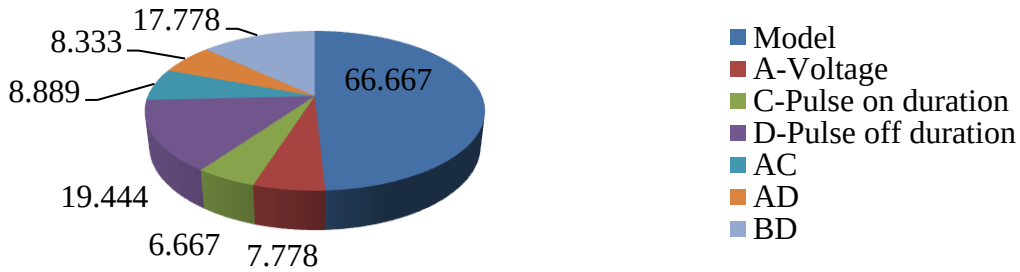

Figure 4. 3: Percentage contribution of process variables

4.2.4 ANALYSIS OF MATERIAL REMOVAL RATE (MRR)

The ANOVA summary recommended that the quadric model is statistically significant for analysis of MRR and linear terms of voltage, pulse on duration and pulse off duration, interaction terms of voltage, current, pulse on duration and pulse off duration are significant model terms. Hence, analysis of MRR is extended for these terms only as their values of "Probability > F" less than 0.05. The three dimensional surface plots for the MRR with respect to the significant process parameters are shown in Figures 4.5(a-c). In each of these graphs, two process variables are varied while the other two variables are held constant at its middle value. The interaction effect of voltage and pulse on duration on metal removal rate in the form of 3D surface graph at constant peak current of 20ampere and pulse off duration of 45µs is represented in Figure 4.5(a) using design expert software and response surface methodology. From this Figure, it is observed that maximum metal removal rate (0.730mm^3/min) was obtained at the highest voltage (40V) and highest pulse on duration (40µs) combination. The minimum metal removal rate (0.613mm^3/min) was obtained at the lowest voltage (30V) and highest pulse on duration (40µs) combination. It is seen from these graphs that there is slight rise in slope indicating non-linearity in the variation. It is observed that material removal rate increases with increase in voltage and pulse on duration. There is a significant increase in material removal rate with increase in voltage however with increase in pulse on duration there is slight decrease in material removal rate at highest pulse on duration setting of 40µs.

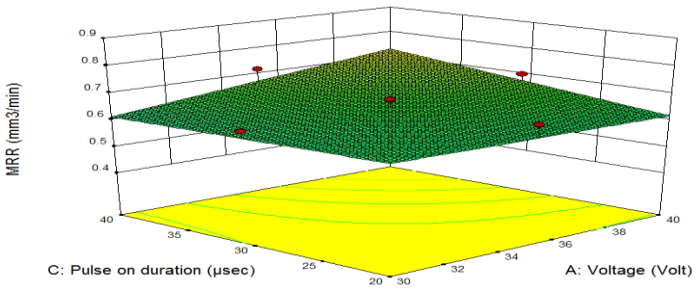

Figure 4.5 a: Interaction effect of voltage and pulse on duration on MRR

Furthermore, Figure 4.5(b) shows the interaction effect of voltage and pulse off duration on MRR in the form of 3D surface graph at constant peak current of 20 ampere and pulse on duration of 30µs obtained from design expert software and response surface methodology. Further it can be observed that maximum MRR value equal to 0.748 mm^3/min was obtained at the highest voltage of 40Vand lowest pulse off duration (30µs) combination. Additionally, the minimum MRR value equal to 0.600 mm^3/min was obtained at the highest voltage (40V) and highest pulse off duration (60µs) combination. It can be interpreted that material removal rate decreases with increase in voltage and

pulse off duration. There is a significant increase in material removal rate with increase in voltage, however with increase in pulse off duration there is a slight decrease in MRR.

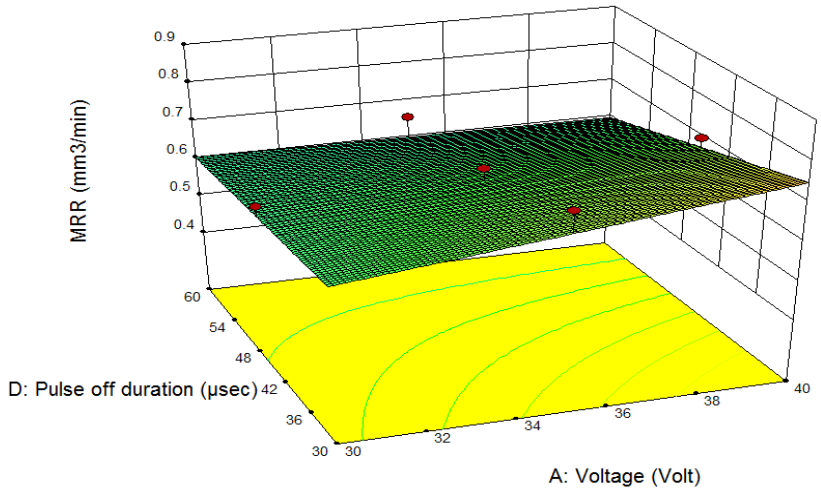

Figure 4.5 b: Interaction effect of voltage and pulse off duration on MRR

Figure 4.5(c) exhibits the interaction effect of peak current and pulse off duration on MRR at constant voltage of 35V and pulse on duration of 30µs. From this Figure, it is witnessed that maximum MRR of 0.748 mm^3/min was achieved at the highest voltage of 40Vand lowest pulse off duration (30µs) combination. The minimum MRR equal to 0.600 mm^3/min was obtained at the maximum voltage (40V) and maximum pulse off duration (60µs) combination. It is observed that material removal rate drops with rise in voltage and pulse off duration. There is a significant escalation in material removal rate with increase in voltage, however with increase in pulse off duration there is a slight decrease in MRR.

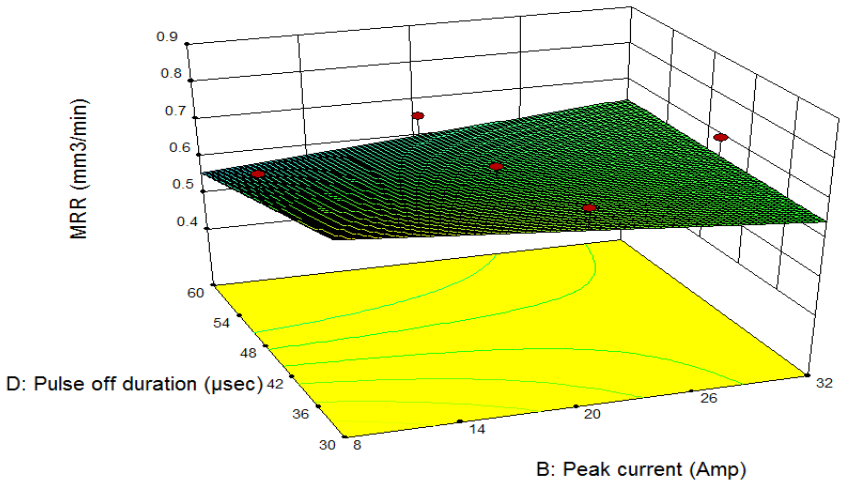

Figure 4.5(c): Interaction effect of voltage and pulse off duration on MRR

Figure 4.5(c) illustrates the interaction outcome of current and pulse off duration on MRR at constant voltage of 35 volts and pulse on duration of 30µs. Furthermore, from this Figure, it is seen that that maximum MRR was obtained at the lowest current (8 ampere) and pulse off duration (30µs). The least MRR was obtained at the lowest current (8 ampere) and highest pulse off duration of 60µs combination. It is observed that surface roughness increases with increase in current and the spark gap. There is a significant increase in MRR with increase in current, however with increase in pulse off duration there is noteworthy reduction in MRR.

4.2.5 ANALYSIS OF OVERCUT (OC)

The percentage contribution of different process variables on OC is presented in Figure 4.5 and it can be seen in this case A, C, D, AB, AC, AD, BC, BD, CD, A^2, B^2, C^2, D^2 are significant model terms. Voltage has a significant effect on OC followed by pulse on duration and pulse off duration.

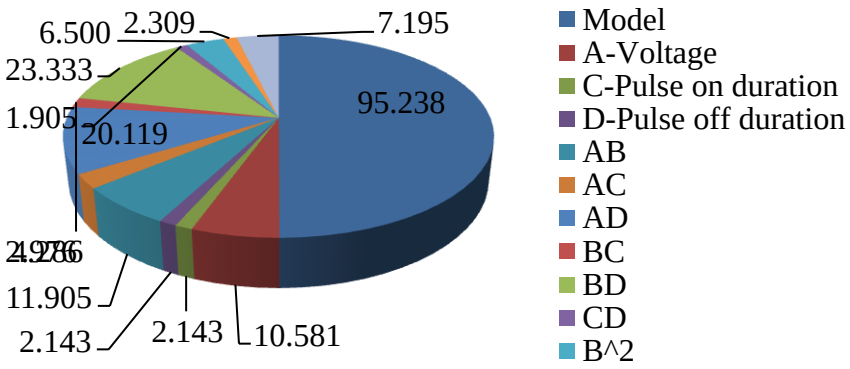

Figure 4. 4: Percentage contribution of process variables

The Analysis of variance summary indicates that the quadric model is statistically significant for OC and linear terms of voltage, pulse on duration and pulse off duration, interaction terms of voltage, peak current and pulse on duration and square terms of peak current, pulse on duration and pulse off duration are significant model terms. Hence, analysis of OC is extended for these terms only. The three dimensional surface plots for the OC with respect to the significant process parameters are shown in Figures (4.6-4.10). In each of these graphs, two machining parameters are varied while the other two parameters are held constant as its middle value. The interaction effect of voltage and current on OC in the form of 3D surface graph at constant pulse on duration of 30µs and pulse off duration of 40µs is represented in Figure 4.6 using design expert software and response surface methodology. From this Figure, it is observed that maximum OC was obtained at the highest current (32 ampere) and highest voltage (40V) combination. The minimum OC was obtained at the highest current (32 amps) and lowest voltage (30V) combination. It can be observed from these graphs that there is significant amount of curvature indicating non-linearity in the variation. It also points towards significant contribution from the interaction of the machining parameters. It is observed that OC increases with increase in current and the voltage. There is significant decrease in OC with increase in current, however with increase in voltage there is slight increase in OC. As for as the current is concerned, more current means more energy available per spark. This higher energy available per spark leads to melting of more material per spark and hence high overcut effect.

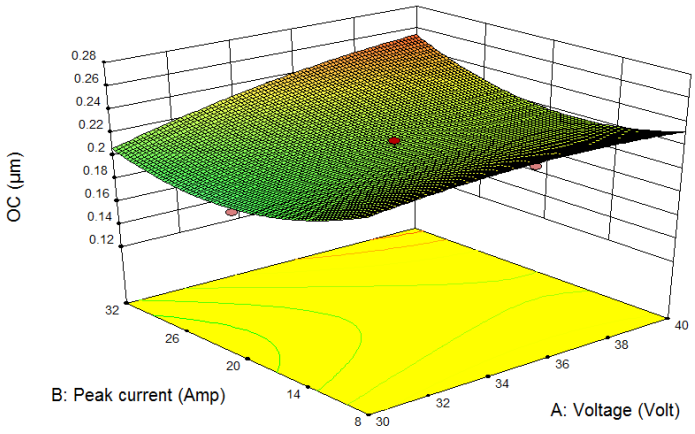

Figure 4. 5: Interaction effect of Voltage and Peak current on OC

At constant peak current of 20 ampere and pulse off duration of 45µs, the interaction effect of voltage and pulse on duration on OC is represented in Figure 4.7. It is observed that maximum OC was found at the highest voltage of (40V) and lowest pulse on

duration of 20µs.The minimum OC was obtained at the lowest voltage (30V) and the highest pulse on duration of (40µs) combination. It indicates significant contribution from the interaction of the machining parameters. It is interesting to note that OC first increases with increase in voltage and the pulse on duration and then decreases. There is a significant increase in OC with increase in voltage however with increase in pulse on duration initially there is increase in OC then reduction on further increment of pulse on duration.

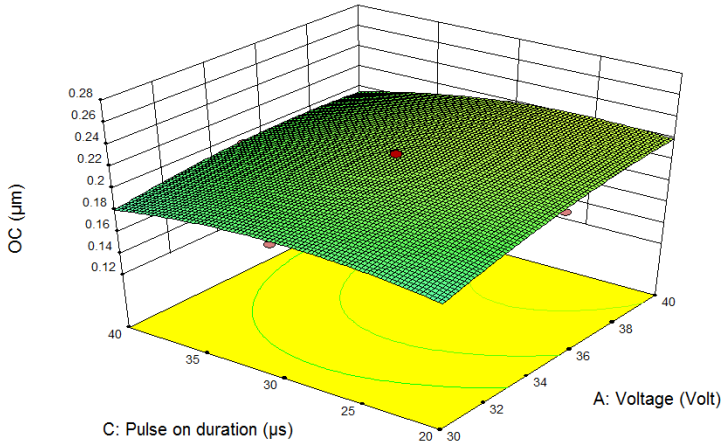

Figure 4. 6: Interaction effect of Voltage and Pulse on duration on OC

On observing the interaction effect of voltage and pulse off duration on OC at constant peak current of 20 ampere and pulse on duration of 30µs is demonstrated in Figure 4.8 it can be seen that maximum OC (0.210µm) was obtained at the highest voltage (40V) and lowest pulse off duration (30µs) combination. The minimum OC (0.149 µm) was determined at the lowest pulse off duration (30µs) and lowest voltage (30V) combination. Furthermore, with the increase in voltage and pulse off duration the value of OC increases initially and then decreases at higher levels of voltage and pulse off duration settings. It is observed that there is substantial increase in OC with increase in voltage and pulse off duration.

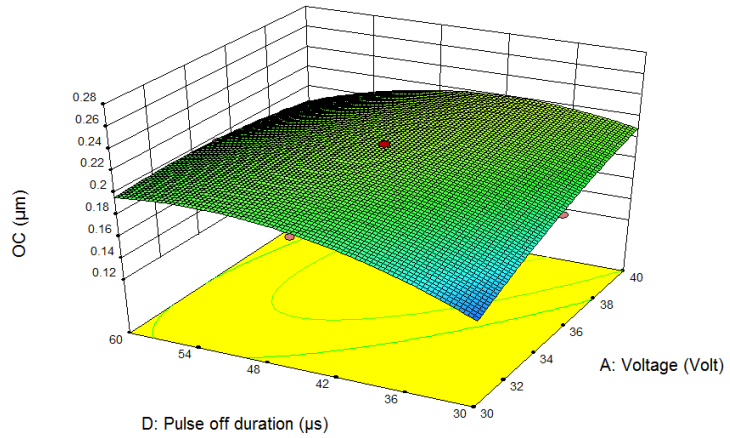

Figure 4. 7: Interaction effect of Voltage and Pulse off duration on OC

Figure 4.9 shows the interaction effect of peak current and pulse on duration on OC at constant voltage of 30 V and pulse off duration of 45µs. The maximum OC value of (0.210µm) was obtained at the highest voltage (40V) and lowest pulse off duration (30µs) combination similarly the minimum OC (0.149 µm) was obtained at the lowest pulse off duration (30µs) and lowest voltage (30 V) combination. Moreover, with the increase in voltage and pulse off duration the value of OC increases initially and then decreases at higher levels of voltage and pulse off duration settings. It is observed that there is significant increase in OC with increase in voltage and pulse off duration.

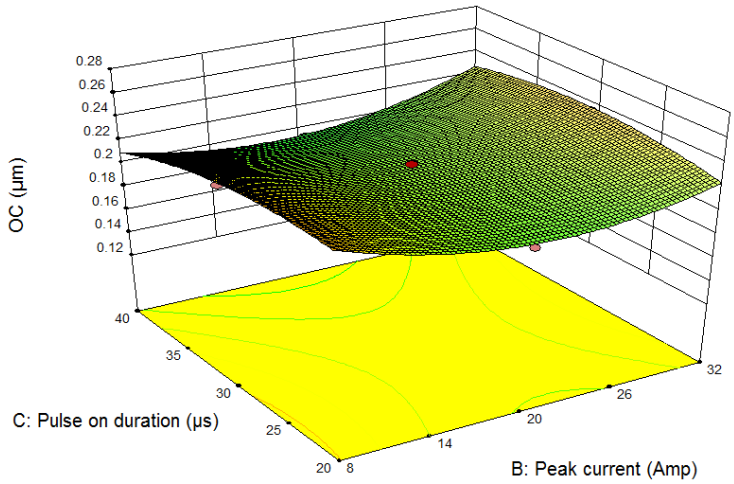

Figure 4. 8: Interaction effect of Peak current and Pulse on duration on OC

Figure 4.10 illustrates the interaction plot of peak current and pulse off duration on OC constant voltage of 35V and pulse on duration of 30µs. From this Figure, it is observed that maximum OC was gained at the lowest peak current of (8 ampere) and highest pulse off duration of 60µs.The minimum OC was achieved at the lowest peak current of

(8ampere) and lowest pulse off duration of (30µs) combination. Moreover, OC first increases with increase in voltage and the pulse on duration and then decreases. There is a significant increase in OC with increase in current however with increase in pulse off duration initially there is increase in OC.

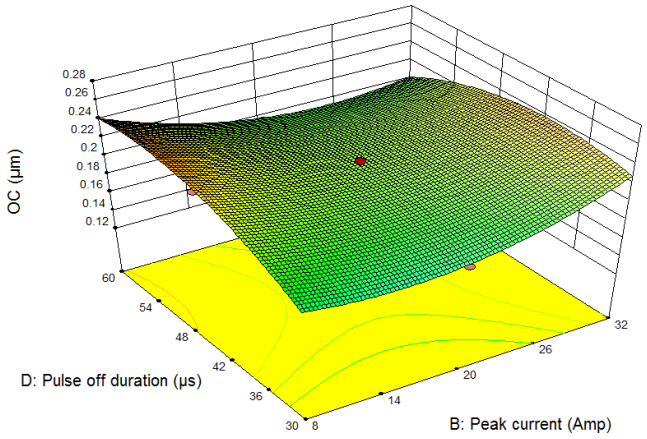

Figure 4. 9: Interaction effect of Peak current and Pulse off duration on OC

The effect of pulse on duration and pulse off duration on OC at constant voltage of 35V and peak current of 20 amperes is represented in Figure 4.10. Additionally, it is observed that maximum OC was achieved at the lowest pulse on duration of (20µs) and highest pulse off duration of 60µs.The minimum OC was attained at the highest pulse on duration of 40µs and lowest pulse off duration of (30µs) combination. However, OC first increases with increase in pulse off duration and the pulse on duration and then decreases. There is a significant increase in OC with increase in pulse on duration nevertheless with increase in pulse off duration initially there is increase in OC but later onwards it starts decreasing.

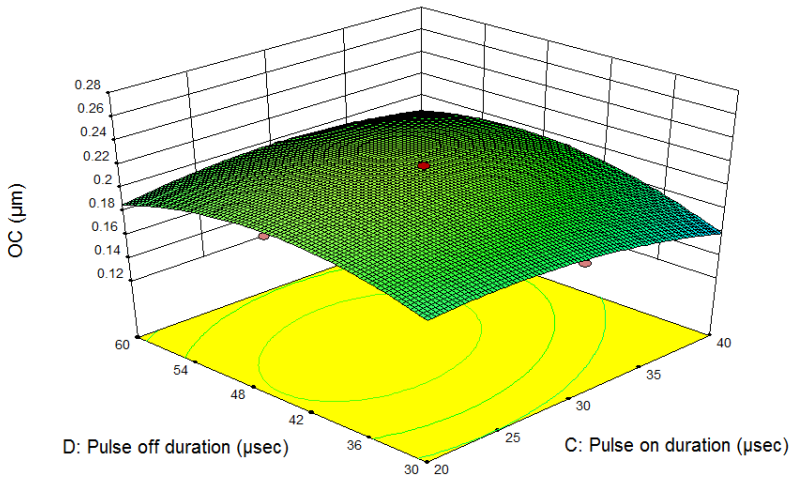

Figure 4. 10: Interaction effect of Pulse on duration and Pulse off duration on OC

The reduced model for RCL after backward elimination process is demonstrated in Table 4.6 in "Appendix 2" and the model F-value of 11.53 indicates that the model is significant. There is only a 0.01% chance that an F-value this large could occur due to noise. The percentage contribution of different process variables on RCL is presented in Figure 4.11.

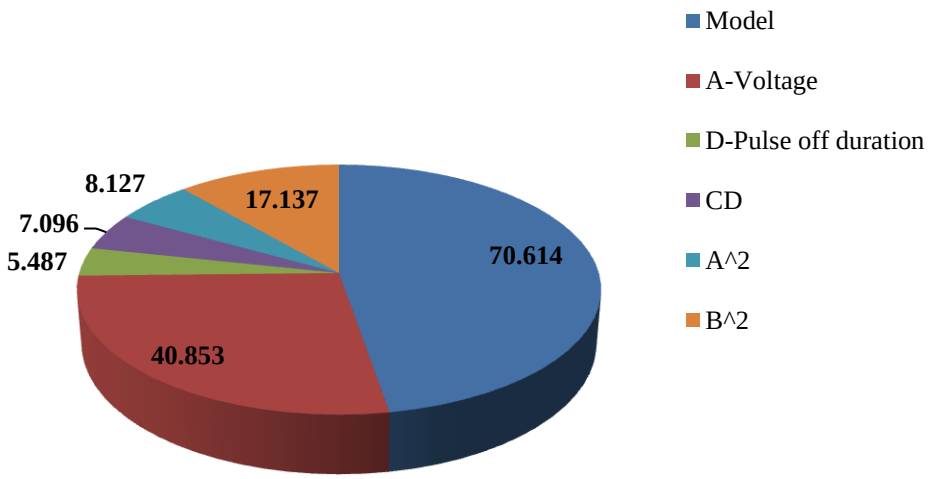

Figure 4. 11: Percentage contribution of process variables

From Figure 4.12, it is observed that maximum RCL was obtained at the highest pulse on duration of (40µs) and highest pulse off duration of 60µs.The minimum RCL was obtained at the highest pulse on duration of 40µs and lowest pulse off duration of (30µs) combination. It is seen that RCL decreases with increase in pulse off duration and with the increase in pulse on duration it also decreases. There is a noteworthy increase in RCL with increase in pulse on duration however with increase in pulse off duration initially there is increase in RCL but later onwards it starts decreasing.

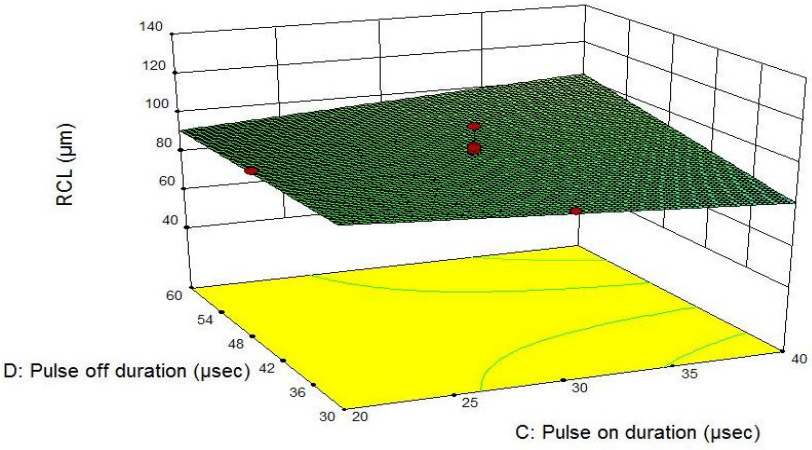

Figure 4. 12: Interaction effect of Pulse on duration and Pulse off duration on RCL

Table 4.7 shows the truncated model for TA after backward elimination process and is presented in "Appendix 3" it can be seen the model F-value of 2699.29 infers the model is significant. The percentage contribution of different process variables on RCL is presented in Figure 4.14 and it can be seen in this case A, B, C, D, AB, AD, BC, BD, CD, A^2, B^2, C^2, D^2 are significant model terms. Peak current has a significant effect on TA followed by pulse off duration, pulse on duration and voltage.

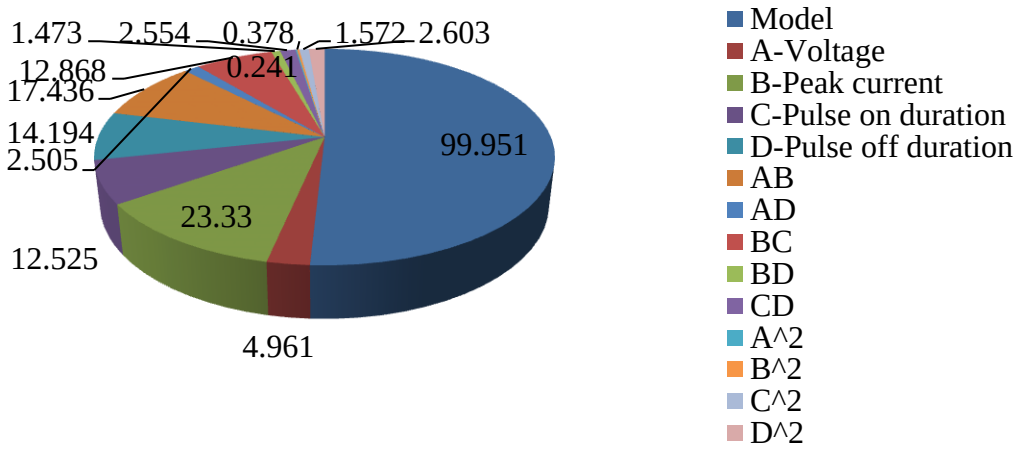

Figure 4.14: Percentage contribution of process variables

It can be observed from Table 4.17 that the interaction terms AB and BC have maximum influence on TA as compared to other interaction terms. Hence interaction plots for only AB and BC have been considered. The interaction effect of peak current and Voltage on TA in the form of 3D surface graph at constant pulse on duration of 30µs and pulse off

duration of 45µs is represented in Figure 4.15. From this Figure, it is observed that maximum TA (3.03951°) was obtained at the highest peak current of 32A and lowest voltage of (30V) combination. The minimum TA (1.5419°) was obtained at the lowest peak current of 8A and highest voltage (40V) combination. Furthermore, with the increase in voltage and peak current the value of TA increases initially and then decreases at higher levels of voltage and peak current settings. It is observed that there is significant increase in TA with increase in voltage and peak current.

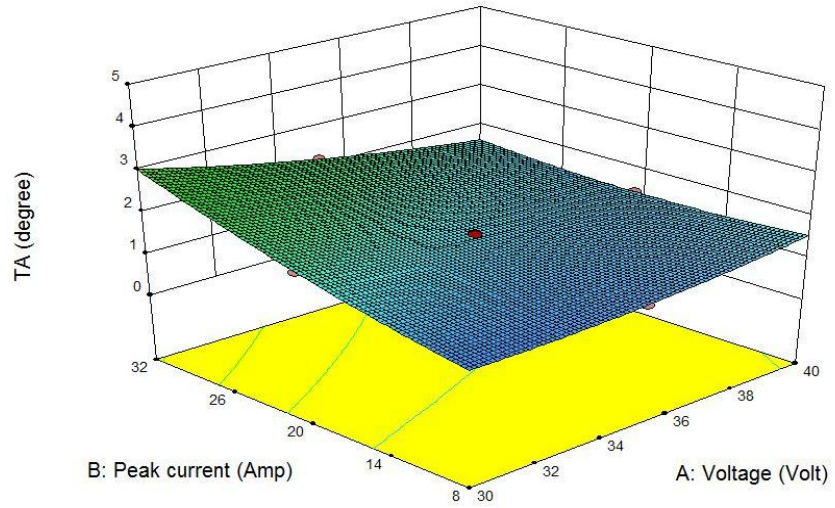

Figure 4.15: Interaction effect of Voltage and Peak current on TA

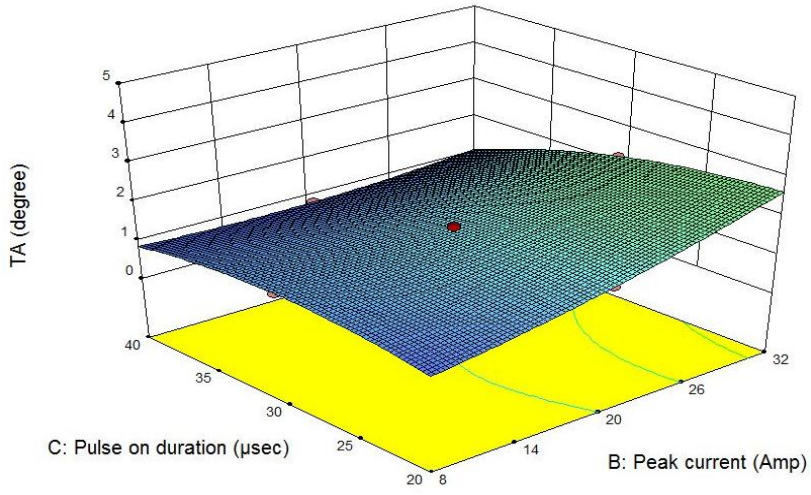

Figure 4.16: Interaction effect of Pulse on duration and Peak current on TA

From Figure 4.16, it is observed that maximum TA (2.634°) was achieved at the highest peak current of 32A and the lowest pulse on duration (20µs) combination. The minimum TA (0.860°) was obtained at the least peak current of 8A and maximum pulse on duration (40µs) combination. Furthermore, with the increase in pulse on duration and peak current the value of TA increases initially and then decreases at higher levels of pulse on

duration and peak current settings. It is observed that there is significant increase in TA with increase in pulse on duration and peak current. Based on Equation 4.5, the effect of input parameters on values of MRR, OC, RCL and TA has been evaluated by computing the values of various constants in Tables (4.4 - 4.7).

The mathematical models of MRR, OC, RCL and TA can be expressed in coded form as follows:

$$MRR = 0.6475 + 0.0275*A + 0.0254*C - 0.044*D + 0.0316*AC - 0.030*AD + 0.0450*BD \quad (4.6)$$

$$OC = 0.214 + 0.012*A - 0.0067*C + 0.0067*D + 0.010*AB - 0.005*AC - 0.018*AD + 0.008*BC - 0.019*BD + 0.006*CD - 0.006*A^2 + 0.023*B^2 - 0.011*C^2 - 0.021*D^2 \quad (4.7)$$

$$RCL = 92.528 - 13.599*A + 4.984*D + 6.012*CD + 13.866*A^2 - 20.135*B^2 \quad (4.8)$$

$$TA = 1.5203 - 0.237*A + 0.513*B - 0.376*C - 0.400*D - 0.471*AB + 0.178*AD - 0.404*BC - 0.137*BD + 0.180*CD + 0.137*A^2 + 0.172*B^2 - 0.349*C^2 + 0.453*D^2 \quad (4.9)$$

4.3 ANN MODELING OF EDM PROCESS

In recent years ANN have been broadly used for various types of applications where statistical methods were traditionally employed. ANNs can be used in the following applications; thermal analysis, pattern recognition (Fukunaga and Hostetler 1975), resource allocation, constraints satisfaction (optimization), credit card application (Ghosh and Reilly 1994), screening, data mining, information retrieval process, data base management, simulation, and robotics control. ANNs proved to be significant tools for modeling, especially when the relationship of the process variables and responses of experimental data relationship is unknown. ANNs can classify and learn associated patterns between input data sets and corresponding target values. After training, ANNs can be utilized to predict the outcome of new independent input data. Based on response surface methodology layout with central composite design 30 data sets as shown in Table 4.8 in “Appendix 4” were used for training and testing data sets. As there is no standard procedure available for selection of training and validation data sets hence 20 sets were selected randomly as training data set and remaining 10 sets as validation. Moreover, similar selection criteria was adopted by (Dhara et al. 2007). In the present investigation the ANN modeling of µ-EDM for fabrication of micro holes has been carried out using a Neural network toolbox in MATLAB. Appropriate selection of number of hidden layers and the number of neurons in the hidden layers leads significant part in the optimization of feed forward network with back propagation configuration. Too few neurons in the hidden layer may lead to under fitting while too many neurons can contribute to over fitting. Before training the neural network, the architecture of the network has been decided; i.e., the number of hidden layers and the number of neurons in each layer. According to Fausett (1994) the back propagation architecture with one hidden layer is sufficient for the majority of applications. Hence, only one hidden layer has been taken. Therefore, extensive training and testing of the network architecture for the chosen

training test was carried out by trial and error. By examining generalization capability of the network in which all training points are well fitted. The optimum architecture is found out by varying the number of neurons in the hidden layers using MATLAB. In this architecture, number of hidden neurons is varied from 1 to 20 and a plot between total average prediction error (%) and number of neurons is made. The number of neurons in the hidden layer is changed and the total average prediction error is calculated for each case. The number of neurons in the hidden layer is 12 for which the total average prediction error is the least. The procedure for determining the number of neurons in the hidden layer is shown graphically in Figure 4.17.

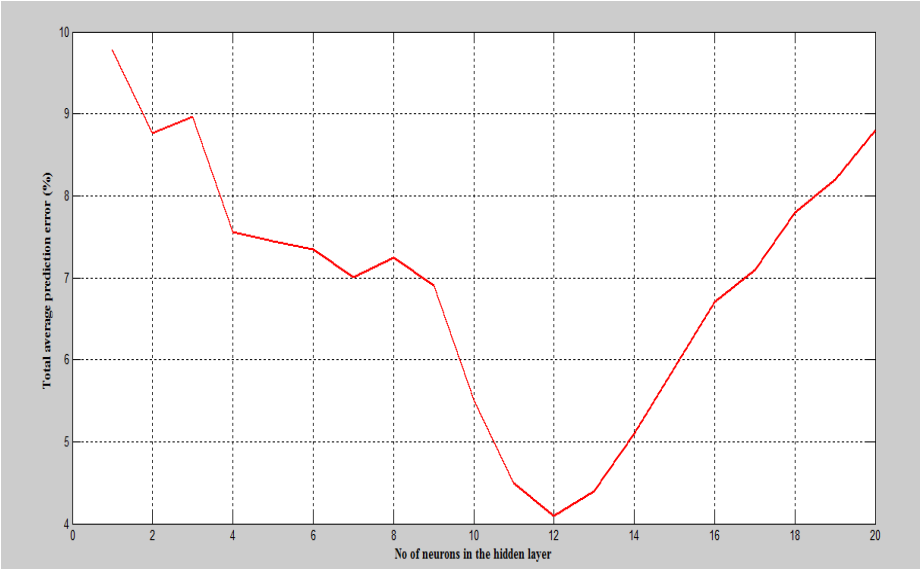

Figure 4. 12: Plot for determining the number of neurons in the hidden layer.

Several models were designed and tested with process parameter in order to determine the optimal architecture for the most suitable activation function and the best training algorithm suitable for the prediction of MRR, OC, RCL and TA in µ-EDM operation.

4.3.1 TRAINING AND TESTING

Testing of the trained network is carried out in two stages. Firstly, it is tested with seen input data sets (training sets). In the second phase, the network is tested with unseen input data sets (testing set). Error value is the numerical difference between the actual value of output and the value predicted by the trained network.

$$\text{Predicted error}(\%) = \frac{(\text{Experimental Value} - \text{Predicted Value}) \times 100}{\text{Experimental Value}} \qquad (4.10)$$

$$\text{Total average prediction error} = \frac{A1+A2+A3+A4}{3} \quad (4.11)$$

where A_1, A_2 ,A_3 and A_4 are the average prediction error in MRR, OC, RCL and TA respectively. A network of structure 4-12-4 is found to be the most suitable network for the present task. The activation function in the hidden layer was the hyperbolic tangent sigmoid transfer function (tansig) and in the output layer was the linear transfer function pure line. The learning algorithm used was the back propagation algorithm. According to Wang et al. (2003) back propagation is a systematic method for training multilayer ANN. Back propagation neural networks apply the error-back procedure for learning. The back-propagation procedure uses a gradient descent method, which adjusts the weight in its original and simplest form by an amount proportional to the partial derivative of the error function (E) with respect to the given weight. It uses gradient-descent method to minimize the total mean square error of the output computed by the network.

$$w_{ij}(t+1) = w_{ij}(t) - \eta \frac{\partial E}{\partial w_{ij}} + \mu \Delta w \quad (4.12)$$

in which η and μ are user-selected, positive constants (between 0 and 1) called learning rate coefficient and momentum term respectively. The Δw is the weight change in earlier layer. The developed model is shown schematically in Figure 4.18.

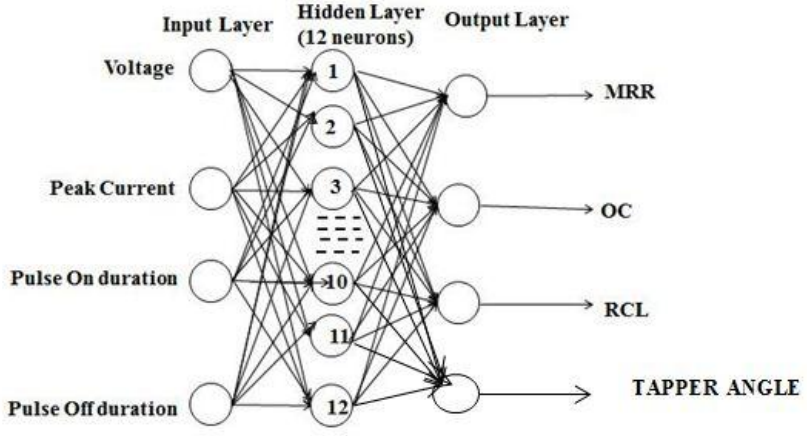

Figure 4. 13: Selected Network Architecture.

Comparison is made for all randomly selected training data sets of each individual output and is as shown in Figures (4.20- 4.23). The figures indicated that the errors were within the acceptable limit, and hence ANN can be effectively used for the prediction of MRR,

OC, RCL and TA in µ-EDM. Further the regression value of 0.9981, 0.99965, 0.99982 and 0.99957 for MRR, OC, RCL and TA have been obtained which signifies the correlation between experimental and predicted values.The regression plot for MRR, OC, RCL and TA have been given in Figure 4.19(a-d).

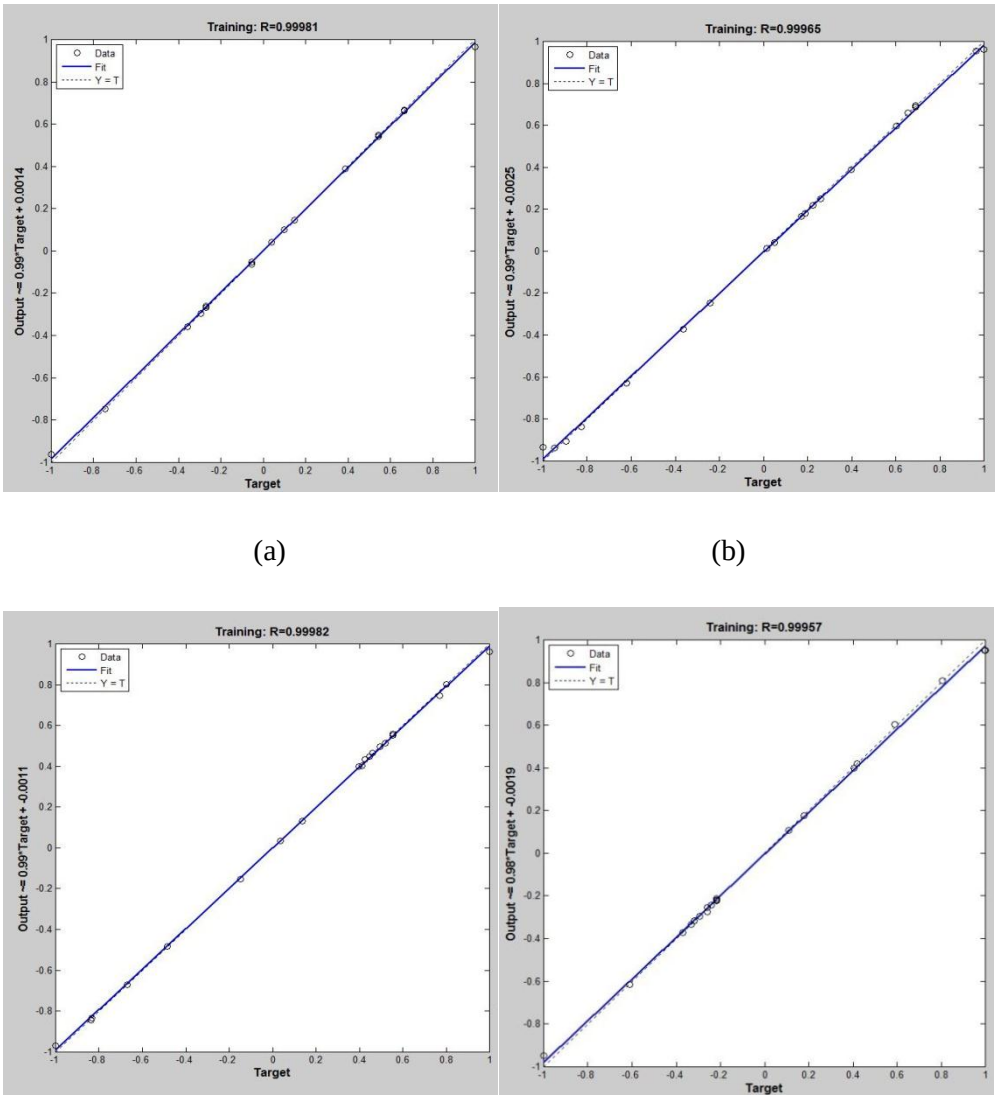

Figure 4. 14:Regression plot for process responses

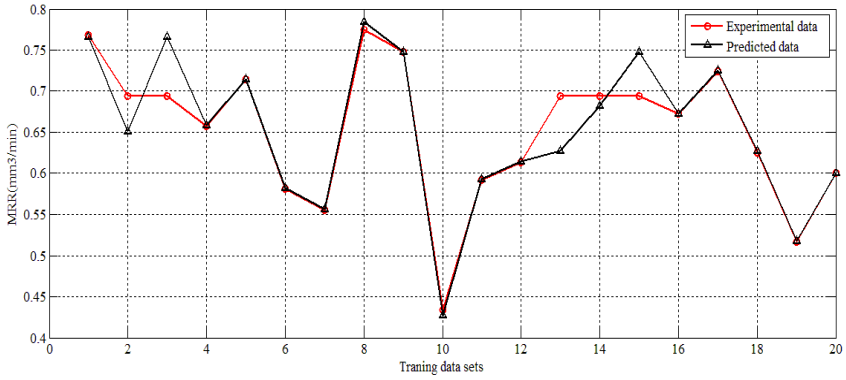

Figure 4. 20: Comparison of experimental and predicted output for MRR for training data sets.

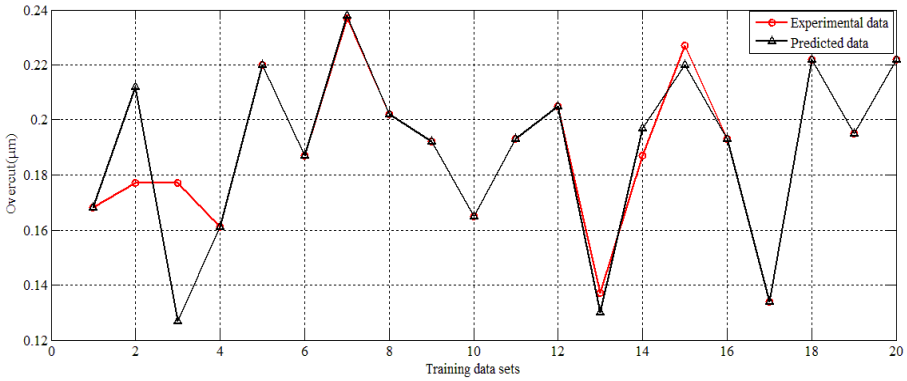

Figure 4. 21 :Comparison of experimental and predicted output for OC for training data sets.

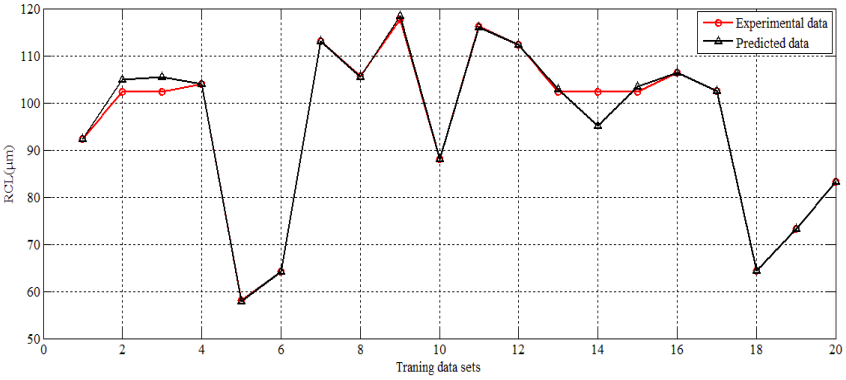

Figure 4. 22:Comparison of experimental and predicted output for (RCL) for training datasets.

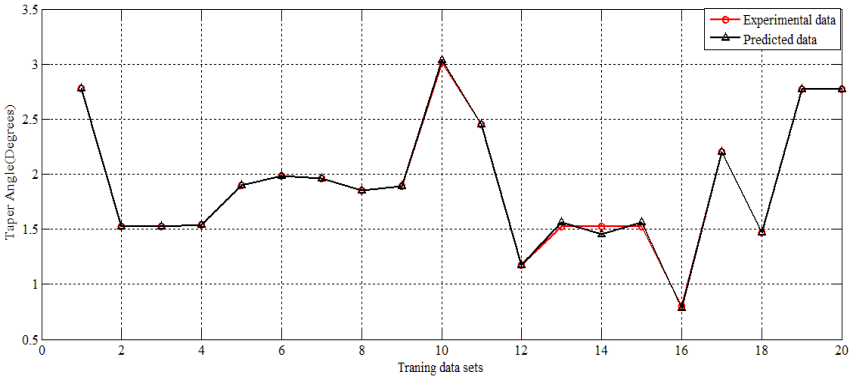

Figure 4. 23 :Comparison of experimental and predicted output for TA for training data sets.

The trained neural network was validated against another set of experimental data, termed as validation data set illustrated in Table 4.9 in "Appendix 5". The errors in prediction are also presented in Table 4.10 in "Appendix 5". It can be seen from Table 4.10 that the model predictions match the experimental data very closely except few data. Moreover, the average error in the prediction was -5.080 % for MRR, -2.752 % for OC, and 0.070 % for RCL and -3.341 % for TA respectively. The predictive efficiency of Neural networks is affected by different factors like noise corruption, spatial distribution and size of the data used to construct the ANN model. Noisy data associated with uncertainties in measurements are generated in the experiments. The noise can be maintained at a very small value if the experiments are carried out with care and using accurate instruments. Another source of error stems from the fact that only finite data are available for training. The total average prediction error of the network was predicted as -11.243 %. The developed ANN model was tested by repeating few experiments randomly from the entire data set for checking the predictive accuracy of the developed model. Table 4.11- 4.12 in "Appendix 6" contains testing of the developed model with experimental data and the predicted output and percentage error in prediction of MRR, OC and RCL were within acceptable limits. It is observed that the total average prediction error is -17.901% which implies level of over prediction. Figure 4.24 shows that the predictions of all responses in µ-EDM process by making use of developed model are in good agreement with the experimental results, i.e., the results indicate that the neural network can very satisfactorily predict the output data.

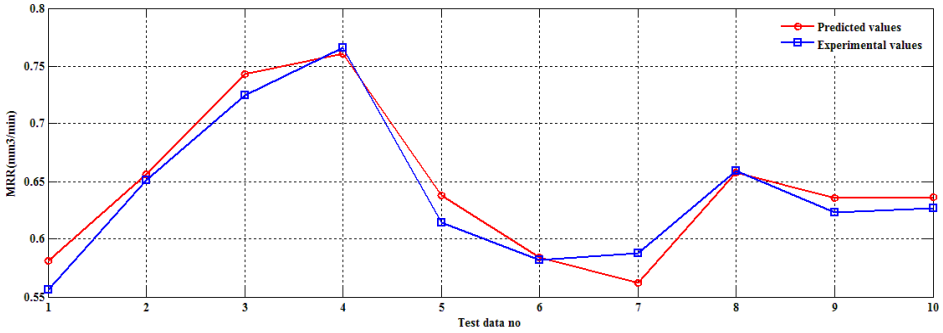
Predicted values
Experimental values
MRR(mm3/min)
Test data no

(a)

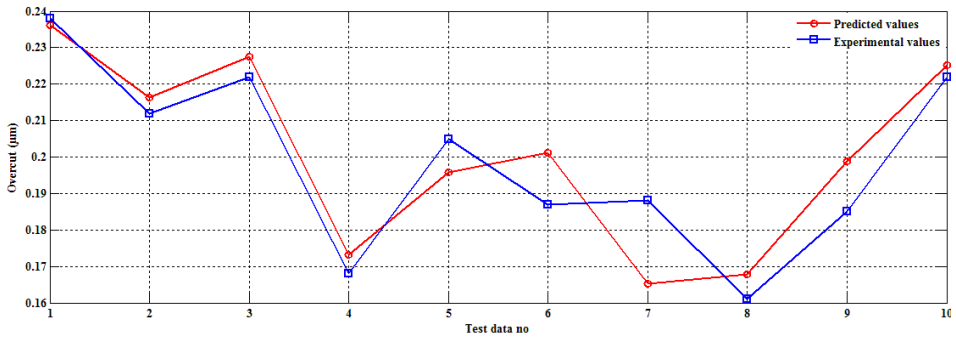
Predicted values
Experimental values
Overcut (µm)
Test data no

(b)

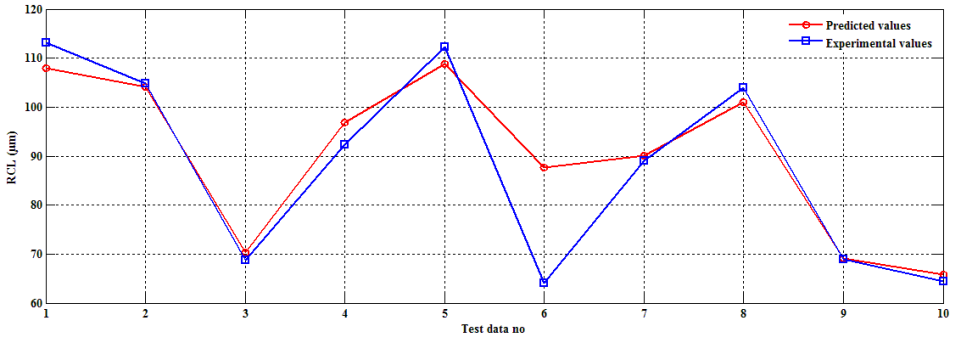
Predicted values
Experimental values
RCL (µm)
Test data no

(c)

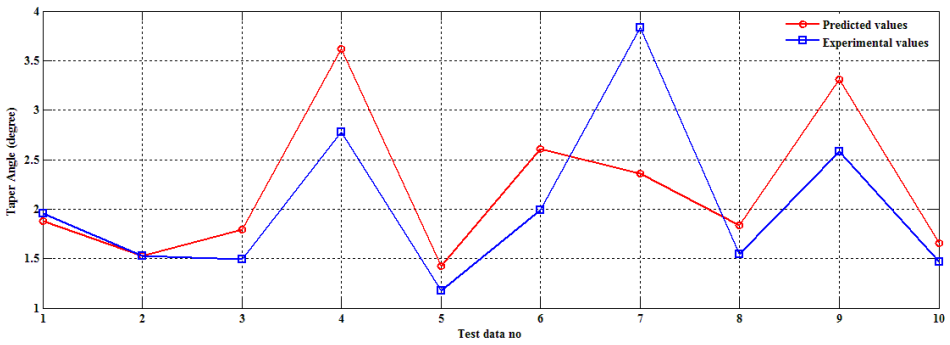

(d)

Figure 4.24: Comparison of experimental and ANN output for process responses for test data set.

4.4 ANFIS MODELING

The adaptive network based fuzzy inference system (ANFIS) is a useful neural network approach for the solution of function approximation problems (Buragohain & Mahanta, 2008). An ANFIS gives the mapping relation between the input and output data by using hybrid learning method to determine the optimal distribution of membership functions (Ying & Pan, 2008). Both artificial neural network (ANN) and fuzzy logic (FL) are used in ANFIS architecture (Avci, 2008). Such framework makes the ANFIS modelling more systematic and less reliant on expert knowledge Once a training data set, is provided the ANFIS method generates a fuzzy inference system (FIS) whose membership function parameters are tuned (adjusted) using either a back propagation algorithm only, or it can be of hybrid type .This inherits fuzzy systems a learning tendency from the data they are modeling. In the present case, the structure of the model comprises of five layers in which each layer is created with several nodes. The inputs of each layer are extended by the nodes from predecessor layer as its case with a neural network. The structure of ANFIS modeling is shown in Figure 4.25. It can be concluded from Figure 4.25 that the network comprises *k* inputs $(X_1, \ldots, X_k)$, in which each one consists of *n* membership functions (MFs). Moreover, a layer with F fuzzy rules along with an output layer is used for construction of this model.

The number of nodes in the first layer is calculated by product of *k* as the number of inputs and *n* as number of MFs *(N=k. n).*

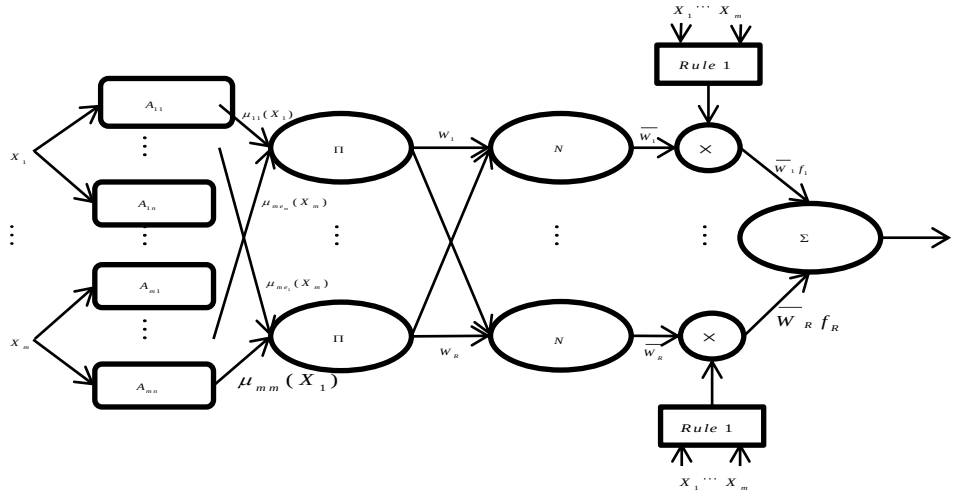

Figure 4. 25: Basic structure of an ANFIS model

Number of nodes in other layers (layers 2–4) relates to number of fuzzy rules (F) (Babajanzade Roshan et al. 2013). The linguistic nodes in layers one and four indicate the input and output linguistic variables, respectively. Nodes in layers two represent membership functions for input variables. Each neuron in the third layer represents one fuzzy rule, with input connections representing prerequisites of the rule and the output connection representing consequences of the rules. Initially, all these layers are fully connected, representing all possible rules. In the present work this technique is used to correlate the mapping relationship between process inputs (e.g., applied voltage (V), peak current (I_p), Pulse On duration (T_{on}) and Pulse off duration (T_{off}) and main outputs (material removal rate, overcut and recast layer thickness). Thus, for each output a separate ANFIS structure can be defined. For example, for MRR the first layer of ANFIS structure is input layer that contains four nodes (for four inputs). The last layer (output layer) has one node that represents values of MRR. Figures 4.26, 4.27 4.28 and 4.29 indicate the proposed ANFIS topography for MRR, OC and RCL and TA respectively.

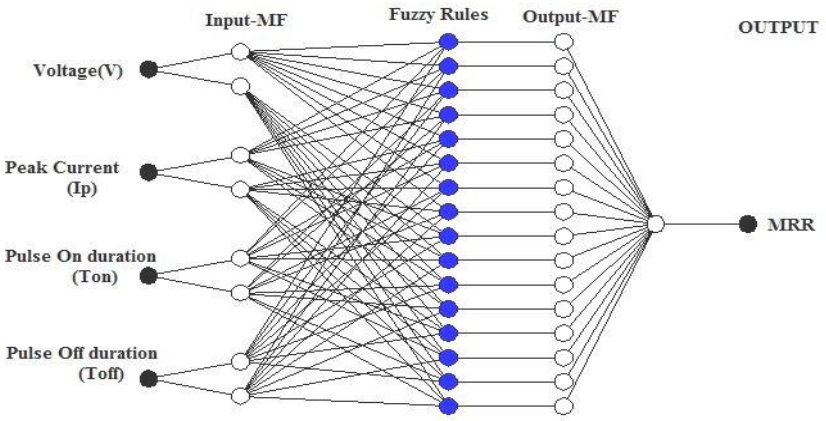

Figure 4. 15:Structure of developed ANFIS model for predicting MRR

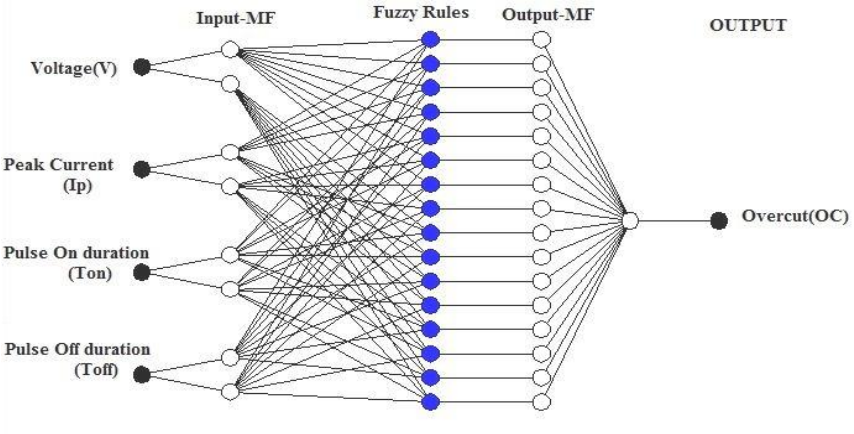

Figure 4. 16:Structure of developed ANFIS model for predicting OC

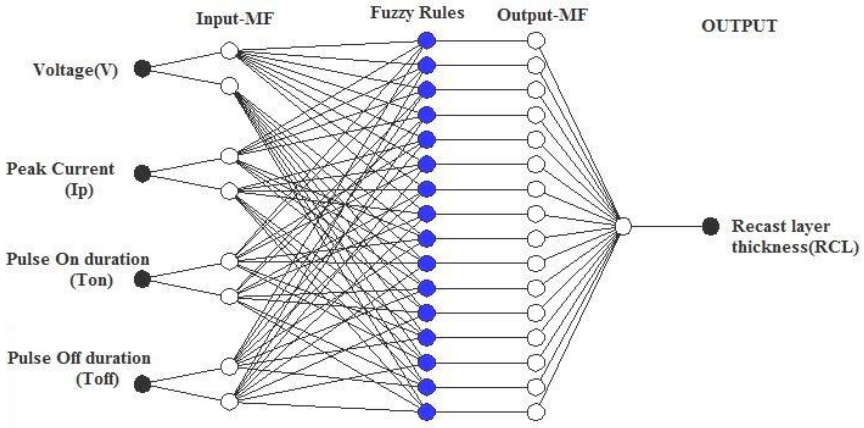

Figure 4. 17:Structure of developed ANFIS model for predicting RCL

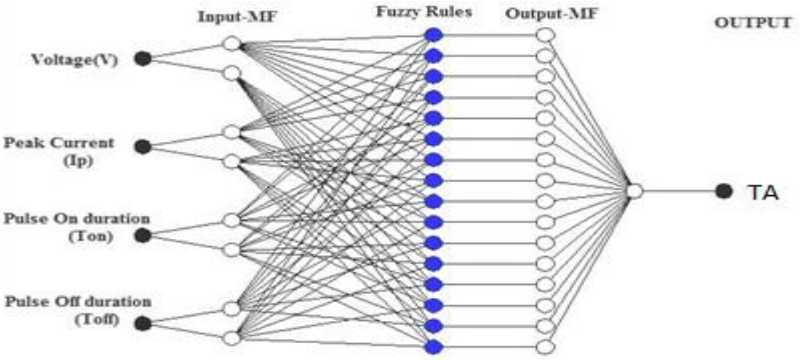

Figure 4. 18:Structure of developed ANFIS model for predicting TA

The layers of ANFIS can be summarized as follows:

Fuzzification layer: In this layer crisp inputs are converted into linguistic terms (such as good, very good, excellent) by using of membership functions. In this research, we have taken four input variables, namely applied voltage (V), peak current (Ip), Pulse On duration (T_{on}) and Pulse off duration (T_{off}). So the output of the layer-1 is given as

$$z_{1,i} = \mu_{aik}(x_i) \tag{4.13}$$

where i=1, 2...n is the number of inputs associated with the ANFIS model and μ_{aik} for *k=1, 2* are the number of input membership functions. Here we have used two membership functions and $z_{1,i}$ in Equation 4.13 corresponds to the output obtained from layer-1. Several types of membership functions are used, for example, triangular, trapezoidal and generalized bell function. In this study, the trapezoidal function for OC and generalized bell function has been selected for MRR and, RCL respectively. Function selection is done on the basis of its lowest value of the average error during testing and training. Total average error can be calculated by the following Eq.4.14.

$$\text{Total average error (TAE)} = \frac{\text{Training error + Validation error}}{2} \tag{4.14}$$

The formulation of the generalized bell function is expressed as follows:

$$\mu_{a_{ik}}(X_i) = \frac{1}{1 + \left| \frac{X_i - c_{ik}}{a_{ik}} \right|^{2b_{ik}}} \tag{4.15}$$

The Eq.(4.15) gives the concept about the generalized bell function which is used as membership function and the parameters such as a_{ik}, b_{ik}, c_{ik} are referred as the promising parameters associated with the fuzzy set. In this case, a_{ik} and b_{ik} vary the width of the curve, and c_{ik} locates the center of the curve. The parameter b_{ik} should be positive.

Product layer: In this layer, firing strengths are generated by multiplying the incoming signals from layer-1 with the fuzzy rules. The output of layer 2 is given by the mathematical expression as

$$z_{2,i} = \omega_l = \prod_{i=1}^{l} \mu_{a_{ik}}(x_i) \qquad (4.16)$$

where *i=1, 2, 3 ... l* are the *l* number of fuzzy based rules.

Normalized layer: In this layer, outputs are normalized and the firing strengths are calculated by using the mathematical formula as

$$z_{3,i} = \overline{\omega}_i = \frac{\omega_i}{\sum_{i=1}^{l} \omega_i} \qquad (4.17)$$

Defuzzification layer: In this layer, Takagi–Sugeno fuzzy type rules (if-then rules) as described in Eq. (4.13) are applied in the weighted output of each node. The node function linked in level-4 in the ANFIS architecture is a linear function, and the output of layer 4 is calculated as

$$z_{4,i} = \overline{\omega}_i (w_1 x_1 + w_2 x_2 + ...w_n x_n + v_i) \qquad (4.18)$$

where w_i and v_i the consequent parameters associated with the fuzzy rule.

Output layer: This layer represents the modeled output by ANFIS network, which is mathematically expressed as

$$z = \frac{\sum_{i=1}^{l} \omega_i z_{4,i}}{\sum_{i=1}^{l} \omega_{4,i}} \qquad (4.19)$$

For the training of the ANFIS model, a hybrid learning algorithm is used. During the first phase of the hybrid learning algorithm, each of the node outputs move forward until

the layer-4 accomplished and the outputs are obtained by using the least-squares procedure. The values of $\{w_i\ n_i,\ v_i\}$ in the Eq. (4.18) remain fixed, the overall output can be stated as a linear combination of these parameters, which is given as

$$z_{5,i=}\sum_{i=1}\overline{\omega}_i o_i = \frac{\sum_i \omega_i o}{\sum_i \omega_i} \tag{4.21}$$

The corresponding value of final output 'o' is given as $o = \overline{\omega}_i(w_1x_1 + w_2x_2 + ...w_nx_n + v_i)$

For this purpose, the MATLAB R2012b package (ANFIS toolbox) has been utilized. Prediction of material removal rate, overcut and recast layer thickness of the Micro-EDM process by ANIFS comprises of three main phases, training validation and testing. Therefore, among 30 data sets mentioned in the design matrix, number of 20 data has been chosen stochastically for the training of ANFIS network. Then the trained network was validated by the other ten remaining data sets that were not involved in training. The training data sets are shown in Table 4.13 in "Appendix 7". Further the testing of model was carried out using the test data sets used during ANN modeling. There are some key factors like fuzzy based rule, the number of MFs, and their type that play significant role for accurate prediction by ANFIS. In the present work, a first order TSK type fuzzy-based rule has been used for the development of predictive models. Total average error (TAE) as mentioned in Equation 4.14 is considered as selection criteria for comparison of all existing networks and final selection is made of the most accurate one. The value of error goal was set at 0.03, and the iteration number was 500 epochs. Various structures were tested of ANFIS model for each response (material removal rate, overcut recast layer thickness and taper angle), it was obtained that structures with 16 numbers of membership functions (2 MFs for each input) had the lowest values of TAE for each response. Network selection with larger number of MFs generally leads to over-fitting and generates higher values than the desired value of TAE. Another vital factor which has a significant effect on the predictive accuracy of ANFIS model is a type of membership functions. In this work various types of MFs namely triangular, trapezoid, generalized bell and Gaussian have been practiced. Table 4.14 represents training and validation error of ANFIS models for different membership functions. TAE for MRR, OC, RCL and TA have been presented in Table 4.15. Results indicated that the trapezoid function leads the lowest values of TAE for MRR, OC RCL and TA, respectively.

Table 4.14: Training and validation error

Type of membership function	MRR		OC		RCL		TA	
	Training error	Validation error	Training error	Validation error	Training error	Validation error	Training error	Validation error
Triangle	0.03099	0.24763	0.02301	0.08744	2.00930	2.00920	0.02046	0.02046
Trapezoid	0.03055	0.23483	0.02296	0.07912	1.94080	1.94060	0.02046	0.02046
Generalized bell	0.30338	0.38966	0.02296	0.07929	1.92890	1.92890	0.02046	0.02046
Gaussian	0.30577	0.24176	0.02296	0.07892	1.94443	1.94420	0.02074	0.20722

Table 4.15: TAE for process responses

Type of membership function	MRR Total Average error	OC Total Average error	RCL Total Average error	TA Total Average error
Triangle	0.020462	0.020462	0.020462	0.020462
Trapezoid	0.020461	0.020461	0.020461	0.020461
Generalized bell	0.020463	0.020463	0.020463	0.020463
Gaussian	0.11398	0.1606	0.13729	0.148945

The developed ANFIS model was tested for checking the predictive accuracy of the developed model. Tables (4.16 - 4.17) in "Appendix 8" contains testing of the developed model with experimental data and the predicted output and percentage error in prediction of MRR, OC and RCL were within acceptable limits. It is observed that the total average prediction error is -7.080 % which implies level of over prediction.

4.4 MULTI-OBJECTIVE OPTIMIZATION USING ETLBO, DE AND ABC

In the present section multi-objective optimization has been carried out using three popular meta-heuristic approaches namely Elitist Teaching learning based optimization, Differential evolution and Artificial Bee colony optimization. Furthermore, pareto optimal sets of solution obtained from each algorithm was ranked using fuzzy based ranking method.

4.4.1 MULTI-OBJECTIVE OPTIMIZATION USING ETLBO

Elitism addresses the problem of losing good solutions during the optimization process due to random effects (Zitzler et al. 2004) . ETLBO resembles the teaching-learning process in a class room for finding out the global optimal solution. Teacher and learners are the two critical components of the algorithm and emphasizes on two basic modes of the learning, through teacher (known as teacher phase) and interacting with the other learners (known as learner phase). In this algorithm a group of learners is considered as population and different subjects taught to the learners are considered as different design variables of the optimization problem. A learner's overall result is equivalent to the value of the objective function (Yu et al. 2014). The concept of elitism has been utilized in most of the evolutionary and swarm intelligence algorithms where during every generation the worst solutions are replaced by the elite solutions. In the ETLBO algorithm, after replacing the worst solutions with elite solutions at the end of learner phase, if the duplicate solutions exist then it is necessary to modify the duplicate solutions in order to avoid trapping in the local optima. In the present work, duplicate solutions are modified by mutation on randomly selected dimensions of the duplicate solutions before executing the next generation. (Rao and Patel 2013). Moreover, in the present work, the effect of the common controlling parameters of the algorithm i.e. population size, number of generations and elite-size on the performance of the algorithm are also investigated by considering different population sizes, number of generations and elite sizes. At this point, it is important to clarify that in the ETLBO algorithm, the solution is updated in the teacher phase as well as in the learner phase. In the duplicate elimination step, if duplicate solutions are present then they are randomly modified. So the total number of function evaluations in the ETLBO algorithm is = {(2 × population size × number of generations) + (function evaluations required for duplicate elimination). TLBO modifies duplicated individuals by mutation on randomly selected dimensions at the end of each generation, whilst the second difference only appears for constrained problems where elitism has been used. There are two versions for replacing the worst individuals. Besides the classical elitism approach has been used in the first TLBO implementation. The elitist method has also been investigated in the second TLBO implementation. The first-half of the population is compared with the second-half. If an individual from the second-half of the population is better than an individual from the first-half, then the individual from the second half replaces the individual from the first-half (Črepinšek et al. 2012). In the entire experimental work, the above formula is used to count the number of function evaluations while conducting experiments with TLBO algorithm. The flow chart of the Elitist TLBO algorithm is shown in Figure.4.30. Guidelines on setting and conducting computational experiments for replication and comparison in evolutionary algorithms are provided by (Črepinšek et al. 2014) . In the present investigation, a computer program has been developed in MATLAB language. The four design variables namely V, I_p , T_{on} and T_{off} are analogues to subjects taught to

learners ie, sub_1,sub_2, sub_3, sub_4 respectively. The limits of search space are defined by taking low and high boundary limits of design parameters as shown in Table 4.1. The process models for the responses obtained through regression analysis (Equations 4.6-4.9) are used as objective functions. The Pareto optimal solution obtained from ETLBO is presented in Table 4.14 in "Appendix 9".

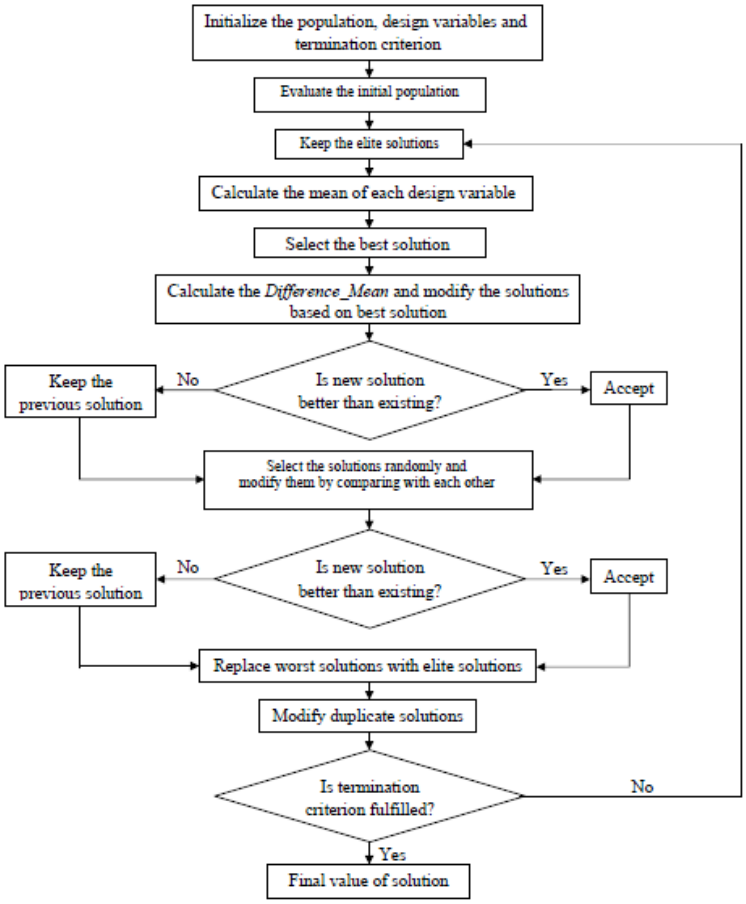

Figure 4. 30: Flow chart for ETLBO

4.4.2 CENTROID BASED FUZZY RANKING METHOD

A centroid based distance method for ranking intuitionistic fuzzy numbers where they are ranked in terms of Euclidean distances from the centroid point to the origin. Ranking intuitionistic fuzzy numbers is one of the fundamental problems of fuzzy decision making. The centroid of a trapezoid is considered to be the balancing point of the trapezoid as shown in Figure 4.31. The trapezoid (APQD) is divided into three plane figures. These three plane figures are a triangle (APB), a rectangle (BPQC), and again a triangle (CQD) respectively. Each centroid point G_1, $G_2$and G_3 are the balancing points of each individual plane figure, and the circumcenter of these centroid points is equidistant from each vertex. Therefore, this point would be a better reference point than the centroid point of the trapezoid. Figure 4.31 represents the circumcenter of centroids

The circumcenter S_A $(x_0, y_0)$of the triangle with vertices G_1, G_2 and G_3 of the membership function of the generalized trapezoidal intuitionistic fuzzy number A is defined as a_1 , a_2 , a_3 , a_4 and w

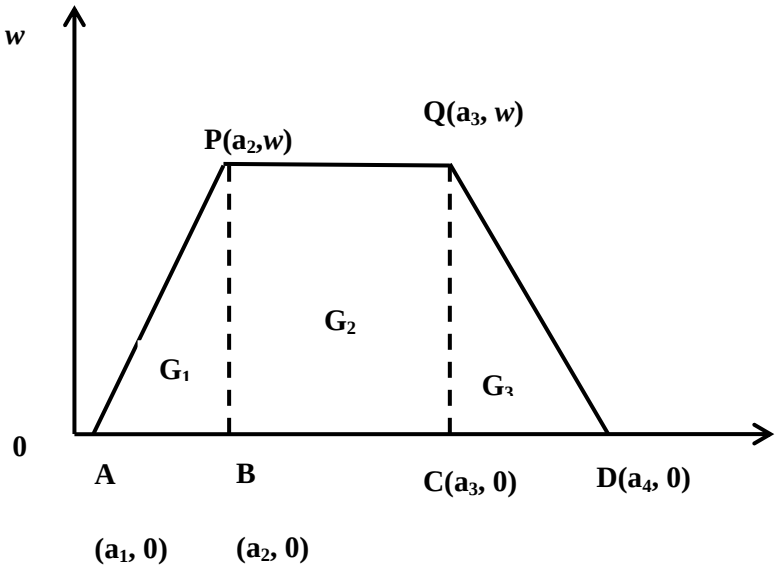

Figure 4.31: Circumcenter of centroids

For this, fuzzy performance importance index(FPII) has been computed which helps in identifying the weaker attributes (Vinodh and Vimal 2011).

Mathematically, FP *II* is expressed as

$$FP\ II = W' \otimes R \tag{4.22}$$

where

W' = attribute's importance weight; R = performance rating

If W' is high, then the transformation [1-W] is low. W is the fuzzy importance weight. The lower the value of FP *II* factor is, the lower the degree of contribution becomes. Similarly, a higher FPII indicates higher ranking. Then, using Eq. 4.22 the FPIIs of each element are calculated. Since fuzzy numbers do not always yield a totally ordered set, all the FPIIs must be ranked. Here, the rank of the fuzzy number is based on the centroid method for membership function (a_1, a_2, a_3, a_4) and the ranking score is expressed by

$$S_A(x_0, y_0) = \left(\frac{a_1 + 2a_2 + 2a_3 + a_4}{6} , \frac{(2a_1 + a_2 - 3a_3)(2a_4 + a_3 - 3a_2) + 5w^2}{12w} \right) \quad (4.23)$$

The ranking of the membership function of the trapezoidal or triangular intuitionistic fuzzy number is defined as

$$R_A = \sqrt{\left(x_0^2 + y_0^2 \right)} \quad (4.24)$$

Next, it is to rank the responses of all 35 feasible non-dominated sorted Pareto solutions (i.e., DMU's), by determining the most efficient combination of design parameters. The ranking has been done by evaluating the fuzzy performance importance index (FPII) and then applying the centroid method (i.e., trapezoidal variation) to give preference values to the output responses in the fuzzy domain. For calculating FPII, all the objectives should be taken on either minimization or maximization scale. The objective function of MRR has been modified into minimization problem at the time of implementing.

4.4.3 MULTI-OBJECTIVE DIFFERENTIAL EVOLUTION

Differential evolution (DE) is a type of evolutionary algorithm developed by investigators (Storn and Price 1997) for optimization problems over a continuous domain. The basic idea of DE is to adapt the search during the evolutionary process. In multi-objective differential evolution (MODE), a Pareto-based approach is presented to implement the selection of the best individuals. Firstly, a population of size, NP, is generated randomly and the fitness functions are evaluated. At a given generation of the evolutionary search, the population is sorted into several ranks based on dominance concept. Secondly, DE operations are carried out over the individuals of the population. The fitness functions of the trial vectors, thus created, are evaluated. One of the key differences between DE and MODE is that the trial vectors are not compared with the corresponding parent vectors. Instead, both the parent vectors and the trial vectors are combined to form a global population of size, 2*NP. Then, the ranking of the global population is carried out after the crowding distance calculation. The best NP individuals are selected based on its ranking and crowding distance. These act as the parent vectors for the next generation. The control parameters of differential evolution are assumed to be scaling factor (F) = 0.5, crossover factor (Cr) = 0.8 and population size (Np) = 25. However, a number of strategies have been proposed by Storn and Price. The (DE/rand/1/bin) strategy for present work has been selected as it is the most successful and the most widely used strategy. In the present investigation, a computer program has been developed in MATLAB language. The flow chart foe MODE has been given in Figure 4.32.

The Pareto optimal solution obtained from MODE is presented in Table 4.15 in "Appendix 10".

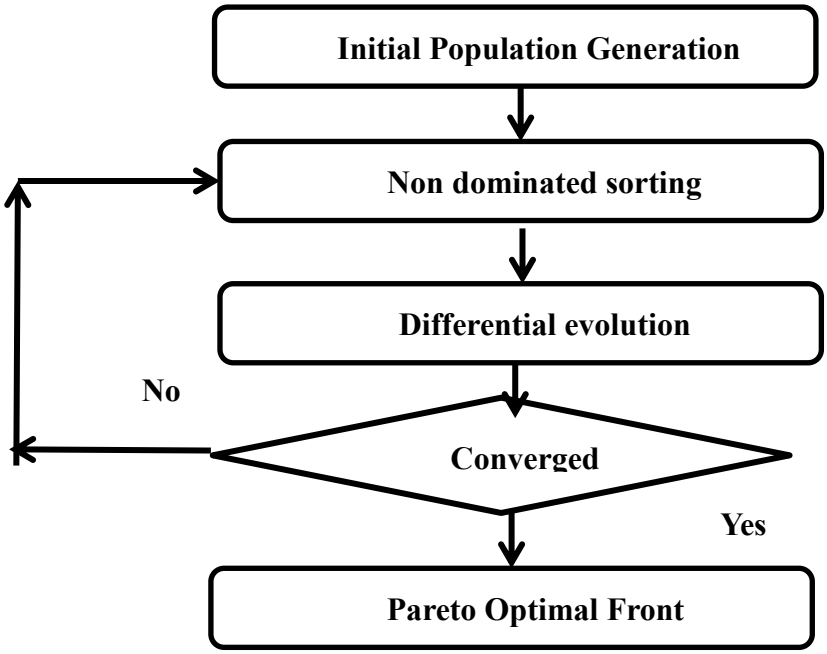

Figure 4.32: Flow chart for MODE

4.4.4 MULTI-OBJECTIVE OPTIMIZATION USING ARTIFICIAL BEE COLONY ALGORITHM

The artificial bee colony algorithm is a new population-based meta-heuristic approach (Karaboga and Akay 2009). It has been used in various complex problems. The algorithm simulates the intelligent foraging behavior of honey bee swarms. The algorithm is very simple and robust. In the ABC algorithm, the colony of artificial bees is classified into three categories: employed bees, onlookers, and scouts. Employed bees are associated with a particular food source that they are currently exploiting or are employed. They carry with them information about this particular source and share the information to onlookers. Onlooker bees are those bees that are waiting on the dance area in the hive for the information to be shared by the employed bees about their food sources and then make the decision to choose a food source. A bee carrying out random search is called a scout. In the ABC algorithm, the first half of the colony consists of the employed artificial bees, and the second half includes the onlookers. For every food source, there is only one employed bee. In other words, the number of employed bees is equal to the number of food sources around the hive. The employed bee whose food source has been exhausted by the bees becomes a scout. The position of a food source represents a possible solution to the optimization problem, and the nectar amount of a food source corresponds to the quality (fitness) of the associated solution represented by that food source. Onlookers are placed on the food sources by using a probability-based selection process. As the nectar amount of a food source increases, the probability value with which the food source is preferred by onlookers increases too. As opposed to single-

objective optimization, multi-objective optimization (MO) usually maintain a non-dominated solutions set. In multi-objective optimization, for the absence of preference information, none of the solutions can be said to be better than the others. Therefore, in our algorithm, an External Archive (EA) is created to keep a historical record of the non-dominated vectors found along the search process. In the initialization phase, the external archive will be initialized. After initializing the solutions and calculating the value of every solution they are sorted based on non-domination. Then each solution is compared with every other solution in the population to find which one is non-dominated solution. Then all non-dominated solutions are put in the external archive. In the onlooker bees 'phase, a comprehensive new learning strategy is used to produce the new solutions. For each bee, it randomly chooses *m* dimensions and learns from a non-dominated solution which is randomly selected from EA. The other dimensions learn from the other non-dominated solutions. The Control Parameters of ABC algorithm considered are number of colony size (Np) = 25, while the number of food sources equals the half of the colony size (Food Number) = Np/2, and Abandonment Limit Parameter which can be defined as a food source which could not be improved through "limit" trials is abandoned by its employed bee. The value of Abandonment Limit Parameter has been taken as 100 and has been calculated using (Np*D) where D is no of decision variables. The Pareto optimal solution obtained from MOABC is presented in Table 4.16 in "Appendix 11".

4.5 COMPARISON OF ETLBO, MODE AND MOABC ON THE BASIS OF NUMBER OF FUNCTION ELVALUATIONS

In the field of optimization, a common platform is essential to compare the performance of different algorithms. Therefore, for maintaining the consistency in comparison of ETLBO, MODE and MOABC, the number of function evaluations has been set as 24000 evaluations. The same number of function evaluations has been previously used by many researchers for comparing the performance of different algorithms for standard benchmark functions. The numbers of function evaluations for ETLBO, MODE and MOABC have been calculated using Equations (4.11-4.13) respectively.

$$\text{Number of function evaluations for (ETLBO)} = (2 * \text{Population size} * \text{Number of generations}) + (\text{Function evaluations required for duplicate elimination}) \quad (4.25)$$

where Population size = 25 ; Number of generations = 4700

$$\text{Function evaluations required for duplicate elimination} = 5000$$

$$\text{Number of function evaluations for(MODE)} = (\text{Population size} * \text{Maximum Number of generations}) \quad (4.26)$$

where Population size =25; Maximum Number of generations = 9600

Number of function evaluations for (MOABC) = (2*Colony size(N_p)*Maximum Number of cycles) (4.27)

Colony size(N_p) = 25 ; Maximum Number of cycles = 4800

For maintaining consistency in comparison of ETLBO, MODE and MOABC the number of function evaluations was set to 240000 evaluations for each algorithm. The results of optimization of µ-EDM process using ETLBO and MODE and MOABC are presented in Table 4.17.

Table 4. 17: Optimization results

Response	ETLBO			MODE			MOABC		
	Best	Mean	Worst	Best	Mean	Worst	Best	Mean	Worst
MRR (mm^3/min)	0.369	0.339	0.278	0.357	0.378	0.278	0.273	0.2669	0.211
OC(µm)	0.098	0.0885	0.119	0.133	0.128	0.118	0.028	0.0951	0.081
RCL(µm)	112.6	88.447	65.253	98.33	90.258	65.406	97.641	83.958	86.052
TA(degree)	1.56	1.6805	1.892	0.504	1.865	1.92	2.778	3.39	3.576

The Best, Mean and the Worst solution set has been calculated. From Table 4.17 it can be observed that ETLBO yielded maximum MRR value of 0.369 mm^3/min along with minimum value of TA of 1.56°, while MOABC yielded minimum values of OC and RCL as 0.028 and 97.641 respectively. However, the mean values of solutions yielded by ETLBO, MODE and MOABC for all process responses were entirely different. For case of MRR the mean value was highest for ELTBO while for OC and RCL the mean value was highest for MODE and for case of TA it was highest for MOABC.

4.6 FABRICATION OF MICRO-HOLES IN INCONEL 718 USING GRAPHITE

4.6.1 EXPERIMENTAL DETAILS

In the second phase of experimental investigation, fabrication of micro-holes has been carried out using graphite as tool electrode whereas Inconel 718 with exactly similar dimensions as stated in section 4.2.2 was used as work piece material using a micro-EDM operation. Experiments were carried out on AGIETRON 250 C machine as shown in Figure 4.1. Based on initial investigations, four process parameters were selected as the source voltage (V), Peak current (I_p), Pulse on duration (T_{on}) and Pulse off duration

(T_{off}), because they have a direct effect on the performance parameters such as material removal rate, hole overcut and recast layer thickness. The experimental layout was based on the face centered, central composite design (CCD). The levels of parameters selected (Table 4.18) are also based on preliminary experiments and literature survey.

Table 4. 18: Process parameters and their levels for machining experiments

Process parameters	Units	Low	High
Voltage(V)	Volt	30	40
Peak Current (I_p)	Ampere	8	32
Pulse on duration (T_{on})	µs	20	40
Pulse off duration (T_{off})	µs	30	60

EDM 3033 oil was used as dielectric, and it was kept same for entire experimentation. Total 30 holes were drilled (Figure 4.33 and Figure 4.34). The machining time (T_m), recast layer thickness (RCL) and overcut (OC) and taper angle (TA) were measured. The tool material used was fine graphite of 0.5 mm diameter.

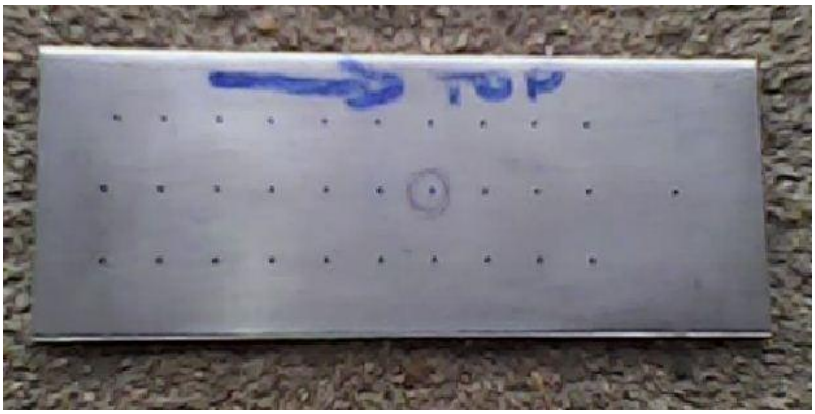

Figure 4. 33: Inconel 718 workpiece

The hole overcut, and recast layer thickness were scanned using (JEOL JSM6480LV) built Scanning electron microscope. The input process variables and their limits in the experiments are given in Table 4.18. For determining the machined hole overcut, the diameter of the hole at the entrance side was measured in four different positions as indicated in Figure 4.34. An average value was considered for measuring RCL. Based on response surface methodology layout with central composite design 30 data sets as shown in Table 4.19 in “Appendix 12” were obtained out of which 20 random sets will be used for training network and remaining 10 sets were fed to the trained network as validation sets to inspect the predictive accuracy of the ANN and ANFIS models.

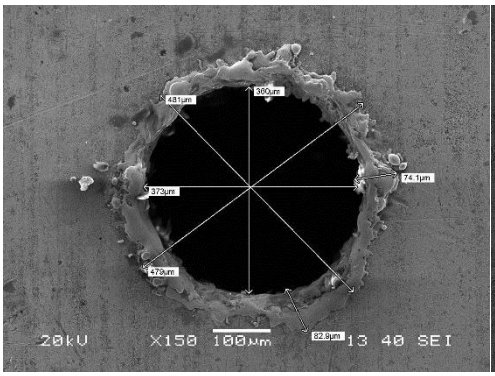

1st Hole Top view

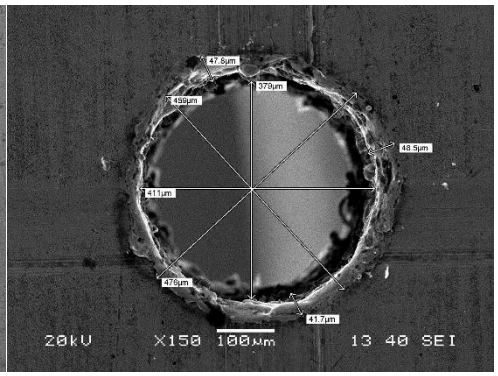

1st Hole Bottom view

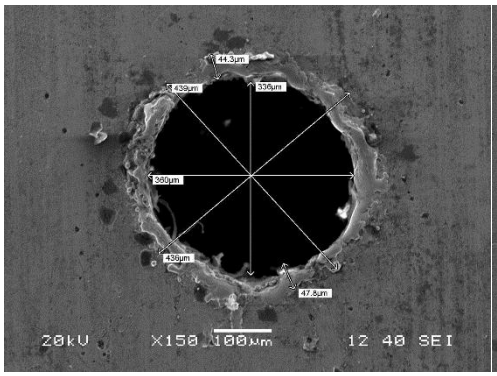

2nd Hole Top view

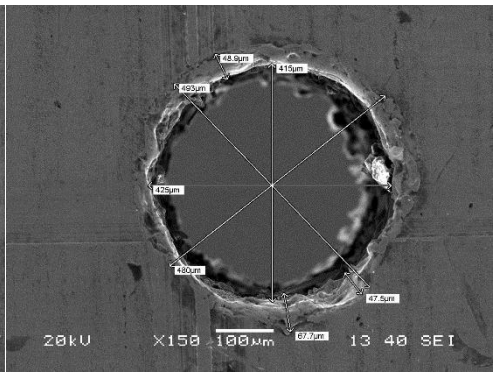

2nd Hole Bottom view

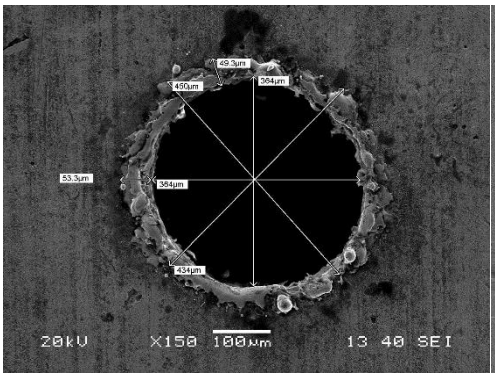

3rd Hole Top view

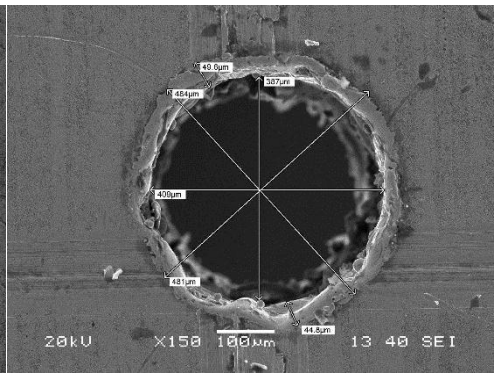

3rd Hole Bottom view

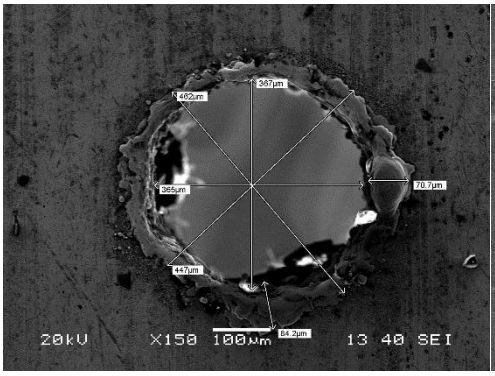

4th Hole Top view

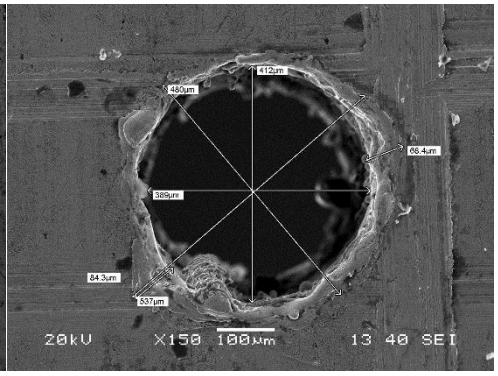

4th Hole Bottom view

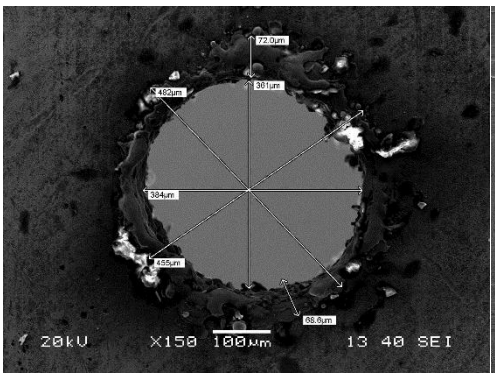

5th Hole Top view

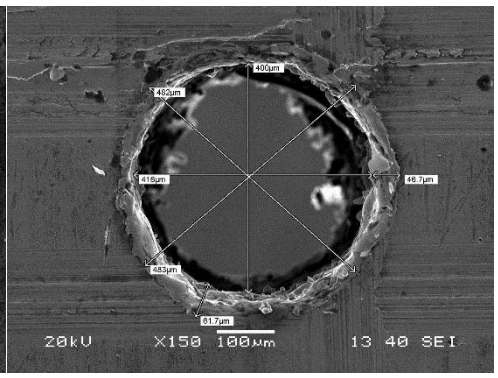

5th Hole Bottom view

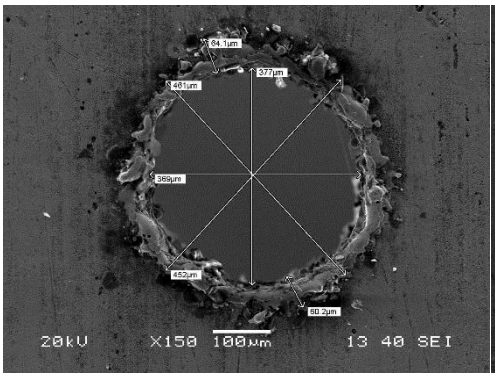

6th Hole Top view

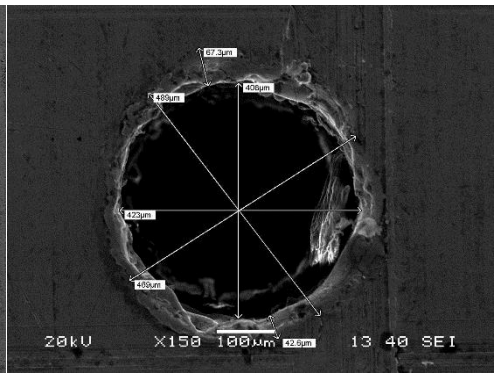

6th Hole Bottom view

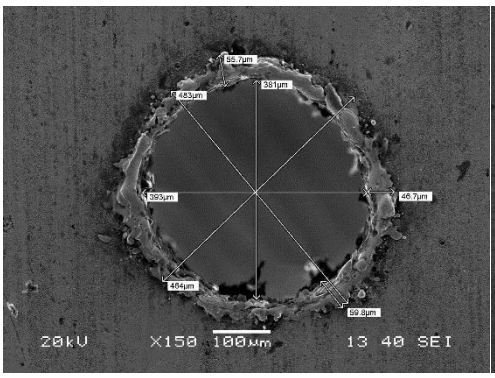

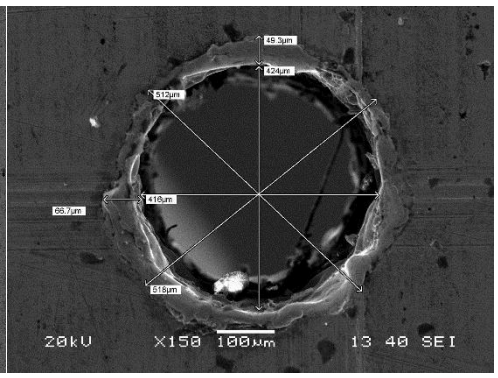

7th Hole Top view

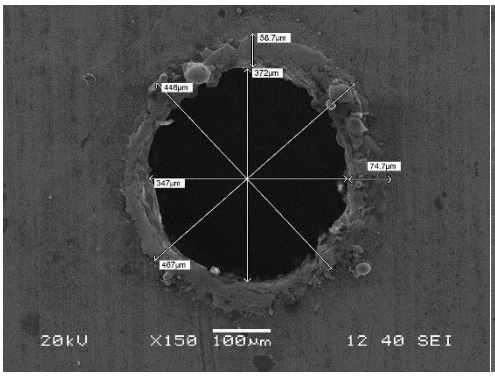

7th Hole Bottom view

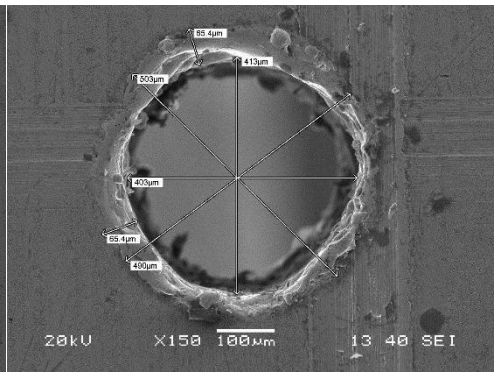

8th Hole Top view

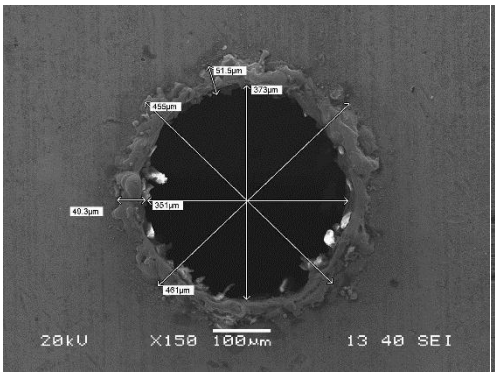

8th Hole Bottom view

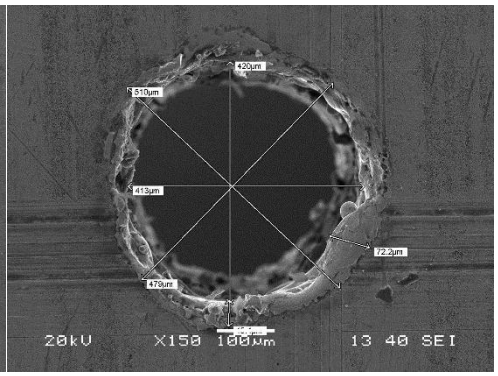

9th Hole Top view

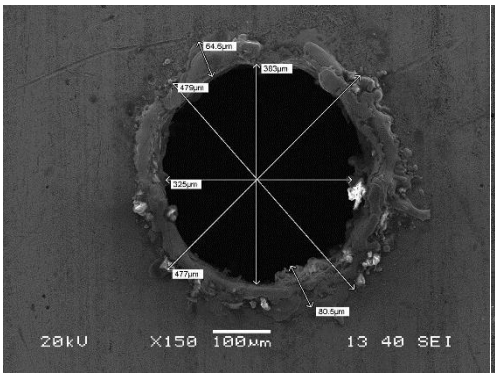

9th Hole Bottom view

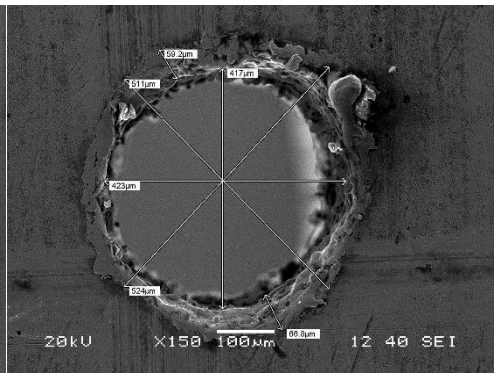

10th Hole Top view

10th Hole Bottom view

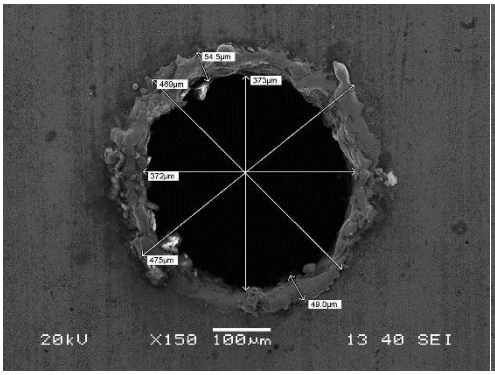

11th Hole Top view

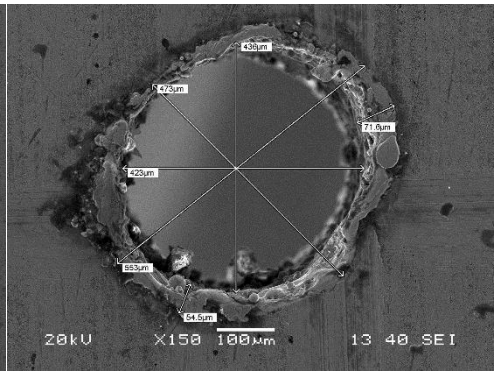

11th Hole Bottom view

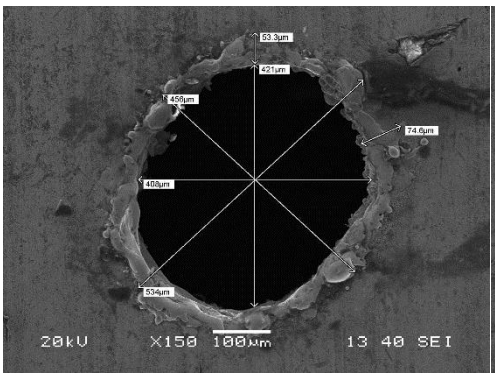

12th Hole Top view

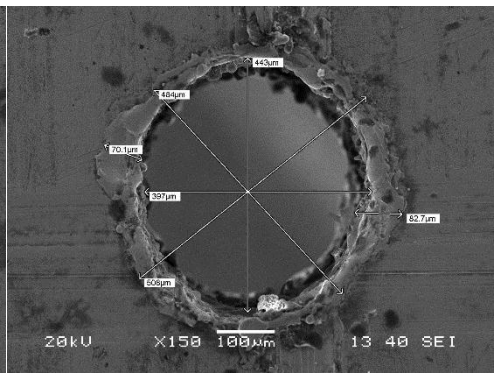

12th Hole Bottom view

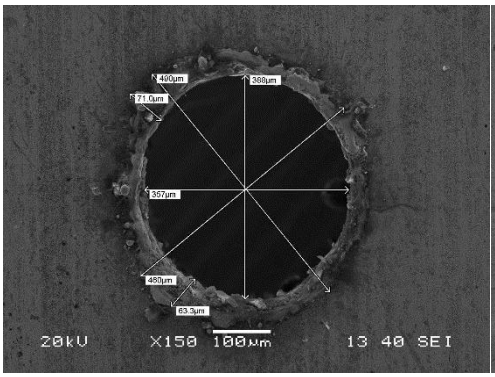

13th Hole Top view

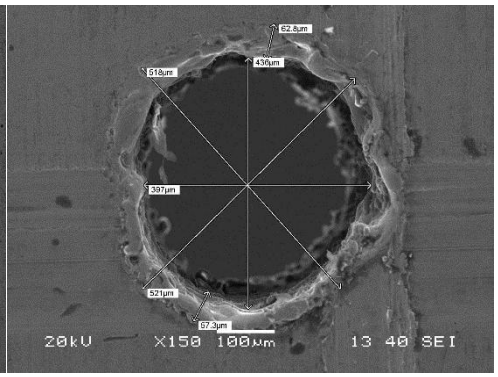

13th Hole Bottom view

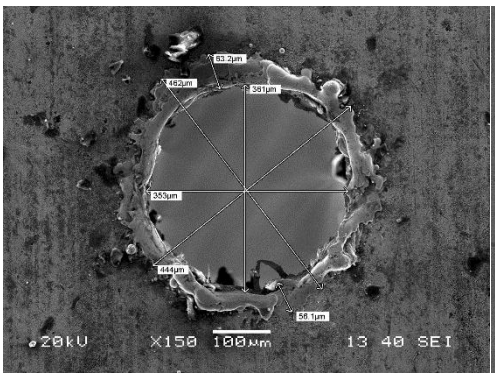

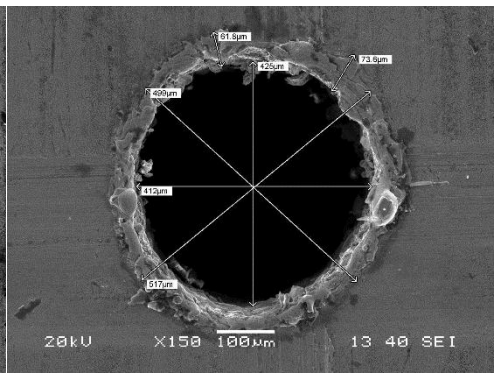

14th Hole Top view

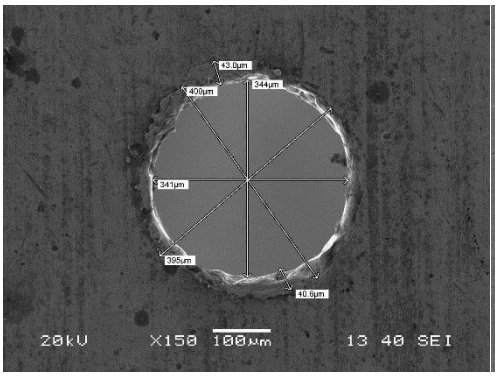

14th Hole Bottom view

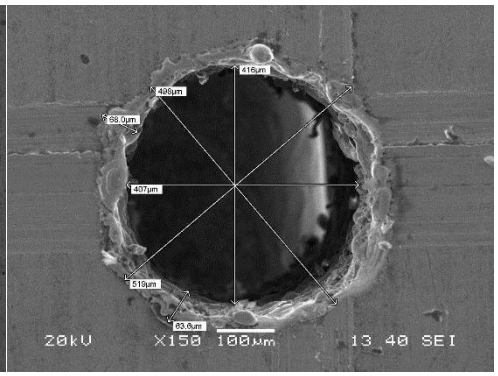

15th Hole Top view

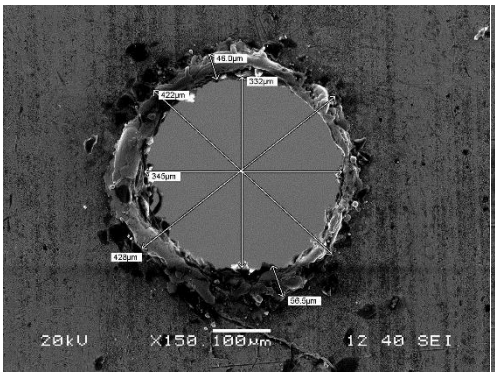

15th Hole Bottom view

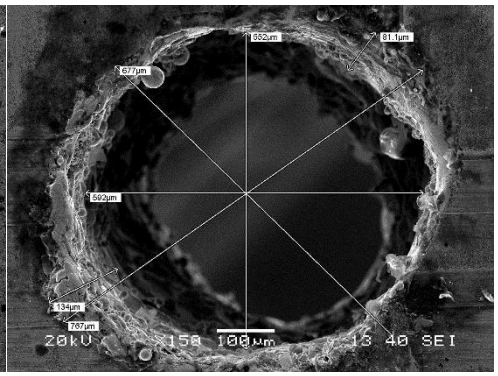

16th Hole Top view

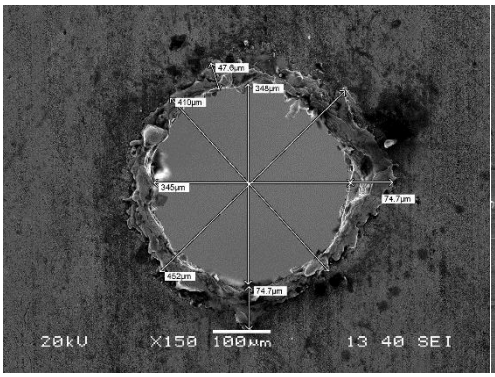

16th Hole Bottom view

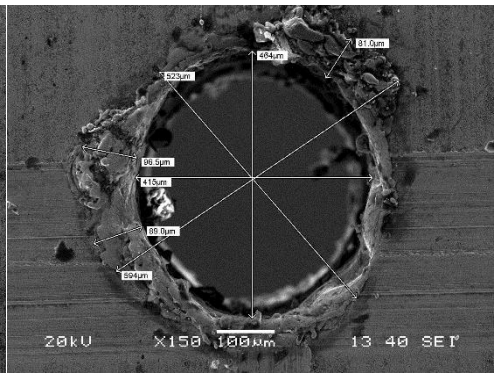

17th Hole Top view

17th Hole Bottom view

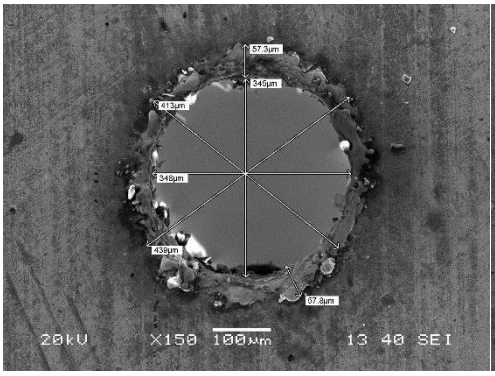

18th Hole Top view

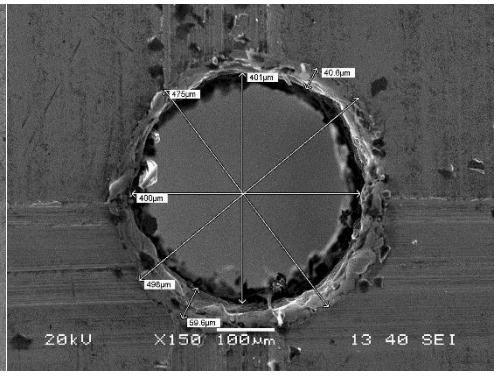

18th Hole Bottom view

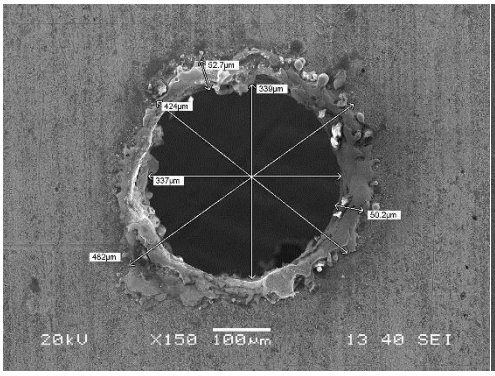

19th Hole Top view

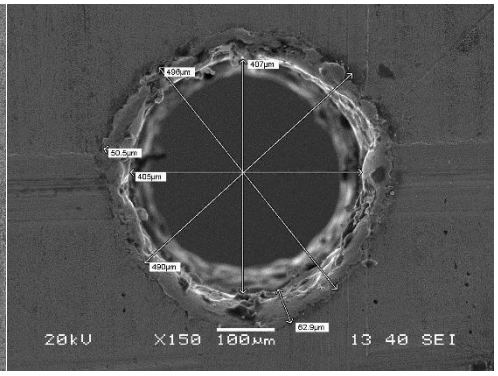

19th Hole Bottom view

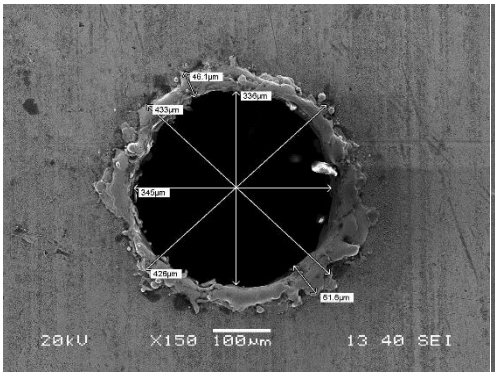

20th Hole Top view

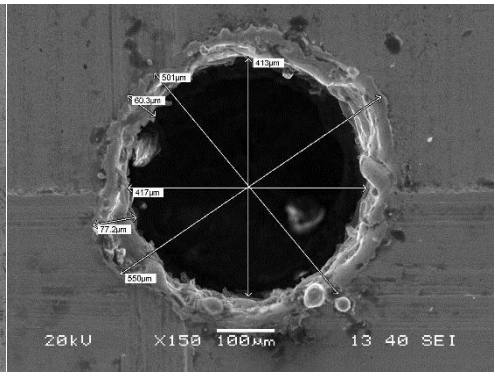

20th Hole Bottom view

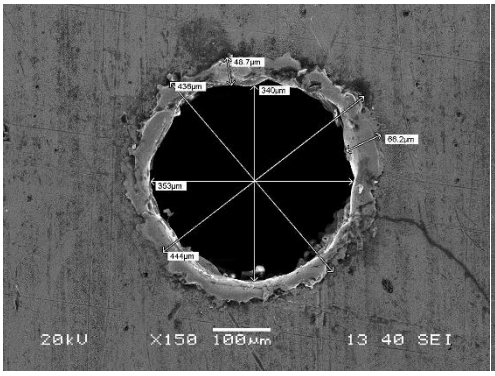

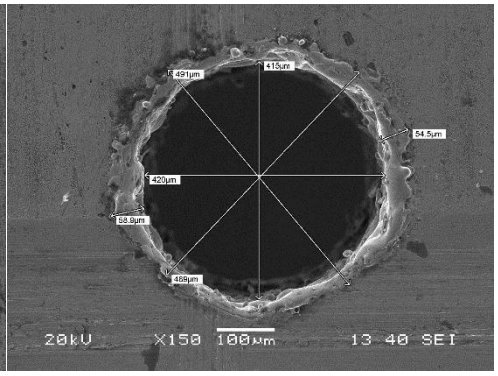

21st Hole Top view

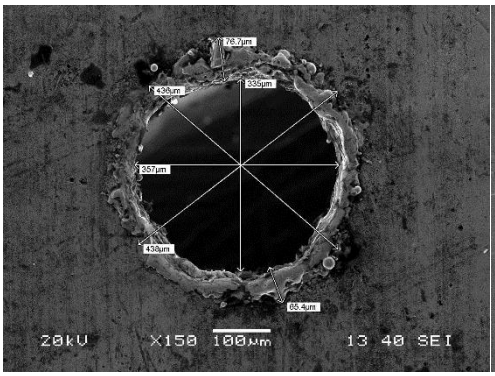

21st Hole Bottom view

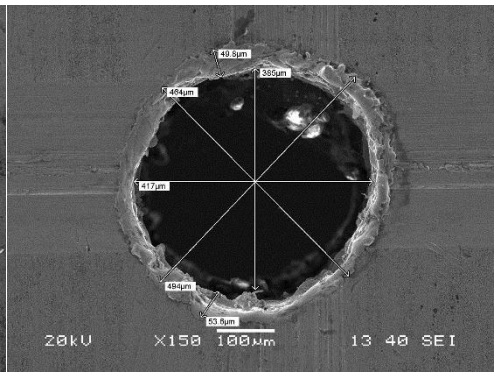

22nd Hole Top view

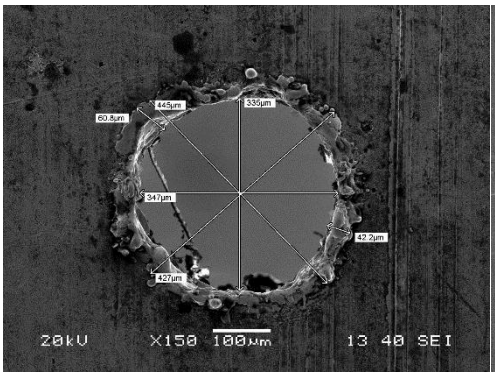

22nd Hole Bottom view

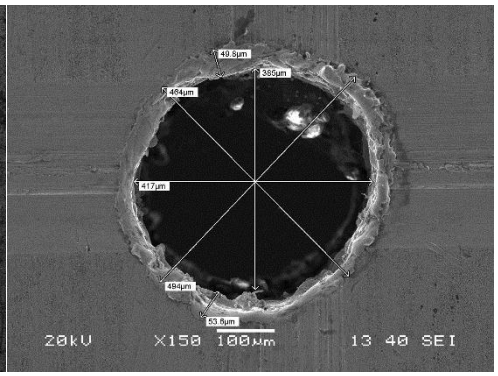

23rd Hole Top view

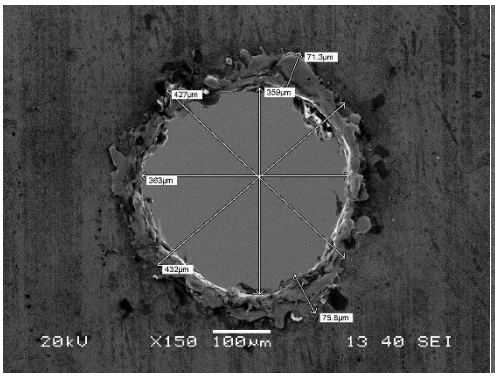

23rd Hole Bottom view

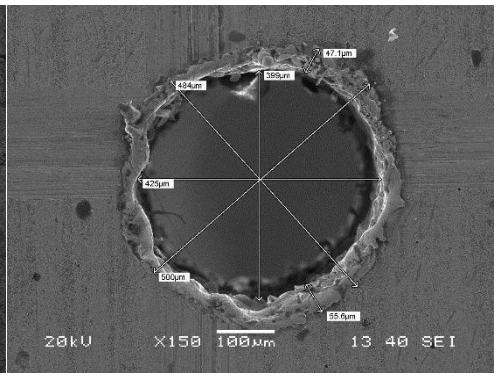

24th Hole Top view

24th Hole Bottom view

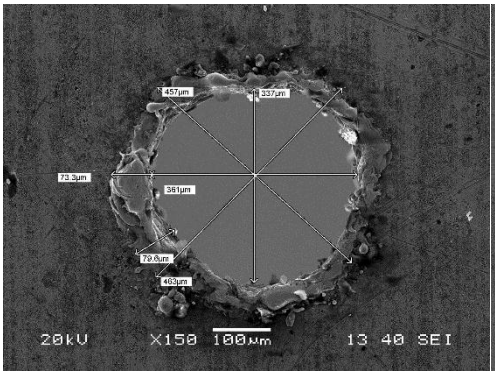

25th Hole Top view

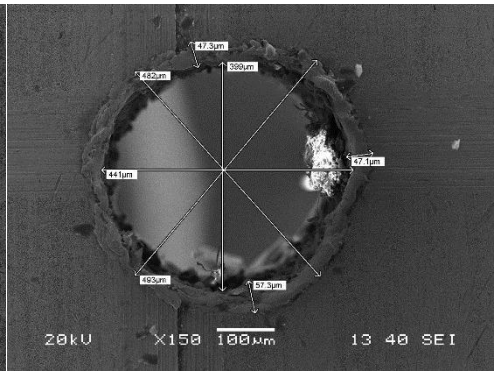

25th Hole Bottom view

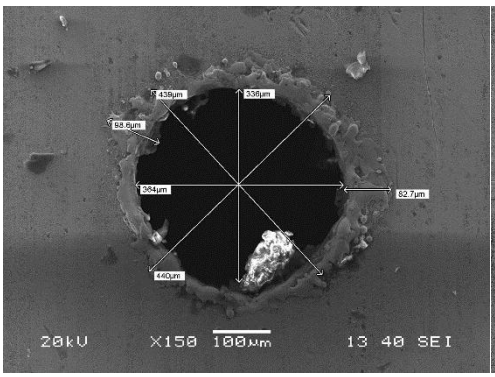

26th Hole Top view

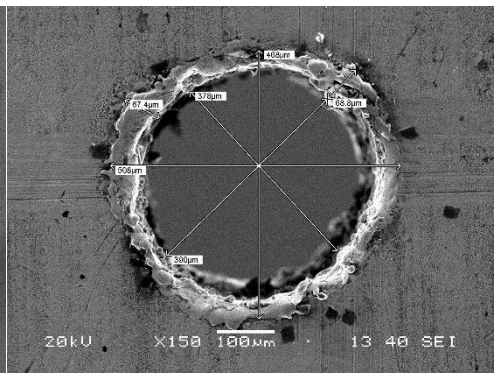

26th Hole Bottom view

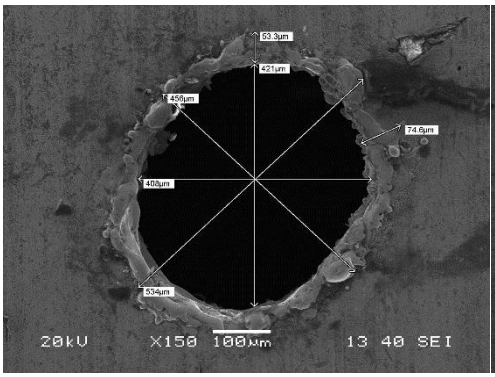

27th Hole Top view

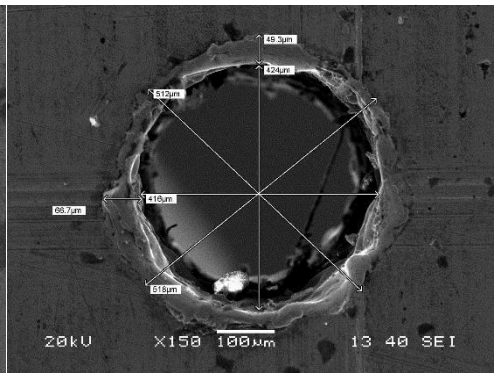

27th Hole Bottom view

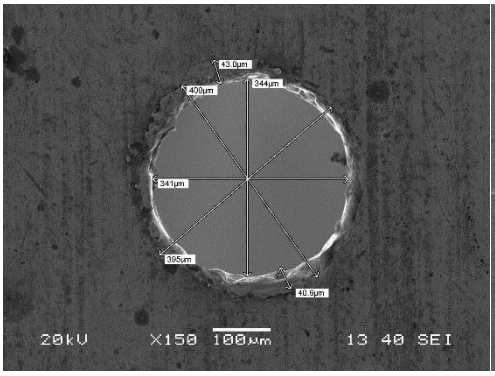

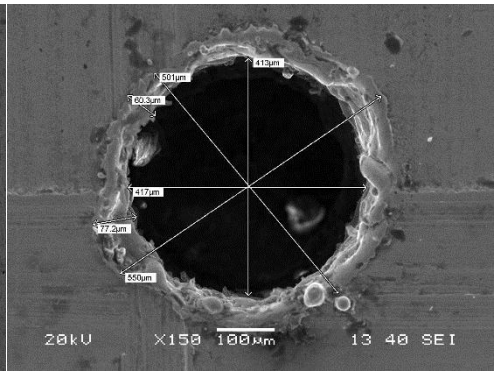

28th Hole Top view

28th Hole Bottom view

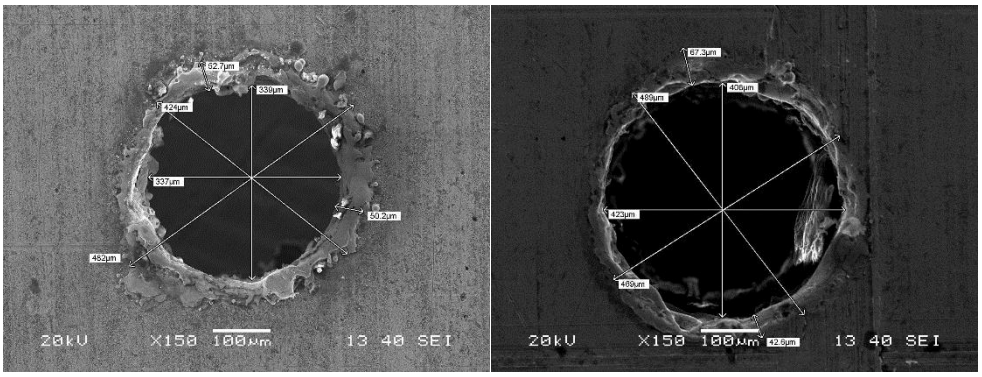

29th Hole Top view

29th Hole Bottom view

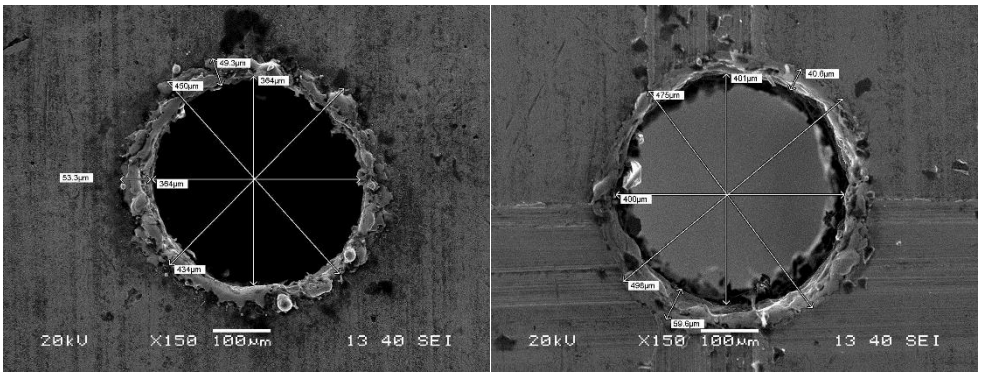

30th Hole Top view

30th Hole Bottom view

Figure 4. 19: SEM Images of Micro Holes

4.6.2 RESPONSE SURFACE METHODOLOGY

The coefficients of regression model can be estimated from the experimental results by Design expert software. The significant terms in the model were found by analysis of variance at 5% level of significance by backward elimination process. The regression coefficients are calculated using the coded units. The regression coefficients calculated for the models and corresponding P-values are shown in Table 4.20-4.23 in Appendixes 13 14 and 15 respectively. Further the percentage contribution of different process variables can be observed from these tables.

The mathematical model correlating process responses like MRR, OC, RCL and TA with the process control parameters is developed as:

$$MRR = 0.611184 - 0.0406111*A - 0.0178332*B + 0.0240555*C - 0.0101251*AB + 0.0237501*AC + 0.0102501*CD - 0.0393682*A^2 - 0.0243687*B^2 + 0.0196313*C^2 + 0.0976318*D^2 \quad (4.28)$$

$$OC = 0.199208 + 0.00871044*C + 0.030281*A^2 + 0.0233018*B^2 - 0.03445*D^2 \quad (4.29)$$

$$RCL = 93.5161 + 2.2610*A - 8.6045*B + 2.8142*BC - 3.0592*CD - 9.9295*D^2 \quad (4.30)$$

$$TA = 2.6206 + 0.551095*B + 0.474145*C + 0.326236*D - 0.395418*AB + 0.233005*AC + 0.119183*AD + 0.13538*BC + 0.252853*BD + 0.3831*CD - 1.42422*A^2 + 1.5411*B^2 - 1.01638*C^2 + 0.55205*D^2 \quad (4.31)$$

Analysis of variance (ANOVA) was carried out to check the adequacy of the developed models. Table 4.20 in "Appendix 13" shows the ANOVA for MRR after applying backward elimination process and as it can be seen from Table 4.20 that it comprises of only significant terms. The p value for the model is lowers than 0.05 (i.e. at 95% confidence level) indicates that the developed model is statistically significant. Further the model F-value of 43.73 implies the model is significant. There is only a 0.01% chance that an F-value this large could occur due to noise. In this case A, B, C, AB, AC, CD are significant model terms. The same and similar analyses were carried out for OC, RCL and TA. Furthermore, after backward elimination process the R-Squared value for MRR, OC, RCL and TA were found to be 0.9584, 0.8399, 0.8591and 0.9997 respectively. However, the truncated models have lower R-Squared value than that of full quadratic model exhibiting significance of relationship between the response and the variables. This shows that second order models can explain the variation in the MRR, OC, RCL and TA up to the extent of 95.84 %, 83.99%, 85.91% and 99.97% respectively. The "Predicted R-Squared" values are in reasonable agreement with the "Adjusted R-Squared "values. The percentage contribution of different process variables on MRR is presented in Figure 4.35 and it can be seen that voltage has a significant effect on MRR followed by pulse on duration and peak current.

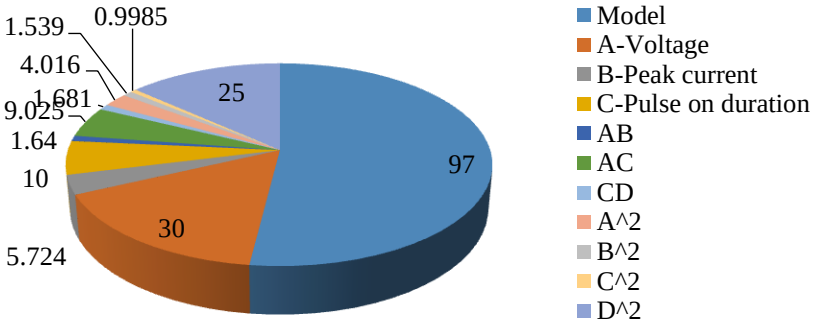

Figure 4. 35: Percentage contribution of process variables

Figure 4.36 shows the percentage contribution of different process variables on OC and it can be seen that pulse on duration has a significant effect on OC. Furthermore, the square terms of voltage, peak current and pulse off duration are also found to be significant. However, it is interesting to note that there are no significant interaction terms in this model. Further the model F-value of 7.33 implies the model is significant. There is only a 0.05% chance that an F-value this large could occur due to noise.

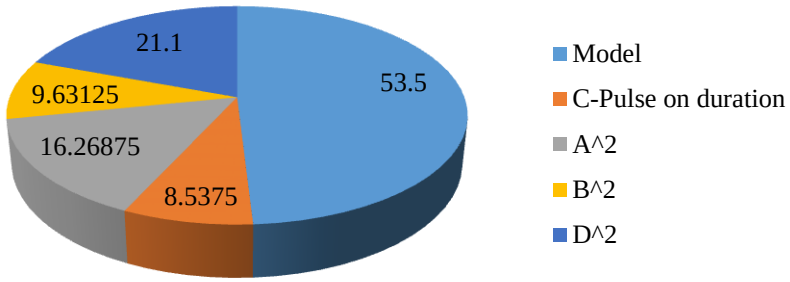

Figure 4.36: Percentage contribution of process variables

Figure 4.37 illustrates percentage contribution of different process variables on RCL and it can be observed that that peak current is found to be most significant effect on RCL followed by voltage. Furthermore, pulse off duration in square terms has a significant effect on RCL while BC and CD are found to be significant the interaction terms. Further the model F-value of 29.26 implies the model is significant.

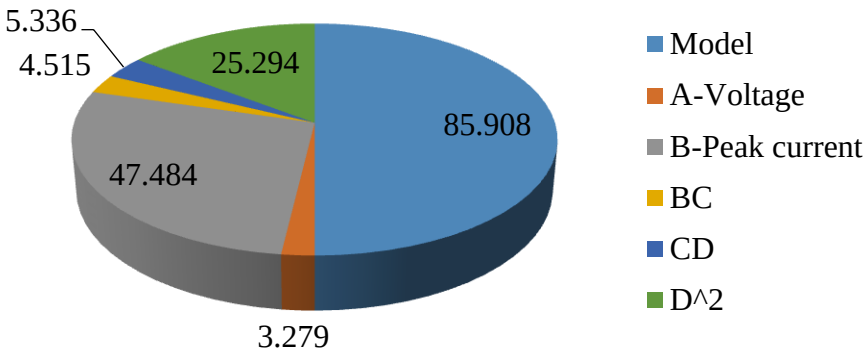

Figure 4.37: Percentage contribution of process variables

On observing Figure 4.38 and it can be witnessed that that peak current is found to be most significant effect on TA followed by pulse on duration and pulse off duration. Furthermore, AB, AC, AD, BC, BD, CD are identified as significant the interaction terms. Further the model F-value of 4598.32 implies the model is significant.

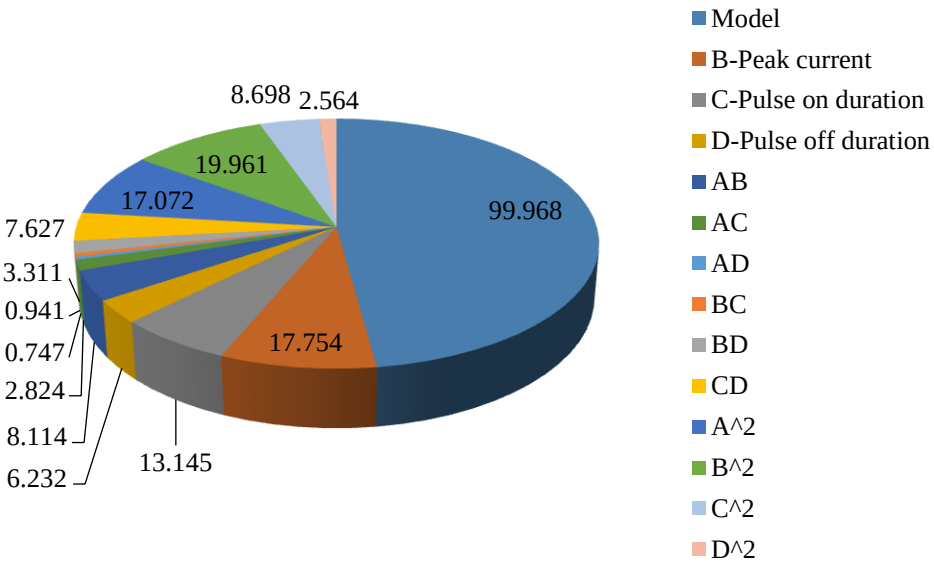

Figure 4.38: Percentage contribution of process variables

4.6.3 EFFECT OF PROCESS VARIABLES ON MRR

It can be observed from Table 4.20 that the interaction terms AB, AC and CD have significant contribution on MRR. The three dimensional surface plots for the MRR with respect to the significant interaction terms are shown in Figures 4.39, 4.40 and 4.41. In each of these graphs, two process variables are varied while the other two variables are

held constant at its middle value. Figure 4.39 shows the interaction effect of voltage and peak current on MRR in at constant pulse on duration of 30µs and pulse off duration of 45µs. It is observed that maximum MRR value of 0.6115 mm^3/min was achieved at the voltage of 32 V and lowest peak current (8A) combination. The minimum MRR value of 0.4863 mm^3/min was obtained at the highest voltage (40V) and highest peak current of (32A) combination. It is observed that material removal rate initially increases with increase in voltage and peak current then it decreases with further increase in voltage and peak current. There is a significant rise in material removal rate with increase in voltage, however with rise in pulse off duration there is a slight drop in MRR.

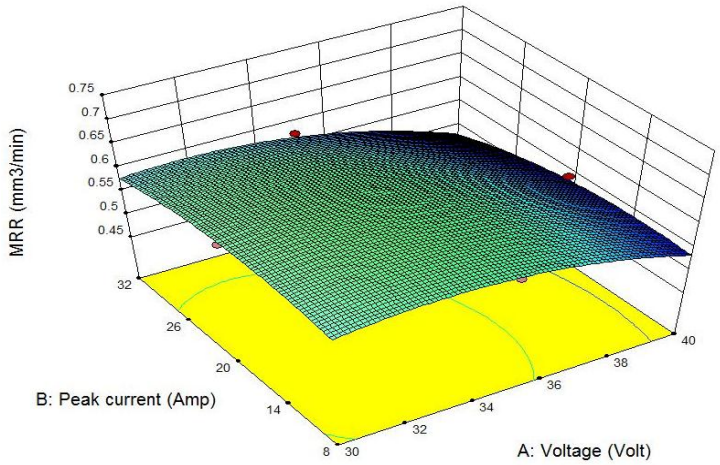

Figure 4.39: Interaction effect of voltage and peak current on MRR

Figure 4.40 indicates the interaction effect of voltage and pulse on duration on MRR at constant peak current of 20 A and pulse off duration of 45 µs. Additionally, it is interesting to note that the maximum MRR was obtained at the lowest voltage (30V) and highest pulse on duration (40µs). Further, the minimum MRR was obtained at the highest voltage (40V) and lowest pulse off duration of 20µs combination. It is seen that MRR increases with increase in voltage and the pulse on duration.

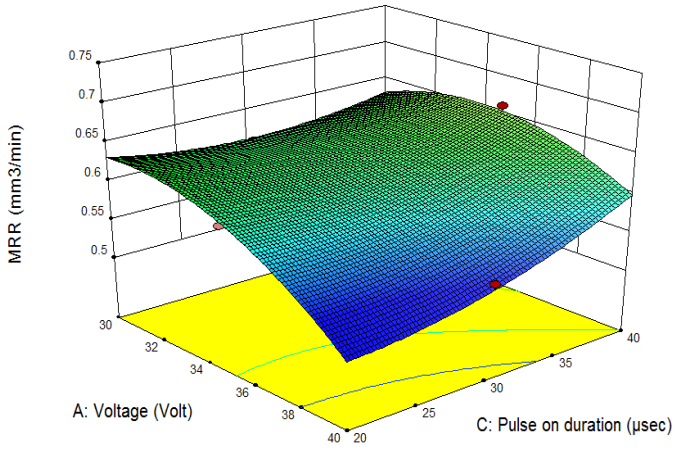

Figure 4.40: Interaction effect of voltage and pulse on duration on MRR

Figure 4.41 illustrates the interaction effect of pulse on duration and pulse off duration on MRR at constant peak current of 20 A and voltage of 35. The maximum MRR value of 0.760mm^3/min was achieved at the highest values of pulse on duration and pulse off duration. Also it was observed that with the increase in pulse on duration the MRR increases, while it initially decreases and then increases with increase in pulse off duration.

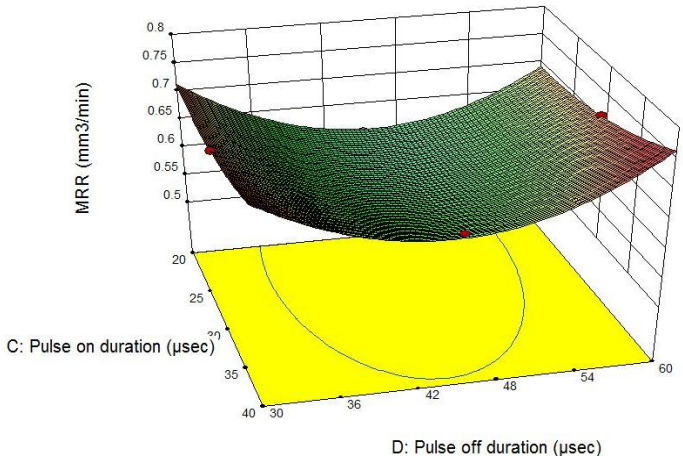

Figure 4.41: Interaction effect of pulse on duration and pulse off duration on MRR

4.6.4 EFFECT OF PROCESS VARIABLES ON RCL

Figure 4.42 presents the interaction effect of pulse on duration and peak current on RCL at constant voltage of 35 V and pulse on duration of 45 µs. The minimum RCL value of 82.265 µm was attained at the peak value of peak current (32A) and least value of pulse on duration (20µs). Additionally, it was observed that with the increase in peak current

the RCL decreases linearly, while it varies proportionally with pulse on duration. With the increase in both peak current and pulse on duration RCL decreases.

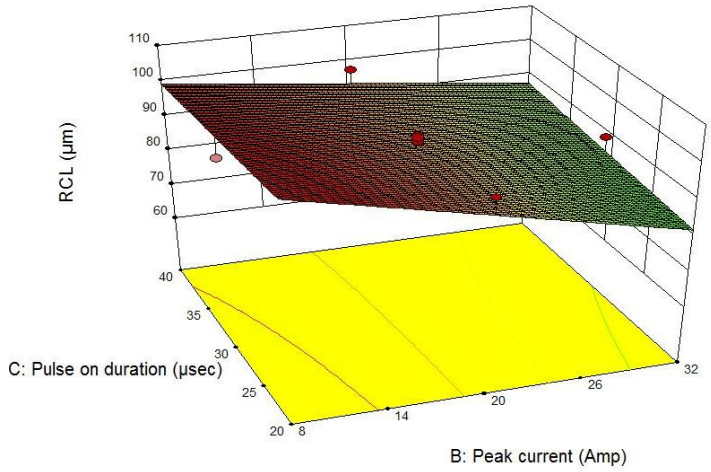

Figure 4.42: Interaction effect of pulse on duration and peak current on RCL

At constant voltage of 35 V and peak current of 20 the interaction effect of pulse on duration and pulse off duration on RCL is represented in Figure 4.43. It is further observed that least RCL value of 80.604 µm was found at the lowest values of pulse on duration (20µs) and pulse off duration (30µs) correspondingly. Besides it was observed that with the increase in pulse on duration RCL increases proportionally, while it initially increases with increase in pulse off duration and decreases with any further increase in pulse off duration. Moreover, the increase in both pulse on duration and pulse off duration RCL initially increases then it starts declining with further increase in pulse on duration and pulse off duration.

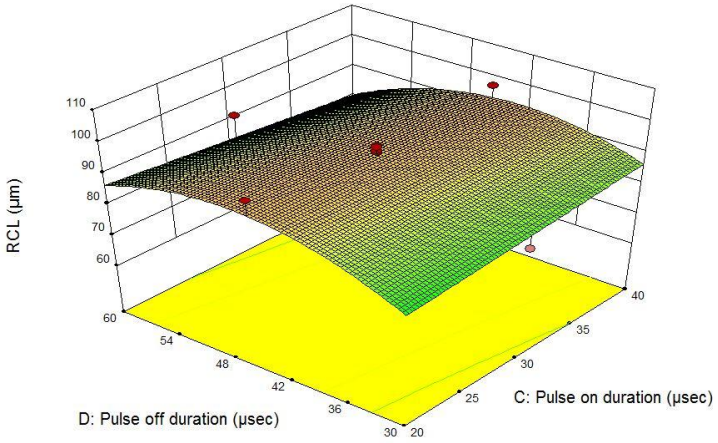

Figure 4.43: Interaction effect of pulse on duration and pulse off duration on RCL

4.6.5 EFFECT OF PROCESS VARIABLES ON TA

From Figure 4.44, it is observed that minimum TA value of 1.716° was obtained at the lowest values of voltage (30V) and peak current (8A) respectively. Furthermore, it was observed that with the increase in peak current TA initially increases then it decreases non-linearly, at the middle level of peak current setting and again increases at high level voltage settings. However, with the increase in voltage the value of TA goes on increasing up to maximum value of 3.306°. Additionally, with the increase in both voltage and peak current simultaneously the value of TA goes on increasing and starts decreasing for higher values of peak current and voltage.

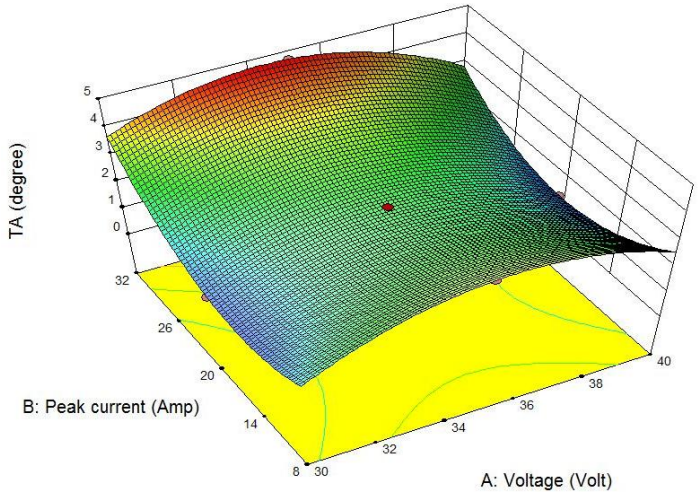

Figure 4.44: Interaction effect of voltage and peak current on TA

Figure 4.45 demonstrates the interaction effect of voltage and pulse on duration on TA at constant peak current of 20A and pulse off duration of 45µs. It can be observed that with the increase in voltage the value of TA firstly goes on increasing but it starts to decline for higher level voltage settings. However exactly similar trend was also observed for pulse on duration. Furthermore, when voltage and pulse on duration where increased simultaneously, the value of TA initially increases then it decreases for higher level settings of voltage and pulse on duration.

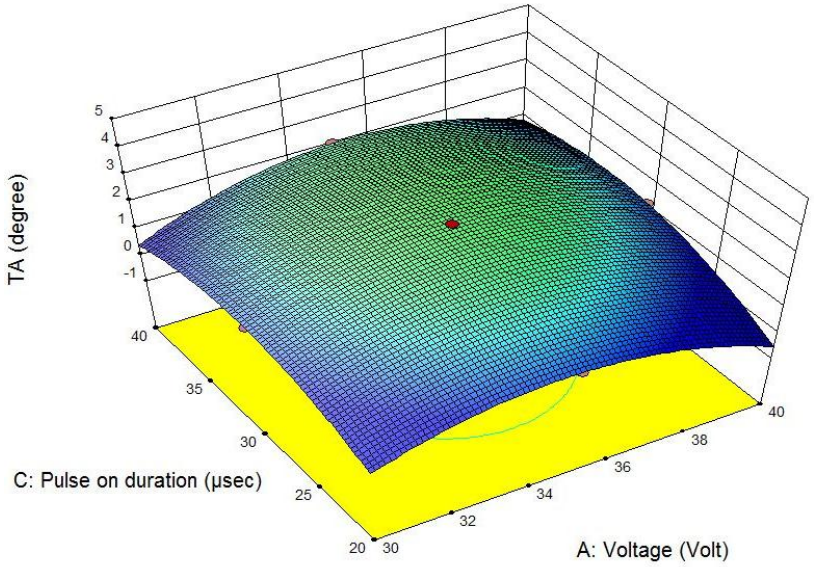

Figure 4.45: Interaction effect of voltage and pulse on duration on TA

From Figure 4.46 it can be observed that with the rise in peak current the value of TA initially goes on declining but it starts to rise for higher level peak current settings. However, with the increase in pulse on duration the value of TA indicates linearly increasing trend. Likewise, when peak current and pulse off duration where increased simultaneously, the value of TA initially decreases then it increases for higher level settings of peak current and pulse off duration.

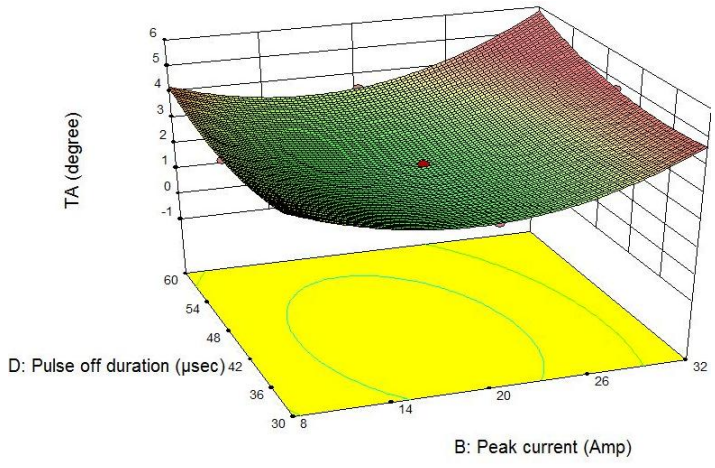

Figure 4.46 Interaction effect of peak current and pulse off duration on TA

From Figure 4.47 it can be perceived that with the increase in pulse off duration the value of TA initially goes on reducing but it starts to grow for higher level pulse off duration settings. But with the increase in pulse on duration the value of TA increases with increase in pulse on duration. Furthermore, when pulse on duration and pulse off duration

where increased simultaneously, the value of TA initially increases and then decreases for higher level settings of pulse on duration and pulse off duration.

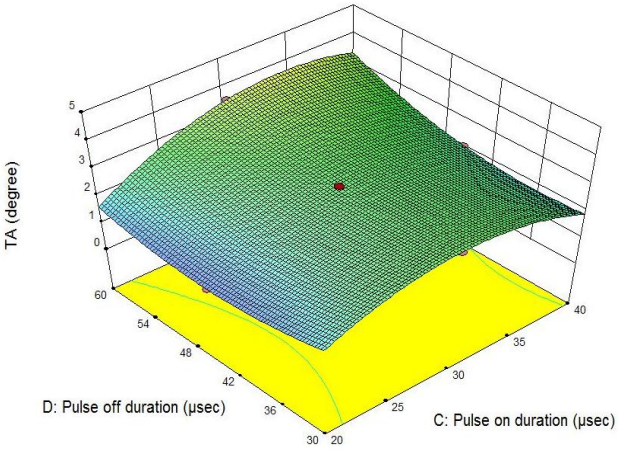

Figure 4.47 Interaction effect of pulse on duration and pulse off duration on TA

4.7 ANN MODELING:

Nowadays Artificial Neural Network (ANN) is widely used for optimization, prediction and image processing etc., ANN is one of the powerful data modeling tool provoked from the operation of human nervous system. It is a multiprocessor computing system, with simple processing elements. It is called as neurons, with a high degree of interconnection and simple scalar messages carried through the system. The main processing element is named as neuron. The information that is contained in each neuron is first weighed *(w_{ij}),* and summed up and considered as a net function *(u_i).* Then the value from the net function is transferred by a transfer function *(f(u))* with activation value (a_i), to the next neuron. Each input is given a relative weight, which affects the impact of the input neurons. It has an adaptive coefficient that determines the strength of the input data.

4.7.1 THE NETWORK ARCHITECTURE

ANN architecture consists of many neurons interconnected, and this net forms a processing system. The layers consist of processing elements that are called as neurons. A network with 4x12x1x4 architecture, which means 4 input (Voltage, Peak current, Pulse on duration and Pulse off duration neurons in the input layer, 12 neurons in the hidden layer and 4 outputs (MRR, Overcut, Recast layer thickness, and Taper Angle) in the output layer. Generally, in the multi-layer feed forward network, the size of hidden layers is one of the most important considerations when solving problems. One hidden layer was adopted in this model. The inputs and outputs are normalized to gain better results. To train the developed model, 20 data sets were used which are tabulated in Table 4.24 in "Appendix 16". To test the ANN model, 10 data sets were used. A

MATLAB program has been written to train, validate and test the model. The topology and training parameters are given in Table 4.24.

Table 4. 24: ANN topology and its training parameters

Parameters	Values
Number of input neurons	4
Number of hidden layers	1
Number of neurons in each hidden layer	12
Number of output neuron	4
Momentum factor	0.09
Learning rate	0.001
Number of iterations	500

During training phase, the regression value of 0.99981, 0.99981, 0.99985 and 0.99965 for MRR, OC, RCL and TA have been obtained which signifies the fair correlation between experimental and predicted values.The regression plot for MRR, OC, RCL and TA have been given in Figure 4.48. Hence ANN can be effectively used for the prediction of MRR, OC, RCL and TA in µ-EDM.

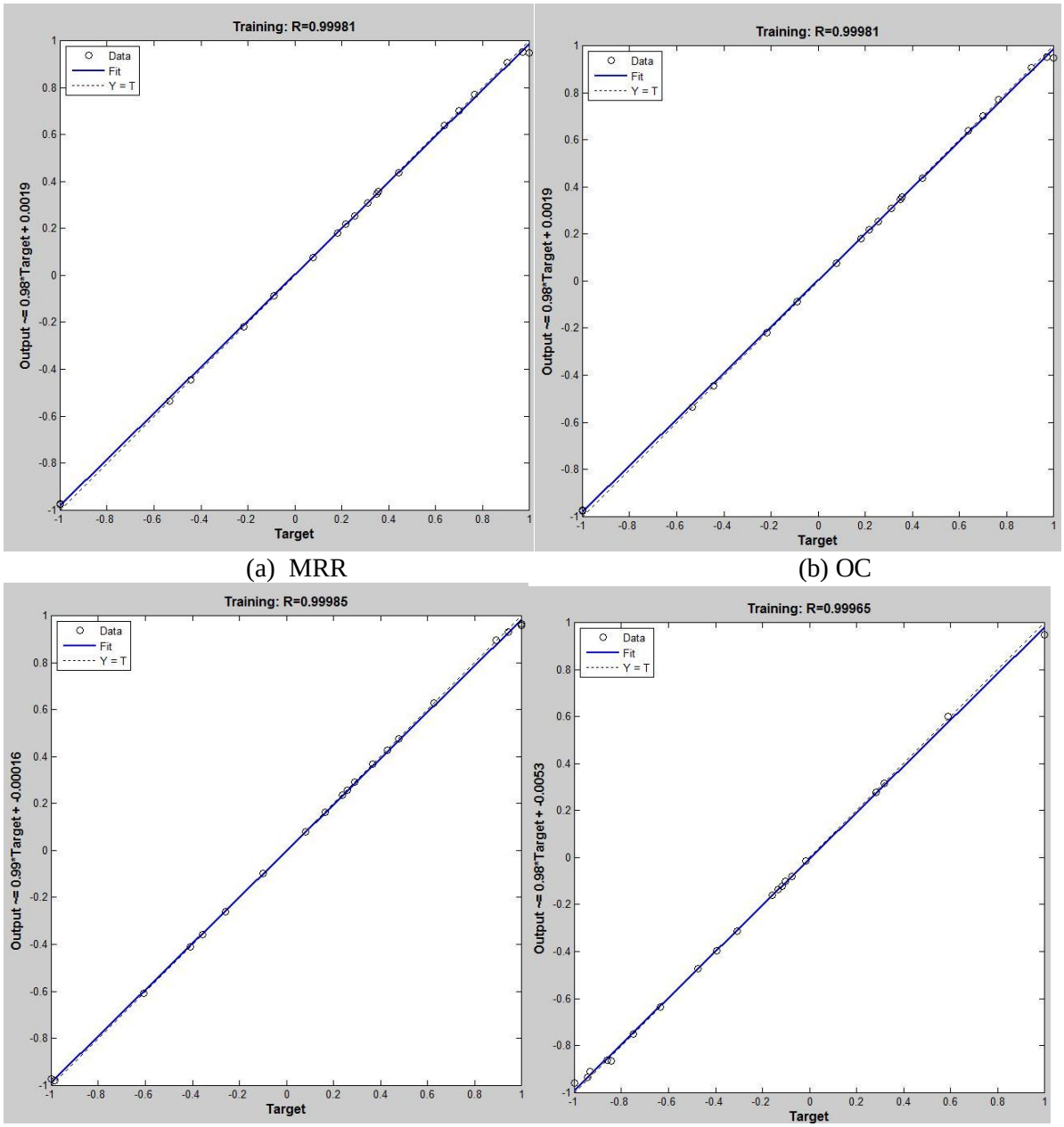

(a) MRR (b) OC

(c) RCL (d)TA

Figure 4.48: Regression plot for MRR, OC, RCL and TA

The trained neural network was validated against another set of experimental data, termed as validation data set illustrated in Table 4.25 in "Appendix 17". The errors in prediction are also presented in Table 4.26 "Appendix 17". It can be seen from Table 4.27 that the model predictions match the experimental data very closely except few data. Moreover, the average error in the prediction was 1.057 % for MRR, 9.303 % for OC, and -0.252 % for RCL and -23.090 % for TA respectively. The total average prediction error of the network was predicted as -12.983 % which indicates that the model is over predicting the values. The developed ANN model was tested by repeating few experiments randomly from the entire data set for checking the

predictive accuracy of the developed model. Figures (4.31- 4.34) indicated the errors between predicted and experimental values for all process responses.

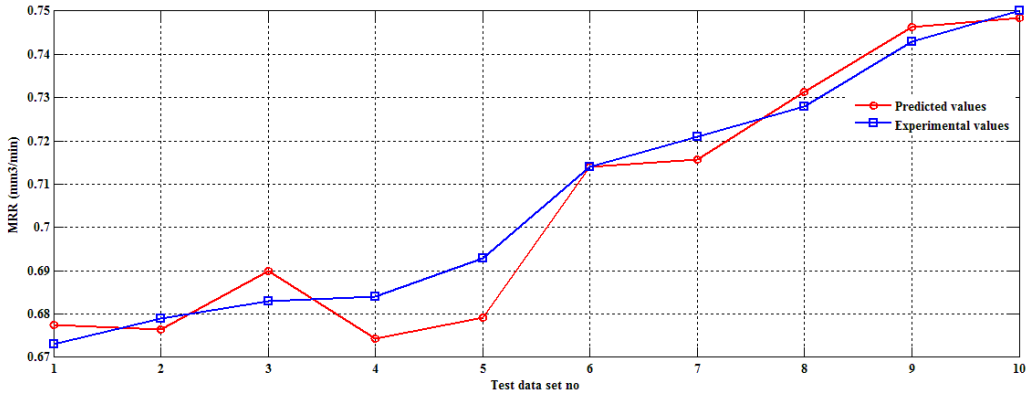

Figures 4.31: Errors between predicted and experimental values of MRR during testing

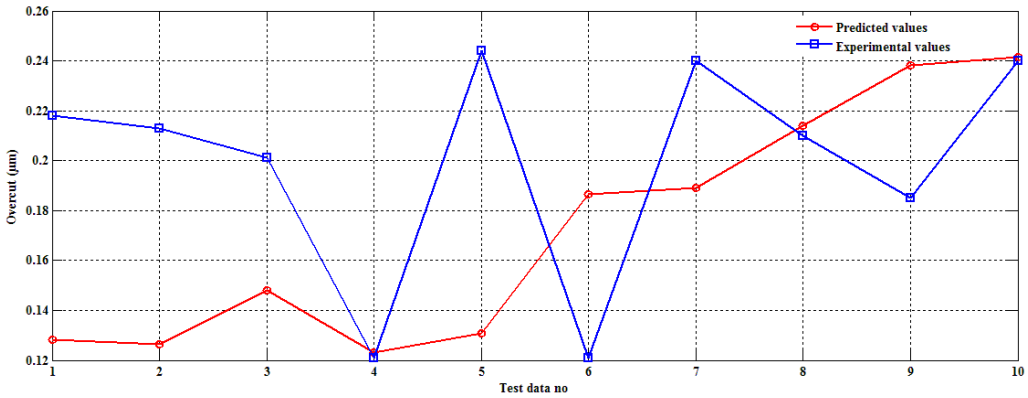

Figures 4.32: Errors between predicted and experimental values of OC during testing

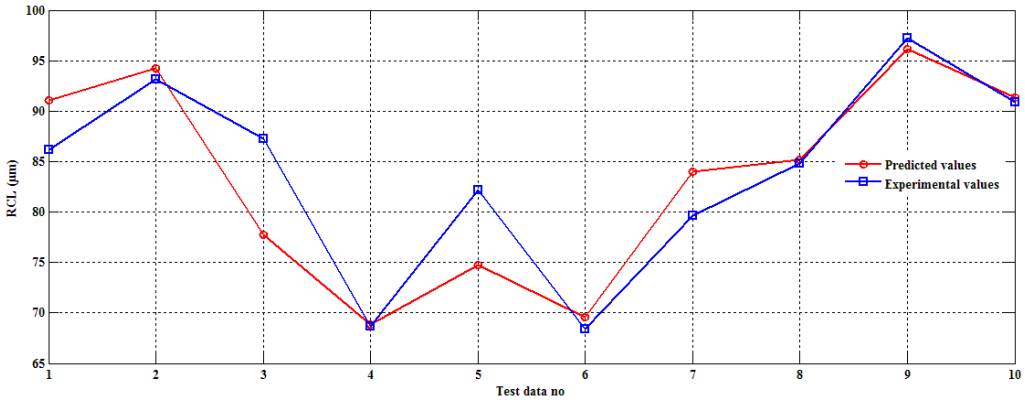

Figures 4.33: Errors between predicted and experimental values of RCL during testing

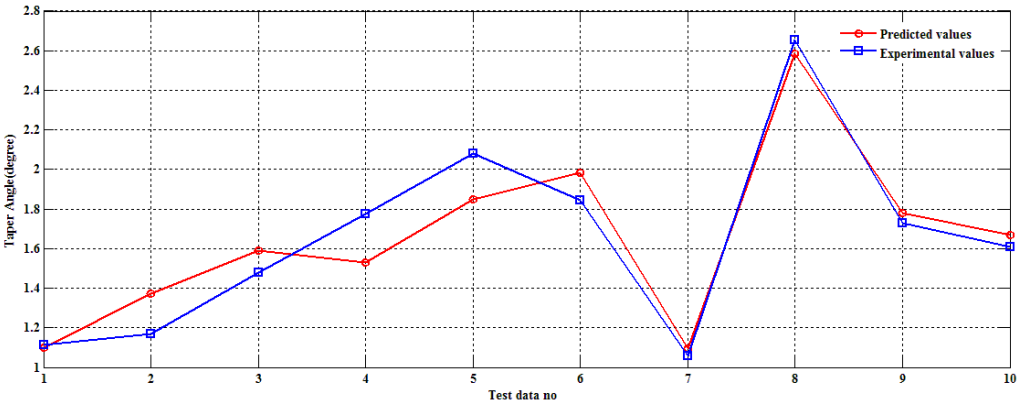

Figures 4.34: Errors between predicted and experimental values of TA during testing

Table (4.27 - 4.28) in "Appendix 18" contains testing of the developed model with experimental data and the predicted output and percentage error in prediction of MRR, OC and RCL were within acceptable limits. It is observed that the total average prediction error is 4.908 % which is implies level of over prediction.

4.8 ANFIS MODELING

The adaptive neuro-fuzzy inference system has been used to predict MRR, OC RCL and TA. For this purpose, the MATLAB 2012b package (ANFIS toolbox) has been utilized. Prediction of MRR, OC, RCL and TA of the micro-EDM process by ANIFS comprises of three main phases, training and testing. A similar methodology was adopted as mentioned in section 4.4. However, for the purpose of comparing the predictive tendency with ANN model same data was used for training, validation and testing as it was used for development of ANN. Total average error (TAE) as mentioned in Equation 4.14 is considered as selection criteria for comparison of all existing networks and final selection is made of the most accurate one. The value of error goal was set at 0.03, and the iteration number was 500 epochs. Various structures were tested of ANFIS model for each response (material removal rate, overcut recast layer thickness and taper angle), it was obtained that structures with 16 numbers of membership functions (2 MFs for each input) had the lowest values of TAE for each response. In this work various types of MFs namely triangular, trapezoid, generalized bell and Gaussian have been practiced. Table 4.29 represents training and validation error of ANFIS models for different membership functions.

TAE for MRR, OC, RCL and TA have been presented in Table 4.30. Results indicated that the generalized bell function leads the lowest values of TAE for MRR, OC RCL and TA, respectively.

Table 4.29: Training and validation error

Type of membership function	MRR		OC		RCL		TA	
	Training error	Validation error	Training error	Validation error	Training error	Validation error	Training error	Validation error
Triangle	0.01463	0.01463	0.01745	0.01744	4.29320	4.29270	0.35751	0.35748
Trapezoid	0.01352	0.01352	0.01413	0.01412	3.68910	3.38620	0.34938	0.34938
Generalized bell	0.01328	0.01328	0.00992	0.00992	3.25470	3.25390	0.31822	0.31802
Gaussian	0.01347	0.01346	0.01333	0.01332	3.58430	3.58140	0.33718	0.33708

Table 4.30: TAE for process responses

Type of membership function	MRR Total Average error	OC Total Average error	RCL Total Average error	TA Total Average error
Triangle	0.014631	0.017445	4.29295	0.357495
Trapezoid	0.013521	0.014127	3.53765	0.34938
Generalized bell	0.013275	0.009916	3.2543	0.31812
Gaussian	0.013464	0.013326	3.58285	0.33713

The developed ANFIS model was tested for checking the predictive accuracy of the developed model. Tables (4.31 - 4.32) contains testing of the developed model with experimental data and the predicted output and percentage error in prediction of MRR, OC and RCL were within acceptable limits. It is observed that the total average prediction error is -6.629 % which implies level of over prediction.

Table 4.31: Testing of the developed model with experimental data.

Process Parameters				MRR (mm^3/min)		OC(μm)		RCL(μm)		TA(degrees)	
V	I_p	T_{on}	T_{off}	Exp	ANFIS	Exp	ANFIS	Exp	ANFIS	Exp	ANFIS
35	20	20	45	0.670	0.673	0.218	0.205	86.158	89.977	1.116	1.112
40	20	30	45	0.672	0.679	0.213	0.222	93.155	92.763	1.150	1.171
30	8	40	60	0.681	0.683	0.201	0.201	87.249	86.348	1.379	1.479
30	32	20	30	0.584	0.684	0.121	0.121	68.627	68.739	1.476	1.776
35	8	30	45	0.690	0.693	0.244	0.244	82.143	88.674	2.081	2.081
30	32	40	60	0.712	0.714	0.121	0.121	68.408	68.422	1.824	1.844
35	20	40	45	0.721	0.721	0.240	0.233	79.665	84.094	1.060	1.060
35	20	30	45	0.728	0.716	0.210	0.215	84.857	87.734	2.653	2.196
40	8	20	30	0.740	0.743	0.185	0.185	97.222	97.120	1.731	1.731
35	20	30	45	0.750	0.716	0.240	0.215	90.882	87.734	1.610	2.196

Table 4.32: Errors in Prediction of Responses during testing

(V)	(I_p)	(T_{on})	(T_{off})	% Error in Prediction of MRR	% Error in Prediction of OC	% Error in Prediction of RCL	% Error in Prediction of TA
35	20	20	45	-0.448	6.055	-4.432	0.358
40	20	30	45	-1.042	-4.085	0.421	-1.826
30	8	40	60	-0.294	0.000	1.032	-7.252
30	32	20	30	-17.123	-0.083	-0.162	-20.325
35	8	30	45	-0.435	0.123	-7.951	0.000
30	32	40	60	-0.281	0.000	-0.021	-1.096
35	20	40	45	0.000	2.958	-5.559	0.000
35	20	30	45	1.690	-2.190	-3.390	17.214
40	8	20	30	-0.405	-0.054	0.105	0.000
35	20	30	45	4.573	10.583	3.464	-36.416
Average (%) of error				-1.376	1.331	-1.649	-4.934
Total average prediction error (%) = -6.629							

4.9 MULTIOBJECTIVE OPTIMIZATION USING ETLBO MODE AND MOABC

The process of optimizing simultaneously a collection of objective functions is called as multi-objective optimization (MOO). In the present section multi-objective optimization has been carried out using three meta-heuristic approaches namely Elitist Teaching learning based optimization, Differential evolution and Artificial Bee colony optimization. Furthermore, pareto optimal sets of solution obtained from each algorithm have been ranked using centroid based Fuzzy ranking method as discussed in section 4.4.2. The regression Equations (4.28- 4.31) obtained from ANOVA analysis haven used

for formulating the objective functions. In present multi-objective optimization regime only MRR have to maximized while OC, RCL and ta have to minimized. The tuning parameters for each algorithm were same as discussed in sections 4.4.1, 4.4.3 and 4.4.4. The results obtained from MOETLBO, MODE and MOABC after applying centroid based Fuzzy ranking method have been presented in Tables 4.33-4.35 in "Appendix (19 - 21)". For maintaining consistency in comparison of ETLBO, MODE and MOABC the number of function evaluations was set to 240000 evaluations for each algorithm. The results of optimization of μ-EDM process using ETLBO and MODE and MOABC are presented in Table 4.36 in "Appendix 22". From statistical point of view, the Best, Mean and the Worst solution set have been calculated. From Table 4.36 it can be observed that for MRR and OC, MOETLBO yielded the best i.e., maximum value of MRR and minimum value of OC. However, for RCL and TA the minimum value was obtained from MODE and MOABC. Furthermore, when mean value of solutions obtained from different algorithms was compared it has been observed that for MRR and RCL the mean value obtained from MOETLBO was higher than that of MODE and MOABC. Additionally, for the case of OC the mean value of solutions for MODE and MOABC was same, while for TA the mean value of solutions obtained from MODE was higher than MOETLBO and MOABC. Hence from the above results it can be concluded that none of algorithms ensure the best solutions for all process responses which justifies the existence of no free lunch theorems still holds valid for multi-objective regime.

4.9 FABRICATION OF MICRO-HOLE IN INCONEL-718 USING PLATINUM AS TOOL ELECTRODE

4.9.1. EXPERIMENTAL DETAILS

In third phase of experimentation the fabrication of micro-hole has been carried out in Inconel 718 with platinum as electrode tool material in micro-EDM operation. The experimental set up is given in Figure 4.1. The platinum electrode used is shown in Figure 4.35. The workpiece image is shown in Figure 4.36. Additionally, SEM images of micro-holes are given in Figure 4.37.

The Experimental condition for micro-hole machining on Inconel 718 are given in Table 4.37.

Table 4. 37: Experimental condition

Machine Tool	AGIETRON 250 C
Workpiece	25×15×1 mm Inconel 718 plate
Tool electrode	Platinum tool of diameter 0.5mm
Dielectric fluid	EDM 3033 oil
Polarity	Positive (workpiece '+ve' and tool '-ve')
Pulse-on time	20 to 40 µs
Pulse-off time	30 to 60 µs
Peak current	8 to 32 A
Voltage	30 to 40 V

Figure 4. 20:Platinum electrode

Figure 4. 21: Inconel 718 workpiece

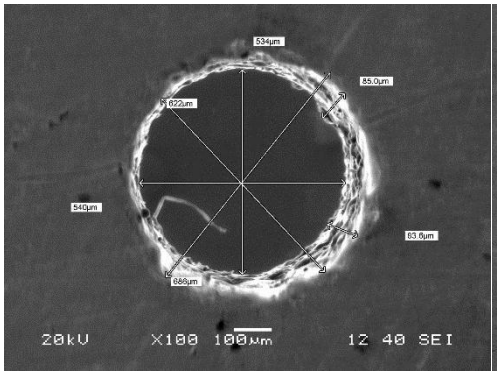

1st Hole Top view

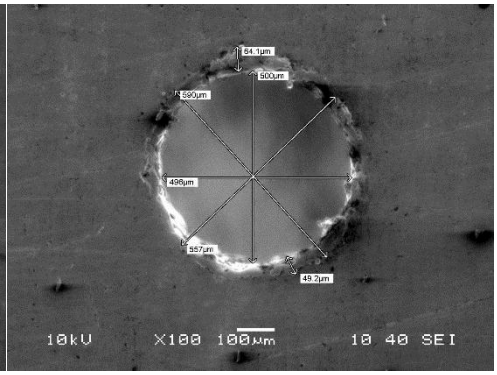

1st Hole Bottom view

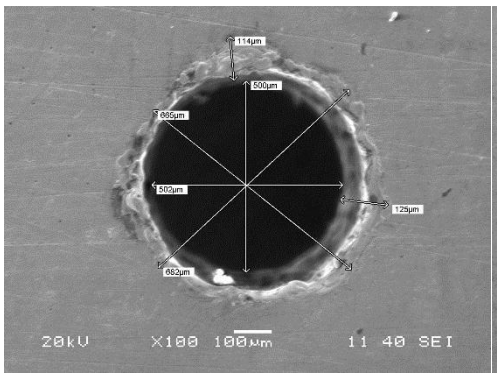

2nd Hole Top view

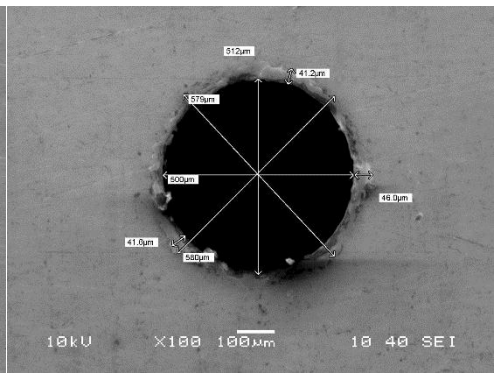

2nd Hole Bottom view

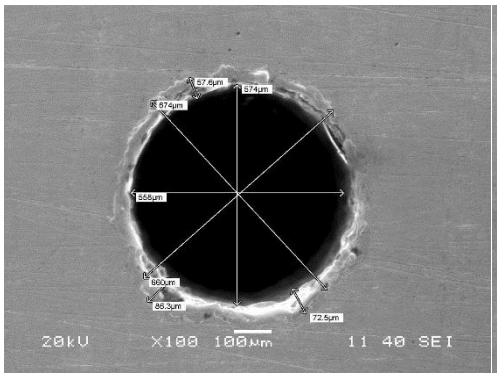

3rd Hole Top view

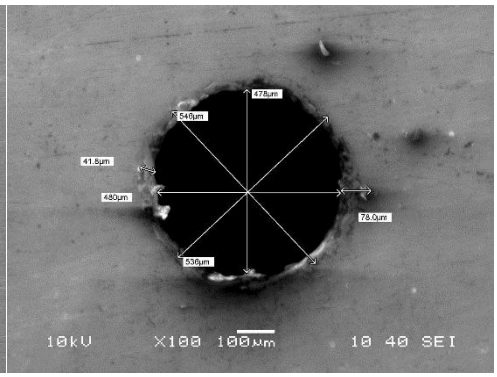

3rd Hole Bottom view

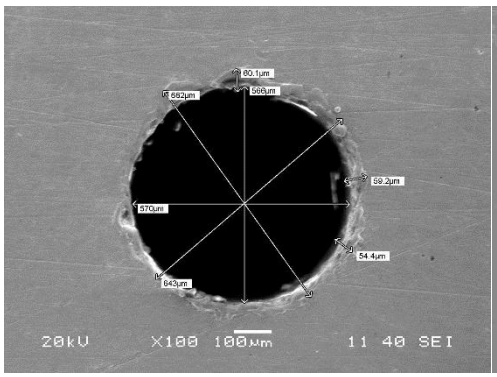

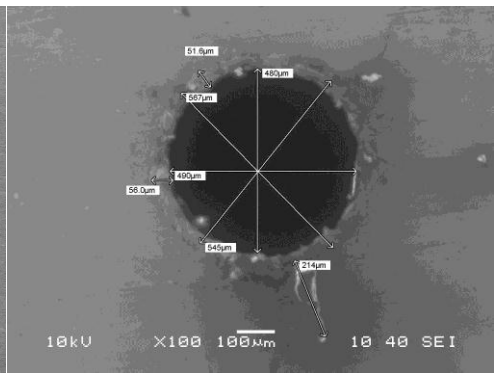

4th Hole Top view

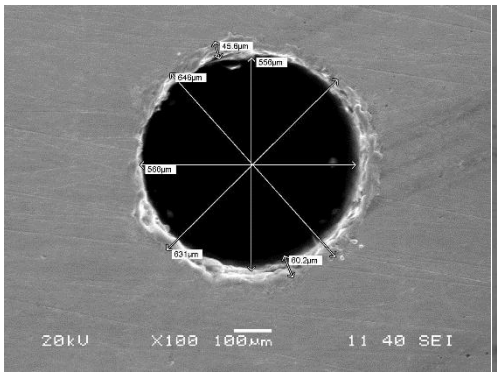

4th Hole Bottom view

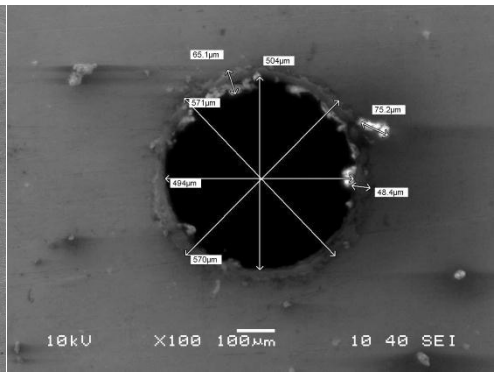

5th Hole Top view

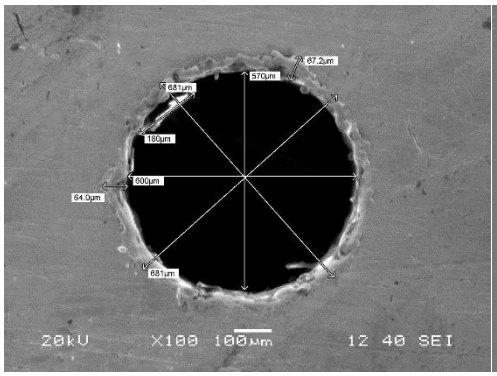

5th Hole Bottom view

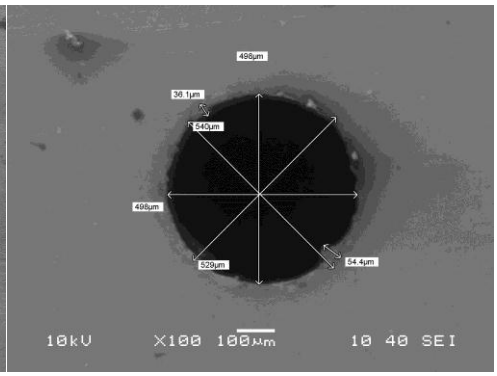

6th Hole Top view

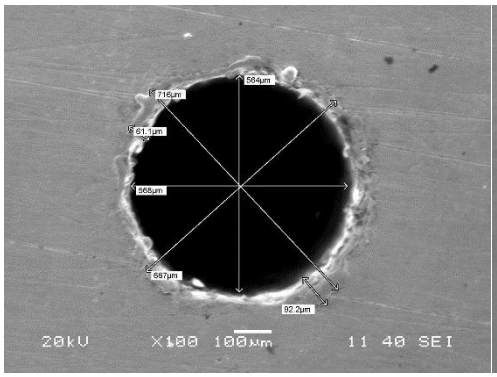

6th Hole Bottom view

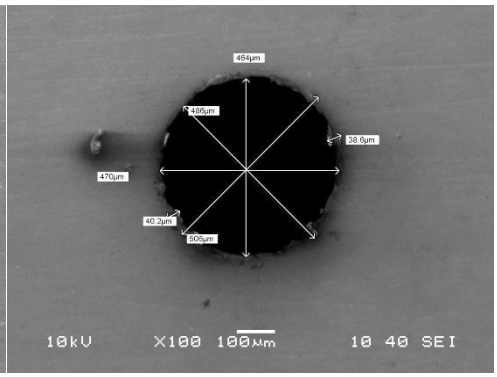

7th Hole Top view

7th Hole Bottom view

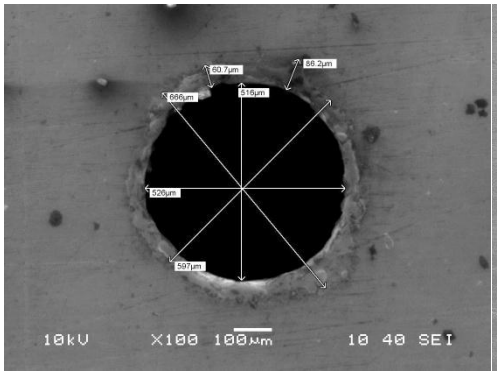

8th Hole Top view

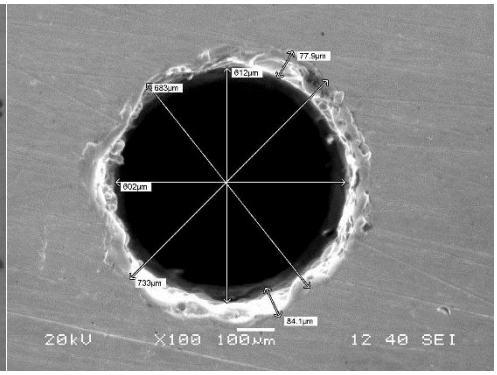

8th Hole Bottom view

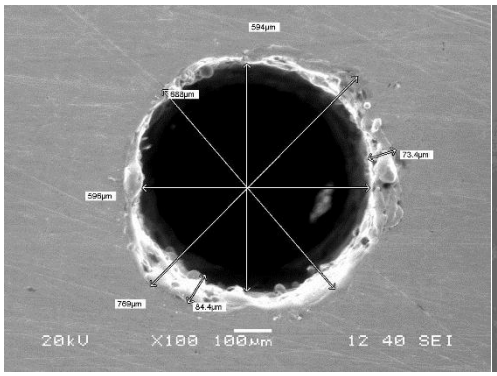

9th Hole Top view

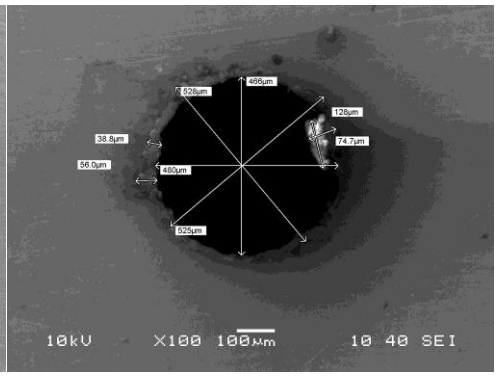

9th Hole Bottom view

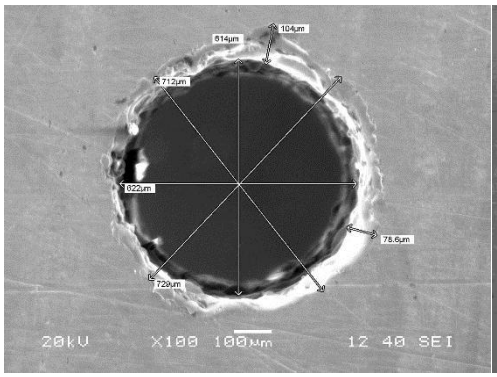

10th Hole Top view

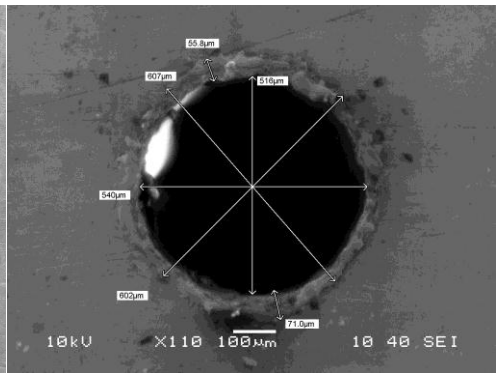

10th Hole Bottom view

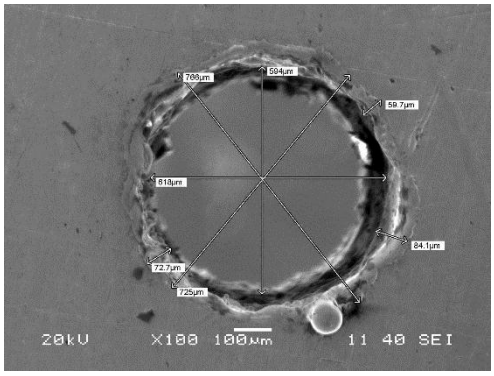

11th Hole Top view

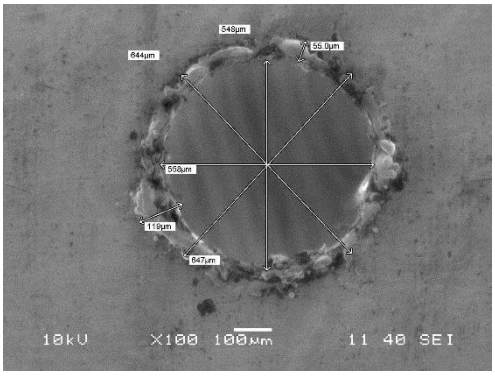

11th Hole Bottom view

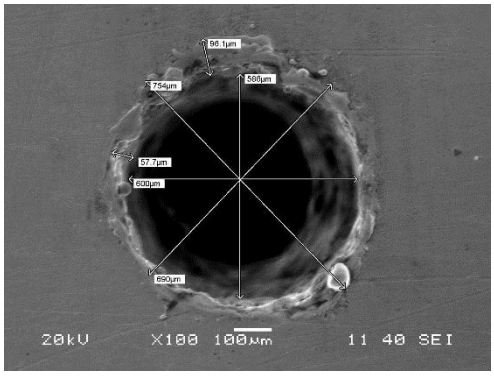

12th Hole Top view

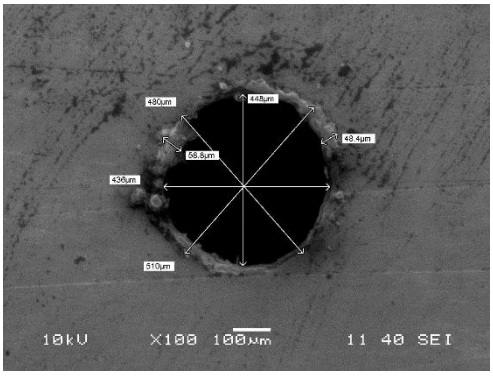

12th Hole Bottom view

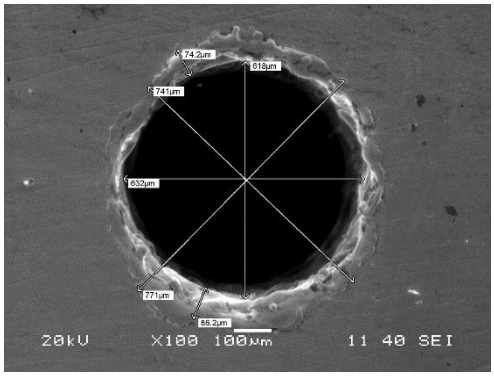

13th Hole Top view

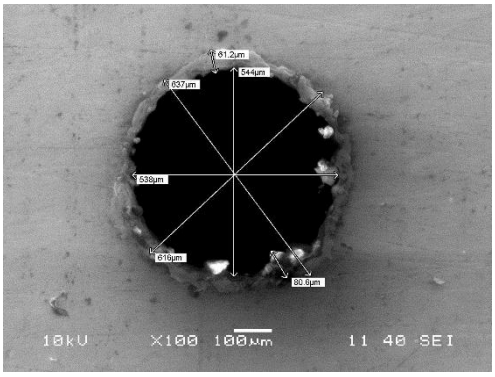

13th Hole Bottom view

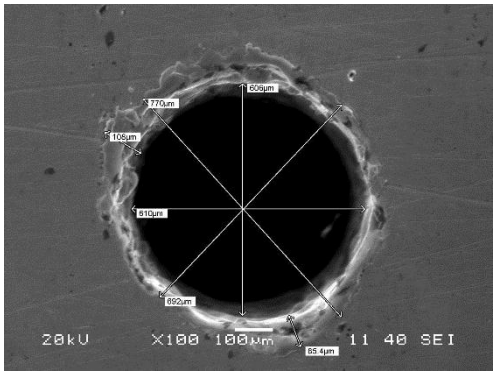

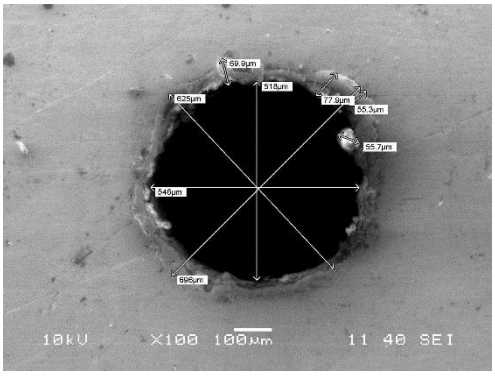

14th Hole Top view

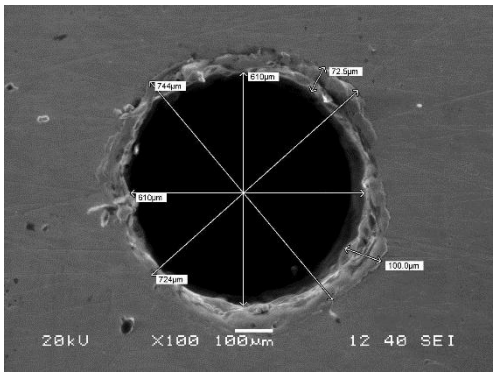

14th Hole Bottom view

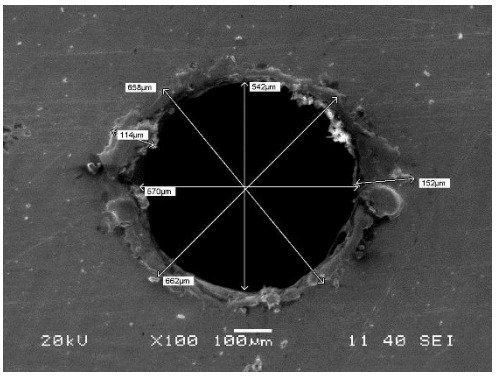

15th Hole Top view

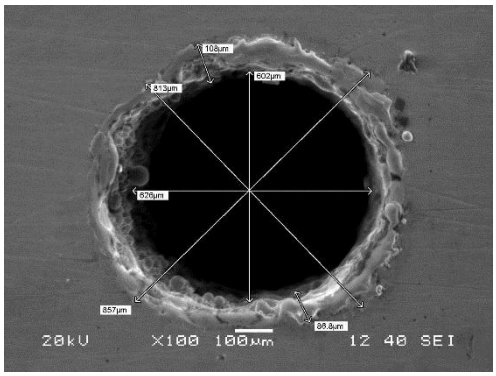

15th Hole Bottom view

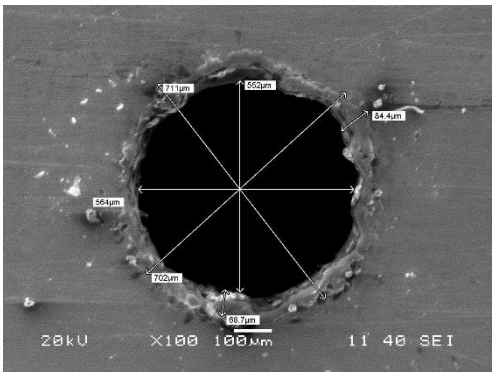

16th Hole Top view

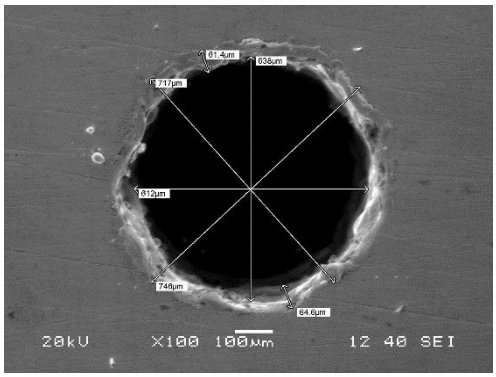

16th Hole Bottom view

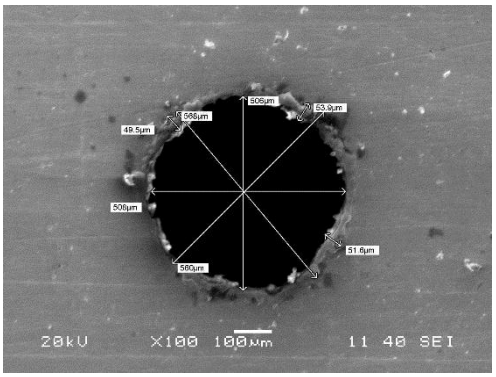

17th Hole Top view

17th Hole Bottom view

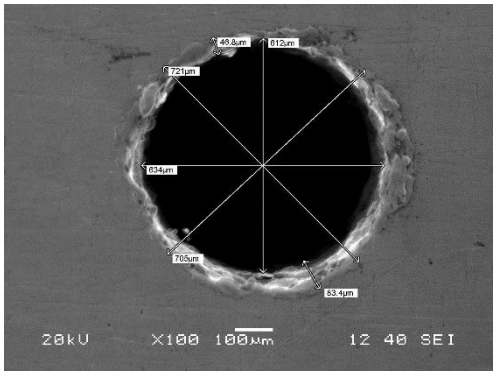

18th Hole Top view

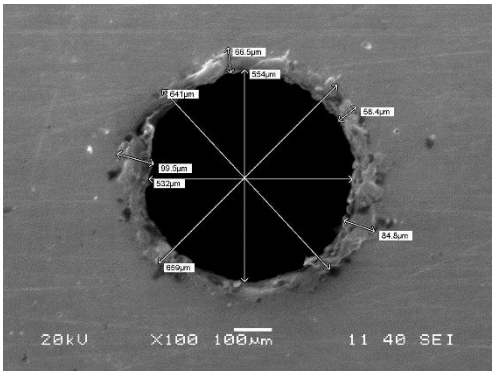

18th Hole Bottom view

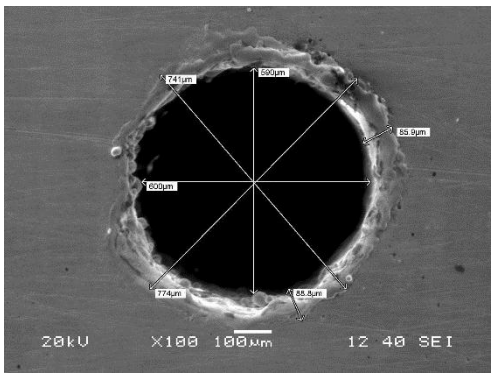

19th Hole Top view

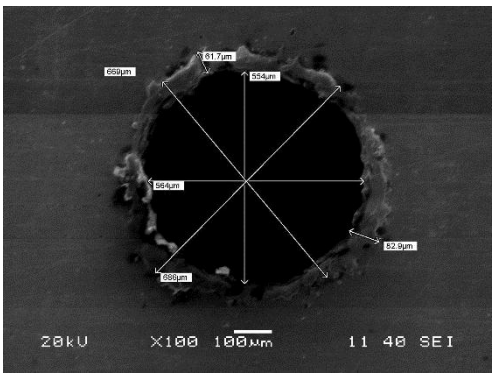

19th Hole Bottom view

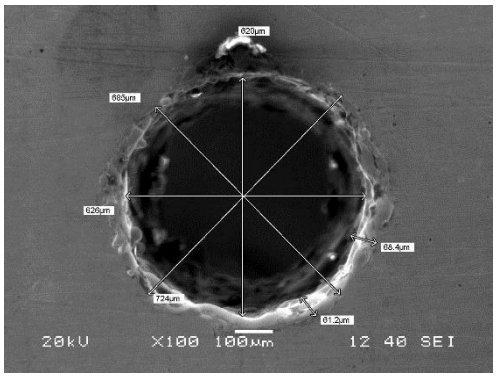

20th Hole Top view

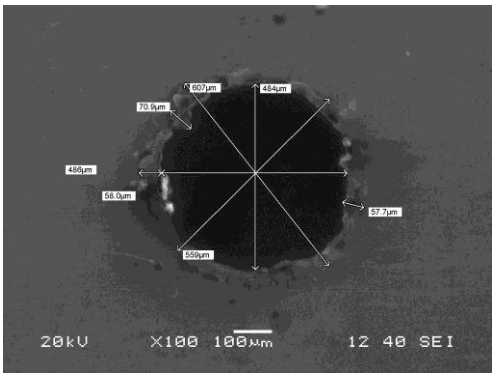

20th Hole Bottom view

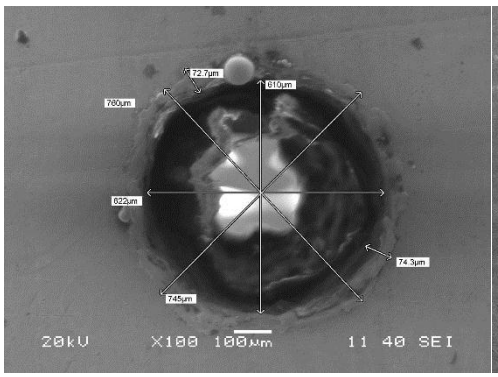

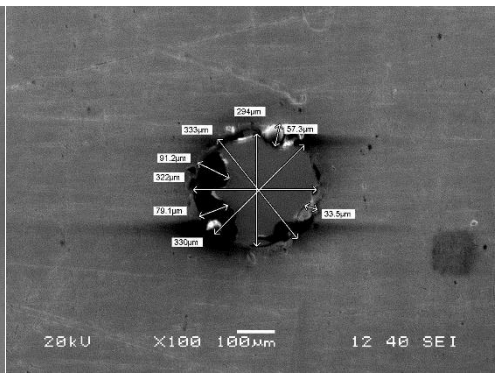

21st Hole Top view

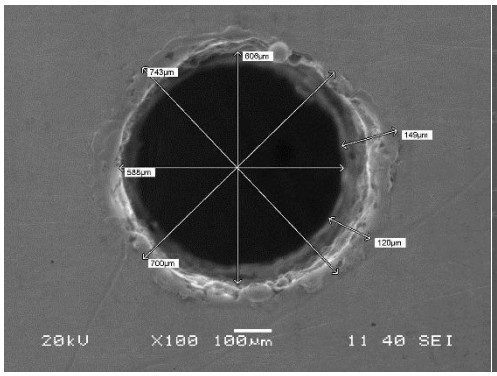

21st Hole Bottom view

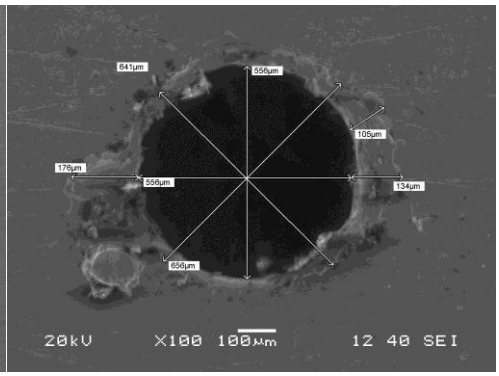

22nd Hole Top view

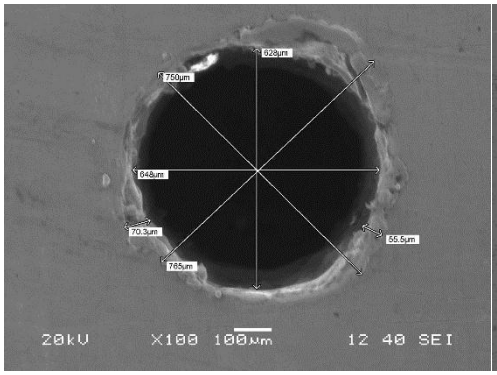

22nd Hole Bottom view

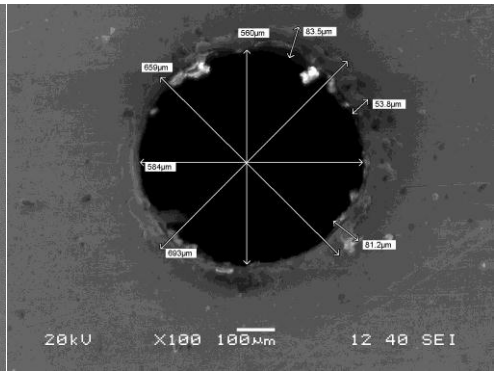

23rd Hole Top view

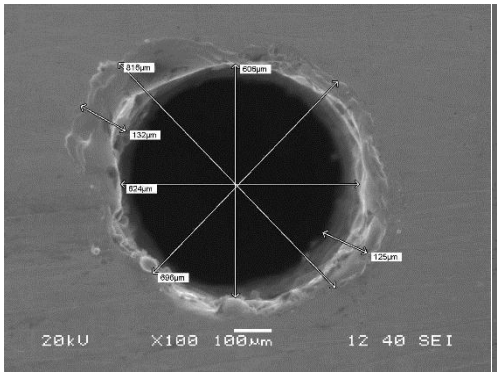

23rd Hole Bottom view

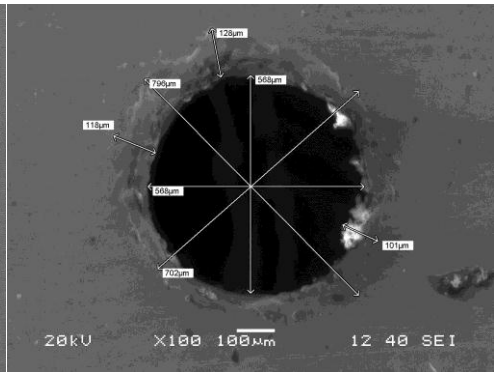

24th Hole Top view

24th Hole Bottom view

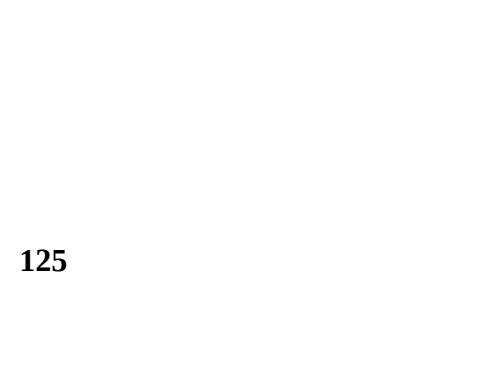

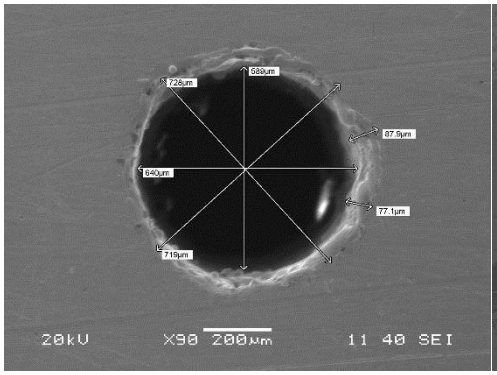

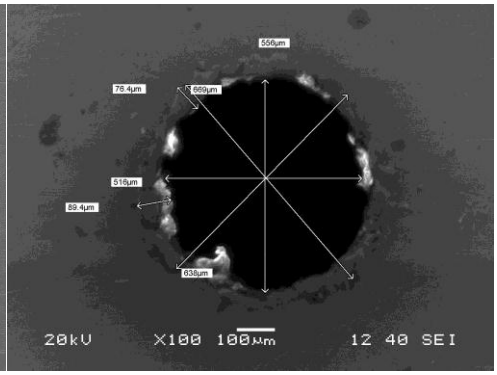

25th Hole Top view

25th Hole Bottom view

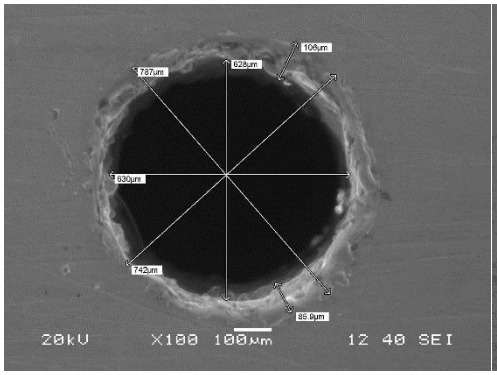

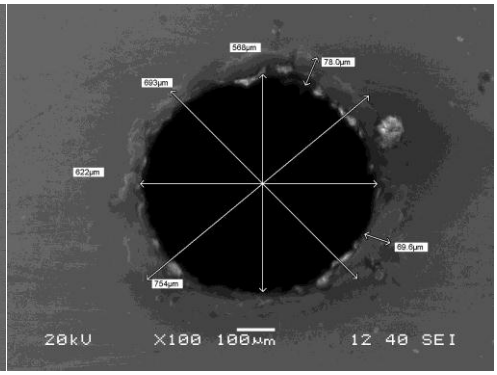

26th Hole Top view

26th Hole Bottom view

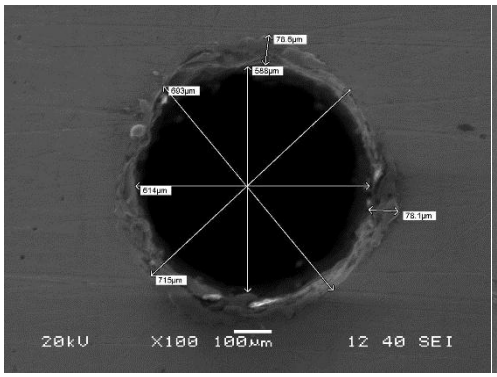

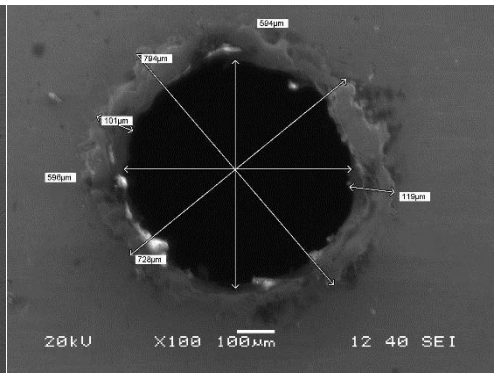

27th Hole Top view

27th Hole Bottom view

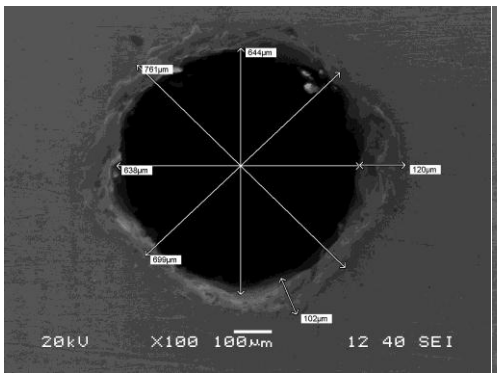

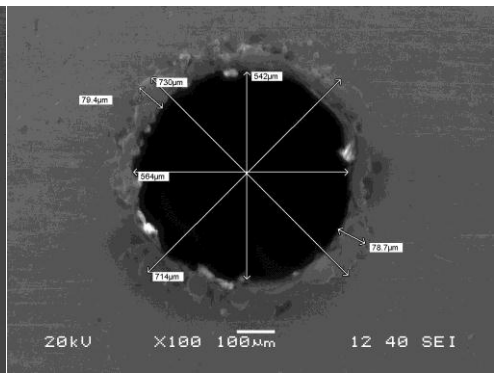

28th Hole Top view

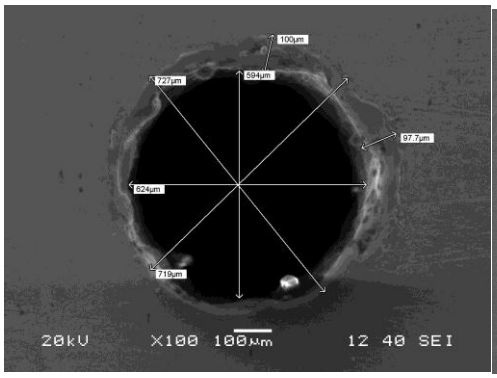

28th Hole Bottom view

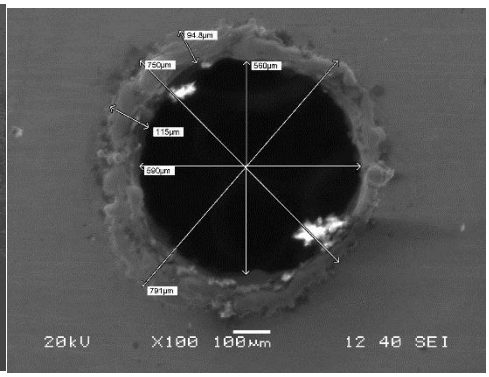

29th Hole Top view

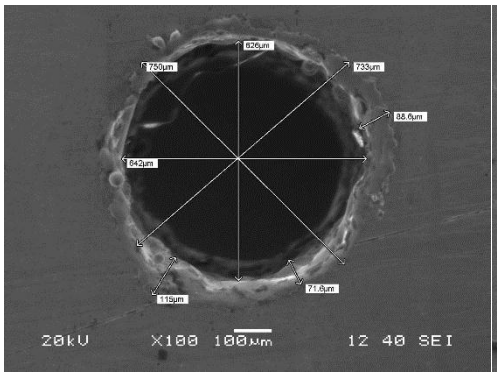

29th Hole Bottom view

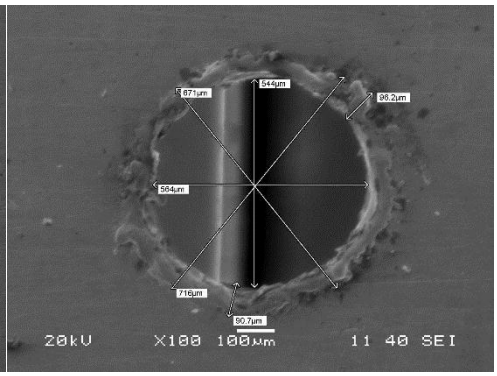

30th Hole Top view

30th Hole Bottom view

Figure 4. 22:SEM images of micro holes

4.9.2 RESPONSES SURFACE METHODOLOGY USING MULTIPLE REGRESSION ANALYSIS

The experimental layout was based on the central composite design (CCD). The design consists of 30 experiments with 16 (2^4) factorial points, eight star points to form a central composite design with $\alpha = \pm 2$, six center points for replication. The design was generated and analyzed using design expert software package. The experimental design matrix and output response values by experiment are shown in Table 4.38 in "Appendix 23". In this section, multiple regression models are developed to predict different process responses like MRR, RCL, TA and OC to improve the quality characteristics of the hole. Multiple regressions is commonly used as a traditional technique to predict the various machining processes. To solve the regression Equation, a matrix is formulated to determine the regression coefficients. The regression coefficients are used to estimate the MRR and overcut. The multiple regression analysis is used when more than two parameters are considered. In multiple regression analysis, linear equation is given by:

$$Y = a_0 + a_1 x_1 + a_2 x_2 + a_3 x_3 + \ldots\ldots n\ x_n$$

where $a_0\ a_1,\ a_2$ *and* a_3 are the regression coefficients and $x_1,\ x_2\ x_3$ *and* x_n are the predicted variables. Analysis of variance (ANOVA) was carried out to check the adequacy of the developed models. Table 4.39 shows the ANOVA for MRR after applying backward elimination process and as it can be observed from Table 4.39 that it comprises of only significant terms. The p value for the model is lowers than 0.05 (i.e. at 95% confidence level) indicates that the developed model is statistically significant. Further the model F-value of 50.41 implies the model is significant. There is only a 0.01% chance that an F-value this large could occur due to noise. In this case A, B, C, AC, AD, BC, BD, CD are significant model terms. The same and similar analyses were carried out for OC, RCL and TA. Furthermore, after backward elimination process the R-Squared value for MRR, OC, RCL and TA were found to be 0.9727, 0.9883, 0.9855 and 0.9140 respectively. However, the truncated models have lower R-Squared value than that of full quadratic model exhibiting significance of relationship between the response and the variables. This shows that second order models can explain the variation in the MRR, OC, RCL and TA up to the extent of 97.27%, 98.83%, 98.55% and 91.40 % respectively. The "Predicted R-Squared" values are in reasonable agreement with the "Adjusted R-Squared "values.

Table 4. 39: Analysis of Variance for MRR

Source	Sum of Squares	DOF	Mean Square	F Value	p-value Prob > F	Percentage contribution
Model	0.15	12	0.013	50.41	<0.0001	93.750
A-Voltage	2.902E-003	1	2.902E-003	11.55	0.0034	1.814
B-Peak current	0.023	1	0.023	91.68	< 0.0001	14.375
C-Pulse on duration	6.008E-003	1	6.008E-003	23.91	0.0001	3.755
AB	0.013	1	0.013	52.60	< 0.0001	8.125
AD	4.519E-003	1	4.519E-003	17.98	0.0006	2.824
BC	2.038E-003	1	2.038E-003	8.11	0.0111	1.274
BD	0.032	1	0.032	127.88	< 0.0001	20.000
CD	0.024	1	0.024	95.07	< 0.0001	15.000
A^2	0.012	1	0.012	47.22	< 0.0001	7.500
B^2	3.789E-003	1	3.789E-003	15.07	0.0012	2.368
C^2	2.231E-003	1	2.231E-003	8.88	0.0084	1.394
D^2	0.027	1	0.027	107.14	< 0.0001	16.875
Residual	4.272E-003	17	2.513E-004			
Lack of Fit	3.234E-003	12	2.695E-004	1.30	0.4113	Insignificant
Pure Error	1.038E-003	5	2.077E-004			
Corrected Total	0.16	29			R-Squared	0.9727
					Adj R-Squared	0.9534
					Pred R-Squared	0.9213

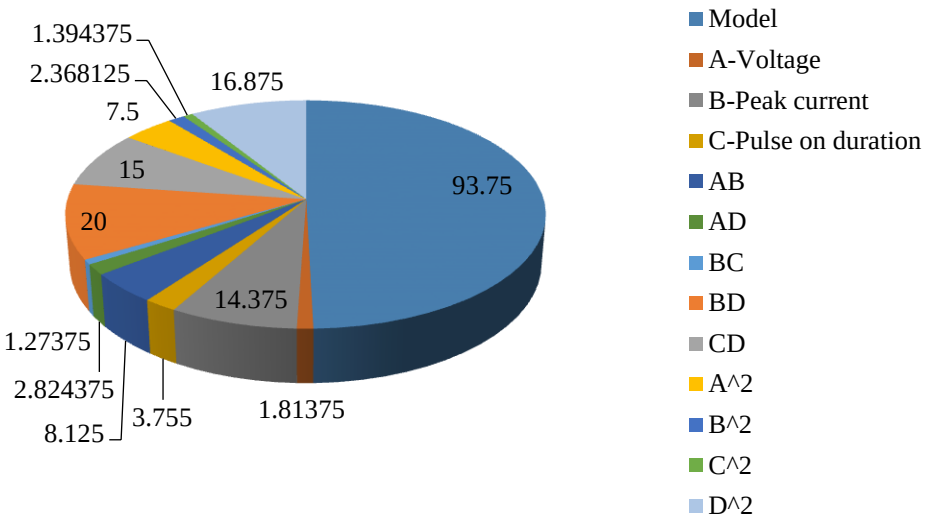

Figure 4. 38: Percentage contribution of process variables

On observing Table 4.39, it can be perceived that the interaction terms BD and CD significantly influence the MRR as their percentage contribution is 20 and 15 % respectively.

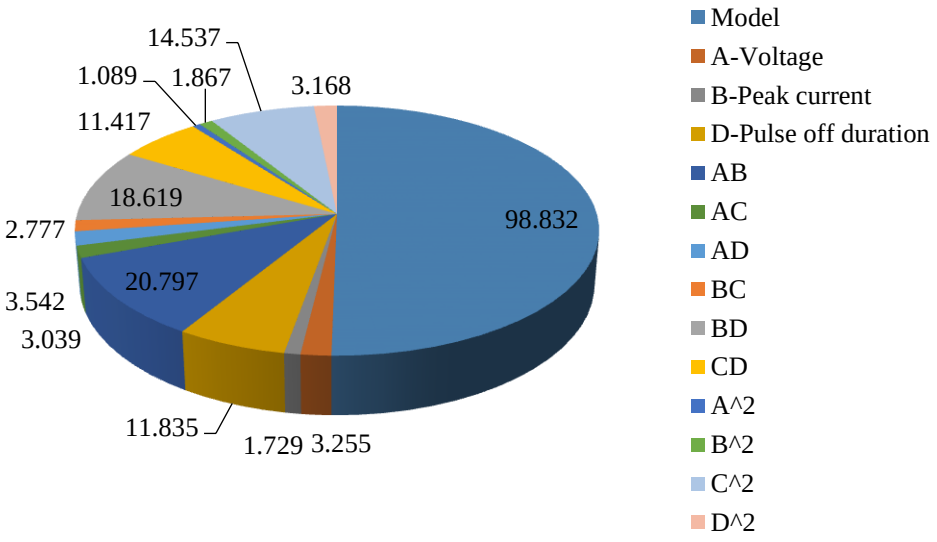

Figure 4. 39: Percentage contribution of process variables

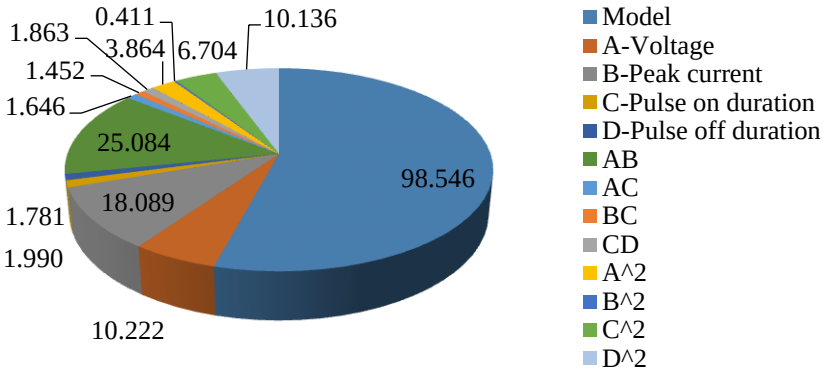

Figure 4. 40: Percentage contribution of process variables

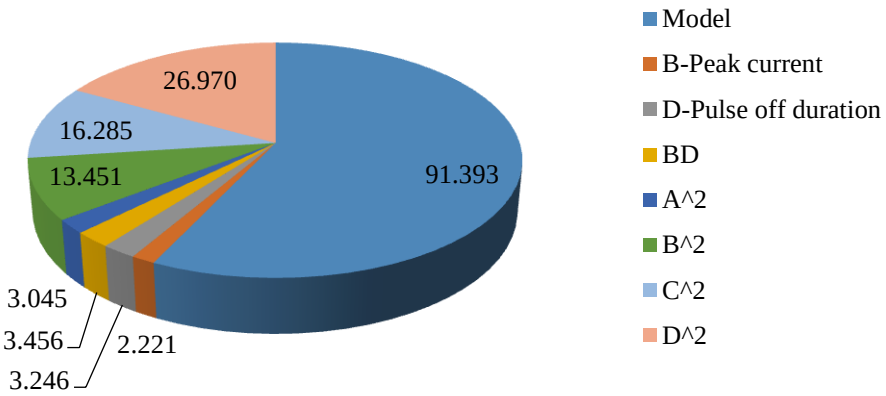

Figure 4. 41: Percentage contribution of process variables

4.9.3 ARTIFICIAL NEURAL NETWORK PREDICTION MODEL FOR PROCESS RESPONSES

ANN is one of the powerful data modeling tool provoked from the operation of human nervous system. It is a multiprocessor computing system, with simple processing elements. It is called as neurons, with a high degree of interconnection and simple scalar messages carried through the system. The main processing element is named as neuron. The information that is contained in each neuron is first weighed (w_{ij}), and summed up and considered as a net function (u_i). Then the value from the net function is transferred by a transfer function ($f(u)$) with activation value (a_i), to the next neuron. Each input is given a relative weight, which affects the impact of the input neurons. It has an adaptive coefficient that determines the strength of the input data.

4.9.4 THE NETWORK ARCHITECTURE

ANN architecture consist of many neurons interconnected, and this net forms a processing system. The Layers consist of processing elements that are called as neurons. A network with 4x12x1x4 architecture, which means 4 input (voltage, peak current, pulse on duration and pulse off duration neurons in the input layer, 12 neurons in the hidden layer and 4 outputs (MRR and Overcut, Recast layer thickness, and Taper Angle) in the output layer. Generally, in the multi-layer feed forward network, the size of hidden layers is one of the most important considerations when solving problems. Two hidden layers were adopted in this model. The inputs and outputs are normalized to gain better results. To train the developed model, 20 data sets were used which are tabulated in Table 4.40 in "Appendix 27". To train the developed model, 20 data sets were used. To test the ANN model, 10 data sets were used. A MATLAB program is written to train, test and predict the MRR and overcut values. The topology and training parameters are given in Table 4.41.

Table 4. 41: ANN topology and its training parameters

Parameters	Values
Number of input neurons	4
Number of hidden layers	1
Number of neurons in each hidden layer	12
Number of output neuron	1
Momentum factor	0.9
Learning rate	0.001
Number of iterations	500

The comparison has been done by randomly selected training data sets of each individual output and is as shown in Figures 4.42-4.45. The Figures indicated that the errors were within the acceptable limit, and hence ANN can be effectively used for the prediction of MRR, OC and RCL and Taper Angle in µ-EDM. Properly trained back-propagation network tends to give reasonable answers when presented with inputs that have never been fed before to it.

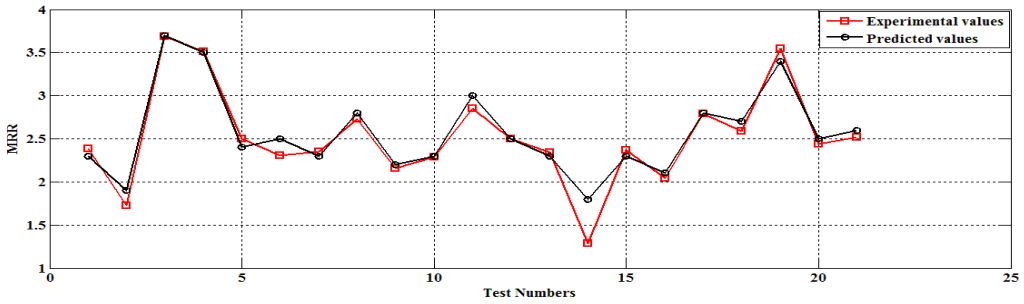

Figure 4. 42: Comparison of experimental and ANN output for MRR for training data.

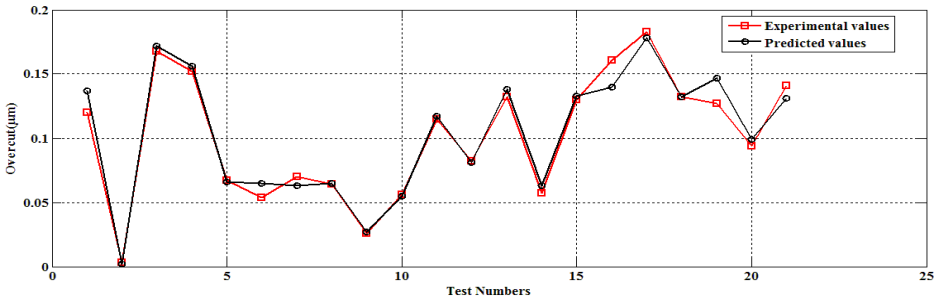

Figure 4.43:Comparison of experimental and ANN output for OC for training data

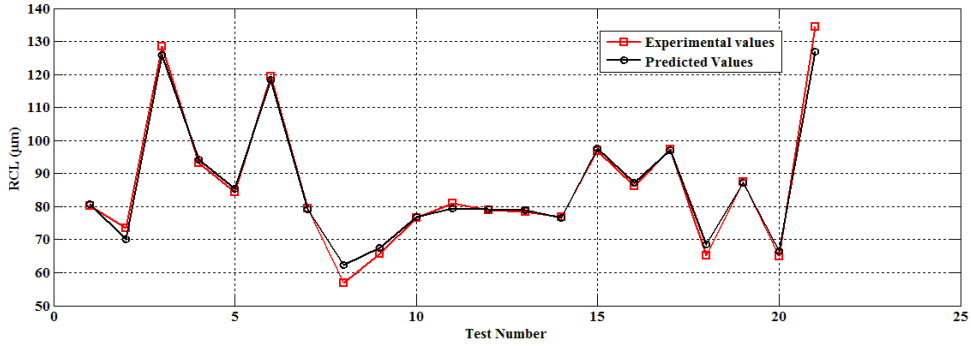

Figure 4. 44: Comparison of experimental and ANN output for RCL for training data

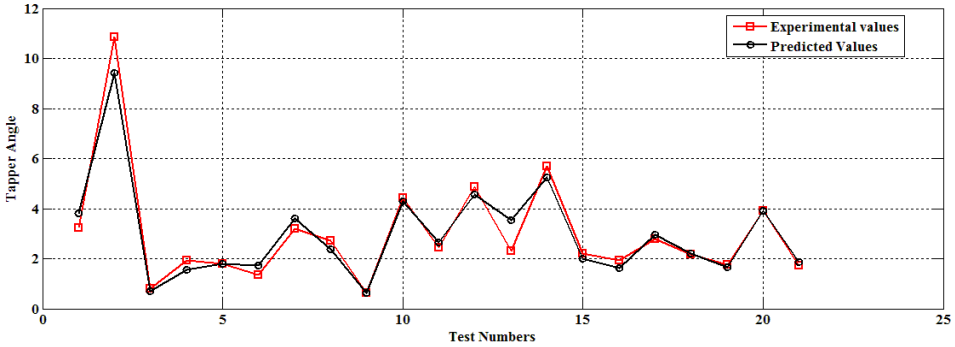

Figure 4. 45: Comparison of experimental and ANN output for TA for training data

The trained neural network was validated against another set of experimental data, termed as validation data set illustrated in Table 4.42 in "Appendix 28". The errors in prediction are also presented in Table 4.43. It can be seen from Table 4.43 in "Appendix 28" that the model predictions match the experimental data very closely except few data. Moreover, the average error in the prediction was -1.558 % for MRR, -0.535 % for OC, and 2.890 % for RCL and -11.515 % for TA respectively. The total average prediction error of the network was predicted as -10.719 % which indicates that the model is over predicting the values. The developed ANN model was tested by repeating few experiments randomly from the entire data set for checking the predictive accuracy of the developed model. Figures (4.46- 4.49) indicated the errors between predicted and experimental values for all process responses.

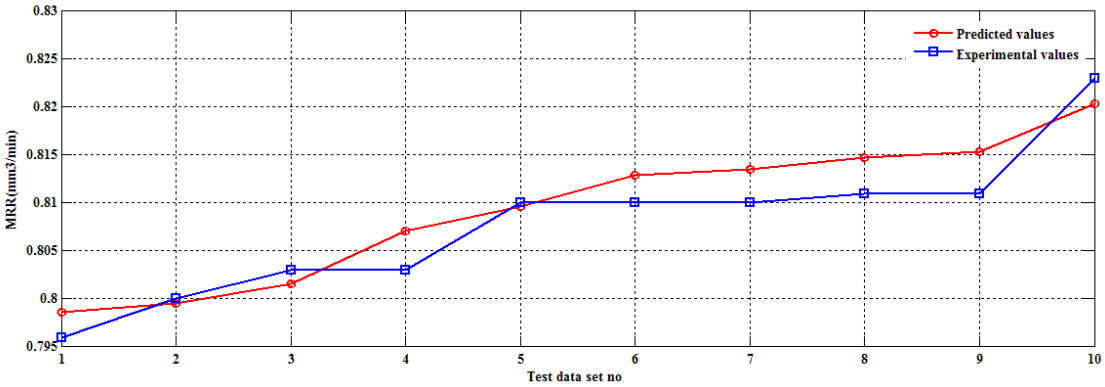

Figures 4.46: Errors between predicted and experimental values of MRR during testing

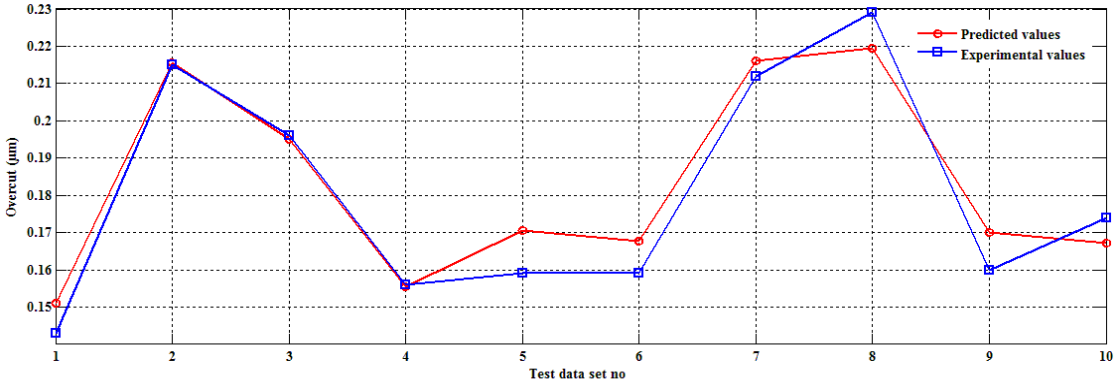

Figures 4.47: Errors between predicted and experimental values of OC during testing

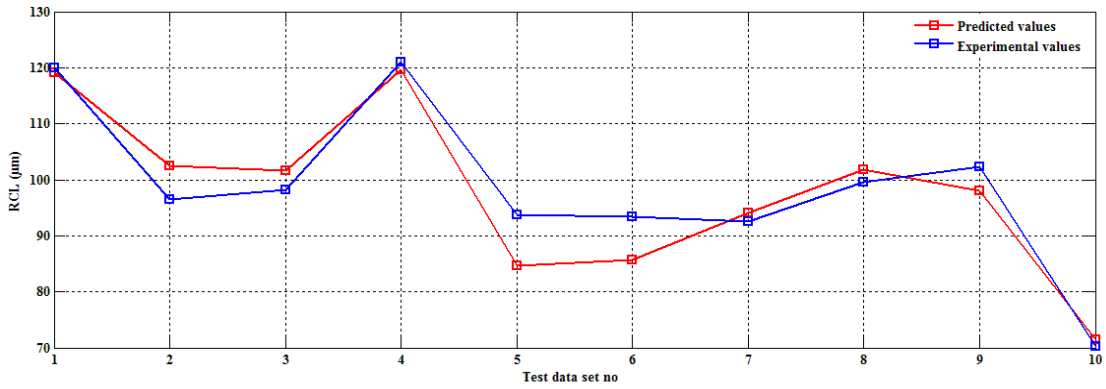

Figures 4.48: Errors between predicted and experimental values of RCL during testing

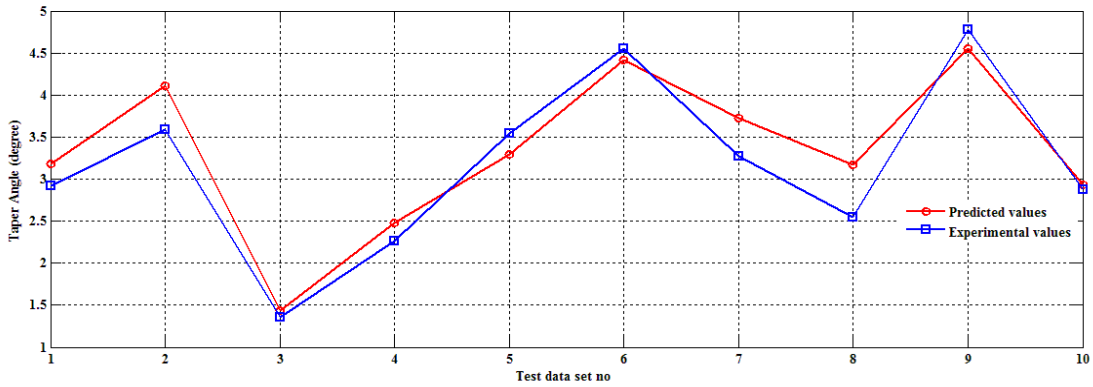

Figures 4.49: Errors between predicted and experimental values of TA during testing

Table (4.44 - 4.45) in "Appendix 29" contains testing of the developed model with experimental data and the predicted output and percentage error in prediction of MRR, OC, RCL and TA were within acceptable limits. It is observed that the total average prediction error is -7.492 % which is implies level of over prediction.

4.10 ANFIS MODELING

The adaptive neuro-fuzzy inference system has been used to predict MRR, OC, RCL and TA. For this purpose, the MATLAB 2012b package (ANFIS toolbox) has been utilized. Prediction of MRR, OC, RCL and TA of the micro-EDM process by ANIFS comprises of three main phases, training, validation and testing. A similar methodology was adopted as mentioned in section 4.4. However, for the purpose of comparing the predictive tendency with ANN model same data was used for training, validation and testing as it was used for development of ANN model. Total average error (TAE) as mentioned in Equation 4.14 is considered as selection criteria for comparison of all existing networks and final selection is made of the most accurate one. The value of error goal was set at 0.03, and the iteration number was 500 epochs. Various structures were

tested of ANFIS model for each response (material removal rate, overcut recast layer thickness and taper angle), it was obtained that structures with 16 numbers of membership functions (2 MFs for each input) had the lowest values of TAE for each response. In this work various types of MFs namely triangular, trapezoid, generalized bell and Gaussian have been practiced. Table 4.56 represents training and validation error of ANFIS models for different membership functions. TAE for MRR, OC, RCL and TA have been presented in Table 4.57.

Table 4.56: Training and validation error

Type of membership function	MRR		OC		RCL		TA	
	Training error	Validation error	Training error	Validation error	Training error	Validation error	Training error	Validation error
Triangle	0.00871	0.00871	0.02160	0.02160	2.38990	2.38740	0.68635	0.68628
Trapezoid	0.00544	0.00543	0.02059	0.02059	2.13580	2.13560	0.56457	0.56406
Generalized bell	0.00272	0.00271	0.02042	0.02042	2.08010	2.18000	0.49767	0.49767
Gaussian	0.00537	0.00536	0.02061	0.02060	2.12680	2.12660	0.56775	0.56754

Table 4.57: TAE for process responses

Type of membership function	MRR Total Average error	OC Total Average error	RCL Total Average error	TA Total Average error
Triangle	0.008708	0.021602	2.38865	1.20513
Trapezoid	0.005436	0.020586	2.1357	1.07814
Generalized bell	0.002714	0.02042	2.13005	1.07524
Gaussian	0.005364	0.020605	2.1267	1.07365

Results indicated that the generalized bell function leads the lowest values of TAE for MRR, OC TA, while for RCL Gaussian function yielded lowest value of TAE.The developed ANFIS model was tested for checking the predictive accuracy of the developed model. Tables (4.58 -4.59) in “Appendix 30” contains testing of the developed

model with experimental data and the predicted output and percentage error in prediction of MRR, OC and RCL were within acceptable limits. It is observed that the total average prediction error is -5.548 % which implies level of over prediction.

4.10.1 MULTI-OBJECTIVE OPTIMIZATION

The present work is aimed to maximize the MRR and to maintaining a minimum value for Overcut effect Recast layer thickness and Taper angle. It is difficult to obtain the same, as both MRR as well as other process responses increase simultaneously. Thus, there is a conflict and consequently, it became an ideal problem to be tackled using a multi-objective optimization. In the present section multi-objective optimization has been carried out using three meta-heuristic approaches namely Elitist Teaching learning based optimization, Differential evolution and Artificial Bee colony optimization. Furthermore, pareto optimal sets of solution obtained from each algorithm have been ranked using centroid based Fuzzy ranking method as discussed in section 4.4.2. The regression Equations (4.32- 4.35) obtained from ANOVA analysis haven used for formulating the objective functions. In present multi-objective optimization regime only MRR have to maximized while OC, RCL and ta have to minimized. The tuning parameters for each algorithm were same as discussed in sections 4.4.1, 4.4.3 and 4.4.4. The results obtained from MOETLBO, MODE and MOABC after applying centroid based fuzzy ranking method have been presented in Tables 4.60-4.62 in "Appendixes 31-33". In this multi-objective optimization problem, equal weights have been considered, for giving equal significance to all the four objectives MRR, OC, RCL and TA and. Thus, W_{MRR}, W_{OC}, W_{RCL} W_{TA} are all equal to 1/4. For maintaining consistency in comparison of MOETLBO, MODE and MOABC the number of function evaluations was set to 240000 evaluations for each algorithm. The results of optimization of µ-EDM process using MOETLBO and MODE and MOABC are presented in Table 4.63.

Table 4.63: Optimization results

Response	MOETLBO			MODE			MOABC		
	Best	Mean	Worst	Best	Mean	Worst	Best	Mean	Worst
MRR ($mm^{3/}$min)	0.716	0.587	0.543	0.651	0.463	0.310	0.648	0.517	0.224
OC(µm)	0.156	0.160	0.169	0.160	0.167	0.180	0.170	0.170	0.169
RCL(µm)	145.155	79.624	52.180	147.799	92.965	57.578	150.513	108.364	69.715
TA (degree)	0.465	2.363	2.021	0.097	2.506	0.629	4.104	6.402	6.725

The Best, Mean and the Worst solution set has been calculated. From Table 4.63 it can be observed that MOETLBO yielded maximum MRR value of 0.716 mm^3/min and

minimum values of OC and RCL as 0.156 µm and 145.155 µm respectively. MODE yielded minimum values of TA as 0.097°. Furthermore, when mean value of solutions obtained from different algorithms was compared it has been observed that for MRR the mean value obtained from MOETLBO was higher than that of MODE and MOABC. Additionally, for the case of OC, RCL and TA the mean value of solutions obtained from for MOABC was higher than that of MOETLBO and MODE. Hence from the above results it can be concluded that none of algorithms ensures the best solutions for all process responses which justifies the existence of no free lunch theorems still holds valid for multi-objective regime.

4.10.2RESULTS AND DISCUSSIONS

The total average prediction error obtained from ANN and ANFIS models for different combinations of workpiece and electrode materials have been tabulated in Table 4.64. Furthermore, it can be observed from the Table 4.64 that with exactly same training, validation and testing data sets developed ANN and ANFIS models yielded different total average prediction error during testing of models. However, the predictive accuracy of ANFIS models is better than ANN models for fabrication of micro holes using copper and platinum as electrode materials, while for Graphite as electrode material the predictive accuracy of ANN model was found to be superior to ANFIS model. Additionally, both models yielded negative total average prediction error which indicates slight level of over prediction.

Table 4.64: ANN and ANFIS models results

S.No	Workpiece	Tool	ANN Model	ANFIS Model
			Total average prediction error	Total average prediction error
1	Inconel 718	Copper	-17.901%	-7.080 %
2	Inconel 718	Graphite	4.908 %	-6.629 %
3	Inconel 718	Platinum	-7.492 %	-5.548 %

4.11 CONCLUSIONS

In the present investigation, fabrication of micro-holes in Inconel-718 has been carried out using copper, graphite and platinum as electrode tool material. Micro-holes are fabricated as per the Central composite design using response surface methodology. MRR, the thickness of recast layer, radial overcut and taper of the micro-hole have been measured as the responses. On visual inspection it was found that for higher pulse on time, the exit portion of the micro-hole has not been uniformly machined. As pulse-on time increases, the tool wear at the front tip of the tool also increases rapidly resulting eventually in a round or non-uniform shape at the front of the tool and causes uneven machining at the exit or bottom portion of the micro-hole.

1. Results of Multi-objective optimization using MOETLBO, MODE and MOABC indicated that when comparisons are done on the basis of equal no of function evolutions and same population size none of the algorithms guarantees a perfect solution satisfying different conflicting objectives simultaneously. Since "no free lunch theorems" still holds, therefore none of the above mentioned algorithms should be treated superior. Hence on the basis of priority for a certain response the process engineer can selected the Pareto optimal solutions obtained from different methods.
2. It has been found that neural configuration with feed-forward back propagation of 4-12-4 structure was found to give reasonably good prediction accuracy. It was found that average error in the prediction of developed model was very small indeed while doing the micro-EDM operation in Inconel-718 using copper as electrode. It was, -1.052 % for MRR, -1.097 % for OC, -3.667 % for RCL and -12.085 % for TA with the total average prediction error as -17.901 % for fabrication of micro-holes.
3. For fabrication of micro-hole in Inconel 718 with graphite as electrode, the error was less than that of copper. It was, 0.215 % for MRR, 5.44 % for OC, and 0.582 % for RCL and -1.334 % for TA with the total average prediction error as 4.908 % for developed ANN model.

4. For fabrication of micro-hole in Inconel 718 with platinum as electrode, the total average prediction error of -7.492 % was observed. It was, -0.205 % for MRR, -1.792 % for OC, and 0.843 % for RCL and -6.339 % for TA for developed ANN model.
5. During modeling of MRR, OC, RCL and TA by ANFIS, the 2-2-2-2 structure was selected as the best topography due to its lowest total average error and faster performance. The total average prediction error for different combination of electrode materials with Inconel 718 as workpiece material was found to be -7.080 % for copper, -6.629 % for graphite and -5.548 % for platinum.

CHAPTER 5

EXPERIMENTAL INVESTIGATION OF MICRO HOLE DRILLING ON TITANUIM GRADE 5

5.1 INTRODUCTION

The continuous introduction of new materials and the endless demands for engineers to produce complicated shapes within tighter tolerances in many industrial applications is gradually increasing. From this point of view, machining special materials such as titanium is present great importance. The usage of titanium and its alloys is increasing in many industrial and commercial applications because of these materials excellent properties such as a high strength–weight ratio, high temperature strength and exceptional corrosion resistance. The alloys are extensively used in aerospace, biomedical applications and in many corrosive environments. Titanium alloys have found very wide application areas of aerospace, such as jet engine and airframe components, automotive, medicine and dentistry due to their excellent corrosion resistance, lightweight and mechanical properties (Hascalık and Caydas2007). However, the machinability of titanium and its alloys is considered to be rather poor owing to several inherent properties of materials. Poor thermal conductivity, chemically reactivity and low elastic modulus are the common problems. The conventional machining processes are unable to provide good machining characteristics on titanium alloys. Titanium alloys are generally used for a component which requires the greatest reliability and therefore the surface integrity must be maintained. Therefore, when machining any component, it is essential to satisfy surface integrity requirements. In the present investigation, fabrication of micro-holes in Titanium alloy (Ti–6Al–4V) has been carried out using copper, graphite and platinum as electrode tool material. Micro-holes are fabricated as per the Central composite design using response surface methodology. MRR, the thickness of recast layer, radial overcut and taper angle of the micro-hole have been measured as the responses. The qualities of micro-holes have been investigated. Response surface methodology (RSM) was used to identify the effects of process variables on process responses. Further, artificial neural network modeling has been carried out for prediction

of process responses. Multi-objective optimization using metaheuristic algorithms like MOETLBO, MODE and MOABC have been carried out

5.2 EXPERIMENTAL DETAILS

Experimentation Investigation using Titanium alloy (Ti–6Al–4V) as workpiece material has been carried out in three different phases. In first phase fabrication of micro holes was drilled by using electrolytic copper in the form of cylindrical rod, whereas in the second and third phase micro holes have been drilled using Graphite and Platinum.

5.2.1 DESIGN OF EXPERIMENTS

The experimental layout was based on the central composite design (CCD). The design consists of 30 experiments with 16 (2^4) factorial points, eight star points to form a central composite design with $\alpha=\pm2$, six centre points for replication. The design was generated and analyzed using Design Expert software package. Table 5.1 presents process factors and their levels.

Table 5. 1:Process parameters and their levels for machining experiments

Process parameters	Symbol	Units	Low	High
Voltage (V)	A	Volt	30	60
Peak Current (I_p)	B	Ampere	10	40
Pulse on duration (T_{on})	C	µs	40	80
Pulse off duration (T_{off})	D	µs	20	30

5.2.2 EXPERIMENTAL SETUP and MATERIALS USED

In present investigation fabrication of micro holes was carried out using sinking EDM machine with built in computer numeric control as mentioned in previous chapter. The holes were fabricated on a rectangular shaped work piece specimen made of Titanium alloy (Ti–6Al–4V) having a mean thickness of 1 mm, length 25 mm, and width 15 mm which is presented in Figure 5.1.

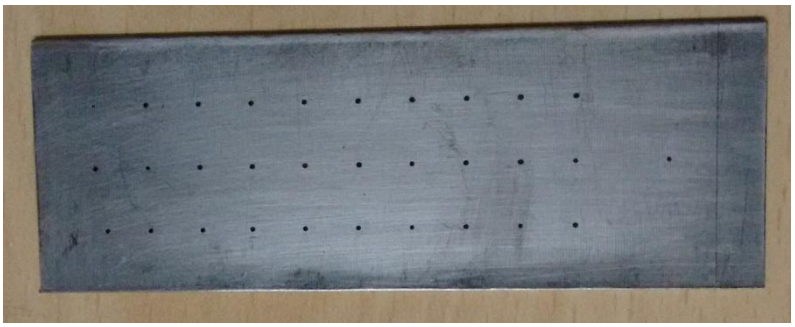

Figure 5. 1:Titanium workpiece

The physical properties of workpiece have been presented in Table 5.2. Electrolytic copper in the form of cylinder with 0.5mm diameter was used as tool material.

Electrolyte was fed externally to the cutting zone through the dielectric pumping system incorporated with machine. EDM 3033 oil was used as a dielectric instead of distilled water because of its low resistivity and electrochemical action. Based on preliminary experimental runs, the source voltage (V), Peak current (I_p), Pulse on duration (T_{on}) and Pulse off duration (T_{off}) were selected as four significant process parameters. The machining time (T_m), recast layer thickness (RCL), Overcut (OC) and taper of micro-hole were measured. The hole overcut and recast layer thickness were examined using Scanning electron microscope. The measurement was done from various positions and an average value has been considered. For determining machined hole overcut, the diameter of hole at entrance side was measured by scanning electron microscope.

Table 5. 2:Properties of Titanium

Work material	Ti–6Al–4V
Hardness (HV20)	600
Melting point (8C)	1660
Ultimate tensile strength (MPa)	832
Yield strength (MPa)	745
Impact-toughness (J)	34
Elastic modulus (GPa)	113

The microscopic view of micro drilled holes measured from both top and the bottom surface of workpiece are shown in Figure 5.2.

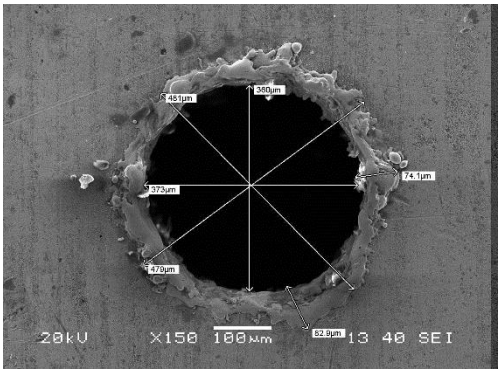

1st Hole Top view

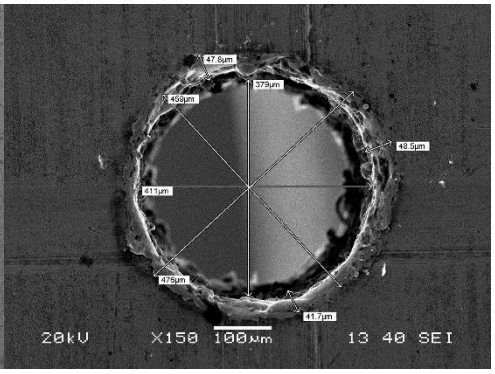

1st Hole Bottom view

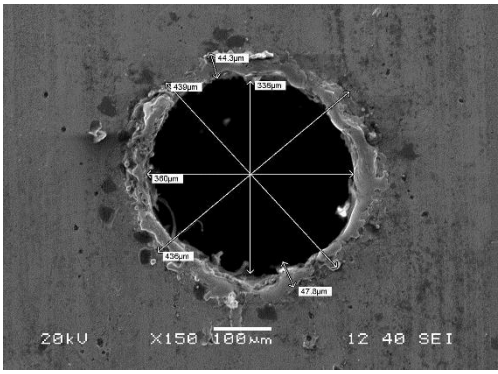

2nd Hole Top view

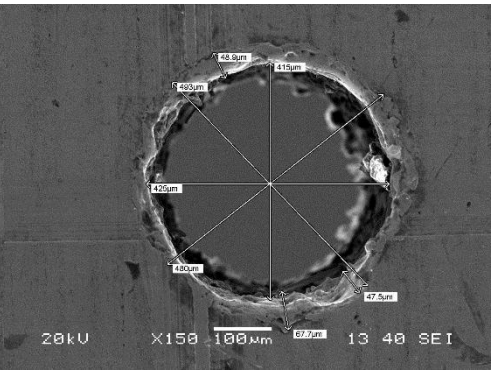

2nd Hole Bottom view

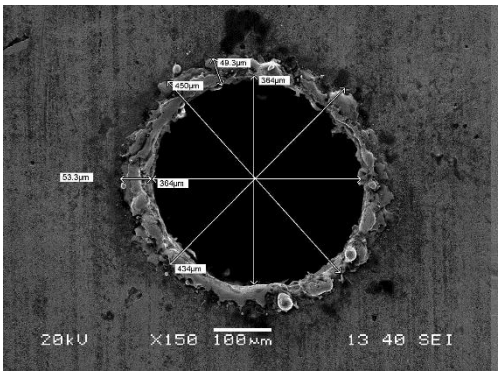

3rd Hole Top view

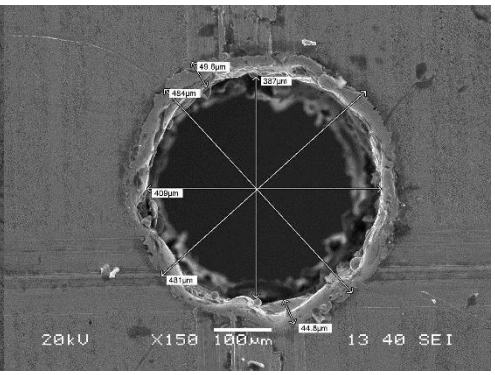

3rd Hole Bottom view

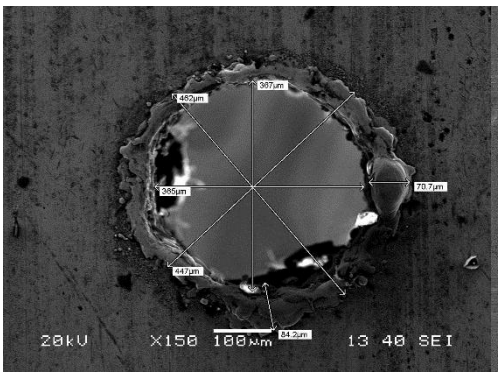

4th Hole Top view

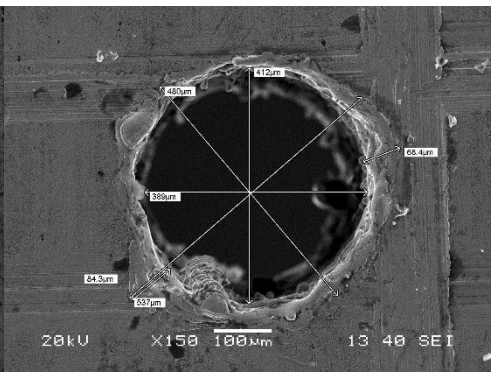

4th Hole Bottom view

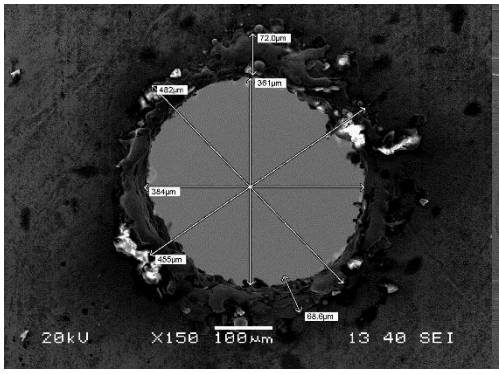

5th Hole Top view

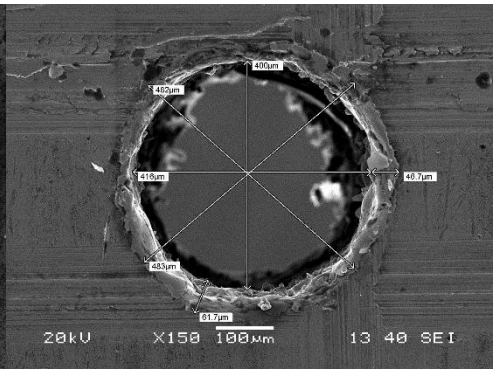

5th Hole Bottom view

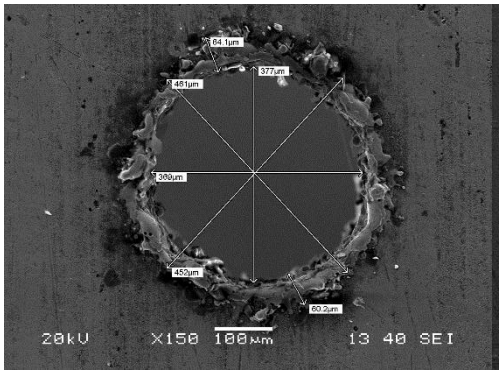

6th Hole Top view

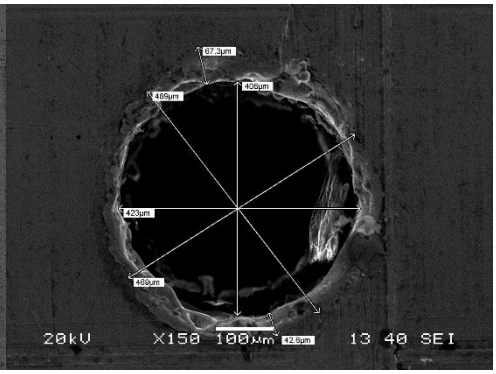

6th Hole Bottom view

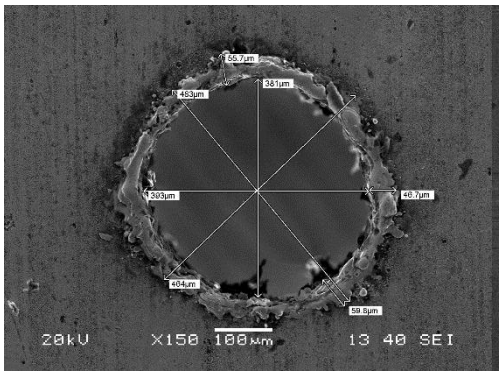

7th Hole Top view

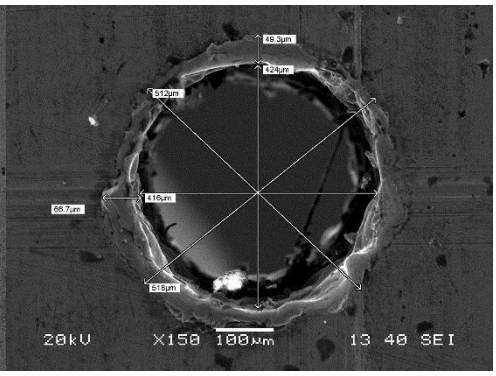

7th Hole Bottom view

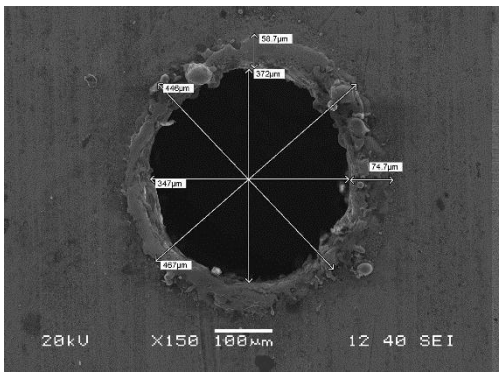

8th Hole Top view

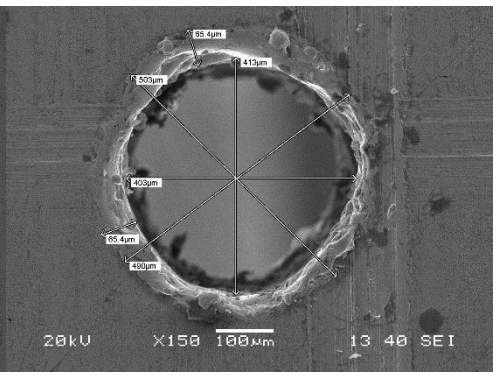

8th Hole Bottom view

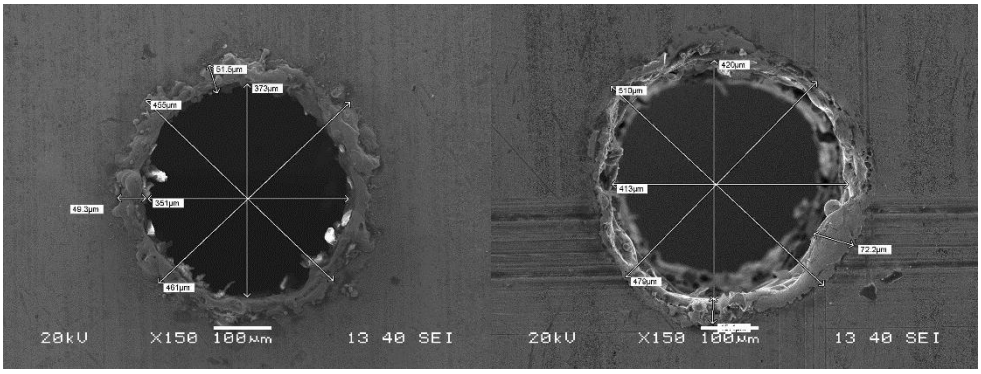

9th Hole Top view 9th Hole Bottom view

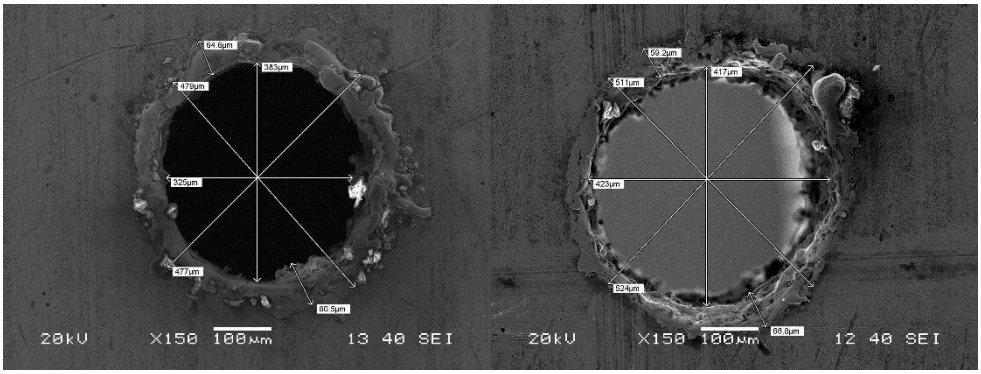

10th Hole Top view 10th Hole Bottom view

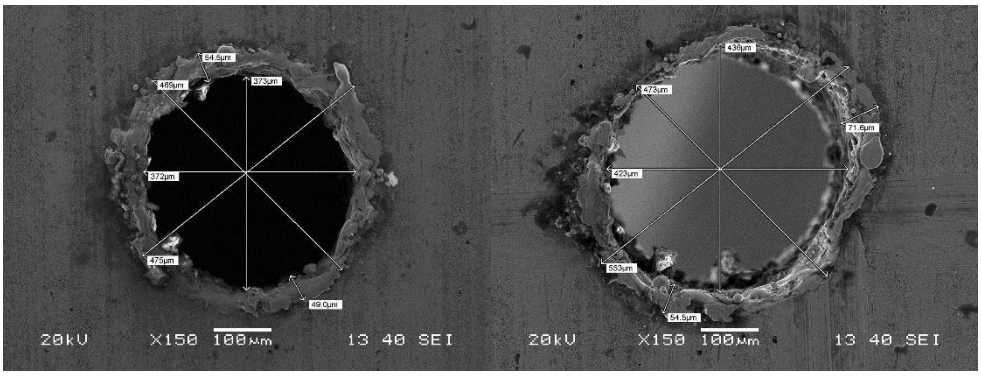

11th Hole Top view 11th Hole Bottom view

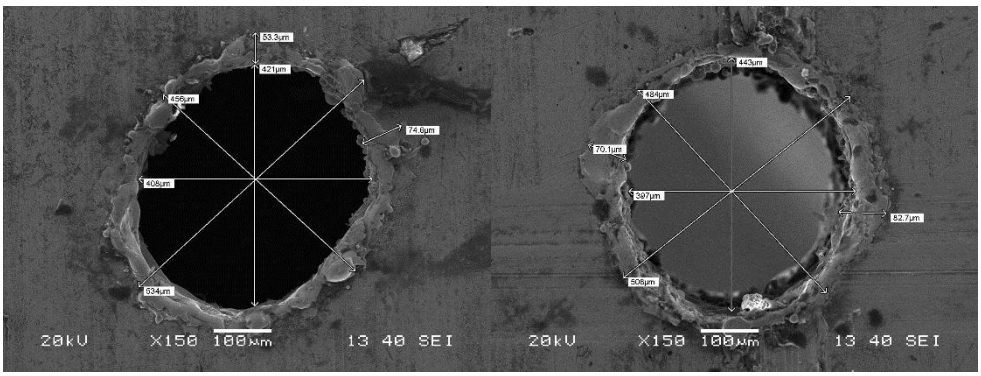

12th Hole Top view 12th Hole Bottom view

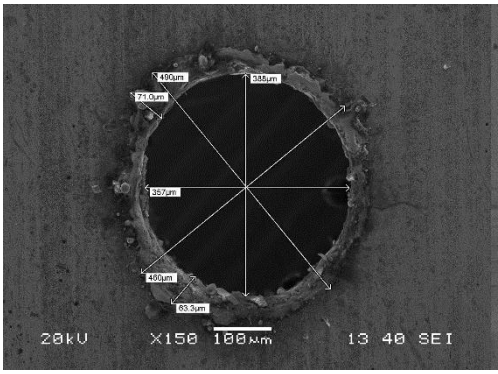

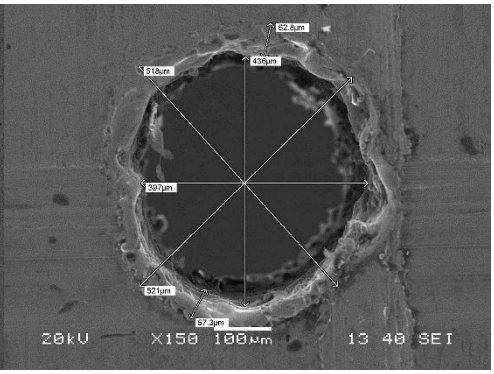

13th Hole Top view

13th Hole Bottom view

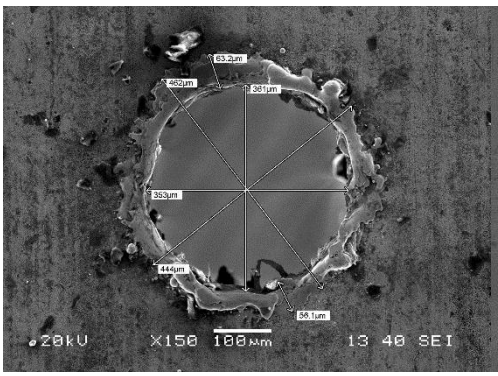

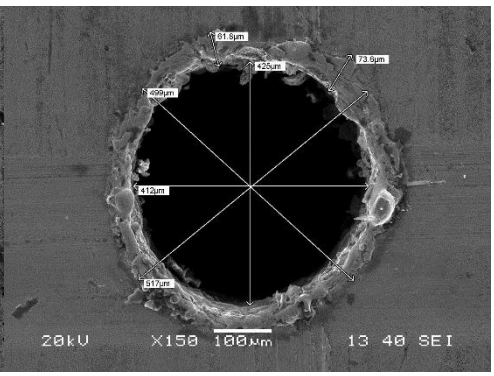

14th Hole Top view

14th Hole Bottom view

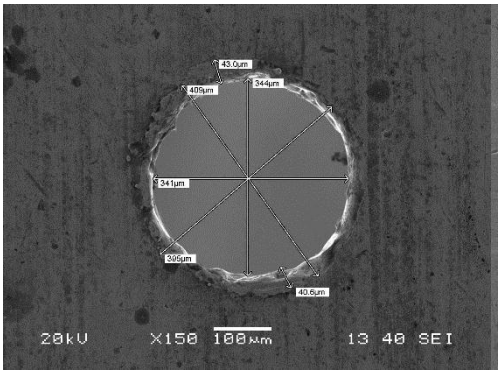

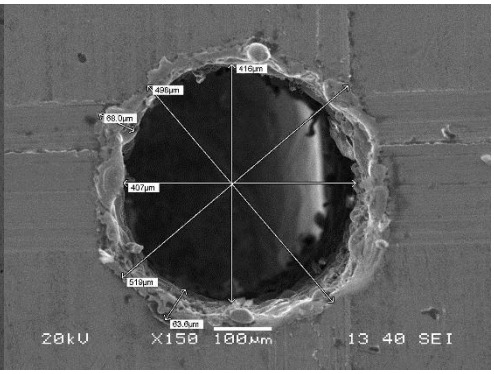

15th Hole Top view

15th Hole Bottom view

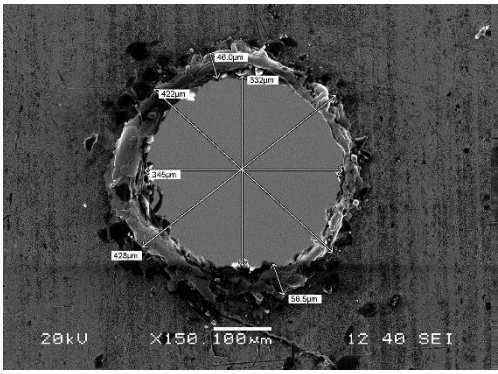

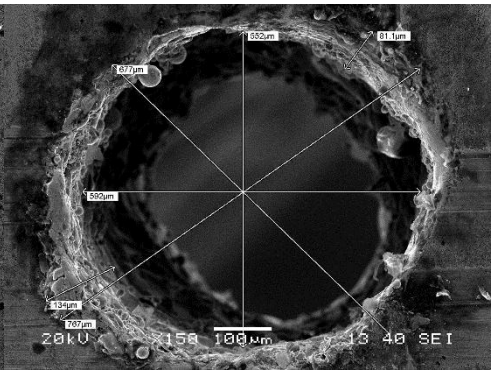

16th Hole Top view

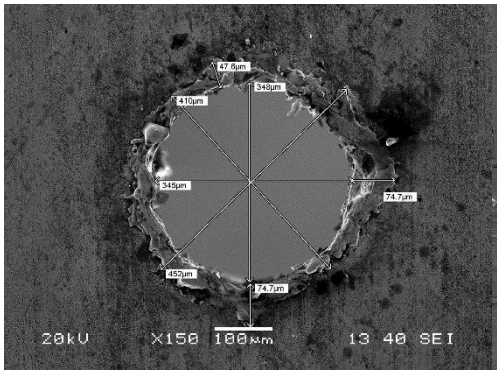

16th Hole Bottom view

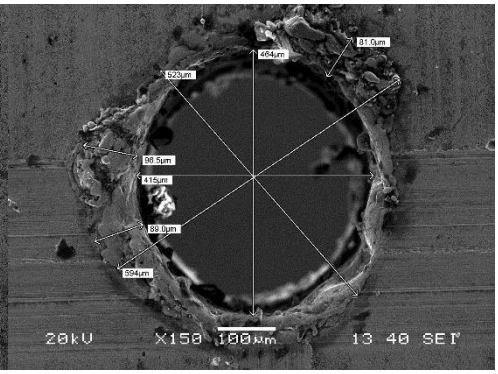

17th Hole Top view

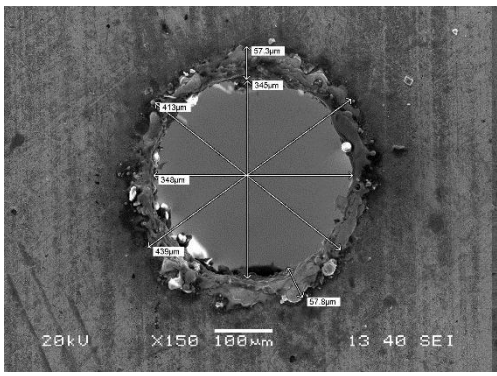

17th Hole Bottom view

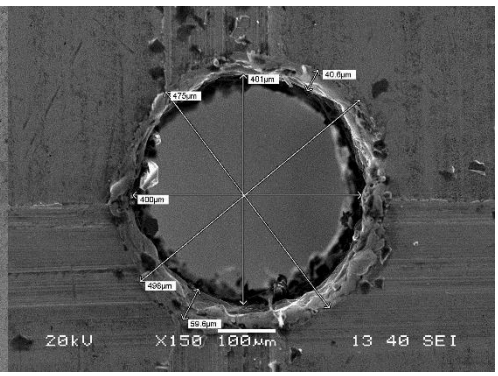

18th Hole Top view

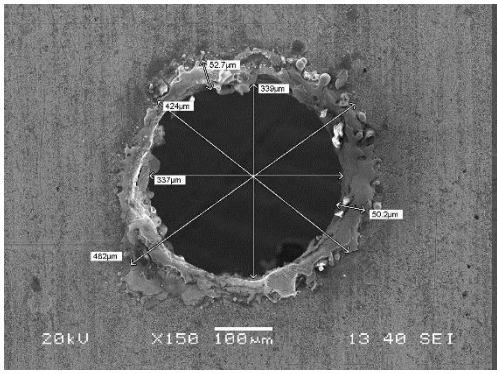

18th Hole Bottom view

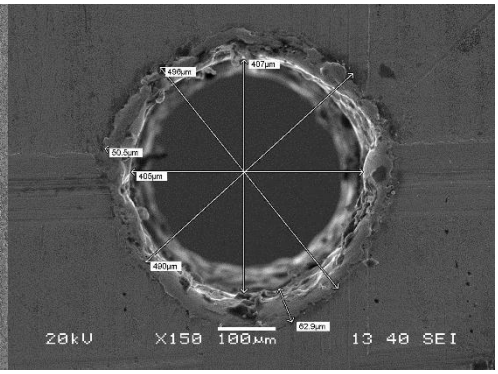

19th Hole Top view

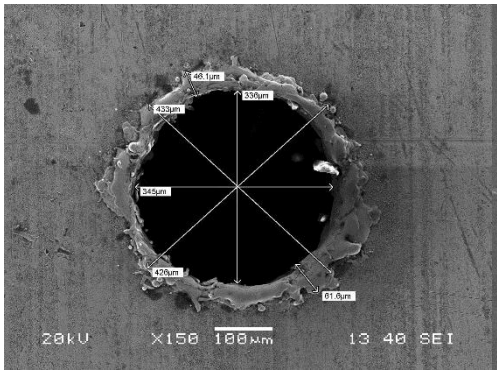

19th Hole Bottom view

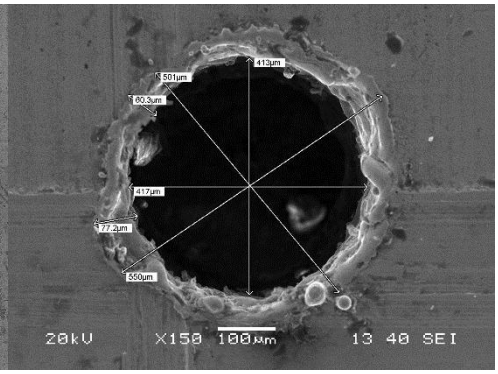

20th Hole Top view

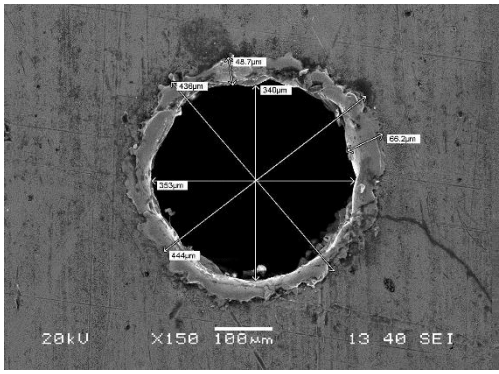

20th Hole Bottom view

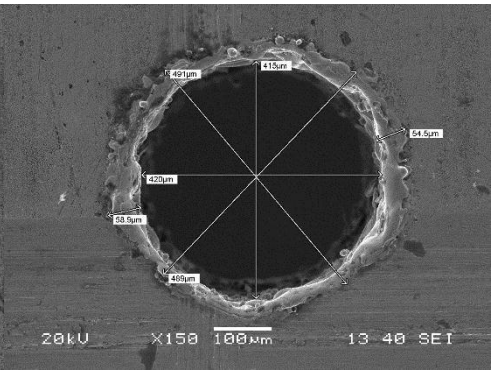

21st Hole Top view

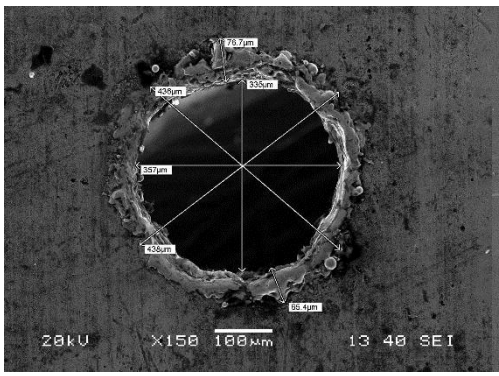

21st Hole Bottom view

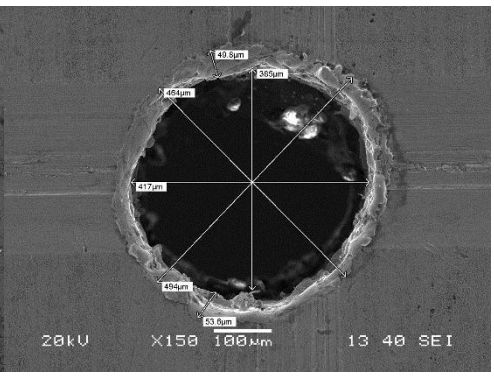

22nd Hole Top view

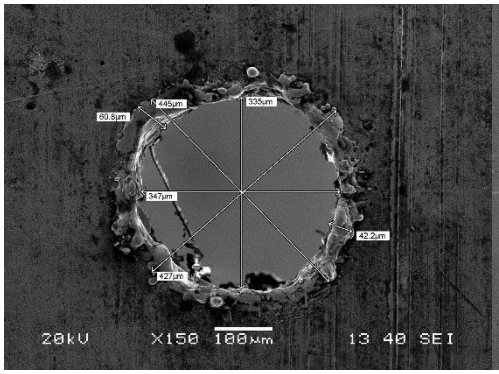

22nd Hole Bottom view

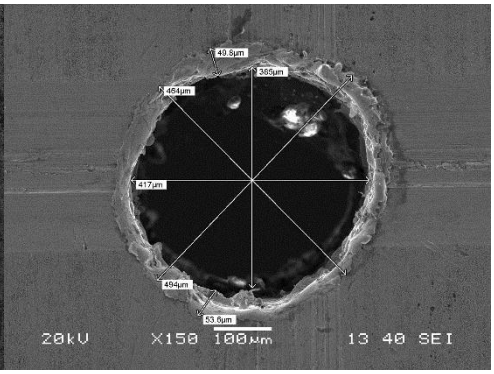

23rd Hole Top view

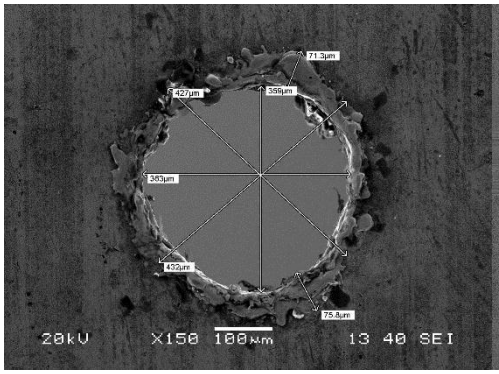

23rd Hole Bottom view

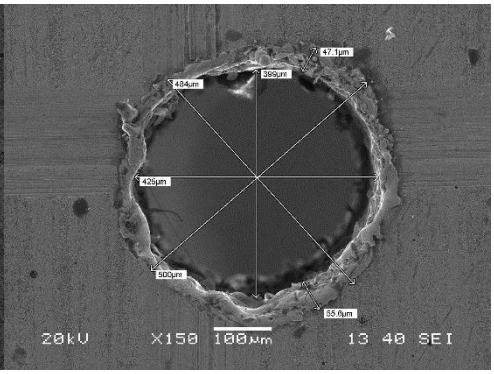

24th Hole Top view

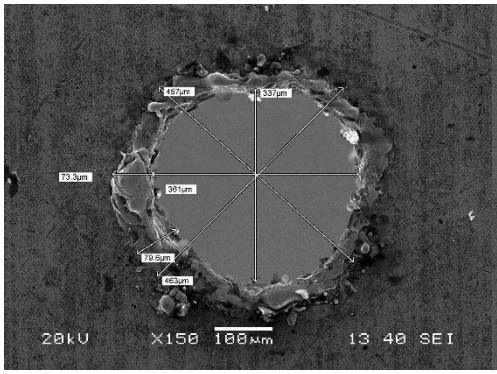

24th Hole Bottom view

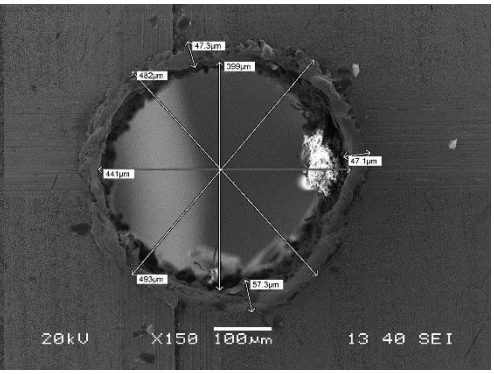

25th Hole Top view

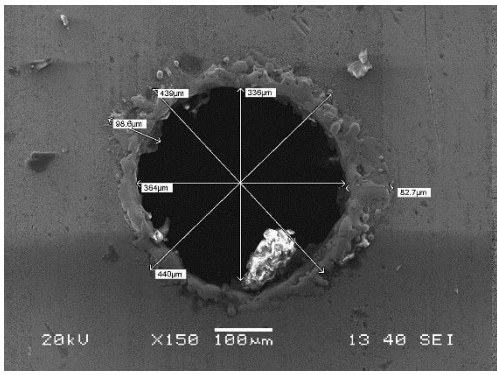

25th Hole Bottom view

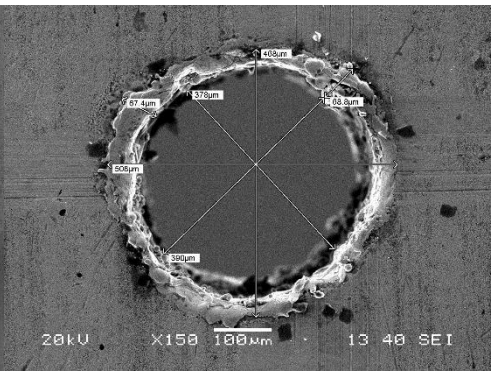

26th Hole Top view

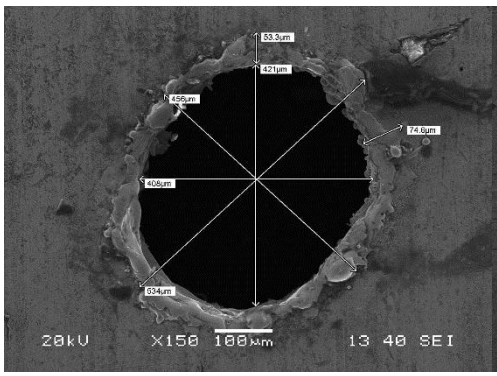

26th Hole Bottom view

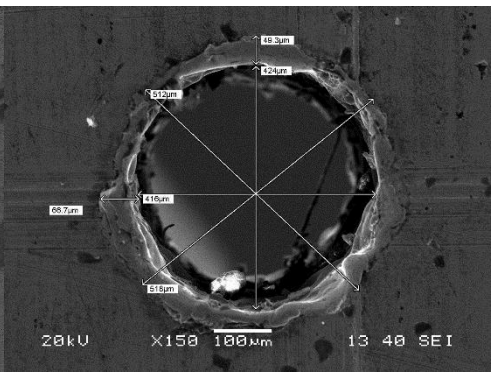

27th Hole Top view

27th Hole Bottom view

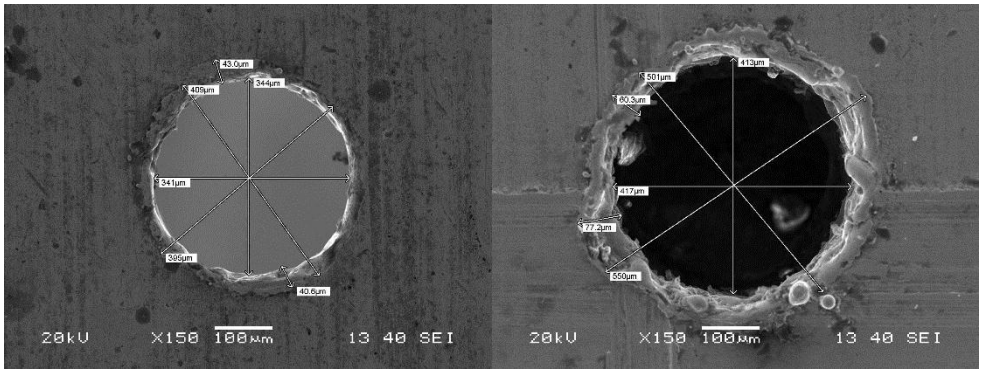

28th Hole Top view 28th Hole Bottom view

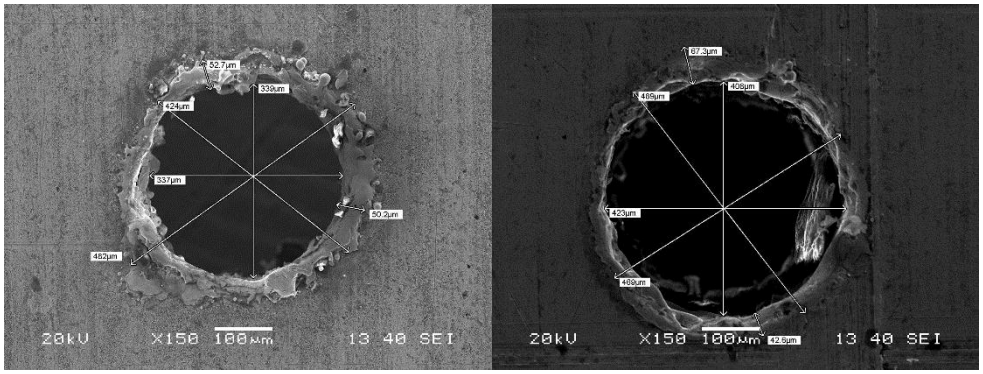

29th Hole Top view 29th Hole Bottom view

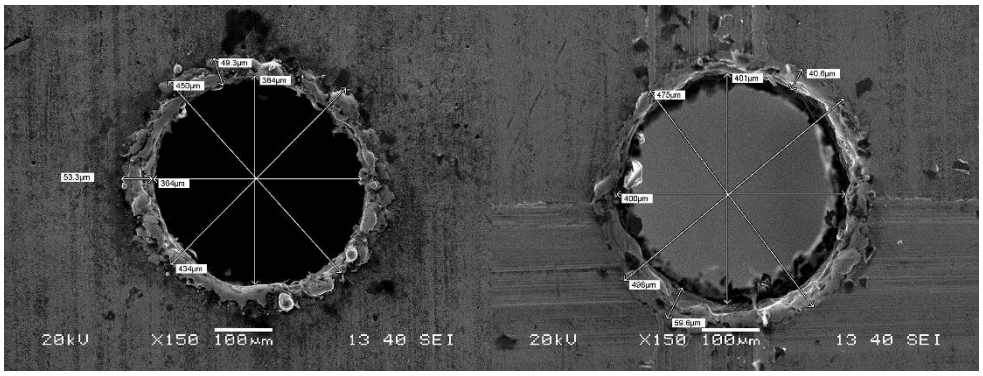

30th Hole Top view 30th Hole Bottom view

Figure 5. 2: SEM Images of Micro Holes

MRR was calculated considering the geometry of micro-hole and machining time. The value of OC was calculated by diametric difference of tool as well as machined. The MRR has been determined as the average volume of the material removed to the machining time and generally expressed in cubic millimeter per minute. MRR, OC, RCL and Taper angle has been calculated using Equation (4.1-4.3) as discussed in previous chapter. Based on response surface methodology layout with central composite design 30 data sets as shown in Table 5.3 in "Appendix 34" were obtained out of which 20 random sets will be used for training network and remaining 10 sets were fed to the trained

network as validation sets to inspect the predictive accuracy of the ANN and ANFIS models.

5.2.3 RESPONSE SURFACE ANALYSIS OF PROCESS RESPONSES

Analysis of variance technique (ANOVA) was used for checking the adequacy of developed models, it has observed that calculated F-ratios were larger than the tabulated values at a 95% confidence level. Hence, the models are considered to be adequate. Furthermore, the determination coefficient (R^2) indicates the goodness of fit for the model. The coefficients of regression model can be estimated from the experimental results by Design expert software. The significant terms in the model were found by analysis of variance at 5% level of significance by backward elimination process. The regression coefficients are calculated using the coded units. The regression coefficients calculated for the models and corresponding P-values are shown in Table 5.4-5.5 in Appendix 35-36. Further the percentage contribution of different process variables can be observed from these tables. The mathematical model correlating process responses like MRR, OC, RCL and TA with the process control parameters is developed as:

$$MRR = 0.906032 - 0.00387672 * A - 0.0406828 * B + 0.000506428 * A * B - 1.13045e-005 * A * C - 0.000206351 * B * D + 7.70474e-005 * C * D + 0.000554719 * B^2 \quad (5.1)$$

$$OC = -0.165399 + 0.00948715 * B + 0.0145738 * D + 3.70404e-005 * A * B + 6.95799e-006 * A * C - 0.000368751 * B * D - 6.38092e-006 * C * D \quad (5.2)$$

$$RCL = 153.628 - 1.82539 * B - 1.77687 * D + 0.00508037 * A * D + 0.0206207 * B * C + 0.0028784 * C * D - 0.00463502 * C^2 \quad (5.3)$$

$$TA = -22.154 + 0.50326 * A - 0.0874608 * B + 0.137319 * C + 0.670229 * D - 0.00369827 * A * B - 0.00529682 * A * D - 0.00549821 * C * D - 0.00349002 * A^2 + 0.00549267 * B^2 \quad (5.4)$$

Response Surface Analysis for MRR

Analysis of variance (ANOVA) was carried out to check the adequacy of the developed models. Table 5.4 in “Appendix 35” shows the ANOVA for MRR after applying backward elimination process and as it can be seen from Table 4.20 that it comprises of only significant terms. The p value for the model is lowers than 0.05 (i.e. at 95% confidence level) indicates that the developed model is statistically significant. Further the model F-value of 11.19 implies the model is significant. There is only a 0.01% chance that an F-value this large could occur due to noise. In this case A, B, AB, AC, BD and CD are significant model terms. The similar analyses were carried out for OC, RCL

and TA. Furthermore, after backward elimination process the R-Squared value for MRR, OC, RCL and TA were found to be 0.7807, 0.7485, 0.7086 and 0.9642 respectively. However, the truncated models have lower R-Squared value than that of full quadratic model exhibiting significance of relationship between the response and the variables. This shows that second order models can explain the variation in the MRR, OC, RCL and TA up to the extent of 78.07 %, 74.85 %, 70.86% and 96.42% respectively. The "Predicted R-Squared" values are in reasonable agreement with the "Adjusted R-Squared "values.

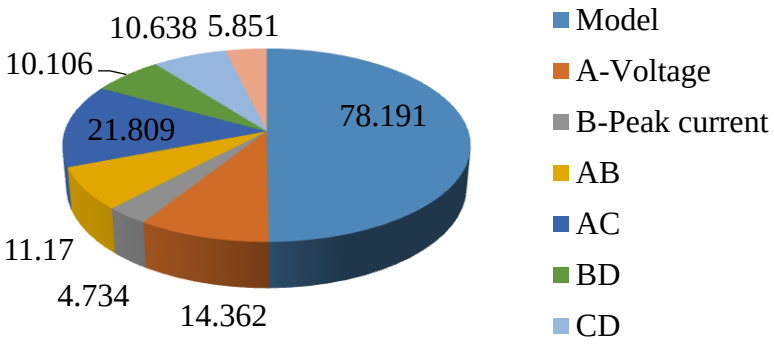

Figure 5. 3Percentage contribution of process variables

It can be observed from Table 5.4 in "Appendix 35" that the interaction terms AB, AC, BD and CD have significant contribution on MRR. The three dimensional surface plots for the MRR with respect to the significant interaction terms are shown in Figures 5.4 - 5.7 In each of these graphs, two process variables are varied while the other two variables are held constant at its middle value. Further, the interaction effect of voltage and peak current on MRR at constant pulse on duration of 60 µs and pulse off duration of 25µs is presented in Figure 5.4. It is observed that maximum MRR value of 1.013 mm^3/min was obtained at the voltage of 60V and lowest peak current (40A) combination. The least MRR value of 0.5424 mm^3/min was obtained at the lowest voltage (30V) and highest peak current of (40A) combination. It is observed that material removal rate increases with increase in voltage and peak current there is a significant increase in material removal rate with increase in voltage, however with increase in peak current there is a slight decline in MRR.

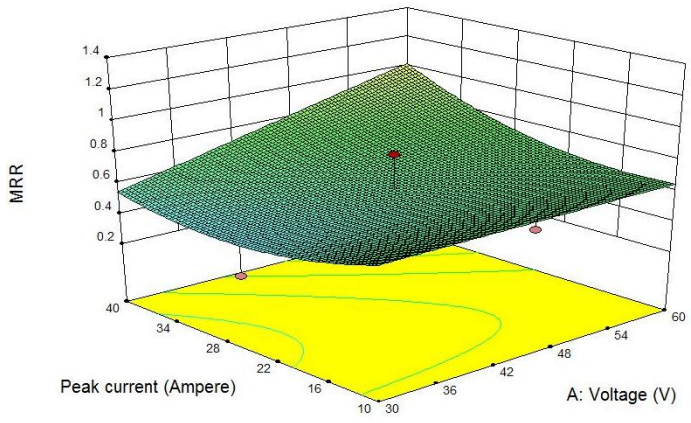

Figure 5. 4 Interaction effect of voltage and peak current on MRR

Figure 5.5 shows the interaction effect of voltage and pulse on duration on MRR at constant peak current of 20 A and pulse off duration of 25. From this Figure, it is observed that maximum MRR was attained at the highest voltage (60V) and highest pulse on duration (80µs). The least MRR was obtained at the lowest voltage (30V) and highest pulse off duration of 80µs combination. It indicates significant contribution from the interaction terms of the process variables. It is witnessed that MRR increases with increase in voltage and the pulse on duration.

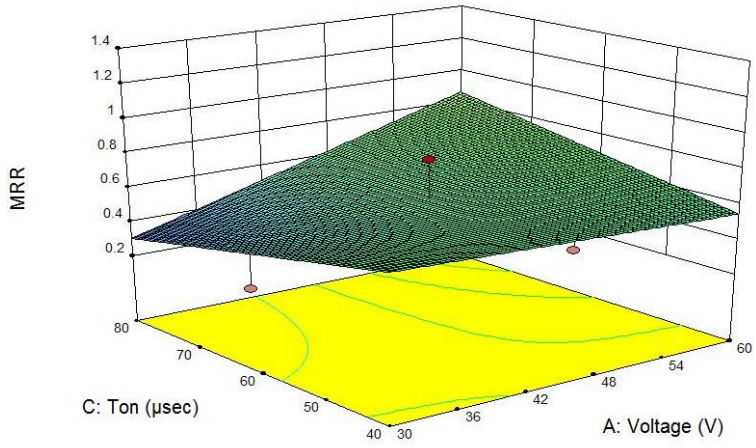

Figure 5. 5 Interaction effect of voltage and pulse on duration on MRR

At constant pulse on duration of 60 µs and voltage of 45 V the interaction effect of peak current and pulse off duration on MRR in is represented in Figure 5.6. It is observed that

maximum MRR value of 0.885 mm^3/min was found at the highest value of peak current and lowest value of pulse off duration. Furthermore, it was observed that with the increase in pulse off duration the MRR increases, while it initially decreases and then increases with increase in peak current.

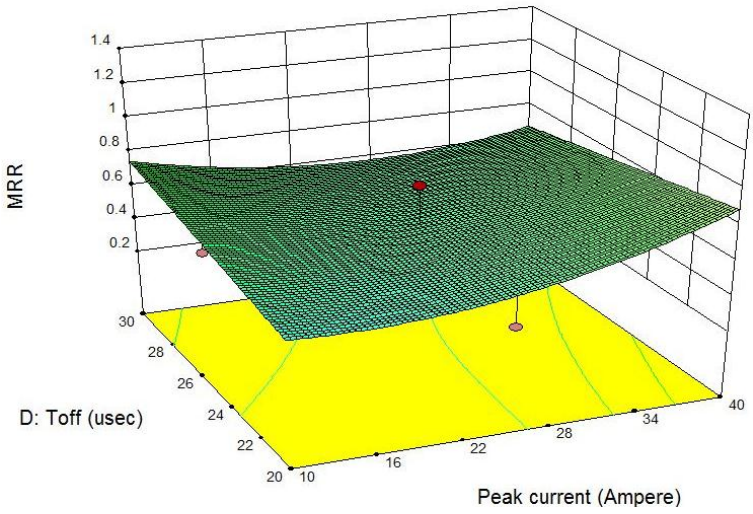

Figure 5. 6 Interaction effect of peak current and pulse off duration on MRR

From Figure 5.7, it is observed that maximum MRR value of 0.695mm^3/min was obtained at the highest values of pulse on duration and pulse off duration. Also, it was observed that with the increase in pulse on duration the MRR increases, while it initially decreases and then increases with increase in pulse off duration.

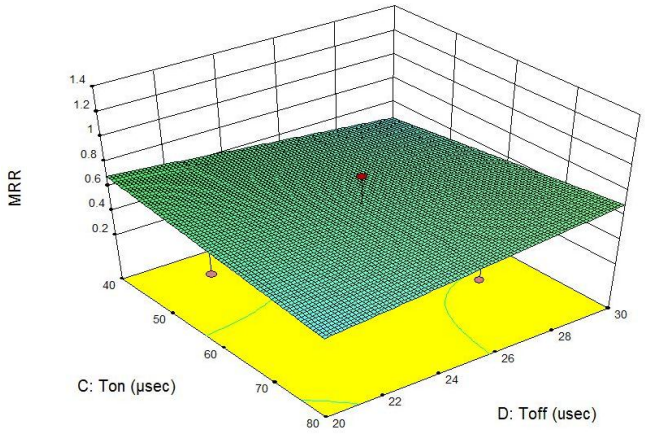

Figure 5. 7 Interaction effect of pulse on duration and pulse off duration on MRR

Response Surface Analysis for Overcut

The percentage contribution of different process variables on OC is presented in Figure 5.8 and it can be seen that peak current has a significant effect on OC. Additionally; the interaction terms AB, AC, BD and CD are also found to be significant. Nonetheless, the interaction terms AC and CD are more significant as compared to other significant terms as their percentage contribution are 27.85%, 14.28% respectively. Further the model F-value of 11.41 implies the model is significant. There is only a 0.01% chance that an F-value this large could occur due to noise. The truncated model for OC after applying backward elimination method has been tabulated in Table 5.5 in Appendix 35.

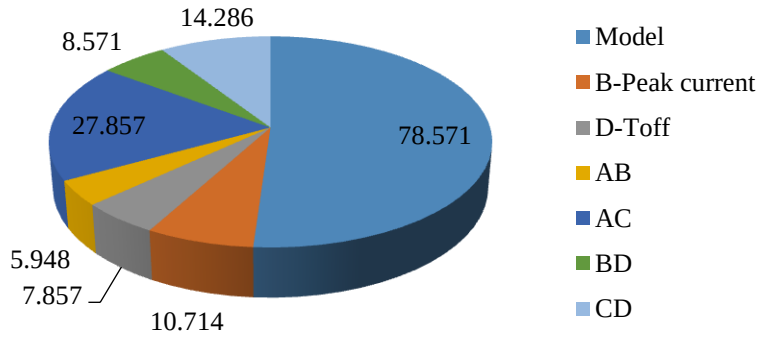

Figure 5. 8 Percentage contribution of process variables

Figure 5.9 shows the interaction effect of voltage and pulse on duration on OC at constant peak current of 25A and pulse off duration of 25 µs. From this Figure, it is observed that maximum OC was obtained at highest voltage (60V) and highest pulse on duration of 80µs combination. The minimum OC was attained at the highest voltage (60V) and lowest pulse on duration of 40µs combination. It is observed that OC increases with increase in pulse on duration and the voltage. There is significant decrease in OC with increase in pulse on duration, however with increase in voltage there is slight increase in OC.

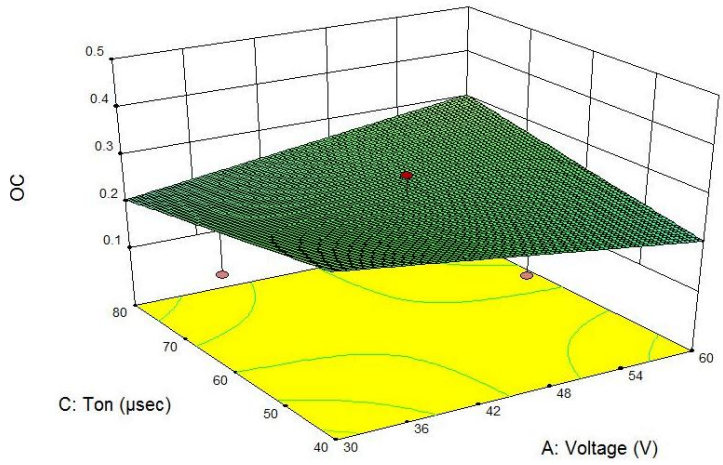

Figure 5. 9: Interaction effect of voltage and pulse on duration on OC

From Figure 5.10, it is witnessed that maximum OC was obtained at the lowest pulse on duration of (40µs) and highest pulse off duration of 30µs.The minimum OC was attained at the highest pulse on duration of 80µs and lowest pulse off duration of (20µs) combination. It is observed that OC first increases with increase in pulse off duration and the pulse on duration and then decreases. There is a significant increase in OC with increase in pulse on duration however with increase in pulse off duration initially there is increase in OC but later onwards it starts decreasing.

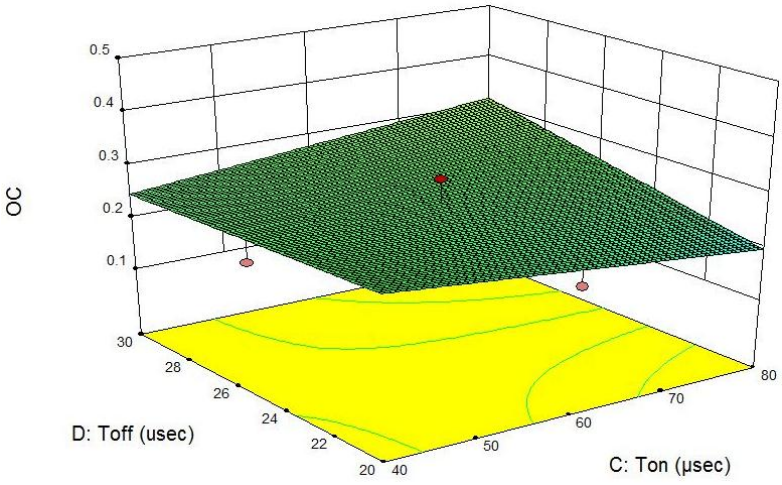

Figure 5. 10: Interaction effect of pulse on duration and pulse off duration on OC

Response Surface Analysis for RCL

The truncated model for RCL after backward elimination process is shown in Table 5.6 in "Appendix 36" and yielded a model F-value of 9.32 which implies that the model is significant. The percentage contribution of different process variables on RCL is presented in Figure 5.11.

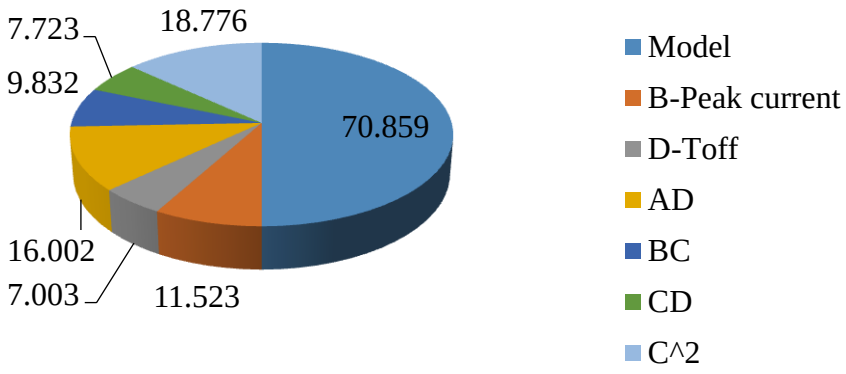

Figure 5. 11: Percentage contribution of process variables

It can be observed from Figure 5.11 among different interaction terms AD has highest contribution of 16.002%. The interaction effect of voltage and pulse off duration on RCL in the form of 3D surface graph at constant pulse on duration of 60µs and peak current of 25 A is represented in Figure 5.12. From this Figure, it is perceived that minimum RCL value of 59.051 µm was obtained at the highest values of voltage (60V) and pulse off duration (30µs) respectively. Additionally, it was observed that with the increase in voltage duration RCL increases linearly, while it initially increases with increase in pulse off duration and decreases with further increase in pulse off duration. With the increase in both pulse on duration and pulse off duration RCL initially increases then it starts decreasing with further increase in pulse on duration and pulse off duration.

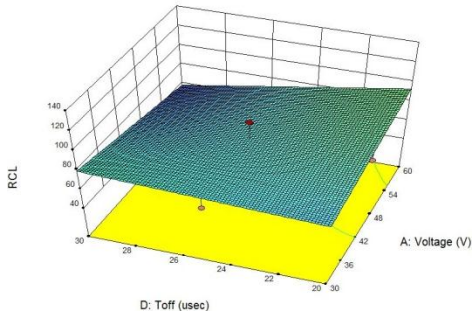

Figure 5. 12: Interaction effect of pulse on duration and pulse off duration on RCL

Response Surface Analysis for TA

The backward elimination process discards the insignificant terms to adjust the fitted quadratic model. The model, with rest of the terms after elimination, is presented in Table 5.7 in "Appendix 36". After backward elimination, the values of R-Squared and Adjusted R-Squared 0.9642 and 0.9481 respectively. The truncated model has lower R^2 than that of full quadratic model, exhibiting significance of relationship between the response and the variables and the terms of the adequate model after the elimination are A, B, C and D. The percentage contribution of different process variables on TA is presented in Figure 5.13 and it can be observed that that pulse off duration is found to be most significant effect on TA followed by voltage, pulse on duration and peak current. Furthermore, AB, AD, CD are found to be significant the interaction terms. However, among different interaction terms AB has highest percentage contribution of 30.199%.

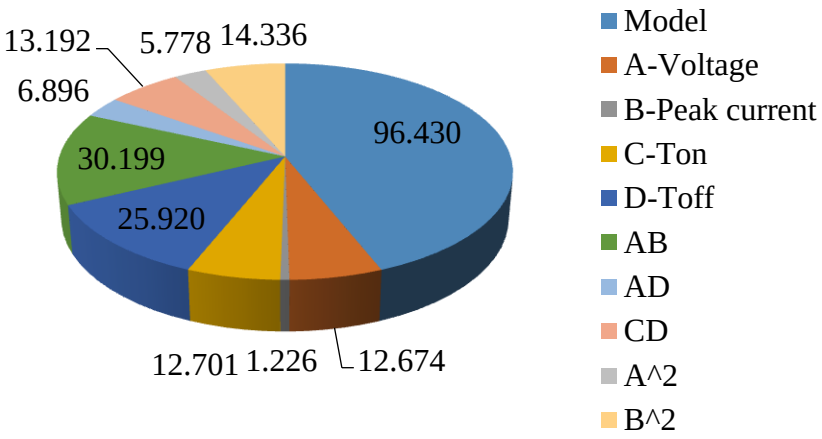

Figure 5. 13: Percentage contribution of process variables

At constant pulse on duration of 60µs and pulse off duration of 25µs the interaction effect of voltage and peak current on TA is represented in Figure 5.14. From Figure 5.14, it is observed that minimum TA value of 0.700° was attained at the highest values of voltage (60V) and peak current (40A) respectively. Also, it was observed that with the increase in peak current TA initially increases then it decreases non-linearly, at the middle level of peak current setting and again increases at high level voltage settings. However, with the increase in voltage the value of TA goes on increasing up to maximum value of 1.806°. Additionally, with the increase in both voltage and peak current simultaneously the value of TA goes on increasing and starts decreasing for higher values of peak current and voltage.

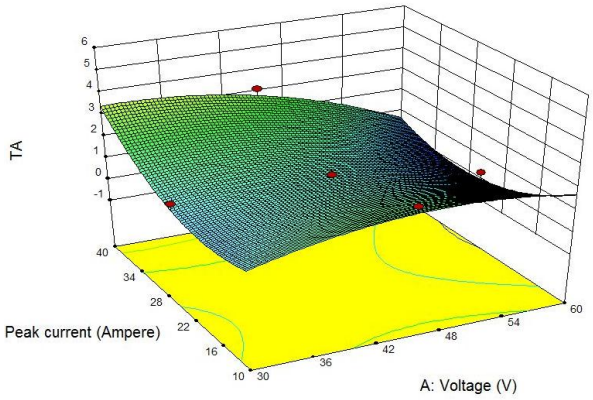

Figure 5. 14 : Interaction effect of Voltage and Peak current on TA

5.3 ANN MODELING OF EDM PROCESS

Artificial intelligence (AI) predictions have been getting interest to a large extent in order to solve problems that are scarcely solved by the use of conventional methods. They have been referring to have the ability to be trained like humans, by accumulating knowledge through recurring learning activities. For that reason, the intention of this research is to propose multiple input single output models using the AI approaches to predict the responses such as MRR, OC, RCL and TA. A feed-forward neural network with four input neurons, one hidden layer and one output neuron is used and the architecture of the model. The activation function in the hidden layer is the hyperbolic tangent sigmoid transfer function, which standardizes or normalizes the data and hence the transformed data lie between -1 and 1. The activation function in the hidden layer was the hyperbolic tangent sigmoid transfer function (tansig) and in the output layer was the linear transfer function pure line. The training algorithm selected is the back-propagation because the algorithm yields fastest training. Weights are randomly initialized, and the learning rate and momentum parameter were set at 0.001 and 0.09 respectively. The data set obtain from experiments are divide randomly in to three subsets namely; training, testing and validation sets, in 50%, 40% and 10% of the total data, respectively shown in Table 5.8 in Appendix 37. The training set is used to calculate the gradient and to form the weight factors and bias. The testing data is used to minimize the MSE while training and stop the training after appropriate epoch. The remaining 10% validation data set is used to calculate the prediction error to estimate the accuracy of the models on the unseen data set, In the present investigation the ANN modeling of µ-EDM for fabrication of micro holes has been carried out using a Neural network toolbox in MATLAB. Appropriate selection of number of hidden layers and the number of neurons in the hidden layers leads significant part in the optimization of feed forward network with back propagation

configuration. During training phase, the regression value of 0.99701, 0.99902, 0.9997 and 0.99965 for MRR, OC, RCL and TA have been obtained which signifies the fair correlation between experimental and predicted values.The regression plot for MRR, OC, RCL and TA have been given in Figure 5.15 (a-d). Hence ANN can be effectively used for the prediction of MRR, OC, RCL and TA in µ-EDM.

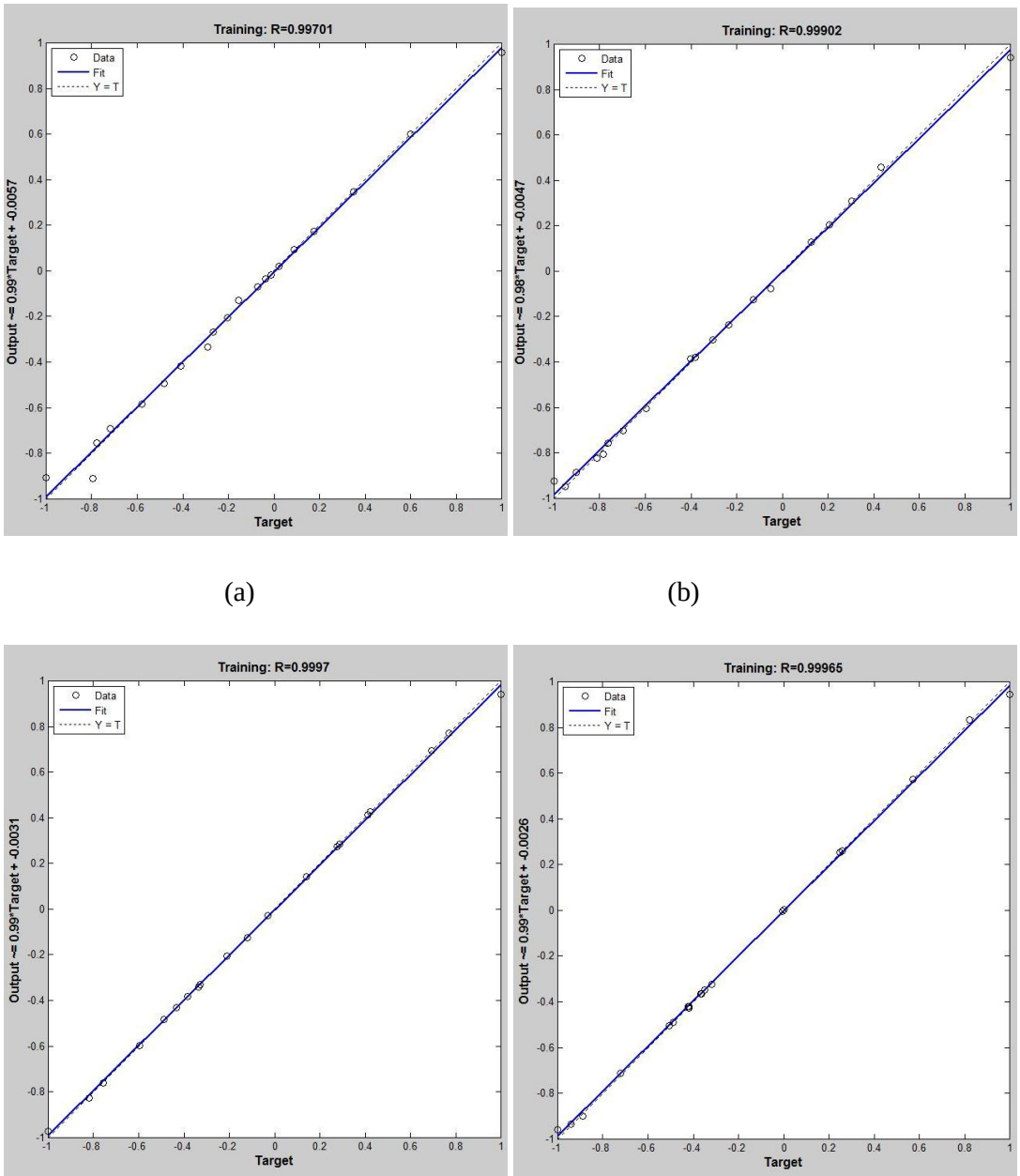

(a) (b)

(c) (d)

Figure 5. 15 (a-d): Regression plot for MRR, OC, RCL and TA

The trained neural network was validated against another set of experimental data, termed as validation data set illustrated in Table 5.9 in "Appendix 38". The errors in prediction are also presented in Table 5.10 in "Appendix 38". It can be seen from Table 5.10 that the model predictions match the experimental data very closely except few data. Moreover, the average error in the prediction was -0.775 % for MRR, 4.996 % for OC, and -2.583 % for RCL and -14.402 % for TA respectively. The total average prediction error of the network was predicted as -12.764 % which indicates that the model is over predicting the values. The developed ANN model was tested by repeating few experiments randomly from the entire data set for checking the predictive accuracy of the developed model. Figures (5.16- 5.19) indicated the errors between predicted and experimental values for all process responses during testing.

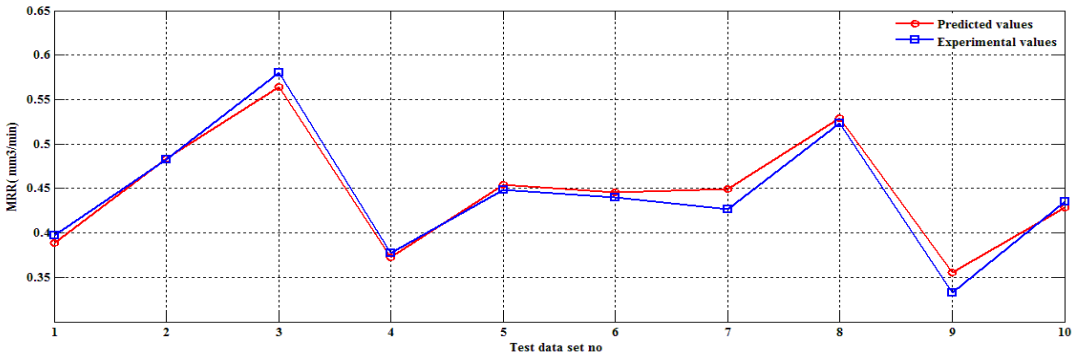

Figure 5. 16: Errors between predicted and experimental values of MRR during testing

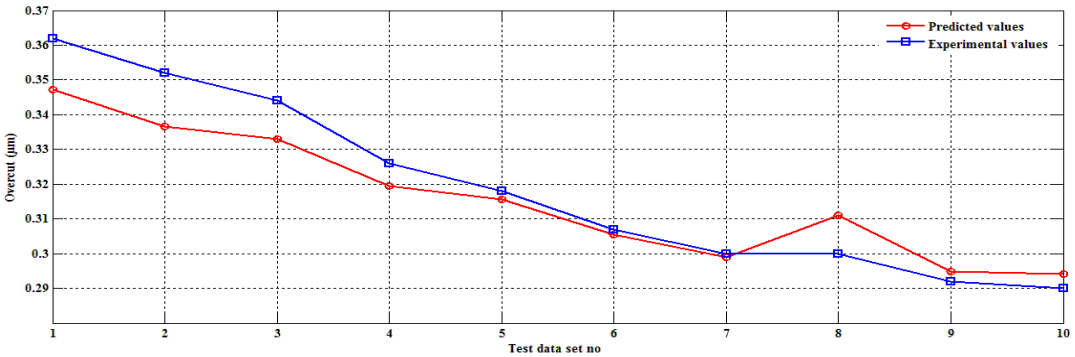

Figure 5. 17: Errors between predicted and experimental values of OC during testing

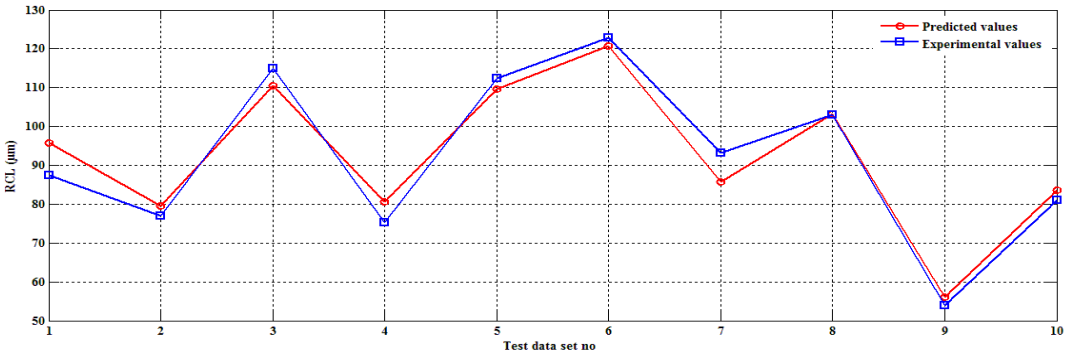

Figure 5. 18: Errors between predicted and experimental values of RCL during testing

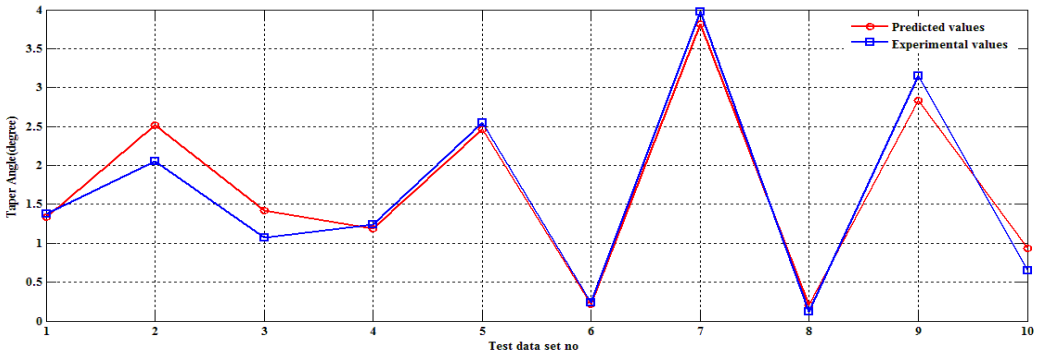

Figure 5. 19: Errors between predicted and experimental values of TA during testing

Table (5.11 – 5.12) in "Appendix 39" contains testing of the developed model with experimental data and the predicted output and percentage error in prediction of MRR, OC and RCL were within acceptable limits. It is observed that the total average prediction error is -15.322 % which is implies level of over prediction.

5.4 ANFIS MODELING

ANFIS has been used to predict MRR, OC RCL and TA. For this purpose, the MATLAB 2012b package (ANFIS toolbox) has been utilized. Prediction of MRR, OC, RCL and TA of the micro-EDM process by ANIFS comprises of three main phases, training and testing. A similar methodology was adopted as mentioned in section 4.4. However, for the purpose of comparing the predictive tendency with ANN model same data was used for training, validation and testing as it was used for development of ANN. Total average error (TAE) as mentioned in Equation 4.14 is considered as selection criteria for comparison of all existing networks and final selection is made of the most accurate one. The value of error goal was set at 0.03, and the iteration number was 500 epochs. In this work various types of MFs namely triangular, trapezoid, generalized bell and Gaussian have been practiced. Table 5.13 represents training and validation error of ANFIS models

for different membership functions. TAE for MRR, OC, RCL and TA have been presented in Table 5.14. Results indicated that the generalized bell function leads the lowest values of TAE for MRR, OC RCL and TA, respectively.

Table 5.13: Training and validation error

Type of membership function	MRR		OC		RCL		TA	
	Training error	Validation error	Training error	Validation error	Training error	Validation error	Training error	Validation error
Triangle	0.038361	0.03836	0.026284	0.026283	6.1114	6.1108	0.67067	0.67066
Trapezoid	0.037118	0.037113	0.025406	0.025403	5.3883	5.3858	0.64795	0.64786
Generalized bell	0.035493	0.035493	0.0249	0.0249	4.3544	4.3544	0.59505	0.59505
Gaussian	0.036787	0.036781	0.025261	0.025258	5.2356	5.2327	0.64252	0.64242

Table 5.14: TAE for process responses

Type of membership function	MRR Total Average error	OC Total Average error	RCL Total Average error	TA Total Average error
Triangle	0.038361	0.026284	6.1111	0.670665
Trapezoid	0.037116	0.025405	5.38705	0.647905
Generalized bell	0.035493	0.0249	4.3544	0.59505
Gaussian	0.036784	0.02526	5.23415	0.64247

The developed ANFIS model was tested for checking the predictive accuracy of the developed model. Tables (5.15 – 5.16) in "Appendix 40 "contains testing of the developed model with experimental data and the predicted output and percentage error in prediction of MRR, OC and RCL were within acceptable limits. It is observed that the total average prediction error is -14.191 % which implies level of over prediction.

5.5 MULTIOBJECTIVE OPTIMIZATION

The process of optimizing simultaneously a collection of objective functions is called as multi-objective optimization (MOO). In the present section multi-objective optimization has been carried out using three meta-heuristic approaches namely Elitist Teaching learning based optimization, Differential evolution and Artificial Bee colony optimization. Furthermore, pareto optimal sets of solution obtained from each algorithm have been ranked using centroid based Fuzzy ranking method as discussed in section 4.4.2. The regression Equations (5.1-5.4) obtained from ANOVA analysis haven used for

formulating the objective functions. In present multi-objective optimization regime only MRR have to maximized while OC, RCL and ta have to minimized. The tuning parameters for each algorithm were same as discussed in sections 4.4.1, 4.4.3 and 4.4.4. The objective, in this work, is to find the optimal combination of input parameters that provides maximum MRR and minimum OC, RCL and TA respectively. Because of the conflicting nature of performance measures, a single combination of input parameters does not serve the purpose. As a result, a set of optimal solutions (i.e., pareto-optimal solutions) is obtained instead of a single optimal combination. The results obtained from MOETLBO, MODE and MOABC after applying centroid based Fuzzy ranking method have been presented in Tables 5.17- 5.19 in Appendixes (41-43). The results of optimization of µ-EDM process using ETLBO and MODE and MOABC are presented in Table 5.20 in "Appendix 44". From statistical point of view, the Best, Mean and the Worst solution set have been calculated. From Table 5.20 it can be observed that for MRR OC and TA, MOETLBO yielded the best i.e., maximum value of MRR and minimum value of OC and TA. However, for RCL the minimum value was obtained from MOABC. Hence from the above results it can be concluded that none of algorithms ensure the best solutions for all process responses which justifies the existence of no free lunch theorems still holds valid for multi-objective regime.

5.6 FABRICATION OF MICRO-HOLES IN TITANIUM USING GRAPHITE AS TOOL ELECTRODE

5.6.1 EXPERIMENTAL DETAILS

In the second phase of experimental investigation, fabrication of micro-holes has been carried out using graphite as tool electrode whereas Titanium alloy (Ti 6Al-4V) with exactly similar dimensions as stated in section 5.2.2 was used as work piece material using a micro-EDM operation. Further, in order to investigate the effects of applied voltage (V), peak current (Ip), Pulse On duration (Ton) and Pulse off duration (T_{off}) on the material removal rate (MRR), Overcut (OC) and Recast layer thickness (RCL) Taper angle (TA). Based on initial investigations, four process parameters were selected as the source voltage (V), Peak current (I_P), Pulse on duration (Ton) and Pulse off duration (T_{off}), because they have a direct effect on the performance parameters such as material removal rate, hole overcut and recast layer thickness. The experimental layout was based on the face centered, central composite design (CCD). The levels of parameters selected were same as tabulated (Table 5.21) are also based on preliminary experiments and literature survey. EDM oil was used as dielectric, and it was kept same for entire experimentation. Total 30 holes were drilled (Fig 5.20). The machining time (Tm), recast layer thickness (RCL) and overcut (OC) were measured. The tool material used was fine graphite of 0.5mm diameter.

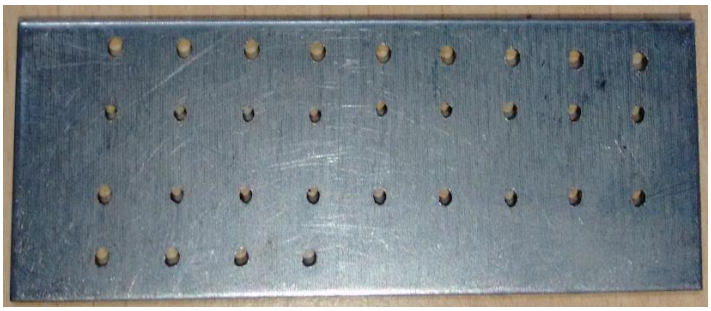

Figure 5. 20: Titanium workpiece

The hole overcut, and recast layer thickness were scanned using (JEOL JSM6480LV) built Scanning electron microscope. Based on response surface methodology layout with central composite design 30 data sets as shown in Table 5.21 in “Appendix 45” were obtained out of which 20 random sets were used for training network and remaining 10 sets were fed to the trained network as validation sets to inspect the predictive accuracy of the network model. Figure 5.21 presents the SEM images of all fabricated micro holes.

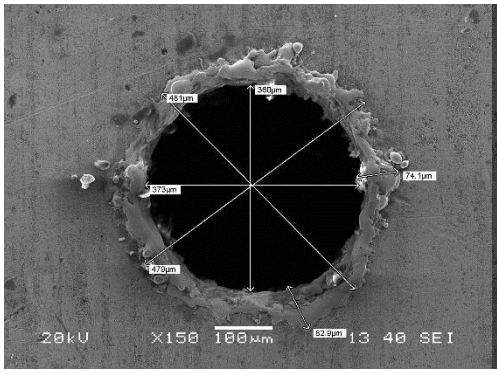

1st Hole Top view

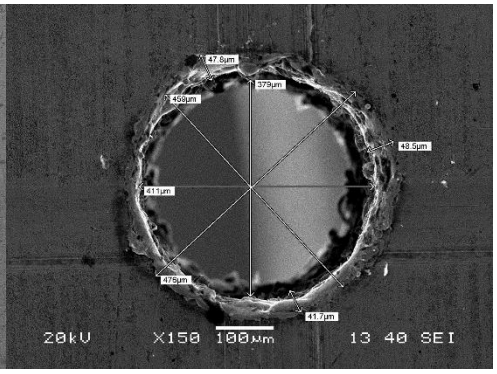

1st Hole Bottom view

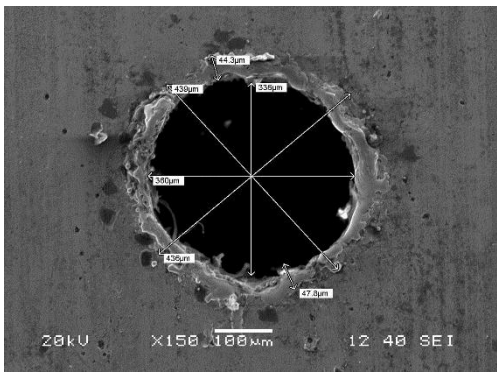

2nd Hole Top view

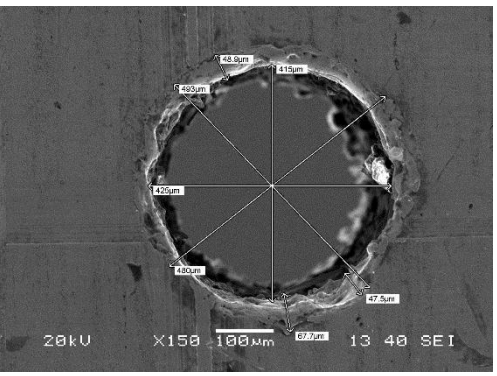

2nd Hole Bottom view

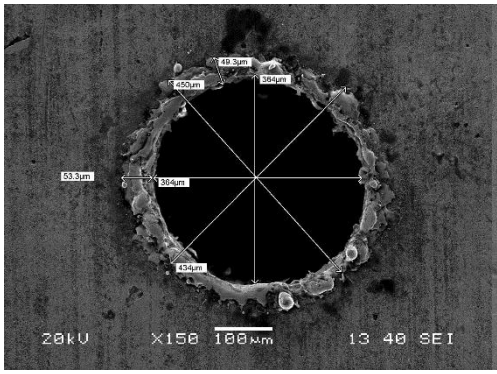

3rd Hole Top view

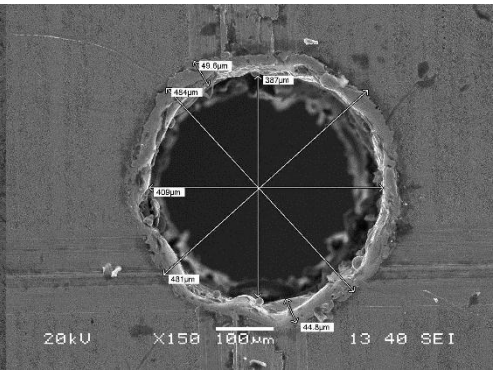

3rd Hole Bottom view

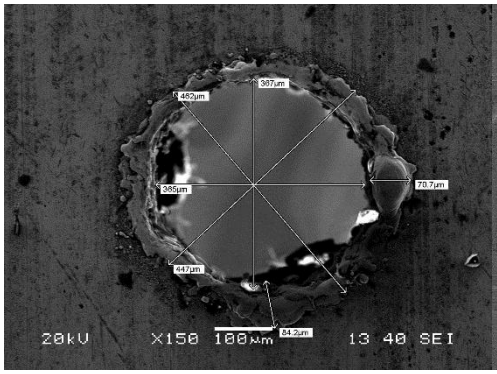

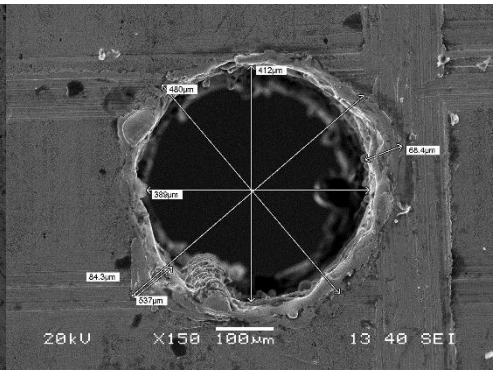

4th Hole Top view

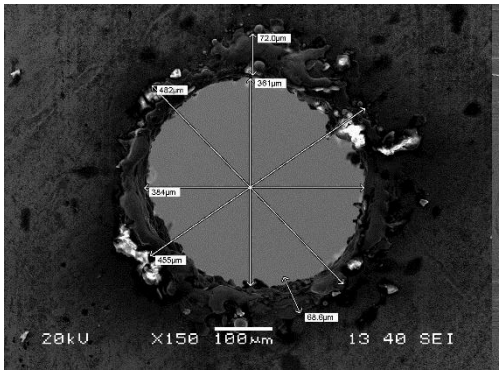

4th Hole Bottom view

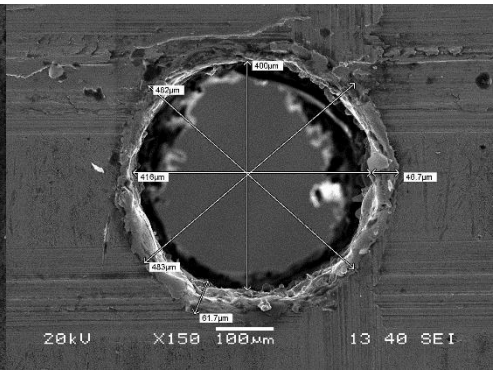

5th Hole Top view

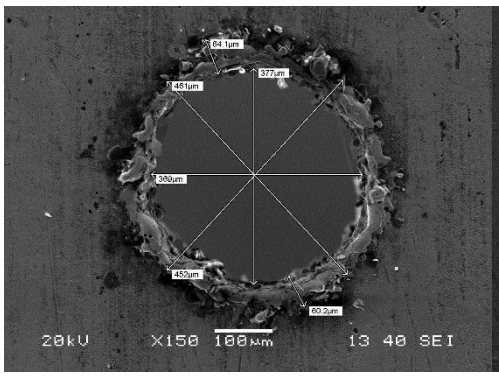

5th Hole Bottom view

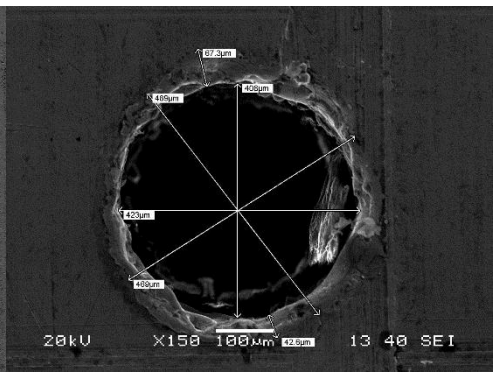

6th Hole Top view

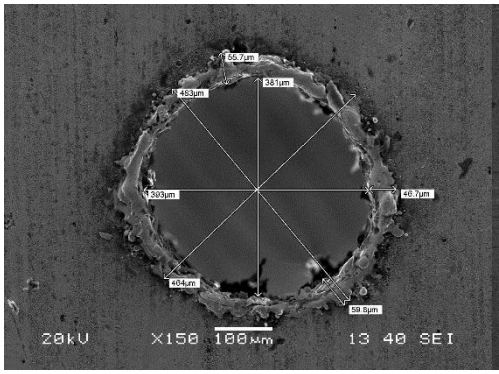

6th Hole Bottom view

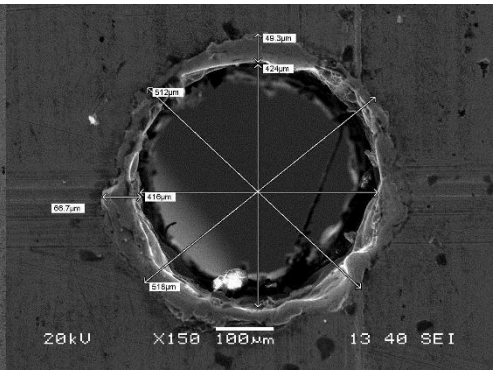

7th Hole Top view

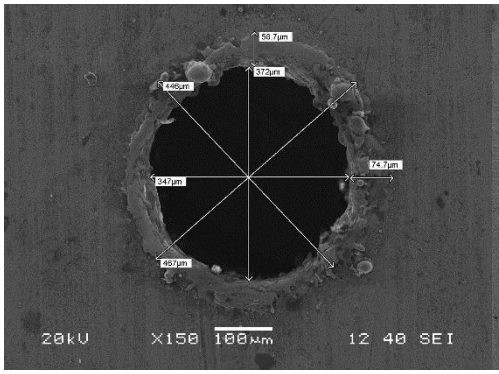

7th Hole Bottom view

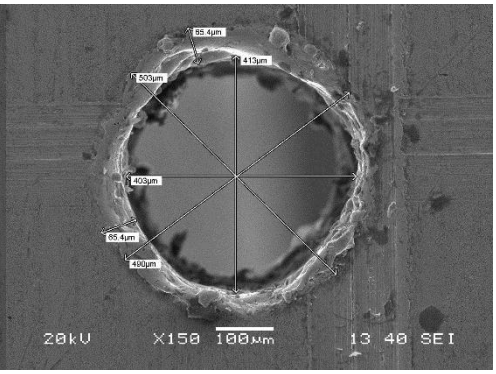

8th Hole Top view

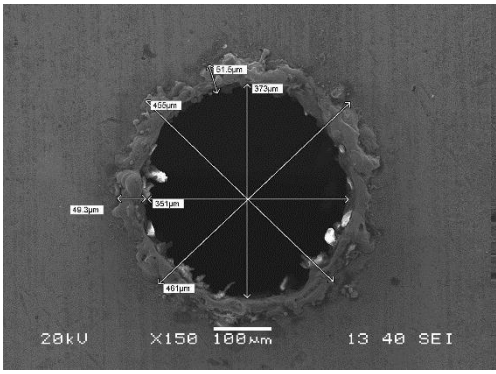

8th Hole Bottom view

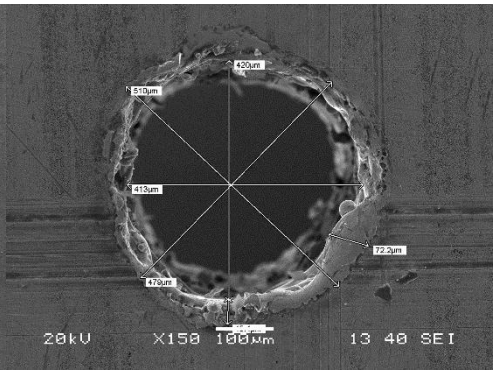

9th Hole Top view

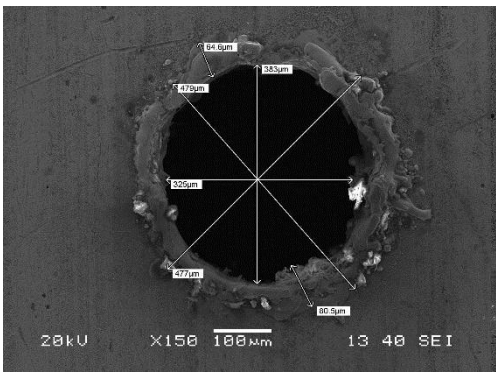

9th Hole Bottom view

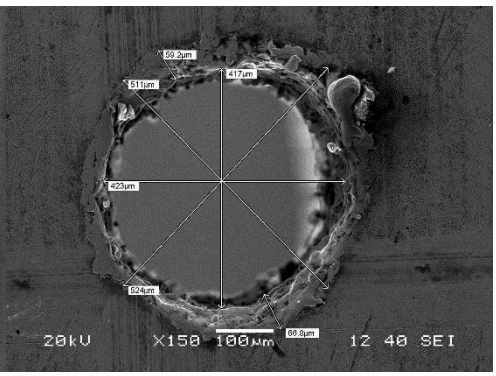

10th Hole Top view

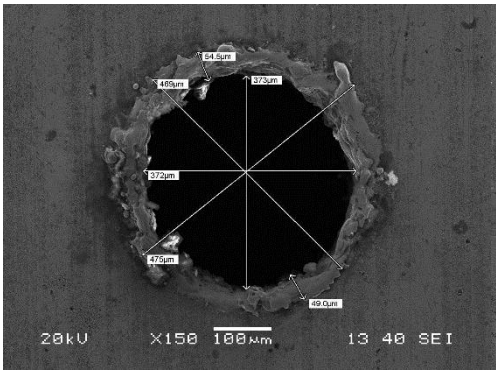

10th Hole Bottom view

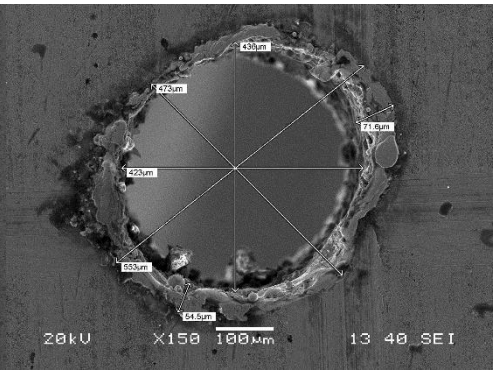

11th Hole Top view

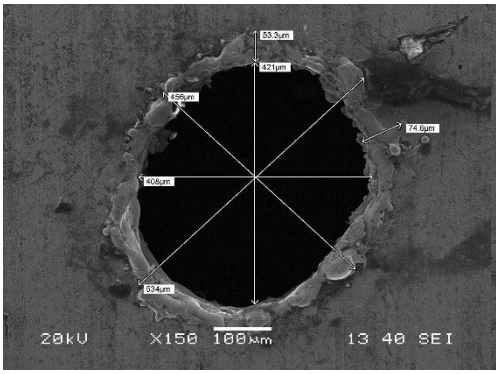

11th Hole Bottom view

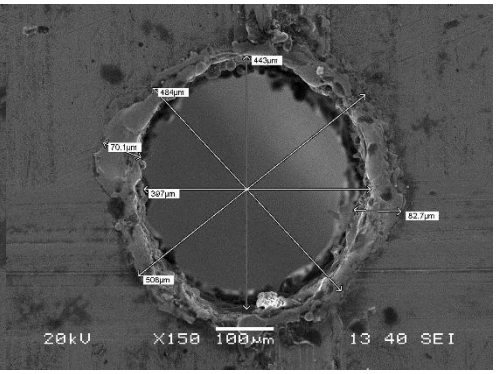

12th Hole Top view

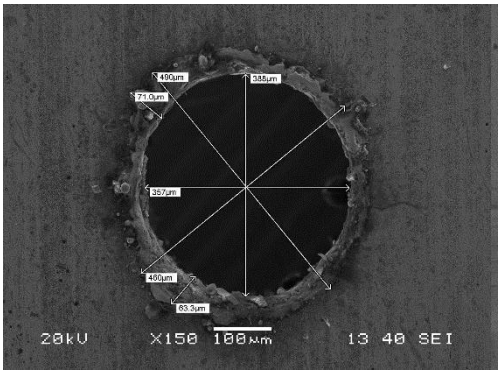

12th Hole Bottom view

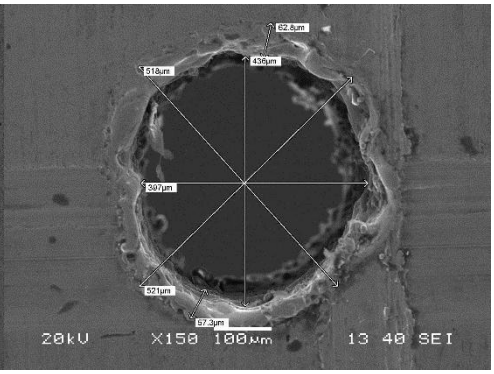

13th Hole Top view

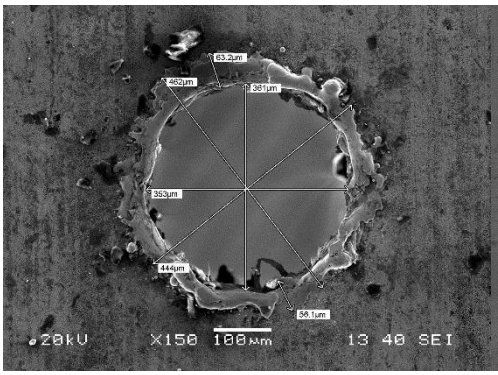

13th Hole Bottom view

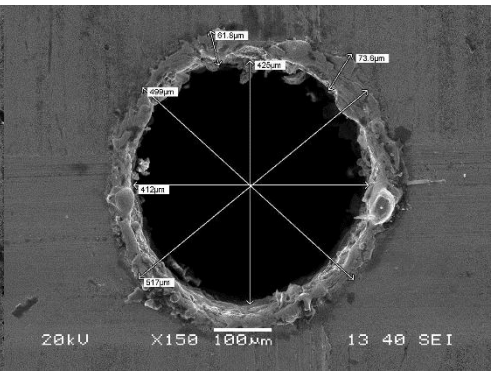

14th Hole Top view

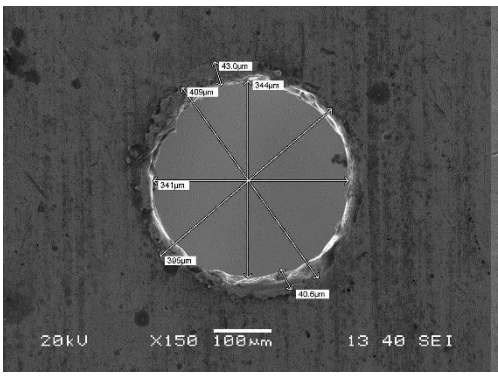

14th Hole Bottom view

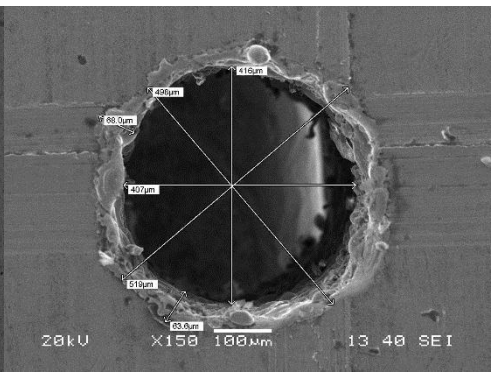

15th Hole Top view

15th Hole Bottom view

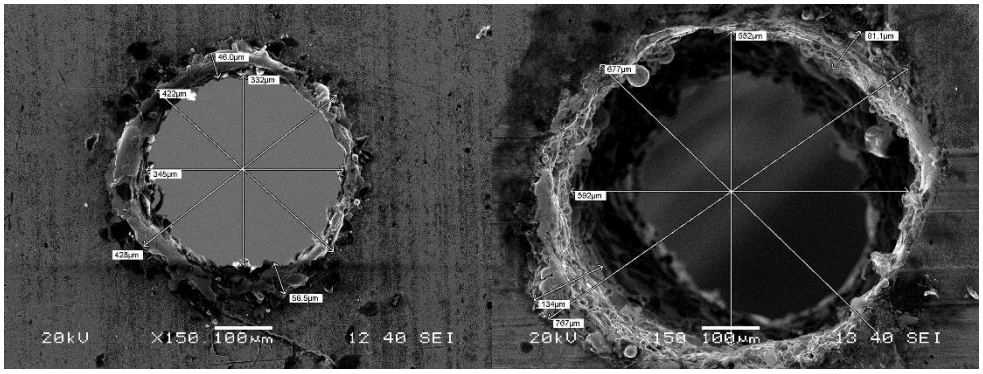

16th Hole Top view 16th Hole Bottom view

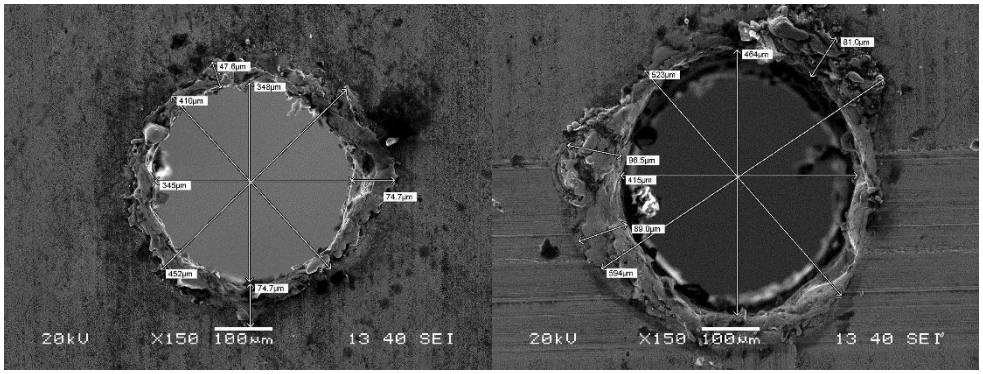

17th Hole Top view 17th Hole Bottom view

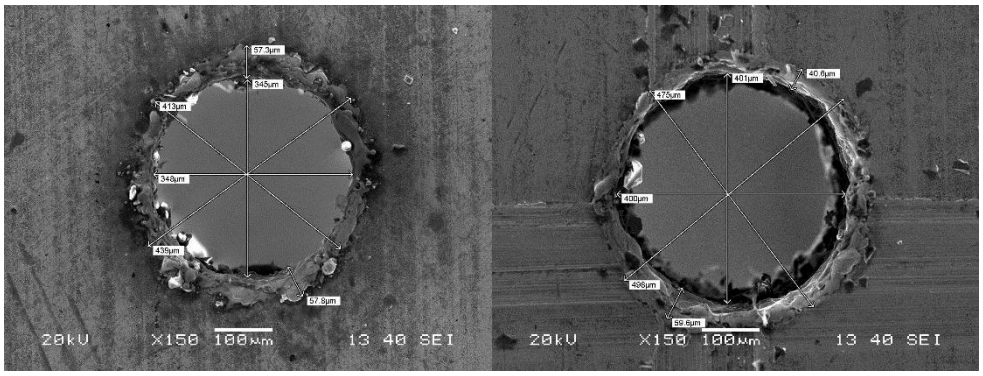

18th Hole Top view 18th Hole Bottom view

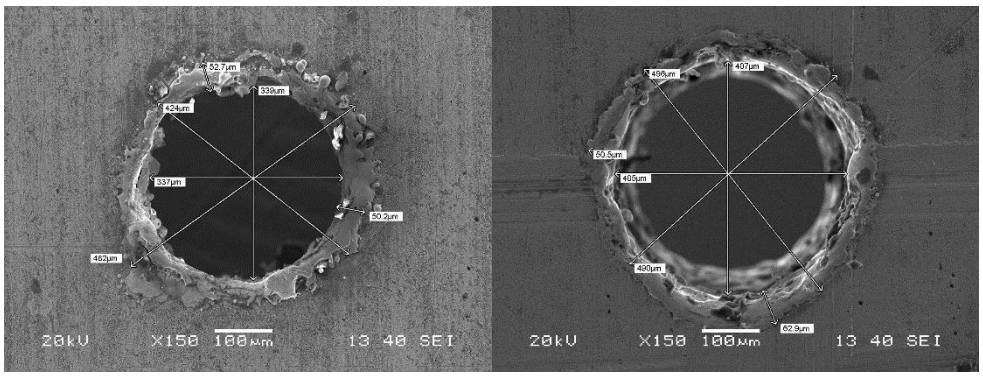

19th Hole Top view 19th Hole Bottom view

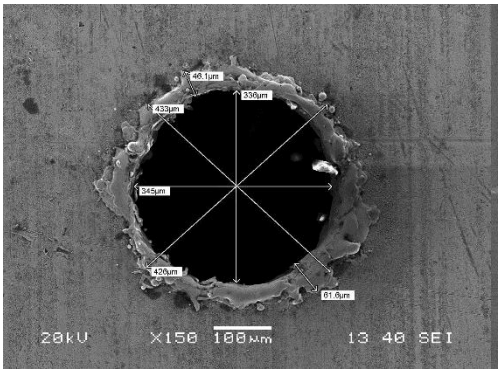

20th Hole Top view

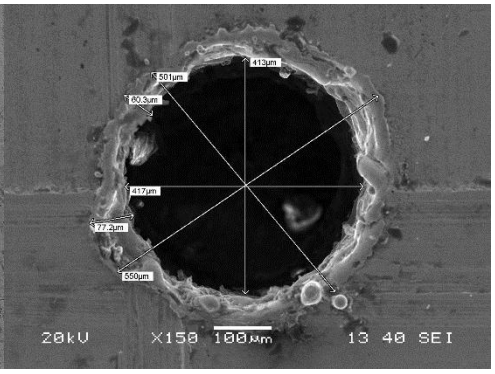

20th Hole Bottom view

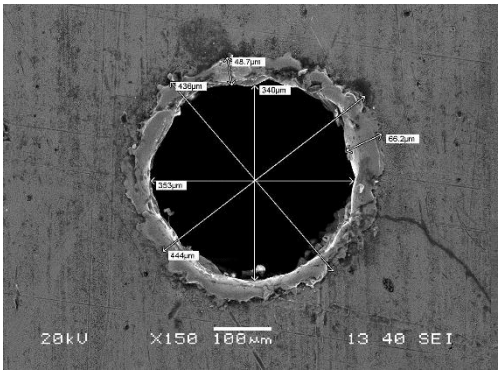

21st Hole Top view

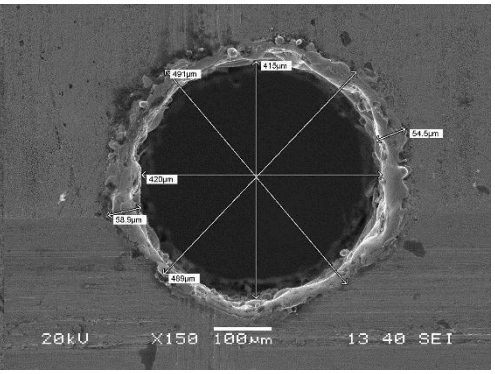

21st Hole Bottom view

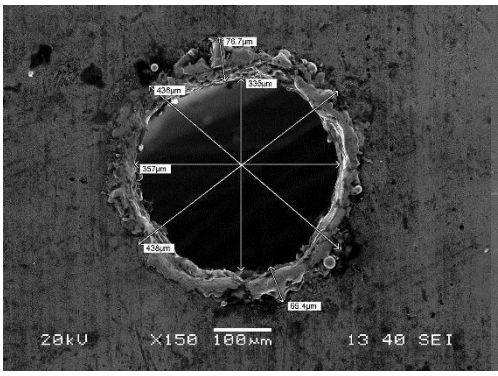

22nd Hole Top view

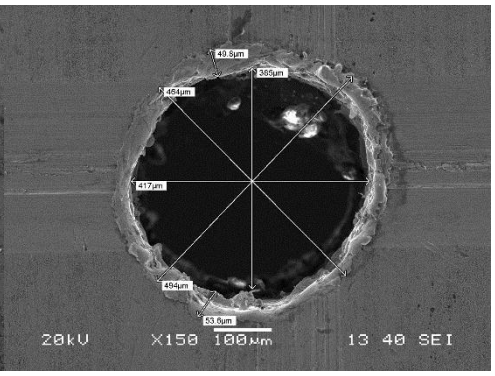

22nd Hole Bottom view

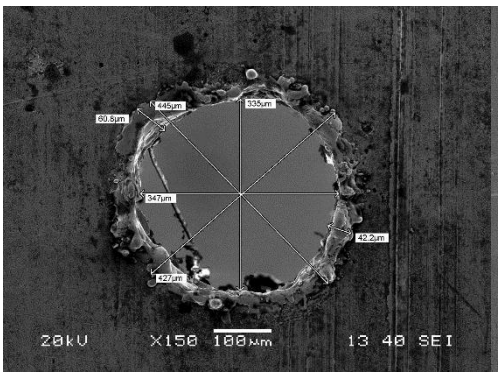

23rd Hole Top view

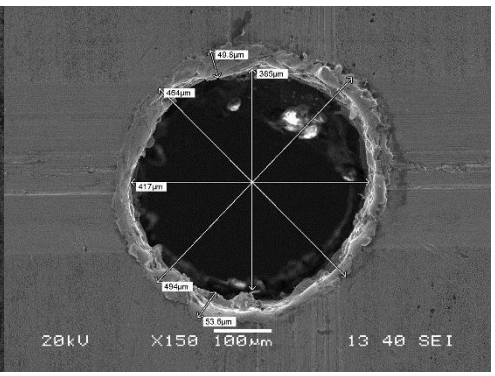

23rd Hole Bottom view

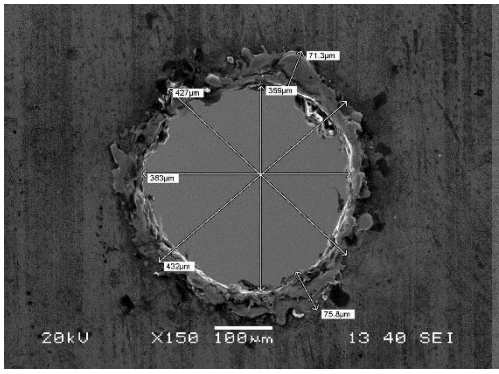

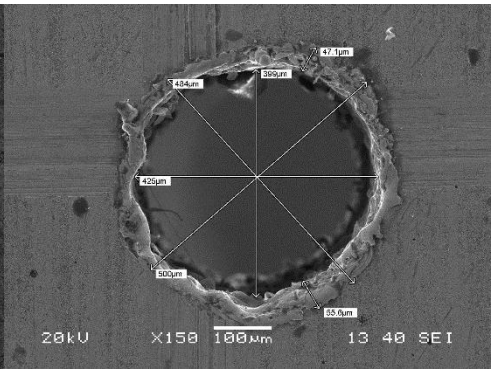

24th Hole Top view

24th Hole Bottom view

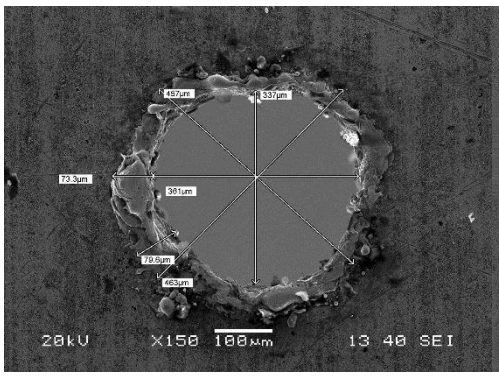

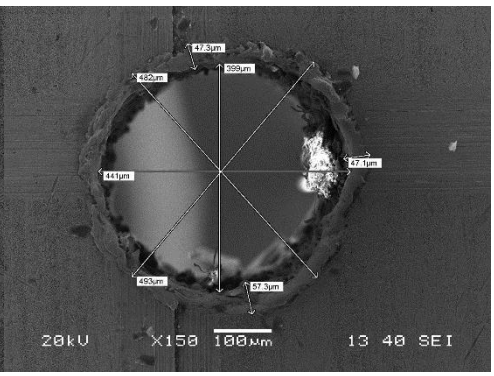

25th Hole Top view

25th Hole Bottom view

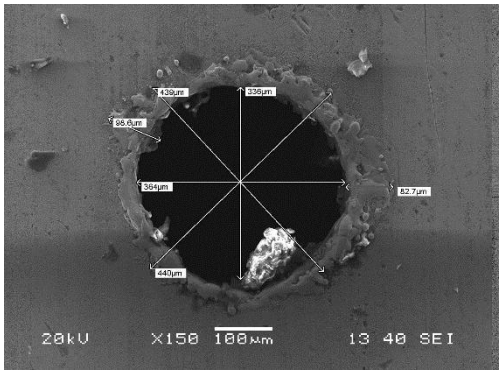

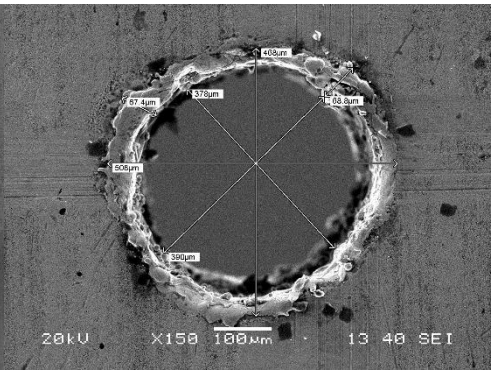

26th Hole Top view

26th Hole Bottom view

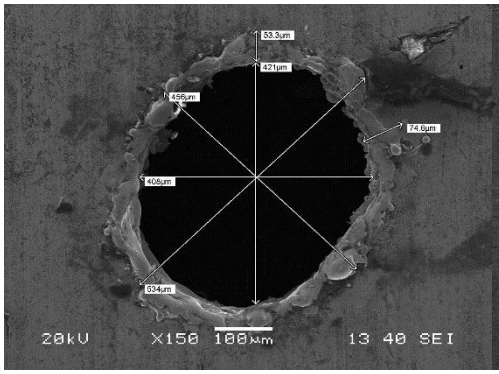

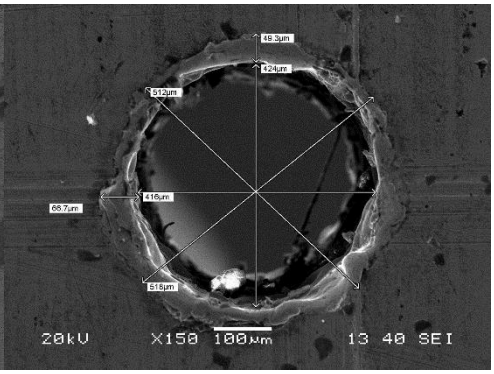

27th Hole Top view 27th Hole Bottom view

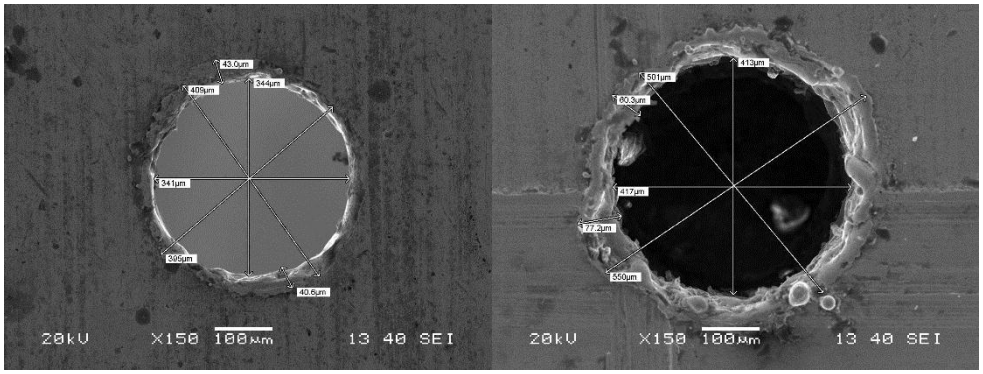

28th Hole Top view 28th Hole Bottom view

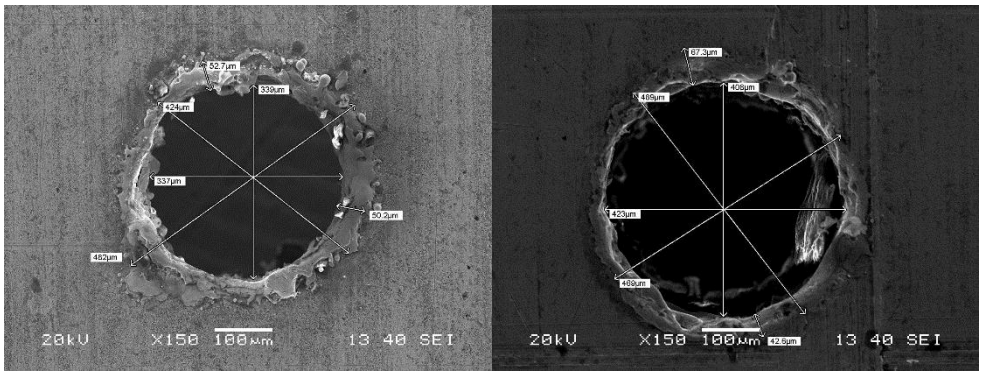

29th Hole Top view 29th Hole Bottom view

30th Hole Top view 30th Hole Bottom view

Figure 5. 21: SEM Images of Micro Holes

5.6.2 RESPONSE SURFACE ANALYSIS OF PROCESS RESPONSES

Based on the experimental data gathered, statistical regression analysis enabled to study the correlation of process parameters with the process responses. In this study, for four variables under consideration, a polynomial regression is used for modeling. For

simplicity, a quadratic model of all responses is proposed. The effects of these variables and the interaction between them were included in this analyses and the developed model is expressed as interaction equation: The unknown coefficients are determined from the experimental data as presented in Table 5.21. The mathematical model correlating process responses like MRR, OC, RCL and TA with the process control parameters is developed as:

$$MRR = 0.58707 - 0.00513478 * A - 0.0114774 * B + 0.000438389 * A * B - 5.25041e\text{-}006 * A * C - 0.000192821 * B * D + 3.82977e\text{-}005 * C * D \quad (5.5)$$

$$OC = 1.10364 - 0.0184954 * C - 0.0228189 * D + 0.000147102 * A * B + 0.000162349 * A * C + 0.000243434 * A * D - 0.0004473 * B * D + 0.000432031 * C * D - 0.000200004 * A^2 + 0.000126543 * B^2 \quad (5.6)$$

$$RCL = 153.628 - 1.82539 * B - 1.77687 * D + 0.00508037 * A * D + 0.0206207 * B * C + 0.0028784 * C * D - 0.00463502 * C^2 \quad (5.7)$$

$$TA = 2.24067 + 0.800158 * A - 0.133417 * B + 0.379744 * C - 2.2702 * D - 0.00228824 * A * C - 0.00720662 * A^2 + 0.00321756 * B^2 - 0.00228902 * C^2 + 0.0475926 * D^2 \quad (5.8)$$

Response Surface Analysis of MRR

The F ratios are calculated for 95% level of confidence and the factors having p-value more than 0.05 are considered. For the appropriate fitting of MRR, the non-significant terms are eliminated by the backward elimination process. The regression model is revaluated by determining the unknown coefficients, which are tabulated in Table 5.22. The model made to represent MRR depicts the most influencing parameters in order of significance. The percentage contributions of different variables have been presented in Figure 5.22.

Table 5. 22:ANOVA for MRR (After backward elimination)

Source	Sum of Squares	DOF	Mean Square	F Value	p-value Prob > F	Percentage Contribution
Model	0.77	6	0.13	13.00	< 0.0001	77
A-Voltage	0.12	1	0.12	12.43	0.0018	12
B-Peak Current	0.048	1	0.048	4.81	0.0386	4.8
AB	0.16	1	0.16	15.73	0.0006	16
AC	0.22	1	0.22	22.52	< 0.0001	22
BD	0.098	1	0.098	9.88	0.0046	9.8
CD	0.13	1	0.13	12.65	0.0017	13
Residual	0.23	23	9.894E-003			
Lack of Fit	0.18	18	0.010	1.08	0.5151	Insignificant
Pure Error	0.047	5	9.341E-003			
Corrected Total	1.00	29				

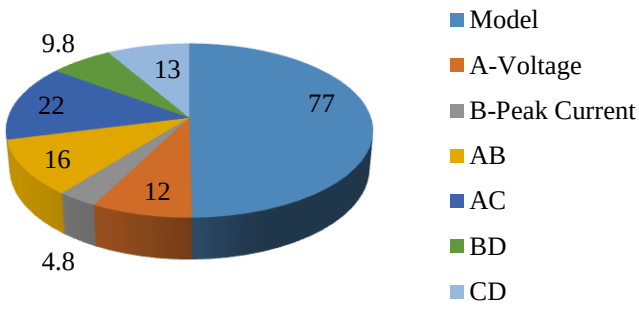

Figure 5. 22: Percentage contribution of process variables

From Table 5.22, it can be observed that the interaction terms AB, AC and CD significantly influence the MRR as their percentage contribution is 16, 22 and 13 % respectively. From Figure 5.23, it is observed that maximum MRR value of 0.709 mm^3/min was obtained at the highest voltage of 60 V and highest peak current (40A) combination. The minimum MRR value of 0.357mm^3/min was obtained at the lowest voltage (30V) and highest peak current of (40A) combination. It is observed that material removal rate initially increases with increase in voltage and peak current then it decreases with further increase in voltage and peak current. There is a significant increase in material removal rate with increase in voltage, however with increase in peak current there is a slight decrease in MRR.

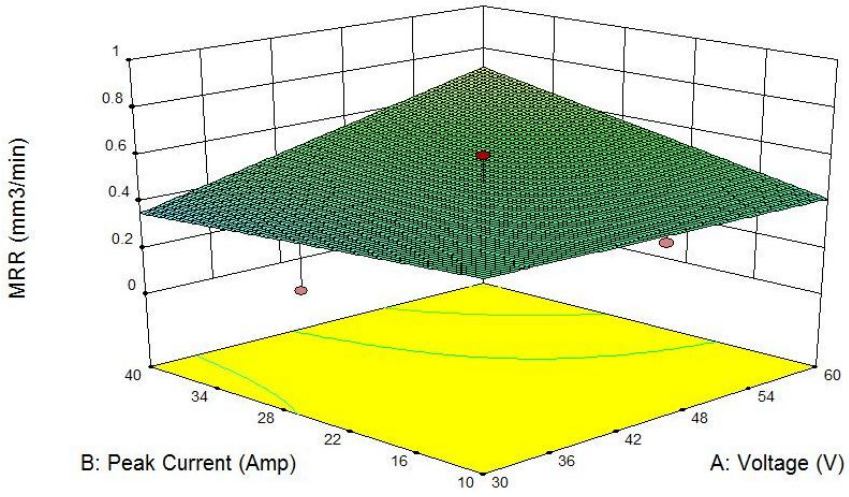

Figure 5. 23: Interaction effect of voltage and peak current on MRR

At constant peak current of 25A and pulse off duration of 25 µs the interaction effect of voltage and pulse on duration on MRR represented in Figure 5.24. It is observed that maximum MRR was found at the lowest voltage (30V) and highest pulse on duration

(80µs). The minimum MRR was obtained at the highest voltage (60V) and lowest pulse off duration of 40µs combination. It also points towards most significant contribution from the interaction terms of the process variables. It is observed that MRR increases with increase in voltage and the pulse on duration.

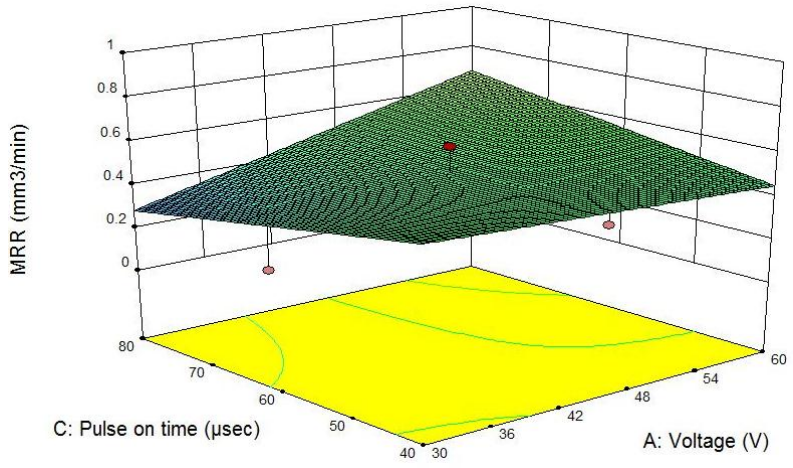

Figure 5. 24: Interaction effect of voltage and pulse on duration on MRR

Figure 5.25 displays the interaction effect of pulse on duration and pulse off duration on MRR in the form of 3D surface graph at constant peak current of 20 A and voltage of 35 V. Furthermore, it is observed that maximum MRR value of 0.570mm^3/min was obtained at the highest values of pulse on duration and pulse off duration. In addition, it was also observed that with the increase in pulse on duration the MRR increases, while it initially decreases and then increases with increase in pulse off duration.

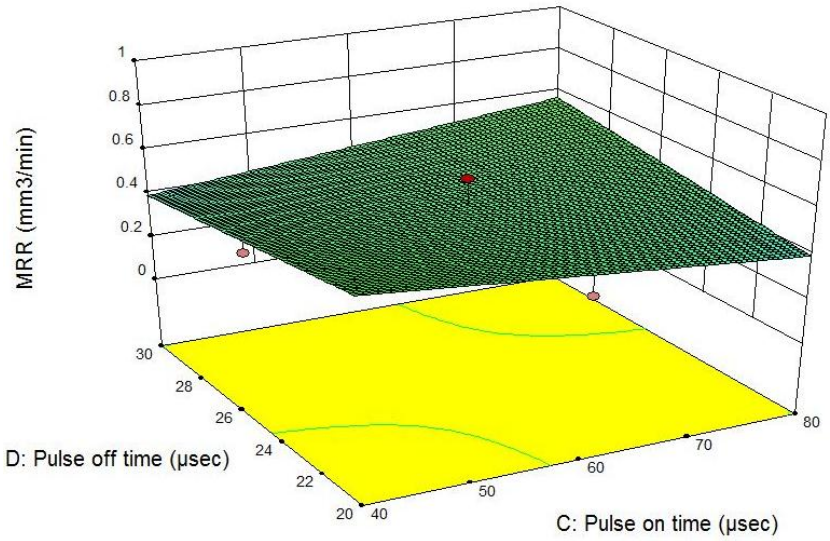

Figure 5. 25: Interaction effect of pulse on duration and pulse off duration on MRR

Response Surface Analysis of OC

For the appropriate fitting of OC, the non-significant terms are eliminated by the backward elimination process. The regression model is revaluated by determining the unknown coefficients, which are tabulated in Table 5.23 in "Appendix 46". The model made to represent OC depicts the most influencing parameters in order of significance.

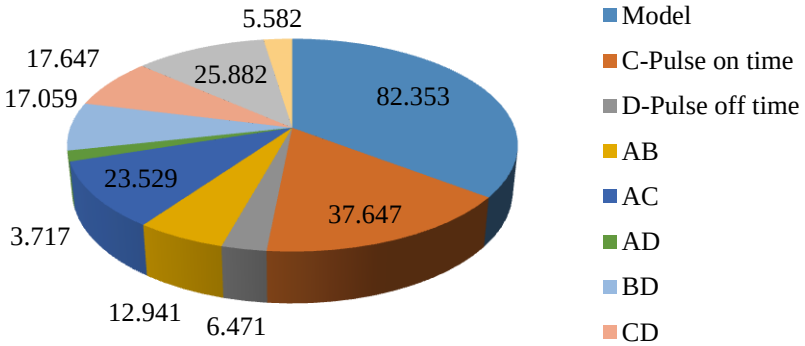

Figure 5. 26: Percentage contribution of process variables

Figure 5.26 shows the percentage contribution of different process variables on OC, pulse on duration has a significant effect on OC. Additionally, among different interaction

terms AB. AC, AD, BD and CD the percentage contribution of AC is found to more influential owing to highest percentage contribution of 23.52%. Further F-value of the model 12.88 indicates that the model is significant. There is only a 0.05% chance that an F-value this large could occur due to noise. At constant peak current of 25 ampere and pulse off duration of 25µs is represented in Figure 5.27. From this Figure, it is observed that maximum OC was obtained at the highest voltage of (60V) and lowest pulse on duration of 40µs.The minimum OC was attained at the lowest voltage (30V) and highest pulse on duration of (80µs) combination. It indicates significant contribution from the interaction of the machining parameters. It is witnessed that OC first increases with increase in voltage and the pulse on duration and then decreases. There is a noteworthy increase in OC with increase in voltage however with increase in pulse on duration initially there is increase in OC then reduction on further increment of pulse on duration.

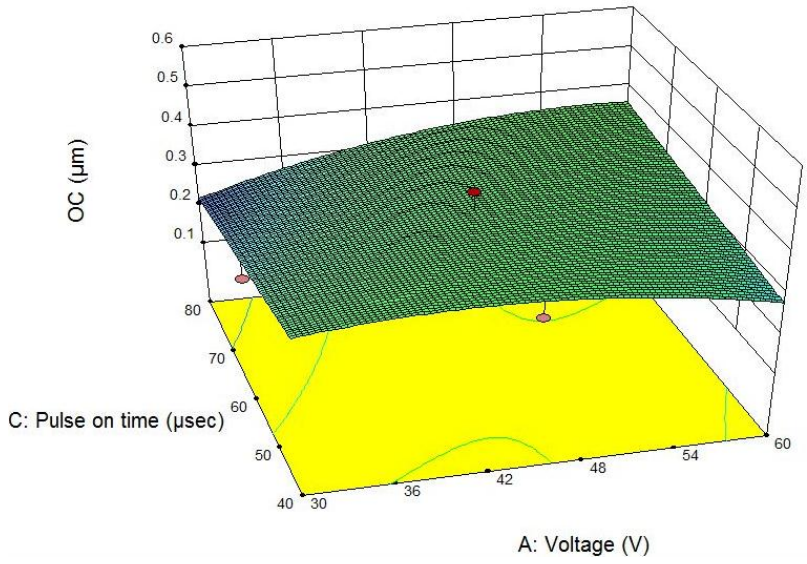

Figure 5. 27: Interaction effect of Voltage and Pulse on duration on OC

Response Surface Analysis of RCL

For the proper fitting of RCL, the non-significant terms are eliminated by the backward elimination process. The truncated model for RCL after backward elimination process is presented in Table 5.24 in "Appendix 47" and it can be seen that the model F-value of 9.51 implies the model is significant. There is only a 0.01% chance that an F-value this large could occur due to noise. The percentage contribution of different process variables on RCL is presented in Figure 5.28.

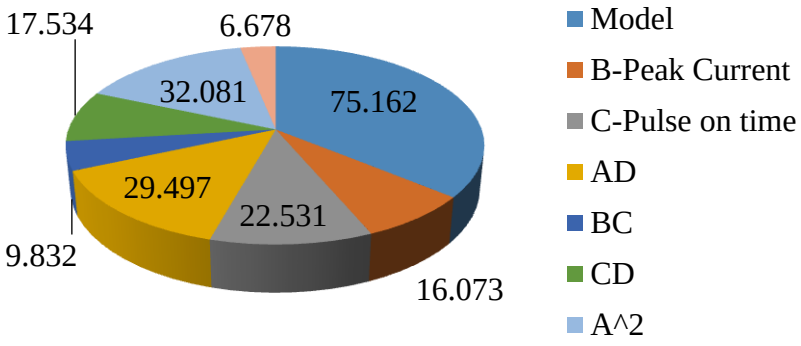

Figure 5. 28: Percentage contribution of process variables

Furthermore, among different interaction terms AB. BC and CD the percentage contribution of AD is found to more influential owing to highest percentage contribution of 29.49%. Figure 5.29 shows the interaction effect of voltage and pulse off duration on RCL at constant peak current of 25 A and pulse on duration of 60 µs. From this Figure, it is observed that minimum RCL value of 58.40 µm was obtained at the highest values of voltage and pulse off duration. Furthermore, it was observed that with the increase in pulse off duration RCL increases linearly, while it non linearly increases with increase in voltage, with the increase in both voltage and pulse off duration RCL decreases.

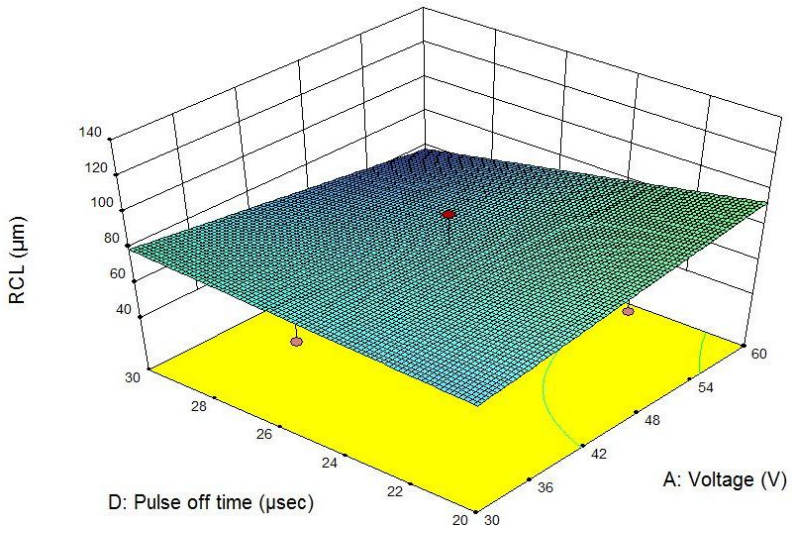

Figure 5. 29: Interaction effect of Voltage and Pulse off duration on RCL

Response Surface Analysis of TA

The non-significant terms are eliminated by the backward elimination process. The truncated model for TA after backward elimination process is presented in Table 5.25 in "Appendix 48" and it can be seen that the model F-value of 9.51 denotes the model significance. There is only a 0.01% chance that an F-value this large could occur due to noise. The percentage contribution of different process variables on TA is presented in Figure 5.30 and it can be perceived that voltage has a significant effect on TA. Also, the square terms of voltage, peak current pulse on duration and pulse off duration are also found to be significant. However, it is interesting to note that there are no significant interaction terms in this model. Further the model F-value of 21.30 implies the model is significant. There is only a 0.01% chance that an F-value this large could occur due to noise.

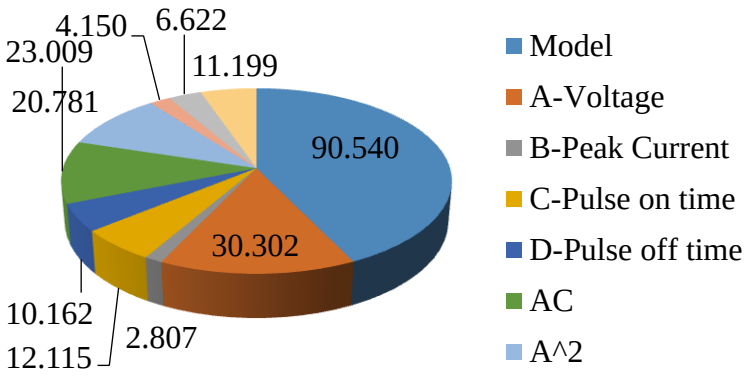

Figure 5. 30: Percentage contribution of process variables

5.6.3 ANN MODELING:

ANN architecture consist of many neurons interconnected, and this net forms a processing system. The Layers consist of processing elements that are called as neurons. A network with 4x12x4 architecture, which means 4 input (Voltage, Peak current, Pulse on duration and Pulse off duration neurons in the input layer, 12 neurons in the hidden layer and 4 outputs (MRR and Overcut, Recast layer thickness, and Taper Angle) in the output layer. Generally, in the multi-layer feed forward network, the size of hidden layers is one of the most important considerations when solving problems. Two hidden layers were adopted in this model. The inputs and outputs are normalized to gain better results. To train the developed model, 20 data sets were used which are tabulated in Table 5.26 in "Appendix 49". A MATLAB© program is written to train, test and predict the MRR and overcut values. Properly trained back-propagation network tends to give reasonable answers when presented with inputs that have never been fed before to it. During training phase, the regression value of 0.99885, 0.99703, 0.99967 and 0.999843 for MRR, OC,

RCL and TA have been obtained which signifies the fair correlation between experimental and predicted values.The regression plot for MRR, OC, RCL and TA have been given in Figure 5.31(a-d). Hence ANN can be effectively used for the prediction of MRR, OC, RCL and TA in µ-EDM.

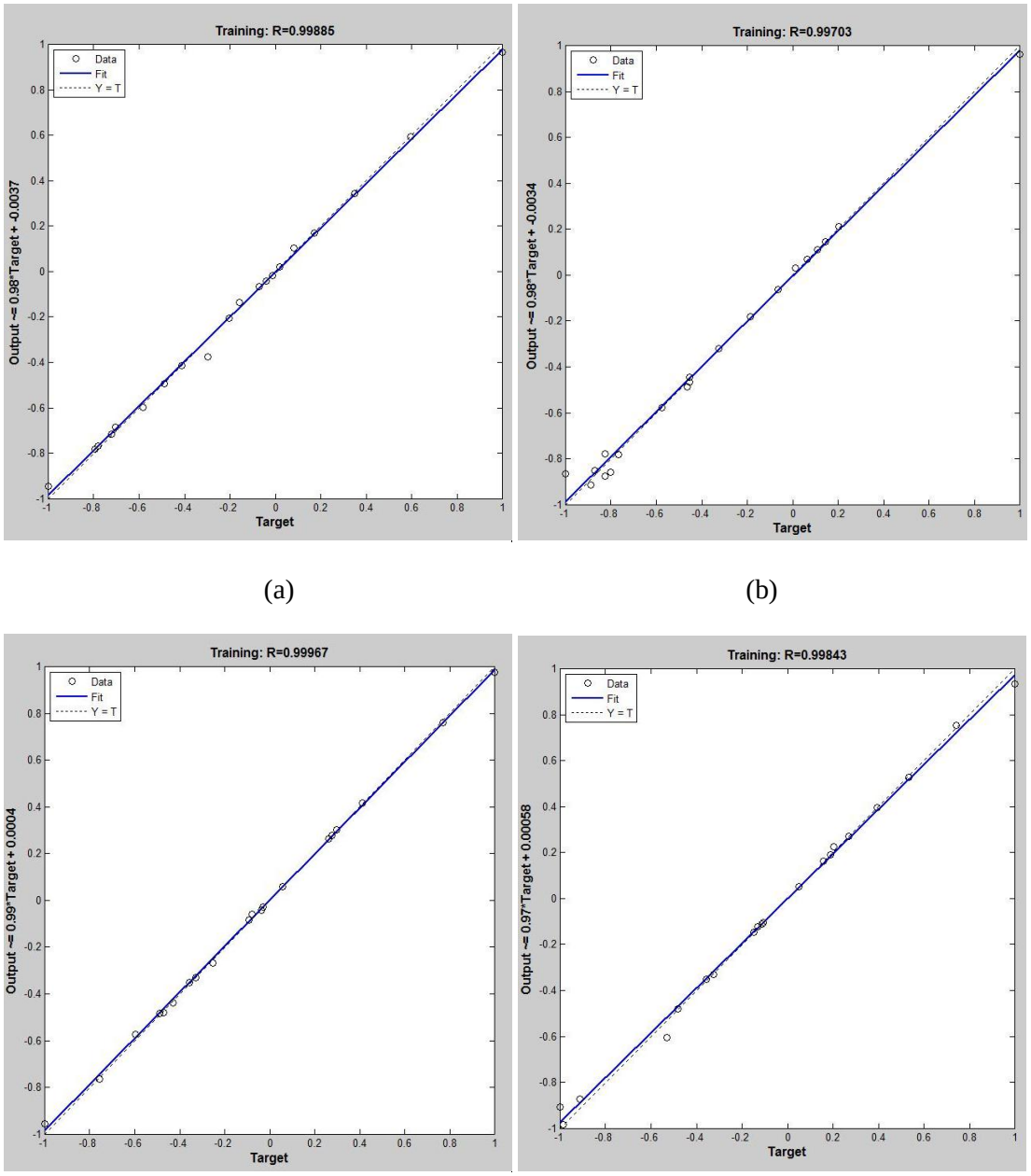

Figure 5. 31(a-d): Regression plot for MRR, OC, RCL and TA

The trained neural network was validated against another set of experimental data, termed as validation data set illustrated in Table 5.27 in "Appendix 50". The errors in prediction are also presented in Table 5.27. It can be seen from Table 5.28 in "Appendix 50" that the model predictions match the experimental data very closely except few data.

Moreover, the average error in the prediction was -19.150 % for MRR, 0.391 % for OC, and 4.343 % for RCL and 15.038 % for TA respectively. The total average prediction error of the network was predicted as 0.621 % which indicates that the model is over predicting the values. The developed ANN model was tested by repeating few experiments randomly from the entire data set for checking the predictive accuracy of the developed model. Figures (5.32- 5.35) indicated the errors between predicted and experimental values for all process responses.

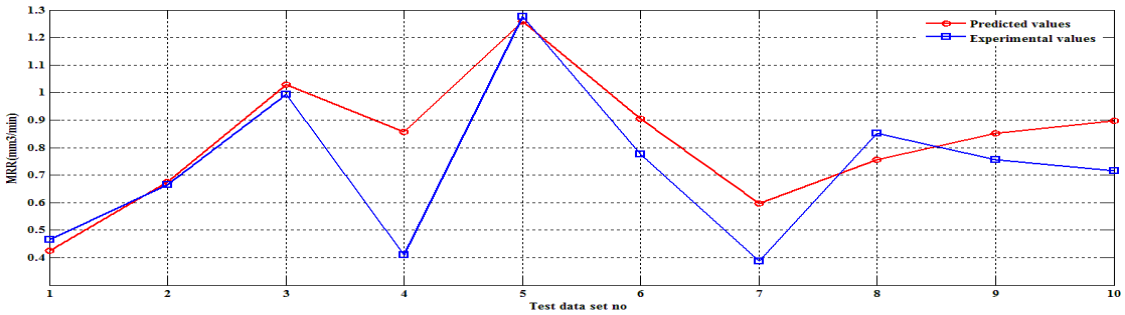

Figure 5. 32: Errors between predicted and experimental values of MRR during testing

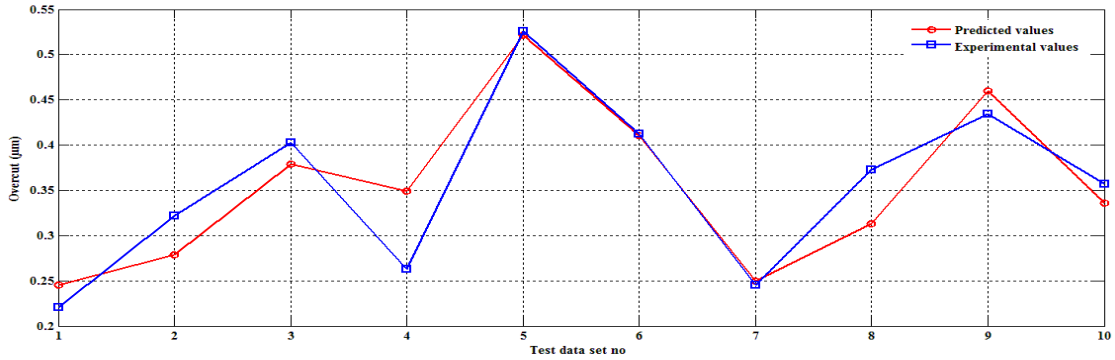

Figure 5. 33: Errors between predicted and experimental values of OC during testing

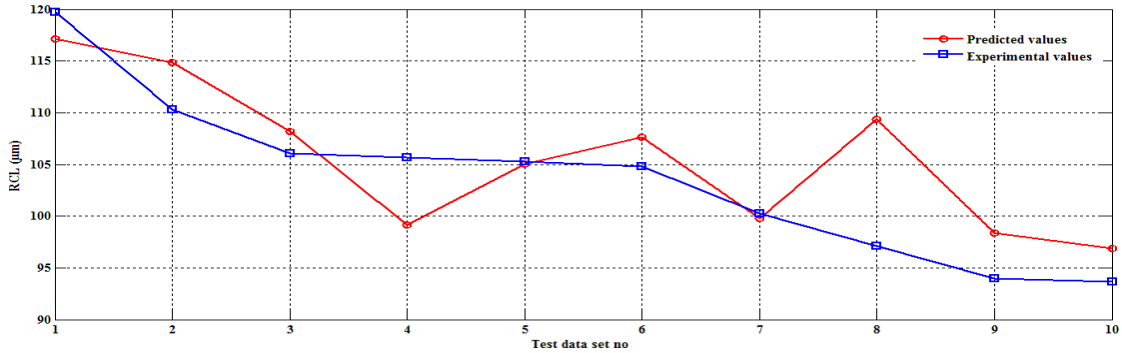

Figure 5. 34: Errors between predicted and experimental values of RCL during testing

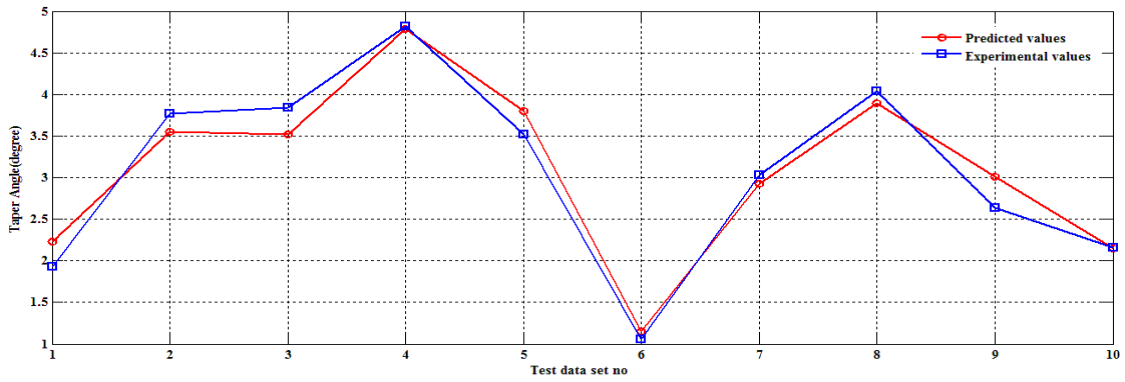

Figure 5. 35: Errors between predicted and experimental values of TA during testing

Table (5.29 – 5.30) in "Appendix 51" contains testing of the developed model with experimental data and the predicted output and percentage error in prediction of MRR, OC and RCL were within acceptable limits. It is observed that the total average prediction error is - 4.377 % which is implies level of over prediction.

5.6.4 ANFIS MODELING

The prediction of MRR, OC RCL and TA has been carried out using ANFIS and MATLAB 2012b package (ANFIS toolbox) has been used. Prediction of MRR, OC, RCL and TA of the micro-EDM process by ANIFS comprises of three main phases, training, validation and testing. A similar methodology was adopted as mentioned in section 4.4. However, for the purpose of comparing the predictive tendency with ANN model same data was used for training, validation and testing as it was used for development of ANN. Total average error (TAE) as mentioned in Equation 4.14 is considered as selection criteria for comparison of all existing networks and final selection is made of the most accurate one. The value of error goal was set at 0.03, and the iteration number was 500 epochs. Various structures were tested of ANFIS model for each response (material removal rate, overcut recast layer thickness and taper angle), it was obtained that structures with 16 numbers of membership functions (2 MFs for each input) had the lowest values of TAE for each response. In this work various types of MFs namely triangular, trapezoid, generalized bell and Gaussian have been practiced. Table 5.31 in "Appendix 52" represents training and validation error of ANFIS models for different membership functions. TAE for MRR, OC, RCL and TA have been presented in Table 5.32 in "Appendix 52". Results indicated that the generalized bell function leads the lowest values of TAE for MRR, OC RCL and TA, respectively. The developed ANFIS model was tested for checking the predictive accuracy of the developed model. Tables

(5.33 – 5.34) in "Appendix 53" contains testing of the developed model with experimental data and the predicted output and percentage error in prediction of MRR, OC and RCL were within acceptable limits. It is observed that the total average prediction error is -7.519 % which implies level of over prediction.

5.6.5 MULTI-OBJECTIVE OPTIMIZATION

The process of optimizing simultaneously a collection of objective functions is called as multi-objective optimization (MOO). In the present section multi-objective optimization has been carried out using three meta-heuristic approaches namely Elitist Teaching learning based optimization, Differential evolution and Artificial Bee colony optimization. Furthermore, pareto optimal sets of solution obtained from each algorithm have been ranked using centroid based Fuzzy ranking method as discussed in section 4.4.2. The regression Equations (5.5-5.8) obtained from ANOVA analysis haven used for formulating the objective functions. In present multi-objective optimization regime only MRR have to maximized while OC, RCL and ta have to minimized. The tuning parameters for each algorithm were same as discussed in sections 4.4.1, 4.4.3 and 4.4.4. The results obtained from MOETLBO, MODE and MOABC after applying centroid based Fuzzy ranking method have been presented in Tables 5.35-5.37 in Appendixes (54-56). The results of optimization of µ-EDM process using ETLBO and MODE and MOABC are presented in Table 5.38.

Table 5.38: Optimization results

Response	MOETLBO			MODE			MOABC		
	Best	Mean	Worst	Best	Mean	Worst	Best	Mean	Worst
MRR (mm^3/min)	0.478	0.387	0.311	0.550	0.488	0.409	0.344	0.266	0.209
OC(µm)	0.252	0.271	0.273	0.346	0.394	0.384	2.228	2.393	2.384
RCL(µm)	97.111	79.335	61.623	94.298	75.871	57.960	99.030	82.609	67.112
TA(degree)	1.708	2.374	3.069	0.714	1.611	2.079	3.338	3.637	4.092

From Table 5.38 it can be observed that for MRR, RCL and TA, MODE yielded the best i.e., maximum value of MRR and minimum values of RCL and TA. However, for OC the minimum value was obtained from MOETLBO. Furthermore, when mean value of solutions obtained from different algorithms was compared it has been observed that for MRR the mean value obtained from MODE was higher than that of MOETLBO and MOABC. Additionally, for the case of OC, RCL and TA the mean value of solutions obtained from MOABC was higher than MOETLBO and MODE. Hence from the above results it can be concluded that none of algorithms ensure the best solutions for all

process responses which justifies the existence of no free lunch theorems still holds valid for multi-objective regime.

5.7. FABRICATION OF MICRO-HOLE IN TITANIUM USING PLATINUM AS TOOL ELECTRODE

5.7.1. EXPERIMENTAL DETAILS

In third phase of experimentation the fabrication of micro-hole has been carried out in Titanium with platinum as electrode tool material in micro-EDM operation. The platinum electrode used is shown in Fig. 5.36. The work-piece and SEM images of micro-holes are given in Figure 5.37 and Figure 5.38 respectively. The Experimental condition for micro-hole machining on Titanium are given in Table 5.39.

Table 5. 39: Experimental condition

Machine Tool	AGIETRON 250 C
Workpiece	25×15×1 mm Titanium plate
Tool electrode	Platinum tool of diameter 0.5mm diameter
Dielectric fluid	EDM oil 3033
Polarity	Positive (workpiece '+ve' and tool '-ve')
Pulse-on time	40 to 80 µs
Pulse-off time	20 to 30 µs
Peak current	10 to 40 amps
Gap voltage	30 to 60 volts

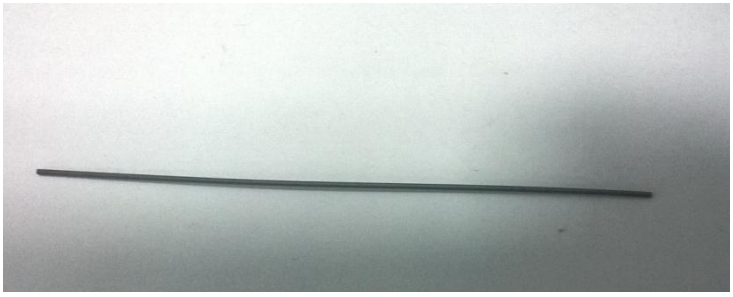

Figure 5. 36: Platinum electrode

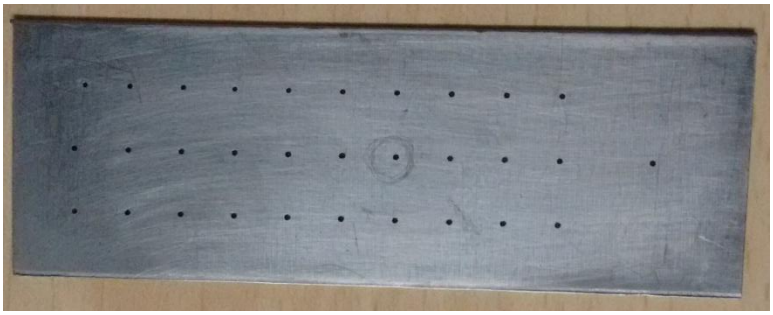

Figure 5. 37: Titanium workipece

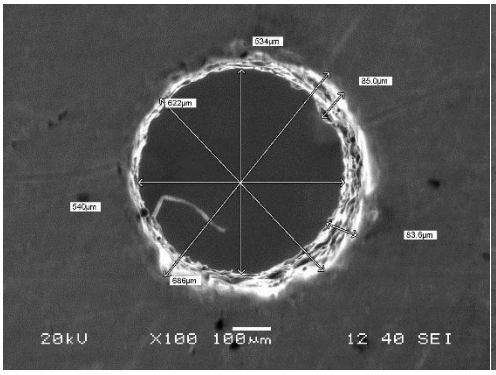

1st Hole Top view

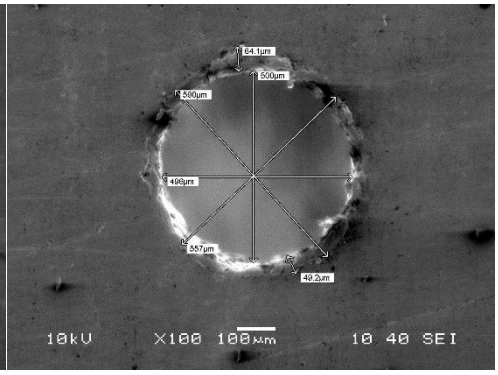

1st Hole Bottom view

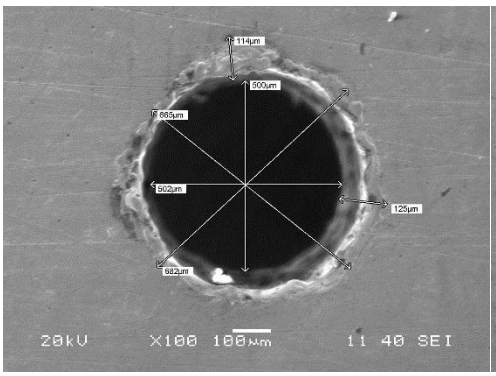

2nd Hole Top view

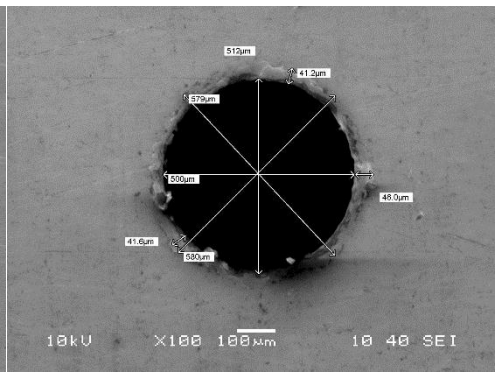

2nd Hole Bottom view

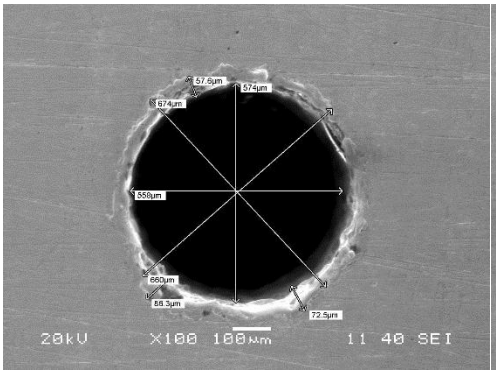

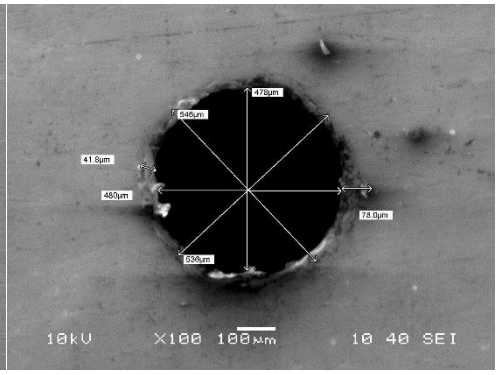

3rd Hole Top view

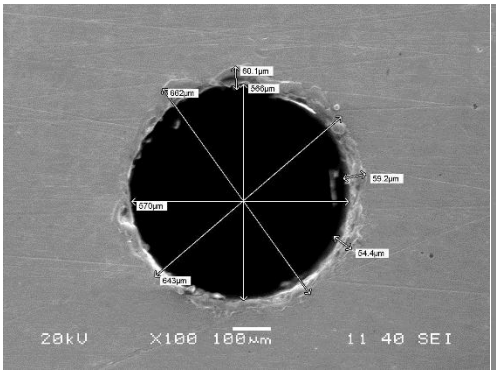

3rd Hole Bottom view

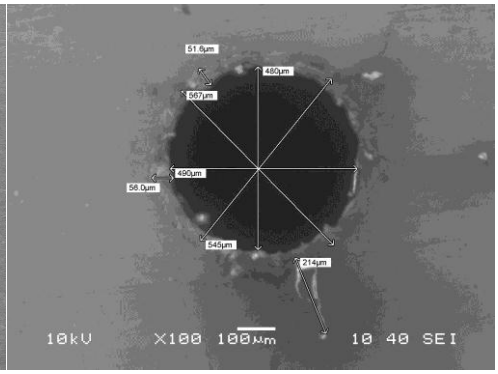

4th Hole Top view

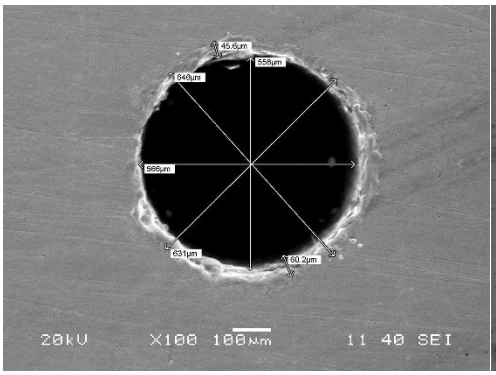

4th Hole Bottom view

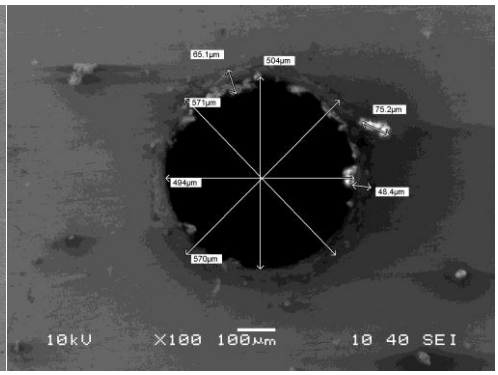

5th Hole Top view

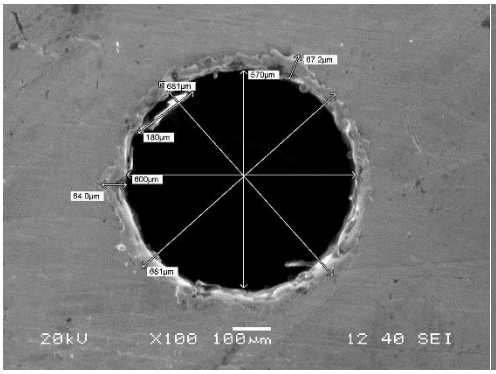

5th Hole Bottom view

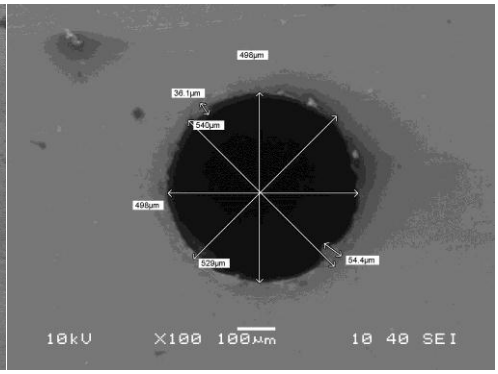

6th Hole Top view

6th Hole Bottom view

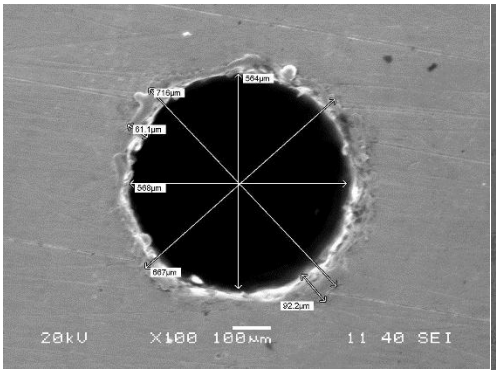

7th Hole Top view

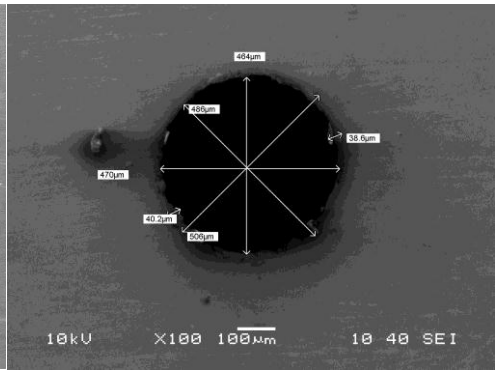

7th Hole Bottom view

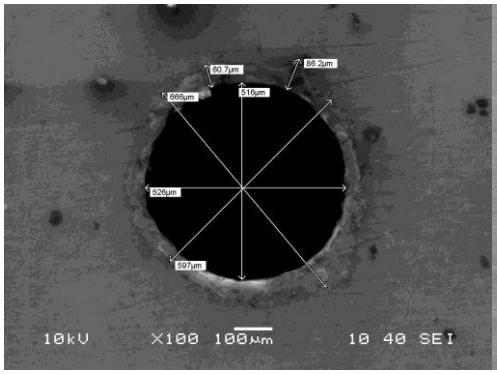

8th Hole Top view

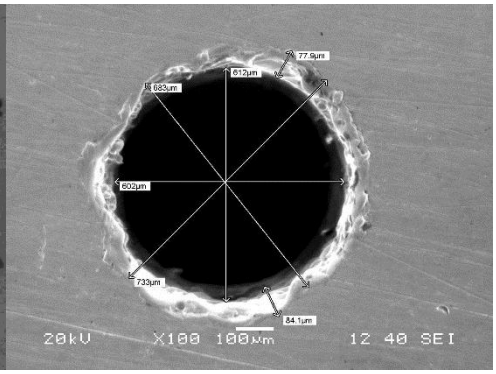

8th Hole Bottom view

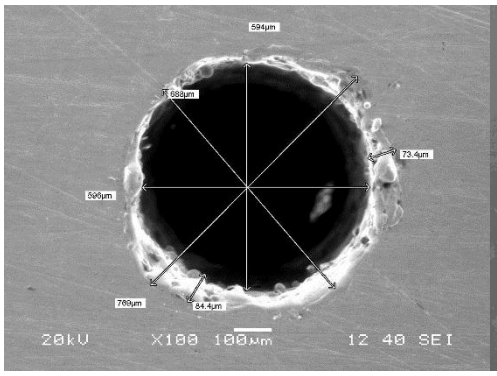

9th Hole Top view

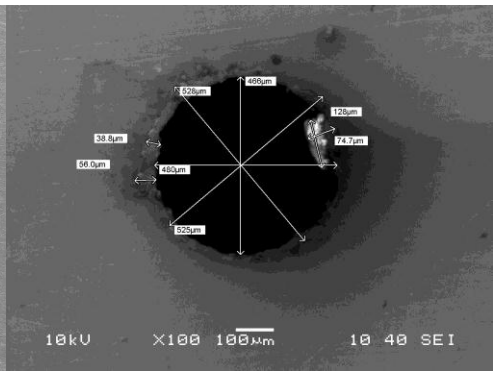

9th Hole Bottom view

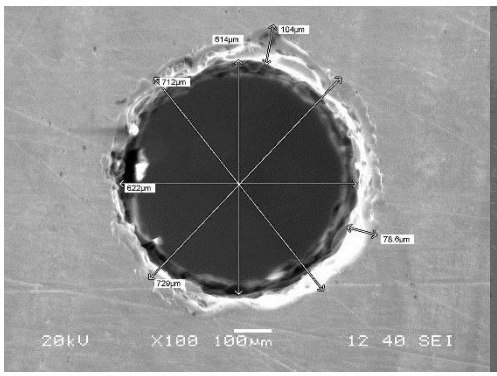

10th Hole Top view

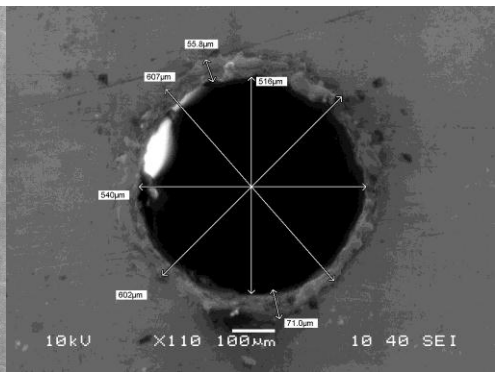

10th Hole Bottom view

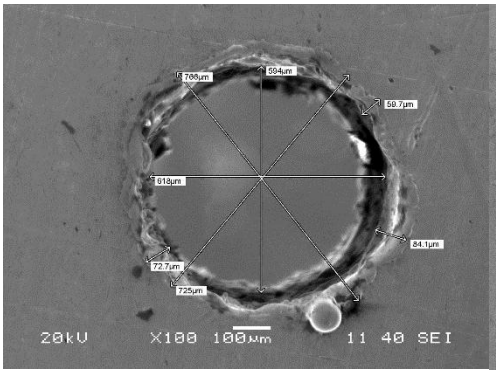

11th Hole Top view

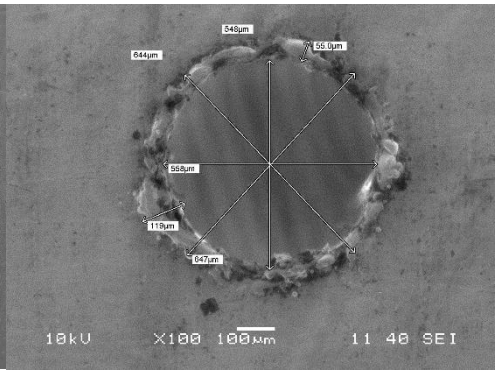

11th Hole Bottom view

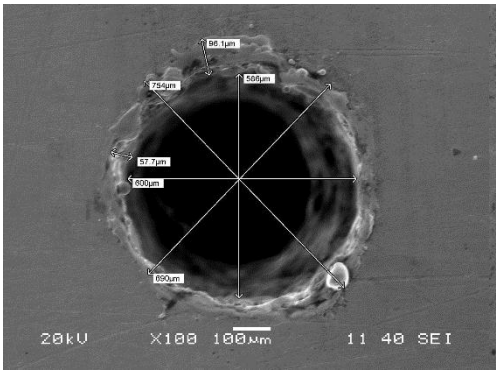

12th Hole Top view

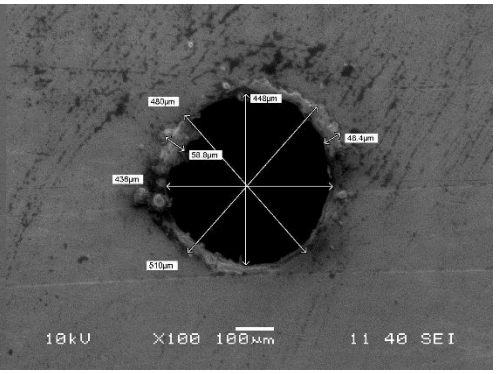

12th Hole Bottom view

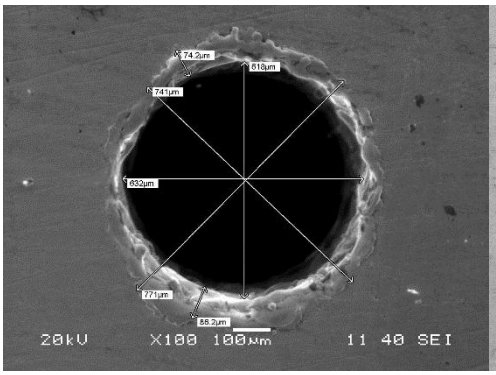

13th Hole Top view

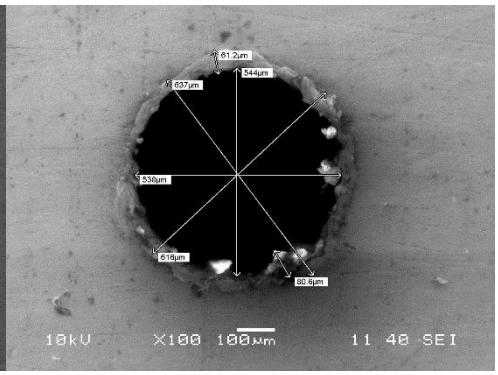

13th Hole Bottom view

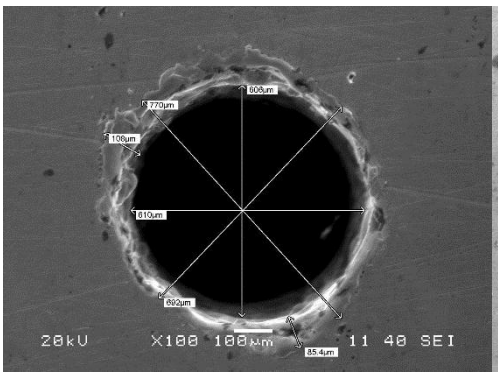

14th Hole Top view

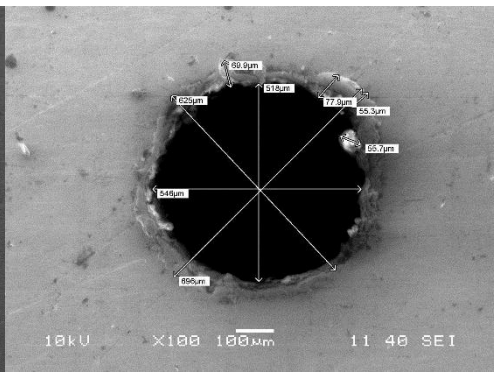

14th Hole Bottom view

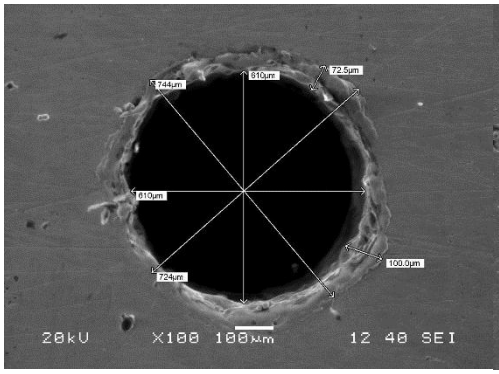

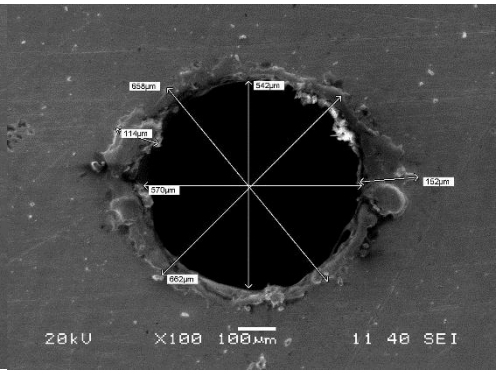

15th Hole Top view

15th Hole Bottom view

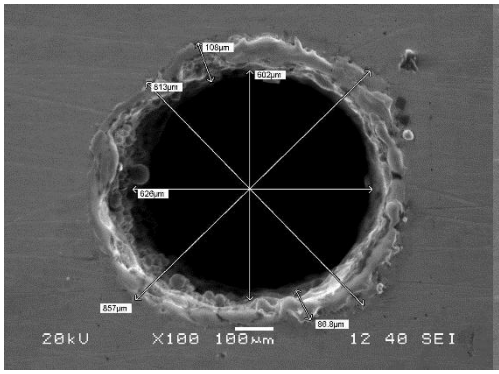

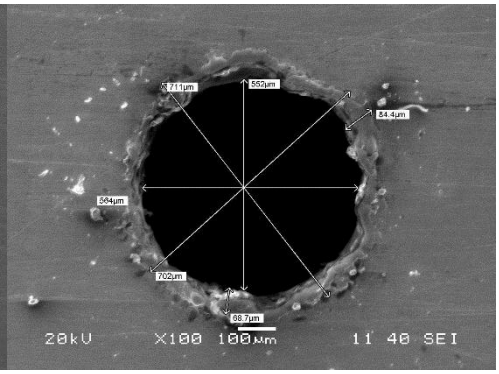

16th Hole Top view

16th Hole Bottom view

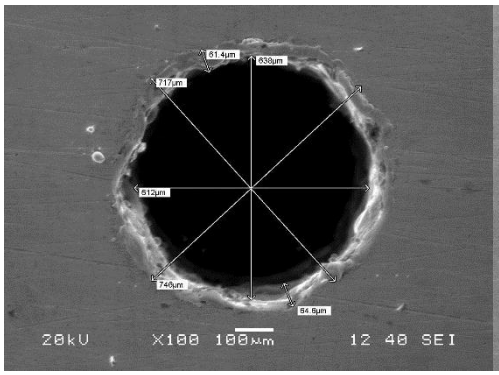

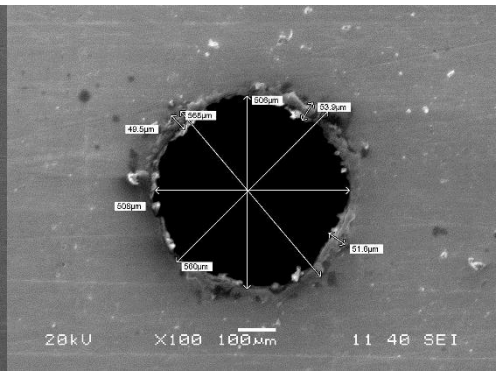

17th Hole Top view

17th Hole Bottom view

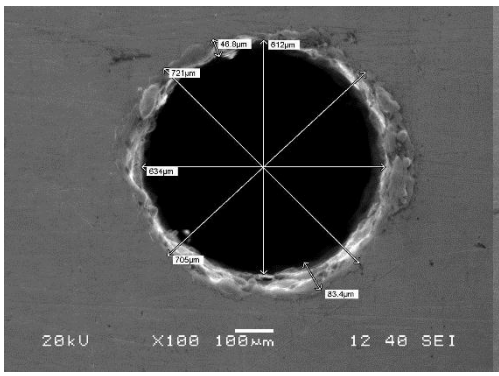

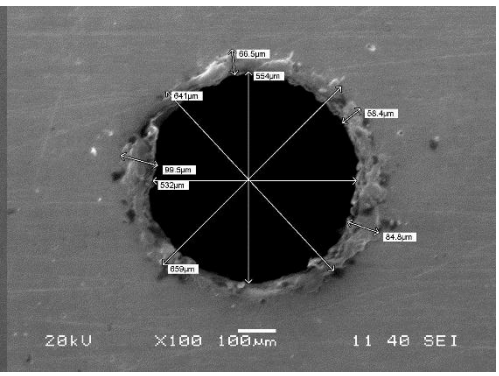

18th Hole Top view

18th Hole Bottom view

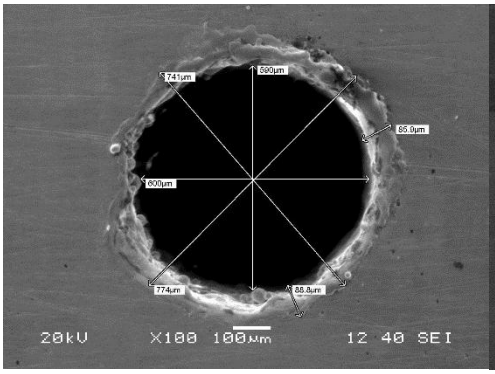

19th Hole Top view

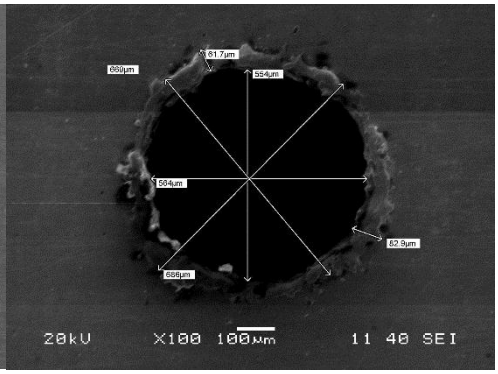

19th Hole Bottom view

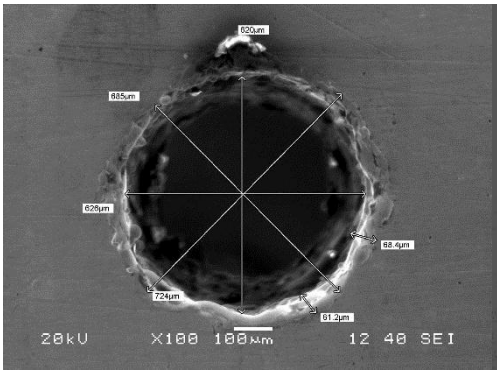

20th Hole Top view

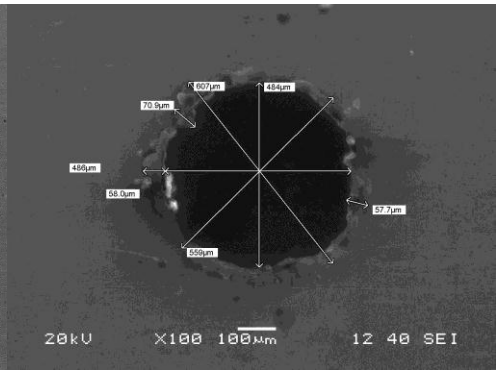

20th Hole Bottom view

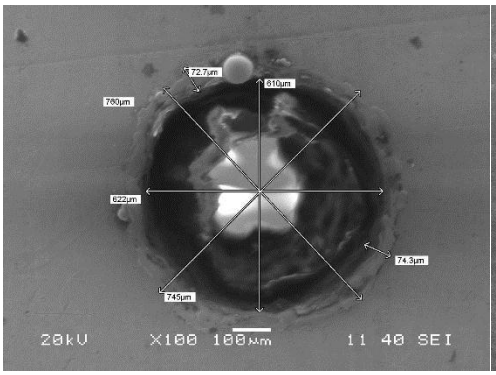

21st Hole Top view

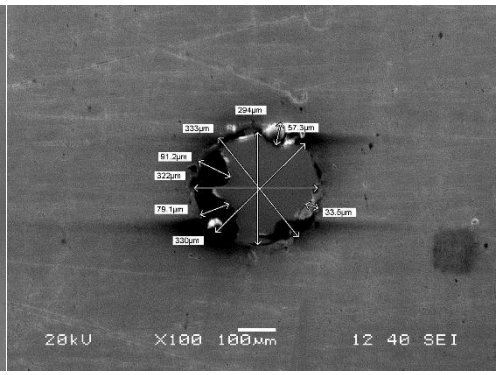

21st Hole Bottom view

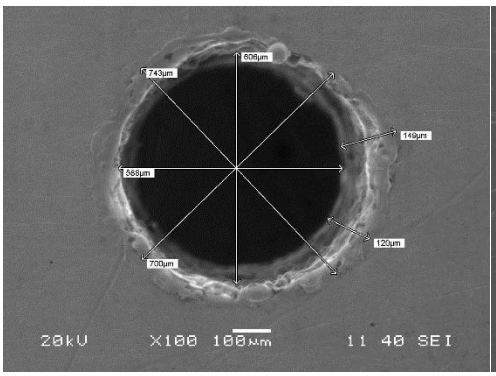

22nd Hole Top view

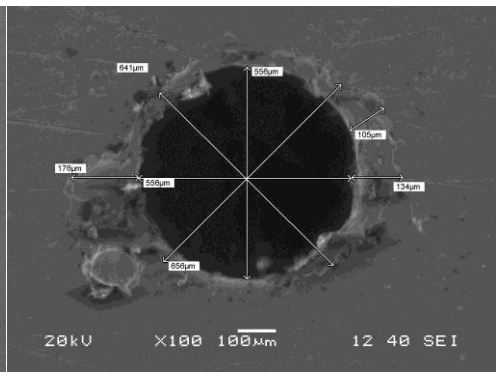

22nd Hole Bottom view

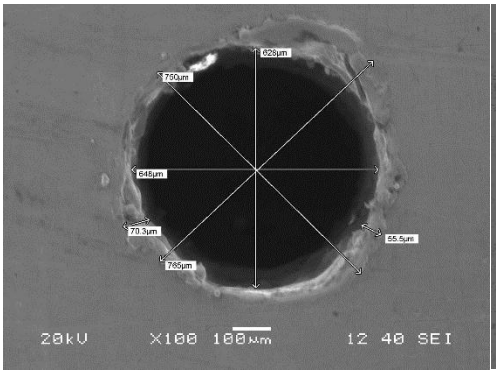

23rd Hole Top view

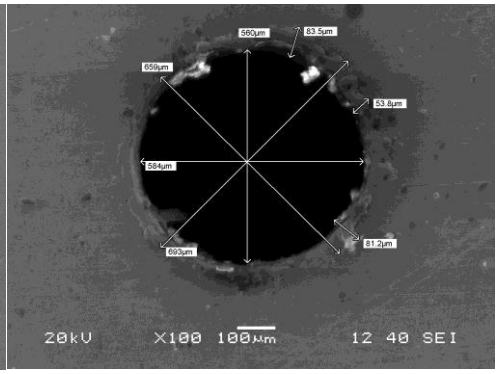

23rd Hole Bottom view

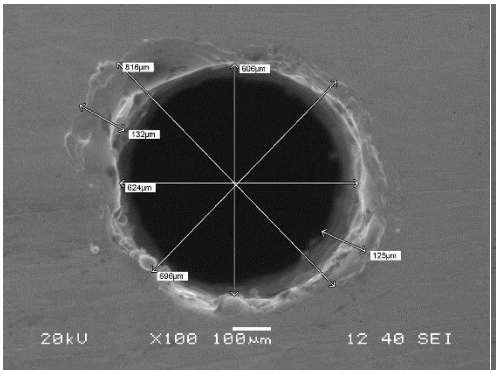

24th Hole Top view

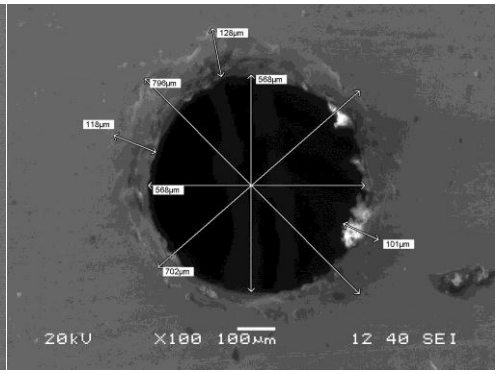

24th Hole Bottom view

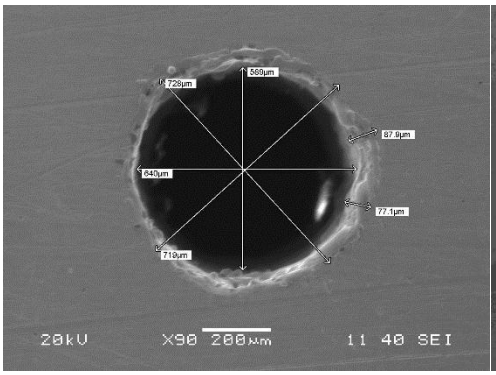

25th Hole Top view

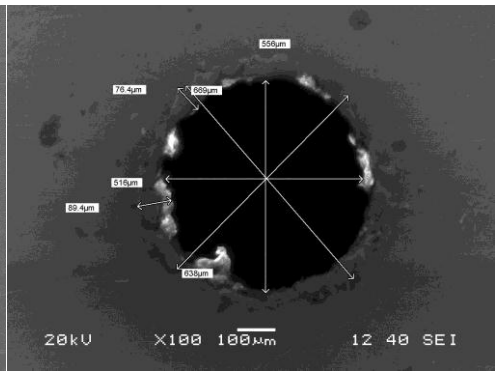

25th Hole Bottom view

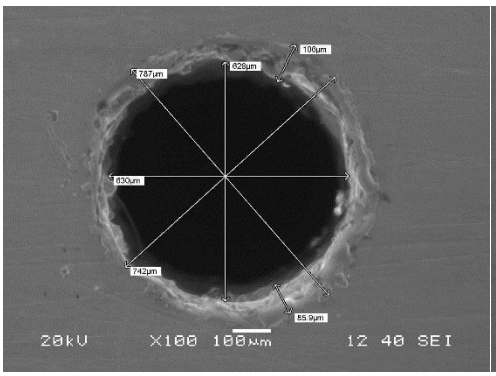

26th Hole Top view

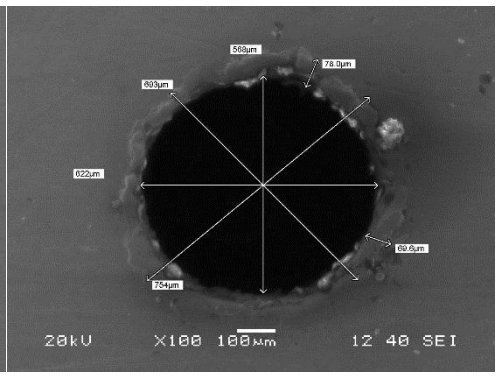

26th Hole Bottom view

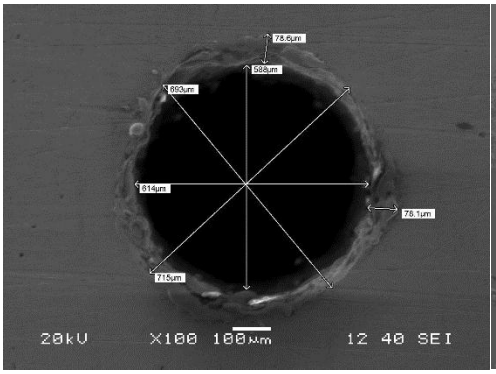

27th Hole Top view

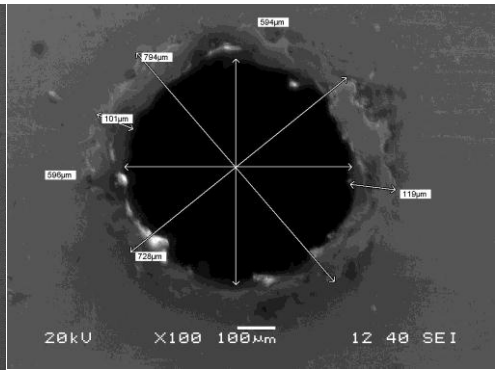

27th Hole Bottom view

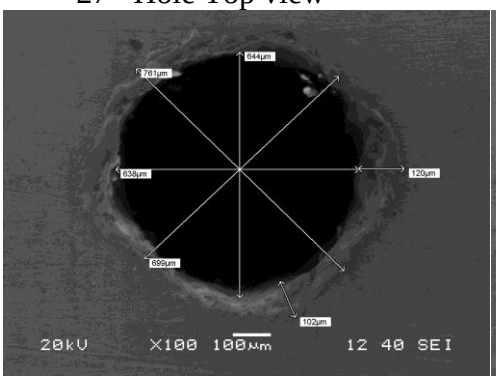

28th Hole Top view

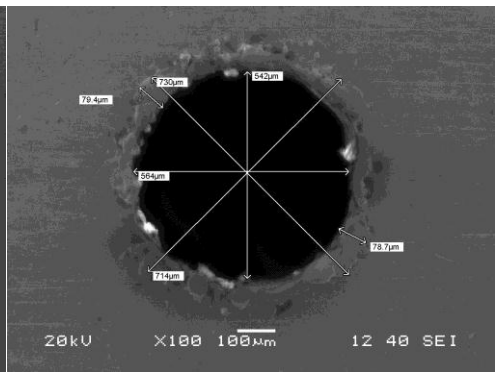

28th Hole Bottom view

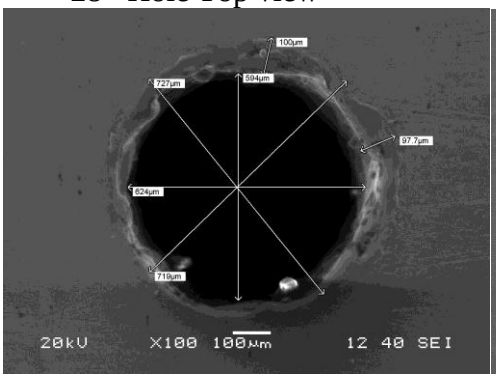

29th Hole Top view

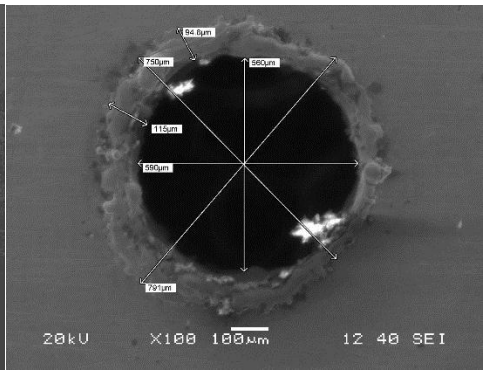

29th Hole Bottom view

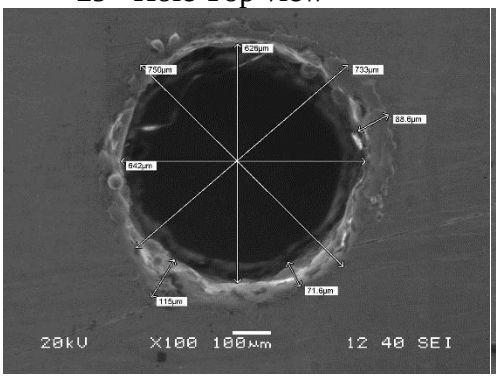

30th Hole Top view

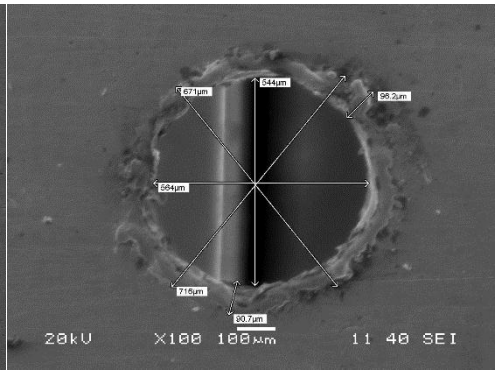

30th Hole Bottom view

Figure 5. 38: SEM Images of Micro Holes

Observance of SEM images of Micro holes: On observing the top and bottom views of SEM micrographs of machined micro-holes at different machining conditions. For higher pulse on time, the exit portion of the micro-hole has not been uniformly machined. As pulse-on time increases, the tool wear at the front tip of the tool also increases rapidly resulting eventually in a round or non-uniform shape at the front of the tool and causes uneven machining at the exit or bottom portion of the micro-hole. The Experimental condition for micro-hole machining on Inconel 718 are given in Table 5.40 in "Appendix 57".

5.7.2 PREDICTION MODEL FOR PROCESS RESPONSES USING RSM

The experimental layout was based on the central composite design (CCD). The design consists of 30 experiments with 16 (2^4) factorial points, eight star points to form a central composite design with $\alpha=\pm2$, seven centre points for replication. The design was generated and analyzed using statistical 9.1 software package. The experimental design matrix and output response values by experiment are shown in Table 5.40. In this section, multiple regression models are developed to predict different process responses like MRR, RCL, Taper effect and OC to improve the quality characteristics of the hole. Multiple regressions are commonly used as a traditional technique to predict the various machining processes. To solve the regression Equation, a matrix is formulated to determine the regression coefficients. The regression coefficients are used to estimate the MRR and overcut. The predicted MRR and overcut values are compared with experimental values. The multiple regression analysis is used when more than two parameters are considered Analysis of variance technique (ANOVA) was used for checking the adequacy of developed models, it was observed that calculated F-ratios were larger than the tabulated values at a 95% confidence level; hence, the models are considered to be adequate. Furthermore, the determination coefficient (R^2) indicates the goodness of fit for the model. For all the four cases, the calculated values of the determination coefficient (R^2) and adjusted determination coefficient (adj. R^2) are more than 80% and 70%, respectively, which indicates a high significance of the model. The mathematical models of MRR, OC, RCL and TA can be expressed in coded form as follows:

$$MRR = 0.951334 - 0.00407056 * A - 0.042717 * B + 0.000531749 * A * B - 1.18697e-005 * A * C - 0.000216669 * B * D + 8.08997e-005 * C * D + 0.000582454 * B^2 \quad (5.9)$$

$$OC = 0.60932 - 0.0153044 * C + 9.82065e-005 * A * B + 0.000172746 * A * C - 0.00048034 * B * D + 0.000294378 * C * D - 0.000132735 * A^2 + 0.000193116 * B^2 \quad (5.10)$$

$$RCL = 352.336 - 2.66444 * B - 7.01052 * C - 0.159991 * A * D + 0.0331344 * B * C + 0.0931311 * C * D + 0.0477689 * A^2 + 0.0317873 * C^2 \quad (5.11)$$

$$TA = -15.4803 + 0.559877 * A - 0.0973002 * B + 0.391577 * D - 0.00411433 * A * B - 0.00589271 * A * D - 0.000215873 * C * D - 0.00388265 * A^2 + 0.00611059 * B^2 \quad (5.12)$$

Table 5.41 displays the ANOVA for OC after applying backward elimination process and as it can be seen from Table 5.41 that it comprises of only significant terms. Further the model F-value of 12.53 implies the model is significant. In this case C, AB, AC, BD and CD are found to be significant model terms. The percentage contribution of different process variables on MRR is presented in Figure 5.39. However, the interaction terms BD and CD are more significant as compared to other significant terms as their percentage contribution are 32.85%, 35.26 % respectively.

Table 5. 41: Analysis of Variance for MRR (after backward elimination)

Source	Squares	DOF	Square	Value	Prob > F	Percentage Contribution
Model	1.66	7	0.24	12.53	< 0.0001	80.193
C-Pulse on duration	1.02	1	1.02	54.20	< 0.0001	49.275
AB	0.21	1	0.21	11.19	0.0029	10.145
AC	0.45	1	0.45	23.69	< 0.0001	21.739
BD	0.68	1	0.68	35.72	< 0.0001	32.850
CD	0.73	1	0.73	38.35	< 0.0001	35.266
A^2	0.43	1	0.43	22.50	< 0.0001	20.773
B^2	0.33	1	0.33	17.60	0.0004	15.942
Residual	0.42	22	0.019			80.193
Lack of Fit	0.30	17	0.018	0.76	0.6945	
Pure Error	0.12	5	0.023			
Corrected Total	2.07	29		R-Squared	0.7995	
				Adj R-Squared	0.7357	
				Pred R-Squared	0.7133	

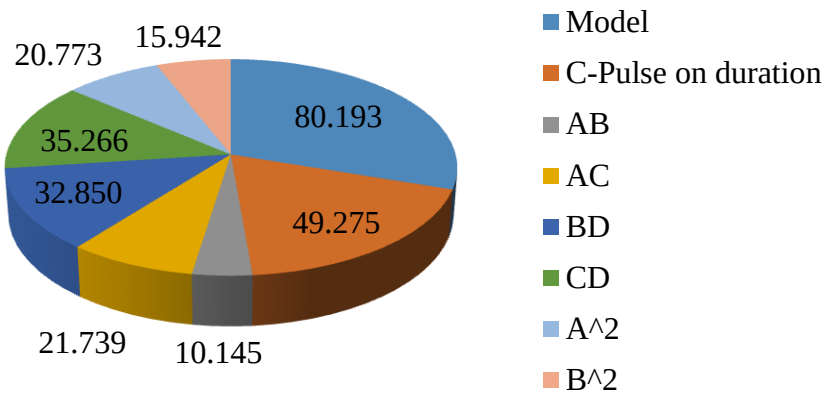

Figure 5. 39: Percentage contribution of process variables

From Figure 5.40, it is observed that maximum MRR value of 0.935mm^3/min was obtained at the highest value of peak current and lowest value of pulse off duration. Furthermore, it was observed that with the increase in pulse off duration the MRR increases, while it initially decreases and then increases with increase in peak current.

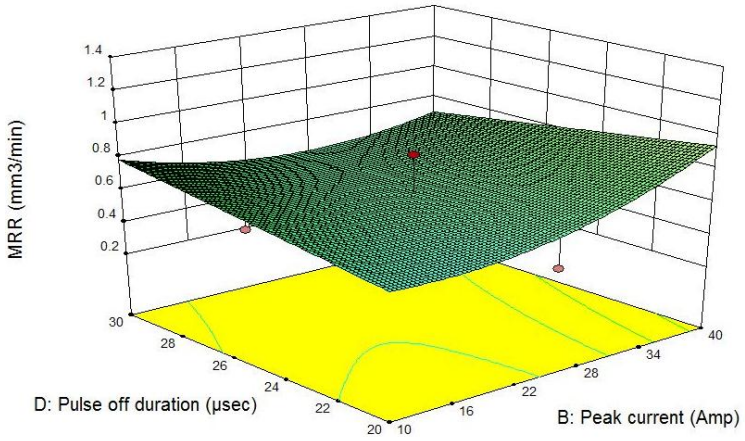

Figure 5. 40: Interaction effect of peak current and pulse off duration on MRR

Figure 5.41 shows the interaction effect of pulse on duration and pulse off duration on MRR at constant peak current of 25 A and voltage of 45 V. From this Figure, it is observed that maximum MRR value of 0.729 mm^3/min was obtained at the lowest values of pulse on duration and pulse off duration. Furthermore, it was observed that with the increase in pulse on duration the MRR increases, while it initially decreases and then increases with increase in pulse off duration.

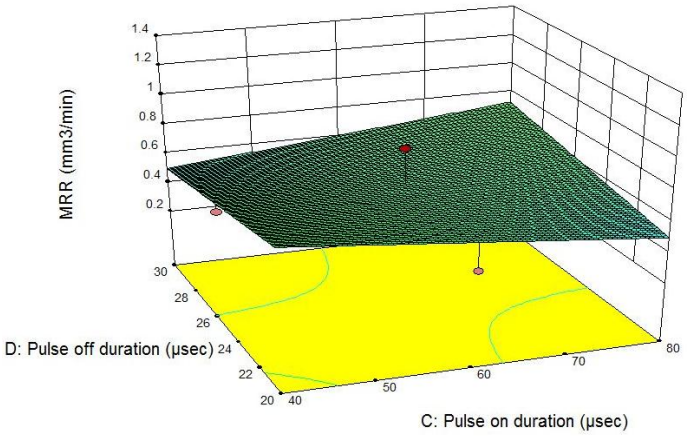

Figure 5. 41: Interaction effect of pulse on duration and pulse off duration on MRR

Response Surface Analysis for OC

Figure 5.42 shows the percentage contribution of different process variables on OC and it is found that pulse on duration has a significant effect on OC. Furthermore, the interaction terms AB, AC, BD and CD are also found to be significant. However, the interaction terms AC and CD are more significant as compared to other significant terms as their percentage contribution are 28.75%, 38.75% respectively. Further the model F-value of 13.86 implies the model is significant. There is only a 0.01% chance that an F-value this large could occur due to noise. The truncated model for OC after applying backward elimination method has been tabulated in Table 5.42 in "Appendix 58."

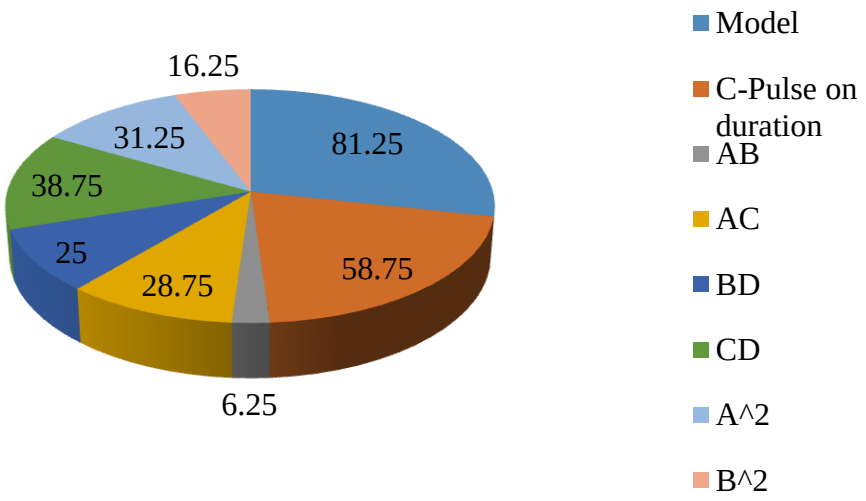

Figure 5. 42: Percentage contribution of process variables

At constant peak current of 25A and pulse off duration of 25 µs the interaction effect of voltage and pulse on duration on OC is represented in Figure 5.43. It is observed that maximum OC was obtained at maximum voltage (60V) and highest pulse on duration of 80µs combination. The minimum OC was obtained at the highest voltage (60V) and lowest pulse on duration of 40µs combination. It is observed that OC increases with increase in pulse on duration and the voltage. There is significant decrease in OC with increase in pulse on duration, however with increase in voltage there is slight increase in OC.

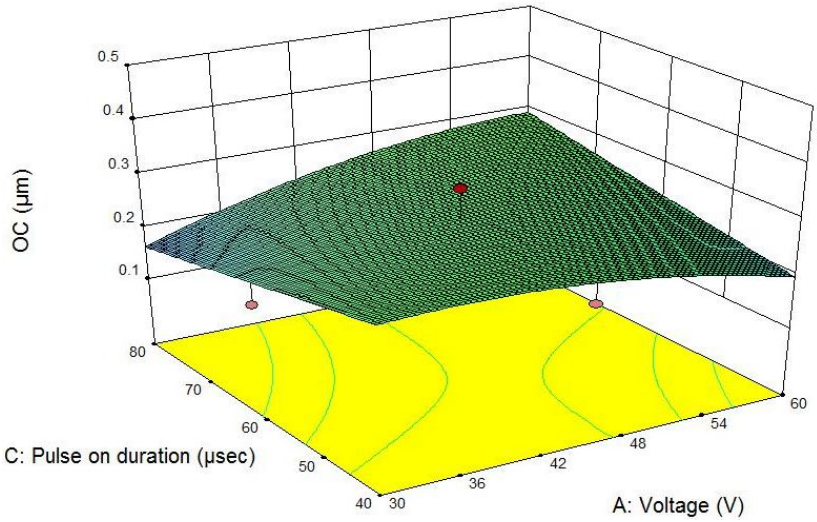

Figure 5. 43: Interaction effect of voltage and pulse on duration on OC

Figure 5.44 demonstrates the interaction effect of pulse on duration and pulse off duration on OC at constant voltage of 45V and peak current of 25 A. From this Figure, it is observed that maximum OC was obtained at the lowest pulse on duration of (40µs) and highest pulse off duration of 30µs.The minimum OC was obtained at the highest pulse on duration of 80µs and lowest pulse off duration of (20µs) combination. It is observed that OC first increases with increase in pulse off duration and the pulse on duration and then decreases. There is a significant increase in OC with increase in pulse on duration however with increase in pulse off duration initially there is increase in OC but later onwards it starts decreasing.

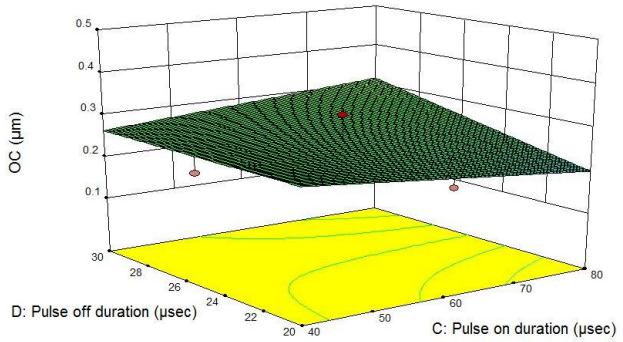

Figure 5. 44: Interaction effect of pulse on duration and pulse off duration on OC

Response Surface Analysis for RCL

Table 5.43 in "Appendix 59" shows the truncated model for RCL after backward elimination process and it can be observed the model F-value of 9.51 denotes the model is significant. There is only a 0.01% chance that an F-value this large could occur due to noise. The percentage contribution of different process variables on RCL is presented in Figure 5.45.

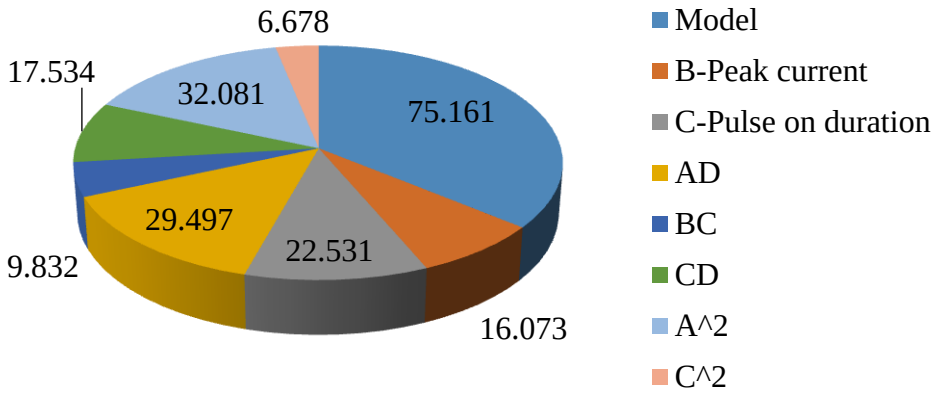

Figure 5. 45: Percentage contribution of process variables

It can be observed from Figure 5.45 among different interaction terms AD has highest contribution of 29.49%. Figure 5.46 shows the interaction effect of voltage and pulse off duration on RCL at constant pulse on duration of 60µs and peak current of 25 A is represented in Figure 5.46. Additionally, it is observed that minimum RCL value of 80.99 µm was obtained at the highest values of voltage (60V) and pulse off duration (30µs) respectively. Moreover, it was observed that with the increase in voltage duration RCL increases linearly, while it initially increases with increase in pulse off duration and decreases with further increase in pulse off duration. With the increase in both pulse on duration and pulse off duration RCL initially increases then it starts decreasing with further increase in pulse on duration and pulse off duration.

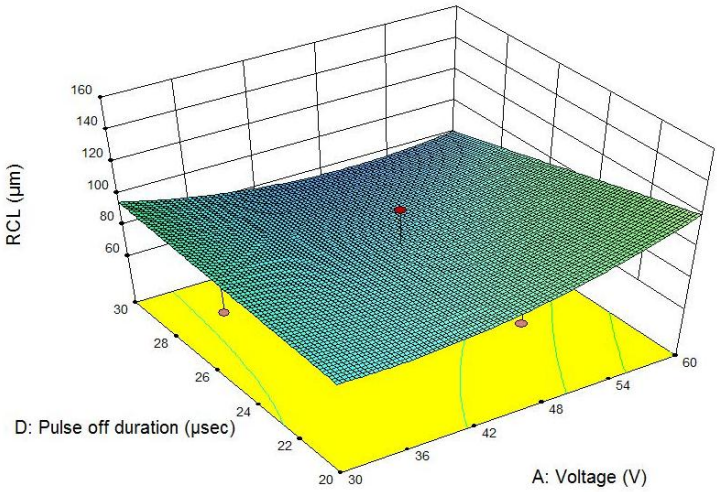

Figure 5. 46: Interaction effect of voltage and pulse off duration on RCL

Response Surface Analysis for TA

The backward elimination process eliminates the insignificant terms to adjust the fitted quadratic model. The model, with rest of the terms after elimination, is presented in Table 5.44 in "Appendix 60". After backward elimination, the values of R-Squared and Adj R-Squared 0.9642 and 0.9481 respectively. The truncated model has lower R^2 than that of full quadratic model, exhibiting significance of relationship between the response and the variables and the terms of the adequate model after the elimination are A, B, C and D.

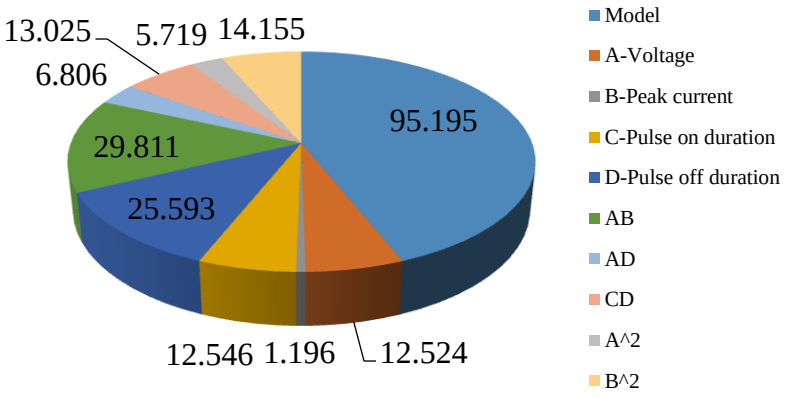

Figure 5. 47:Percentage contribution of process variables

The percentage contribution of different process variables on TA is presented in Figure 5.47 and it can be observed that that pulse off duration is found to be most significant effect on TA followed by voltage, pulse on duration and peak current. Furthermore, AB, AD, CD are found to be significant the interaction terms. However, among different interaction terms AB has highest percentage contribution of 29.811%. Further the model F-value of 59.89 implies the model is significant. There is only a 0.01% chance that an F-value this large could occur due to noise. At constant pulse on duration of 60µs and pulse off duration of 25µs the interaction effect of voltage and peak current on TA is represented in Figure 5.48. From this Figure, it is observed that minimum TA value of 3.76° was obtained at the highest values of voltage (60V) and peak current (40A) respectively. Furthermore, it was observed that with the increase in peak current TA initially increases then it decreases non-linearly, at the middle level of peak current setting and again increases at high level voltage settings. However, with the increase in voltage the value of TA goes on increasing up to maximum value of 0.80°. Additionally, with the increase in both voltage and peak current simultaneously the value of TA goes on increasing and starts decreasing for higher values of peak current and voltage.

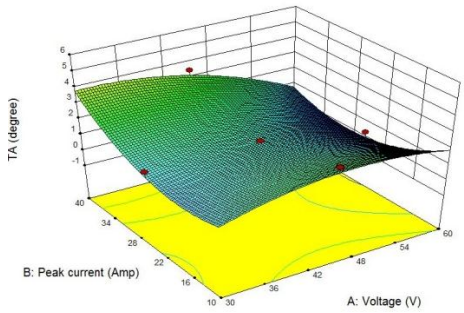

Figure 5. 48: Interaction effect of Voltage and Peak current on TA

5.8 ARTIFICIAL NEURAL NETWORK PREDICTION MODEL FOR PROCESS RESPONSES

5.8.1 THE NETWORK ARCHITECTURE

A network with 4x12x 4 architecture, which means 4 input (Voltage, Peak current, Pulse on duration and Pulse off duration neurons in the input layer, 12 neurons in the hidden layer and 4 outputs (MRR and Overcut, Recast layer thickness, and Taper Angle) in the output layer. Generally, in the multi-layer feed forward network, the size of hidden layers is one of the most important considerations when solving problems. Two hidden layers were adopted in this model. The inputs and outputs are normalized to gain better results. The data set obtain from experiments are divide randomly in to three subsets namely; training, testing and validation sets, in 50%, 40% and 10% of the total data, respectively shown in Table 5.46 in "Appendix 61". A MATLAB program is written to train, test and predict the MRR and overcut values. The topology and training parameters are given in Table 5.45. Properly trained back-propagation network tends to give reasonable answers when presented with inputs that have never been fed before to it.

Table5.45: ANN topology and its training parameters

Parameters	Values
Number of input neurons	4
Number of hidden layers	1
Number of neurons in hidden layer	12
Number of output neuron	4
Momentum factor	0.9
Learning rate	0.001
Number of iterations	500

During training phase, the regression value of 0.99882, 0.99928, 0.99918 and 0.9994 for MRR, OC, RCL and TA have been obtained which signifies the fair correlation between experimental and predicted values.The regression plot for MRR, OC, RCL and TA have been given in Figure 5.49(a-d). Hence ANN can be effectively used for the prediction of MRR, OC, RCL and TA in µ-EDM.

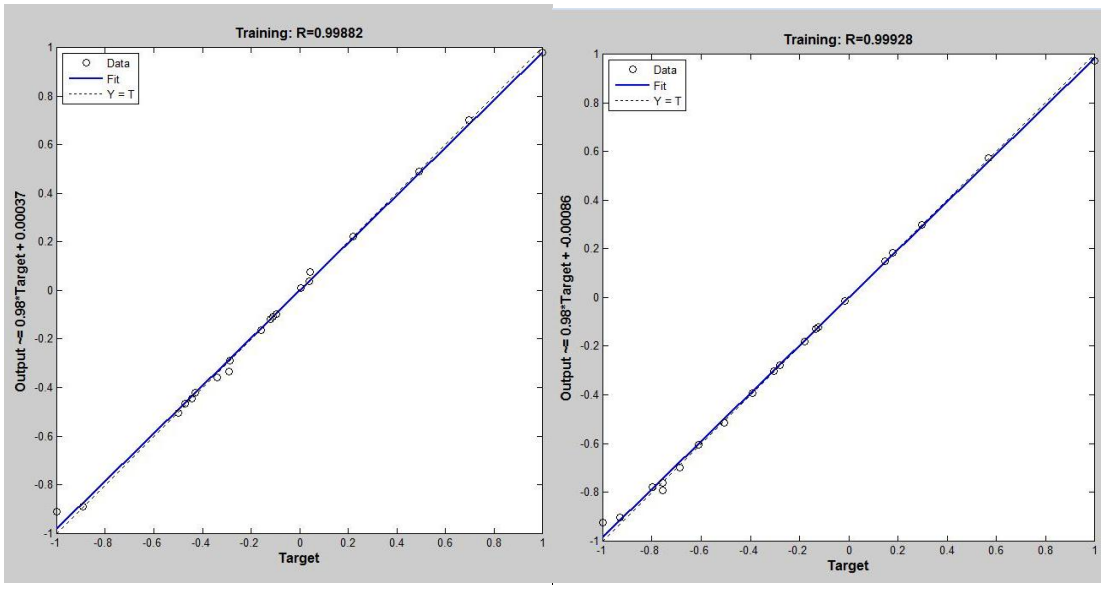

(a) (b)

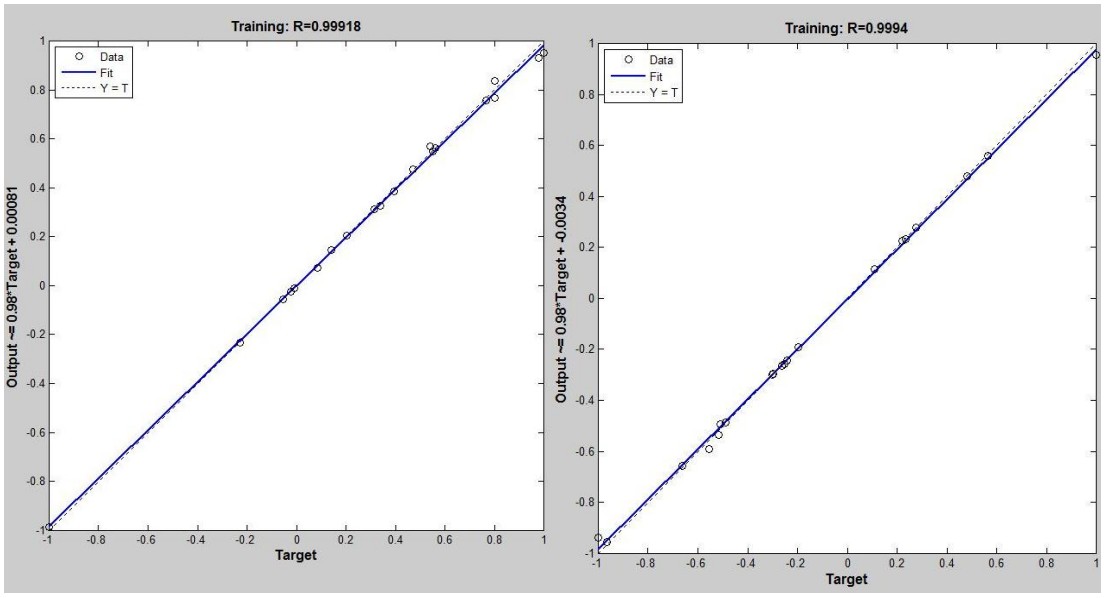

(c) (d)

Figure 5. 49 (a-d): Regression plot for MRR, OC, RCL and TA

The trained neural network was validated against another set of experimental data, termed as validation data set illustrated in Table 5.47 in "Appendix 62". The errors in prediction are also presented in Table 5.48 in "Appendix 62". It can be seen from Table 5.48 that the model predictions match the experimental data very closely except few data. Moreover, the average error in the prediction was 2.213 % for MRR, -3.700 % for OC, and -0.295 % for RCL and -8.067 % for TA respectively. The total

average prediction error of the network was predicted as -9.849 % which indicates that the model is over predicting the values. The developed ANN model was tested by repeating few experiments randomly from the entire data set for checking the predictive accuracy of the developed model. Figures (5.50- 5.53) indicated the errors between predicted and experimental values for all process responses during testing.

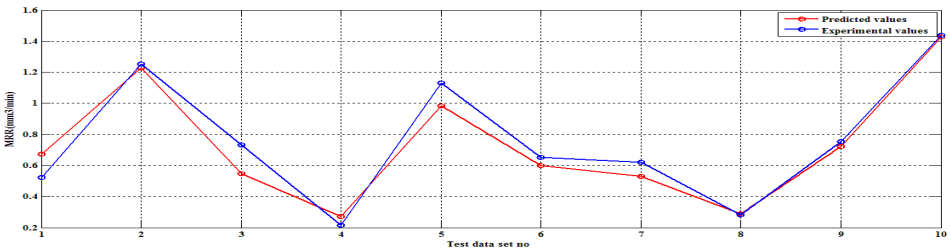

Figure 5. 50: Errors between predicted and experimental values of MRR during testing

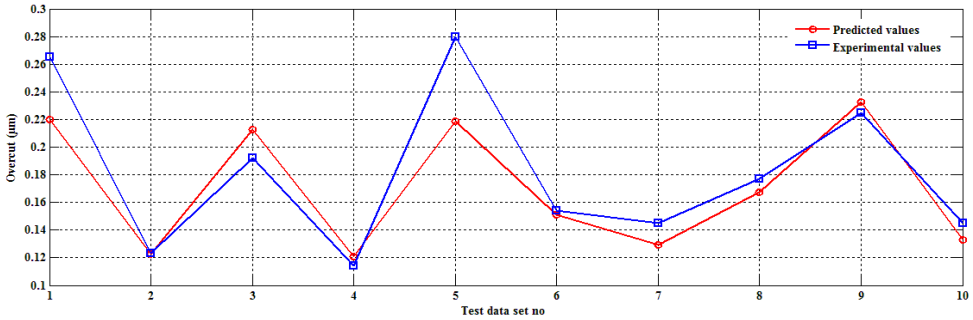

Figure 5. 51: Errors between predicted and experimental values of OC during testing

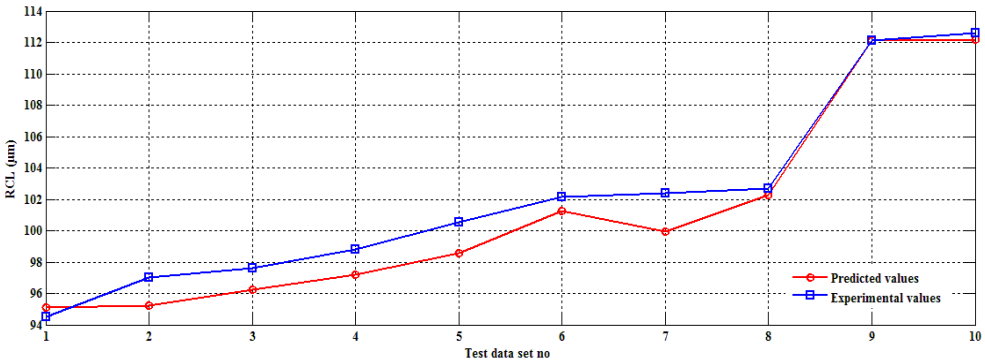

Figure 5. 52 Errors between predicted and experimental values of RCL during testing

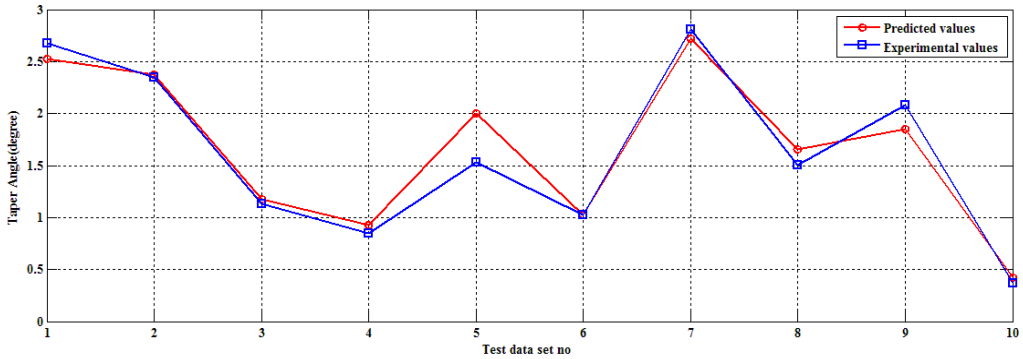

Figure 5. 53: Errors between predicted and experimental values of RCL during testing

Table (5.49 – 5.50) in "Appendix 63" contains testing of the developed model with experimental data and the predicted output and percentage error in prediction of MRR, OC and RCL were within acceptable limits. It is observed that the total average prediction error is 1.743 % which is implies level of over prediction.

5.8.2 ANFIS MODELING

Prediction of MRR, OC, RCL and TA of the micro-EDM process by ANIFS comprises of three main phases, training and testing. However, for the purpose of comparing the predictive tendency with ANN model same data was used for training, validation and testing as it was used for development of ANN. Total average error (TAE) as mentioned in Equation 4.14 is considered as selection criteria for comparison of all existing networks and final selection is made of the most accurate one. The value of error goal was set at 0.03, and the iteration number was 500 epochs. In this work various types of MFs namely triangular, trapezoid, generalized bell and Gaussian have been practiced. Table 5.51 in "Appendix 64" represents training and validation error of ANFIS models for different membership functions. TAE for MRR, OC, RCL and TA have been presented in Table 5.52 in "Appendix 64". Results indicated that the generalized bell function leads the lowest values of TAE for MRR, OC RCL and TA, respectively. The developed ANFIS model was tested for checking the predictive accuracy of the developed model. Tables (5.53 –5.54) in "Appendix 65" contains testing of the developed model with experimental data and the predicted output and percentage error in prediction of MRR, OC and RCL were within acceptable limits. It is observed that the total average prediction error is -19.441 % which implies level of over prediction.

5.8.3 MULTIOBJECTIVE OPTIMIZATION

In the present section multi-objective optimization has been carried out using three meta-heuristic approaches namely Elitist Teaching learning based optimization, Differential evolution and Artificial Bee colony optimization. Furthermore, Pareto optimal sets of solution obtained from each algorithm have been ranked using centroid based Fuzzy

ranking method as discussed in section 4.4.2. The regression Equations (5.5-5.8) obtained from ANOVA analysis haven used for formulating the objective functions. In present multi-objective optimization regime only MRR have to maximized while OC, RCL and ta have to minimized. The tuning parameters for each algorithm were same as discussed in sections 4.4.1, 4.4.3 and 4.4.4. The objective, in this work, is to find the optimal combination of input parameters that provides maximum MRR and minimum OC, RCL and TA respectively. Because of the conflicting nature of performance measures, a single combination of input parameters does not serve the purpose. As a result, a set of optimal solutions (i.e., pareto-optimal solutions) is obtained instead of a single optimal combination. The results obtained from MOETLBO, MODE and MOABC after applying centroid based Fuzzy ranking method have been presented in Tables 5.55- 5.57 in Appendixes (66-68). The results of optimization of µ-EDM process using ETLBO and MODE and MOABC are presented in Table 5.58. From Table 5.58 it can be observed that for MRR, MOETLBO yielded the best i.e., maximum value of MRR. The minimum value of OC and TA was yielded by MOABC. However, for RCL the minimum value was obtained from MODE. Hence from the above results it can be concluded that none of algorithms ensure the best solutions for all process responses which justifies the existence of no free lunch theorems still holds valid for multi-objective regime.

Table 5.58: Optimization results

Response	MOETLBO			MODE			MOABC		
	Best	Mean	Worst	Best	Mean	Worst	Best	Mean	Worst
MRR (mm^3/min)	0.460	0.684	0.624	0.777	0.608	0.399	0.454	0.709	0.874
OC(µm)	0.267	0.258	0.135	0.166	0.131	0.265	0.142	0.133	0.172
RCL(µm)	92.886	88.736	89.674	49.616	77.404	80.375	112.170	113.783	131.363
TA(degree)	2.253	1.673	0.206	5.881	3.598	4.6717	1.449	4.056	6.859

5.9 RESULTS AND DISCUSSIONS

The total average prediction error obtained from ANN and ANFIS models for different combinations of workpiece and electrode materials have been tabulated in Table 5.59. Furthermore, it can be observed from the Table 5.59 that with exactly same training, validation and testing data sets developed ANN and ANFIS models yielded different total average prediction error during testing of models.

However, the predictive accuracy of ANFIS models is very close with ANN models for fabrication of micro holes using copper and graphite as electrode materials, while for platinum as electrode material the predictive accuracy of ANN model was found to be superior to ANFIS model. Additionally, both models yielded negative total average prediction error which indicates slight level of over prediction.

Table 5.59: Comparison of ANN and ANFIS models

S.No	Workpiece	Tool	ANN Model	ANFIS Model
			Total average prediction error	Total average prediction error
1	Titanium Grade 5	Copper	-15.322	-14.191
2	Titanium Grade 5	Graphite	-4.377	--7.519
3	Titanium Grade 5	Platinum	1.743	-19.441

5.10 CONCLUSIONS

In the present investigation, fabrication of micro-holes in Titanium Grade 5 has been carried out using copper, graphite and platinum as electrode tool material. Micro-holes are fabricated as per the Central composite design using response surface methodology. MRR, the thickness of recast layer, radial overcut and taper of the micro-hole have been measured as the responses.

1. Results of Multi-objective optimization using MOETLBO, MODE and MOABC indicated that when comparisons are done on the basis of equal no of function evolutions and same population size none of the algorithms guarantees a perfect solution satisfying different conflicting objectives simultaneously. Since "no free lunch theorems" still holds, therefore none of the above mentioned algorithms should be treated superior. Hence on the basis of priority for a certain response the process engineer can selected the Pareto optimal solutions obtained from different methods.
2. It has been found that neural configuration with feed-forward back propagation of 4-12-4 structure was found to give reasonably good prediction accuracy. It was found that average error in the prediction of developed model was very small indeed while doing the micro-EDM operation in Titanium Grade 5 using platinum as electrode. It was, 1.044 % for MRR, 4.549 % for

OC, 1.021 % for RCL and -4.871 % for TA with the total average prediction error as 1.743 % for fabrication of micro-holes.

3. For fabrication of micro-hole in Titanium Grade 5 with graphite as electrode, the error observed was, 0.956 % for MRR, -0.863 % for OC, and -2.035 % for RCL and -2.4 436% for TA with the total average prediction error as 4.908 % for developed ANN model.
4. For fabrication of micro-hole in Titanium Grade 5 with copper as electrode, the total average prediction error of -7.492 % was observed. It was, -0.860 % for MRR, 0.928 % for OC, and -1.104 % for RCL and -14.285 % for TA for developed ANN model.
5. During modeling of MRR, OC, RCL and TA by ANFIS, the 2-2-2-2 structure was selected as the best topography due to its lowest total average error and faster performance. The total average prediction error for different combination of electrode materials with Inconel 718 as workpiece material was found to be -14.191 % for copper, -7.519 % for graphite and -19.441 % for platinum.

CHAPTER 6

FEA MODELING

6.1 INTRODUCTION

For the reason that the challenges triggered by means of advanced technologies, the micro electrical discharge machining (µEDM) procedure is without doubt one of the quality alternatives for machining of high-strength and wear resistant materials. Inconel 718 and Titanium Grade5 are the high strength and corrosion resistant aerospace material that have widespread applications in mould industries. As a result of rapid, repetitive spark discharges from a pulsating direct-current power supply between the workpiece and the tool submerged into a dielectric liquid the material removal takes place. During each discharge, extreme heat is generated, causing simultaneous melting and evaporation of the work material. Depending on the plasma flushing efficiency (%PFE), the breakdown of the plasma channel causes exceptionally violent suction and serious mass bubbling of a percentage of the liquid material and expulsion from the liquid cavity. The metal left in the crater gets re-solidified, which is called the "white layer" or "recast layer", and develops a residual stress that often leads to micro cracks. The heat affected zone (HAZ) is located just below the recast layer. The micro cracks formed in the white layer might penetrate into the heat affected zone. Moreover; this layer is softer than the underlying base material. The nature of an ED machined surface is turning out to be more imperative to fulfil the expanding demands of refined segment execution, life span and dependability. Optimum utilization of the µ-EDM process requires the selection of an appropriate set of machining parameters that would result in the minimum thickness of the recast layer and the depth of heat affected zone (Shabgard et al. 2013) . Several studies have been carried out to determine optimum ED machining parameter combinations from the aspect of surface integrity (Alfano and Crisÿeld 2001). However, these studies were based on the use of experimental approaches and statistical analyses. In a few studies, mainly numerical models have been developed to analyse the outputs of the EDM process, using FE or analytical methods(Das et al. 2003) .For instance, (Ben Salah et al. 2006) developed a numerical model to study the

temperature distribution in the EDM process, for prediction of the material removal rate using the thermal model. They reported that taking into account the thermal conductivity of workpiece material was of crucial importance to the accuracy of the numerical results and gave a better correlation with experimental observations. (Marafona and Chousal 2006) employed an FE model for predicting removed material from both anode and cathode. They reported that the anode material removal efficiency was smaller than that of the cathode because there was a high amount of energy going to the anode and also a fast cooling of this material. They stated that this phenomenon could be explained by the differences of thermal conductivity of the cathode and anode. (Joshi and Pande 2009)introduced an intelligent process modeling and optimization of EDM process. In their model, FEM was used to estimate the output parameters of EDM process including MRR and %TWR. The dependency of material properties on the temperature and spark radius to the discharge duration has been emphasized in their investigation. Considering the existing tendency for improving the quality of EDMed product, it is essential to develop numerical models to estimate the relationship between the predominant EDM machining parameters and the resulting machined surface integrity, i.e., white layer thickness and depth of HAZ. In Kansal's study (Kansal et al. 2008) an axisymmetric two dimensional model for powder mixed dielectric has been developed using finite element method. The temperature distribution in the workpiece material using ANSYS software has been determined from the thermal model. The material removal rate is estimated from the temperature profiles. Theoretical findings are found compatible with the performed experimental results. It's assumed that once the workpiece material reaches its melting point, then such elements are assumed to be eroded due. Electrical discharge process was simulated by using transient thermal analysis. In this chapter an axisymmetric three-dimensional model for temperature distribution in the micro electrical discharge machining process has been developed using the Finite element method to estimate the MRR by using a combination of different electrode materials during fabrication of micro holes in Inconel 718 and Titanium 5 as workpiece materials. Additionally, the effect of process variables like pulse on duration and peak current on plasma flushing efficiency has been carried out. Developed model includes variation of plasma channel radius and transfer of heat from the channel by the electrical discharge. Effect of generated energy in plasma channel on workpiece removal was theoretically investigated by using different process parameters like voltage, current, pulse on duration and pulse off duration.

6.2 THERMAL ANALYSIS OF THE EDM PROCESS

During the process, high electric potential applied between cathode and anode ionizes the dielectric medium producing a plasma arc. The primary mechanism of material removal

in EDM process is the thermal heating of the work surface due to intense heat generated by the plasma. The highly charged ionized particles of the plasma raise the temperature of the electrodes (tool, work) beyond their melting point, sometimes even more than that of boiling point. For the thermal analysis of the process, conduction is thus considered as the primary mode of heat transfer between the ions of plasma and the molecules of work–tool. In the present work, Fourier heat conduction equation with necessary boundary conditions is taken as the governing equation. Transient nonlinear analysis of the single-spark operation of µ-EDM process has been carried out. During the process, spark discharges may occur over work surface at locations where the inter-electrode gap is minimum. All discharges can be considered to be identical. The present analysis is thus carried out for a single-spark operation. A small cylindrical portion of the workpiece around the spark is chosen for analysis. The two-dimensional axisymmetric process continuum and the associated boundary conditions is shown in Figure 6.1.

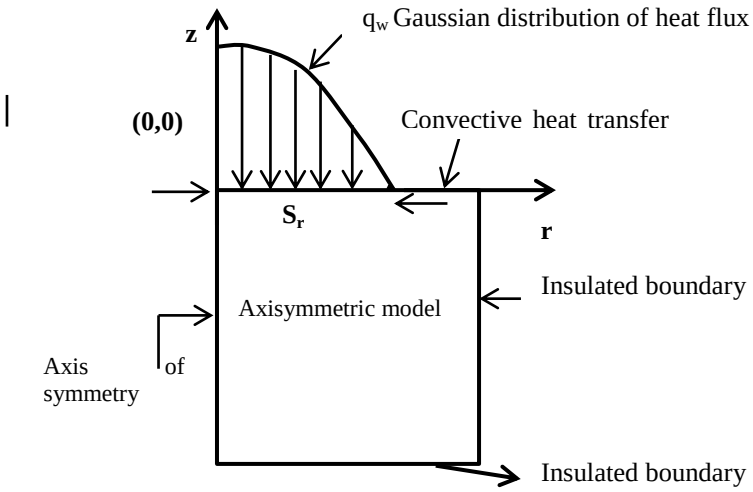

Figure 6. 1:Boundary conditions for solution

6.2.1 ASSUMPTIONS

The following assumptions have been made during the thermal analysis

1. The model is developed for a single spark.
2. The material properties of the workpiece and tool are temperature dependent.

3. The spark radius is assumed to be a function of discharge current and time.
4. Flushing efficiency is considered to be 100%. There is no deposition of recast layer on the machined surfaces.
5. Only a fraction of total spark energy is dissipated as heat into the workpiece; the rest is lost into the dielectric convection and radiation.
6. Heat flux is assumed to be Gaussian-distributed. The zone of influence of the spark is assumed to be axisymmetric in nature.
7. The effects of spark gap on discharge characteristics are negligible.
8. The phase changes during the analysis are neglected.

6.2.2 GOVERNING EQUATION

For the thermal analysis of EDM process, Fourier heat conduction equation is taken as the governing equation

$$\frac{1}{r}\frac{\partial}{\partial r}\left(K_t r \frac{\partial T}{\partial r}\right)+\frac{\partial}{\partial z}\left(K_t \frac{\partial T}{\partial z}\right)=\rho C_p \frac{\partial T}{\partial t} \tag{6.1}$$

where r and z are the coordinates of cylindrical work domain; T is temperature; K_t is thermal conductivity; ρ is density; C_p is specific heat capacity of workpiece material.

6.2.3 BOUNDARY CONDITIONS

Figure 6.1 shows the associated boundary conditions applied. In µ-EDM process, the workpiece is immersed in dielectric medium; the temperature of the domain is thus assumed to be ambient temperature (T_a) to start with. The boundaries of the domain away from the spark domain are considered as insulated. Heat flux (q_w) is applied on the top surface of the workpiece where the spark occurs.

6.2.4 HEAT INPUT

Important factors which contribute to the accurate calculation of material removal rate in single-spark µ-EDM modeling include the amount of heat input, radius of plasma spark, and thermo physical properties of material. Researchers have assumed two forms of heat input models, viz. point source model or uniformly distributed heat flux model. Both these are simplistic as in actual practice neither is there a point source (like laser beam) nor is there any uniform (constant) application of heat on the workpiece. A spark radius exists at the cathode electrode. Consideration of average thermo physical material properties and constant µ-EDM spark radius make the reported models simplistic and restrict their further applicability. In this present work, the Gaussian distribution of heat input proposed by (Patel et al. 1989) has been used to approximate the heat from the plasma. The heat q_w entering the workpiece due to µ-EDM spark is represented by the following equation:

$$q_w(r) = q_o \exp\left\{-4.5\left(\frac{r}{s_r}\right)^2\right\} \quad (6.2)$$

Using this equation, the maximum heat flux q_o can be calculated as below.

$$q_0 = \frac{4.56 F_c V I}{\pi s_r^2} \quad (6.3)$$

where F_c is the fraction of total µ-EDM spark power going to the cathode; V is discharge voltage (V); I is discharge current (A); S_r is spark radius (µm) at the work surface.

6.2.5 SPARK RADIUS

Spark radius is an important factor in the modeling of µ-EDM process. In practice, it is extremely difficult to experimentally measure spark radius due to very short pulse duration in the order of few microseconds. (Ikai and Hashiguchi 1995) have derived a semi empirical equation of spark radius namely "equivalent heat input radius" as a function of discharge current (I) and spark on time (T_{on}), which is more realistic as compared to other approaches.

This equation is as follows:

$$S_r = (2.04e-3) I^{0.43} T_{on}^{0.44} \quad (6.4)$$

In the present work, this approach has been used to calculate equivalent heat input at cathode using Equations. 6.2, 6.3, and 6.4. The heat flux equation derived and used for further analysis in this work is as follows:

$$q_w(t) = \frac{3.4878 \times 10^5 F_c V I^{0.14}}{T_{on}^{0.88}} \exp\left\{-4.5\left(\frac{t}{T_{on}}\right)^{0.88}\right\} \quad (6.5)$$

where T_{on} is time at the end of electric discharge (μs).

6.2.6 ENERGY DISTRIBUTION

Energy distribution is another important factor in the thermal analysis of µ-EDM process. The total spark power gets divided into three parts, a portion conducted away by the cathode, portion conducted away by the anode, and the rest being dissipated in the dielectric. Few experimental studies have been reported in literature to determine these fractions of heat. (DiBitonto et al. 1989) recommended that the energy distribution should be chosen as 18.3% for cathode (F_c) and 8±1% for anode (F_a) for good correlation between analytical and experimental results. In the present work, the F_c value has been taken as 0.183.

6.3 MODELING PROCEDURE USING ANSYS

The governing equation (Equation 1) with boundary conditions mentioned earlier was solved by FEM to predict the temperature distribution at the end of each transient heat transfer analysis cycle. A 3-D continuum of size 0.5×0.3×0.03 mm was considered for the analysis. Thermal solid element (Brick node 278) with an element size of 10μm was used for the discretization of the continuum. The thermal properties of Inconel 718 and Titanium 5 used during modeling are given in Table 6.1. The temperature profiles obtained from the FE analysis were used to calculate the amount of material removed from the specimen.

Table 6. 1:Thermal properties of Inconel 718 and Titanium 5

Thermal properties	Symbol	Units	Inconel 718	Titanium 5
Thermal conductivity	K	W/Mk	14.5	7.62
Specific Heat	C	J/KgK	435	490
Density	ρ	Kg/m^3	8190	4900
Melting point	K	Kelvin	1609	1923

6.3.1 DETERMINATION OF MRR

The theoretical crater volume is defined by the parabolic geometry as described by the following equation

$$V_C(FEA) = \frac{1}{2}\pi d_c r_c^2 \tag{6.6}$$

where d_c=Depth of crater in μm; r_c= radius of crater in μm. Referring to Figure 6.4 it can be seen that the crater follows a parabolic curve. It may be noted that for more precise calculation of crater volume, element volumes were defined after modeling was over. The cavity volume obtained from ANSYS has been tabulated in 6th column of Table 6.2 and 6.3 respectively. Furthermore, FEA (MRR) for single spark has been calculated using the following equation.

$$MRR = \frac{V_C \times 60}{(T_{on} + T_{off}) \times 10^3} \tag{6.7}$$

where V_C = Volume of Crater in mm^3; T_{on}= Pulse on duration; T_{off} = Pulse off duration.

Further MRR for multi-discharge have been calculated as

$$MRR_{(multi-discharge)} = MRR_{(single\ spark)} \times No\ of\ pulses \tag{6.8}$$

$$No\ of\ pulses = \frac{T_{machining}}{T_{on} + T_{off}} \quad (6.9)$$

The experimental sets have been taken in such a manner that none of sets must be repeated and resulted in unique sets which have been tabulated in Tables 6.2 and Table 6.3 respectively for Inconel 718 and Titanium Grade 5.

Table 6. 2: MRR with different process parameters (Inconel 718)

Voltage (V)	Peak current (I_p)	Pulse on duration (T_{on})	Pulse off duration (T_{off})	Spark radius (S_r) µm	Volume of cavity (V_c) in (mm^3)	FEA MRR (mm^3/ min)	Exp. MRR (mm^3/ min	Exp. MRR (mm^3/ min	Exp. MRR (mm^3/ min)
							Copper	Graphite	Platinum
30	8	20	30	18.639	7.96E-04	0.955	0.766	0.421	0.761
	20	30	45	33.037	4.98E-04	0.799	0.748	0.370	0.668
	32	40	30	45.893	6.23E-04	0.834	0.458	0.417	0.629
35	20	20	45	27.639	4.82E-04	0.745	0.659	0.366	0.603
		30	45	33.037	1.44E-03	1.151	0.651	0.358	0.611
		40	45	37.496	9.00E-04	0.835	0.673	0.414	0.662
40	8	20	30	18.639	6.03E-04	0.723	0.715	0.415	0.603
	20	30	45	33.037	9.84E-04	0.787	0.627	0.383	0.538
	32	40	60	45.893	9.87E-04	0.692	0.601	0.381	0.677

Table 6. 3:MRR with different process parameters (Titanium 5)

Voltage (V)	Peak current (I_p)	Pulse on duration (T_{on})	Pulse off duration (T_{off})	Spark radius (S_r) µm	Volume of cavity (V_c) in (mm^3)	FEA MRR (mm^3/ min)	Exp. MRR (mm^3/ min	Exp. MRR (mm^3/ min	Exp. MRR (mm^3/min)
							Copper	Graphite	Platinum
30	10	40	30	27.831	3.97E-14	0.984	0.448	0.852	0.406
	25	60	25	49.332	1.28E-13	0.361	0.142	0.27	0.283
	40	80	20	68.529	9.99E-14	0.957	0.204	0.387	0.895
45	25	40	25	41.272	5.78E-14	0.694	0.284	0.539	0.566
		60	25	49.332	8.27E-14	0.798	0.377	0.715	0.754
		80	25	55.989	9.00E-14	0.663	0.263	0.499	0.652
60	10	80	30	37.756	8.04E-14	1.755	0.397	0.755	1.129
	25	60	25	49.332	8.57E-14	0.659	0.27	0.513	0.539
	40	80	20	68.529	1.26E-13	1.902	0.580	1.101	1.156

6.4 MODEL VALIDATION AND RESULTS

Simulation has been carried out by considering the parameters in Table 6.2 and Table 6.3 for Inconel 718 and Titanium 5 respectively. Furthermore, spark radius has been calculated using Equation (4). As a result of a single spark a shallow shape crater has been formed. The volume of the crater equals that of the removed material by the spark. After thermal modeling elements showing the temperature more than melting temperature were killed from the complete mesh of the work domain for further analysis. Figure 6.2 shows The temperature distribution in Inconel 718 with V=30V, I=20 Amp, S_r= 33.037µm and T_{on} =30µs is shown in Figure 6.2.

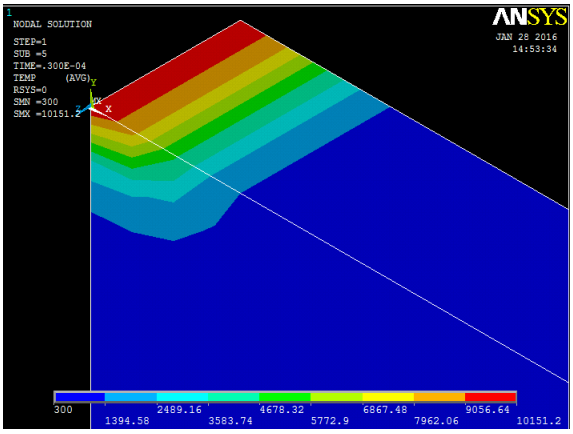

Figure 6. 2:Temperature distribution in Inconel 718 with V=30V, I=20Amp,Sr=33.037µm.

Figure 6.3 depicts the temperature distribution in workpiece after removing elements reaching temperature equal to or higher than the melting point of Inconel 718. Joshi proposed a method for calculating volume of cavity that was based on coordinates of nodes. It was employed for two dimensional geometries of workpiece. But in present modeling a three dimensional geometry has been considered which restricts the use of coordinate based method of cavity calculation. However, volume of cavity can be directly obtained from ANSYS by defining volume tables prior to thermal analysis. The temperature distribution of melted cavity has been shown in Figure 6.4.

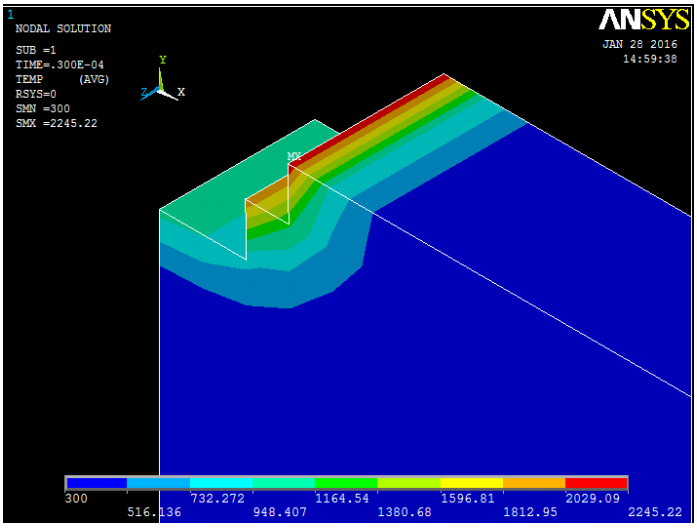

Figure 6. 3: Temperature distribution in Inconel 718

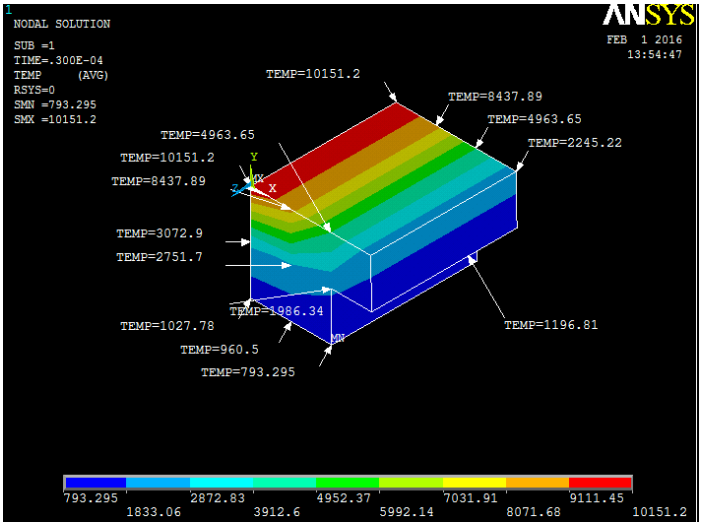

Figure 6. 4: Temperature distribution in melted cavity

By employing similar methodology temperature distributions considering Titanium 5 as workpeice material for parametric setting value of 30V, 25Amp, Ton= 60µs and S_r = 49.332 µm has been shown in Figure 6.5 – 6.7.

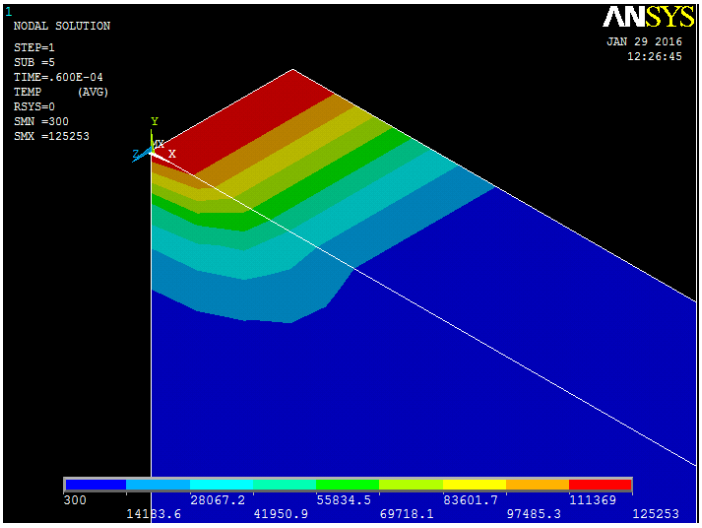

Figure 6. 5:Temperature distribution in Titanium 5 with V=30V I=25Amp, Sr =49.332 µm.

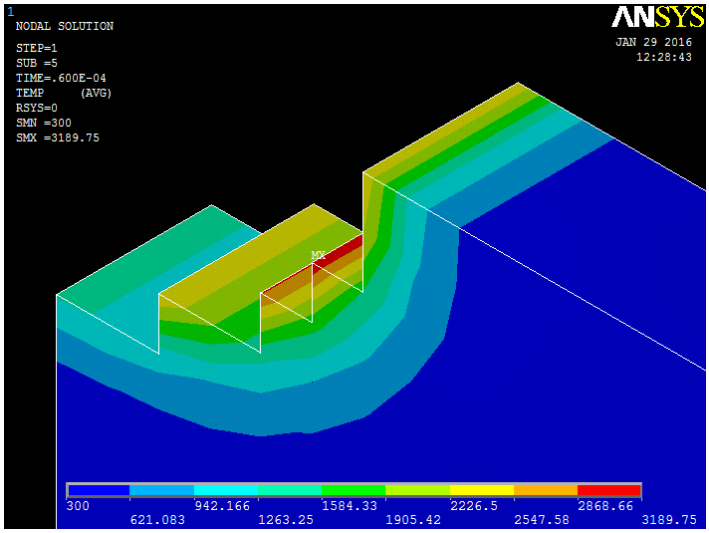

Figure 6. 6:Temperature distribution in Titanium

As it can be seen from Figure 6.7 The temperature distribution in single spark for V = 30V, I = 25Amp, and T_{on} = 60 μs is shown in Fig.6.7. It can be observed that the temperature tends to decrease when measured in radial direction as well as along the depth of cavity.

6.5 EFFECT OF VARIATION IN PROCESS PARAMETERS FOR INCONEL 718 AND TITANIUM 5

The distribution of temperature and its level in the melted cavity depends upon various process parameters such as voltage, peak current, pulse on duration and pulse off duration. The effect of variation of these process parameters on the temperature isotherms is explained below.

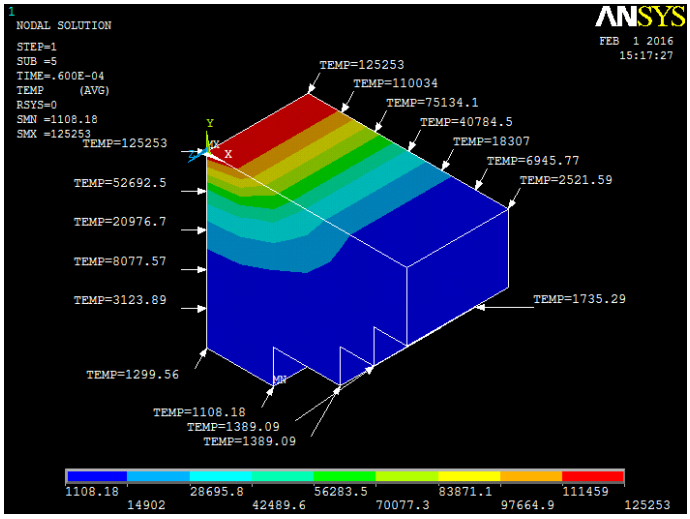

Figure 6.7:Temperature distribution in cavity

6.5.1 EFFECT OF VARIATION IN CURRENT

The variation of the surface temperature with distance (along radius and depth of melted cavity) has been plotted for three different values of peak current i.e, (8, 20 and 32 Amp) for Inconel 718 and (10, 25 and 40 Amp) for Titanium 5 are shown in Figures 6.8 - 6.11.

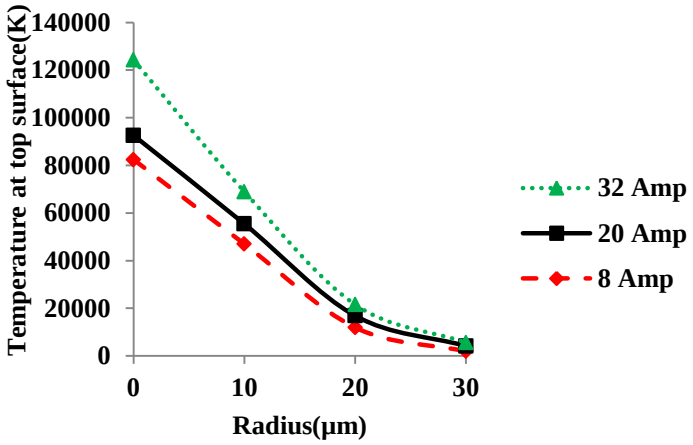

Figure 6. 8:Variation of temperature in radial reduction with peak current (Inconel718).

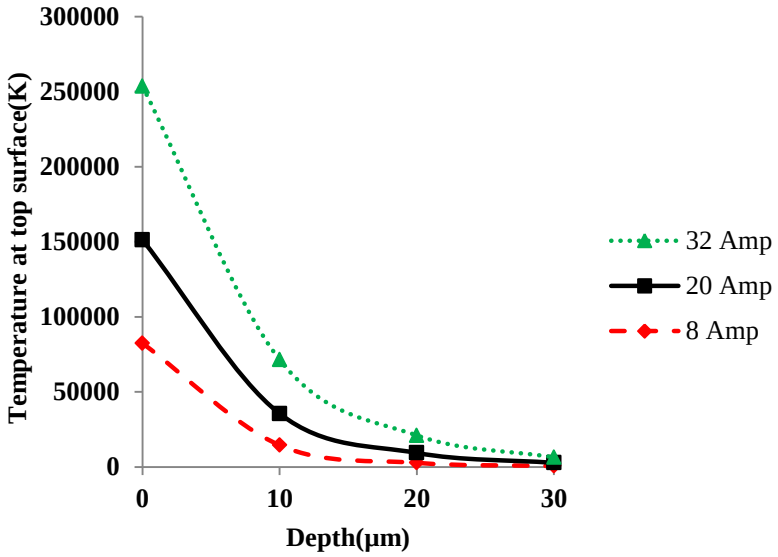

Figure 6. 9:Variation of temperature along the depth direction with peak current (Inconel718)

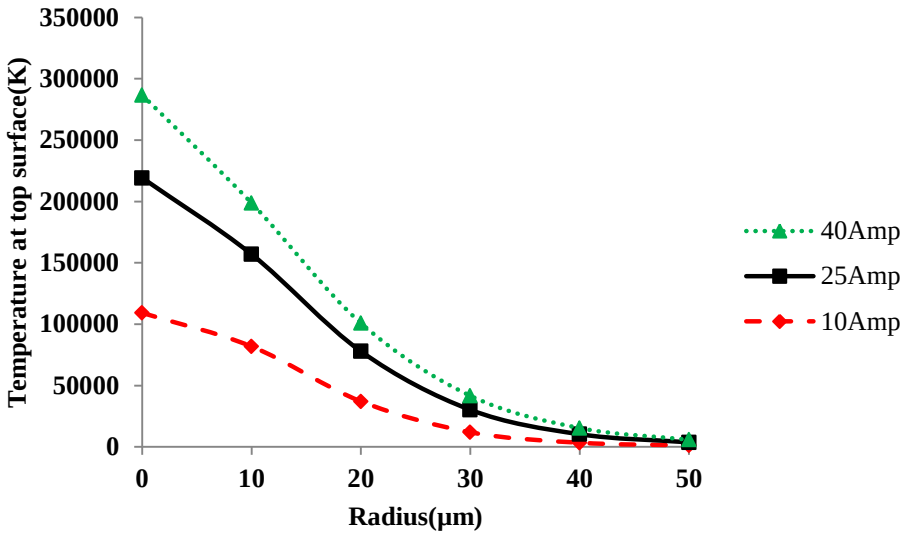

Figure 6. 10:Variation of temperature in radial direction at 30V with peak current (Titanium 5)

Referring to Figures (6.8 and 6.10) it can be observed that the top surface temperature goes on increasing with increase in current for both workpiece materials. This is due to the fact that; the current is a function of the heat energy transferred to the workpiece. The larger the current, the greater the heat energy generated and transferred to the workpiece. Further, from these figures it can be seen that the distribution of temperature follows the shape of Gaussian curve (bell shape).

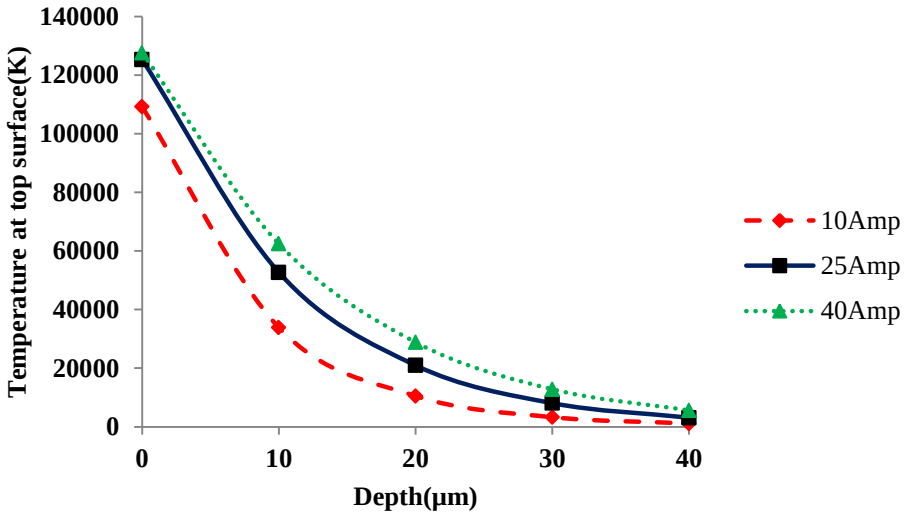

Figure 6. 11:Variation of temperature in depth direction at 30V with peak current (Titanium 5)

The considerable temperature gradient along the radial direction can be seen up to the radius of 30µm.The temperature variation along the depth of the melted cavity is shown in Figures (6.9 and 6.11). It can be observed that the temperature is maximum at the top

surface and decreases as we proceed downward. No variation in temperature is observed after a depth of 30µm for Inconel 718 and 40µm for Titanium 5. Hence it can be concluded that the material removal rate is more along the radial direction than along the depth resulting in shallow craters.

6.5.2 EFFECT OF VARIATION IN PULSE ON DURATION

The effect of variation in pulse duration on surface temperature distribution in melted cavity in Inconel 718 as well as Titanium 5 along radius and depth are plotted in Figures (6.12 -6.15) respectively. From the trend of variation in surface temperature along the radius of the both workpiece materials, it can be observed that with increase in pulse duration, the surface temperature also increases. It is obvious because, if heat is supplied for a longer time period, the temperature will be high.

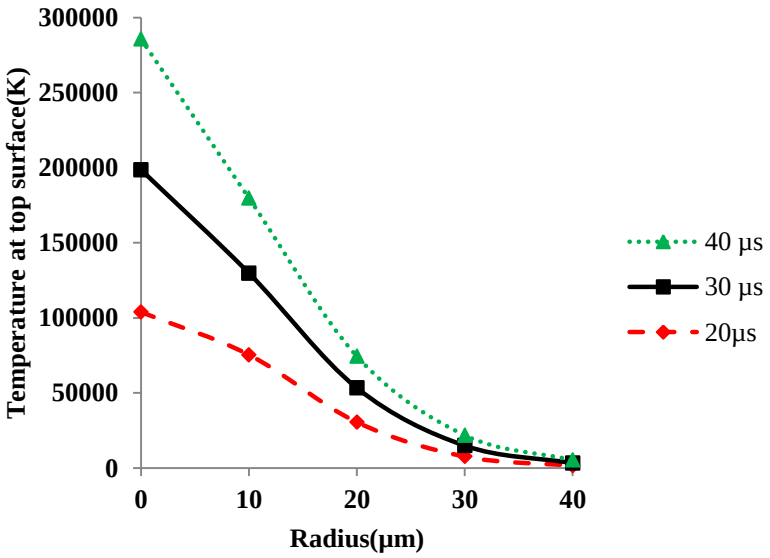

Figure 6. 12:Variation of temperature in radial direction with pulse on time (Inconel 718 at V = 35 V, I = 20 Amp and Toff = 45 µs

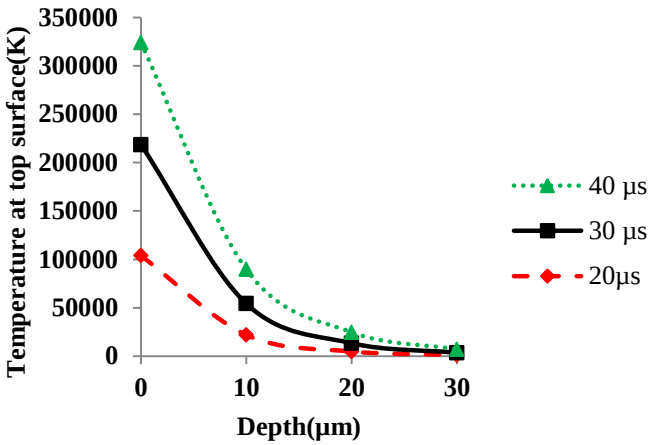

Figure 6. 13:Variation of temperature in depth direction with pulse duration (Inconel 718 at V = 35 V, I = 20 Amp and Toff = 45µs)

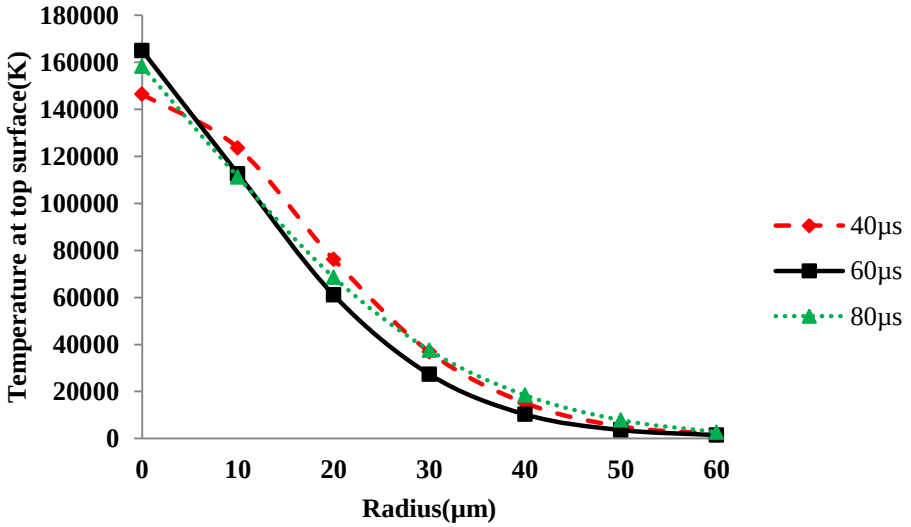

Figure 6. 14:Variation of temperature in radial direction in radial direction with pulse duration (Titanium 5 at V = 45 V, I = 25 Amp and Toff = 45 µs),

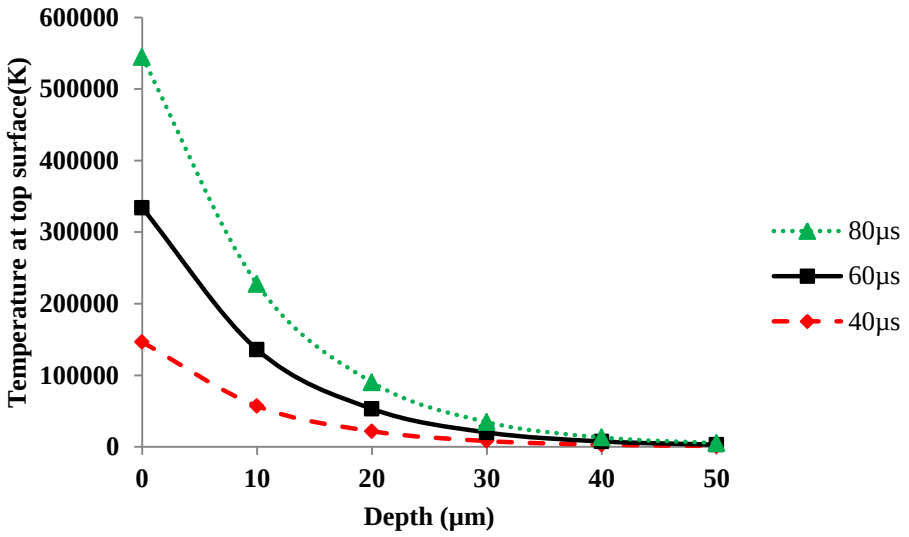

Figure 6. 15:Variation of temperature in depth direction with pulse duration (Titanium 5 at V = 45 V, I = 25 Amp and Toff = 45 µs),

The temperature is very high near the point of spark. It decreases slowly as we move away from the tip of workpiece. It can be seen that the temperature variation is high up to the radius of about 20µm for Inconel 718 and 30µm for Titanium 5. Beyond 20µm and 30µm the rate of decrement is high. The reason being that as the heat flux is given for a longer period on workpiece surface; the temperature near the centre will be high.

6.5.3 TEMPERATURE DISTRIBUTION IN VOLTAGE FOR INCONEL 718 AND TITANIUM 5

The effect of variation in voltage on surface temperature distribution in melted cavity in Inconel 718 as well as Titanium 5 along radius and depth are plotted in Figures (6.16 - 6.18) respectively. From the trend of variation in surface temperature along the radius of the both workpiece materials, it can be observed that with increase in voltage, the surface temperature also increases. It is obvious because, if heat is supplied for a longer time period, the temperature will be high.

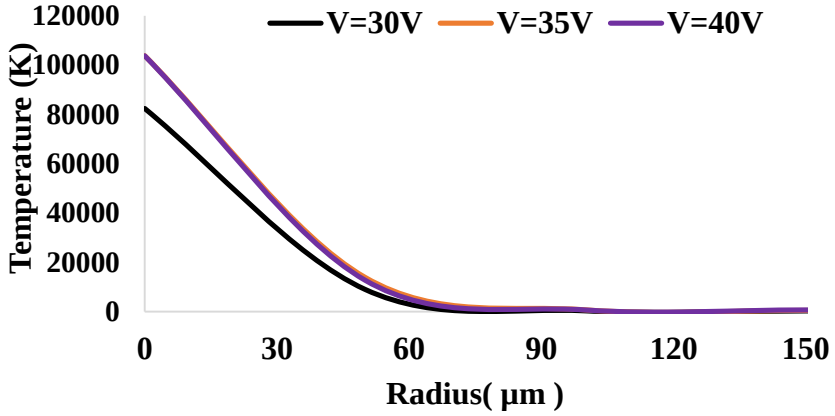

Figure 6. 16 :Variation of temperature in radial direction in radial direction with voltage

(Inconel 718)

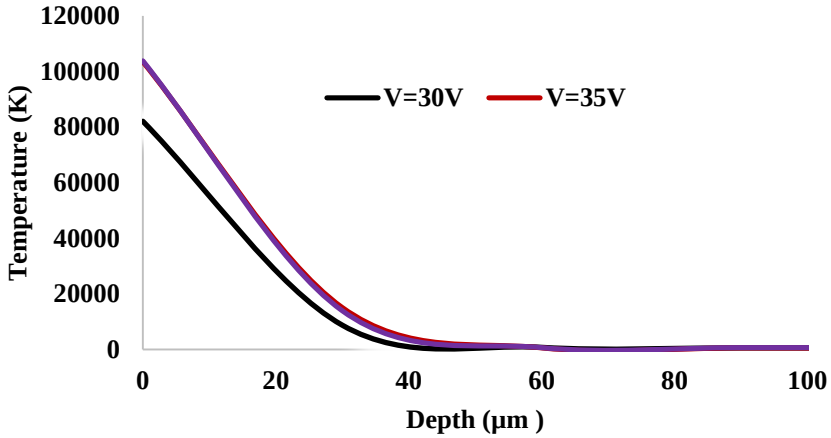

Figure 6.17: Variation of temperature in radial direction in radial direction with voltage(Titanium718)

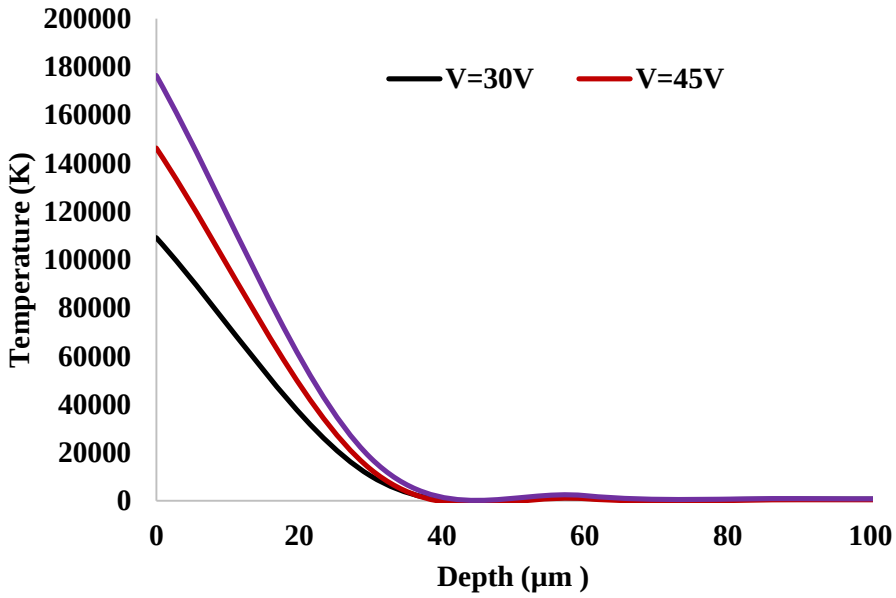

Figure 6. 18: Variation of temperature in depth direction with pulse duration (Titanium 5

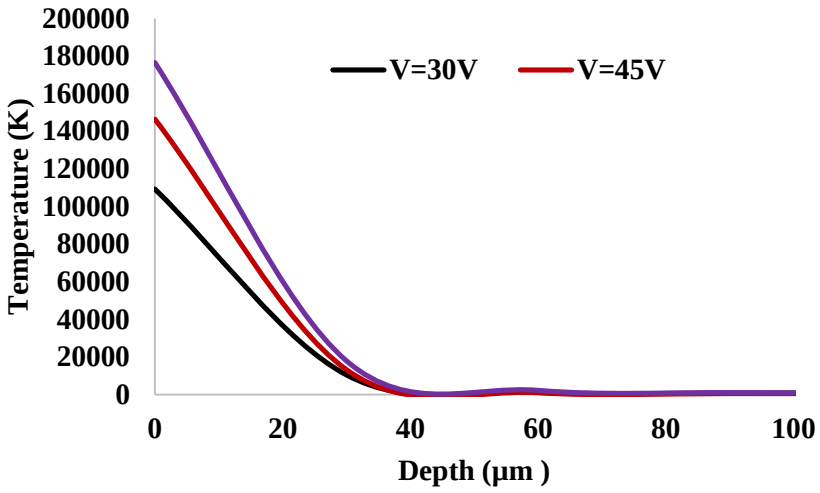

Figure 6. 19: Variation of temperature in depth direction with pulse duration (Titanium 5

FEM modeling was validated with experimental data for MRR given in Table 6.2 and 6.3 The experimental sets have been selected in such a way that none of sets must be repeated and resulted in unique sets Inconel 718 and Titanium Grade 5. Modeling was carried for single discharge Pulse on duration (T_{on}), Voltage (V), Peak current(Ip) and spark radius(Sr) are the variables. Experiment was carried out for multi-discharge in the same set up as discussed in Chapter 3..MRR in single discharge is converted to equivalent multi-discharge and was compared with theoretical modeling .The comparison of MRR obtained by FEA and experiment is shown in Figure 6.16 and 6.17 during micro hole fabrication in Inconel 718 and Titanium 5 respectively. There is some difference between simulation and experiment. It was observed that the error in MRR was varying from 5% to 18.44% for Titanium Grade 5 and 6.38% to 20.33% for Inconel-718. It can be observed from these Figures that the MRR obtained using copper for Inconel 718 and platinum for Titanium Grade 5 indicates a very close matching with MRR obtained from FEA. However, the MRR obtained from FEA was higher than experimental MRR because the µ-EDM process is governed by different factors such as ignition delays, high frequency of sparks, flushing efficiency, and phase change of electrodes, dielectric medium, and random behaviour of debris particles. It is very difficult to incorporate these factors into the process models during FEA modeling.

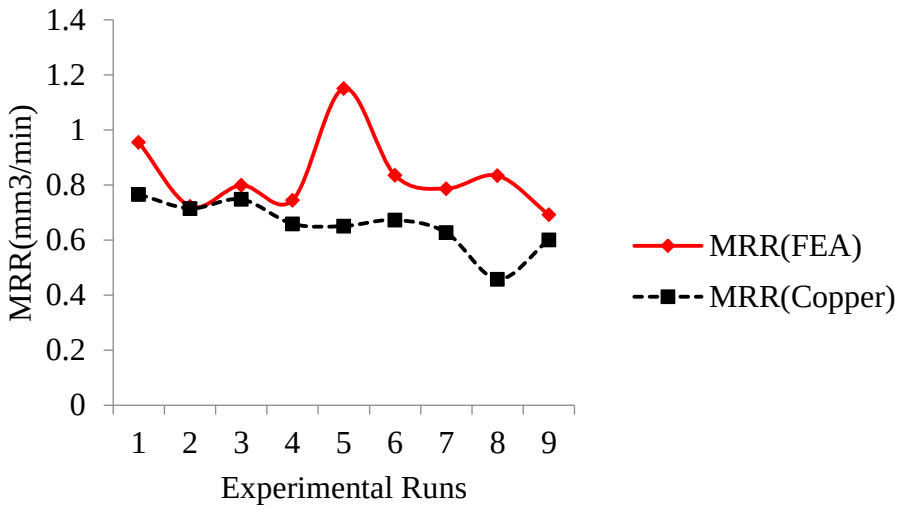

Figure 6. 16:Comparison of MRR obtained by FEA in Inconel 718 using Copper as electrode

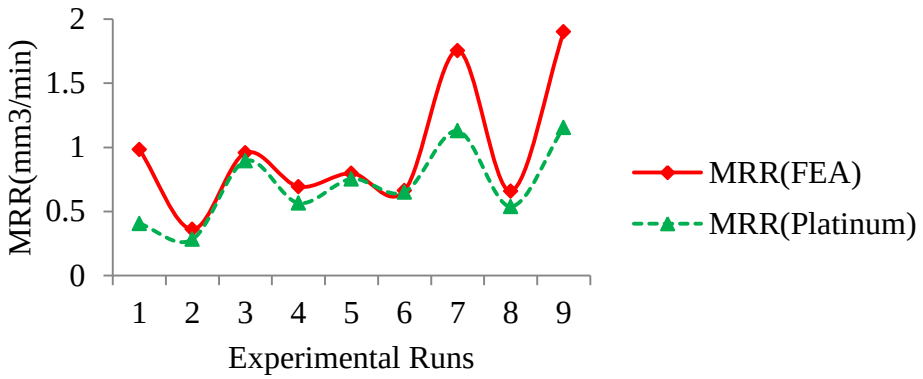

Figure 6. 17:Comparison of MRR obtained by FEA in Titanium 5.

CONCLUSION

Finite element simulation and modeling were carried out for a single spark to determine temperature distribution in melted cavity and MRR. The variation of temperature distribution in radial and depth direction with different process parameters has been determined for Inconel 718 and Titanium grade 5. Theoretical cavity volume was calculated for different process parameter settings for both workpiece materials and it was found that Titanium 5 exhibited higher cavity volume then Inconel 718. Furthermore, the MRR obtained using platinum as tool electrode during fabrication of micro holes in Inconel 718 and Titanium Grade 5 indicated a close match with MRR obtained using FEA.

CHAPTER 7

PERFORMANCE ANALYSIS OF ELECTRODE MATERIALS

7.1 INTRODUCTION

Micro-EDM operation for a given workpiece materials is influenced by different electrode materials. In case of fabrication of micro hole, the characteristics of micro hole are also influenced by the electrode material. Material removal rate, Overcut, recast layer thickness and Taper angle vary with change in tool electrode material. In present investigation the effect of change of electrode material on the fabrication of micro-hole in Inconel 718 and Titanium has been investigated. Copper, graphite and platinum are considered as electrode material.

7.2 ANALYSIS OF OUTPUT PERFORMANCE USING INCONEL 718 AS WORKPIECE MATERIAL

MRR, Overcut, Recast Layer thickness and Taper angle are investigated in the fabrication of micro-hole in Inconel 718 using Copper, graphite and platinum as electrode material. Further a comparative study has been carried out in order to investigate the effect of process variables on process responses.

7.2.1 PERFORMANCE OF DIFFERENT ELECTRODES MATERIALS ON MRR

The experimental data on MRR for different operating conditions are listed in Table 7.1. The different operating combinations with different electrode materials yielded varying amount of MRR as in Table 7.1. The variation of MRR for different combination of process parameters with respect to voltage is given in (Table 7.1) and is shown in Figure 7.1 Furthermore, the effect of process variables like Voltage, Peak current, Pulse on duration and Pulse off duration with respect to MRR have been shown in Figures 7.1-7.4 respectively.

Table 7. 2: MRR for different electrodes with combination of process parameters

S. No	Parameters				Material Removal Rate (MRR) mm^3/min		
	Voltage (V)	Peak current (I_p)	Pulse on duration (T_{on})	Pulse off duration (T_{off})	Copper	Graphite	Platinum
1	30	8	20	30	0.766	0.807	0.961
2	30	8	40	60	0.556	0.683	0.926
3	30	8	20	60	0.784	0.805	0.833
4	30	8	40	30	0.538	0.636	0.888
5	30	20	30	45	0.748	0.753	0.868
6	30	32	20	30	0.588	0.684	0.823
7	30	32	20	60	0.427	0.538	0.888
8	30	32	40	60	0.593	0.714	0.910
9	30	32	40	30	0.458	0.588	0.829
10	35	8	30	45	0.614	0.693	0.800
11	35	20	30	45	0.651	0.750	0.811
12	35	20	30	30	0.682	0.796	0.989
13	35	20	30	45	0.766	0.818	0.811
14	35	20	30	45	0.627	0.728	0.810
15	35	20	30	45	0.659	0.669	0.810
16	35	20	30	45	0.682	0.773	0.810
17	35	20	30	45	0.748	0.799	0.810
18	35	20	40	45	0.673	0.721	0.862
19	35	20	20	45	0.659	0.673	0.803
20	35	20	30	60	0.689	0.832	0.911
21	35	32	30	45	0.725	0.799	0.776
22	40	8	20	30	0.715	0.743	0.803
23	40	8	20	60	0.627	0.665	0.796
24	40	8	40	30	0.623	0.654	0.900
25	40	8	40	60	0.518	0.538	0.909
26	40	20	30	45	0.627	0.679	0.738
27	40	32	40	60	0.601	0.622	0.877
28	40	32	40	30	0.816	0.845	0.996
29	40	32	20	60	0.582	0.598	0.736
30	40	32	20	30	0.725	0.824	0.770

7.2.1.1 *EFFECT OF VOLTAGE VARIATION ON MRR*

Referring to Figure 7.1 it can be observed that MRR is maximum for platinum as electrode material followed by graphite and copper respectively. The maximum MRR obtained using platinum as electrode was 0.996 mm^3/min. Additionally Figure 7.1depicts that there is a significant rise in MRR for all three electrode materials at voltage setting of 35 V. However, a decreasing trend can be seen when voltage reaches to 40V.

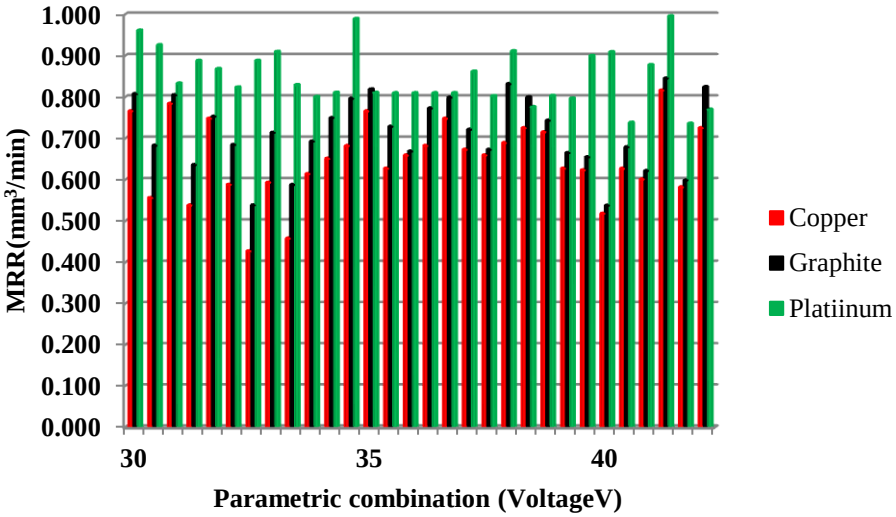

Figure 7.1 Variation of MRR for different electrodes as per process parameters

7.2.1.2 *EFFECT OF CURRENT VARIATION ON MRR*

The variation of MRR for different combination of process parameters with respect to current is shown in form of bar graph in Figure 7.2. The experimental data on MRR for effect of current variation on MRR different operating conditions are listed in Table 7.2. Further the effect of current variation on MRR is shown in Figure 7.2 and it can be observed that platinum as electrode material shows maximum MRR followed by graphite and copper. It can be observed that with increase in current settings MRR tends to increase for platinum while it tends to decrease for the case of graphite and copper for maximum current setting of 32 amperes.

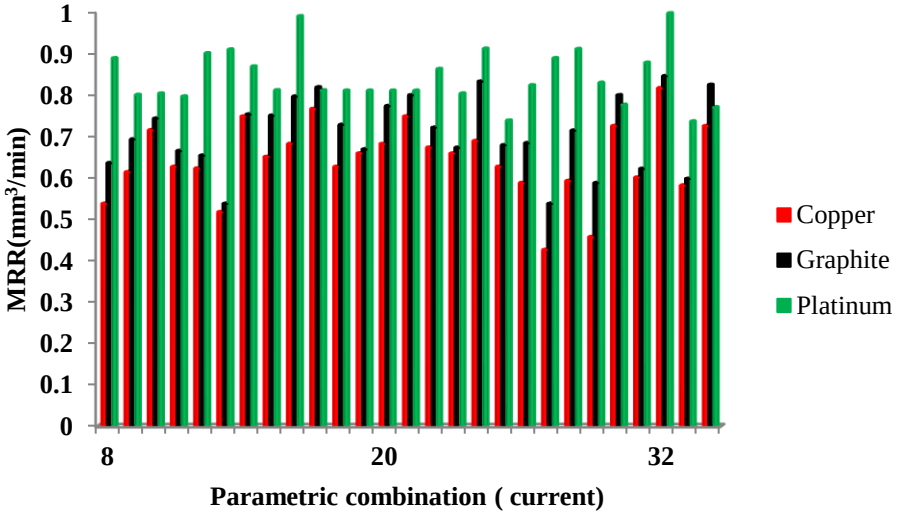

Figure 7.2 Variation of MRR with respect to voltage

Table 7. 2: MRR for different electrodes with variation in current

S. No	Parameters				Material Removal Rate (MRR) mm^3/min		
	Peak current (I_p)	Voltage (V)	Pulse on duration (T_{on})	Pulse off duration (T_{off})	Copper	Graphite	Platinum
1	8	30	20	30	0.766	0.807	0.961
2	8	30	40	60	0.556	0.683	0.926
3	8	30	20	60	0.784	0.805	0.833
4	8	30	40	30	0.538	0.636	0.888
5	8	35	30	45	0.614	0.693	0.8
6	8	40	20	30	0.715	0.743	0.803
7	8	40	20	60	0.627	0.665	0.796
8	8	40	40	30	0.623	0.654	0.9
9	8	40	40	60	0.518	0.538	0.909
10	20	30	30	45	0.748	0.753	0.868
11	20	35	30	45	0.651	0.75	0.811
12	20	35	30	30	0.682	0.796	0.989
13	20	35	30	45	0.766	0.818	0.811
14	20	35	30	45	0.627	0.728	0.81
15	20	35	30	45	0.659	0.669	0.81
16	20	35	30	45	0.682	0.773	0.81
17	20	35	30	45	0.748	0.799	0.81
18	20	35	40	45	0.673	0.721	0.862
19	20	35	20	45	0.659	0.673	0.803
20	20	35	30	60	0.689	0.832	0.911
21	20	40	30	45	0.627	0.679	0.738
22	32	35	30	45	0.725	0.799	0.776
23	32	40	40	60	0.601	0.622	0.877
24	32	40	40	30	0.816	0.845	0.996
25	32	40	20	60	0.582	0.598	0.736
26	32	40	20	30	0.725	0.824	0.77
27	32	30	20	30	0.588	0.684	0.823
28	32	30	20	60	0.427	0.538	0.888
29	32	30	40	60	0.593	0.714	0.91
30	32	30	40	30	0.458	0.588	0.829

Further the effect of current variation on MRR is shown in Figure 7.2 and it can be observed that platinum as electrode material shows maximum MRR followed by graphite and copper. It can be observed that with increase in current settings MRR tends to increase for platinum while it tends to decrease for the case of graphite and copper for maximum current setting of 32 amperes.

7.2.1.3 EFFECT OF PULSE ON DURATION VARIATION ON MRR

The variation of MRR for different combination of process parameters with respect to pulse on duration is shown in form of bar graph in Figure 7.3 and the different experimental conditions are listed in Table 7.3. The variation of MRR with respect to pulse on duration is shown in Figure 7.3 and it can be observed that platinum as electrode material shows highest MRR during different pulse on duration settings. Furthermore, it can be observed that there is a significant rise in MRR as the pulse on duration tends to reach 40µs.Copper as electrode material exhibited the least MRR value of 0.427 mm^3/min at 20 µs pulse on duration.

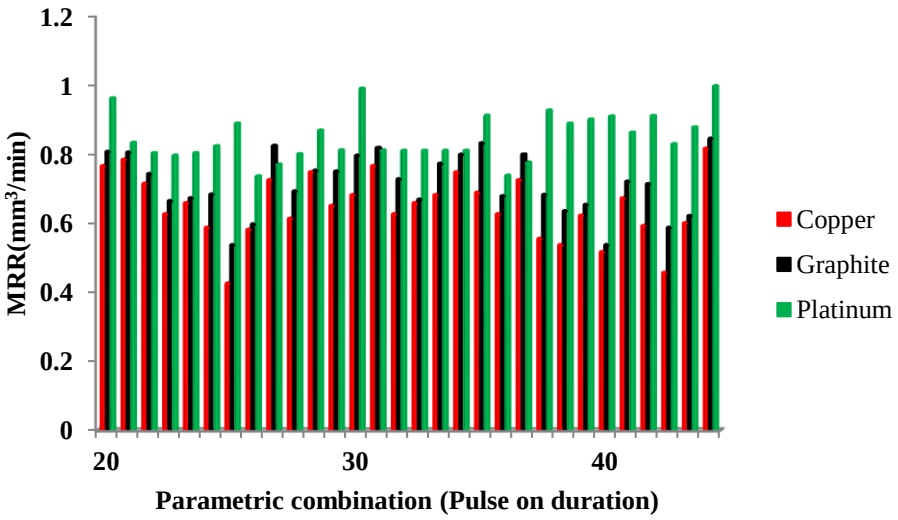

Figure 7.3 Variation of MRR with respect to pulse on duration

Table 7. 3: MRR for different electrodes with variation in Pulse on duration (T_{on})

S. No	Parameters				Material Removal Rate (MRR) mm^3/min		
	Pulse on duration (T_{on})	Peak current (I_p)	Voltage (V)	Pulse off duration (T_{off})	Copper	Graphite	Platinum
1	20	8	30	30	0.766	0.807	0.961
2	20	8	30	60	0.784	0.805	0.833
3	20	8	40	30	0.715	0.743	0.803
4	20	8	40	60	0.627	0.665	0.796
5	20	20	35	45	0.659	0.673	0.803
6	20	32	40	60	0.582	0.598	0.736
7	20	32	40	30	0.725	0.824	0.77
8	20	32	30	30	0.588	0.684	0.823
9	20	32	30	60	0.427	0.538	0.888
10	30	8	35	45	0.614	0.693	0.8
11	30	20	30	45	0.748	0.753	0.868
12	30	20	35	45	0.651	0.75	0.811
13	30	20	35	30	0.682	0.796	0.989
14	30	20	35	45	0.766	0.818	0.811
15	30	20	35	45	0.627	0.728	0.81
16	30	20	35	45	0.659	0.669	0.81
17	30	20	35	45	0.682	0.773	0.81
18	30	20	35	45	0.748	0.799	0.81
19	30	20	35	60	0.689	0.832	0.911
20	30	20	40	45	0.627	0.679	0.738
21	30	32	35	45	0.725	0.799	0.776
22	40	8	30	30	0.538	0.636	0.888
23	40	8	40	30	0.623	0.654	0.9
24	40	8	40	60	0.518	0.538	0.909
25	40	20	35	45	0.673	0.721	0.862
26	40	32	40	60	0.601	0.622	0.877
27	40	32	40	30	0.816	0.845	0.996
28	40	32	30	60	0.593	0.714	0.91
29	40	32	30	30	0.458	0.588	0.829
30	40	8	30	60	0.556	0.683	0.926

7.2.1.4 EFFECT OF PULSE OFF DURATION VARIATION ON MRR

The variation of MRR for different combination of process parameters with respect to pulse off duration is shown in form of bar graph in Figure 7.4 and the different experimental conditions are listed in Table 7.4. The variation of MRR with respect to pulse off duration is shown in Figure 7.4 and it can be observed here that platinum as electrode material exhibits higher MRR as compared to graphite and copper respectively. Moreover, it can be observed that for pulse off duration settings of 45µs there was sudden fall in the MRR trend for the case of platinum electrode.

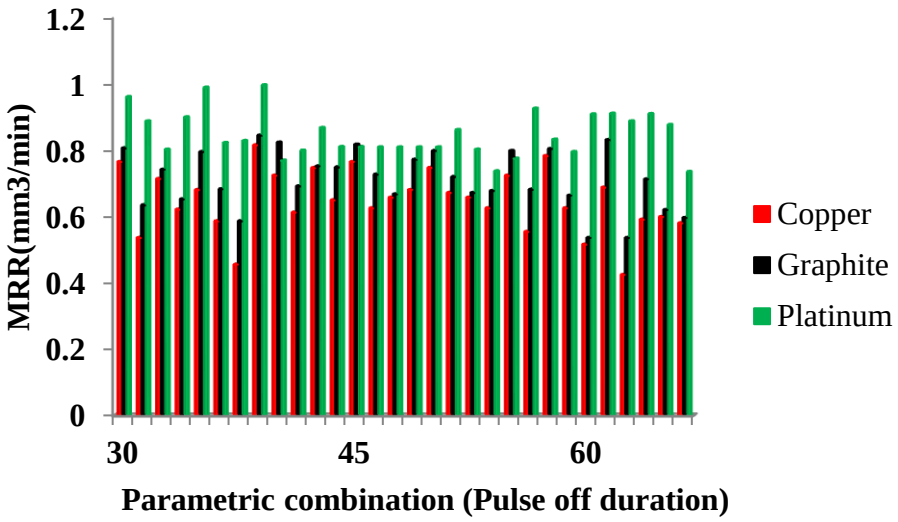

Figure 7.4 Variation of MRR with respect to pulse off duration

Table 7. 4: MRR for different electrodes with variation in Pulse off duration (T_{off})

S. No	Parameters				Material Removal Rate (MRR) mm^3/min		
	Pulse off duration (T_{off})	Pulse On duration T_{on}	Peak current (I_p)	Voltage (V)	Copper	Graphite	Platinum
1	30	20	8	30	0.766	0.807	0.961
2	30	20	8	40	0.715	0.743	0.803
3	30	20	32	40	0.725	0.824	0.77
4	30	20	32	30	0.588	0.684	0.823
5	30	30	20	35	0.682	0.796	0.989
6	30	40	8	30	0.538	0.636	0.888
7	30	40	8	40	0.623	0.654	0.9
8	30	40	32	30	0.458	0.588	0.829
9	30	40	32	40	0.816	0.845	0.996
10	45	20	20	35	0.659	0.673	0.803
11	45	30	8	35	0.614	0.693	0.8
12	45	30	20	30	0.748	0.753	0.868
13	45	30	20	35	0.651	0.75	0.811
14	45	30	20	35	0.766	0.818	0.811
15	45	30	20	35	0.627	0.728	0.81
16	45	30	20	35	0.659	0.669	0.81
17	45	30	20	35	0.682	0.773	0.81
18	45	30	20	35	0.748	0.799	0.81
19	45	30	20	40	0.627	0.679	0.738
20	45	30	32	35	0.725	0.799	0.776
21	45	40	20	35	0.673	0.721	0.862
22	60	20	32	40	0.582	0.598	0.736
23	60	20	32	30	0.427	0.538	0.888
24	60	20	8	40	0.627	0.665	0.796
25	60	30	20	35	0.689	0.832	0.911
26	60	40	8	40	0.518	0.538	0.909
27	60	40	32	40	0.601	0.622	0.877
28	60	40	32	30	0.593	0.714	0.91
29	60	40	8	30	0.556	0.683	0.926
30	60	20	8	30	0.784	0.805	0.833

7.2.2 PERFORMANCE OF DIFFERENT ELECTRODES MATERIALS ON OC

The performance of various electrodes is also analyzed from the overcut point of view. In micro-EDM process, the size of the machined hole with different electrodes varies due to end erosion, side erosion and stiffness/tension of the various electrodes. During machining process, overcut occurs due to side erosion and removal of debris. Since overcut leads to oversizing of holes it should be as the least as possible. Overcut is also one of the major parameters to be considered to evaluate the machining performance of die-sinking micro- EDM. The experimental results of obtained overcut during fabrication of micro holes on Inconel 718 as work piece material for different operating conditions are tabulated in Table 7.5.

7.2.2.1 EFFECT OF VOLTAGE VARIATION ON OC

The variation of OC for different combination of process parameters with respect to voltage is shown in form of bar graph in Figure 7.5 and the different experimental conditions are listed in Table 7.5. The effect of voltage variation on OC is presented in Figure 7.5 it can be seen that for operating voltage setting of 30V, graphite depicted minimum overcut effect, while at the operating voltage of 35 V copper showed least overcut. It is interesting to note that at 40V platinum exhibited least overcut.

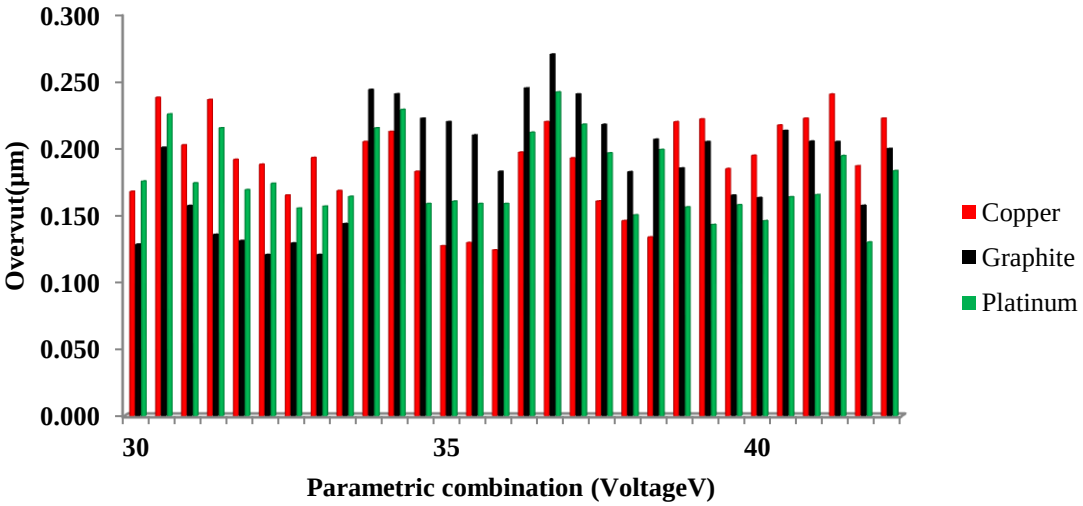

Figure 7.5: Variation of OC with respect to Voltage

Table 7. 5: OC for different electrodes with combination of process parameters

S. No.	Parameters				Overcut(μm)		
	Voltage (V)	Peak current (I_p)	Pulse on duration (T_{on})	Pulse off duration (T_{off})	Copper	Graphite	Platinum
1	30	8	20	30	0.168	0.129	0.175
2	30	8	40	60	0.238	0.201	0.225
3	30	8	20	60	0.202	0.157	0.174
4	30	8	40	30	0.236	0.136	0.215
5	30	20	30	45	0.192	0.131	0.169
6	30	32	20	30	0.188	0.121	0.174
7	30	32	20	60	0.165	0.129	0.155
8	30	32	40	60	0.193	0.121	0.157
9	30	32	40	30	0.168	0.144	0.164
10	35	8	30	45	0.205	0.244	0.215
11	35	20	30	45	0.212	0.240	0.229
12	35	20	30	30	0.183	0.222	0.159
13	35	20	30	45	0.127	0.220	0.160
14	35	20	30	45	0.130	0.210	0.159
15	35	20	30	45	0.124	0.183	0.159
16	35	20	30	45	0.197	0.245	0.212
17	35	20	30	45	0.220	0.270	0.242
18	35	20	40	45	0.193	0.240	0.218
19	35	20	20	45	0.161	0.218	0.196
20	35	20	30	60	0.146	0.182	0.150
21	35	32	30	45	0.134	0.207	0.199
22	40	8	20	30	0.220	0.185	0.156
23	40	8	20	60	0.222	0.205	0.143
24	40	8	40	30	0.185	0.165	0.158
25	40	8	40	60	0.195	0.163	0.146
26	40	20	30	45	0.217	0.213	0.164
27	40	32	40	60	0.222	0.205	0.165
28	40	32	40	30	0.240	0.205	0.194
29	40	32	20	60	0.187	0.157	0.130
30	40	32	20	30	0.222	0.200	0.183

7.2.2.2 EFFECT OF CURRENT VARIATION ON OC

The variation of OC for different combination of process parameters with respect to current is shown in form of bar graph in Figure 7.6 and the different experimental conditions are listed in Table 7.6. The effect of current variation on OC is presented in Figure 7.6 it can be observed that all electrode materials showed a nonlinear trend with irregular fluctuations in overcut values. However, copper as electrode material exhibited least overcut during the current setting of 20 amperes while graphite showed the least overcut effect at 32 amperes current setting.

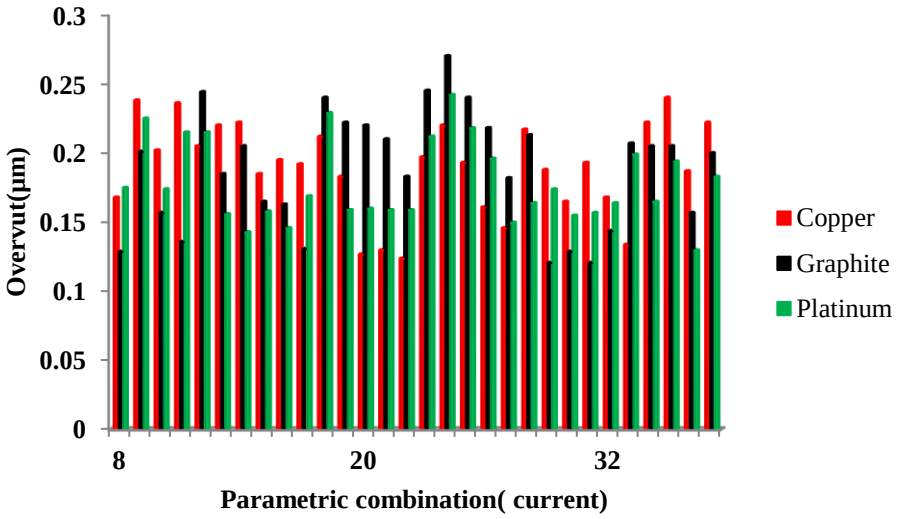

Figure 7.6 Variation of OC with respect to current

Table 7. 6: OC for different electrodes with variation in Peak current (I_p)

S. No.	Parameters				Overcut(μm)		
	Peak current (I_p)	Voltage (V)	Pulse on duration (T_{on})	Pulse off duration (T_{off})	Copper	Graphite	Platinum
1	8	30	20	30	0.168	0.129	0.175
2	8	30	40	60	0.238	0.201	0.225
3	8	30	20	60	0.202	0.157	0.174
4	8	30	40	30	0.236	0.136	0.215
5	8	35	30	45	0.205	0.244	0.215
6	8	40	20	30	0.22	0.185	0.156
7	8	40	20	60	0.222	0.205	0.143
8	8	40	40	30	0.185	0.165	0.158
9	8	40	40	60	0.195	0.163	0.146
10	20	30	30	45	0.192	0.131	0.169
11	20	35	30	45	0.212	0.24	0.229
12	20	35	30	30	0.183	0.222	0.159
13	20	35	30	45	0.127	0.22	0.16
14	20	35	30	45	0.13	0.21	0.159
15	20	35	30	45	0.124	0.183	0.159
16	20	35	30	45	0.197	0.245	0.212
17	20	35	30	45	0.22	0.27	0.242
18	20	35	40	45	0.193	0.24	0.218
19	20	35	20	45	0.161	0.218	0.196
20	20	35	30	60	0.146	0.182	0.15
21	20	40	30	45	0.217	0.213	0.164
22	32	40	40	60	0.222	0.205	0.165
23	32	40	40	30	0.24	0.205	0.194
24	32	40	20	60	0.187	0.157	0.13
25	32	40	20	30	0.222	0.2	0.183
26	32	30	20	30	0.188	0.121	0.174
27	32	30	20	60	0.165	0.129	0.155
28	32	30	40	60	0.193	0.121	0.157
29	32	30	40	30	0.168	0.144	0.164
30	32	35	30	45	0.134	0.207	0.199

7.2.2.3 EFFECT OF PULSE ON DURATION VARIATION ON OC

The variation of OC for different combination of process parameters with respect to current is shown in form of bar graph in Figure 7.7 and the different experimental conditions are given in Table 7.7. The effect of pulse on duration variation on OC is presented in Figure 7.7 it can be observed that graphite exhibited higher overcut as compared to platinum and copper during the different pulse on duration settings.

However, during the pulse on duration setting of 30µs, copper showed least overcut effect.

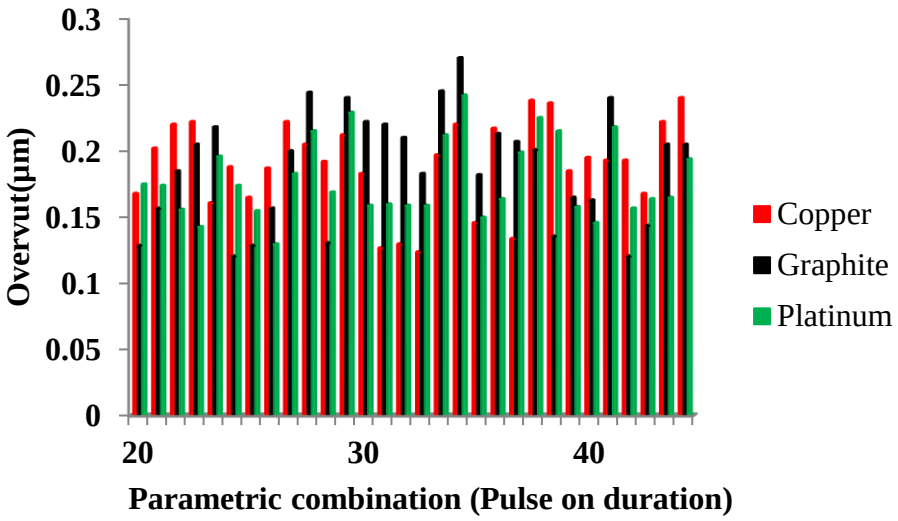

Figure 7.7 Variation of OC with respect to pulse on duration

Table 7. 7: OC for different electrodes with variation in Pulse on duration (T_{on})

S. No.	Parameters				Overcut(µm)		
	Pulse on duration (T_{on})	Peak current (I_p)	Voltage (V)	Pulse off duration (T_{off})	Copper	Graphite	Platinum
1	30	8	20	30	0.168	0.129	0.175
2	30	8	40	60	0.238	0.201	0.225
3	30	8	20	60	0.202	0.157	0.174
4	30	8	40	30	0.236	0.136	0.215
5	30	20	30	45	0.192	0.131	0.169
6	30	32	20	30	0.188	0.121	0.174
7	30	32	20	60	0.165	0.129	0.155
8	30	32	40	60	0.193	0.121	0.157
9	30	32	40	30	0.168	0.144	0.164
10	35	20	30	45	0.212	0.24	0.229
11	35	20	30	30	0.183	0.222	0.159
12	35	20	30	45	0.127	0.22	0.16
13	35	20	30	45	0.13	0.21	0.159
14	35	20	30	45	0.124	0.183	0.159
15	35	20	30	45	0.197	0.245	0.212
16	35	20	30	45	0.22	0.27	0.242
17	35	20	40	45	0.193	0.24	0.218
18	35	20	20	45	0.161	0.218	0.196
19	35	20	30	60	0.146	0.182	0.15
20	35	32	30	45	0.134	0.207	0.199
21	35	8	30	45	0.205	0.244	0.215
22	40	20	30	45	0.217	0.213	0.164
23	40	32	40	60	0.222	0.205	0.165
24	40	32	40	30	0.24	0.205	0.194
25	40	32	20	60	0.187	0.157	0.13
26	40	32	20	30	0.222	0.2	0.183
27	40	8	20	30	0.22	0.185	0.156
28	40	8	20	60	0.222	0.205	0.143
29	40	8	40	30	0.185	0.165	0.158
30	40	8	40	60	0.195	0.163	0.146

7.2.2.4 EFFECT OF PULSE OFF DURATION VARIATION ON OC

The variation of OC for different combination of process parameters with respect to pulse off duration is shown in form of bar graph in Figure 7.8 the different experimental conditions are given in Table 7. 8. The effect of pulse off duration on OC is presented in Figure 7.8 and it can be observed that for pulse off duration setting of 30µs, graphite showed least overcut but as there is rise in pulse off duration value to 45µs, it showed a rise in overcut value at the same time copper exhibited least overcut effect followed by platinum.

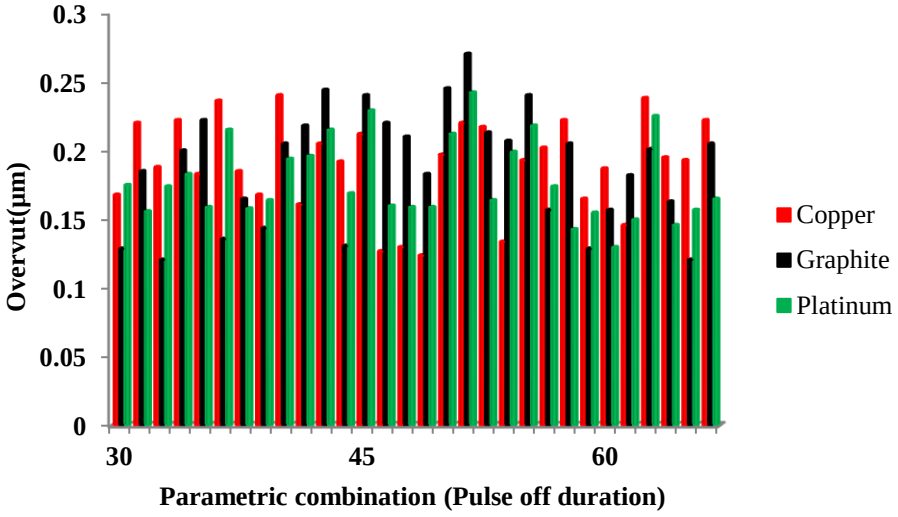

Figure 7.8 Variation of OC with respect to pulse off duration

Table 7. 8: OC for different electrodes with variation in Pulse off duration (T_{off})

S. No.	Parameters				Overcut(μm)		
	Pulse off duration (T_{off})	Peak current (I_p)	Pulse on duration (T_{on})	Voltage (V)	Copper	Graphite	Platinum
1	30	8	20	30	0.168	0.129	0.175
2	30	8	40	30	0.236	0.136	0.215
3	30	32	20	30	0.188	0.121	0.174
4	30	32	40	30	0.168	0.144	0.164
5	30	32	40	40	0.24	0.205	0.194
6	30	20	30	35	0.183	0.222	0.159
7	30	32	20	40	0.222	0.2	0.183
8	30	8	20	40	0.22	0.185	0.156
9	30	8	40	40	0.185	0.165	0.158
10	45	20	30	30	0.192	0.131	0.169
11	45	20	30	35	0.212	0.24	0.229
12	45	20	30	35	0.127	0.22	0.16
13	45	20	30	35	0.13	0.21	0.159
14	45	20	30	35	0.124	0.183	0.159
15	45	20	30	35	0.197	0.245	0.212
16	45	20	30	35	0.22	0.27	0.242
17	45	20	40	35	0.193	0.24	0.218
18	45	20	20	35	0.161	0.218	0.196
19	45	32	30	35	0.134	0.207	0.199
20	45	8	30	35	0.205	0.244	0.215
21	45	20	30	40	0.217	0.213	0.164
22	60	32	40	40	0.222	0.205	0.165
23	60	32	20	40	0.187	0.157	0.13
24	60	8	20	40	0.222	0.205	0.143
25	60	8	40	40	0.195	0.163	0.146
26	60	8	40	30	0.238	0.201	0.225
27	60	8	20	30	0.202	0.157	0.174
28	60	32	20	30	0.165	0.129	0.155
29	60	32	40	30	0.193	0.121	0.157
30	60	20	30	35	0.146	0.182	0.15

7.2.3 PERFORMANCE OF DIFFERENT ELECTRODES MATERIALS ON RCL

Due to rapid local heating and quenching and random attack of the spark, a multi layered surface is created on the workpiece. The top most layer also termed as recast layer or white layer is formed by molten metal which is not flushed away by the dielectric, but resolidifies on the sample's machined surface during cooling. It is found that the recast layer is quite hard and that non-etchable. RCL significantly affects fatigue strength and shortens service life (Abu Zeid, 1997). The experimental results of RCL during fabrication of micro holes on Inconel 718 as work piece material for different operating conditions are presented in Table 7.9.

7.2.3.1 EFFECT OF VOLTAGE VARIATION ON RCL

The variation of RCL for different combination of process parameters as per Table 7.9 is shown in form of bar graph in Figure 7.9. The effect of voltage variation on RCL is presented in Figure 7.9 it can be observed that at first level of voltage variation i.e., 30V Copper electrode depicts higher recast layer followed by Graphite and Platinum. But as the operating voltage reaches to 35 V a rise can be seen for platinum superseding Graphite, while at the same time Copper still exhibiting maximum RCL. Similarly, an unusual observation can be seen when the voltage reaches to 40V, now Platinum as electrode material depicts highest RCL followed by Graphite and Copper

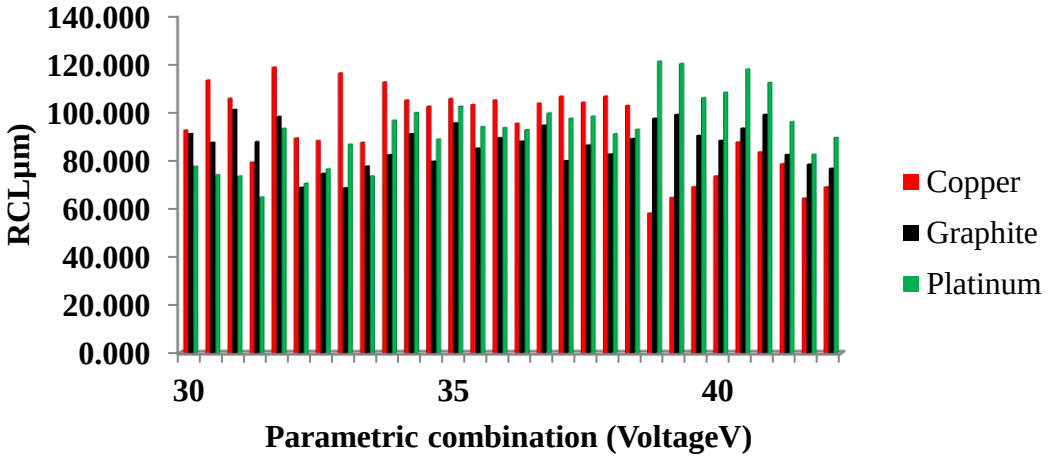

Figure 7.9: Variation of RCL with respect to Voltage

Table 7. 9: RCL for different electrodes with variation in Voltage

S. No.	Parameters				RCL (μm)		
	Voltage (V)	Peak current (I_p)	Pulse on duration (T_{on})	Pulse off duration (T_{off})	Copper	Graphite	Platinum
1	30	8	20	30	92.370	90.825	77.284
2	30	8	40	60	113.079	87.249	73.773
3	30	8	20	60	105.555	100.891	73.224
4	30	8	40	30	79.032	87.548	64.568
5	30	20	30	45	118.483	97.999	93.076
6	30	32	20	30	89.041	68.627	70.268
7	30	32	20	60	87.999	74.391	76.234
8	30	32	40	60	116.060	68.408	86.494
9	30	32	40	30	87.249	77.429	73.262
10	35	8	30	45	112.308	82.143	96.414
11	35	20	30	45	104.857	90.882	99.627
12	35	20	30	30	102.237	79.441	88.591
13	35	20	30	45	105.472	95.326	102.250
14	35	20	30	45	102.943	84.857	93.723
15	35	20	30	45	104.857	89.191	93.360
16	35	20	30	45	95.173	87.741	92.474
17	35	20	30	45	103.514	94.341	99.474
18	35	20	40	45	106.391	79.665	97.287
19	35	20	20	45	103.891	86.158	98.128
20	35	20	30	60	106.408	82.365	90.840
21	35	32	30	45	102.560	88.810	92.657
22	40	8	20	30	57.926	97.222	120.976
23	40	8	20	60	64.348	98.833	119.973
24	40	8	40	30	68.854	90.141	105.791
25	40	8	40	60	73.287	88.070	108.054
26	40	20	30	45	87.390	93.155	117.724
27	40	32	40	60	83.250	98.843	112.098
28	40	32	40	30	78.322	82.204	95.809
29	40	32	20	60	64.077	78.177	82.307
30	40	32	20	30	68.791	76.422	89.284

7.2.3.2 EFFECT OF CURRENT VARIATION ON RCL

The variation of RCL for different combination of process parameters with respect to current is shown in form of bar graph in Figure 7.10 and the different experimental set with variation of current on RCL is given in Table 7.10. The variation of RCL with respect to current is shown in Figure 7.10 and it can be observed that copper as electrode material overall showed higher RCL as compared to graphite and platinum except initial current setting value of 8 amperes. The least RCL was observed as 57.926 µm at 8 amperes for the case of copper.

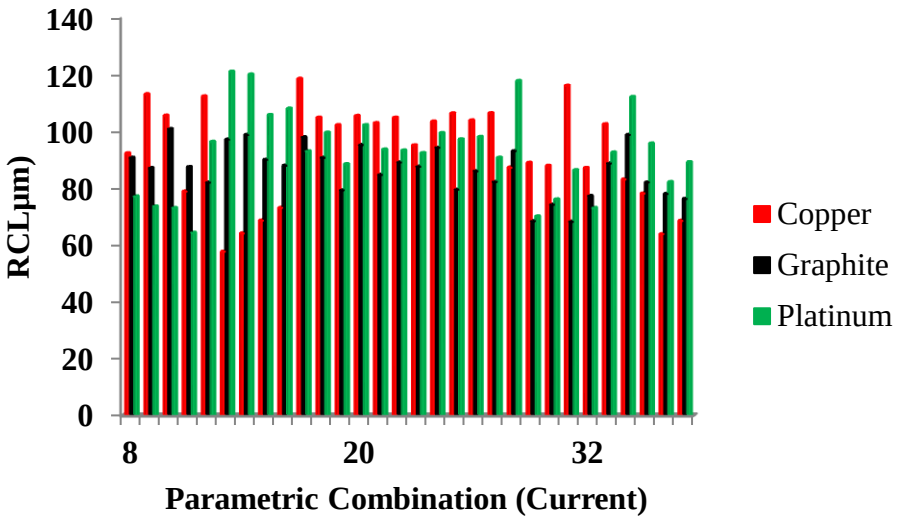

Figure 7.10: Variation of RCL with respect to current

Table 7. 10: RCL for different electrodes with variation in Peak current (I_p)

S. No.	Parameters				RCL (μm)		
	Peak current (I_p)	Voltage (V)	Pulse on duration (T_{on})	Pulse off duration (T_{off})	Copper	Graphite	Platinum
1	8	30	20	30	92.37	90.825	77.284
2	8	30	40	60	113.079	87.249	73.773
3	8	30	20	60	105.555	100.891	73.224
4	8	30	40	30	79.032	87.548	64.568
5	8	35	30	45	112.308	82.143	96.414
6	8	40	20	30	57.926	97.222	120.976
7	8	40	20	60	64.348	98.833	119.973
8	8	40	40	30	68.854	90.141	105.791
9	8	40	40	60	73.287	88.07	108.054
10	20	30	30	45	118.483	97.999	93.076
11	20	35	30	45	104.857	90.882	99.627
12	20	35	30	30	102.237	79.441	88.591
13	20	35	30	45	105.472	95.326	102.25
14	20	35	30	45	102.943	84.857	93.723
15	20	35	30	45	104.857	89.191	93.36
16	20	35	30	45	95.173	87.741	92.474
17	20	35	30	45	103.514	94.341	99.474
18	20	35	40	45	106.391	79.665	97.287
19	20	35	20	45	103.891	86.158	98.128
20	20	35	30	60	106.408	82.365	90.84
21	20	40	30	45	87.39	93.155	117.724
22	32	40	40	60	83.25	98.843	112.098
23	32	40	40	30	78.322	82.204	95.809
24	32	40	20	60	64.077	78.177	82.307
25	32	40	20	30	68.791	76.422	89.284
26	32	30	20	30	89.041	68.627	70.268
27	32	30	20	60	87.999	74.391	76.234
28	32	30	40	60	116.06	68.408	86.494
29	32	30	40	30	87.249	77.429	73.262
30	32	35	30	45	102.56	88.81	92.657

7.2.3.3 EFFECT OF PULSE ON DURATION VARIATION ON RCL

The variation of RCL for different combination of process parameters with respect to pulse on duration is shown in form of bar graph in Figure 7.11. The variation of RCL with respect to pulse on duration is shown in Figure 7.11 and is presented in Table 7.11 and it can be observed that at initial pulse on duration setting value of 20 µs copper showed least RCL, while at the same setting platinum exhibited highest RCL. Further increase in pulse on duration resulted in higher RCL values for copper and platinum respectively.

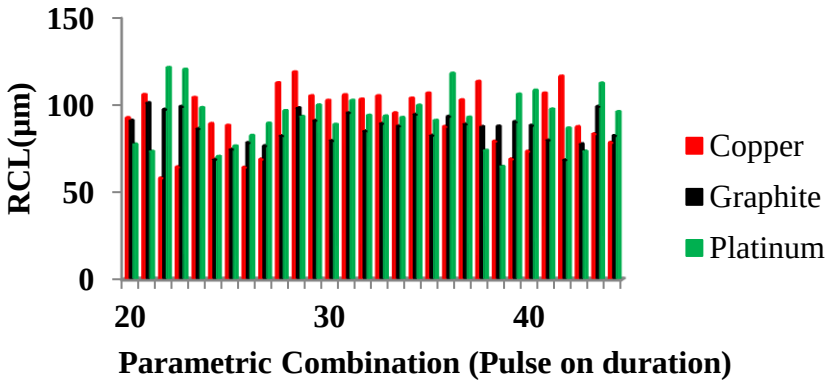

Figure 7.11 Variation of RCL with respect to Pulse on duration

Table 7. 11: RCL for different electrodes with variation in Pulse on duration (T_{on})

S. No.	Parameters				RCL (µm)		
	Pulse on duration (T_{on})	Peak current (I_p)	Voltage (V)	Pulse off duration (T_{off})	Copper	Graphite	Platinum
1	20	8	30	30	92.37	90.825	77.284
2	20	8	30	60	105.555	100.891	73.224
3	20	8	40	30	57.926	97.222	120.976
4	20	8	40	60	64.348	98.833	119.973
5	20	20	35	45	103.891	86.158	98.128
6	20	32	40	60	64.077	78.177	82.307
7	20	32	40	30	68.791	76.422	89.284
8	20	32	30	30	89.041	68.627	70.268
9	20	32	30	60	87.999	74.391	76.234
10	30	8	35	45	112.308	82.143	96.414
11	30	20	30	45	118.483	97.999	93.076
12	30	20	35	45	104.857	90.882	99.627
13	30	20	35	30	102.237	79.441	88.591
14	30	20	35	45	105.472	95.326	102.25

S. No.	Parameters				RCL (µm)		
	Pulse on duration (T_{on})	Peak current (I_p)	Voltage (V)	Pulse off duration (T_{off})	Copper	Graphite	Platinum
15	30	20	35	45	102.943	84.857	93.723
16	30	20	35	45	104.857	89.191	93.36
17	30	20	35	45	95.173	87.741	92.474
18	30	20	35	45	103.514	94.341	99.474
19	30	20	35	60	106.408	82.365	90.84
20	30	20	40	45	87.39	93.155	117.724
21	30	32	35	45	102.56	88.81	92.657
22	40	8	40	30	68.854	90.141	105.791
23	40	8	40	60	73.287	88.07	108.054
24	40	20	35	45	106.391	79.665	97.287
25	40	32	40	60	83.25	98.843	112.098
26	40	32	40	30	78.322	82.204	95.809
27	40	32	30	60	116.06	68.408	86.494
28	40	32	30	30	87.249	77.429	73.262
29	40	8	30	60	113.079	87.249	73.773
30	40	8	30	30	79.032	87.548	64.568

7.2.3.4 EFFECT OF PULSE OFF DURATION VARIATION ON RCL

The variation of RCL for different combination of process parameters with respect to pulse off duration is shown in form of bar graph in Figure 7.12 and is represented in Table 7.12. The effect of pulse off duration variation on RCL is presented in Figure 7.12 it can be observed that for initial pulse off duration setting of 30µs copper showed least RCL, while platinum as highest. Similarly, at pulse off duration value of 45 µs copper showed higher RCL value followed by platinum and graphite respectively.

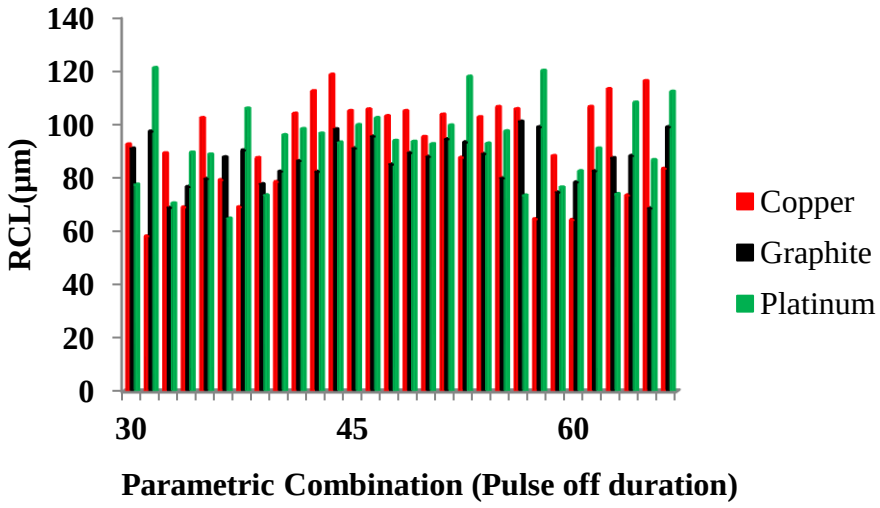

Figure 7.12: Variation of RCL with respect to Pulse off duration

Table 7. 12: RCL for different electrodes with variation in Pulse off duration (T_{off})

S. No.	Parameters				RCL (µm)		
	Pulse off duration (T_{off})	Pulse on duration (T_{on})	Peak current (I_p)	Voltage (V)	Copper	Graphite	Platinum
1	30	20	8	30	92.37	90.825	77.284
2	30	20	8	40	57.926	97.222	120.976
3	30	40	32	30	87.249	77.429	73.262
4	30	40	8	40	68.854	90.141	105.791
5	30	30	20	35	102.237	79.441	88.591
6	30	40	8	30	79.032	87.548	64.568
7	30	40	32	40	78.322	82.204	95.809
8	30	20	32	40	68.791	76.422	89.284
9	30	20	32	30	89.041	68.627	70.268
10	45	20	20	35	103.891	86.158	98.128
11	45	30	8	35	112.308	82.143	96.414
12	45	30	20	30	118.483	97.999	93.076
13	45	30	20	35	104.857	90.882	99.627
14	45	30	20	35	105.472	95.326	102.25
15	45	30	20	35	102.943	84.857	93.723
16	45	30	20	35	104.857	89.191	93.36
17	45	30	20	35	95.173	87.741	92.474
18	45	30	20	35	103.514	94.341	99.474
19	45	30	20	40	87.39	93.155	117.724
20	45	30	32	35	102.56	88.81	92.657
21	45	40	20	35	106.391	79.665	97.287
22	60	40	32	40	83.25	98.843	112.098
23	60	40	32	30	116.06	68.408	86.494
24	60	40	8	30	113.079	87.249	73.773
25	60	20	8	30	105.555	100.891	73.224
26	60	20	8	40	64.348	98.833	119.973
27	60	20	32	40	64.077	78.177	82.307
28	60	20	32	30	87.999	74.391	76.234
29	60	30	20	35	106.408	82.365	90.84
30	60	40	8	40	73.287	88.07	108.054

7.2.4 PERFORMANCE OF DIFFERENT ELECTRODES MATERIALS ON TA

The entrance and exit diameters of the machined holes were not the same due to the corner wear of the electrode in addition to linear wear. Therefore, the taper angle was measured to evaluate the dimensional accuracy of the micro-holes. The taper angle in micro- holes fabricated by electrodes copper graphite and platinum for different combinations of process parameter is given in Table 7.13.

7.2.4.1 EFFECT OF VOLTAGE VARIATION ON TA

The variation of TA for different combination of process parameters (Table 7.4) with respect to voltage variation is shown in the form of bar graph in Figure 7.13. Referring to Figure 7.13 it can be observed that for operating voltage of 30V graphite exhibit's least TA followed by platinum and copper. Furthermore, with further increase in operating voltage i.e., 35V copper indicates least TA preceded by graphite and platinum. In addition to that at highest voltage level setting of 40V graphite yielded least TA followed by copper and platinum respectively.

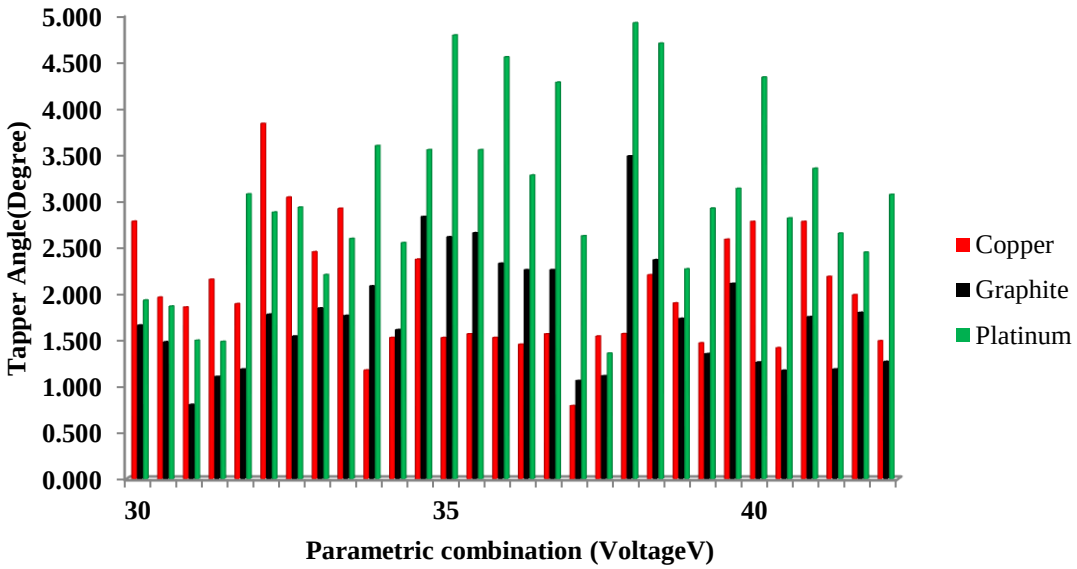

Figure 6. 13: Variation of TA with respect to Voltage

Table 7. 13: TA for different electrodes with combination of process parameters

S. No.	Parameters				TA(degree)		
	Voltage (V)	Peak current (I_p)	Pulse on duration (T_{on})	Pulse off duration (T_{off})	Copper	Graphite	Platinum
1	30	8	20	30	2.777	1.659	1.930
2	30	8	40	60	1.960	1.479	1.864
3	30	8	20	60	1.853	0.802	1.495
4	30	8	40	30	2.153	1.105	1.483
5	30	20	30	45	1.890	1.185	3.072
6	30	32	20	30	3.831	1.776	2.876
7	30	32	20	60	3.037	1.541	2.930
8	30	32	40	60	2.449	1.844	2.203
9	30	32	40	30	2.917	1.763	2.592
10	35	8	30	45	1.174	2.081	3.592
11	35	20	30	45	1.525	1.610	2.548
12	35	20	30	30	2.369	2.828	3.548
13	35	20	30	45	1.525	2.610	4.782
14	35	20	30	45	1.565	2.653	3.548
15	35	20	30	45	1.525	2.326	4.548
16	35	20	30	45	1.453	2.256	3.274
17	35	20	30	45	1.565	2.256	4.274
18	35	20	40	45	0.788	1.060	2.621
19	35	20	20	45	1.541	1.112	1.357
20	35	20	30	60	1.567	3.481	4.915
21	35	32	30	45	2.201	2.363	4.695
22	40	8	20	30	1.897	1.731	2.264
23	40	8	20	60	1.467	1.350	2.918
24	40	8	40	30	2.584	2.109	3.131
25	40	8	40	60	2.775	1.260	4.331
26	40	20	30	45	1.415	1.171	2.813
27	40	32	40	60	2.775	1.750	3.348
28	40	32	40	30	2.184	1.185	2.650
29	40	32	20	60	1.987	1.796	2.445
30	40	32	20	30	1.490	1.266	3.067

7.2.4.2 EFFECT OF CURRENT VARIATION ON TA

The variation of TA for different combination of process parameters (Table 7.14) with respect to voltage variation is shown in the form of bar graph in Figure 7.14. The variation of TA with respect to current is shown in Figure 7.14 and it can be observed that except for few parametric combinations at 8 ampere platinum as electrode material showed highest TA as compared to copper and graphite. However, the least TA was shown by graphite for majority of runs.

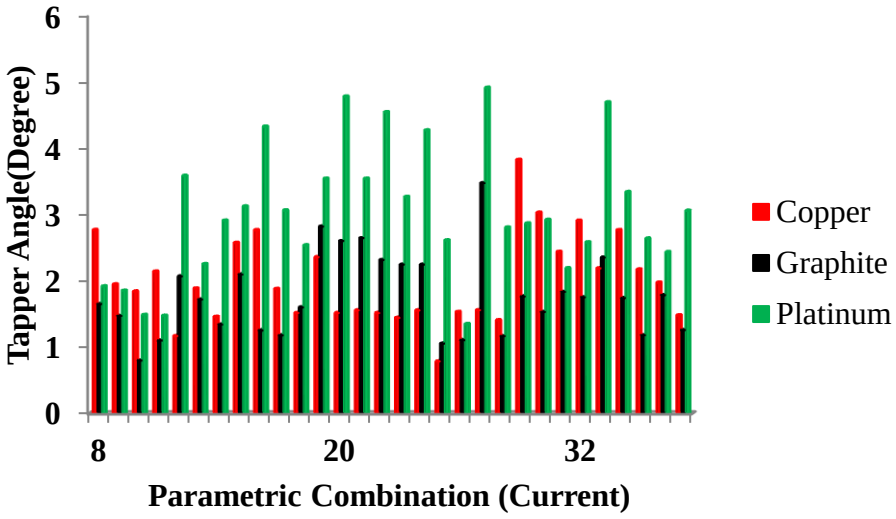

Figure 7 14: Variation of TA with respect to current

Table 7. 14: TA for different electrodes with variation in Peak current (I_p)

S. No.	Parameters				TA(degree)		
	Peak current (I_p)	Voltage (V)	Pulse on duration (T_{on})	Pulse off duration (T_{off})	Copper	Graphite	Platinum
1	8	30	20	30	2.777	1.659	1.93
2	8	30	40	60	1.96	1.479	1.864
3	8	30	20	60	1.853	0.802	1.495
4	8	30	40	30	2.153	1.105	1.483
5	8	35	30	45	1.174	2.081	3.592
6	8	40	20	30	1.897	1.731	2.264
7	8	40	20	60	1.467	1.35	2.918
8	8	40	40	30	2.584	2.109	3.131
9	8	40	40	60	2.775	1.26	4.331
10	20	35	30	45	1.525	1.61	2.548
11	20	35	30	30	2.369	2.828	3.548
12	20	35	30	45	1.525	2.61	4.782
13	20	35	30	45	1.565	2.653	3.548
14	20	35	30	45	1.525	2.326	4.548
15	20	35	30	45	1.453	2.256	3.274
16	20	35	30	45	1.565	2.256	4.274
17	20	35	40	45	0.788	1.06	2.621
18	20	35	20	45	1.541	1.112	1.357
19	20	35	30	60	1.567	3.481	4.915
20	20	40	30	45	1.415	1.171	2.813
21	20	30	30	45	1.89	1.185	3.072
22	32	35	30	45	2.201	2.363	4.695
23	32	40	40	60	2.775	1.75	3.348
24	32	40	40	30	2.184	1.185	2.65
25	32	40	20	60	1.987	1.796	2.445
26	32	40	20	30	1.49	1.266	3.067
27	32	30	20	30	3.831	1.776	2.876
28	32	30	20	60	3.037	1.541	2.93
29	32	30	40	60	2.449	1.844	2.203
30	32	30	40	30	2.917	1.763	2.592

7.2.4.3 EFFECT OF PULSE ON DURATION ON TA

The variation of TA for different combination of process parameters with respect to pulse on duration is shown in form of bar graph in Figure 7.15 and is given in Table 7.15. The effect of pulse on duration variation on TA is presented in Figure7.15 it can be observed that platinum showed higher taper angle during each level of parametric combination, while graphite showed the least TA except for few cases at 30µs pulse on duration setting.

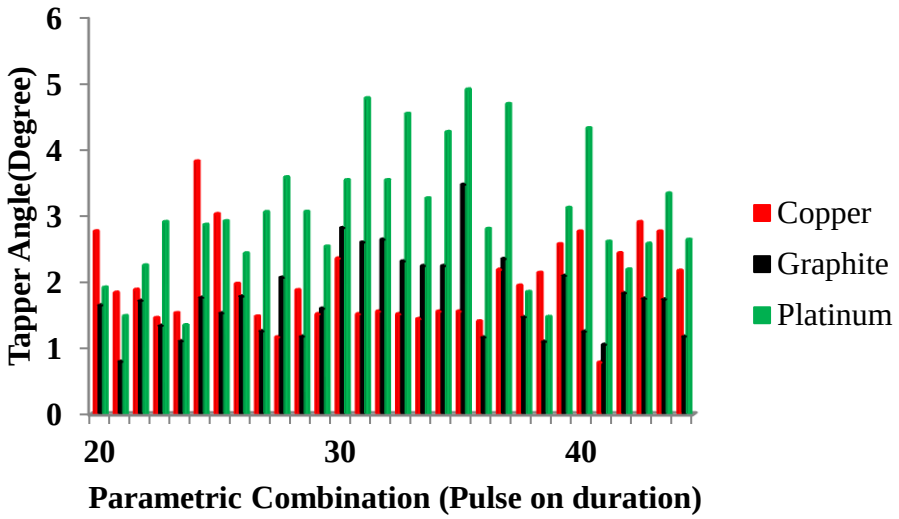

Figure 7. 15: Variation of TA with respect to Pulse on duration

Table 7. 15: TA for different electrodes with variation in Pulse on duration (T_{on})

S. No.	Parameters				TA(degree)		
	Pulse on duration (T_{on})	Peak current (I_p)	Voltage (V)	Pulse off duration (T_{off})	Copper	Graphite	Platinum
1	20	8	30	30	2.777	1.659	1.93
2	20	8	30	60	1.853	0.802	1.495
3	20	8	40	30	1.897	1.731	2.264
4	20	20	35	45	1.541	1.112	1.357
5	20	8	40	60	1.467	1.35	2.918
6	30	8	35	45	1.174	2.081	3.592
7	20	32	40	60	1.987	1.796	2.445
8	20	32	40	30	1.49	1.266	3.067
9	20	32	30	30	3.831	1.776	2.876
10	20	32	30	60	3.037	1.541	2.93
11	30	20	35	45	1.525	1.61	2.548
12	30	20	35	30	2.369	2.828	3.548
13	30	20	35	45	1.525	2.61	4.782
14	30	20	35	45	1.565	2.653	3.548
15	30	20	35	45	1.525	2.326	4.548
16	30	20	35	45	1.453	2.256	3.274
17	30	20	35	45	1.565	2.256	4.274
18	30	20	35	60	1.567	3.481	4.915
19	30	20	40	45	1.415	1.171	2.813
20	30	20	30	45	1.89	1.185	3.072
21	30	32	35	45	2.201	2.363	4.695
22	40	20	35	45	0.788	1.06	2.621
23	40	8	40	30	2.584	2.109	3.131
24	40	8	40	60	2.775	1.26	4.331
25	40	32	40	60	2.775	1.75	3.348
26	40	32	40	30	2.184	1.185	2.65
27	40	32	30	60	2.449	1.844	2.203
28	40	32	30	30	2.917	1.763	2.592
29	40	8	30	60	1.96	1.479	1.864
30	32	30	40	30	2.917	1.763	2.592

7.2.4.4 EFFECT OF PULSE OFF DURATION ON TA

The variation of OC for different combination of process parameters with respect to pulse off duration is shown in form of bar graph in Figure 7.16 and is presented in Table7.16. The variation of TA with respect to pulse off duration is shown in Figure 7.16 and it can be observed that except for few combinations at pulse of duration setting of 30 µs, platinum marked highest TA while copper marked the least TA of 0.788 degree at 45 µs setting of pulse off duration.

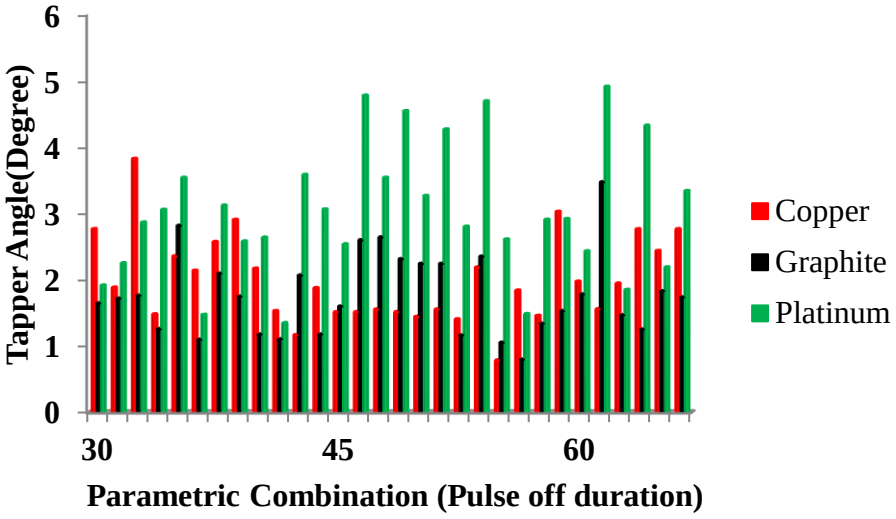

Figure 7. 16 Variation of TA with respect to Pulse off duration

Table 7. 16: TA for different electrodes with variation in Pulse off duration (T_{off})

S. No.	Parameters				TA(degree)		
	Pulse off duration (T_{off})	Pulse on duration (T_{on})	Peak current (I_p)	Voltage (V)	Copper	Graphite	Platinum
1	30	20	8	30	2.777	1.659	1.93
2	30	40	32	30	2.917	1.763	2.592
3	30	20	8	40	1.897	1.731	2.264
4	30	20	32	40	1.49	1.266	3.067
5	30	20	32	30	3.831	1.776	2.876
6	30	30	20	35	2.369	2.828	3.548
7	30	40	8	40	2.584	2.109	3.131
8	30	40	32	40	2.184	1.185	2.65
9	45	20	20	35	1.541	1.112	1.357
10	45	30	8	35	1.174	2.081	3.592
11	45	30	20	35	1.525	1.61	2.548
12	45	30	20	35	1.525	2.61	4.782
13	45	30	20	35	1.565	2.653	3.548
14	45	30	20	35	1.525	2.326	4.548
15	45	30	20	35	1.453	2.256	3.274
16	45	30	20	35	1.565	2.256	4.274
17	45	30	20	40	1.415	1.171	2.813
18	45	30	20	30	1.89	1.185	3.072
19	45	30	32	35	2.201	2.363	4.695
20	45	40	20	35	0.788	1.06	2.621
21	60	20	32	40	1.987	1.796	2.445
22	60	20	32	30	3.037	1.541	2.93
23	60	30	20	35	1.567	3.481	4.915
24	60	40	8	40	2.775	1.26	4.331
25	60	40	32	40	2.775	1.75	3.348
26	60	20	8	40	1.467	1.35	2.918
27	60	40	32	30	2.449	1.844	2.203
28	60	40	8	30	1.96	1.479	1.864
29	60	20	8	30	1.853	0.802	1.495
30	32	30	40	30	2.917	1.763	2.592

7.3 ANALYSIS OF OUTPUT PERFORMANCE USING TITANIUM AS WORKPIECE MATERIAL

In present investigation, comparison of MRR, Overcut, Recast Layer thickness and Taper angle with respect to voltage current, pulse on duration, pulse off duration for copper graphite and platinum electrode are given.

7.3.1 PERFORMANCE OF DIFFERENT ELECTRODES MATERIALS ON MRR

The MRR using copper graphite and platinum as electrodes are presented in Table 7.17.

7.3.1.1 EFFECT OF VOLTAGE VARIATION ON MRR

The variation of MRR for different process combinations with respect to variation in voltage is shown in Figure 7.17. Figure 7.17 show the variation of voltage along with MRR obtained using different electrode materials. The variation of MRR with respect to voltage is shown in Figure 7.17 and it can be seen that for different voltage settings platinum marks highest MRR, while copper as electrode material exhibits least MRR among the three electrode materials. It can also be observed that for platinum MRR rises nonlinearly, as the voltage increases. The variation of MRR with respect to voltage is shown in Figure 7.17 and it can be seen that for different operating voltage settings platinum marks highest MRR, while copper as electrode material exhibits least MRR among the three electrode materials. It can also be observed that for platinum MRR rises nonlinearly, as the voltage increases.

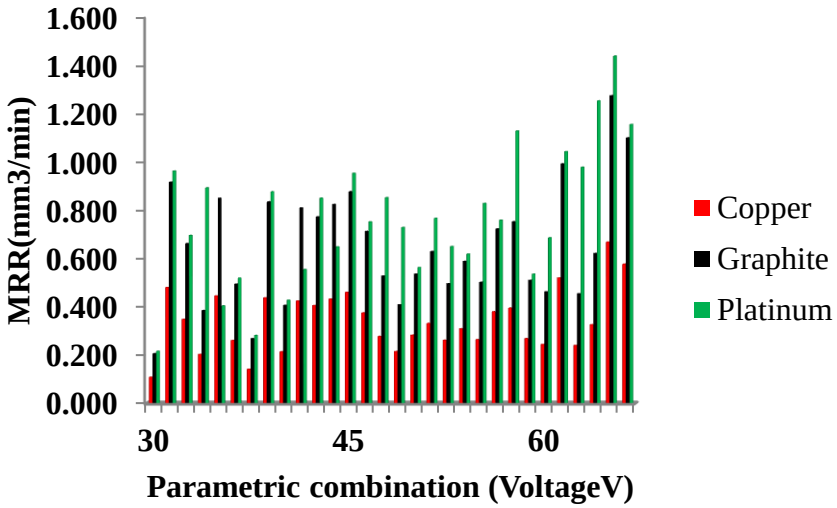

Figure 7. 17 : Variation of MRR with respect to Voltage

Table 7. 17: MRR for different electrodes with combination of process parameters

S. No.	Parameters				Material Removal Rate (MRR) mm^3/min		
	Voltage (V)	Peak current (I_p)	Pulse on duration (T_{on})	Pulse off duration (T_{off})	Copper	Graphite	Platinum
1	30	10	80	20	0.149	0.207	0.217
2	30	40	40	20	0.483	0.918	0.964
3	30	10	80	30	0.350	0.665	0.699
4	30	40	80	20	0.204	0.387	0.895
5	30	10	40	30	0.448	0.852	0.406
6	30	40	40	30	0.262	0.497	0.522
7	30	25	60	25	0.142	0.270	0.283
8	30	10	40	20	0.440	0.837	0.879
9	30	40	80	30	0.215	0.409	0.429
10	45	25	60	25	0.427	0.812	0.557
11	45	25	60	25	0.408	0.775	0.852
12	45	25	60	25	0.435	0.826	0.651
13	45	25	60	25	0.463	0.879	0.955
14	45	25	60	25	0.377	0.715	0.754
15	45	25	60	25	0.279	0.531	0.854
16	45	25	60	20	0.216	0.411	0.731
17	45	25	40	25	0.284	0.539	0.566
18	45	40	60	25	0.333	0.632	0.769
19	45	25	80	25	0.263	0.499	0.652
20	45	10	60	25	0.311	0.591	0.621
21	45	25	60	30	0.266	0.505	0.831
22	60	40	40	30	0.382	0.725	0.761
23	60	10	80	30	0.397	0.755	1.129
24	60	25	60	25	0.270	0.513	0.539
25	60	10	80	20	0.245	0.465	0.689
26	60	40	40	20	0.523	0.994	1.044
27	60	10	40	20	0.241	0.457	0.980
28	60	10	40	30	0.328	0.624	1.254
29	60	40	80	30	0.671	1.275	1.439
30	60	40	80	20	0.580	1.101	1.156

7.3.1.2 EFFECT OF CURRENT VARIATION ON MRR

The variation of MRR for different combination of process parameters with respect to current is shown in form of bar graph in Figure 7.18 and is shown in Table 7.18. Figure

7.18 shows the effect of current variation on MRR, and as it can be inferred from Figure 7.18 that among different electrode materials i.e. platinum, copper and graphite, platinum depicts higher MRR followed by graphite and copper. Furthermore, there is a marginal rise in MRR when current variation is increased from 10 amperes to 25 amperes for the case of platinum electrode, while for the case of graphite, MRR initially tends to rise for 10-25 ampere current variation range and falls down nonlinearly when the variation in current range is 40 amperes.

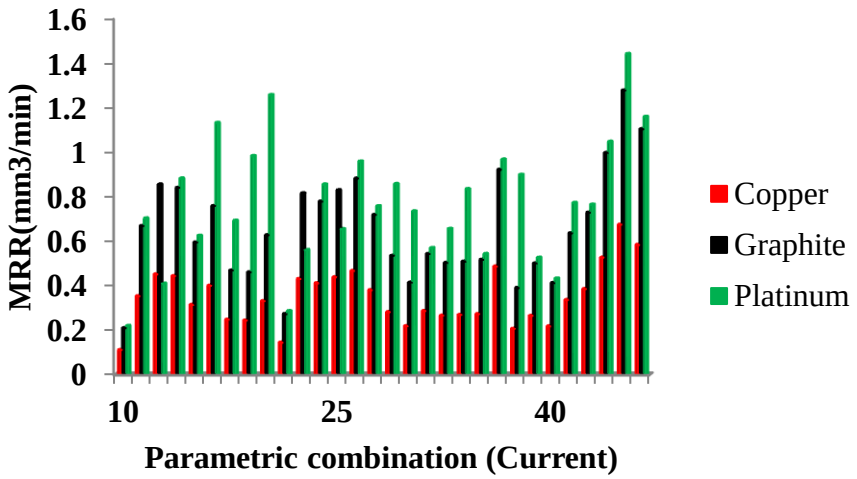

Figure 7. 18: Variation of MRR with respect to current

Table 7. 18: MRR for different electrodes with variation in Peak current (I_p)

S. No.	Parameters				Material Removal Rate (MRR) mm^3/min		
	Peak current (I_p)	Voltage (V)	Pulse on duration (T_{on})	Pulse off duration (T_{off})	Copper	Graphite	Platinum
1	10	30	80	20	0.149	0.207	0.217
2	10	30	80	30	0.35	0.665	0.699
3	10	30	40	20	0.44	0.837	0.879
4	10	60	40	20	0.241	0.457	0.98
5	10	45	60	25	0.311	0.591	0.621
6	10	60	80	30	0.397	0.755	1.129
7	10	60	40	30	0.328	0.624	1.254
8	10	60	80	20	0.245	0.465	0.689
9	10	30	40	30	0.448	0.852	0.406
10	25	30	60	25	0.142	0.27	0.283
11	25	45	60	25	0.427	0.812	0.557
12	25	45	60	25	0.408	0.775	0.852
13	25	45	60	25	0.435	0.826	0.651
14	25	45	60	25	0.463	0.879	0.955
15	25	45	60	25	0.377	0.715	0.754
16	25	45	60	25	0.279	0.531	0.854
17	25	45	60	20	0.216	0.411	0.731
18	25	45	40	25	0.284	0.539	0.566
19	25	45	80	25	0.263	0.499	0.652
20	25	45	60	30	0.266	0.505	0.831
21	25	60	60	25	0.27	0.513	0.539
22	40	30	80	30	0.215	0.409	0.429
23	40	45	60	25	0.333	0.632	0.769
24	40	60	40	30	0.382	0.725	0.761
25	40	60	40	20	0.523	0.994	1.044
26	40	60	80	30	0.671	1.275	1.439
27	40	60	80	20	0.58	1.101	1.156
28	40	30	40	20	0.483	0.918	0.964
29	40	30	80	20	0.204	0.387	0.895
30	40	30	40	30	0.262	0.497	0.522

7.3.1.3 EFFECT OF PULSE ON DURATION VARIATION ON MRR

The variation of MRR for different combination of process parameters with respect to pulse on duration is shown in form of bar graph in Figure 7.19 and is shown in Table7.19 . Figure 7.19 shows the variation of pulse on duration with respect to MRR, further it can be observed that platinum as electrode material exhibit's higher MRR throughout the variation of pulse on duration setting in the range of 40-80µs. Next to platinum, graphite depicts lower MRR followed by copper as least MRR.

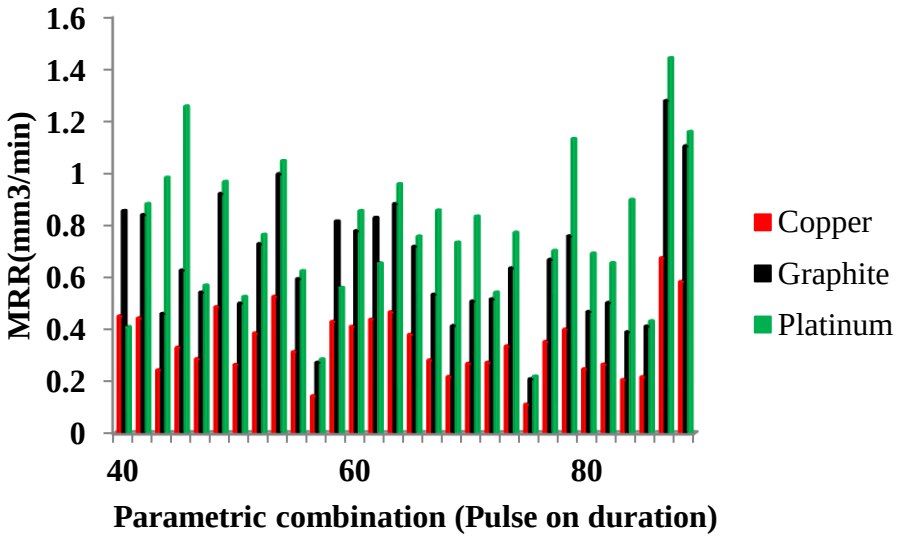

Figure 7. 19: Variation of MRR with respect to pulse on duration

Table 7. 19: MRR for different electrodes with variation in Pulse on duration (T_{on})

S. No.	Parameters				Material Removal Rate (MRR) mm^3/min		
	Pulse on duration (T_{on})	Voltage (V)	Peak current (I_p)	Pulse off duration (T_{off})	Copper	Graphite	Platinum
1	40	30	40	30	0.262	0.497	0.522
2	40	60	40	20	0.523	0.994	1.044
3	40	30	10	20	0.44	0.837	0.879
4	40	60	10	20	0.241	0.457	0.98
5	40	45	25	25	0.284	0.539	0.566
6	40	30	10	30	0.448	0.852	0.406
7	40	60	40	30	0.382	0.725	0.761
8	40	30	40	20	0.483	0.918	0.964
9	40	60	10	30	0.328	0.624	1.254
10	60	45	10	25	0.311	0.591	0.621
11	60	30	25	25	0.142	0.27	0.283
12	60	45	25	25	0.427	0.812	0.557
13	60	45	25	25	0.408	0.775	0.852
14	60	45	25	25	0.435	0.826	0.651
15	60	45	25	25	0.463	0.879	0.955
16	60	45	25	25	0.377	0.715	0.754
17	60	45	25	25	0.279	0.531	0.854
18	60	45	25	20	0.216	0.411	0.731
19	60	45	25	30	0.266	0.505	0.831
20	60	60	25	25	0.27	0.513	0.539
21	60	45	40	25	0.333	0.632	0.769
22	80	45	25	25	0.263	0.499	0.652
23	80	30	40	30	0.215	0.409	0.429
24	80	60	40	30	0.671	1.275	1.439
25	80	60	40	20	0.58	1.101	1.156
26	80	30	40	20	0.204	0.387	0.895
27	80	60	10	30	0.397	0.755	1.129
28	80	60	10	20	0.245	0.465	0.689
29	80	30	10	20	0.149	0.207	0.217
30	80	30	10	30	0.35	0.665	0.699

7.3.1.4 EFFECT OF PULSE OFF DURATION VARIATION ON MRR

The variation of MRR for different combination of process parameters with respect to pulse off duration is shown in form of bar graph in Figure 7.20 and is presented in Table 7.20. The effect of pulse off duration variation on MRR is shown in Figure 7.20 and it can be observed that platinum as electrode material exhibit's a higher value of MRR as compared to Copper and Graphite for different pulse off duration settings i.e.20-30 µs. However, a nonlinear trend was observed for all cases of electrode materials.

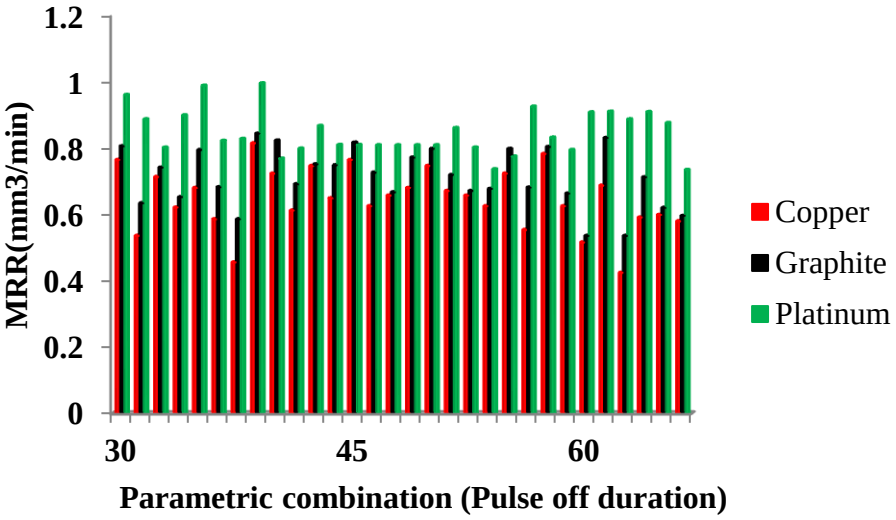

Figure 7. 20: Variation of MRR with respect to Pulse off duration

Table 7. 20: MRR for different electrodes with variation in Pulse off duration (T_{off})

S. No.	Parameters				Material Removal Rate (MRR) mm^3/min		
	Pulse off duration (T_{off})	Pulse on duration (T_{on})	Voltage (V)	Peak current (I_p)	Copper	Graphite	Platinum
1	20	40	60	40	0.523	0.994	1.044
2	20	80	60	10	0.245	0.465	0.689
3	20	80	30	10	0.149	0.207	0.217
4	20	80	60	40	0.58	1.101	1.156
5	20	80	30	40	0.204	0.387	0.895
6	20	60	45	25	0.216	0.411	0.731
7	20	40	30	40	0.483	0.918	0.964
8	20	40	30	10	0.44	0.837	0.879
9	20	40	60	10	0.241	0.457	0.98
10	25	40	45	25	0.284	0.539	0.566
11	25	60	45	10	0.311	0.591	0.621
12	25	60	30	25	0.142	0.27	0.283
13	25	60	45	25	0.427	0.812	0.557
14	25	60	45	25	0.408	0.775	0.852
15	25	60	45	25	0.435	0.826	0.651
16	25	60	45	25	0.463	0.879	0.955
17	25	60	45	25	0.377	0.715	0.754
18	25	60	45	25	0.279	0.531	0.854
19	25	60	60	25	0.27	0.513	0.539
20	25	60	45	40	0.333	0.632	0.769
21	25	80	45	25	0.263	0.499	0.652
22	30	80	30	40	0.215	0.409	0.429
23	30	80	60	40	0.671	1.275	1.439
24	30	80	60	10	0.397	0.755	1.129
25	30	80	30	10	0.35	0.665	0.699
26	30	40	30	40	0.262	0.497	0.522
27	30	40	30	10	0.448	0.852	0.406
28	30	40	60	40	0.382	0.725	0.761
29	30	40	60	10	0.328	0.624	1.254
30	30	60	45	25	0.266	0.505	0.831

7.3.2 PERFORMANCE OF DIFFERENT ELECTRODES MATERIALS ON OC

The overcuts of micro-holes for different electrodes are given in Table 7.21. The variation of overcut for different combination of process parameters in Table 7.21 is shown in Figure 7.21.

7.3.2.1 EFFECT OF VOLTAGE VARIATION ON OC

The variation of MRR for different combination of process parameters with respect to pulse on duration is shown in form of bar graph in Figure 7.21. The variation of OC with respect to voltage is shown in Figure 7.21 and it can be observed that the overcut effect is maximum for graphite. During the considered voltage settings of 30-60V, graphite shows maximum OC, followed by copper and platinum. Since overcut effect is undesirable it should be as least as possible from accuracy point of view. Referring to Figure 7.21 it can be observed that platinum as electrode material shows least overcut along with non-linearly declining trend as it reaches to highest level of voltage variation of 60V.

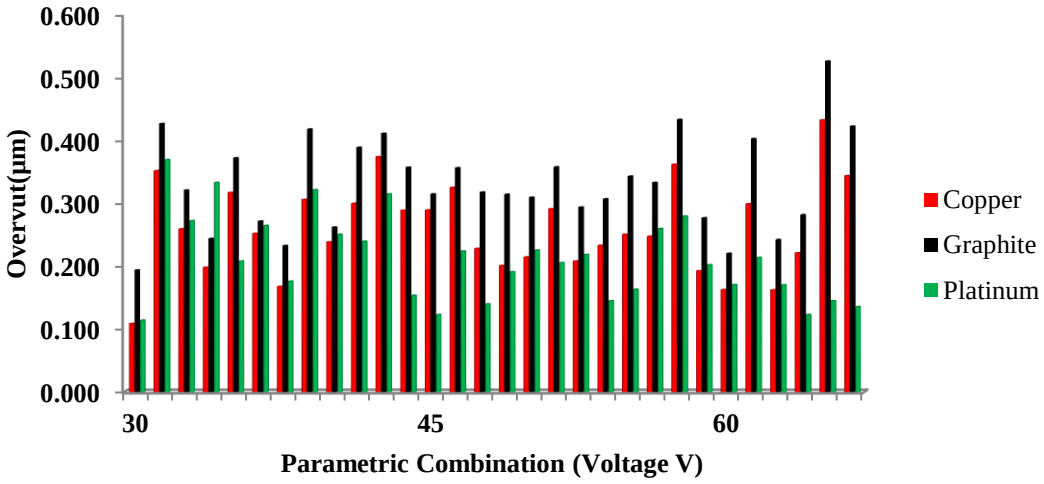

Figure 7.21: Variation of OC with respect to Voltage

Table 7. 21: OC for different electrodes with combination of process parameters

S. No.	Parameters				Overcut(μm)		
	Voltage (V)	Peak current (I_p)	Pulse on duration (T_{on})	Pulse off duration (T_{off})	Copper	Graphite	Platinum
1	30	10	80	20	0.109	0.195	0.114
2	30	40	40	20	0.352	0.427	0.370
3	30	10	80	30	0.260	0.322	0.273
4	30	40	80	20	0.199	0.245	0.334
5	30	10	40	30	0.318	0.373	0.209
6	30	40	40	30	0.253	0.272	0.265
7	30	25	60	25	0.168	0.233	0.177
8	30	10	40	20	0.307	0.418	0.322
9	30	40	80	30	0.239	0.263	0.251
10	45	25	60	25	0.300	0.389	0.240
11	45	25	60	25	0.375	0.412	0.315
12	45	25	60	25	0.290	0.358	0.154
13	45	25	60	25	0.270	0.315	0.123
14	45	25	60	25	0.326	0.357	0.225
15	45	25	60	25	0.229	0.318	0.140
16	45	25	60	20	0.202	0.315	0.192
17	45	25	40	25	0.215	0.310	0.226
18	45	40	60	25	0.292	0.358	0.206
19	45	25	80	25	0.209	0.295	0.219
20	45	10	60	25	0.234	0.308	0.145
21	45	25	60	30	0.251	0.344	0.164
22	60	40	40	30	0.248	0.232	0.261
23	60	10	80	30	0.362	0.434	0.280
24	60	25	60	25	0.193	0.277	0.203
25	60	10	80	20	0.163	0.221	0.171
26	60	40	40	20	0.300	0.403	0.215
27	60	10	40	20	0.163	0.243	0.171
28	60	10	40	30	0.222	0.282	0.123
29	60	40	80	30	0.433	0.526	0.145
30	60	40	80	20	0.344	0.423	0.136

7.3.2.2 EFFECT OF CURRENT VARIATION ON OC

The variation of OC for different combination of process parameters with respect to current is shown in form of bar graph in Figure 7.22 and is shown in Table 7.22. Figure 7.22 depicts the effect of current variation on overcut, and it can be observed that among different electrode materials, platinum shows the least overcut effect followed by copper and graphite. Furthermore, the variations in overcut values are found to be minimum for the case of platinum, while irregular variations are observed for the considered current values for the case of copper and graphite.

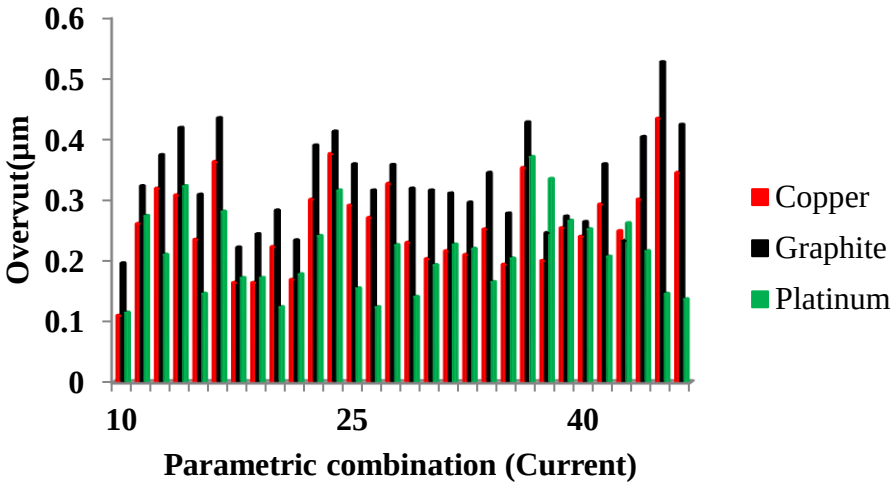

Figure 7.22: Variation of OC with respect to current

Table 7. 22: OC for different electrodes with variation in Peak current (I_p)

S. No.	Parameters				Overcut(μm)		
	Peak current (I_p)	Voltage (V)	Pulse on duration (T_{on})	Pulse off duration (T_{off})	Copper	Graphite	Platinum
1	10	30	80	20	0.109	0.195	0.114
2	10	30	80	30	0.26	0.322	0.273
3	10	30	40	30	0.318	0.373	0.209
4	10	60	40	20	0.163	0.243	0.171
5	10	60	40	30	0.222	0.282	0.123
6	10	30	40	20	0.307	0.418	0.322
7	10	60	80	20	0.163	0.221	0.171
8	10	45	60	25	0.234	0.308	0.145
9	25	30	60	25	0.168	0.233	0.177
10	25	45	60	25	0.3	0.389	0.24
11	25	45	60	25	0.375	0.412	0.315
12	25	45	60	25	0.29	0.358	0.154
13	25	45	60	25	0.27	0.315	0.123
14	25	45	60	25	0.326	0.357	0.225
15	25	45	60	25	0.229	0.318	0.14
16	25	45	60	20	0.202	0.315	0.192
17	25	45	40	25	0.215	0.31	0.226
18	25	45	80	25	0.209	0.295	0.219
19	25	45	60	30	0.251	0.344	0.164
20	25	60	60	25	0.193	0.277	0.203
21	40	30	80	20	0.199	0.245	0.334
22	40	30	80	30	0.239	0.263	0.251
23	40	45	60	25	0.292	0.358	0.206
24	40	30	40	30	0.253	0.272	0.265
25	40	60	40	30	0.248	0.232	0.261
26	40	60	40	20	0.3	0.403	0.215
27	40	60	80	30	0.433	0.526	0.145
28	40	60	80	20	0.344	0.423	0.136
29	40	30	40	20	0.352	0.427	0.37
30	40	60	80	20	0.344	0.423	0.136

7.3.2.3 EFFECT OF PULSE ON DURATION VARIATION ON OC

The variation of OC for different combination of process parameters with respect to pulse on duration is shown in form of bar graph in Figure 7.23. The effect of pulse on duration variation on Overcut is shown in Figure 7.23 and it can be observed that graphite as electrode material exhibit's a higher value of OC as compared to Copper and Platinum. Further the range of variation in OC for platinum electrode was comparatively less.

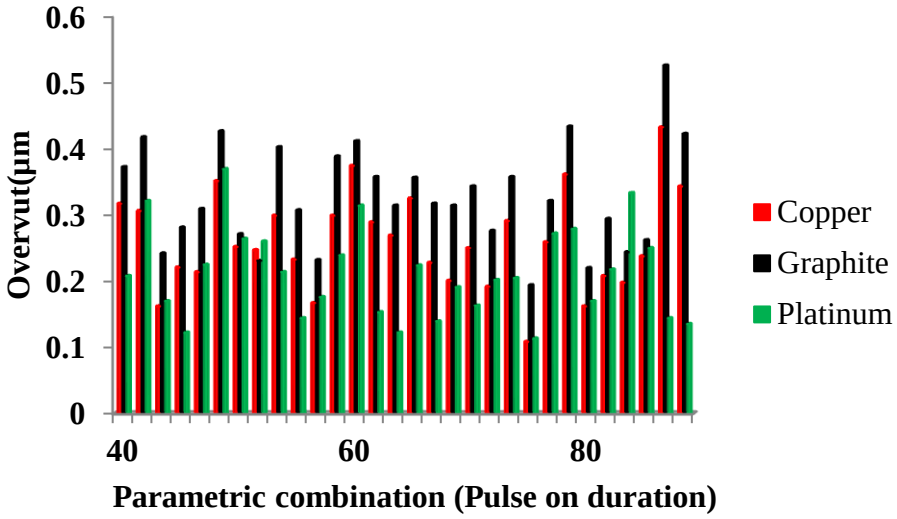

Figure 7.23: Variation of OC with respect to pulse on duration

Table 7. 23: OC for different electrodes with variation in Pulse on duration (T_{on})

S. No.	Parameters				Overcut(μm)		
	Pulse on duration (T_{on})	Peak current (I_p)	Voltage (V)	Pulse off duration (T_{off})	Copper	Graphite	Platinum
1	40	10	30	30	0.318	0.373	0.209
2	40	10	60	30	0.222	0.282	0.123
3	40	40	30	30	0.253	0.272	0.265
4	40	40	30	20	0.352	0.427	0.37
5	40	40	60	20	0.3	0.403	0.215
6	60	10	45	25	0.234	0.308	0.145
7	60	25	30	25	0.168	0.233	0.177
8	60	25	45	25	0.3	0.389	0.24
9	60	25	45	25	0.375	0.412	0.315
10	60	25	45	25	0.29	0.358	0.154
11	60	25	45	25	0.27	0.315	0.123
12	60	25	45	25	0.326	0.357	0.225
13	60	25	45	25	0.229	0.318	0.14
14	60	25	45	20	0.202	0.315	0.192
15	60	25	45	30	0.251	0.344	0.164
16	60	25	60	25	0.193	0.277	0.203
17	80	25	45	25	0.209	0.295	0.219
18	80	40	30	20	0.199	0.245	0.334
19	80	40	30	30	0.239	0.263	0.251
20	60	40	45	25	0.292	0.358	0.206
21	80	10	30	30	0.26	0.322	0.273
22	80	10	60	20	0.163	0.221	0.171
23	80	40	60	30	0.433	0.526	0.145
24	80	40	60	20	0.344	0.423	0.136
25	40	60	40	30	0.248	0.232	0.261
26	40	60	40	20	0.3	0.403	0.215
27	40	60	80	30	0.433	0.526	0.145
28	40	60	80	20	0.344	0.423	0.136
29	40	30	40	20	0.352	0.427	0.37
30	40	60	80	20	0.344	0.423	0.136

7.3.2.4 EFFECT OF PULSE OFF DURATION VARIATION ON OC

The variation of OC for different combination of process parameters with respect to pulse off duration is shown in form of bar graph in Figure 7.24 and is given in Table7.24. The effect of pulse off duration variation on Overcut is shown in Figure 7.24 and it can be observed that for initial pulse of duration setting value of 20 µs, platinum as electrode material exhibit's a lower value of OC as compared to Copper and Graphite. Further the range of variation in OC for platinum electrode was considerably steady as it was significantly irregular for copper and graphite for entire range of pulse off duration.

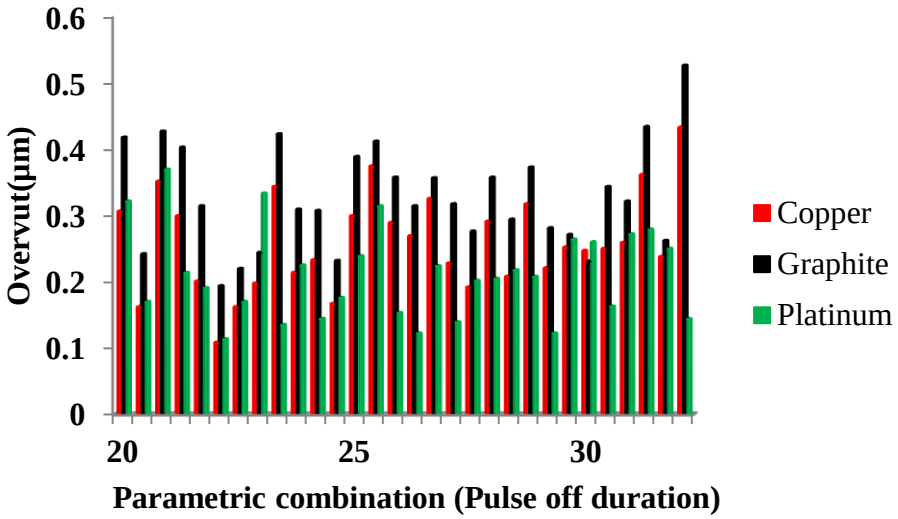

Figure 7.24: Variation of OC with respect to Pulse off duration

Table 7. 24: OC for different electrodes with variation in Pulse off duration (T_{off})

S. No.	Parameters				Overcut(μm)		
	Pulse off duration (T_{off})	Pulse on duration (T_{on})	Peak current (I_p)	Voltage (V)	Copper	Graphite	Platinum
1	20	60	25	45	0.202	0.315	0.192
2	20	80	40	60	0.344	0.423	0.136
3	20	80	10	60	0.163	0.221	0.171
4	20	80	40	30	0.199	0.245	0.334
5	20	40	40	60	0.3	0.403	0.215
6	20	40	40	30	0.352	0.427	0.37
7	25	60	10	45	0.234	0.308	0.145
8	25	60	25	30	0.168	0.233	0.177
9	25	60	25	45	0.3	0.389	0.24
10	25	60	25	45	0.375	0.412	0.315
11	25	60	25	45	0.29	0.358	0.154
12	25	60	25	45	0.27	0.315	0.123
13	25	60	25	45	0.326	0.357	0.225
14	25	60	25	45	0.229	0.318	0.14
15	25	60	25	60	0.193	0.277	0.203
16	25	80	25	45	0.209	0.295	0.219
17	25	60	40	45	0.292	0.358	0.206
18	30	60	25	45	0.251	0.344	0.164
19	30	80	40	30	0.239	0.263	0.251
20	30	80	10	30	0.26	0.322	0.273
21	30	80	40	60	0.433	0.526	0.145
22	30	40	10	30	0.318	0.373	0.209
23	30	40	10	60	0.222	0.282	0.123
24	30	40	40	30	0.253	0.272	0.265
25	40	60	40	30	0.248	0.232	0.261
26	40	60	40	20	0.3	0.403	0.215
27	40	60	80	30	0.433	0.526	0.145
28	40	60	80	20	0.344	0.423	0.136
29	40	30	40	20	0.352	0.427	0.37
30	40	60	80	20	0.344	0.423	0.136

7.3.3 PERFORMANCE OF DIFFERENT ELECTRODES MATERIALS ON RCL

The RCL using copper graphite and platinum as electrodes for different combination of process parameters is given in Table 7.25.

7.3.3.1 EFFECT OF VOLTAGE VARIATION ON RCL

The variation of RCL for different combination of process parameters with respect to voltage is shown in form of bar graph in Figure 7.25. The effect of voltage variation on RCL can be seen from Figures 7.25 and from here it can be inferred that for all level of voltage variation i.e., 30-60V platinum shows maximum RCL with a nonlinearly rising trend. Furthermore, copper marks least RCL among the electrode materials considered here. It can be further observed that there is drastic rise in RCL value at highest voltage setting of 60V for copper graphite and platinum respectively.

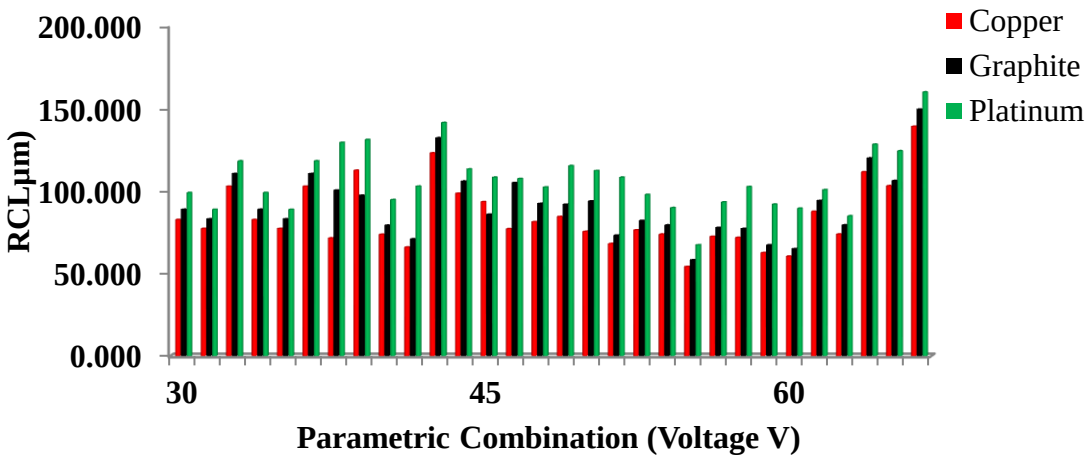

Figure 7.25: Variation of RCL with respect to Voltage

Table 7. 25: RCL for different electrodes with combination of process parameters

S. No.	Parameters				RCL (µm)		
	Voltage (V)	Peak current (I_p)	Pulse on duration (T_{on})	Pulse off duration (T_{off})	Copper	Graphite	Platinum
1	30	10	80	20	82.444	88.627	98.811
2	30	40	40	20	77.054	82.833	88.612
3	30	10	80	30	102.610	110.306	118.002
4	30	40	80	20	71.254	100.224	129.194
5	30	10	40	30	112.343	97.143	130.942
6	30	40	40	30	73.486	78.997	94.509
7	30	25	60	25	65.796	70.731	102.665
8	30	10	40	20	122.819	132.030	141.242
9	30	40	80	30	98.328	105.703	113.077
10	45	25	60	25	93.282	85.682	108.083
11	45	25	60	25	76.879	104.820	107.274
12	45	25	60	25	81.125	92.185	102.133
13	45	25	60	25	84.265	91.680	115.123
14	45	25	60	25	75.237	93.680	112.125
15	45	25	60	25	67.898	72.990	108.083
16	45	25	60	20	76.174	81.887	97.600
17	45	25	40	25	73.615	79.136	89.657
18	45	40	60	25	54.007	58.058	67.108
19	45	25	80	25	72.245	77.663	93.082
20	45	10	60	25	71.652	77.026	102.400
21	45	25	60	30	62.419	67.100	91.782

S. No.	Parameters				RCL (µm)		
	Voltage (V)	Peak current (I_p)	Pulse on duration (T_{on})	Pulse off duration (T_{off})	Copper	Graphite	Platinum
22	60	40	40	30	60.281	64.802	89.323
23	60	10	80	30	87.439	93.997	100.555
24	60	25	60	25	73.663	79.188	84.712
25	60	10	80	20	111.382	119.736	128.089
26	60	40	40	20	102.958	106.055	124.152
27	60	10	40	20	138.965	149.387	159.810
28	60	10	40	30	84.380	90.709	97.037
29	60	40	80	30	97.915	105.259	112.602
30	60	40	80	20	114.950	123.571	132.193

7.3.3.2 EFFECT OF CURRENT VARIATION ON RCL

The variation of RCL for different combination of process parameters with respect to current is shown in form of bar graph in Figure 7.26 and is given in Table7.26 . The effect of current variation on RCL is shown in Figure 7.26 and it can be observed that platinum as electrode material exhibit's a sudden rise and fall in RCL value for current setting of 10Amp, while attains a stagnant value for middle level setting of current i.e. 25Amp and beyond it shows a nonlinear rise and finally starts declining for higher level setting of current at 40Amp.It was also observed that graphite shows a nonlinear reducing trend for current variation range of 25 Amp to 40Amp. Copper as electrode material shows a rise for initial current setting of 10 Amp and starts falling down with further increase in current setting value to 25 Amp and finally starts rising for current level setting
of 40 Amp.

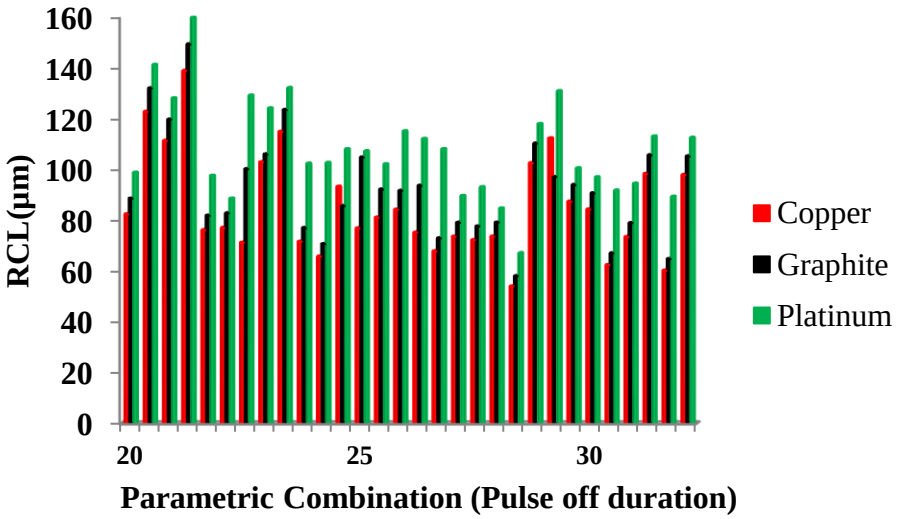

Figure 7.26: Variation of RCL with respect to current

Table 7. 26: RCL for different electrodes with variation in Peak current (I_p)

S. No.	Parameters				RCL (µm)		
	Peak current (I_p)	Voltage (V)	Pulse on duration (T_{on})	Pulse off duration (T_{off})	Copper	Graphite	Platinum
1	10	30	80	20	82.444	88.627	98.811
2	10	30	80	30	102.61	110.306	118.002
3	10	60	80	30	87.439	93.997	100.555
4	10	60	40	20	138.965	149.387	159.81
5	10	60	40	30	84.38	90.709	97.037
6	10	30	40	20	122.819	132.03	141.242
7	10	60	80	20	111.382	119.736	128.089
8	10	30	60	25	71.652	77.026	102.4
9	10	30	40	30	112.343	97.143	130.942
10	25	30	60	25	65.796	70.731	102.665
11	25	45	60	25	93.282	85.682	108.083
12	25	45	60	25	76.879	104.82	107.274
13	25	45	60	25	81.125	92.185	102.133
14	25	45	60	25	84.265	91.68	115.123
15	25	45	60	25	75.237	93.68	112.125
16	25	45	60	25	67.898	72.99	108.083
17	25	45	60	20	76.174	81.887	97.6
18	25	45	40	25	73.615	79.136	89.657
19	25	45	80	25	72.245	77.663	93.082
20	25	45	60	30	62.419	67.1	91.782
21	25	60	40	30	60.281	64.802	89.323
22	40	60	60	25	73.663	79.188	84.712
23	40	60	40	20	102.958	106.055	124.152
24	40	60	80	30	97.915	105.259	112.602
25	40	60	80	20	114.95	123.571	132.193
26	40	30	40	20	77.054	82.833	88.612
27	40	45	80	20	71.254	100.224	129.194
28	40	30	40	30	73.486	78.997	94.509
29	40	30	80	30	98.328	105.703	113.077
30	40	45	60	25	54.007	58.058	67.108

7.3.3.3 EFFECT OF PULSE ON DURATION VARIATION ON RCL

The variation of RCL for different combination of process parameters with respect to pulse on duration is shown in form of bar graph in Figure 7.27 and is given in Table7.27. Figure 7.27 depicts the effect of pulse on duration on RCL, and it can be observed that among different electrode materials, copper shows the lower values of RCL followed by graphite and platinum. However, all electrodes showed a nonlinear trend throughout the entire range of pulse on duration variation.

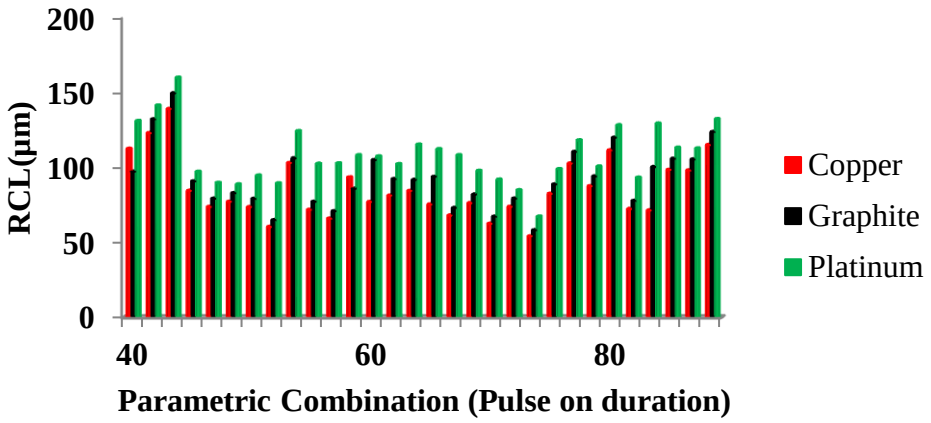

Figure 7.27: Variation of RCL with respect to pulse on duration

7.3.3.4 EFFECT OF PULSE OFF DURATION VARIATION ON RCL

The variation of RCL for different combination of process parameters with respect to pulse on duration is shown in form of bar graph in Figure 7.28 and is given in Table7.28.The effect of pulse off duration variation on RCL is shown in Figure 7.28 and it can be observed platinum as electrode material showed higher value of RCL as compared to copper and graphite for initial pulse off duration setting value of 20µs but as the pulse off duration increases to 25 µs a sudden fall in RCL value was also observed .However for pulse on duration setting value of 30µs copper as electrode material exhibited highest RCL value.

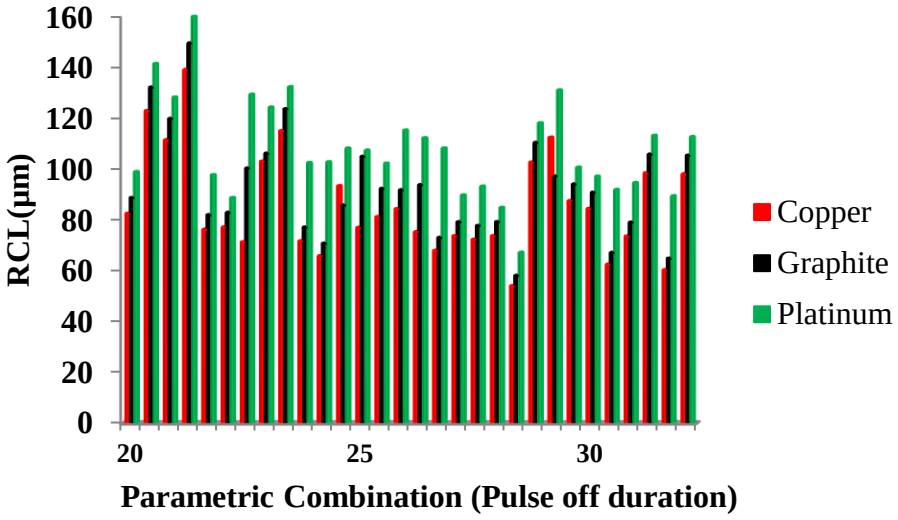

Figure 7.28: Variation of RCL with respect to pulse on duration

Table 7. 28: RCL for different electrodes with variation in Pulse on duration (T_{on})

S. No.	Parameters				RCL (µm)		
	Pulse off duration (T_{off})	Pulse on duration (T_{on})	Peak current (I_p)	Voltage (V)	Copper	Graphite	Platinum
1	20	30	10	80	82.444	88.627	98.811
2	20	30	10	40	122.819	132.03	141.242
3	20	60	10	40	138.965	149.387	159.81
4	20	60	40	40	102.958	106.055	124.152
5	20	60	10	80	111.382	119.736	128.089
6	20	60	40	80	114.95	123.571	132.193
7	20	45	40	80	71.254	100.224	129.194
8	20	30	40	40	77.054	82.833	88.612
9	25	30	10	60	71.652	77.026	102.4
10	25	30	25	60	65.796	70.731	102.665
11	25	45	25	60	93.282	85.682	108.083
12	25	45	25	60	76.879	104.82	107.274
13	25	45	25	60	81.125	92.185	102.133
14	25	45	25	60	84.265	91.68	115.123
15	25	45	25	60	75.237	93.68	112.125
16	25	45	25	60	67.898	72.99	108.083
17	25	45	25	40	73.615	79.136	89.657
18	25	45	25	80	72.245	77.663	93.082
19	25	45	40	60	54.007	58.058	67.108
20	25	45	40	60	54.007	58.058	67.108
21	25	60	25	60	73.663	79.188	84.712
22	30	30	40	40	73.486	78.997	94.509
23	30	30	40	80	98.328	105.703	113.077
24	30	30	40	80	98.328	105.703	113.077
25	30	60	40	80	97.915	105.259	112.602
26	30	60	10	80	87.439	93.997	100.555
27	30	60	10	40	84.38	90.709	97.037
28	30	45	25	60	62.419	67.1	91.782
29	30	30	10	80	102.61	110.306	118.002
30	30	30	10	40	112.343	97.143	130.942

7.3.4 PERFORMANCE OF DIFFERENT ELECTRODES MATERIALS ON TA

The taper angle (TA) in micro-holes fabricated using copper graphite and platinum as electrodes for different combination of process parameters is given in Table 7.29.

7.3.4.1 EFFECT OF VOLTAGE VARIATION ON TA

Taper angle was assessed for all the experimental runs. The typical variation of TA (of the eroded hole) influenced by parametric combinations of three levels of gap voltage (30, 45 and 60V) is shown in Figures 7.29. Referring to Figure 7.29 it can be observed that graphite indicates highest TA during the considered values of voltage variation. Additionally, it can be observed that platinum and copper showed marginal difference in TA.

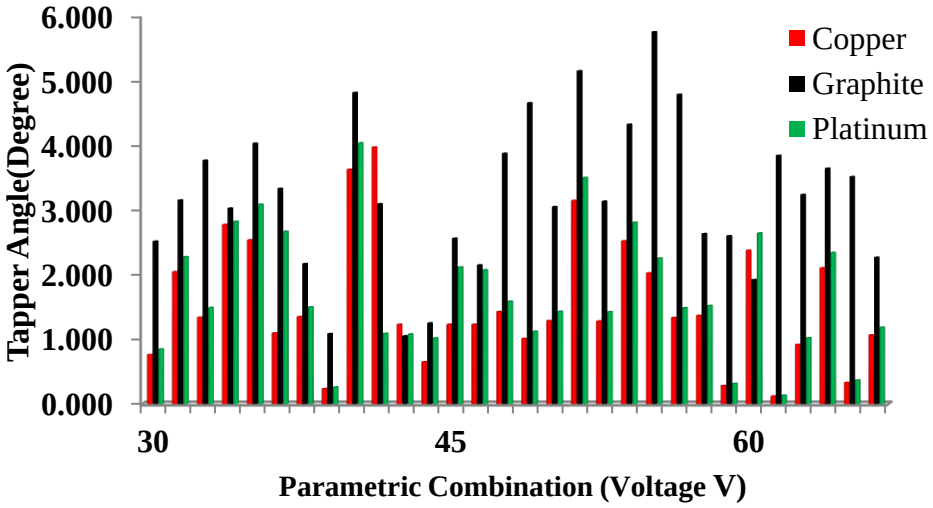

Figure 7. 29: Variation of TA with respect to Voltage

Table 7. 29: TA for different electrodes with combination of process parameters

S. No.	Parameters				TA(degree)		
	Voltage (V)	Peak current (I_p)	Pulse on duration (T_{on})	Pulse off duration (T_{off})	Copper	Graphite	Platinum
1	30	10	80	20	0.766	2.524	0.852
2	30	40	40	20	2.052	3.158	2.283
3	30	10	80	30	1.345	3.772	1.496
4	30	40	80	20	2.781	3.032	2.830
5	30	10	40	30	2.544	4.034	3.094
6	30	40	40	30	1.102	3.337	2.676
7	30	25	60	25	1.354	2.178	1.507
8	30	10	40	20	0.234	1.090	0.261
9	30	40	80	30	3.631	4.816	4.040
10	45	25	60	25	3.974	3.100	1.095
11	45	25	60	25	1.235	1.056	1.084
12	45	25	60	25	0.652	1.257	1.023
13	45	25	60	25	1.236	2.568	2.125
14	45	25	60	25	1.236	2.157	2.084
15	45	25	60	25	1.433	3.877	1.595
16	45	25	60	20	1.015	4.656	1.129
17	45	25	40	25	1.292	3.056	1.437
18	45	40	60	25	3.151	5.149	3.505
19	45	25	80	25	1.287	3.140	1.431
20	45	10	60	25	2.528	4.326	2.813
21	45	25	60	30	2.034	5.750	2.263
22	60	40	40	30	1.342	4.786	1.493
23	60	10	80	30	1.373	2.640	1.527
24	60	25	60	25	0.283	2.606	0.315
25	60	10	80	20	2.383	1.930	2.651
26	60	40	40	20	0.119	3.846	0.132
27	60	10	40	20	0.923	3.243	1.027
28	60	10	40	30	2.112	3.647	2.350
29	60	40	80	30	0.331	3.520	0.368
30	60	40	80	20	1.070	2.275	1.190

7.3.4.2 EFFECT OF CURRENT VARIATION ON TA

The variation of TA for different combination of process parameters with respect to current is shown in form of bar graph in Figure 7.30 and is given in Table7.30. Figure 7.30 shows the effect of current variation on taper angle it can be observed that graphite as electrode material shows highest taper angle variation for current settings of 10Amp,

25Amp and 40 Amp, Copper and platinum showed a nonlinear trend of taper angle variation throughout the current setting variation of 10Amp to 40 Amp.

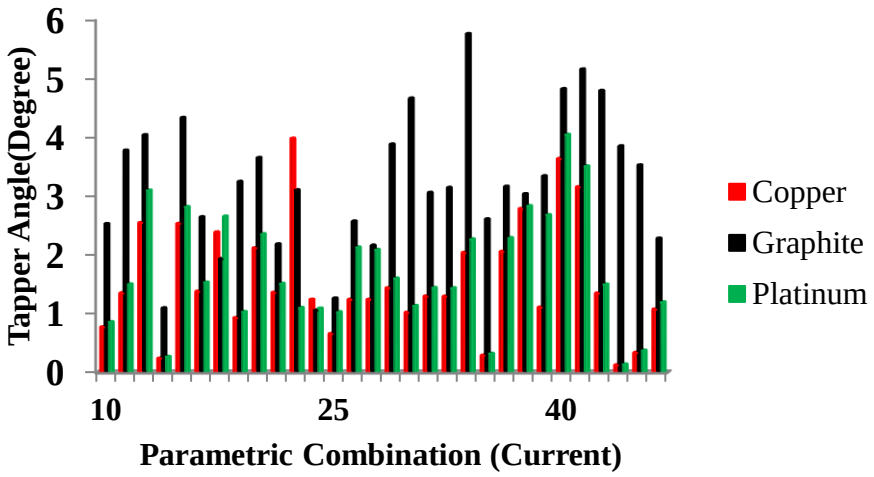

Figure 7. 30: Variation of TA with respect to current

Table 7. 30: TA for different electrodes with variation in Peak current (I_p)

S. No.	Parameters				TA(degree)		
	Peak current (I_p)	Voltage (V)	Pulse on duration (T_{on})	Pulse off duration (T_{off})	Copper	Graphite	Platinum
1	10	30	80	20	0.766	2.524	0.852
2	10	30	80	30	1.345	3.772	1.496
3	10	30	40	30	2.544	4.034	3.094
4	10	30	40	20	0.234	1.09	0.261
5	10	45	60	25	2.528	4.326	2.813
6	10	60	40	20	0.923	3.243	1.027
7	10	60	40	30	2.112	3.647	2.35
8	10	60	80	30	1.373	2.64	1.527
9	10	60	80	20	2.383	1.93	2.651
10	25	30	60	25	1.354	2.178	1.507
11	25	45	60	25	3.974	3.1	1.095
12	25	45	60	25	1.235	1.056	1.084
13	25	45	60	25	0.652	1.257	1.023
14	25	45	60	25	1.236	2.568	2.125
15	25	45	60	25	1.236	2.157	2.084
16	25	45	60	25	1.433	3.877	1.595
17	25	45	60	20	1.015	4.656	1.129
18	25	45	40	25	1.292	3.056	1.437
19	25	45	80	25	1.287	3.14	1.431
20	25	45	60	30	2.034	5.75	2.263
21	25	60	60	25	0.283	2.606	0.315
22	40	45	60	25	3.151	5.149	3.505
23	40	60	40	30	1.342	4.786	1.493
24	40	60	40	20	0.119	3.846	0.132
25	40	60	80	30	0.331	3.52	0.368
26	40	60	80	20	1.07	2.275	1.19
27	40	30	40	20	2.052	3.158	2.283
28	40	30	80	20	2.781	3.032	2.83
29	40	30	40	30	1.102	3.337	2.676
30	40	40	80	20	1.07	2.275	1.19

7.3.4.3 EFFECT OF PULSE ON DURATION VARIATION ON TA

The variation of TA for different combination of process parameters with respect to pulse on duration is shown in form of bar graph in Figure 7.31 and is given in Table7.31. Figure 7.31 shows the effect of Pulse on duration variation on taper angle it can be observed that platinum as electrode material showed a least taper angle for similar pulse on duration setting of 40 µs when compared with copper and graphite. As higher taper angle affects the quality of micro hole, platinum as electrode material exhibits lowest taper angle throughout the entire range of pulse on duration settings should be preferred.

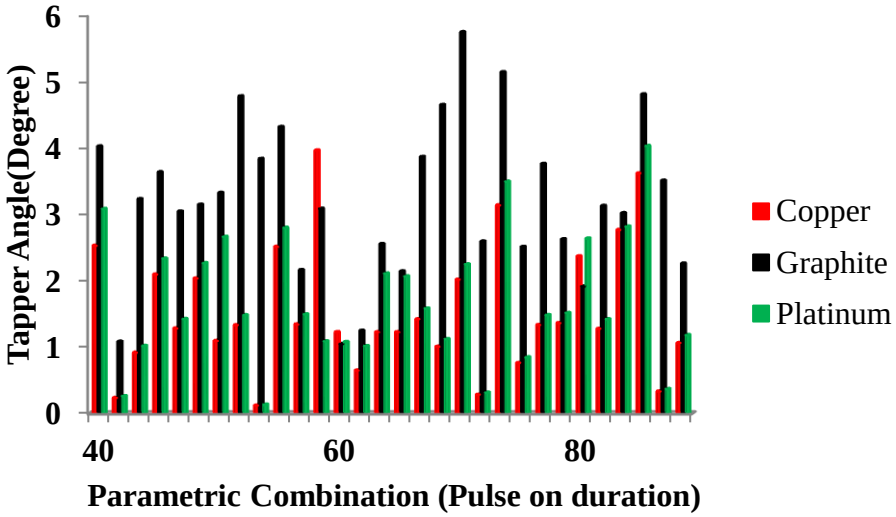

Figure 7. 31: Variation of TA with respect to pulse on duration

Table 7. 31: TA for different electrodes with variation in Pulse on duration (T_{on})

S. No.	Parameters				TA(degree)		
	Pulse on duration (T_{on})	Peak current (I_p)	Voltage (V)	Pulse off duration (Toff)	Copper	Graphite	Platinum
1	30	10	80	20	0.766	2.524	0.852
2	30	10	80	30	1.345	3.772	1.496
3	30	10	40	30	2.544	4.034	3.094
4	30	10	40	20	0.234	1.09	0.261
5	30	25	60	25	1.354	2.178	1.507
6	30	40	40	20	2.052	3.158	2.283
7	30	40	80	20	2.781	3.032	2.83
8	30	40	40	30	1.102	3.337	2.676
9	45	25	60	25	3.974	3.1	1.095
10	45	25	60	25	1.235	1.056	1.084
11	45	40	60	25	3.151	5.149	3.505
12	45	25	60	25	0.652	1.257	1.023
13	45	25	60	25	1.236	2.568	2.125
14	45	25	60	25	1.236	2.157	2.084
15	45	25	60	25	1.433	3.877	1.595
16	45	10	60	25	2.528	4.326	2.813
17	45	25	60	20	1.015	4.656	1.129
18	45	25	40	25	1.292	3.056	1.437
19	45	25	80	25	1.287	3.14	1.431
20	45	25	60	30	2.034	5.75	2.263
21	60	25	60	25	0.283	2.606	0.315
22	60	40	40	30	1.342	4.786	1.493
23	60	40	40	20	0.119	3.846	0.132
24	60	40	80	30	0.331	3.52	0.368
25	60	40	80	20	1.07	2.275	1.19
26	60	10	40	20	0.923	3.243	1.027
27	60	10	40	30	2.112	3.647	2.35
28	60	10	80	30	1.373	2.64	1.527
29	60	10	80	20	2.383	1.93	2.651
30	60	10	60	25	0.283	2.606	0.215

7.3.4.4 EFFECT OF PULSE OFF DURATION VARIATION ON TA

The variation of TA for different combination of process parameters with respect to pulse on duration is shown in form of bar graph in Figure 7.32 and is given in Table7.32. Figure 7.32 shows the effect of Pulse off variation on taper angle it can be observed that Copper as electrode material exhibited a lower values of taper angle when compared with graphite and platinum. It was also observed that platinum reaches to higher value of taper angle for pulse off duration setting at 30µs. Furthermore, graphite as electrode material showed highest taper angle during the pulse off duration range of 25-30 µs.

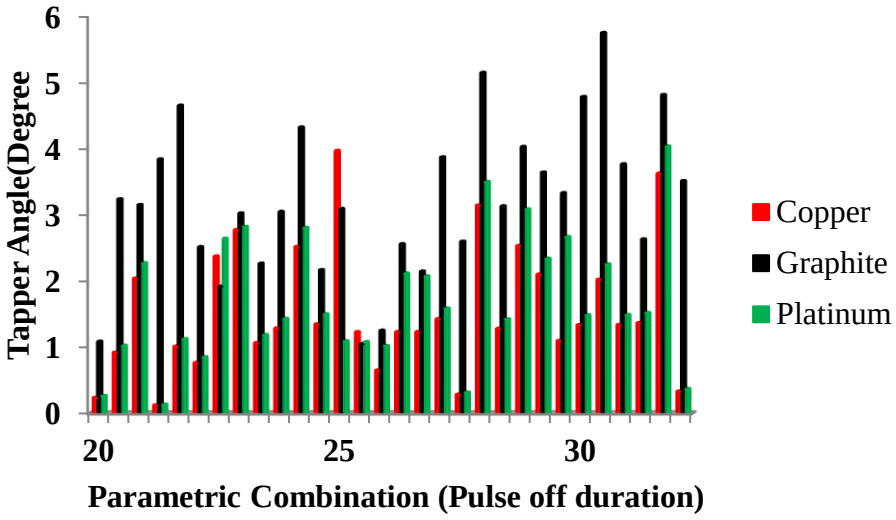

Figure 7. 32: Variation of TA with respect to pulse off duration

Table 7. 32: TA for different electrodes with variation in Pulse on duration (T_{on})

S. No.	Parameters				TA(degree)		
	Pulse off duration (Toff)		Peak current (I_p)	Voltage (V)	Copper	Graphite	Platinum
1	20	30	10	80	0.766	2.524	0.852
2	20	30	10	40	0.234	1.09	0.261
3	20	60	40	80	1.07	2.275	1.19
4	20	60	10	80	2.383	1.93	2.651
5	20	60	10	40	0.923	3.243	1.027
6	20	30	40	40	2.052	3.158	2.283
7	20	30	40	80	2.781	3.032	2.83
8	20	45	25	60	1.015	4.656	1.129
9	20	60	40	40	0.119	3.846	0.132
10	25	45	25	60	3.974	3.1	1.095
11	25	30	25	60	1.354	2.178	1.507
12	25	45	25	60	1.235	1.056	1.084
13	25	45	40	60	3.151	5.149	3.505
14	25	45	25	60	0.652	1.257	1.023
15	25	45	25	60	1.236	2.568	2.125
16	25	45	25	60	1.236	2.157	2.084
17	25	45	25	60	1.433	3.877	1.595
18	25	60	10	60	0.283	2.606	0.215
19	25	45	10	60	2.528	4.326	2.813
20	25	45	25	40	1.292	3.056	1.437
21	25	45	25	80	1.287	3.14	1.431
22	25	60	25	60	0.283	2.606	0.315
23	30	60	40	40	1.342	4.786	1.493
24	30	30	40	40	1.102	3.337	2.676
25	30	60	40	80	0.331	3.52	0.368
26	30	60	10	40	2.112	3.647	2.35
27	30	60	10	80	1.373	2.64	1.527
28	30	45	25	60	2.034	5.75	2.263
29	60	10	80	20	2.383	1.93	2.651
30	60	10	60	25	0.283	2.606	0.215

CONCLUSION

Based on the experimental results, an analysis was made to identify the performance of various electrodes during fabrication of micro holes considering Inconel 718 as well as titanium as workpiece materials. It was found that that platinum followed by graphite and copper as electrode material exhibited higher MRR for both the workpiece materials but on the other hand platinum showed higher values of OC,RCL and TA respectively when compared to graphite and copper.

CHAPTER 8

CONCLUSION

Modeling of micro-EDM operation has been carried out for fabrication of micro-holes in Inconel-718 and Titanium Grade-5 using copper, graphite and platinum as electrode material. Multi-objective optimization techniques such as ETLBO, MODE, MOABC have been used in order to determine optimum process parameters. Experimental investigations have been performed using Response Surface Methodology (RSM) based on central composite design. Predictions techniques like ANN and ANFIS have been used to determine different machinability criteria such as MRR, OC, RCL and TA of micro-hole. The voltage, peak current, pulse-on duration and pulse-off durations have been considered as process parameters. The different conclusions made from the above investigations are as follows:

1. Multi-objective optimization using MOETLBO, MODE and MOABC indicated that when comparisons are done on the basis of equal no function evaluations and same population size, none of the optimization technique yielded solutions satisfying various conflicting objectives. On the basis of priority for a certain response the process engineer can select the parameters from the pareto optimal solutions when the responses are conflicting in nature.
2. A feed forward back propagation of 4-12-4 structure of neural configuration gave reasonable prediction accuracy. The total average prediction error of -17.901% for copper, 4.908% for graphite and -7.492 % for platinum was obtained during fabrication of micro holes in Inconel 718 as workpiece.

3. During modeling of process responses by ANFIS, the 2-2-2-2 structure was found to be best topography due to its lowest prediction error and faster performance. According to

this structure for majority of cases the Generalized Bell Function type of membership function was selected for modeling of MRR, OC, RCL and TA because of its lower values of total average error rather than other types. The total average prediction error of -7.080% for copper, -6.629 % for graphite and -5.548 % for platinum was obtained during fabrication of micro holes in Inconel 718 as workpiece.

4. FEM modeling has been carried out to determine MRR using ANSYS software in Inconel-718 and Titanium grade 5 for different combination of process parameters.

5. FEM modeling for MRR has been validated with experiments. It was observed that the error in MRR was varying from 5% to 18.44% for Titanium Grade 5 and 6.38% to 20.33% for Inconel-718.

CONTRIBUTION TO RESEARCH

This research work offers new insights into the performance of micro-µ-EDM of Inconel 718 and Titanium5 using different electrodes. The optimum process parameters have been identified to determine multi-objective machinability criteria such as MRR, angle of taper of micro-hole, the thickness of recast-layer and overcut for fabrication of micro-holes. ANN and ANFIS modeling have been developed to determine multi-responses for different combination of process parameters with reasonable accuracy. Theoretical FEM modeling has been compared with experiments for fabrication of micro-holes.

SCOPE FOR FURTHER RESEARCH

During fabrication of micro holes using µ-EDM process, further research can be done using different materials such as composite and ceramic materials. Further, tool wear analysis can be adopted to evaluate the performance of the different electrode materials. An in-depth study can be done to understand the influence of properties of electrodes as they affect the output performance. Geometry prediction using simulation of µ-EDM process can be done considering more realistic process dynamics for the better understanding of the influence of machining parameters on the responses. Future study can concentrate on producing new composite electrodes with specific properties suitable to produce micro-holes.

APPENDIX 1

Table 4. 4 Truncated model for OC. (After elimination)

Source	Sum of Squares	DOF	Mean Square	F Value	p-value Prob > F	Percentage Contribution (%)
Model	0.020	12	1.674E-003	139.32	< 0.0001	95.238
A	2.222E-003	1	2.222E-003	52.20	< 0.0001	10.581
C	4.500E-004	1	4.500E-004	10.57	0.0047	2.143
D	4.500E-004	1	4.500E-004	10.57	0.0047	2.143
AB	2.500E-003	1	2.500E-003	58.72	< 0.0001	11.905
AC	9.000E-004	1	9.000E-004	21.14	0.0003	4.286
AD	4.225E-003	1	4.225E-003	99.24	< 0.0001	20.119
BC	6.250E-004	1	6.250E-004	14.68	0.0013	2.976
BD	4.900E-003	1	4.900E-003	115.10	< 0.0001	23.333
CD	4.000E-004	1	4.000E-004	9.40	0.0070	1.905
B^2	1.365E-003	1	1.365E-003	32.07	< 0.0001	6.500
C^2	4.848E-004	1	4.848E-004	11.39	0.0036	2.309
D^2	1.511E-003	1	1.511E-003	35.48	< 0.0001	7.195
Residual	7.237E-004	17	4.257E-005			
Lack of Fit	6.532E-004	12	5.443E-005	3.86	0.0731	Insignificant
Pure Error	7.053E-005	5	1.411E-005			
Corrected Total	0.021	29			R-Squared	0.9652
					Adjusted R-Squared	0.9407
					Predicted R-Squared	0.8619

APPENDIX 2

Table 4. 5 :Truncated model for RCL. (After elimination)

Source	Sum of Squares	DOF	Mean Square	F Value	p-value Prob > F	Percentage Contribution (%)
Model	5754.51	5	1150.90	11.53	< 0.0001	70.614
A-Voltage	3329.20	1	3329.20	33.36	< 0.0001	40.853
D-Pulse off duration	447.13	1	447.13	4.48	0.0448	5.487
CD	578.31	1	578.31	5.80	0.0241	7.096
A^2	662.33	1	662.33	6.64	0.0166	8.127
B^2	1396.57	1	1396.57	14.00	0.0010	17.137
Residual	2394.77	24	99.78			
Lack of Fit	2032.39	19	106.97	1.48	0.3543	Insignificant
Pure Error	362.39	5	72.48			
Corrected Total	8149.28	29			R-Squared	0.7061
					Adjusted R-Squared	0.6449
					Predicted R-Squared	0.5285

APPENDIX 3

Table 4. 6:Truncated model for TA. (After elimination)

Source	Sum of Squares	DOF	Mean Square	F Value	p-value Prob > F	Percentage Contribution
Model	20.35	13	1.57	2699.29	< 0.0001	99.951
A-Voltage	1.01	1	1.01	1747.09	< 0.0001	4.961
B-Peak current	4.75	1	4.75	8181.25	< 0.0001	23.330
C-Pulse on duration	2.55	1	2.55	4399.76	< 0.0001	12.525
D-Pulse off duration	2.89	1	2.89	4983.48	< 0.0001	14.194
AB	3.55	1	3.55	6120.04	< 0.0001	17.436
AD	0.51	1	0.51	879.24	< 0.0001	2.505
BC	2.62	1	2.62	4522.15	< 0.0001	12.868
BD	0.30	1	0.30	520.54	< 0.0001	1.473
CD	0.52	1	0.52	897.81	< 0.0001	2.554
A^2	0.049	1	0.049	85.06	< 0.0001	0.241
B^2	0.077	1	0.077	133.36	< 0.0001	0.378
C^2	0.32	1	0.32	546.75	< 0.0001	1.572
D^2	0.53	1	0.53	918.65	< 0.0001	2.603
Residual	9.281E-003	16	5.800E-004			
Lack of Fit	8.735E-004	11	7.940E-005	0.047	1.0000	Insignificant
Pure Error	8.407E-003	5	1.681E-003			
Corrected Total	20.36	29			R-Squared	0.9995
					Adjusted R-Squared	0.9992
					Predicted R^2	0.9993

APPENDIX 4

Table 4. 7:Data sets for neural network model

S. No	Parameters				(MRR) in mm^3/min	(OC) in µm	RCL) in µm	(TA)in degrees
	Voltage (V)	Peak current (I_p)	Pulse on duration (T_{on})	Pulse off duration (T_{off})				
1	30	8	20	30	0.766	0.168	92.370	2.777
2	30	8	40	60	0.556	0.238	113.079	1.960
3	30	8	20	60	0.784	0.202	105.555	1.853
4	30	8	40	30	0.538	0.236	79.032	2.153
5	30	20	30	45	0.748	0.192	118.483	1.890
6	30	32	20	30	0.588	0.188	89.041	3.831
7	30	32	20	60	0.427	0.165	87.999	3.037
8	30	32	40	60	0.593	0.193	116.060	2.449
9	30	32	40	30	0.458	0.168	87.249	2.917
10	35	8	30	45	0.614	0.205	112.308	1.174
11	35	20	30	45	0.651	0.212	104.57	1.525
12	35	20	30	30	0.682	0.183	102.237	2.369
13	35	20	30	45	0.766	0.127	105.472	1.525
14	35	20	30	45	0.627	0.130	102.943	1.565
15	35	20	30	45	0.659	0.124	104.857	1.525
16	35	20	30	45	0.682	0.197	95.173	1.453
17	35	20	30	45	0.748	0.220	103.514	1.565
18	35	20	40	45	0.673	0.193	106.391	0.788
19	35	20	20	45	0.659	0.161	103.891	1.541
20	35	20	30	60	0.689	0.146	106.408	1.567
21	35	32	30	45	0.725	0.134	102.560	2.201
22	40	8	20	30	0.715	0.220	57.926	1.897
23	40	8	20	60	0.627	0.222	64.348	1.467
24	40	8	40	30	0.623	0.185	68.854	2.584
25	40	8	40	60	0.518	0.195	73.287	2.775
26	40	20	30	45	0.627	0.217	87.390	1.415
27	40	32	40	60	0.601	0.222	83.250	2.775
28	40	32	40	30	0.816	0.240	78.322	2.184
29	40	32	20	60	0.582	0.187	64.077	1.987
30	40	32	20	30	0.725	0.222	68.791	1.490

APPENDIX 5

Table 4. 8:Validation of the Developed Model with Experimental Data.

Process Parameters				MRR (mm^3/min)		OC(μm)		RCL(μm)		TA(degrees)	
V	I_p	T_{on}	T_{off}	Exp	ANN	Exp	ANN	Exp	ANN	Exp	ANN
30	32	40	30	0.458	0.600	0.168	0.168	87.249	96.816	2.917	3.020
30	32	20	60	0.427	0.465	0.165	0.201	87.999	101.336	3.037	3.807
35	20	30	45	0.651	0.662	0.212	0.202	104.857	102.654	1.525	1.625
30	8	20	60	0.784	0.757	0.202	0.200	105.555	101.811	1.853	1.891
40	8	20	30	0.715	0.671	0.220	0.228	57.926	59.936	1.897	2.545
40	32	20	60	0.582	0.559	0.187	0.188	64.077	64.889	1.987	2.037
30	8	40	30	0.538	0.563	0.236	0.233	79.032	74.433	2.153	1.681
30	32	40	60	0.593	0.728	0.193	0.179	116.060	114.067	2.449	2.027
40	32	40	60	0.601	0.692	0.222	0.230	83.250	80.199	2.775	2.757
30	32	20	30	0.588	0.471	0.188	0.210	89.041	77.194	3.831	3.793

Table 4. 9:Errors in Prediction of Responses during validation

(V)	(I_p)	(T_{on})	(T_{off})	% Error in Prediction of MRR	% Error in Prediction of OC	% Error in Prediction of RCL	% Error in Prediction of TA
30	32	40	30	-31.110	0.119	-10.965	-3.523
30	32	20	60	-8.854	-21.673	-15.156	-25.367
35	20	30	45	-1.755	4.577	2.101	-6.573
30	8	20	60	3.495	0.924	3.547	-2.051
40	8	20	30	6.107	-3.826	-3.469	-34.150
40	32	20	60	3.922	-0.711	-1.267	-2.496
30	8	40	30	-4.703	1.219	5.819	21.910
30	32	40	60	-22.744	7.171	1.717	17.213
40	32	40	60	-15.121	-3.480	3.665	0.634
30	32	20	30	19.961	-11.844	13.305	0.995
Average (%) of error				-5.080	-2.752	-0.070	-3.341
Total average prediction error (%) = -11.2434							

APPENDIX 6

Table 4. 10: Testing of the Developed Model with Experimental Data.

Process Parameters				MRR (mm^3/min)		OC(μm)		RCL(μm)		TA (degrees)	
V	I_p	T_{on}	T_{off}	Exp	ANN	Exp	ANN	Exp	ANN	Exp	ANN
30	8	40	60	0.556	0.581	0.238	0.236	113.079	107.955	1.960	1.874
35	20	30	45	0.651	0.656	0.212	0.216	104.857	104.063	1.525	1.529
40	32	20	30	0.725	0.743	0.222	0.228	68.791	70.362	1.490	1.796
30	8	20	30	0.766	0.761	0.168	0.173	92.370	96.767	2.777	3.617
35	8	30	45	0.614	0.638	0.205	0.196	112.308	108.773	1.174	1.421
40	32	20	60	0.582	0.584	0.187	0.201	64.077	87.742	1.987	2.609
30	32	20	30	0.588	0.562	0.188	0.165	89.041	90.067	3.831	2.356
35	20	20	45	0.659	0.658	0.161	0.168	103.891	101.016	1.541	1.836

Table 4. 11: Errors in Prediction of Responses during testing

(V)	(I_p)	(T_{on})	(T_{off})	% Error in Prediction of MRR	% Error in Prediction of OC	% Error in Prediction of RCL	% Error in Prediction of TA
30	8	40	60	-4.561	0.801	4.531	4.365
35	20	30	45	-0.805	-2.084	0.758	-0.246
40	32	20	30	-2.469	-2.507	-2.283	-20.532
30	8	20	30	0.655	-3.123	-4.760	-30.258
35	8	30	45	-3.937	4.468	3.148	-21.063
40	32	20	60	-0.375	-7.533	-36.932	-31.325
30	32	20	30	4.371	12.162	-1.153	38.514
35	20	20	45	0.174	-4.210	2.768	-19.142
40	8	40	30	-2.077	-7.461	-0.398	-28.099
40	8	20	60	-1.492	-1.483	-2.350	-13.070
Average (%) of error				-1.052	-1.097	-3.667	-12.085
Total average prediction error (%) = -17.901							

APPENDIX 7

Table 4.13: Training data sets

S. No	Parameters				Material Removal Rate (MRR) in mm^3/min	Overcut (OC) in µm	Recast layer thickness (RCL) in µm	Taper Angle (TA) in degrees
	Voltage (V)	Peak current (I_p)	Pulse on duration (T_{on})	Pulse off duration (T_{off})				
1	35	20	30	45	0.682	0.197	95.173	1.453
2	35	20	30	45	0.627	0.13	102.943	1.565
3	30	20	30	45	0.748	0.192	118.483	1.89
4	40	32	40	30	0.816	0.24	78.322	2.184
5	30	8	20	30	0.766	0.168	92.37	2.777
6	35	20	40	45	0.673	0.193	106.391	0.788
7	35	8	30	45	0.614	0.205	112.308	1.174
8	40	20	30	45	0.627	0.217	87.39	1.415
9	40	8	20	60	0.627	0.222	64.348	1.467
10	40	32	20	30	0.725	0.222	68.791	1.49
11	35	20	30	45	0.659	0.124	104.857	1.525
12	35	20	30	45	0.766	0.127	105.472	1.525
13	35	20	20	45	0.659	0.161	103.891	1.541
14	35	20	30	45	0.748	0.22	103.514	1.565
15	35	20	30	60	0.689	0.146	106.408	1.567
16	30	8	40	60	0.556	0.238	113.079	1.96
17	35	32	30	45	0.725	0.134	102.56	2.201
18	35	20	30	30	0.682	0.183	102.237	2.369
19	40	8	40	30	0.623	0.185	68.854	2.584
20	40	8	40	60	0.518	0.195	73.287	2.775

APPENDIX 8

Table 4.16: Testing of the developed model with experimental data.

Process Parameters				MRR (mm^3/min)		OC(μm)		RCL(μm)		TA(degrees)	
V	I_p	T_{on}	T_{off}	Exp	ANFIS	Exp	ANFIS	Exp	ANFIS	Exp	ANFIS
30	32	40	30	0.556	0.556	0.238	0.238	113.079	113.079	1.960	1.960
30	32	20	60	0.651	0.691	0.212	0.166	104.857	103.150	1.525	1.552
35	20	30	45	0.725	0.725	0.222	0.222	68.791	68.92	1.490	1.490
30	8	20	60	0.766	0.766	0.168	0.168	92.370	92.371	2.777	2.777
40	8	20	30	0.614	0.615	0.205	0.205	112.308	112.302	1.174	1.139
40	32	20	60	0.582	0.481	0.187	0.224	64.077	112.422	1.987	1.281
30	8	40	30	0.588	0.517	0.188	0.176	89.041	122.367	3.831	4.928
30	32	40	60	0.659	0.657	0.161	0.157	103.891	102.151	1.541	1.602
40	32	40	60	0.623	0.623	0.185	0.185	68.854	68.854	2.584	2.584
30	32	20	30	0.627	0.627	0.222	0.222	64.348	64.348	1.467	1.467

Table 4.17: Errors in Prediction of Responses during testing

(V)	(I_p)	(T_{on})	(T_{off})	% Error in Prediction of MRR	% Error in Prediction of OC	% Error in Prediction of RCL	% Error in Prediction of TA
30	8	40	60	0.000	0.000	0.000	0.000
35	20	30	45	-6.175	21.698	1.628	-1.790
40	32	20	30	0.000	0.000	-0.001	0.000
30	8	20	30	0.000	0.000	-0.001	0.000
35	8	30	45	-0.081	0.098	0.005	2.964
40	32	20	60	17.320	-19.572	-75.448	35.526
30	32	20	30	12.041	6.489	-37.427	-28.630
35	20	20	45	0.258	2.547	1.675	-3.926
40	8	40	30	0.000	0.000	0.000	0.000
40	8	20	60	0.000	0.000	-0.001	0.007
Average (%) of error				2.336	1.126	-10.957	0.415
Total average prediction error (%) = -7.080							

APPENDIX 9

Table 4. 12:Pareto-optimal solutions obtained from ETLBO

V	I_p	T_{on}	T_{off}	MRR	OC	RCL	TA	Rank
30.033	27.413	39.992	59.995	0.369	0.098	112.665	1.56	1
30.857	8.027	39.995	59.601	0.366	0.132	108.182	0.964	2
30.037	32	20.561	59.995	0.357	0.072	102.94	3.039	3
30.111	31.973	20.026	59.605	0.356	0.072	102.379	3.02	4
32.945	8.001	39.992	59.979	0.354	0.127	103.192	1.082	5
30.907	31.9	20.149	59.877	0.362	0.073	100.624	2.888	6
30.933	31.915	20.149	59.846	0.362	0.073	100.559	2.886	7
30.006	8.001	39.989	33.237	0.346	0.046	99.263	1.247	8
30.06	8	20.063	59.933	0.359	0.134	99.255	0.543	9
30.006	8	39.997	30	0.343	0.028	97.926	1.477	10
30.006	8	20	57.706	0.357	0.133	98.833	0.504	11
32.945	31.993	20	59.999	0.376	0.075	95.569	2.613	12
33.017	31.968	20	59.998	0.377	0.075	95.379	2.601	13
30.88	8.001	39.997	30	0.327	0.032	95.879	1.443	14
32.945	8.001	39.989	33.237	0.297	0.057	92.128	1.188	15
32.914	8.02	20.532	59.979	0.378	0.134	92.595	0.711	16
32.945	8	39.992	30	0.29	0.041	90.79	1.396	17
35.173	31.993	20.026	59.999	0.392	0.077	89.698	2.355	18
35.647	31.999	20.146	59.789	0.394	0.079	88.41	2.305	19
39.997	31.999	39.992	59.979	0.311	0.081	86.493	0.779	20
32.945	8.004	20	30.016	0.315	0.075	85.307	1.698	21
39.998	27.714	39.997	59.995	0.312	0.082	85.608	0.857	22
39.951	32	39.992	57.785	0.301	0.089	85.728	0.685	23
37.276	31.993	20.001	59.999	0.407	0.079	83.749	2.16	24
37.415	31.963	20.039	59.849	0.407	0.08	83.325	2.144	25
39.997	8	39.992	57.753	0.303	0.106	82.229	1.639	26
37.276	8	39.997	30.003	0.213	0.059	78.972	1.448	27
39.951	31.993	20	59.999	0.425	0.08	75.67	1.983	28
39.998	27.714	20.021	59.995	0.426	0.085	74.645	1.77	29
39.997	27.431	39.998	30.003	0.163	0.118	73.149	1.117	30
39.997	8	20	59.995	0.428	0.126	72.184	1.361	31
39.935	8.001	20.052	33.237	0.294	0.125	66.218	1.658	32
39.937	8.004	20	30.016	0.278	0.118	65.452	1.887	33
40	8.004	20.546	30.016	0.275	0.118	65.406	1.92	34
40	8.004	20	30	0.278	0.119	65.253	1.892	35

APPENDIX 10

Table 4. 13: Pareto-optimal solutions obtained from MODE

V	I_p	T_{on}	T_{off}	MRR	OC	RCL	TA	Rank
39.782	8.106	20.186	59.702	0.608	0.191	103.850	1.415	1
39.961	8.419	20.124	59.202	0.605	0.191	103.555	1.340	2
39.900	9.251	24.032	55.867	0.591	0.196	100.307	2.418	3
39.975	10.061	21.431	57.628	0.594	0.193	101.129	1.553	4
39.951	9.928	32.926	59.429	0.621	0.202	96.390	3.675	5
36.794	11.708	20.869	54.452	0.634	0.197	97.788	1.112	6
31.102	9.884	24.050	49.336	0.671	0.206	94.793	1.966	7
39.938	15.872	20.400	41.653	0.575	0.197	93.633	0.537	8
34.553	9.085	39.991	56.816	0.720	0.215	91.101	2.301	9
34.553	9.085	39.991	55.816	0.719	0.215	91.091	2.255	10
39.919	17.529	20.419	42.442	0.571	0.197	92.221	0.459	11
39.954	18.813	21.284	47.254	0.566	0.197	91.581	0.746	12
39.763	19.892	20.117	41.228	0.569	0.198	89.921	0.320	13
35.424	18.812	37.829	54.555	0.673	0.214	86.851	2.444	14
32.679	14.795	39.985	52.419	0.708	0.219	87.250	1.588	15
39.613	23.290	22.284	46.890	0.558	0.200	87.362	1.199	16
38.161	26.386	24.918	55.622	0.574	0.202	85.170	2.585	17
32.841	20.702	22.869	43.989	0.647	0.207	86.143	1.593	18
34.627	22.656	22.051	47.904	0.631	0.204	85.810	1.448	19
32.198	23.591	21.499	43.301	0.659	0.207	83.362	1.524	20
37.154	28.654	22.350	52.073	0.590	0.203	82.390	2.188	21
39.776	29.761	21.983	44.646	0.543	0.202	81.566	1.765	22
32.567	29.081	39.242	50.972	0.685	0.222	79.682	3.259	23
39.481	30.792	21.618	44.911	0.548	0.202	80.535	1.871	24
32.930	29.093	23.173	49.090	0.640	0.208	79.650	2.798	25
39.992	31.922	21.963	43.494	0.535	0.203	79.661	2.081	26
30.160	31.962	39.984	33.246	0.684	0.230	78.871	2.916	27
30.599	31.485	38.104	54.744	0.682	0.223	77.453	4.277	28
31.854	30.099	23.018	50.227	0.652	0.209	78.468	3.079	29
30.692	31.176	38.088	49.948	0.678	0.224	77.673	3.917	30
30.599	31.985	38.104	54.744	0.682	0.223	77.171	4.417	31
33.405	31.639	23.351	51.328	0.633	0.209	78.041	3.412	32
30.182	31.702	38.020	51.017	0.680	0.224	77.126	4.130	33
30.248	31.986	22.595	52.787	0.672	0.210	76.528	3.611	34
30.080	31.990	21.153	35.705	0.677	0.213	74.371	3.146	35

APPENDIX 11

Table 4. 14:Pareto-optimal solutions obtained from MOABC

V	I_p	T_{on}	T_{off}	MRR	OC	RCL	TA	Rank
39.997	8.039	25.051	49.049	0.725	0.155	145.392	0.443	1
39.870	8.515	25.874	46.958	0.721	0.156	144.378	0.768	2
39.735	8.460	25.213	47.439	0.720	0.156	142.867	0.725	3
39.714	9.240	26.693	45.993	0.718	0.157	141.630	1.226	4
39.501	9.602	28.301	43.916	0.707	0.158	138.569	1.556	5
39.555	9.765	29.753	39.216	0.695	0.160	134.100	2.162	6
39.040	11.173	30.848	44.350	0.696	0.160	129.996	2.317	7
38.757	10.158	31.639	40.082	0.674	0.159	126.120	2.274	8
38.975	14.622	24.688	46.537	0.715	0.160	122.851	3.414	9
37.470	12.003	25.699	50.661	0.684	0.156	117.405	2.621	10
36.582	8.514	31.709	48.346	0.649	0.158	119.057	0.882	11
37.700	14.812	29.590	47.933	0.685	0.160	116.052	3.520	12
36.800	12.217	27.522	50.276	0.674	0.157	114.758	2.726	13
38.636	16.646	24.494	38.884	0.715	0.164	112.937	4.410	14
37.854	19.281	24.027	41.464	0.697	0.164	106.054	4.327	15
35.398	8.494	34.735	49.419	0.633	0.161	108.496	0.927	16
39.325	20.403	24.600	56.097	0.672	0.157	104.344	4.703	17
36.467	29.595	28.624	42.359	0.594	0.167	94.695	1.484	18
35.553	31.636	26.771	45.394	0.558	0.164	93.285	0.215	19
35.514	32.000	26.253	45.299	0.554	0.164	92.618	0.028	20
35.134	19.129	36.328	55.609	0.656	0.160	87.292	4.821	21
30.025	8.335	38.913	52.332	0.637	0.185	89.894	1.105	22
35.129	22.212	28.249	32.222	0.659	0.167	83.217	5.592	23
36.078	31.161	35.647	42.751	0.563	0.165	87.949	0.593	24
35.156	19.960	36.549	35.753	0.625	0.163	81.650	5.206	25
34.379	15.761	36.694	34.032	0.609	0.162	79.722	5.317	26
34.026	16.666	34.983	31.766	0.614	0.162	77.454	5.960	27
34.892	17.229	37.578	33.491	0.609	0.162	75.559	5.612	28
35.707	31.838	22.914	56.061	0.494	0.153	77.301	1.040	29
36.282	19.200	36.810	30.914	0.615	0.163	72.259	6.230	30
35.673	31.938	22.320	59.986	0.463	0.148	67.174	1.784	31
34.939	31.720	22.181	59.997	0.468	0.147	66.983	1.945	32
34.445	17.280	39.495	30.664	0.586	0.161	61.277	6.317	33
34.255	18.940	39.722	30.079	0.587	0.161	57.713	6.532	34
34.692	20.225	39.960	30.078	0.588	0.161	56.391	6.461	35

APPENDIX 12

Table 4. 15:Design matrix and experimental results

S. No	Parameters				Material Removal Rate (MRR) in mm^3/min	Overcut (OC) in µm	Recast layer thickness (RCL) in µm	Taper Angle (TA) in degrees
	Voltage (V)	Peak current (I_p)	Pulse on duration (T_{on})	Pulse off duration (T_{off})				
1	30	8	20	30	0.807	0.129	90.825	1.659
2	30	8	40	60	0.683	0.201	87.249	1.479
3	30	8	20	60	0.805	0.157	100.891	0.802
4	30	8	40	30	0.636	0.136	87.548	1.105
5	30	20	30	45	0.753	0.131	97.999	1.185
6	30	32	20	30	0.684	0.121	68.627	1.776
7	30	32	20	60	0.538	0.129	74.391	1.541
8	30	32	40	60	0.714	0.121	68.408	1.844
9	30	32	40	30	0.588	0.144	77.429	1.763
10	35	8	30	45	0.693	0.244	82.143	2.081
11	35	20	30	45	0.750	0.240	90.882	1.610
12	35	20	30	30	0.796	0.222	79.441	2.828
13	35	20	30	45	0.818	0.220	95.326	2.610
14	35	20	30	45	0.728	0.210	84.857	2.653
15	35	20	30	45	0.669	0.183	89.191	2.326
16	35	20	30	45	0.773	0.245	87.741	2.256
17	35	20	30	45	0.799	0.270	94.341	2.256
18	35	20	40	45	0.721	0.240	79.665	1.060
19	35	20	20	45	0.673	0.218	86.158	1.112
20	35	20	30	60	0.832	0.182	82.365	3.481
21	35	32	30	45	0.799	0.207	88.810	2.363
22	40	8	20	30	0.743	0.185	97.222	1.731
23	40	8	20	60	0.665	0.205	98.833	1.350
24	40	8	40	30	0.654	0.165	90.141	2.109
25	40	8	40	60	0.538	0.163	88.070	1.260
26	40	20	30	45	0.679	0.213	93.155	1.171
27	40	32	40	60	0.622	0.205	98.843	1.750
28	40	32	40	30	0.845	0.205	82.204	1.185
29	40	32	20	60	0.598	0.157	78.177	1.796
30	40	32	20	30	0.824	0.200	76.422	1.266

APPENDIX 13

Table 4. 16: Truncated model for MRR

Source	Sum of Squares	DOF	Mean Square	F Value	p-value Prob > F	Percentage contribution
Model	0.097	10	9.719E-003	43.73	< 0.0001	97
A-Voltage	0.030	1	0.030	133.56	< 0.0001	30
B-Peak current	5.724E-003	1	5.724E-003	25.75	< 0.0001	5.724
C-Pulse on duration	0.010	1	0.010	46.86	< 0.0001	10
AB	1.640E-003	1	1.640E-003	7.38	0.0137	1.64
AC	9.025E-003	1	9.025E-003	40.60	< 0.0001	9.025
CD	1.681E-003	1	1.681E-003	7.56	0.0127	1.681
A^2	4.016E-003	1	4.016E-003	18.07	0.0004	4.016
B^2	1.539E-003	1	1.539E-003	6.92	0.0165	1.539
C^2	9.985E-004	1	9.985E-004	4.49	0.0474	0.9985
D^2	0.025	1	0.025	111.11	< 0.0001	25
Residual	4.223E-003	19	2.223E-004			
Lack of Fit	4.222E-003	14	3.016E-004	1139.92	< 0.0001	Significant
Pure Error	1.323E-006	5	2.645E-007			
Corrected Total	0.10	29			R-Squared	0.9584
					Adj R-Squared	0.9364
					PredR-Squared	0.8766

APPENDIX 14

Table 4. 17: Truncated model for OC

Source	Sum of Squares	DOF	Mean Square	F Value	p-value Prob > F	Percentage Contribution
Model	8.560E-003	4	2.140E-003	7.33	0.0005	53.5
C-Pulse on duration	1.366E-003	1	1.366E-003	4.68	0.0403	8.5375
A^2	2.603E-003	1	2.603E-003	8.92	0.0062	16.26875
B^2	1.541E-003	1	1.541E-003	5.28	0.0302	9.63125
D^2	3.376E-003	1	3.376E-003	11.57	0.0023	21.1
Residual	7.294E-003	25	2.918E-004			
Lack of Fit	5.242E-003	20	2.621E-004	0.64	0.7851	Insignificant
Pure Error	2.053E-003	5	4.105E-004			
Corrected Total	0.016	29			R-Squared	0.8399
					Adj R-Squared	0.7663
					PredR-Squared	0.7508

Table 4. 22: Truncated model for RCL

Source	Sum of Squares	DOF	Mean Square	F Value	p-value Prob > F	Percentage contribution
Model	2411.08	5	482.22	29.26	< 0.0001	85.908
A-Voltage	92.02	1	92.02	5.58	0.0266	3.279
B-Peak current	1332.69	1	1332.69	80.87	< 0.0001	47.484
BC	126.72	1	126.72	7.69	0.0106	4.515
CD	149.75	1	149.75	9.09	0.0060	5.336
D^2	709.89	1	709.89	43.08	< 0.0001	25.294
Residual	395.51	24	16.48			
Lack of Fit	352.62	19	18.56	2.16	0.2005	Insignificant
Pure Error	42.88	5	8.58			
Corrected Total	2806.58	29			R-Squared	0.8591
					Adj R-Squared	0.8297
					Pred R-Squared	0.7783

APPENDIX 15

Table 4. 18: Truncated model for TA

Source	Sum of Squares	DOF	Mean Square	F Value	p-value Prob > F	Percentage contribution
Model	30.80	13	2.37	4598.32	< 0.0001	99.968
B-Peak current	5.47	1	5.47	10609.61	0.0001	17.754
C-Pulse on duration	4.05	1	4.05	7853.60	< 0.0001	13.145
D-Pulse off duration	1.92	1	1.92	3718.00	< 0.0001	6.232
AB	2.50	1	2.50	4855.18	< 0.0001	8.114
AC	0.87	1	0.87	1685.87	< 0.0001	2.824
AD	0.23	1	0.23	441.08	< 0.0001	0.747
BC	0.29	1	0.29	569.12	< 0.0001	0.941
BD	1.02	1	1.02	1985.31	< 0.0001	3.311
CD	2.35	1	2.35	4557.41	< 0.0001	7.627
A^2	5.26	1	5.26	10199.57	< 0.0001	17.072
B^2	6.15	1	6.15	11942.33	< 0.0001	19.961
C^2	2.68	1	2.68	5194.41	< 0.0001	8.698
D^2	0.79	1	0.79	1532.48	< 0.0001	2.564
Residual	8.244E-003	16	5.153E-004			
Lack of Fit	5.728E-003	11	5.207E-004	1.03	0.5214	Insignificant
Pure Error	2.516E-003	5	5.032E-004			
Corrected Total	30.81	29			R^2	0.9997
					$AdjR^2$	0.9995
					$PredR^2$	0.9993

APPENDIX 16

Table 4.24: Training data sets

S. No	Parameters				(MRR) in mm^3/min	(OC) in µm	RCL) in µm	(TA)in degrees
	Voltage (V)	Peak current (I_p)	Pulse on duration (T_{on})	Pulse off duration (T_{off})				
1	30	32	20	60	0.538	0.129	74.391	1.541
2	40	8	40	60	0.538	0.163	88.07	1.26
3	30	32	40	30	0.588	0.144	77.429	1.763
4	40	32	20	60	0.598	0.157	78.177	1.796
5	40	32	40	60	0.622	0.205	98.843	1.75
6	30	8	40	30	0.636	0.136	87.548	1.105
7	40	8	40	30	0.654	0.165	90.141	2.109
8	40	8	20	60	0.665	0.205	98.833	1.35
9	35	20	30	45	0.669	0.183	89.191	2.326
10	35	20	20	45	0.673	0.218	86.158	1.112
11	40	20	30	45	0.679	0.213	93.155	1.171
12	30	8	40	60	0.683	0.201	87.249	1.479
13	30	32	20	30	0.684	0.121	68.627	1.776
14	35	8	30	45	0.693	0.244	82.143	2.081
15	30	32	40	60	0.714	0.121	68.408	1.844
16	35	20	40	45	0.721	0.24	79.665	1.06
17	35	20	30	45	0.728	0.21	84.857	2.653
18	40	8	20	30	0.743	0.185	97.222	1.731
19	35	20	30	45	0.75	0.24	90.882	1.61
20	30	20	30	45	0.753	0.131	97.999	1.185

APPENDIX 17

Table 4.25: Validation of the Developed Model with Experimental Data.

Process Parameters				MRR (mm^3/min)		OC(μm)		RCL(μm)		TA(degrees)	
V	I_p	T_{on}	T_{off}	Exp	ANN	Exp	ANN	Exp	ANN	Exp	ANN
35	20	30	45	0.773	0.774	0.245	0.245	87.741	89.531	2.256	1.523
35	20	30	30	0.796	0.783	0.222	0.161	79.441	78.906	2.828	0.873
35	20	30	45	0.799	0.779	0.270	0.264	94.341	97.428	2.256	2.695
35	32	30	45	0.799	0.790	0.207	0.182	88.810	91.373	2.363	1.279
30	8	20	60	0.805	0.820	0.157	0.144	100.891	98.171	0.802	2.532
30	8	20	30	0.807	0.793	0.129	0.130	90.825	91.251	1.659	2.584
35	20	30	45	0.818	0.815	0.220	0.234	95.326	97.557	2.610	3.008
40	32	20	30	0.824	0.809	0.200	0.146	76.422	79.890	1.266	2.034
35	20	30	60	0.832	0.837	0.182	0.149	82.365	78.176	3.481	1.061
40	32	40	30	0.845	0.811	0.205	0.195	82.204	78.448	1.185	2.146

Table 4.26: Errors in Prediction of Responses

(V)	(I_p)	(T_{on})	(T_{off})	% Error in Prediction of MRR	% Error in Prediction of OC	% Error in Prediction of RCL	% Error in Prediction of TA
35	20	30	45	-0.140	0.032	-2.041	32.506
35	20	30	30	1.690	27.549	0.673	69.124
35	20	30	45	2.488	2.288	-3.272	-19.458
35	32	30	45	1.115	12.222	-2.886	45.872
30	8	20	60	-1.900	8.447	2.696	-215.731
30	8	20	30	1.709	-1.144	-0.469	-55.756
35	20	30	45	0.313	-6.313	-2.340	-15.244
40	32	20	30	1.766	26.820	-4.538	-60.649
35	20	30	60	-0.544	18.170	5.086	69.528
40	32	40	30	4.071	4.959	4.569	-81.092
Average (%) of error				1.057	9.303	-0.252	-23.090
Total average prediction error (%) = -12.983							

APPENDIX 18

Table 4.27: Testing of the Developed Model with Experimental Data.

Process Parameters				MRR (mm^3/min)		OC(µm)		RCL(µm)		TA(degrees)	
V	I_p	T_{on}	T_{off}	Exp	ANN	Exp	ANN	Exp	ANN	Exp	ANN
35	20	20	45	0.673	0.677	0.218	0.137	86.158	91.056	1.112	1.101
40	20	30	45	0.679	0.676	0.213	0.168	93.155	94.244	1.171	1.373
30	8	40	60	0.683	0.690	0.201	0.138	87.249	77.762	1.479	1.592
30	32	20	30	0.684	0.674	0.121	0.135	68.627	68.809	1.776	1.528
35	8	30	45	0.693	0.679	0.244	0.131	82.143	74.753	2.081	1.848
30	32	40	60	0.714	0.714	0.121	0.175	68.408	69.559	1.844	1.982
35	20	40	45	0.721	0.716	0.240	0.224	79.665	83.994	1.060	1.095
35	20	30	45	0.728	0.731	0.210	0.213	84.857	85.172	2.653	2.587
40	8	20	30	0.743	0.746	0.185	0.239	97.222	96.165	1.731	1.778
35	20	30	45	0.750	0.748	0.240	0.241	90.882	91.360	1.610	1.668

Table 4.28: Errors in Prediction of Responses during Testing

(V)	(I_p)	(T_{on})	(T_{off})	% Error in Prediction of MRR	% Error in Prediction of OC	% Error in Prediction of RCL	% Error in Prediction of TA
35	20	20	45	-0.665	37.134	-5.684	1.021
40	20	30	45	0.371	21.034	-1.169	-17.214
30	8	40	60	-1.023	31.211	10.874	-7.643
30	32	20	30	1.417	-11.758	-0.266	13.953
35	8	30	45	2.002	46.197	8.996	11.173
30	32	40	60	0.005	-44.874	-1.682	-7.479
35	20	40	45	0.733	6.509	-5.434	-3.335
35	20	30	45	-0.458	-1.284	-0.371	2.501
40	8	20	30	-0.447	-29.224	1.087	-2.712
35	20	30	45	0.217	-0.503	-0.526	-3.606
Average (%) of error				0.215	5.444	0.582	-1.334
Total average prediction error (%) = 4.908							

APPENDIX 19

Table 4.33: Pareto-optimal solutions obtained from MOETLBO

V	I_p	T_{on}	T_{off}	MRR	OC	RCL	TA	Rank
39.993	8.059	20.012	59.948	0.606	0.191	104.137	1.364	1
39.995	8.049	20.016	59.748	0.605	0.193	103.137	1.354	2
39.976	10.494	20.102	59.084	0.598	0.191	101.668	1.036	3
39.986	12.792	20.029	57.599	0.591	0.192	99.266	0.738	4
39.993	12.950	20.019	54.785	0.589	0.193	98.496	0.685	5
39.306	13.137	20.864	54.630	0.596	0.194	97.692	0.983	6
39.992	18.220	20.044	49.740	0.573	0.195	92.741	0.348	7
39.168	20.413	20.126	55.950	0.584	0.195	91.601	0.541	8
39.998	19.991	20.007	39.597	0.565	0.198	89.780	0.258	9
39.995	23.121	20.195	53.771	0.563	0.196	89.054	0.593	10
39.814	27.172	23.413	55.268	0.549	0.199	85.352	2.152	11
39.594	24.720	21.150	41.906	0.557	0.200	85.570	0.870	12
30.220	20.750	20.128	44.673	0.692	0.207	85.243	0.967	13
39.997	29.993	20.457	59.207	0.551	0.197	84.066	1.722	14
39.976	29.330	24.923	45.866	0.537	0.204	82.337	2.509	15
39.871	29.371	21.963	39.813	0.540	0.203	81.490	1.581	16
36.909	31.169	25.330	46.228	0.580	0.208	79.523	3.274	17
39.997	31.968	25.503	38.815	0.528	0.207	79.861	2.866	18
39.290	31.259	22.660	45.194	0.548	0.203	80.176	2.312	19
36.490	31.480	25.242	46.048	0.586	0.209	79.059	3.360	20
39.971	30.982	21.553	44.250	0.539	0.202	80.506	1.798	21
35.503	28.042	20.400	39.484	0.620	0.205	80.488	1.466	22
39.530	31.451	22.006	41.697	0.544	0.204	79.692	2.028	23
33.484	31.870	26.741	43.587	0.618	0.213	77.382	3.938	24
35.758	31.651	24.087	41.277	0.596	0.209	78.084	3.111	25
34.713	31.834	25.351	41.124	0.605	0.212	77.644	3.525	26
30.897	31.960	29.771	36.428	0.634	0.220	76.588	4.280	27
31.826	31.885	27.857	39.427	0.630	0.217	76.659	4.130	28
32.906	31.867	26.236	39.596	0.623	0.214	76.886	3.838	29
34.141	30.894	22.933	40.539	0.621	0.210	77.771	2.862	30
30.323	31.868	27.321	41.111	0.643	0.217	75.935	4.231	31
30.570	31.994	27.199	35.959	0.639	0.218	75.887	4.162	32
30.304	29.079	21.911	35.423	0.669	0.213	77.154	2.674	33
30.005	31.998	20.217	35.326	0.686	0.213	74.105	2.905	34
30.005	31.998	20.092	35.326	0.688	0.212	74.078	2.869	35

APPENDIX 20

Table 4.34: Pareto-optimal solutions obtained from MODE

V	I_p	T_{on}	T_{off}	MRR	OC	RCL	TA	Rank
39.995	13.530	20.459	53.971	0.542	0.204	96.463	1.463	1
39.998	13.569	20.425	53.986	0.543	0.204	96.442	1.448	2
39.917	15.751	20.799	54.514	0.536	0.204	94.324	1.473	3
39.297	16.683	20.205	50.045	0.545	0.206	92.590	1.156	4
39.048	17.002	20.494	48.660	0.546	0.207	91.899	1.237	5
39.709	19.902	20.609	52.741	0.530	0.206	90.080	1.340	6
39.694	19.514	20.337	46.779	0.530	0.207	89.602	1.096	7
39.872	20.238	23.996	41.177	0.505	0.211	87.991	2.053	8
39.708	20.169	20.158	45.109	0.529	0.207	88.812	1.011	9
39.882	21.838	25.511	46.085	0.500	0.212	86.699	2.585	10
39.538	20.847	22.302	41.628	0.516	0.210	87.502	1.661	11
39.858	24.000	21.793	41.056	0.506	0.211	84.759	1.632	12
34.960	22.659	20.086	44.249	0.596	0.213	84.216	1.481	13
39.494	25.131	21.657	42.973	0.512	0.211	83.710	1.770	14
37.690	25.352	20.880	44.199	0.546	0.212	82.846	1.762	15
37.117	27.564	23.081	44.654	0.538	0.215	80.511	2.775	16
33.438	25.605	21.918	42.277	0.595	0.217	80.468	2.464	17
39.949	30.716	27.115	40.815	0.478	0.217	78.971	3.713	18
37.311	31.357	32.208	47.818	0.525	0.223	77.522	4.909	19
40.000	31.992	27.326	40.769	0.475	0.218	77.952	3.987	20
33.793	28.671	25.441	45.944	0.567	0.220	78.078	3.825	21
38.604	30.043	23.868	40.849	0.506	0.216	78.739	3.103	22
33.578	31.619	30.214	54.454	0.562	0.224	75.986	5.494	23
31.538	31.985	31.015	59.377	0.581	0.225	75.170	6.013	24
31.985	31.803	29.250	52.282	0.574	0.225	75.004	5.432	25
31.250	30.742	32.086	47.680	0.575	0.229	75.240	5.062	26
32.353	30.177	22.040	47.548	0.605	0.219	76.298	3.529	27
32.003	29.282	20.587	46.360	0.623	0.218	76.848	2.915	28
30.806	30.617	39.998	42.924	0.608	0.237	75.521	3.724	29
31.774	30.016	21.334	44.120	0.617	0.219	75.814	3.286	30
32.572	31.802	24.276	42.598	0.583	0.222	74.574	4.311	31
31.716	31.899	25.381	41.468	0.585	0.224	74.133	4.596	32
31.350	31.988	25.590	43.080	0.588	0.225	73.971	4.729	33
30.306	30.372	20.078	43.746	0.646	0.220	74.744	3.142	34
30.364	32.000	21.068	40.971	0.633	0.222	73.040	3.802	35

APPENDIX 21

Table 4.35: Pareto-optimal solutions obtained from MOABC

V	I_p	T_{on}	T_{off}	MRR	OC	RCL	TA	Rank
39.976	10.040	20.173	59.875	0.567	0.201	101.081	0.846	1
39.226	10.540	20.173	59.875	0.577	0.202	100.269	0.919	2
39.392	12.679	20.186	59.437	0.568	0.202	98.215	1.114	3
32.806	11.813	20.208	59.357	0.652	0.208	96.028	1.168	4
39.946	14.926	23.681	58.546	0.536	0.205	94.791	0.131	5
30.069	13.329	20.085	59.975	0.675	0.211	93.549	1.378	6
30.069	14.329	20.085	59.975	0.674	0.211	92.601	1.382	7
30.301	15.201	20.236	59.351	0.669	0.211	91.678	1.300	8
39.883	18.527	20.716	50.396	0.538	0.205	91.044	1.049	9
37.836	20.202	21.406	53.253	0.563	0.208	88.847	0.733	10
37.274	22.485	21.702	57.860	0.568	0.208	87.248	0.509	11
33.407	20.714	21.240	47.461	0.618	0.214	85.562	0.435	12
38.106	24.970	21.505	52.047	0.549	0.209	84.345	0.345	13
39.650	26.099	24.208	46.815	0.508	0.212	83.088	0.428	14
31.914	25.943	22.329	57.855	0.625	0.215	81.516	0.358	15
39.437	28.325	23.754	43.563	0.507	0.213	80.790	0.642	16
39.205	29.215	25.509	43.476	0.504	0.215	79.915	1.189	17
39.747	29.631	25.849	39.562	0.493	0.216	79.693	1.262	18
36.636	29.769	27.417	41.623	0.535	0.220	78.284	1.838	19
39.997	31.997	27.378	41.898	0.485	0.217	77.965	1.918	20
34.528	28.639	24.798	43.842	0.571	0.219	78.311	1.397	21
33.044	27.547	23.177	44.469	0.599	0.218	78.668	0.980	22
31.348	26.740	23.472	43.877	0.614	0.220	78.568	1.041	23
30.252	28.417	21.935	58.746	0.644	0.217	78.749	0.808	24
37.104	31.686	26.545	41.588	0.528	0.219	76.846	2.061	25
30.287	27.588	24.818	39.820	0.611	0.223	77.132	1.612	26
34.550	31.495	28.789	42.041	0.556	0.224	76.015	2.514	27
31.221	29.091	24.480	43.650	0.607	0.222	76.409	1.698	28
31.417	31.575	39.977	33.160	0.610	0.238	76.660	1.454	29
34.050	31.995	28.789	42.041	0.561	0.224	75.387	2.674	30
33.515	31.393	26.406	43.880	0.573	0.222	75.535	2.324	31
32.519	31.767	30.081	40.741	0.572	0.227	74.994	2.798	32
31.884	31.346	34.136	43.955	0.583	0.230	75.186	2.595	33
30.244	31.992	30.330	42.187	0.589	0.229	73.784	3.003	34
30.241	31.991	27.110	42.171	0.599	0.226	73.543	2.844	35

APPENDIX 22

Table 4.36: Optimization results

Response	MOETLBO			MODE			MOABC		
	Best	Mean	Worst	Best	Mean	Worst	Best	Mean	Worst
MRR (mm^3/min)	0.606	0.596	0.688	0.542	0.555	0.633	0.567	0.577	0.599
OC(µm)	0.191	0.204	0.212	0.204	0.216	0.222	0.201	0.216	0.226
RCL(µm)	104.137	84.260	74.078	94.463	81.900	73.04	101.081	83.208	73.543
TA(degree)	1.364	2.209	2.869	1.463	2.970	3.802	0.846	1.392	2.844

APPENDIX 23

Table 4.38. Experimental design matrix along with results

S. No	Parameters				Material Removal Rate (MRR) in mm^3/min	Overcut (OC) in µm	Recast layer thickness (RCL) in µm	Taper Angle (TA) in degrees
	Voltage (V)	Peak current (I_p)	Pulse on duration (T_{on})	Pulse off duration (T_{off})				
1	30	8	20	30	0.961	0.175	77.284	1.930
2	30	8	40	60	0.926	0.225	73.773	1.864
3	30	8	20	60	0.833	0.174	73.224	1.495
4	30	8	40	30	0.888	0.215	64.568	1.483
5	30	20	30	45	0.868	0.169	93.076	3.072
6	30	32	20	30	0.823	0.174	70.268	2.876
7	30	32	20	60	0.888	0.155	76.234	2.930
8	30	32	40	60	0.910	0.157	86.494	2.203
9	30	32	40	30	0.829	0.164	73.262	2.592
10	35	8	30	45	0.800	0.215	96.414	3.592
11	35	20	30	45	0.811	0.229	99.627	2.548
12	35	20	30	30	0.989	0.159	88.591	3.548
13	35	20	30	45	0.811	0.160	102.250	4.782
14	35	20	30	45	0.810	0.159	93.723	3.548
15	35	20	30	45	0.810	0.159	93.360	4.548
16	35	20	30	45	0.810	0.212	92.474	3.274
17	35	20	30	45	0.810	0.242	99.474	4.274
18	35	20	40	45	0.862	0.218	97.287	2.621
19	35	20	20	45	0.803	0.196	98.128	1.357
20	35	20	30	60	0.911	0.150	90.840	4.915
21	35	32	30	45	0.776	0.199	92.657	4.695
22	40	8	20	30	0.803	0.156	120.976	2.264
23	40	8	20	60	0.796	0.143	119.973	2.918
24	40	8	40	30	0.900	0.158	105.791	3.131
25	40	8	40	60	0.909	0.146	108.054	4.331
26	40	20	30	45	0.738	0.164	117.724	2.813
27	40	32	40	60	0.877	0.165	112.098	3.348
28	40	32	40	30	0.996	0.194	95.809	2.650
29	40	32	20	60	0.736	0.130	82.307	2.445
30	40	32	20	30	0.770	0.183	89.284	3.067

APPENDIX 24

Table 4. 41: Analysis of Variance for OC

Source	Sum of Squares	DOF	Mean Square	F Value	p-value Prob > F	Percentage contribution
Model	3.893E-003	13	2.994E-004	103.94	< 0.0001	98.832
A	1.282E-004	1	1.282E-004	44.49	< 0.0001	3.255
B	6.809E-005	1	6.809E-005	23.63	0.0002	1.729
D	4.662E-004	1	4.662E-004	161.84	< 0.0001	11.835
AB	8.192E-004	1	8.192E-004	284.36	< 0.0001	20.797
AC	1.197E-004	1	1.197E-004	41.54	< 0.0001	3.039
AD	1.395E-004	1	1.395E-004	48.44	< 0.0001	3.542
BC	1.094E-004	1	1.094E-004	37.97	< 0.0001	2.777
BD	7.334E-004	1	7.334E-004	254.57	< 0.0001	18.619
CD	4.497E-004	1	4.497E-004	156.09	< 0.0001	11.417
A^2	4.291E-005	1	4.291E-005	14.90	0.0014	1.089
B^2	7.354E-005	1	7.354E-005	25.53	0.0001	1.867
C^2	5.726E-004	1	5.726E-004	198.75	< 0.0001	14.537
D^2	1.248E-004	1	1.248E-004	43.32	< 0.0001	3.168
Residual	4.609E-005	16	2.881E-006			
Lack of Fit	3.385E-005	11	3.077E-006	1.26	0.4251	Insignificant
Pure Error	1.224E-005	5	2.448E-006			
Corrected Total	3.939E-003	29			R-Squared	0.9883
					Adj R-Squared	0.9788
					Pred R-Squared	0.9644

APPENDIX 25

Table 4. 19: Analysis of Variance for RCL

Source	Sum of Squares	DOF	Mean Square	F Value	p-value Prob > F	Percentage contribution
Model	9308.40	12	775.70	95.99	< 0.0001	98.546
A-Voltage	965.55	1	965.55	119.49	< 0.0001	10.222
B-Peak current	1708.65	1	1708.65	211.44	< 0.0001	18.089
C-Pulse on duration	187.95	1	187.95	23.26	0.0002	1.990
D-Pulse off duration	168.24	1	168.24	20.82	0.0003	1.781
AB	2369.38	1	2369.38	293.21	< 0.0001	25.084
AC	155.47	1	155.47	19.24	0.0004	1.646
BC	137.13	1	137.13	16.97	0.0007	1.452
CD	175.98	1	175.98	21.78	0.0002	1.863
A^2	365.03	1	365.03	45.17	< 0.0001	3.864
B^2	38.80	1	38.80	4.80	0.0427	0.411
C^2	633.26	1	633.26	78.37	< 0.0001	6.704
D^2	957.39	1	957.39	118.48	< 0.0001	
Residual	137.37	17	8.08			
Lack of Fit	98.74	12	8.23	1.06	0.5098	Insignificant
Pure Error	38.64	5	7.73			
Corrected Total	9445.77	29			R-Squared	0.9855
					Adj R-Squared	0.9752
					Pred R-Squared	0.9615

APPENDIX 26

Table 4. 43: Analysis of Variance for TA

Source	Sum of Squares	DOF	Mean Square	F Value	p-value Prob > F	Percentage contribution
Model	95.46	7	13.64	33.38	< 0.0001	91.393
B-Peak current	2.32	1	2.32	5.67	0.0263	2.221
D-Pulse off duration	3.39	1	3.39	8.29	0.0087	3.246
BD	3.61	1	3.61	8.84	0.0070	3.456
A^2	3.18	1	3.18	7.79	0.0106	3.045
B^2	14.05	1	14.05	34.40	< 0.0001	13.451
C^2	17.01	1	17.01	41.64	< 0.0001	16.285
D^2	28.17	1	28.17	68.97	< 0.0001	26.970
Residual	8.99	22	0.41			
Lack of Fit	6.83	17	0.40	0.93	0.5923	Insignificant
Pure Error	2.16	5	0.43			
Corrected Total	104.45	29			R-Squared	0.9140
					Adj R-Squared	0.8866
					Pred R-Squared	0.8323

APPENDIX 27

Table 4.40: Training data sets

S. No	Parameters				(MRR) in mm^3/min	(OC) in µm	(RCL) µm	(TA)in degrees
	Voltage (V)	Peak current (I_p)	Pulse on duration (T_{on})	Pulse off duration (T_{off})				
1	40	32	20	60	0.736	0.130	82.307	2.445
2	40	20	30	45	0.738	0.164	117.724	2.813
3	40	32	20	30	0.77	0.183	89.284	3.067
4	35	32	30	45	0.776	0.199	92.657	4.695
5	40	8	20	60	0.796	0.143	119.973	2.918
6	35	8	30	45	0.80	0.215	96.414	3.592
7	35	20	20	45	0.803	0.196	98.128	1.357
8	40	8	20	30	0.803	0.156	120.976	2.264
9	35	20	30	45	0.810	0.159	93.723	3.548
10	35	20	30	45	0.812	0.159	93.36	4.548
11	35	20	30	45	0.814	0.212	92.474	3.274
12	35	20	30	45	0.810	0.242	99.474	4.274
13	35	20	30	45	0.815	0.229	99.627	2.548
14	35	20	30	45	0.811	0.16	102.25	4.782
15	30	32	20	30	0.823	0.174	70.268	2.876
16	30	32	40	30	0.829	0.164	73.262	2.592
17	30	8	20	60	0.833	0.174	73.224	1.495
18	35	20	40	45	0.862	0.218	97.287	2.621
19	30	20	30	45	0.868	0.169	93.076	3.072
20	40	32	40	60	0.877	0.165	112.098	3.348

APPENDIX 28

Table 4. 42:Validation of the Developed Model with Experimental Data

Process Parameters				MRR (mm^3/min)		OC(µm)		RCL(µm)		TA(degrees)	
V	I_p	T_{on}	T_{off}	Exp	ANN	Exp	ANN	Exp	ANN	Exp	ANN
30	8	40	30	0.888	0.951	0.215	0.212	64.568	67.352	1.483	1.645
30	32	20	60	0.888	0.898	0.155	0.161	76.234	68.305	2.930	4.724
40	8	40	30	0.900	0.904	0.158	0.165	105.791	104.519	3.131	3.022
40	8	40	60	0.909	0.932	0.146	0.155	108.054	106.113	4.331	4.508
30	32	40	60	0.910	0.955	0.157	0.177	86.494	78.367	2.203	4.447
35	20	30	60	0.911	0.909	0.150	0.157	90.840	84.804	4.915	4.861
30	8	40	60	0.926	0.935	0.225	0.212	73.773	82.349	1.864	2.209
30	8	20	30	0.961	0.983	0.175	0.160	77.284	74.239	1.930	2.007
35	20	30	30	0.989	0.960	0.159	0.164	88.591	92.644	3.548	2.037
40	32	40	30	0.996	0.990	0.194	0.166	95.809	80.453	2.650	1.637

Table 4.43: Errors in Prediction of Responses

(V)	(I_p)	(T_{on})	(T_{off})	% Error in Prediction of MRR	% Error in Prediction of OC	% Error in Prediction of RCL	% Error in Prediction of TA
30	8	40	30	-7.069	1.576	-4.311	-10.892
30	32	20	60	-1.134	-3.946	10.401	-61.220
40	8	40	30	-0.422	-4.587	1.202	3.490
40	8	40	60	-2.528	-6.121	1.796	-4.091
30	32	40	60	-4.912	-12.762	9.397	-101.864
35	20	30	60	0.206	-4.522	6.645	1.091
30	8	40	60	-0.955	5.698	-11.624	-18.482
30	8	20	30	-2.330	8.338	3.940	-4.010
35	20	30	30	2.921	-3.410	-4.575	42.597
40	32	40	30	0.639	14.389	16.027	38.227
Average (%) of error				-1.558	-0.535	2.890	-11.515
Total average prediction error (%) = -10.719							

APPENDIX 29

Table 4.44: Testing of the Developed Model with Experimental Data.

Process Parameters				MRR (mm^3/min)		OC(μm)		RCL(μm)		TA(degrees)	
V	I_p	T_{on}	T_{off}	Exp	ANN	Exp	ANN	Exp	ANN	Exp	ANN
40	8	20	60	0.796	0.799	0.143	0.151	119.973	119.044	2.918	3.176
35	8	30	45	0.800	0.800	0.215	0.216	96.414	102.570	3.592	4.106
35	20	20	45	0.803	0.802	0.196	0.195	98.128	101.624	1.357	1.433
40	8	20	30	0.803	0.807	0.156	0.155	120.976	119.595	2.264	2.478
35	20	30	45	0.810	0.810	0.159	0.171	93.723	84.633	3.548	3.290
35	20	30	45	0.810	0.813	0.159	0.168	93.360	85.653	4.548	4.413
35	20	30	45	0.810	0.814	0.212	0.216	92.474	94.050	3.274	3.728
35	20	30	45	0.811	0.815	0.229	0.219	99.627	101.789	2.548	3.171
35	20	30	45	0.811	0.815	0.160	0.170	102.250	98.026	4.782	4.557
30	32	20	30	0.823	0.820	0.174	0.167	70.268	71.497	2.876	2.929

Table 4.45: Errors in Prediction of Responses during Testing

(V)	(I_p)	(T_{on})	(T_{off})	% Error in Prediction of MRR	% Error in Prediction of OC	% Error in Prediction of RCL	% Error in Prediction of TA
40	8	20	60	-0.328	-5.668	0.775	-8.856
35	8	30	45	0.062	-0.271	-6.385	-14.313
35	20	20	45	0.179	0.445	-3.563	-5.581
40	8	20	30	-0.515	0.373	1.142	-9.436
35	20	30	45	0.041	-7.303	9.698	7.285
35	20	30	45	-0.361	-5.481	8.255	2.971
35	20	30	45	-0.438	-1.920	-1.704	-13.873
35	20	30	45	-0.462	4.215	-2.170	-24.435
35	20	30	45	-0.543	-6.200	4.131	4.695
30	32	20	30	0.315	3.891	-1.749	-1.843
Average (%) of error				-0.205	-1.792	0.843	-6.339
Total average prediction error (%) = -7.492							

APPENDIX 30

Table 4.58: Testing of the developed model with experimental data.

Process Parameters				MRR (mm^3/min)		OC(µm)		RCL(µm)		TA(degrees)	
V	I_p	T_{on}	T_{off}	Exp	ANFIS	Exp	ANFIS	Exp	ANFIS	Exp	ANFIS
40	8	20	60	0.796	0.796	0.143	0.143	119.973	119.973	2.918	2.918
35	8	30	45	0.800	0.811	0.215	0.215	96.414	96.414	3.592	3.215
35	20	20	45	0.803	0.802	0.196	0.196	98.128	98.128	1.357	1.363
40	8	20	30	0.803	0.803	0.156	0.156	120.976	120.976	2.264	2.264
35	20	30	45	0.810	0.808	0.159	0.154	93.723	96.818	3.548	3.705
35	20	30	45	0.810	0.808	0.159	0.154	93.360	93.453	4.548	3.705
35	20	30	45	0.810	0.807	0.212	0.214	92.474	96.233	3.274	3.705
35	20	30	45	0.811	0.812	0.229	0.224	99.627	96.245	2.548	3.705
35	20	30	45	0.811	0.812	0.160	0.164	102.250	96.567	4.782	3.705
30	32	20	30	0.823	0.823	0.174	0.174	70.268	70.268	2.876	2.875

Table 4.59: Errors in Prediction of Responses during testing

(V)	(I_p)	(T_{on})	(T_{off})	% Error in Prediction of MRR	% Error in Prediction of OC	% Error in Prediction of RCL	% Error in Prediction of TA
40	8	20	60	0.000	0.000	0.000	0.010
35	8	30	45	-1.388	0.000	0.000	10.507
35	20	20	45	0.075	0.000	0.000	-0.413
40	8	20	30	0.000	0.000	0.000	0.013
35	20	30	45	0.198	-21.698	-3.302	-4.411
35	20	30	45	0.198	-21.698	-3.704	18.547
35	20	30	45	0.198	8.726	-4.698	-13.149
35	20	30	45	0.321	15.502	2.820	-45.389
35	20	30	45	0.321	-20.938	5.312	22.532
30	32	20	30	0.000	0.000	0.000	0.031
Average (%) of error				-0.008	-4.011	-0.357	-1.172
Total average prediction error (%) = -5.548							

APPENDIX 31

Table 4.60: Pareto-optimal solutions obtained from MOETLBO

V	I_p	T_{on}	T_{off}	MRR	OC	RCL	TA	Rank
39.814	8.034	27.066	47.805	0.716	0.156	145.155	0.465	1
39.308	8.100	26.715	47.268	0.704	0.156	140.853	0.532	2
39.613	8.333	22.335	51.511	0.720	0.152	135.981	0.682	3
39.613	8.333	22.335	52.511	0.719	0.152	134.818	0.732	4
38.467	8.373	25.719	52.136	0.692	0.154	129.920	0.790	5
37.689	8.153	25.413	50.234	0.677	0.154	126.503	0.608	6
37.191	8.411	21.910	52.917	0.673	0.151	115.074	0.883	7
36.573	8.422	21.873	54.581	0.661	0.151	108.751	1.038	8
35.573	8.422	21.873	53.581	0.651	0.153	104.940	0.987	9
39.922	31.980	23.470	44.882	0.585	0.178	97.208	0.172	10
38.898	31.900	23.765	39.777	0.599	0.179	91.421	0.118	11
35.705	31.917	22.852	49.251	0.536	0.161	85.710	0.157	12
37.046	31.947	22.255	51.513	0.523	0.160	83.402	0.289	13
36.137	31.943	21.480	37.323	0.603	0.174	78.830	0.409	14
38.131	31.978	20.957	55.901	0.496	0.157	75.710	0.837	15
34.888	31.948	21.298	57.688	0.479	0.150	69.814	1.294	16
36.423	31.944	20.825	58.649	0.468	0.150	66.574	1.448	17
36.260	21.799	39.864	30.747	0.598	0.163	59.452	6.049	18
34.611	31.911	20.275	59.999	0.459	0.147	61.287	1.828	19
35.768	31.989	20.283	59.999	0.455	0.147	61.081	1.744	20
33.832	18.699	39.994	30.004	0.584	0.161	56.512	6.568	21
33.937	25.445	39.995	30.508	0.586	0.163	56.367	5.222	22
33.861	22.489	39.994	30.004	0.589	0.162	55.355	6.183	23
35.753	24.021	39.996	30.005	0.588	0.164	54.804	5.752	24
33.937	25.195	39.995	30.008	0.585	0.163	54.912	5.434	25
33.937	26.195	39.995	30.008	0.582	0.163	54.866	5.058	26
34.160	28.696	39.977	30.024	0.569	0.164	54.689	3.873	27
34.713	29.151	39.929	30.342	0.565	0.165	54.981	3.532	28
35.637	27.263	39.998	30.116	0.575	0.165	53.770	4.521	29
34.682	29.902	39.931	30.045	0.559	0.165	54.140	3.167	30
34.986	30.634	39.998	30.005	0.552	0.165	53.376	2.713	31
36.191	31.049	39.932	30.300	0.548	0.168	53.479	2.337	32
36.017	30.328	39.998	30.005	0.554	0.167	52.574	2.875	33
36.514	31.037	39.998	30.008	0.548	0.168	52.343	2.403	34
36.444	31.604	39.999	30.003	0.543	0.169	52.180	2.021	35

APPENDIX 32

Table 4.61: Pareto-optimal solutions obtained from MODE

V	I_p	T_{on}	T_{off}	MRR	OC	RCL	TA	Rank
40.000	8.002	27.150	45.827	0.651	0.160	147.799	0.097	1
39.967	8.026	24.097	45.158	0.659	0.159	146.047	0.080	2
39.994	8.042	20.115	37.179	0.677	0.159	134.995	0.455	3
39.413	9.018	20.362	47.813	0.653	0.156	132.425	0.795	4
38.792	9.347	21.480	52.357	0.631	0.155	125.062	1.517	5
38.476	8.792	20.456	49.287	0.634	0.155	124.679	0.823	6
38.537	9.586	20.082	37.312	0.645	0.159	119.277	1.342	7
37.495	12.338	32.701	40.625	0.564	0.165	114.825	2.389	8
37.808	10.007	22.576	57.080	0.602	0.154	111.049	2.842	9
38.779	8.038	20.003	60.000	0.622	0.148	109.844	2.386	10
38.976	10.596	20.055	59.998	0.607	0.150	105.881	3.872	11
37.993	12.419	20.063	59.297	0.577	0.152	96.992	4.553	12
37.910	15.791	20.091	58.136	0.544	0.155	93.337	5.323	13
37.974	15.043	20.025	59.999	0.546	0.153	90.286	5.666	14
40.000	32.000	20.029	40.314	0.359	0.197	93.417	0.869	15
39.994	31.999	20.154	39.578	0.363	0.197	93.099	0.864	16
38.018	17.687	20.062	59.940	0.512	0.155	86.409	6.188	17
39.145	31.734	20.077	40.805	0.358	0.192	90.778	0.656	18
35.551	17.775	20.423	59.056	0.501	0.156	79.105	6.018	19
36.743	20.386	20.222	59.416	0.466	0.156	78.672	6.235	20
37.708	31.716	39.079	39.895	0.315	0.181	82.282	0.487	21
38.249	31.022	21.065	57.109	0.267	0.168	80.184	2.290	22
37.164	31.694	20.083	35.680	0.385	0.190	79.636	0.369	23
39.126	31.968	20.094	58.164	0.234	0.169	76.943	1.994	24
34.442	19.084	20.065	59.988	0.480	0.156	71.833	6.457	25
34.153	19.763	20.122	59.998	0.472	0.157	71.039	6.497	26
39.995	32.000	20.194	30.100	0.411	0.207	76.874	0.050	27
39.995	32.000	20.194	30.099	0.411	0.207	76.873	0.050	28
37.106	31.373	21.925	31.313	0.402	0.192	75.530	0.389	29
37.932	32.000	20.051	59.998	0.216	0.163	68.748	2.624	30
36.647	30.123	20.052	59.998	0.266	0.159	67.521	3.765	31
34.270	29.704	20.060	59.998	0.292	0.157	66.510	4.062	32
36.518	31.165	20.064	60.000	0.240	0.159	66.745	3.184	33
36.728	29.307	39.517	30.654	0.348	0.179	61.492	1.900	34
36.385	31.533	39.999	30.024	0.310	0.180	57.578	0.629	35

APPENDIX 33

Table 4.62: Pareto-optimal solutions obtained from MOABC

V	I_p	T_{on}	T_{off}	MRR	OC	RCL	TA	Rank
39.855	8.008	26.969	45.804	0.648	0.170	150.513	4.104	1
39.977	8.541	24.155	43.444	0.657	0.170	148.631	4.374	2
39.821	8.115	22.503	46.125	0.661	0.167	146.575	4.163	3
39.828	8.346	23.087	51.069	0.656	0.166	144.100	4.718	4
39.977	8.030	20.350	46.055	0.672	0.166	144.370	4.093	5
39.546	8.206	23.239	52.075	0.650	0.166	141.108	4.780	6
38.583	8.551	24.004	45.616	0.629	0.168	137.329	4.457	7
39.100	8.153	22.175	52.370	0.642	0.164	135.457	4.802	8
38.990	8.332	20.700	52.304	0.641	0.163	131.313	4.901	9
38.820	8.087	21.401	55.452	0.633	0.162	127.229	5.312	10
38.520	10.048	20.322	51.473	0.625	0.165	124.004	5.773	11
37.836	10.053	21.009	49.537	0.616	0.166	122.539	5.566	12
37.839	10.050	20.555	54.549	0.607	0.163	115.491	6.310	13
38.536	8.006	20.035	59.978	0.618	0.158	112.109	6.368	14
37.555	11.714	20.699	54.242	0.593	0.165	111.375	7.068	15
37.446	11.048	21.112	57.796	0.587	0.163	106.213	7.557	16
37.740	13.501	20.400	56.068	0.575	0.165	105.393	8.149	17
37.528	15.174	20.315	55.186	0.559	0.167	102.747	8.465	18
37.344	15.787	20.574	55.547	0.549	0.167	100.847	8.699	19
39.974	31.989	23.298	40.296	0.350	0.206	104.369	3.152	20
37.319	10.767	20.042	59.977	0.580	0.160	98.023	8.011	21
36.660	13.453	20.060	58.457	0.556	0.163	93.592	8.765	22
36.896	18.729	20.563	57.909	0.499	0.167	89.826	9.743	23
38.561	31.988	20.619	44.789	0.325	0.195	95.509	3.370	24
36.801	31.948	21.746	47.211	0.311	0.187	94.303	3.705	25
35.913	15.189	20.604	58.992	0.532	0.165	88.078	9.481	26
36.649	18.776	20.115	58.154	0.496	0.167	86.957	9.821	27
39.401	31.982	20.978	35.519	0.378	0.209	91.575	3.371	28
36.443	19.534	20.348	59.847	0.476	0.165	81.885	10.369	29
36.551	21.716	20.171	59.031	0.446	0.167	81.302	10.059	30
36.831	31.864	20.464	54.522	0.264	0.178	83.568	5.114	31
36.907	24.732	20.367	59.318	0.390	0.168	79.187	9.637	32
37.438	31.737	20.130	59.022	0.231	0.173	74.538	6.476	33
37.978	31.985	20.050	59.960	0.216	0.173	72.969	6.618	34
35.809	31.954	20.044	59.998	0.224	0.169	69.715	6.725	35

APPENDIX 34

Table 5.3: Design matrix and experimental results

KS. No	Parameters				Material Removal Rate (MRR) in mm^3/min	Overcut (OC) in µm	Recast layer thickness (RCL) in µm	Taper Angle (TA) in degrees
	Voltage (V)	Peak current (I_p)	Pulse on duration (T_{on})	Pulse off duration (T_{off})				
1	30	10	80	20	0.149	0.109	82.444	0.766
2	30	40	40	20	0.483	0.352	77.054	2.052
3	30	10	80	30	0.350	0.260	102.610	1.345
4	30	40	80	20	0.204	0.199	71.254	2.781
5	30	10	40	30	0.448	0.318	112.343	2.544
6	30	40	40	30	0.262	0.253	73.486	1.102
7	30	25	60	25	0.142	0.168	65.796	1.354
8	30	10	40	20	0.440	0.307	122.819	0.234
9	30	40	80	30	0.215	0.239	98.328	3.631
10	45	25	60	25	0.427	0.300	93.282	3.974
11	45	25	60	25	0.408	0.375	76.879	1.235
12	45	25	60	25	0.435	0.290	81.125	0.652
13	45	25	60	25	0.463	0.270	84.265	1.236
14	45	25	60	25	0.377	0.326	75.237	1.236
15	45	25	60	25	0.279	0.229	67.898	1.433
16	45	25	60	20	0.216	0.202	76.174	1.015
17	45	25	40	25	0.284	0.215	73.615	1.292
18	45	40	60	25	0.333	0.292	54.007	3.151
19	45	25	80	25	0.263	0.209	72.245	1.287
20	45	10	60	25	0.311	0.234	71.652	2.528
21	45	25	60	30	0.266	0.251	62.419	2.034
22	60	40	40	30	0.382	0.248	60.281	1.342
23	60	10	80	30	0.397	0.362	87.439	1.373
24	60	25	60	25	0.270	0.193	73.663	0.283
25	60	10	80	20	0.245	0.163	111.382	2.383
26	60	40	40	20	0.523	0.300	102.958	0.119
27	60	10	40	20	0.241	0.163	138.965	0.923
28	60	10	40	30	0.328	0.222	84.380	2.112
29	60	40	80	30	0.671	0.433	97.915	0.331
30	60	40	80	20	0.580	0.344	114.950	1.070

APPENDIX 35

Table 5. 3: ANOVA for MRR (after backward elimination)

Source	Sum of Squares	DOF	Mean Square	F Value	p-value Prob > F	Percentage contribution
Model	1.47	7	0.21	11.19	< 0.0001	78.191
A-Voltage	0.27	1	0.27	14.18	0.0011	14.362
B-Peak current	0.089	1	0.089	4.74	0.0406	4.734
AB	0.21	1	0.21	11.07	0.0031	11.170
AC	0.41	1	0.41	21.71	0.0001	21.809
BD	0.19	1	0.19	10.15	0.0043	10.106
CD	0.20	1	0.20	10.47	0.0038	10.638
B^2	0.11	1	0.11	5.98	0.0230	5.851
Residual	0.41	22	0.019			
Lack of Fit	0.31	17	0.018	0.86	0.6318	
Pure Error	0.11	5	0.021			
Corrected Total	1.88	29			R-Squared	0.7807
					Adj R-Squared	0.7109
					Pred R-Squared	0.6622

Table 5. 4: ANOVA for OC (after backward elimination)

Source	Sum of Squares	DOF	Mean Square	F Value	p-value Prob > F	Percentage contribution
Model	0.11	6	0.018	11.41	< 0.0001	78.571
B-Peak current	0.015	1	0.015	9.82	0.0047	10.714
D-Toff	0.011	1	0.011	7.21	0.0132	7.857
AB	8.327E-003	1	8.327E-003	5.39	0.0294	5.948
AC	0.039	1	0.039	25.42	< 0.0001	27.857
BD	0.012	1	0.012	7.93	0.0098	8.571
CD	0.020	1	0.020	12.69	0.0017	14.286
Residual	0.036	23	1.544E-003			
Lack of Fit	0.029	18	1.594E-003	1.17	0.4708	
Pure Error	6.817E-003	5	1.363E-003			
Corrected Total	0.14	29			R-Squared	0.7485
					Adj R-Squared	0.6829
					Pred R-Squared	0.6273

APPENDIX 36

Table 5. 6: ANOVA for RCL (after backward elimination)

Source	Sum of Squares	DOF	Mean Square	F Value	p-value Prob > F	Percentage Contribution
Model	8615.30	6	1435.88	9.32	0.0001	70.859
B-Peak current	1400.99	1	1400.99	9.09	0.0062	11.523
D-Toff	851.46	1	851.46	5.53	0.0277	7.003
AD	1945.60	1	1945.60	12.63	0.0017	16.002
BC	1195.43	1	1195.43	7.76	0.0105	9.832
CD	938.93	1	938.93	6.10	0.0214	7.723
C^2	2282.89	1	2282.89	14.82	0.0008	18.776
Residual	3543.02	23	154.04			
Lack of Fit	2683.89	18	149.10	0.87	0.6302	
Pure Error	859.13	5	171.83			
Corrected Total	12158.32	29			R-Squared	0.7086
					Adj R-Squared	0.6326
					Pred R-Squared	0.5736

Table 5. 7: ANOVA for TA (After backward elimination)

Source	Sum of Squares	DOF	Mean Square	F Value	p-value Prob > F	Percentage Contribution
Model	35.38	9	3.93	59.89	< 0.0001	96.430
A-Voltage	4.65	1	4.65	70.92	< 0.0001	12.674
B-Peak current	0.45	1	0.45	6.82	0.0167	1.226
C-Ton	4.66	1	4.66	71.03	< 0.0001	12.701
D-Toff	9.51	1	9.51	144.94	< 0.0001	25.920
AB	11.08	1	11.08	168.80	< 0.0001	30.199
AD	2.53	1	2.53	38.47	< 0.0001	6.896
CD	4.84	1	4.84	73.70	< 0.0001	13.192
A^2	2.12	1	2.12	32.36	< 0.0001	5.778
B^2	5.26	1	5.26	80.16	< 0.0001	14.336
Residual	1.31	20	0.066			
Lack of Fit	1.03	15	0.069	1.22	0.4444	Insignificant
Pure Error	0.28	5	0.056			
Corrected Total	36.69	29			R-Squared	0.9642
					Adj R-Squared	0.9481
					Pred R-Squared	0.9210

APPENDIX 37

Table 5.8: Training data sets

S. No	Parameters				(MRR) in mm^3/min	(OC) in µm	RCL) in µm	(TA)in degrees
	Voltage (V)	Peak current (I_p)	Pulse on duration (T_{on})	Pulse off duration (T_{off})				
1	60	40	80	30	0.671	0.433	97.915	0.331
2	45	25	60	25	0.408	0.375	76.879	1.235
3	60	10	80	30	0.397	0.362	87.439	1.373
4	30	40	40	20	0.483	0.352	77.054	2.052
5	60	40	80	20	0.58	0.344	114.95	1.07
6	45	25	60	25	0.377	0.326	75.237	1.236
7	30	10	40	30	0.448	0.318	112.343	2.544
8	30	10	40	20	0.44	0.307	122.819	0.234
9	45	25	60	25	0.427	0.3	93.282	3.974
10	60	40	40	20	0.523	0.3	102.958	0.119
11	45	40	60	25	0.333	0.292	54.007	3.151
12	45	25	60	25	0.435	0.29	81.125	0.652
13	45	25	60	25	0.463	0.27	84.265	1.236
14	30	10	80	30	0.35	0.26	102.61	1.345
15	30	40	40	30	0.262	0.253	73.486	1.102
16	45	25	60	30	0.266	0.251	62.419	2.034
17	60	40	40	30	0.382	0.248	60.281	1.342
18	30	40	80	30	0.215	0.239	98.328	3.631
19	45	10	60	25	0.311	0.234	71.652	2.528
20	45	25	60	25	0.279	0.229	67.898	1.433

APPENDIX 38

Table 5.9: Validation of the Developed Model with Experimental Data.

Process Parameters				MRR (mm^3/min)		OC(μm)		RCL(μm)		TA(degrees)	
V	I_p	T_{on}	T_{off}	Exp	ANN	Exp	ANN	Exp	ANN	Exp	ANN
60	10	40	30	0.328	0.270	0.222	0.193	84.380	78.171	2.112	1.583
45	25	40	25	0.284	0.264	0.215	0.168	73.615	80.572	1.292	0.685
45	25	80	25	0.263	0.266	0.209	0.211	72.245	71.923	1.287	2.328
45	25	60	20	0.216	0.224	0.202	0.171	76.174	86.855	1.015	1.332
30	40	80	20	0.204	0.221	0.199	0.177	71.254	72.049	2.781	2.764
60	25	60	25	0.270	0.277	0.193	0.189	73.663	81.024	0.283	0.333
30	25	60	25	0.142	0.163	0.168	0.137	65.796	68.354	1.354	1.662
60	10	80	20	0.245	0.239	0.163	0.196	111.382	122.929	2.383	2.455
60	10	40	20	0.241	0.217	0.163	0.151	138.965	132.094	0.923	0.342
30	10	80	20	0.149	0.170	0.109	0.129	82.444	73.990	0.766	1.716

Table 5.10: Errors in Prediction of Responses

(V)	(I_p)	(T_{on})	(T_{off})	% Error in Prediction of MRR	% Error in Prediction of OC	% Error in Prediction of RCL	% Error in Prediction of TA
60	10	40	30	17.555	12.920	7.359	25.038
45	25	40	25	6.891	22.054	-9.451	46.955
45	25	80	25	-0.961	-0.820	0.446	-80.919
45	25	60	20	-3.622	15.101	-14.022	-31.236
30	40	80	20	-8.552	10.952	-1.116	0.622
60	25	60	25	-2.619	2.071	-9.993	-17.620
30	25	60	25	-14.805	18.413	-3.888	-22.744
60	10	80	20	2.281	-20.020	-10.367	-3.019
60	10	40	20	9.986	7.648	4.944	62.907
30	10	80	20	-13.906	-18.361	10.254	-124.000
Average (%) of error				-0.775	4.996	-2.583	-14.402
Total average prediction error (%) = -12.764							

APPENDIX 39

Table 5.11: Testing of the Developed Model with Experimental Data

Process Parameters				MRR (mm^3/min)		OC(µm)		RCL(µm)		TA(degrees)	
V	I_p	T_{on}	T_{off}	Exp	ANN	Exp	ANN	Exp	ANN	Exp	ANN
60	10	80	30	0.397	0.389	0.362	0.347	87.439	95.684	1.373	1.340
30	40	40	20	0.483	0.484	0.352	0.337	77.054	79.604	2.052	2.520
60	40	80	20	0.580	0.565	0.344	0.333	114.950	110.442	1.070	1.421
45	25	60	25	0.377	0.373	0.326	0.320	75.237	80.649	1.236	1.187
30	10	40	30	0.448	0.454	0.318	0.316	112.343	109.654	2.544	2.463
30	10	40	20	0.440	0.446	0.307	0.306	122.819	120.627	0.234	0.213
45	25	60	25	0.427	0.449	0.300	0.299	93.282	85.801	3.974	3.810
60	40	40	20	0.523	0.529	0.300	0.311	102.958	103.240	0.119	0.210
45	40	60	25	0.333	0.356	0.292	0.295	54.007	56.167	3.151	2.835
45	25	60	25	0.435	0.428	0.290	0.294	81.125	83.526	0.652	0.934

Table 5.12: Errors in Prediction of Responses during Testing

(V)	(I_p)	(T_{on})	(T_{off})	% Error in Prediction of MRR	% Error in Prediction of OC	% Error in Prediction of RCL	% Error in Prediction of TA
60	10	80	30	1.988	4.114	-9.429	2.396
30	40	40	20	-0.202	4.390	-3.310	-22.795
60	40	80	20	2.670	3.243	3.922	-32.790
45	25	60	25	1.178	1.983	-7.193	3.962
30	10	40	30	-1.425	0.762	2.394	3.204
30	10	40	20	-1.283	0.477	1.785	8.928
45	25	60	25	-5.190	0.377	8.019	4.120
60	40	40	20	-1.076	-3.647	-0.273	-76.700
45	40	60	25	-6.804	-0.975	-3.999	10.016
45	25	60	25	1.543	-1.440	-2.959	-43.195
Average (%) of error				-0.860	0.928	-1.104	-14.285
Total average prediction error (%) = -15.322							

APPENDIX 40

Table 5.15: Testing of the developed model with experimental data.

Process Parameters				MRR (mm^3/min)		OC(μm)		RCL(μm)		TA(degrees)	
V	I_p	T_{on}	T_{off}	Exp	ANFIS	Exp	ANFIS	Exp	ANFIS	Exp	ANFIS
60	10	80	30	0.397	0.397	0.362	0.362	87.439	87.346	1.373	1.371
30	40	40	20	0.483	0.483	0.352	0.352	77.054	77.032	2.052	2.054
60	40	80	20	0.580	0.580	0.344	0.344	114.950	114.949	1.070	1.070
45	25	60	25	0.377	0.388	0.326	0.297	75.237	79.477	1.236	1.669
30	10	40	30	0.448	0.448	0.318	0.318	112.343	112.201	2.544	2.541
30	10	40	20	0.440	0.440	0.307	0.307	122.819	122.840	0.234	0.232
45	25	60	25	0.427	0.388	0.300	0.297	93.282	79.477	3.974	1.669
60	40	40	20	0.523	0.523	0.300	0.300	102.958	102.957	0.119	0.119
45	40	60	25	0.333	0.392	0.292	0.300	54.007	53.859	3.151	3.231
45	25	60	25	0.435	0.388	0.290	0.297	81.125	79.477	0.652	1.669

Table 5.16: Errors in Prediction of Responses during testing

(V)	(I_p)	(T_{on})	(T_{off})	% Error in Prediction of MRR	% Error in Prediction of OC	% Error in Prediction of RCL	% Error in Prediction of TA
60	10	80	30	0.000	0.000	0.106	0.138
30	40	40	20	0.000	0.000	0.029	-0.078
60	40	80	20	0.000	0.000	0.001	0.000
45	25	60	25	-2.918	8.896	-5.635	-35.032
30	10	40	30	0.000	0.000	0.126	0.110
30	10	40	20	0.000	0.000	-0.017	0.684
45	25	60	25	9.133	1.000	14.799	58.002
60	40	40	20	0.000	0.000	0.001	0.000
45	40	60	25	-17.568	-2.705	0.275	-2.548
45	25	60	25	10.805	-2.414	2.032	-155.982
Average (%) of error				1.565	-0.522	1.740	-16.974
Total average prediction error (%) = -14.191							

APPENDIX 41

Table 5. 17: Pareto-optimal solutions obtained from MOETLBO

V	I_p	T_{on}	T_{off}	MRR	OC	RCL	TA	Rank
30.000	10.000	40.000	20.000	0.597	0.162	106.020	0.311	1
30.000	10.000	40.000	20.000	0.597	0.162	106.020	0.311	2
30.016	10.043	40.063	20.059	0.596	0.162	105.883	0.294	3
30.309	12.077	40.540	20.002	0.562	0.169	103.934	0.412	4
30.921	14.355	40.123	20.130	0.530	0.178	101.559	0.431	5
30.018	16.310	40.023	20.000	0.502	0.182	99.708	0.648	6
30.023	17.130	40.220	20.000	0.494	0.185	98.896	0.655	7
30.093	17.533	40.316	20.432	0.490	0.189	97.856	0.522	8
30.161	19.358	40.439	20.838	0.473	0.198	95.446	0.387	9
31.010	20.881	43.025	21.106	0.470	0.205	93.893	0.136	10
30.738	22.432	43.498	21.282	0.460	0.210	92.204	0.048	11
30.926	24.798	43.516	21.453	0.454	0.218	89.775	0.151	12
30.995	25.404	45.411	21.788	0.455	0.222	89.050	0.324	13
30.791	23.767	43.665	24.031	0.452	0.229	86.886	0.764	14
30.141	26.293	42.385	23.816	0.438	0.232	84.522	0.841	15
58.745	37.066	72.463	27.297	0.931	0.309	82.353	0.494	16
33.752	33.516	43.577	22.687	0.510	0.249	80.187	1.609	17
43.861	33.565	45.253	24.278	0.635	0.268	79.621	1.818	18
58.584	39.908	76.348	29.181	1.004	0.313	79.839	0.699	19
59.962	39.974	76.468	29.136	1.027	0.315	80.107	0.415	20
59.984	39.948	76.514	29.166	1.027	0.315	80.089	0.404	21
51.616	33.638	46.086	26.076	0.729	0.284	78.312	1.445	22
57.524	37.513	58.222	29.175	0.898	0.305	76.052	1.035	23
30.028	28.539	41.587	29.467	0.421	0.257	73.655	2.655	24
49.748	38.827	57.412	29.152	0.811	0.291	73.828	2.524	25
59.405	38.514	53.916	28.258	0.947	0.308	75.373	0.818	26
42.980	38.648	46.365	26.040	0.700	0.277	72.958	2.963	27
46.359	39.688	59.972	29.813	0.779	0.285	72.786	3.118	28
46.040	39.438	53.700	29.846	0.758	0.284	70.505	3.284	29
43.530	38.299	45.839	28.862	0.688	0.278	69.087	3.391	30
40.427	39.386	44.984	29.467	0.656	0.273	66.397	4.003	31
30.353	38.317	41.431	28.978	0.482	0.255	64.898	4.169	32
32.941	39.311	44.004	29.955	0.534	0.260	64.147	4.543	33
31.924	38.406	41.438	29.483	0.504	0.258	64.291	4.312	34
32.572	39.286	40.992	29.985	0.522	0.259	62.555	4.639	35

APPENDIX 42

Table 5. 18: Pareto-optimal solutions obtained from MODE

V	I_p	T_{on}	T_{off}	MRR	OC	RCL	TA	Rank
30.000	10.000	40.000	20.000	0.497	0.172	103.020	1.689	1
30.000	10.000	40.000	20.000	0.497	0.172	103.020	1.689	2
30.000	11.000	40.000	20.000	0.479	0.175	102.019	1.606	3
30.000	12.723	40.020	20.001	0.451	0.180	100.293	1.489	4
30.000	17.525	40.092	20.003	0.389	0.196	95.490	1.337	5
30.436	18.654	40.040	20.238	0.380	0.202	94.050	1.455	6
30.396	19.270	40.062	20.955	0.374	0.209	92.351	1.663	7
33.000	22.923	40.128	20.297	0.372	0.218	89.970	1.825	8
30.017	24.533	40.174	20.453	0.345	0.221	87.831	1.700	9
30.320	25.829	40.588	20.796	0.345	0.227	86.144	1.936	10
30.320	25.829	40.588	21.796	0.342	0.232	84.638	2.223	11
31.281	30.278	42.190	21.703	0.361	0.244	80.971	2.767	12
46.146	34.912	40.281	20.527	0.594	0.278	79.096	3.046	13
50.410	35.584	44.360	22.775	0.659	0.291	77.375	3.275	14
49.702	37.575	44.021	21.803	0.694	0.295	76.692	3.441	15
59.847	33.161	64.877	28.871	0.743	0.315	77.820	2.073	16
58.851	38.223	67.304	29.558	0.848	0.320	74.952	2.639	17
59.851	38.223	67.304	29.558	0.863	0.321	75.102	2.431	18
54.294	38.260	64.964	29.496	0.778	0.311	73.721	3.565	19
59.851	39.973	67.304	29.558	0.910	0.323	74.336	2.642	20
54.294	39.260	64.964	29.496	0.802	0.311	73.235	3.703	21
59.851	39.973	66.304	29.558	0.908	0.323	74.046	2.667	22
30.117	28.295	40.447	29.591	0.319	0.268	70.388	4.694	23
39.045	34.886	41.854	27.090	0.474	0.276	69.438	4.839	24
40.134	34.608	40.450	28.039	0.479	0.279	67.897	4.988	25
33.107	37.800	47.474	27.831	0.433	0.270	67.219	5.623	26
44.329	35.731	41.063	29.629	0.546	0.289	65.372	5.177	27
45.669	39.178	45.604	29.193	0.636	0.292	65.049	5.384	28
39.806	37.941	41.459	29.464	0.516	0.281	62.962	5.864	29
32.872	38.526	41.460	28.662	0.424	0.269	62.552	6.096	30
41.316	39.516	42.206	29.260	0.568	0.284	62.335	5.977	31
31.916	38.890	42.911	29.693	0.412	0.268	61.237	6.437	32
32.547	39.271	41.467	29.463	0.425	0.269	60.589	6.482	33
31.850	39.605	41.093	29.835	0.416	0.267	59.411	6.686	34
30.655	39.882	40.645	29.961	0.399	0.265	58.532	6.822	35

APPENDIX 43

Table 5. 19: Pareto-optimal solutions obtained from MOABC

V	I_p	T_{on}	T_{off}	MRR	OC	RCL	TA	Rank
30.000	10.000	40.000	20.000	0.597	0.212	93.020	3.689	1
30.000	10.000	40.000	20.000	0.597	0.212	93.020	3.689	2
32.904	10.936	44.108	20.030	0.589	0.217	91.895	4.130	3
30.014	13.800	40.003	20.000	0.535	0.224	89.219	3.433	4
30.514	13.800	40.003	20.500	0.536	0.229	88.516	3.645	5
30.015	16.707	40.002	20.000	0.498	0.233	86.311	3.344	6
30.016	17.634	40.000	20.000	0.488	0.236	85.383	3.335	7
30.016	18.134	40.615	20.500	0.484	0.242	84.165	3.494	8
30.285	19.121	40.039	20.938	0.475	0.248	82.512	3.644	9
30.168	18.467	40.071	22.225	0.479	0.256	81.214	4.000	10
30.613	23.427	42.477	21.286	0.454	0.263	78.112	3.971	11
49.246	27.267	42.589	22.552	0.622	0.303	74.729	4.698	12
39.210	28.096	40.218	20.776	0.533	0.285	74.773	4.556	13
55.066	30.904	41.335	21.529	0.732	0.319	72.968	4.158	14
31.026	25.784	40.322	23.852	0.444	0.282	71.611	4.854	15
32.454	25.286	40.539	25.620	0.453	0.292	69.682	5.392	16
56.516	31.361	43.335	24.025	0.751	0.330	69.907	4.382	17
30.794	28.718	41.056	25.557	0.439	0.294	66.312	5.611	18
54.194	34.051	46.364	24.901	0.774	0.336	66.996	4.996	19
59.991	39.898	45.361	20.721	1.017	0.362	67.783	4.243	20
32.465	26.688	40.380	28.030	0.446	0.304	64.651	6.168	21
53.464	36.430	41.800	24.088	0.811	0.339	64.071	5.204	22
41.058	36.087	40.279	23.558	0.630	0.317	62.994	6.122	23
42.842	36.978	41.857	24.090	0.670	0.323	62.265	6.302	24
30.008	28.172	40.284	29.977	0.417	0.309	59.864	6.793	25
54.927	38.597	46.569	27.641	0.873	0.348	59.489	5.727	26
54.427	39.097	46.069	27.641	0.877	0.348	58.758	5.887	27
59.314	39.229	46.113	27.598	0.956	0.357	59.407	4.996	28
31.886	35.713	40.754	27.175	0.484	0.306	57.056	7.146	29
56.981	39.642	43.446	27.362	0.928	0.353	57.756	5.512	30
42.966	39.430	43.419	29.804	0.692	0.327	52.491	7.892	31
36.147	38.722	40.502	29.449	0.571	0.315	51.196	8.253	32
33.749	39.762	41.722	29.489	0.551	0.311	50.386	8.557	33
32.408	39.938	40.235	29.964	0.527	0.308	48.518	8.807	34
32.408	39.938	40.235	29.964	0.527	0.308	48.518	8.807	35

APPENDIX 44

Table 5.20: Optimization results

Response	MOETLBO			MODE			MOABC		
	Best	Mean	Worst	Best	Mean	Worst	Best	Mean	Worst
MRR (mm^3/min)	0.597	0.632	0.522	0.497	0.534	0.399	0.597	0.613	0.527
OC(µm)	0.162	0.244	0.259	0.172	0.260	0.265	0.212	0.293	0.308
RCL(µm)	106.020	83.391	62.555	103.020	77.404	58.532	93.020	69.873	48.518
TA(degree)	0.311	1.559	4.639	1.689	3.598	6.822	3.689	5.298	8.807

APPENDIX 45

Table 5. 21: Design matrix and experimental results

S. No	Parameters				Material Removal Rate (MRR) in mm^3/min	Overcut (OC) in µm	Recast layer thickness (RCL) in µm	Taper Angle (TA) in degrees
	Voltage (V)	Peak current (I_p)	Pulse on duration (T_{on})	Pulse off duration (T_{off})				
1	30	10	80	20	0.207	0.195	88.627	2.524
2	30	40	40	20	0.918	0.427	82.833	3.158
3	30	10	80	30	0.665	0.322	110.306	3.772
4	30	40	80	20	0.387	0.245	100.224	3.032
5	30	10	40	30	0.852	0.373	97.143	4.034
6	30	40	40	30	0.497	0.272	78.997	3.337
7	30	25	60	25	0.270	0.233	70.731	2.178
8	30	10	40	20	0.837	0.418	132.030	1.090
9	30	40	80	30	0.409	0.263	105.703	4.816
10	45	25	60	25	0.812	0.389	85.682	3.100
11	45	25	60	25	0.775	0.412	104.820	1.056
12	45	25	60	25	0.826	0.358	92.185	1.257
13	45	25	60	25	0.879	0.315	91.680	2.568
14	45	25	60	25	0.715	0.357	93.680	2.157
15	45	25	60	25	0.531	0.318	72.990	3.877
16	45	25	60	20	0.411	0.315	81.887	4.656
17	45	25	40	25	0.539	0.310	79.136	3.056
18	45	40	60	25	0.632	0.358	58.058	5.149
19	45	25	80	25	0.499	0.295	77.663	3.140
20	45	10	60	25	0.591	0.308	77.026	4.326
21	45	25	60	30	0.505	0.344	67.100	5.750
22	60	40	40	30	0.725	0.232	64.802	4.786
23	60	10	80	30	0.755	0.434	93.997	2.640
24	60	25	60	25	0.513	0.277	79.188	2.606
25	60	10	80	20	0.465	0.221	119.736	1.930
26	60	40	40	20	0.994	0.403	106.055	3.846
27	60	10	40	20	0.457	0.243	149.387	3.243
28	60	10	40	30	0.624	0.282	90.709	3.647
29	60	40	80	30	1.275	0.526	105.259	3.520
30	60	40	80	20	1.101	0.423	123.571	2.275

APPENDIX 46

Table 5. 23: ANOVA for OC (After elimination)

Source	Sum of Squares	DOF	Mean Square	F Value	p-value Prob > F	Percentage Contribution
Model	0.14	9	0.016	12.88	< 0.0001	82.353
C-Pulse on time	0.064	1	0.064	51.85	< 0.0001	37.647
D-Pulse off time	0.011	1	0.011	9.36	0.0062	6.471
AB	0.022	1	0.022	17.73	0.0004	12.941
AC	0.040	1	0.040	32.75	< 0.0001	23.529
AD	6.319E-003	1	6.319E-003	5.15	0.0345	3.717
BD	0.029	1	0.029	23.25	0.0001	17.059
CD	0.030	1	0.030	24.32	< 0.0001	17.647
A^2	0.044	1	0.044	35.50	< 0.0001	25.882
B^2	9.490E-003	1	9.490E-003	7.73	0.0116	5.582
Residual	0.025	20	1.228E-003			
Lack of Fit	0.018	15	1.189E-003	0.88	0.6146	Insignificant
Pure Error	6.732E-003	5	1.346E-003			
Corrected Total	0.17	29			R-Squared	0.8529
					Adj R-Squared	0.7866
					Pred R-Squared	0.7549

APPENDIX 47

Table 5.24: ANOVA for RCL (After elimination)

Source	Sum of Squares	DOF	Mean Square	F Value	p-value Prob > F	Percentage Contribution
Model	9138.38	7	1305.48	9.51	< 0.0001	75.162
B-Peak Current	1954.21	1	1954.21	14.24	0.0010	16.073
C-Pulse on time	2739.41	1	2739.41	19.96	0.0002	22.531
AD	3586.37	1	3586.37	26.13	< 0.0001	29.497
BC	1195.43	1	1195.43	8.71	0.0074	9.832
CD	2131.89	1	2131.89	15.53	0.0007	17.534
A^2	3900.56	1	3900.56	28.42	< 0.0001	32.081
C^2	811.89	1	811.89	5.91	0.0236	6.678
Residual	3019.94	22	137.27			
Lack of Fit	2160.81	17	127.11	0.74	0.7093	
Pure Error	859.13	5	171.83			
Corrected Total	12158.32	29			R-Squared	0.7516
					Adj R-Squared	0.6726
					Pred R-Squared	0.6327

APPENDIX 48

Table 5. 25: ANOVA for TA (After elimination)

Source	Sum of Squares	DOF	Mean Square	F Value	p-value Prob > F	Percentage Contribution
Model	29.67	9	3.30	21.30	< 0.0001	90.540
A-Voltage	9.93	1	9.93	64.12	< 0.0001	30.302
B-Peak Current	0.92	1	0.92	5.96	0.0241	2.807
C-Pulse on time	3.97	1	3.97	25.67	< 0.0001	12.115
D-Pulse off time	3.33	1	3.33	21.53	0.0002	10.162
AC	7.54	1	7.54	48.70	< 0.0001	23.009
A^2	6.81	1	6.81	44.00	< 0.0001	20.781
B^2	1.36	1	1.36	8.77	0.0077	4.150
C^2	2.17	1	2.17	14.03	0.0013	6.622
D^2	3.67	1	3.67	23.69	< 0.0001	11.199
Residual	3.10	20	0.15			90.540
Lack of Fit	2.29	15	0.15	0.95	0.5775	Insignificant
Pure Error	0.81	5	0.16			
Corrected Total	32.77	29			R-Squared	0.9055
					Adj R-Squared	0.8630
					Pred R-Squared	0.7907

APPENDIX 49

Table 5.26: Training data sets

S. No	Parameters				(MRR) in mm^3/min	(OC) in µm	RCL) in µm	(TA)in degrees
	Voltage (V)	Peak current (I_p)	Pulse on duration (T_{on})	Pulse off duration (T_{off})				
1	60	40	80	30	1.275	0.526	105.259	3.52
2	60	10	80	30	0.755	0.434	93.997	2.64
3	30	40	40	20	0.918	0.427	82.833	3.158
4	60	40	80	20	1.101	0.423	123.571	2.275
5	30	10	40	20	0.837	0.418	132.03	1.09
6	45	25	60	25	0.775	0.412	104.82	1.056
7	60	40	40	20	0.994	0.403	106.055	3.846
8	45	25	60	25	0.812	0.389	85.682	3.1
9	30	10	40	30	0.852	0.373	97.143	4.034
10	45	25	60	25	0.826	0.358	92.185	1.257
11	45	40	60	25	0.632	0.358	58.058	5.149
12	45	25	60	25	0.715	0.357	93.68	2.157
13	45	25	60	30	0.505	0.344	67.1	5.75
14	30	10	80	30	0.665	0.322	110.306	3.772
15	45	25	60	25	0.531	0.318	72.99	3.877
16	45	25	60	25	0.879	0.315	91.68	2.568
17	45	25	60	20	0.411	0.315	81.887	4.656
18	45	25	40	25	0.539	0.31	79.136	3.056
19	45	10	60	25	0.591	0.308	77.026	4.326
20	45	25	80	25	0.499	0.295	77.663	3.14

APPENDIX 50

Table 5.27: Validation of the Developed Model with Experimental Data.

Process Parameters				MRR (mm^3/min)		OC(µm)		RCL(µm)		TA(degrees)	
V	I_p	T_{on}	T_{off}	Exp	ANN	Exp	ANN	Exp	ANN	Exp	ANN
60	10	40	30	0.624	0.577	0.282	0.261	90.709	107.765	3.647	2.242
60	25	60	25	0.513	0.572	0.277	0.266	79.188	73.584	2.606	2.123
30	40	40	30	0.497	0.539	0.272	0.273	78.997	75.828	3.337	2.726
30	40	80	30	0.409	0.598	0.263	0.277	105.703	69.250	4.816	4.673
30	40	80	20	0.387	0.430	0.245	0.232	100.224	68.315	3.032	2.588
60	10	40	20	0.457	0.479	0.243	0.243	149.387	148.476	3.243	2.095
30	25	60	25	0.270	0.539	0.233	0.219	70.731	79.125	2.178	2.007
60	40	40	30	0.725	0.694	0.232	0.257	64.802	66.800	4.786	4.557
60	10	80	20	0.465	0.401	0.221	0.220	119.736	110.419	1.930	2.026
30	10	80	20	0.207	0.280	0.195	0.200	88.627	96.269	2.524	2.162

Table 5.28: Errors in Prediction of Responses

(V)	(I_p)	(T_{on})	(T_{off})	% Error in Prediction of MRR	% Error in Prediction of OC	% Error in Prediction of RCL	% Error in Prediction of TA
60	10	40	30	7.468	7.390	-18.803	38.527
60	25	60	25	-11.495	4.011	7.077	18.536
30	40	40	30	-8.439	-0.403	4.012	18.322
30	40	80	30	-46.249	-5.417	34.487	2.963
30	40	80	20	-11.156	5.446	31.837	14.635
60	10	40	20	-4.830	-0.103	0.610	35.387
30	25	60	25	-99.757	5.990	-11.867	7.862
60	40	40	30	4.323	-10.694	-3.083	4.790
60	10	80	20	13.861	0.407	7.782	-4.969
30	10	80	20	-35.228	-2.719	-8.622	14.323
Average (%) of error				-19.150	0.391	4.343	15.038
Total average prediction error (%) = 0.621							

APPENDIX 51

Table 5.29: Testing of the Developed Model with Experimental Data.

Process Parameters				MRR (mm^3/min)		OC(μm)		RCL(μm)		TA(degrees)	
V	I_p	T_{on}	T_{off}	Exp	ANN	Exp	ANN	Exp	ANN	Exp	ANN
60	10	80	20	0.465	0.425	0.221	0.245	119.736	117.111	1.930	2.232
30	10	80	30	0.665	0.676	0.322	0.279	110.306	114.834	3.772	3.556
60	40	40	20	0.994	0.929	0.403	0.379	106.055	108.218	3.846	3.523
30	40	80	30	0.409	0.458	0.263	0.349	105.703	99.182	4.816	4.790
60	40	80	30	1.275	1.258	0.526	0.521	105.259	105.003	3.520	3.795
45	25	60	25	0.775	0.704	0.412	0.410	104.820	107.619	1.056	1.147
30	40	80	20	0.387	0.397	0.245	0.249	100.224	99.757	3.032	2.927
30	10	40	30	0.852	0.755	0.373	0.313	97.143	109.321	4.034	3.896
60	10	80	30	0.755	0.752	0.434	0.460	93.997	98.354	2.640	3.014
45	25	60	25	0.715	0.798	0.357	0.336	93.680	96.893	2.157	2.151

Table 5.30: Errors in Prediction of Responses during Testing

(V)	(I_p)	(T_{on})	(T_{off})	% Error in Prediction of MRR	% Error in Prediction of OC	% Error in Prediction of RCL	% Error in Prediction of TA
60	10	80	20	8.662	-10.853	2.193	-15.630
30	10	80	30	-1.603	13.509	-4.105	5.737
60	40	40	20	6.503	5.893	-2.040	8.388
30	40	80	30	-12.000	-32.764	6.169	0.545
60	40	80	30	1.311	0.866	0.243	-7.825
45	25	60	25	9.183	0.426	-2.671	-8.609
30	40	80	20	-2.578	-1.786	0.466	3.471
30	10	40	30	11.333	16.165	-12.536	3.430
60	10	80	30	0.358	-6.000	-4.635	-14.156
45	25	60	25	-11.611	5.918	-3.430	0.295
Average (%) of error				0.956	-0.863	-2.035	-2.436
Total average prediction error (%) = -4.377							

APPENDIX 52

Table 5.31: Training and validation error

Type of membership function	MRR		OC		RCL		TA	
	Training error	Validation error	Training error	Validation error	Training error	Validation error	Training error	Validation error
Triangle	0.10739	0.10738	0.024679	0.024678	8.3549	8.3541	1.0074	1.0071
Trapezoid	0.099189	0.099185	0.02413	0.024129	7.579	7.568	0.90177	0.90166
Generalized bell	0.096482	0.096448	0.02068	0.02068	6.3901	6.3901	0.83827	0.83787
Gaussian	0.099437	0.099434	0.024129	0.024127	7.4924	7.4894	0.90602	0.90589

Table 5.32: TAE for process responses

Type of membership function	MRR	OC	RCL	TA
	Total Average error	Total Average error	Total Average error	Total Average error
Triangle	0.107385	0.024679	8.3545	1.00725
Trapezoid	0.099187	0.02413	7.5735	0.901715
Generalized bell	0.096465	0.02068	6.3901	0.83807
Gaussian	0.099436	0.024128	7.4909	0.905955

APPENDIX 53

Table 5.33: Testing of the developed model with experimental data.

Process Parameters				MRR (mm^3/min)		OC(µm)		RCL(µm)		TA(degrees)	
V	I_p	T_{on}	T_{off}	Exp	ANFIS	Exp	ANFIS	Exp	ANFIS	Exp	ANFIS
60	10	80	20	0.465	0.567	0.221	0.218	119.736	116.555	1.930	1.901
30	10	80	30	0.665	0.665	0.322	0.332	110.306	110.318	3.772	3.772
60	40	40	20	0.994	0.994	0.403	0.410	106.055	105.961	3.846	3.846
30	40	80	30	0.409	0.400	0.263	0.267	105.703	108.142	4.816	5.342
60	40	80	30	1.275	1.275	0.526	0.526	105.259	105.226	3.520	3.520
45	25	60	25	0.775	0.756	0.412	0.401	104.820	106.092	1.056	1.098
30	40	80	20	0.387	0.397	0.245	0.260	100.224	96.251	3.032	3.218
30	10	40	30	0.852	0.852	0.373	0.361	97.143	97.143	4.034	4.034
60	10	80	30	0.755	0.755	0.434	0.432	93.997	94.043	2.640	2.640
45	25	60	25	0.715	0.756	0.357	0.351	93.680	86.092	2.157	2.980

Table 5.34: Errors in Prediction of Responses during testing

(V)	(I_p)	(T_{on})	(T_{off})	% Error in Prediction of MRR	% Error in Prediction of OC	% Error in Prediction of RCL	% Error in Prediction of TA
60	10	80	20	-21.935	1.357	2.656	1.503
30	10	80	30	0.000	-3.230	-0.011	0.000
60	40	40	20	0.000	-1.687	0.089	0.000
30	40	80	30	2.200	-1.521	-2.307	-10.912
60	40	80	30	0.000	0.000	0.032	0.000
45	25	60	25	2.413	2.646	-1.214	-3.974
30	40	80	20	-2.584	-6.171	3.964	-6.121
30	10	40	30	0.000	3.351	0.000	0.000
60	10	80	30	0.000	0.484	-0.048	0.000
45	25	60	25	-5.776	1.653	8.100	-38.141
Average (%) of error				-2.568	-0.312	1.126	-5.765
Total average prediction error (%) = -7.519							

APPENDIX 54

Table 5.35: Pareto-optimal solutions obtained from MOETLBO

V	I_p	T_{on}	Toff	MRR	OC	RCL	TA	Rank
59.849	15.088	75.367	20.779	0.478	0.252	97.111	1.708	1
59.292	18.177	73.308	21.804	0.508	0.281	95.442	1.704	2
59.864	23.952	79.850	20.353	0.577	0.286	94.495	1.264	3
58.352	20.959	79.315	21.574	0.537	0.294	93.477	1.314	4
30.107	23.677	79.997	20.044	0.430	0.180	91.869	2.279	5
30.108	23.673	79.998	20.046	0.430	0.180	91.867	2.278	6
30.104	31.093	71.809	20.470	0.408	0.239	90.001	2.751	7
30.277	22.875	79.702	21.563	0.431	0.195	89.973	1.873	8
30.254	26.575	76.357	21.627	0.419	0.213	89.587	2.106	9
30.013	20.785	40.535	24.026	0.402	0.342	89.220	0.158	10
30.029	21.479	40.829	24.053	0.401	0.341	88.534	0.201	11
30.091	26.412	67.123	24.515	0.405	0.256	86.014	2.017	12
30.141	27.624	71.935	25.377	0.404	0.245	84.243	2.130	13
30.305	33.200	75.506	25.523	0.390	0.242	82.418	2.435	14
30.035	23.884	43.645	25.942	0.390	0.316	83.819	0.771	15
30.179	33.536	67.787	26.987	0.376	0.259	79.442	2.907	16
30.021	26.989	40.681	24.735	0.382	0.333	82.051	0.340	17
30.082	31.847	74.862	28.440	0.382	0.247	78.622	3.181	18
30.031	27.950	40.831	25.178	0.377	0.328	80.476	0.450	19
30.547	32.056	63.847	28.490	0.375	0.266	77.458	3.391	20
30.050	27.815	41.737	27.029	0.372	0.308	78.066	0.957	21
30.449	39.071	70.014	29.418	0.350	0.260	74.203	4.513	22
30.035	28.004	40.792	28.840	0.363	0.290	74.895	1.550	23
30.584	34.952	56.282	29.943	0.351	0.267	72.007	4.117	24
30.234	39.394	61.521	29.987	0.335	0.262	70.785	4.744	25
30.248	39.330	60.078	29.993	0.334	0.263	70.332	4.697	26
30.029	38.390	40.468	24.115	0.350	0.362	71.635	1.159	27
30.207	36.675	48.682	29.904	0.333	0.269	68.158	3.638	28
30.093	39.292	51.352	29.983	0.324	0.267	67.029	4.165	29
30.010	34.262	40.511	29.686	0.334	0.275	67.340	2.363	30
30.107	39.274	47.901	29.986	0.320	0.269	65.535	3.879	31
30.022	37.941	41.297	29.200	0.323	0.283	64.816	2.568	32
30.118	39.528	42.233	29.997	0.314	0.273	62.566	3.326	33
30.003	39.514	40.420	29.997	0.311	0.273	61.622	3.073	34
30.002	39.514	40.412	29.994	0.311	0.273	61.623	3.069	35

APPENDIX 55

Table 5.36: Pareto-optimal solutions obtained from MODE

V	Ip	T_{on}	T_{off}	MRR	OC	RCL	TA	Rank
59.674	12.398	78.207	20.297	0.550	0.346	94.298	0.714	1
59.706	12.409	78.207	20.314	0.551	0.346	94.279	0.701	2
59.344	16.843	75.317	21.500	0.596	0.382	92.689	0.590	3
59.717	19.160	75.944	21.513	0.621	0.390	91.929	0.396	4
30.081	18.481	77.913	20.085	0.540	0.296	90.334	1.353	5
59.773	22.695	78.528	20.823	0.661	0.396	91.399	0.278	6
59.297	20.402	79.152	21.754	0.635	0.402	90.502	0.079	7
59.975	24.668	79.224	21.822	0.682	0.422	89.657	0.056	8
30.414	25.022	77.499	21.514	0.525	0.317	86.998	1.062	9
30.065	21.619	40.091	23.536	0.501	0.457	86.078	0.878	10
30.035	23.772	45.865	24.388	0.497	0.431	83.575	0.190	11
30.427	25.401	55.073	25.705	0.498	0.401	81.424	0.830	12
30.044	27.653	40.055	23.406	0.484	0.459	80.236	0.732	13
30.081	27.954	41.202	24.622	0.480	0.443	78.416	0.546	14
30.083	36.358	64.309	25.598	0.468	0.384	76.473	1.793	15
30.043	28.696	40.028	24.614	0.477	0.447	77.363	0.668	16
30.023	28.779	40.048	25.932	0.471	0.432	75.295	0.488	17
30.178	34.096	60.928	29.234	0.458	0.373	71.685	2.755	18
30.233	37.571	65.051	28.878	0.451	0.373	71.360	3.021	19
30.224	38.951	61.516	28.990	0.442	0.377	69.469	3.155	20
30.100	32.460	40.777	25.557	0.462	0.438	72.459	0.208	21
30.087	33.572	53.264	29.583	0.451	0.377	69.563	2.496	22
30.098	39.461	61.966	29.514	0.436	0.373	68.556	3.469	23
30.300	39.298	61.225	29.994	0.436	0.372	67.742	3.743	24
30.316	39.970	61.712	29.998	0.434	0.373	67.525	3.845	25
30.025	30.706	40.075	27.383	0.458	0.416	71.187	0.016	26
30.248	39.610	40.149	22.231	0.460	0.508	70.130	0.444	27
30.049	39.185	54.272	29.868	0.427	0.375	65.455	3.276	28
30.236	39.724	53.992	29.994	0.426	0.377	64.805	3.442	29
30.027	38.978	48.703	29.933	0.422	0.378	63.205	2.864	30
30.217	39.969	48.762	29.997	0.420	0.380	62.352	3.075	31
30.198	39.718	44.596	29.997	0.416	0.382	60.586	2.635	32
30.061	39.967	41.766	29.987	0.411	0.383	58.911	2.303	33
30.059	39.967	40.847	29.987	0.410	0.384	58.425	2.191	34
30.013	39.973	40.022	29.994	0.409	0.384	57.960	2.079	35

APPENDIX 56

Table 5.37: Pareto-optimal solutions obtained from MOABC

V	I_p	T_{on}	T_{off}	MRR	OC	RCL	TA	Rank
30.336	17.632	79.820	20.031	0.344	2.288	99.030	3.338	1
30.630	20.006	54.140	24.730	0.316	2.412	95.619	2.626	2
30.564	20.477	59.440	25.317	0.318	2.396	94.249	2.939	3
30.118	21.311	48.533	24.509	0.306	2.424	94.762	2.063	4
30.247	26.978	65.363	23.716	0.305	2.372	92.908	3.039	5
30.255	32.690	78.149	22.835	0.302	2.334	92.400	3.193	6
30.166	24.013	40.473	23.784	0.294	2.453	92.399	1.226	7
30.109	23.848	44.405	25.268	0.293	2.430	90.990	1.760	8
30.502	24.506	42.785	25.256	0.292	2.435	90.178	1.698	9
31.245	26.332	73.294	27.795	0.310	2.373	87.349	3.888	10
30.191	27.747	43.942	25.604	0.280	2.427	86.842	1.910	11
30.045	29.375	41.014	23.909	0.278	2.452	87.042	1.465	12
30.548	37.799	69.093	27.259	0.265	2.376	83.573	4.474	13
30.227	29.315	55.051	28.084	0.276	2.387	84.209	3.637	14
30.278	32.978	71.822	29.278	0.274	2.364	82.896	4.780	15
30.385	37.718	68.726	27.668	0.261	2.374	82.921	4.575	16
30.531	30.878	64.953	29.858	0.275	2.373	82.226	5.017	17
30.450	36.295	62.333	27.780	0.261	2.382	81.938	4.416	18
30.466	36.635	69.346	29.343	0.259	2.369	81.112	5.215	19
30.037	29.760	41.275	25.192	0.272	2.438	84.812	1.603	20
30.211	30.942	56.207	29.140	0.267	2.380	81.776	4.275	21
30.505	39.014	69.973	29.790	0.249	2.370	79.695	5.722	22
30.255	39.014	69.973	29.977	0.245	2.366	79.391	5.779	23
30.721	29.839	40.646	26.362	0.272	2.430	82.869	1.928	24
30.084	36.244	51.108	28.178	0.245	2.392	77.941	3.911	25
30.106	38.569	56.387	29.832	0.232	2.374	75.730	5.320	26
30.350	39.040	56.830	29.950	0.233	2.376	75.446	5.522	27
30.041	38.044	40.693	23.614	0.254	2.477	78.843	2.151	28
30.415	39.732	56.045	29.920	0.231	2.378	74.747	5.562	29
30.053	38.438	45.620	29.792	0.222	2.382	71.501	4.435	30
30.187	39.459	43.196	27.674	0.230	2.416	72.611	3.345	31
30.044	39.143	43.936	29.968	0.216	2.381	69.808	4.437	32
30.031	39.899	40.877	29.157	0.215	2.397	68.754	3.727	33
30.018	39.926	41.192	29.986	0.210	2.383	67.644	4.216	34
30.018	39.926	40.192	29.986	0.209	2.384	67.112	4.092	35

APPENDIX 57

Table 5. 40: Design matrix with output responses

S. No	Parameters				Material Removal Rate (MRR) in mm^3/min	Overcut (OC) in µm	Recast layer thickness (RCL) in µm	Taper Angle (TA) in degrees
	Voltage (V)	Peak current (I_p)	Pulse on duration (T_{on})	Pulse off duration (T_{off})				
1	30	10	80	20	0.217	0.114	98.811	0.852
2	30	40	40	20	0.964	0.370	88.612	2.283
3	30	10	80	30	0.699	0.273	118.002	1.496
4	30	40	80	20	0.895	0.334	129.194	2.830
5	30	10	40	30	0.406	0.209	130.942	3.094
6	30	40	40	30	0.522	0.265	94.509	2.676
7	30	25	60	25	0.283	0.177	102.665	1.507
8	30	10	40	20	0.879	0.322	141.242	0.261
9	30	40	80	30	0.429	0.251	113.077	4.040
10	45	25	60	25	0.557	0.240	108.083	1.095
11	45	25	60	25	0.852	0.315	107.274	1.084
12	45	25	60	25	0.651	0.154	102.133	1.023
13	45	25	60	25	0.955	0.123	115.123	2.125
14	45	25	60	25	0.754	0.225	112.125	2.084
15	45	25	60	25	0.854	0.140	108.083	1.595
16	45	25	60	20	0.731	0.192	97.600	1.129
17	45	25	40	25	0.566	0.226	89.657	1.437
18	45	40	60	25	0.769	0.206	67.108	3.505
19	45	25	80	25	0.652	0.219	93.082	1.431
20	45	10	60	25	0.621	0.145	102.400	2.813
21	45	25	60	30	0.831	0.164	91.782	2.263
22	60	40	40	30	0.761	0.261	89.323	1.493
23	60	10	80	30	1.129	0.280	100.555	1.527
24	60	25	60	25	0.539	0.203	84.712	0.315
25	60	10	80	20	0.689	0.171	128.089	2.651
26	60	40	40	20	1.044	0.215	124.152	0.132
27	60	10	40	20	0.980	0.171	159.810	1.027
28	60	10	40	30	1.254	0.123	97.037	2.350
29	60	40	80	30	1.439	0.145	112.602	0.368
30	60	40	80	20	1.156	0.136	132.193	1.190

APPENDIX 58

Table 5. 42: Analysis of Variance for OC (After elimination)

Source	Sum of Squares	DOF	Mean Square	F Value	p-value Prob > F	Percentage Contribution
Model	0.13	7	0.018	13.86	< 0.0001	81.25
C-Pulse on duration	0.094	1	0.094	72.04	< 0.0001	58.75
AB	0.010	1	0.010	7.76	0.0108	6.25
AC	0.046	1	0.046	35.25	< 0.0001	28.75
BD	0.040	1	0.040	30.24	< 0.0001	25
CD	0.062	1	0.062	47.30	< 0.0001	38.75
A^2	0.050	1	0.050	38.13	< 0.0001	31.25
B^2	0.026	1	0.026	19.74	0.0002	16.25
Residual	0.029	22	1.308E-003			
Lack of Fit	0.021	17	1.251E-003	0.83	0.6502	
Pure Error	7.516E-003	5	1.503E-003			
Corrected Total	0.16	29		R-Squared	0.8152	
				Adj R-Squared	0.7564	
				Pred R-Squared	0.7158	

APPENDIX 59

Table 5. 43: Analysis of Variance for RCL (After elimination)

Source	Sum of Squares	DOF	Mean Square	F Value	p-value Prob > F	Percentage Contribution
Model	12085.50	7	1726.50	9.51	< 0.0001	75.161
B-Peak current	2584.44	1	2584.44	14.24	0.0010	16.073
C-Pulse on duration	3622.88	1	3622.88	19.96	0.0002	22.531
AD	4742.97	1	4742.97	26.13	< 0.0001	29.497
BC	1580.96	1	1580.96	8.71	0.0074	9.832
CD	2819.43	1	2819.43	15.53	0.0007	17.534
A^2	5158.49	1	5158.49	28.42	< 0.0001	32.081
C^2	1073.72	1	1073.72	5.91	0.0236	6.678
Residual	3993.88	22	181.54			
Lack of Fit	2857.68	17	168.10	0.74	0.7093	
Pure Error	1136.20	5	227.24			
Corrected Total	16079.38	29				
				R-Squared	0.7516	
				Adj R-Squared	0.6726	
				Pred RSquared	0.6327	

APPENDIX 60

Table 5. 44: Analysis of Variance for TA (After elimination)

Source	Sum of Squares	DOF	Mean Square	F Value	p-value Prob > F	Percentage Contribution
Model	43.78	9	4.86	59.89	< 0.0001	95.195
A-Voltage	5.76	1	5.76	70.92	< 0.0001	12.524
B-Peak current	0.55	1	0.55	6.82	0.0167	1.196
C-Pulse on duration	5.77	1	5.77	71.03	< 0.0001	12.546
D-Pulse off duration	11.77	1	11.77	144.94	< 0.0001	25.593
AB	13.71	1	13.71	168.80	< 0.0001	29.811
AD	3.13	1	3.13	38.47	< 0.0001	6.806
CD	5.99	1	5.99	73.70	< 0.0001	13.025
A^2	2.63	1	2.63	32.36	< 0.0001	5.719
B^2	6.51	1	6.51	80.16	< 0.0001	14.155
Residual	1.62	20	0.081			
Lack of Fit	1.28	15	0.085	1.22	0.4444	
Pure Error	0.35	5	0.070			
Corrected Total	45.41	29		R-Squared	0.9642	
				Adj R-Squared	0.9481	
				Pred R-Squared	0.9210	

APPENDIX 61

Table 5.46: Training data sets

S. No	Parameters				(MRR) in mm^3/min	(OC) in µm	RCL) in µm	(TA)in degrees
	Voltage (V)	Peak current (I_p)	Pulse on duration (T_{on})	Pulse off duration (T_{off})				
1	45	40	60	25	0.769	0.206	67.108	3.505
2	60	25	60	25	0.539	0.203	84.712	0.315
3	30	40	40	20	0.964	0.37	88.612	2.283
4	60	40	40	30	0.761	0.261	89.323	1.493
5	45	25	40	25	0.566	0.226	89.657	1.437
6	45	25	60	30	0.831	0.164	91.782	2.263
7	45	25	80	25	0.652	0.219	93.082	1.431
8	30	40	40	30	0.522	0.265	94.509	2.676
9	60	10	40	30	1.254	0.123	97.037	2.35
10	45	25	60	20	0.731	0.192	97.6	1.129
11	30	10	80	20	0.217	0.114	98.811	0.852
12	60	10	80	30	1.129	0.28	100.555	1.527
13	45	25	60	25	0.651	0.154	102.133	1.023
14	45	10	60	25	0.621	0.145	102.4	2.813
15	30	25	60	25	0.283	0.177	102.665	1.507
16	45	25	60	25	0.852	0.315	107.274	1.084
17	45	25	60	25	0.557	0.24	108.083	1.095
18	45	25	60	25	0.854	0.14	108.083	1.595
19	45	25	60	25	0.754	0.225	112.125	2.084
20	60	40	80	30	1.439	0.145	112.602	0.368

APPENDIX 62

Table 5.47: Validation of the Developed Model with Experimental Data.

Process Parameters				MRR (mm^3/min)		OC(µm)		RCL(µm)		TA(degrees)	
V	I_p	T_{on}	T_{off}	Exp	ANN	Exp	ANN	Exp	ANN	Exp	ANN
60	40	40	20	1.044	0.912	0.215	0.319	124.152	121.623	0.132	0.878
60	10	80	20	0.689	0.652	0.171	0.131	128.089	133.006	2.651	2.469
30	40	80	20	0.895	0.771	0.334	0.306	129.194	115.639	2.830	2.212
30	10	40	30	0.406	0.451	0.209	0.174	130.942	143.479	3.094	3.865
60	40	80	20	1.156	1.112	0.136	0.287	132.193	146.175	1.190	1.050
30	10	40	20	0.879	0.598	0.322	0.310	141.242	129.749	0.261	0.630
60	10	40	20	0.980	1.046	0.171	0.177	159.810	151.401	1.027	0.755
60	40	40	20	1.044	0.912	0.215	0.319	124.152	121.623	0.132	0.878
60	10	80	20	0.689	0.652	0.171	0.131	128.089	133.006	2.651	2.469
30	40	80	20	0.895	0.771	0.334	0.306	129.194	115.639	2.830	2.212

Table 5.48: Errors in Prediction of Responses

(V)	(I_p)	(T_{on})	(T_{off})	% Error in Prediction of MRR	% Error in Prediction of OC	% Error in Prediction of RCL	% Error in Prediction of TA
30	40	80	30	0.961	31.227	-0.762	12.028
45	25	60	25	-0.346	-66.136	-4.002	-25.199
30	10	80	30	10.173	17.433	-4.682	47.363
60	40	40	20	-4.517	-48.455	2.037	1.515
60	10	80	20	5.390	-0.009	-3.839	6.863
30	40	80	20	2.701	8.409	10.492	4.156
30	10	40	30	-10.995	16.696	-0.410	0.949
60	40	80	20	3.793	3.746	-3.012	11.781
30	10	40	20	1.250	3.722	0.349	-141.327
60	10	40	20	13.716	-3.635	0.881	1.203
Average (%) of error				2.213	-3.700	-0.295	-8.067
Total average prediction error (%) = -9.849							

APPENDIX 63

Table 5.49: Testing of the Developed Model with Experimental Data

Process Parameters				MRR (mm^3/min)		OC(μm)		RCL(μm)		TA(degrees)	
V	I_p	T_{on}	T_{off}	Exp	ANN	Exp	ANN	Exp	ANN	Exp	ANN
30	10	80	20	0.217	0.271	0.114	0.121	98.811	97.201	0.852	0.929
60	10	80	30	1.129	0.982	0.280	0.219	100.555	98.542	1.527	2.003
45	25	60	25	0.651	0.599	0.154	0.151	102.133	101.238	1.023	1.028
45	10	60	25	0.621	0.532	0.145	0.129	102.400	99.917	2.813	2.724
30	25	60	25	0.283	0.291	0.177	0.167	102.665	102.278	1.507	1.657
45	25	60	25	0.754	0.722	0.225	0.233	112.125	112.141	2.084	1.848
60	40	80	30	1.439	1.428	0.145	0.133	112.602	112.206	0.368	0.417
30	10	80	20	0.217	0.271	0.114	0.121	98.811	97.201	0.852	0.929
60	10	80	30	1.129	0.982	0.280	0.219	100.555	98.542	1.527	2.003
45	25	60	25	0.651	0.599	0.154	0.151	102.133	101.238	1.023	1.028

Table 5.50: Errors in Prediction of Responses during Testing

(V)	(I_p)	(T_{on})	(T_{off})	% Error in Prediction of MRR	% Error in Prediction of OC	% Error in Predictio n of RCL	% Error in Predicti on of TA
30	40	40	30	-29.199	16.944	-0.651	5.673
60	10	40	30	1.966	0.190	1.839	-0.890
45	25	60	20	25.011	-10.800	1.377	-3.999
30	10	80	20	-24.973	-6.251	1.629	-9.015
60	10	80	30	12.987	21.866	2.002	-31.146
45	25	60	25	7.917	1.970	0.876	-0.523
45	10	60	25	14.404	11.013	2.425	3.173
30	25	60	25	-2.733	5.561	0.377	-9.939
45	25	60	25	4.288	-3.432	-0.014	11.323
60	40	80	30	0.773	8.430	0.351	-13.368
Average (%) of error				1.044	4.549	1.021	-4.871
Total average prediction error (%) = 1.743							

APPENDIX 64

Table 5.51: Training and validation error

Type of membership function	MRR		OC		RCL		TA	
	Training error	Validation error	Training error	Validation error	Training error	Validation error	Training error	Validation error
Triangle	0.10826	0.10825	0.034542	0.034541	6.6714	6.6705	0.57322	0.57318
Trapezoid	0.093549	0.093506	0.033505	0.033503	5.7524	5.4799	0.51104	0.51079
Generalized bell	0.076613	0.076601	0.032693	0.03269	4.9359	4.9334	0.27646	0.27646
Gaussian	0.091463	0.091406	0.33463	0.33461	5.6419	5.6395	0.49769	0.49736

Table 5.52: TAE for process responses

Type of membership function	MRR	OC	RCL	TA
	Total Average error	Total Average error	Total Average error	Total Average error
Triangle	0.108255	0.034542	6.67095	0.5732
Trapezoid	0.093528	0.033504	5.61615	0.510915
Generalized bell	0.076607	0.032692	4.93465	0.27646
Gaussian	0.091435	0.33462	5.6407	0.497525

APPENDIX 65

Table 5.53: Testing of the developed model with experimental data.

Process Parameters				MRR (mm^3/min)		OC(μm)		RCL(μm)		TA(degrees)	
V	I_p	T_{on}	T_{off}	Exp	ANFIS	Exp	ANFIS	Exp	ANFIS	Exp	ANFIS
30	40	40	30	0.522	0.522	0.265	0.265	94.509	94.509	2.676	2.242
60	10	40	30	1.254	1.253	0.123	0.123	97.037	97.037	2.350	2.214
45	25	60	20	0.731	0.673	0.192	0.211	97.600	103.167	1.129	2.958
30	10	80	20	0.217	0.217	0.114	0.114	98.811	98.813	0.852	0.705
60	10	80	30	1.129	1.128	0.280	0.280	100.555	100.555	1.527	1.640
45	25	60	25	0.651	0.687	0.154	0.210	102.133	101.172	1.023	1.098
45	10	60	25	0.621	0.615	0.145	0.145	102.400	103.057	2.813	2.675
30	25	60	25	0.283	0.287	0.177	0.188	102.665	106.459	1.507	1.692
45	25	60	25	0.754	0.687	0.225	0.210	112.125	101.172	2.084	2.080
60	40	80	30	1.439	1.438	0.145	0.145	112.602	112.602	0.368	0.428

Table 5.54: Errors in Prediction of Responses during testing

(V)	(I_p)	(T_{on})	(T_{off})	% Error in Prediction of MRR	% Error in Prediction of OC	% Error in Prediction of RCL	% Error in Prediction of TA
30	40	40	30	0.000	0.000	0.000	16.226
60	10	40	30	0.096	0.000	0.000	5.783
45	25	60	20	7.948	-9.740	-5.704	-162.011
30	10	80	20	0.000	0.000	-0.002	17.289
60	10	80	30	0.124	0.000	0.000	-7.400
45	25	60	25	-5.515	-36.104	0.941	-7.328
45	10	60	25	0.982	0.000	-0.641	4.906
30	25	60	25	-1.555	-6.328	-3.695	-12.276
45	25	60	25	8.899	6.844	9.769	0.206
60	40	80	30	0.090	0.000	0.000	-16.304
Average (%) of error				1.107	-4.533	0.067	-16.091
Total average prediction error (%) = -19.441							

APPENDIX 66

Table 5. 55: Pareto-optimal solutions obtained from MOETLBO

V	I_p	T_{on}	T_{off}	MRR	OC	RCL	TA	Rank
30.796	28.747	44.213	27.740	0.460	0.267	92.886	2.253	1
59.934	29.097	50.909	21.002	0.803	0.236	119.157	0.128	2
35.617	39.191	52.046	29.813	0.619	0.294	71.954	4.446	3
60.000	27.675	67.150	22.115	0.794	0.254	110.728	0.190	4
37.768	28.784	61.117	21.517	0.573	0.240	84.799	1.269	5
59.944	24.109	48.409	21.271	0.722	0.204	125.433	0.017	6
33.502	39.202	52.466	29.815	0.586	0.286	75.210	4.543	7
31.293	12.668	73.370	20.128	0.624	0.135	89.674	0.206	8
59.772	34.153	49.445	22.311	0.903	0.273	108.412	0.159	9
57.339	39.763	52.771	26.886	1.000	0.321	77.030	1.406	10
59.262	26.447	63.668	21.873	0.764	0.242	110.244	0.058	11
52.781	38.865	64.459	28.982	0.914	0.343	74.295	2.194	12
31.396	22.095	48.245	23.165	0.494	0.247	99.360	0.794	13
50.163	39.317	51.678	29.374	0.859	0.317	63.332	2.832	14
43.384	39.236	52.289	29.807	0.746	0.313	64.280	3.803	15
49.813	39.374	47.108	29.810	0.844	0.306	60.914	2.967	16
59.448	22.349	48.271	20.970	0.698	0.197	127.836	0.140	17
31.858	20.174	48.265	20.533	0.511	0.236	102.653	0.267	18
59.942	27.514	50.500	21.024	0.775	0.225	120.988	0.130	19
31.009	22.428	47.544	23.573	0.488	0.250	99.816	0.859	20
56.275	38.749	52.365	28.734	0.947	0.309	69.083	1.562	21
35.408	39.045	57.194	29.358	0.626	0.291	75.271	4.312	22
35.017	38.332	46.974	28.908	0.591	0.295	73.778	4.152	23
31.181	21.184	54.447	22.324	0.508	0.222	94.915	0.543	24
39.567	26.042	51.581	26.015	0.558	0.266	85.493	1.796	25
37.090	23.384	67.843	21.608	0.560	0.203	87.305	0.864	26
59.269	27.014	49.593	22.966	0.755	0.227	111.358	0.033	27
31.971	24.998	65.468	23.931	0.515	0.206	89.562	1.073	28
45.643	35.131	44.442	27.804	0.701	0.293	73.243	2.654	29
40.602	35.566	50.499	28.584	0.644	0.295	71.620	3.221	30
45.192	39.417	56.504	29.378	0.789	0.322	66.217	3.544	31
31.153	19.676	70.522	22.325	0.542	0.168	91.295	0.426	32
36.724	33.485	54.864	22.682	0.591	0.278	82.096	2.083	33
46.089	39.698	54.440	28.795	0.808	0.324	65.861	3.433	34
31.294	12.668	73.369	20.128	0.624	0.135	89.674	0.206	35

APPENDIX 67

Table 5. 56: Pareto-optimal solutions obtained from MODE

V	Ip	T_{on}	T_{off}	MRR	OC	RCL	TA	Rank
51.020	39.952	47.065	29.999	0.777	0.166	49.616	5.881	1
59.629	23.002	44.653	20.226	0.604	0.066	126.420	3.069	2
30.713	24.812	76.139	22.181	0.420	0.034	82.673	3.572	3
54.289	39.657	55.048	29.217	0.841	0.181	56.220	5.112	4
58.830	39.808	56.157	28.637	0.924	0.176	62.456	4.133	5
30.007	28.275	42.328	28.103	0.347	0.151	85.743	5.246	6
33.487	39.932	49.361	21.462	0.529	0.203	69.897	6.211	7
36.722	34.594	44.077	28.336	0.466	0.163	67.694	6.258	8
31.057	39.999	52.696	29.976	0.457	0.153	68.684	7.847	9
39.793	35.344	52.462	27.173	0.537	0.166	64.710	6.019	10
59.830	34.327	57.795	26.508	0.806	0.149	77.548	3.233	11
30.554	23.914	77.574	20.177	0.421	0.004	79.271	3.093	12
30.562	23.911	77.565	20.180	0.421	0.004	79.271	3.095	13
59.732	29.091	56.644	23.834	0.701	0.117	92.709	2.953	14
59.393	25.175	49.651	22.175	0.632	0.086	107.289	3.032	15
52.932	39.717	52.038	29.236	0.815	0.176	54.196	5.402	16
59.730	23.323	45.218	20.200	0.609	0.067	125.584	3.035	17
37.724	37.084	55.227	29.157	0.530	0.165	63.139	6.743	18
59.282	27.194	51.784	20.391	0.665	0.094	111.567	2.939	19
31.790	23.967	44.987	24.421	0.383	0.147	89.536	4.188	20
50.850	39.528	62.888	29.617	0.794	0.201	60.249	5.702	21
42.433	39.774	53.087	28.613	0.648	0.185	56.963	6.861	22
59.671	24.330	46.437	20.748	0.622	0.074	119.686	3.001	23
59.460	27.444	61.904	20.566	0.680	0.105	105.144	2.874	24
31.870	25.158	48.973	23.148	0.389	0.134	85.103	4.013	25
33.092	39.491	58.448	28.569	0.501	0.157	68.999	7.361	26
59.686	27.739	46.943	23.551	0.667	0.092	100.767	2.996	27
45.703	39.092	50.235	26.815	0.690	0.188	60.447	6.169	28
38.943	39.794	52.965	29.181	0.588	0.178	58.576	7.260	29
34.815	28.645	76.913	20.228	0.463	0.050	77.976	3.865	30
49.362	38.332	54.290	29.557	0.727	0.178	54.655	5.790	31
59.751	29.291	64.341	23.056	0.715	0.130	95.560	2.893	32
55.590	38.647	53.404	28.951	0.834	0.169	58.137	4.691	33
31.284	24.009	43.419	24.950	0.375	0.151	91.204	4.267	34
60.000	27.591	66.805	20.713	0.693	0.111	105.424	2.780	35

APPENDIX 68

Table 5. 57: Pareto-optimal solutions obtained from MOABC

V	I_p	T_{on}	T_{off}	MRR	OC	RCL	TA	RANK
30.049	27.962	47.595	29.957	0.454	0.142	112.170	1.449	1
34.991	39.877	56.067	29.245	0.630	0.166	94.503	0.021	2
30.031	39.999	50.702	30.000	0.536	0.151	99.824	0.881	3
59.936	36.897	60.954	26.302	0.976	0.172	108.024	6.571	4
60.000	13.505	41.763	20.516	0.647	0.043	172.526	5.804	5
58.947	16.465	43.286	20.844	0.650	0.055	161.616	6.075	6
52.220	39.967	48.514	29.986	0.900	0.167	80.017	3.568	7
30.074	39.162	56.422	29.765	0.539	0.142	103.244	0.572	8
31.236	25.220	79.839	21.032	0.528	0.013	112.649	3.710	9
59.250	39.952	63.606	29.003	1.045	0.201	97.348	5.904	10
59.329	19.660	59.991	23.624	0.687	0.099	128.753	6.528	11
57.490	24.331	48.016	21.459	0.704	0.089	139.352	6.469	12
37.124	38.414	47.792	29.804	0.623	0.167	89.842	0.504	13
57.156	18.317	44.248	21.439	0.650	0.073	150.772	5.950	14
30.139	29.100	55.568	28.024	0.475	0.126	110.260	1.752	15
48.790	39.453	56.821	29.754	0.847	0.188	84.684	2.801	16
59.999	13.505	41.763	20.516	0.647	0.043	172.521	5.804	17
34.614	34.052	49.841	29.852	0.538	0.151	97.874	1.012	18
59.461	17.010	44.719	20.891	0.656	0.054	159.442	6.253	19
50.074	39.427	48.457	29.962	0.851	0.169	80.472	3.070	20
48.559	29.536	48.170	26.079	0.670	0.144	103.865	4.270	21
52.919	35.092	56.550	28.494	0.820	0.166	92.388	4.623	22
46.627	37.254	60.299	29.680	0.774	0.183	89.474	2.689	23
55.346	18.025	46.139	24.409	0.641	0.099	131.148	5.440	24
45.297	39.855	51.644	29.308	0.791	0.183	83.649	1.888	25
30.035	38.231	50.671	29.960	0.514	0.146	101.552	0.418	26
47.861	31.009	48.226	25.936	0.681	0.150	102.414	4.041	27
57.129	37.308	57.580	27.720	0.935	0.172	97.022	5.596	28
31.115	28.343	76.904	21.812	0.524	0.038	111.787	3.228	29
59.875	22.203	76.735	22.870	0.731	0.125	134.459	6.975	30
44.578	37.172	50.292	29.946	0.722	0.168	84.673	2.152	31
52.994	34.277	63.999	26.314	0.822	0.174	103.110	4.920	32
59.840	33.434	75.460	26.804	0.910	0.196	121.644	6.911	33
59.985	28.860	78.311	21.785	0.826	0.141	137.955	7.244	34
59.025	31.926	77.960	23.572	0.874	0.172	131.363	6.859	35

References

Ahmad, S. and Lajis, M.A., 2013. Electrical discharge machining (EDM) of Inconel 718 by using copper electrode at higher peak current and pulse duration. In *IOP Conference Series: Materials Science and Engineering* (Vol. 50, No. 1, p. 012062). IOP Publishing.

Alfano, G. and Crisfield, M.A., 2001. Finite element interface models for the delamination analysis of laminated composites: mechanical and computational issues. *International journal for numerical methods in engineering*, *50*(7), pp.1701-1736.

Aravind, D., Varun, A., Manu, R., and Mathew, J. 2009."Modeling of micro electric discharge machining process for MRR using artificial neural networks," Proceeding of the Sixth International Conference on Precision, Meso, Micro and Nano Engineering, pp.C16-C19.

Bhattacharyya, B., Gangopadhyay, S. and Sarkar, B.R., 2007. Modelling and analysis of EDM ED job surface integrity. *Journal of Materials Processing Technology*, *189*(1), pp.169-177.

Bigot, S., Ivanov, A., and Popov, K. "A study of the micro EDM electrode wear," Proceedings of the First International Conference on Multi-Material Micro-Manufacture, 4M, pp.355-358, 2005.

Črepinšek, M., Liu, S.H. and Mernik, L., 2012. A note on teaching–learning-based optimization algorithm. *Information Sciences*, *212*, pp.79-93.

Das, S., Klotz, M. and Klocke, F., 2003. EDM simulation: finite element-based calculation of deformation, microstructure and residual stresses. *Journal of Materials Processing Technology*, *142*(2), pp.434-451.

Datta, S., Bandyopadhyay, A. and Pal, P.K., 2008. Grey-based taguchi method for optimization of bead geometry in submerged arc bead-on-plate welding. *The International Journal of Advanced Manufacturing Technology*,*39*(11-12), pp.1136-1143.

Deb, K., Pratap, A., Agarwal, S. and Meyarivan, T.A.M.T., 2002. A fast and elitist multiobjective genetic algorithm: NSGA-II. *Evolutionary Computation, IEEE Transactions on*, *6*(2), pp.182-197.

Dhar, S., Purohit, R., Saini, N., Sharma, A. and Kumar, G.H., 2007. Mathematical modeling of electric discharge machining of cast Al–4Cu–6Si alloy–10wt.% SiC P composites. *Journal of materials processing technology*,*194*(1), pp.24-29.

Dhara, S.K., Kuar, A.S. and Mitra, S., 2008. An artificial neural network approach on parametric optimization of laser micro-machining of die-steel. *The International Journal of Advanced Manufacturing Technology*, *39*(1-2), pp.39-46.

Dutil, Y., Rousse, D.R., Salah, N.B., Lassue, S. and Zalewski, L., 2011. A review on phase-change materials: mathematical modeling and simulations. *Renewable and sustainable Energy reviews*, *15*(1), pp.112-130.

Ekmekci, B., Elkoca, O. and Erden, A., 2005. A comparative study on the surface integrity of plastic mold steel due to electric discharge machining. *Metallurgical and Materials Transactions B*, *36*(1), pp.117-124.

Ekmekci, B., Elkoca, O., Erman Tekkaya, A. and Erden, A., 2005(a). Residual stress state and hardness depth in electric discharge machining: de-ionized water as dielectric liquid. *Machine Science and Technology*, *9*(1), pp.39-61.

Ekmekci, B., Sayar, A., Öpöz, T.T. and Erden, A., 2009. Geometry and surface damage in micro electrical discharge machining of micro-holes. *Journal of Micromechanics and Microengineering*, *19*(10), p.105030.

Ekmekci, B., Tekkaya, A.E. and Erden, A., 2006. A semi-empirical approach for residual stresses in electric discharge machining (EDM). *International Journal of Machine Tools and Manufacture*, *46*(7), pp.858-868.

Esme Ugur, 2010. "Use of grey based Taguchi method in ball burnishing process for the optimization of surface roughness and micro hardness of AA7075 aluminium alloy," Materials and Technology, Vol.44,

Fausett, L. (1994). *Fundamentals of neural networks*. Englewood Cliffs, NJ: Prentice-Hall.

Fukunaga, K. and Hostetler, L.D., 1975. The estimation of the gradient of a density function, with applications in pattern recognition. *Information Theory, IEEE Transactions on*, *21*(1), pp.32-40.

Garg, R.K., Singh, K.K., Sachdeva, A., Sharma, V.S., Ojha, K. and Singh, S., 2010. Review of research work in sinking EDM and WEDM on metal matrix composite materials. *The International Journal of Advanced Manufacturing Technology*, *50*(5-8), pp.611-624.

George, P.M., Raghunath, B.K., Manocha, L.M. and Warrier, A.M., 2004. Modelling of machinability parameters of carbon–carbon composite—a response surface approach. *Journal of materials processing technology*, *153*, pp.920-924.

Ghosh, S. and Reilly, D.L., 1994, January. Credit card fraud detection with a neural-network. In *System Sciences, 1994. Proceedings of the Twenty-Seventh Hawaii International Conference on* (Vol. 3, pp. 621-630). IEEE.

Gopalakannan, S. and Senthilvelan, T., 2013. Application of response surface method on machining of Al–SiC nano-composites. *Measurement*,*46*(8), pp.2705-2715.

Hasçalık, A. and Çaydaş, U., 2007. Electrical discharge machining of titanium alloy (Ti–6Al–4V). *Applied Surface Science*, *253*(22), pp.9007-9016.

Ho, K.H. and Newman, S.T., 2003. State of the art electrical discharge machining (EDM). *International Journal of Machine Tools and Manufacture*,*43*(13), pp.1287-1300.

Ikai, T. and Hashigushi, K., 1995, April. Heat input for crater formation in EDM. In *Proceedings of the International Symposium for Electro-Machining-ISEM XI, EPFL* (pp. 163-170).

Jahan, M.P., San Wong, Y. and Rahman, M., 2010. A comparative experimental investigation of deep-hole micro-EDM drilling capability for cemented carbide (WC-Co) against austenitic stainless steel (SUS 304). *The International Journal of Advanced Manufacturing Technology*, *46*(9-12), pp.1145-1160.

Jahan, M.P., Rahman, M. and Wong, Y.S., 2014. Micro-Electrical Discharge Machining (Micro-EDM): Processes, Varieties, and Applications. *Comprehensive Materials Processing*, *11*, pp.333-371.

Jeswani, M.L., 1981. Effect of the addition of graphite powder to kerosene used as the dielectric fluid in electrical discharge machining. *Wear*, *70*(2), pp.133-139.

Joshi, S.N. and Pande, S.S., 2009. Development of an intelligent process model for EDM. *The International Journal of Advanced Manufacturing Technology*, *45*(3-4), pp.300-317.

Jung, J.H. and Kwon, W.T., 2010. Optimization of EDM process for multiple performance characteristics using Taguchi method and Grey relational analysis. *Journal of Mechanical Science and Technology*, *24*(5), pp.1083-1090.

Kahng, C.H. and Rajurkar, K.P., 1977. Surface characteristics behaviour due to rough and fine cutting by EDM. *Annals of the CIRP*, *26*(1), pp.77-82.

Kansal, H.K., Singh, S. and Kumar, P., 2008. Numerical simulation of powder mixed electric discharge machining (PMEDM) using finite element method. *Mathematical and Computer Modelling*, *47*(11), pp.1217-1237.

Karaboga, D. and Akay, B., 2009. A comparative study of artificial bee colony algorithm. *Applied mathematics and computation*, *214*(1), pp.108-132.

Kruth, J.P., Stevens, L., Froyen, L. and Lauwers, B., 1995. Study of the white layer of a surface machined by die-sinking electro-discharge machining. *CIRP Annals-Manufacturing Technology*, *44*(1), pp.169-172.

Kunieda, M., Lauwers, B., Rajurkar, K.P. and Schumacher, B.M., 2005. Advancing EDM through fundamental insight into the process. *CIRP Annals-Manufacturing Technology*, *54*(2), pp.64-87.

Kurnia, W., Tan, P.C., Yeo, S.H. and Wong, M., 2008. Analytical approximation of the erosion rate and electrode wear in micro electrical discharge machining. *Journal of Micromechanics and Microengineering*,*18*(8), p.085011.

Lin, C.L., Lin, J.L. and Ko, T.C., 2002. Optimisation of the EDM process based on the orthogonal array with fuzzy logic and grey relational analysis method. *The International Journal of Advanced Manufacturing Technology*,*19*(4), pp.271-277.

Lin, T.R., 2002. Optimisation technique for face milling stainless steel with multiple performance characteristics. *The International Journal of Advanced Manufacturing Technology*, *19*(5), pp.330-335.

Lin, Y.C., Chen, Y.F., Wang, D.A. and Lee, H.S., 2009. Optimization of machining parameters in magnetic force assisted EDM based on Taguchi method. *Journal of materials processing technology*, *209*(7), pp.3374-3383.

Liu, H.S., Yan, B.H., Huang, F.Y. and Qiu, K.H., 2005. A study on the characterization of high nickel alloy micro-holes using micro-EDM and their applications. *Journal of Materials Processing Technology*, *169*(3), pp.418-426.

Luis, C.J., Puertas, I. and Villa, G., 2005. Material removal rate and electrode wear study on the EDM of silicon carbide. *Journal of materials processing technology*, *164*, pp.889-896.

Majumder, A., Das, P.K., Majumder, A. and Debnath, M., 2014. An approach to optimize the EDM process parameters using desirability-based multi-objective PSO. *Production and Manufacturing Research*, *2*(1), pp.228-240.

Marafona, J. and Chousal, J.A.G., 2006. A finite element model of EDM based on the Joule effect. *International Journal of Machine Tools and Manufacture*, *46*(6), pp.595-602.

Mathew, J., Somashekhar, K.P., Sooraj, V.S., Subbarao, N. and Ramachandran, N., 2009. Effect of work material and machining conditions on the accuracy and quality of micro holes. *International Journal of Abrasive Technology*, *2*(3), pp.279-298.

Mernik, M., Liu, S.H., Karaboga, D. and Črepinšek, M., 2015. On clarifying misconceptions when comparing variants of the Artificial Bee Colony Algorithm by offering a new implementation. *Information Sciences*, *291*, pp.115-127.

Mitra, S., Paul, G. and Sarkar, S., 2011, January. Experimental Study on Influence of Process Variables on Crater Dimensions in Micro-EDM of γ-Titanium Aluminide. In *International Conference on Advances In Materials And Processing Technologies (AMPT2010)* (Vol. 1315, No. 1, pp. 1181-1186). AIP Publishing.

Mitra, S., Paul, G. and Sarkar, S., 2011, January. Experimental Study on Influence of Process Variables on Crater Dimensions in Micro-EDM of γ-Titanium Aluminide. In *International Conference on Advances In Materials And Processing Technologies (AMPT2010)* (Vol. 1315, No. 1, pp. 1181-1186). AIP Publishing.

Montgomery, D. (1991). *Design and analysis of experiments*. New York: Wiley.

Muthukumar, V., Sureshbabu, A., Venkatasamy, R., and Raajenthiren,M. 2010. "Optimization of the WEDM parameters on machining Incoloy 800 super alloy with multiple quality characteristics," Optimization, Vol.2, No.6, pp.1538-1547,

Natarajan, N. and Arunachalam, R.M., 2011. Optimization of micro-EDM with multiple performance characteristics using Taguchi method and Grey relational analysis. *Journal of Scientific and Industrial Research*, *70*(7), pp.500-5.

No.3, pp.129-135,

Panda, D.K., 2010. Modelling and optimization of multiple process attributes of electrodischarge machining process by using a new hybrid approach of neuro–grey modeling. *Materials and Manufacturing Processes*, *25*(6), pp.450-461.

Patel, M.R., Barrufet, M.A., Eubank, P.T. and DiBitonto, D.D., 1989. Theoretical models of the electrical discharge machining process. II. The anode erosion model. *Journal of applied physics*, *66*(9), pp.4104-4111.

Payal, H.S., Choudhary, R. and Singh, S., 2008. Analysis of electro discharge machined surfaces of EN-31 tool steel. *Journal of scientific and industrial research*, *67*(12), pp.1072-1077.

Pellicer, N., Ciurana, J. and Ozel, T., 2009. Influence of process parameters and electrode geometry on feature micro-accuracy in electro discharge machining of tool steel. *Materials and manufacturing processes*, *24*(12), pp.1282-1289.

Peng, Z.L., Wang, Z.L. and Jin, B.D., 2008, March. Micro-forming process and microstructure of deposit by using micro EDM deposition in air. In *Key Engineering Materials* (Vol. 375, pp. 153-157). Trans Tech Publications.

pp.26-30,

Pradhan, B.B., Masanta, M., Sarkar, B.R. and Bhattacharyya, B., 2009. Investigation of electro-discharge micro-machining of titanium super alloy. *The International Journal of Advanced Manufacturing Technology*, *41*(11-12), pp.1094-1106.

Pradhan, M.K., and Biswas, C.K. 2008. "Modeling of machining parameters for MRR in EDM using response surface methodology," Proceedings of the National Conference on Mechanism Science and Technology:from Theory to Application, 2008, National Institute of Technology, Hamirpur, pp.1-8,

Precision, Meso, Micro and Nano Engineering, pp.C16-C19,

Put, S., Vleugels, J., Van der Biest, O., Trueman, C.S. and Huddleston, J., 2001. Die sink electrodischarge machining of zirconia based composites. *British ceramic transactions*, *100*(5), pp.207-213.

Ramakrishnan, R. and Karunamoorthy, L., 2008. Modeling and multi-response optimization of Inconel 718 on machining of CNC WEDM process. *Journal of materials processing technology*, *207*(1), pp.343-349.

Rao, R.V. and Kalyankar, V.D., 2013. Parameter optimization of modern machining processes using teaching–learning-based optimization algorithm. *Engineering Applications of Artificial Intelligence*, *26*(1), pp.524-531.

Roshan, S.B., Jooibari, M.B., Teimouri, R., Asgharzadeh-Ahmadi, G., Falahati-Naghibi, M. and Sohrabpoor, H., 2013. Optimization of friction stir welding process of AA7075 aluminum alloy to achieve desirable mechanical properties using ANFIS models and simulated annealing algorithm. *The International Journal of Advanced Manufacturing Technology*, *69*(5-8), pp.1803-1818.

Sarkar, S., Ghosh, K., Mitra, S. and Bhattacharyya, B., 2010. An integrated approach to optimization of WEDM combining single-pass and multipass cutting operation. *Materials and Manufacturing Processes*, *25*(8), pp.799-807.

Shabgard, M., Ahmadi, R., Seyedzavvar, M. and Oliaei, S.N.B., 2013. Mathematical and numerical modeling of the effect of input-parameters on the flushing efficiency of plasma channel in EDM process. *International Journal of Machine Tools and Manufacture*, *65*, pp.79-87.

Shabgard, M., Oliaei, S.N.B., Seyedzavvar, M. and Najadebrahimi, A., 2011(a). Experimental investigation and 3D finite element prediction of the white layer thickness, heat affected zone, and surface roughness in EDM process.*Journal of mechanical science and technology*, *25*(12), pp.3173-3183.

Shabgard, M., Seyedzavar, M. and Nadimi, S., 2011(b). A numerical method for predicting depth of heat affected zone in EDM process for AISI H13 tool steel. *J Sci Ind Res*, *70*, pp.493-499.

Shabgard, M.R. and Shotorbani, R.M., 2009. Mathematical modeling of machining parameters in electrical discharge machining of FW4 welded steel. *World Academy of Science, Engineering and Technology*, *52*(63), pp.403-409.

Shen, Xiaolong, Zhaoyang Ning, and Mingjun Zhang. 2012. "The study on optimization of self-adaptive EDM parameters with grey relational analysis," IEIT Journal of Adaptive and Dynamic Computing, Vol.3,

Somashekhar, K.P., Mathew, J. and Ramachandran, N., 2011(b). Multi-objective optimization of micro wire electric discharge machining parameters using grey relational analysis with Taguchi method. *Proceedings of the Institution of Mechanical Engineers, Part C: Journal of Mechanical Engineering Science*, *225*(7), pp.1742-1753.

Somashekhar, K.P., Ramachandran, N. and Mathew, J., 2010. Optimization of material removal rate in micro-EDM using artificial neural network and genetic algorithms. *Materials and Manufacturing Processes*, *25*(6), pp.467-475.

Storn, R. and Price, K., 1997. Differential evolution–a simple and efficient heuristic for global optimization over continuous spaces. *Journal of global optimization*, *11*(4), pp.341-359.

Suganthi, X.H., Natarajan, U., Sathiyamurthy, S. and Chidambaram, K., 2013. Prediction of quality responses in micro-EDM process using an adaptive neuro-fuzzy inference system (ANFIS) model. *The International Journal of Advanced Manufacturing Technology*, *68*(1-4), pp.339-347.

Thao, O. and Joshi, S.S., 2008. Analysis of heat affected zone in the micro-electric discharge machining. *International Journal of Manufacturing Technology and Management*, *13*(2-4), pp.201-213.

Thorani, Y.L.P., Rao, P.P.B. and Shankar, N.R., 2012. Ordering generalized trapezoidal fuzzy numbers. *International Journal of Contemporary Mathematical Sciences*, *7*(12), pp.555-573.

Tiwary, A.P., Pradhan, B.B. and Bhattacharyya, B., 2015. Study on the influence of micro-EDM process parameters during machining of Ti–6Al–4V superalloy. *The International Journal of Advanced Manufacturing Technology*, *76*(1-4), pp.151-160.

Vijayaraj, R., Gowri, S. and Balan, A.S.S., 2009, October. Study on parametric influence, optimization and modeling in micro WEDM of Ti alloy. In *Advanced Materials Research* (Vol. 76, pp. 571-576).

Vinodh, S. and Vimal, K.E.K., 2012. Thirty criteria based leanness assessment using fuzzy logic approach. *The International Journal of Advanced Manufacturing Technology*, *60*(9-12), pp.1185-1195.

Wang, D., Zhao, W.S., Gu, L. and Kang, X.M., 2011. A study on micro-hole machining of polycrystalline diamond by micro-electrical discharge machining. *Journal of Materials Processing Technology*, *211*(1), pp.3-11.

Wang, K., Gelgele, H.L., Wang, Y., Yuan, Q. and Fang, M., 2003. A hybrid intelligent method for modelling the EDM process. *International Journal of Machine Tools and Manufacture*, *43*(10), pp.995-999.

Yang, W.P. and Tarng, Y.S., 1998. Design optimization of cutting parameters for turning operations based on the Taguchi method. *Journal of materials processing technology*, *84*(1), pp.122-129.

Zeid, O.A., 1997. On the effect of electrodischarge machining parameters on the fatigue life of AISI D6 tool steel. *Journal of Materials Processing Technology*, *68*(1), pp.27-32.

Zitzler, E., Laumanns, M. and Bleuler, S., 2004. A tutorial on evolutionary multiobjective optimization. In *Metaheuristics for multiobjective optimisation* (pp. 3-37). Springer Berlin Heidelberg.

DISSEMINATION

1) K. P .Maity and Himanshu Mishra "Optimization of Micro-EDM operation for fabrication of Micro-holes using ANN Proceedings 25th AIMTDR 2012 and 4th International Conf. Jadavpur University.

2) K. P .Maity and Himanshu Mishra. 2013 "Optimization of Micro-EDM operation for fabrication of Micro-holes using ANN. Journal of the Association of Engineers, India, Vol. 83, No. 3 & 4, pp.71-80.

3) Maity, K. and Mishra, H., 2016. ANN modelling and Elitist teaching learning approach for multi-objective optimization of μ -EDM. *Journal of Intelligent Manufacturing*, pp.118.

4) Maity, K. and Mishra, H., ANFIS based prediction and Optimization of Micro-Electric discharge machining process using Whale Optimization Algorithm *Journal of optimization (Communicated)*